Universität Bremen

Small Molecule Activation mediated by Metal-Ligand Cooperation *via* a Dearomatization/Rearomatization Reaction Sequence using Redox Active Pyridine based Ligand-Systems in Transition Metal Complexes

Dissertation towards the academic degree

Doctor rerum naturalium (Dr. rer. nat.)

Submitted to the
Department of Biology and Chemistry
Institute of Inorganic Chemistry and Crystallography
of the Universität Bremen

Rasmus Stichauer
Bremen
September 2023

This work was carried out under the supervision of Prof. Dr. Jens Beckmann and Dr. Matthias Vogt from September 2015 to September 2023 at the Institute of Inorganic Chemistry and Crystallography, Department of Biology and Chemistry of the University Bremen.

1st Referee: Prof. Dr. Jens Beckmann (Universität Bremen)

2nd Referee: Prof. Dr. Anne Staubitz (Universität Bremen)

Date of Defense: 07.11.2023

Eidesstattliche Erklärung

Ich, Rasmus Stichauer

versichere an Eides statt durch meine Unterschrift, dass ich die vorliegende Arbeit selbstständig und ohne fremde Hilfe angefertigt und alle Stellen, die ich wörtlich dem Sinne nach aus Veröffentlichungen entnommen habe, als solche kenntlich gemacht und mich auch keiner anderen als der angegebenen Literatur oder sonstiger Hilfsmittel bedient habe. Die aus fremden Quellen direkt oder indirekt übernommenen Formulierungen und Gedanken – einschließlich Abbildungen, Tabellen etc. – sind als solche kenntlich gemacht. Diese schriftliche Arbeit wurde bisher weder ganz noch in Teilen als Prüfungsleistung vorgelegt.
Ich versichere eidesstattlich, dass ich die vorgenannten Angaben nach bestem Wissen und Gewissen gemacht und dass die Angaben der Wahrheit entsprechen und ich nichts verschwiegen habe.
Die Strafbarkeit einer falschen eidesstattlichen Versicherung ist mir bekannt, namentlich die Strafandrohung gemäß § 156 StGB bis zu drei Jahren Freiheitsstrafe oder Geldstrafe bei vorsätzlicher Begehung der Tat bzw. Gemäß § 161 Abs. 1 StGB bis zu einem Jahr Freiheitsstrafe oder Geldstrafe bei fahrlässiger Begehung.

_____ _____

Ort, Datum Rasmus Stichauer

Danksagung

Als erstes möchte ich Herrn Prof. Dr. Jens Beckmann für die hervorragende Betreuung und Unterstützung während der gesamten Zeit einen großen Dank aussprechen. Auf Grund der engagierten Teilnahme war eine erfolgreiche Umsetzung der Arbeit auch in schwierigen Phasen realisierbar. Des Weiteren möchte ich mich herzlichst bei Dr. Matthias Vogt für die Einführung und Bereitstellung dieses hoch interessanten Forschungsthemas bedanken, sowie für die ausgezeichnete Betreuung, sowohl im Labor, als auch bei den schriftlichen Ausarbeitungen.

Für das Erstellen des zweiten Gutachtens möchte ich mich bei Frau Prof. Dr. Anne Staubitz herzlich bedanken. Bei Frau Prof. Dr. Petra Swiderek möchte ich für die Übernahme des Vorsitzes des Prüfungsausschusses herzlich bedanken.

Auf die Zeit während der Promotion werde ich dank dem starken Zusammenhalt und der stetigen Unterstützung innerhalb der Arbeitsgruppe immer gerne zurückschauen. Mein Dank gilt allen Weggefährten in der Arbeitsgruppe die mir während der Promotion den Rücken gestärkt haben. Zudem allen Mitarbeitern der Universität Bremen die diese Arbeit mit ermöglicht haben. Bei Dr. Enno Lork und Daniel Duvinage möchte ich mich für die Aufnahme und Auswertung vieler Röntgenstrukturanalysen bedanken. Bei Herrn Johannes Stelten bedanke ich mich für die Umsetzung umfangreicher NMR-Messungen, insbesondere der $^{1}H^{1}H$ EXSY NMR-Experimente. Dr. Thomas Dülcks und Dorit Kempken danke ich für die Aufnahme zahlreicher Massenspektren trotz vieler Fehlschläge. Bei Dr. Emanuel Hupf und Dr. Marian Olaru möchte ich mich ebenfalls für das engagierte Miteinander in zahlreichen Gruppenseminaren bedanken, wodurch viele fruchtbare Ergebnisse erzielt wurden. Bei Herrn Prof. Dr. Robert Langer der Martin-Luther-Universität Halle-Wittenberg möchte ich mich für die Durchführung zahlreicher DFT-Berechnungen bedanken. Isabell Heuermann und Lennart Schmiedeken danke ich für die tolle Zusammenarbeit und den vielzähligen Ergebnissen innerhalb Ihrer Arbeiten, die ich mit betreuen durfte. Während meiner Zeit in der Arbeitsgruppe möchte ich mich ganz besonders bei Daniel Duvinage, Dr. Julius Kögel, Dr. Farzin Mostaghimi, Sebastian Holsten, Dr. Truong Giang Do, Dirk Schlüter, Fabio Meyer und Dr. Sinas Furan bedanken, für die unvergessliche Zeit innerhalb und außerhalb der Arbeitsgruppe, die außerordentliche Unterstützung und die legendären „Themen-Abende“. Ganz besonders möchte ich auch Artem Schröder danken, mit

dem ich diesen Weg ab dem Beginn des Studiums zusammen gegangen bin und in dieser Zeit viel miteinander erlebt habe.

Zuletzt möchte ich meinen Eltern, Marlene und 'Helmele', einen riesigen Dank aussprechen, ohne deren Förderung und Unterstützung diese Arbeit nicht möglich gewesen wäre. Meiner Mutter und meinem vor kurzem verstorbenen Vater widme ich diese Arbeit und werde deren Rückhalt immer in Erinnerung behalten.

List of Publications

Published Articles

- R. Stichauer, D. Duvinage, R. Langer, M. Vogt, 'Manganese(I) Tricarbonyl Complexes with Bidentate Pyridine-Based Actor Ligands: Reversible Binding of CO_2 and Benzaldehyde *via* Cooperative C-C and M-O Bond Formation at Ambient Temperature' *Organometallics* **2022**, *41*, 2798-2809.

- I. Heuermann, B. Heitmann, R. Stichauer, D. Duvinage, M. Vogt, 'Rh(I) Complex with a Tridentate Pyridine-Amino-Olefin Actor Ligand-Metal-Ligand Cooperative Activation of CO_2 and Phenylisocyanate under C-C and Rh-E (E = O, N) Bond Formation' *Organometallics* **2019**, *38*, 1787-1799.

- R. Stichauer, M. Vogt, 'Cooperative Binding of SO_2 under M-O and C-S Bond Formation in a Rhenium(I) Complex with Activated Amino- or Iminopyridine Ligand' *Organometallics* **2018**, *37*, 3639-3643.

- R. Stichauer, A. Helmers, J. Bremer, M. Rohdenburg, A. Wark, E. Lork, M. Vogt, 'Rhenium(I) Triscarbonyl Complexes with Redox-Active Amino- and Iminopyridine Ligands: Metal-Ligand Cooperation as Trigger for the Reversible Binding of CO_2 *via* a Dearomatization/Rearomatization Reaction Sequence' *Organometallics* **2017**, *36*, 839-848.

Poster Presentations at Conferences

- R. Stichauer, A. Helmers, J. Bremer, C. Rugen, T. Tüfek, M. Rhodenburg, A. Wark, E. Lork, M. Vogt, '*Rhenium(I) and Manganese(I) Complexes with Bidentate Amino- and Imino-Pyridine Ligands – Metal-Ligand Cooperation as Key for an Unusual CO_2 Binding Mode*', *19th Norddeutsches Doktorandenkolloquium* **2016**, Hamburg, Germany.

- R. Stichauer, M. Vogt, '*Cooperative Binding of C=O and S=O Moieties under M–O and C–X (X = C,S) Bond Formation in Re(I) and Mn(I) Complexes via Dearomatization-Rearomatization Reaction Sequence*', *21th Norddeutsches Doktorandenkolloquium* **2018**, Braunschweig, Germany.

Abstract

This work demonstrates the bifunctional activation of different functional groups, predominantly C-O, C-N and S-O multiple bonds *via* metal-ligand-cooperation (MLC) under concomitant M—Y and C—Z (M = Re, Mn or Rh; Z = C or S; Y = N or O) bond formation triggered by a dearomatization/rearomatization reaction sequence in three different ligand systems based on simple 2-methyl-pyridine ligand frameworks. Eventually, the simple bidentate ligand frameworks showed similar reactivity with respect to the well-known tridentate pincer complexes, which previously showed such reaction sequences. The bond-activation reactions *via* MLC were investigated in rhenium(I), manganese(I) and rhodium(I) complexes. Due to the formation on anionic complexes the presented study also entails the investigation of effects imposed by the alkali counter cations with respect to the bound (activated) substrate in group 7 transition metal complexes (Re and Mn). Moreover, from a synthetic point of view, it is shown that the active dearomatized anionic complexes can be generated via two different synthetic routes: i.e. *via* double deprotonation or two electron reduction. The former contains the potential for the facile *in situ* preparation of such active cooperative species simply by the addition of base, without the need for strong reducing agents such as alkali metals. In addition to the cooperative binding of CO_2, the anionic 2-amino/2-imino-methyl pyridine-based complexes show likewise the activation of further polarized multiple bonds such as aldehydes, ketones, nitriles and SO_2. All activated carbonyl groups also show reversibility of the newly formed C-C and M-O (M = Re, Mn) bonds in exchange reactions of the activated substrate. The tridentate neutral Rh(I)-π complex with the newly developed ligand framework (*dbap-py*) shows, along with the activation of CO_2, a cooperative binding of phenylisocyanate. The focus of the work is on the simplicity of the cooperative ligand frameworks, as well as the extended reactivity scope due to the direct interaction of the counterion with the activated substrate.

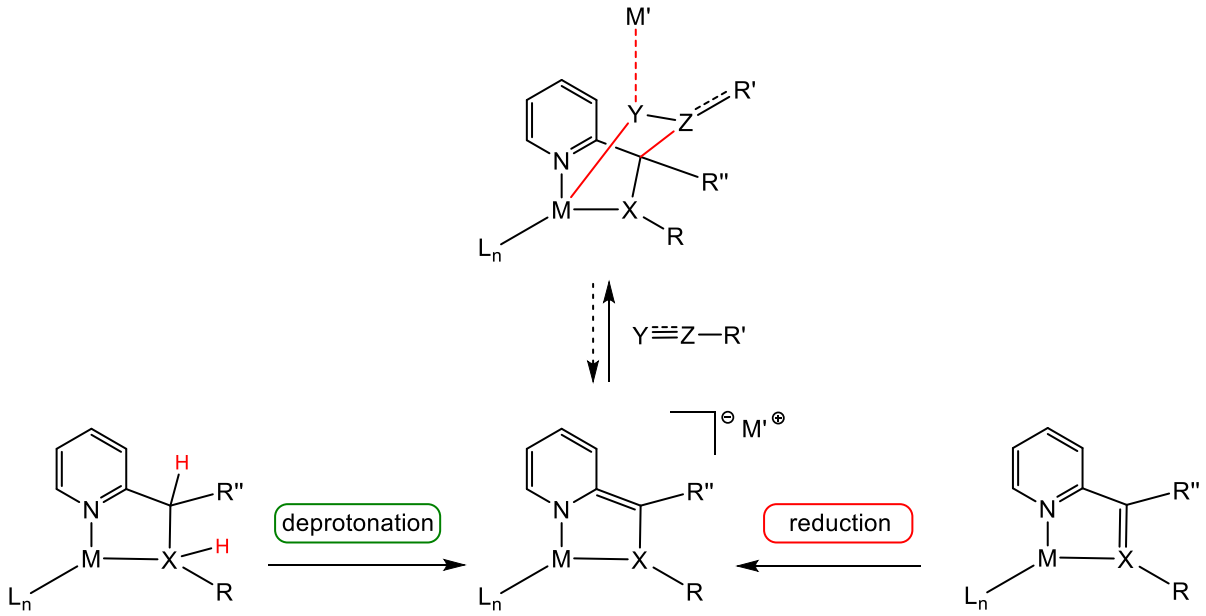

M—Y and C—Z bond formation via MLC and additional interaction of the counterion (M'- - -Y). (M = Mn, Re, Rh; M' = Li, Na, K; X = N, O; #Y = N, O; #Z = C, S; R = lone pair, $Ph^{p\text{-}Me}$, *dbap*; #R' = O, (H, Ph), Ph_2, CH_2-Ph, N-Ph; R" = H, Ph; L = CO, PPh_3) (# = free substrate)

Zusammenfassung

Diese Arbeit zeigt die bifunktionale Aktivierung unterschiedlicher funktioneller Gruppen, vorwiegend C-O, C-N und S-O Mehrfachbindungen, über Metall-Ligand-Kooperation (MLC). Die Aktivierung erfolgt durch M—Y und C—Z (M = Re, Mn oder Rh; Z = C oder S; Y = N oder O) Bindungsbildung, ausgelöst unter einer Dearomatisierungs-/Rearomatisierungs-Reaktionssequenz. Gezeigt werden drei unterschiedliche Ligandensysteme, basierend auf einfachen 2-Methylpyridin Ligandengerüsten. Letztendlich zeigen die einfachen zweizähnigen Ligandengerüste eine ähnliche Reaktivität wie die bekannten dreizähnigen Pinzettenkomplexe, die zuvor derartige Reaktionssequenzen zeigten. Die Bindungsaktivierungsreaktionen mittels MLC wurden in Rhenium(I)-, Mangan(I)- und Rhodium(I)-Komplexen untersucht. Aufgrund der Bildung anionischer Komplexe umfasst die vorliegende Studie auch die Auswirkungen der Alkali-Gegenkationen auf das gebundene (aktivierte) Substrat in Gruppe 7 (Re und Mn) Übergangsmetallkomplexen. Darüber hinaus wird aus synthetischer Sichtweise gezeigt, dass die aktiven desaromatisierten anionischen Komplexe über zwei verschiedene Synthesewege erzeugt werden können: über Doppel-Deprotonierung oder Zwei-Elektronen-Reduktion. Ersteres bietet das Potenzial für eine einfache *in-situ* Herstellung solcher aktiven kooperativer Spezies durch einfache Zugabe einer Base, ohne dass starke Reduktionsmittel wie Alkalimetalle erforderlich sind. Neben der kooperativen Bindung von CO_2 zeigen die anionischen 2-Amino-/2-Imino-methylpyridin basierten Komplexe ebenfalls die Aktivierung weiterer polarisierter Mehrfachbindungen wie Aldehyde, Ketone, Nitrile und SO_2. Alle aktivierten Carbonylgruppen zeigen zusätzlich eine Reversibilität der neu gebildeten C-C und M-O Bindungen (M = Re oder Mn) bei Austauschreaktionen des aktivierten Substrats. Der dreizähnige neutrale Rh(I)-π-Komplex mit dem neu entwickelten Ligandengerüst (*dbap-py*) zeigt neben der Aktivierung von CO_2 eine kooperative Bindung von Phenylisocyanat. Der Schwerpunkt der Arbeit liegt auf der Einfachheit der kooperativen Ligandengerüste sowie dem erweiterten Reaktivitätsvermögen aufgrund der direkten Wechselwirkung des Gegenions mit dem aktivierten Substrat.

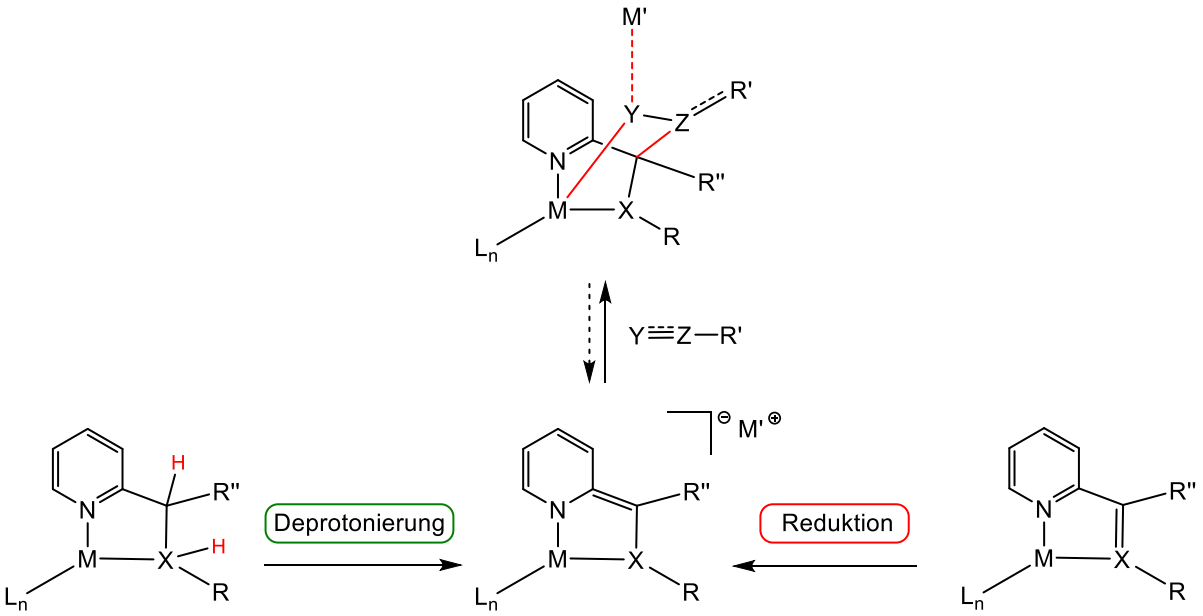

M—Y und C—Z Bindungsbildung durch MLC und zusätzliche Wechselwirkung des Gegenions (M'- - -Y). (M = Mn, Re, Rh; M' = Li, Na, K; X = N, O; #Y = N, O; #Z = C, S; R = freies Elektronenpaar, $Ph^{p\text{-}Me}$, *dbap*; #R' = O, (H,Ph), Ph_2, CH_2-Ph, N-Ph; R'' = H, Ph; L = CO, PPh_3) (# = freies Substrat)

Contents

List of Schemes

List of Figures

List of Charts

1 Introduction

In modern green chemistry, transition metal catalysis is a significant field of research. The motivation of green chemistry is the development of sustainable processes to minimize power consumption and waste for existing or new industrial chemical applications.[1; 2] Many important transition metal complexes were developed in the last decades, which are indispensable for modern industry in catalytic processes such as hydrogenation or hydroformylation of alkenes and C-C coupling catalysts such in the Heck or Suzuki reaction.[3–5] The conventional transition metal catalysis is a widely investigated area and has an important role in sustainable chemistry with relevance, e.g. for the reduction of greenhouse gases or increasing the efficiency of reactions and reducing the energy consumption to minimize the environmental impact. In the last years, a great deal of attention has been payed to the concept of metal-ligand cooperation (MLC) with respect to novel reaction schemes in homogeneous catalysis and bond activation reactions.[6–9] As the name indicates, the substrate activation and the catalytic reaction pathway occur bifunctional in a cooperative mode between the metal and the ligand. In MLC the ligand undergoes reversible structural changes during the catalytic process. In conventional homogeneous transition metal catalysis, the influence of the ligand consists in a certain steric characteristic and/or electronic features, whereas the catalytic reaction process itself occurs at the metal center. Some important catalytic reactions in conventional transition metal catalysis are the oxidative addition, the reductive elimination or the β-hydride elimination (Scheme 1).

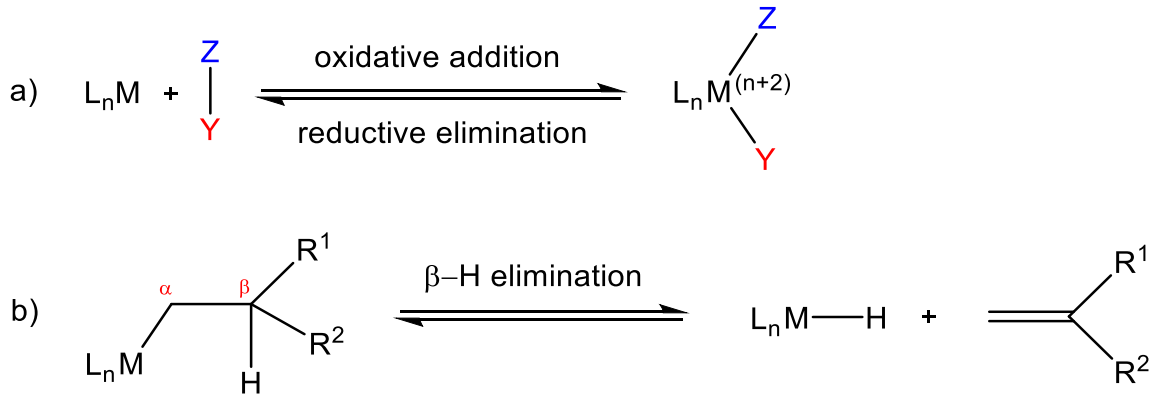

Scheme 1: Important reactions in common homogeneous catalysis reactions with transition metal complexes. a) oxidative addition / reductive elimination. b) β-hydride elimination. (L = ligand; M = metal, Y—Z = substrate, R = organic substituent)

In the course of these fundamental reaction steps the ligand remains unchanged, whereas the metal center undergoes changes in bond modification and/or oxidation state. In case of reaction pathways involving MLC, the bond activation occurs in a different manner (Scheme 2).

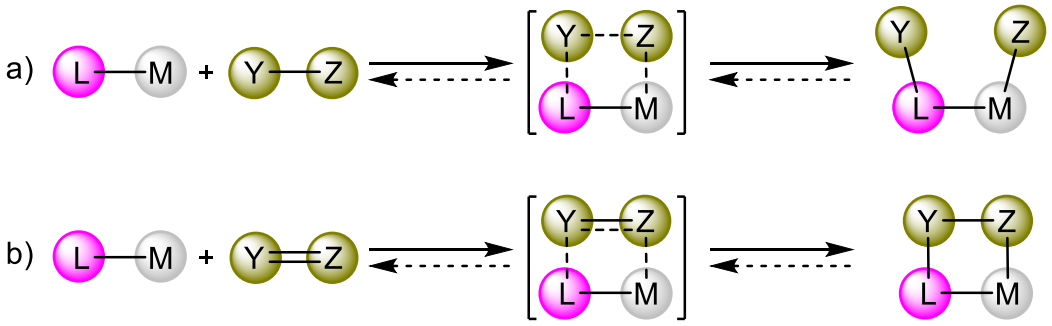

Scheme 2: Bond activation *via* metal-ligand cooperation (MLC). a) Single bond substrate activation b) Multiple bond substrate activation under [2+2]-cycloaddition. L = ligand; M = transition metal; Y—Z = substrate.

The bond activation at the substrate leads to structural modifications in both, the metal center and the ligand. This (chemically) non-innocent behavior of the ligand during the reaction process is to be distinguished from purely redox non-innocent ligands which only provide an exchange of electrons with the metal (i.e. the ligand can function as an electron reservoir), without major structural changes. In many enzymes it is known, that the catalytic pathway occurs *via* such metal-ligand cooperativity.[10; 11] [FeFe]-hydrogenase (**1**) for example, is able to catalyze the heterolytic splitting of H_2.[12; 13] The activation of H_2 occurs *via* MLC between the Fe(II)-center and the amino group in close proximity (Scheme 3). The catalytic mechanism has been vividly discussed and there is still ongoing research.[14]

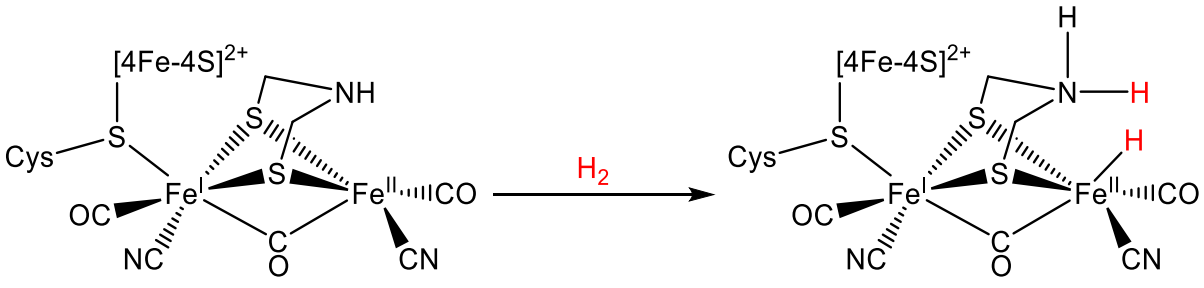

1

Scheme 3: Cooperative H_2 activation in [FeFe]-hydrogenase (**1**).

Bullock *et al.* demonstrated 2013 the reversible heterolytic splitting of H_2 with a structurally similar cationic manganese complex **2**, leading to the manganese hydride complex and protonated amine, with fast exchange of the hydrogen atoms between the manganese and the amino group at room temperature (Scheme 4).[15]

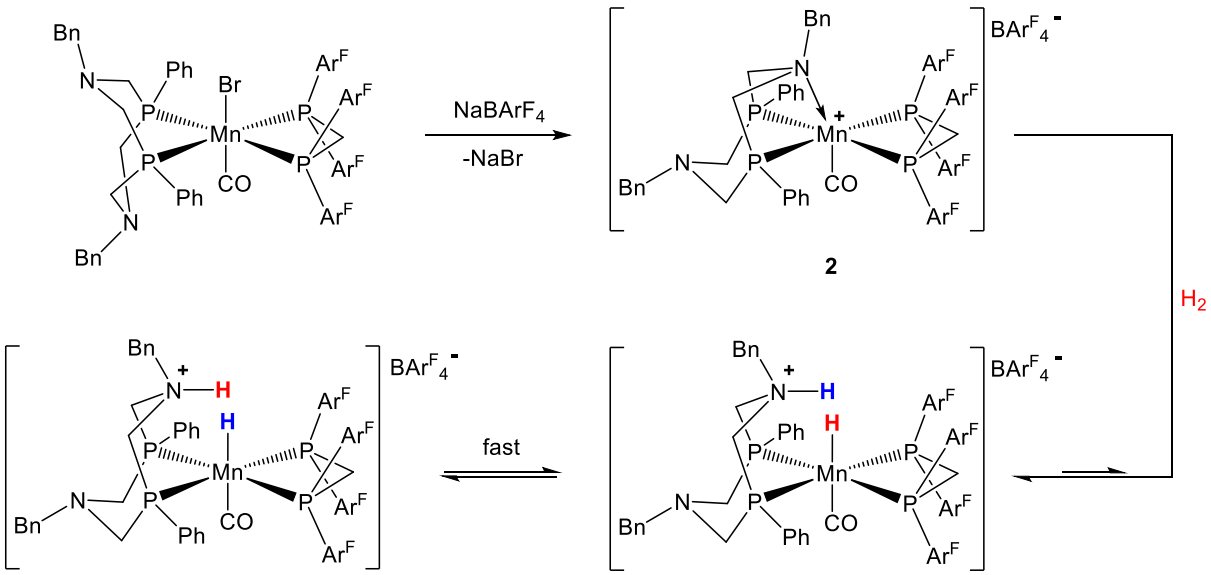

Scheme 4: H_2 activation by [(κ³-$P_2^{Ph}N_2^{Bn}$)Mn(CO)(*bppm*)][Bar^F_4] (**2**) *via* MLC with fast exchange of hydrogen.[15] (*bppm* = $(PAr^F_2)_2CH_2$; Ar^F = 3,5-bis(trifluoromethyl)phenyl)

The activation of small molecules such as H_2 or typical greenhouse gases like CO_2, CH_4 or NO_x is an important field of research and of great significance to make them accessible for economic processes such as substitution of fossil raw materials.[16–24] Over the last years MLC expanded the scope of bond activation reactions and has increased in interest.[8; 9; 25] Because both, the metal and the ligand take part in the reaction, there are more opportunities to adjust and improve the environment for the substrate of interest. There are typically four general types of cooperation in substrate binding/activation *via* MLC. (Scheme 5). In the first mode the ligand acts as a Lewis base (Scheme 5 a); In the second mode as a Lewis acid (Scheme 5 b). In the third mode, a key driving force of the substrate activation occur *via* a dearomatization/ rearomatization sequence of the ligand (Scheme 5 c). Generally, the formal oxidation state of the metal center remains unchanged. The activation of the substrate can occur stepwise or in a concerted manner. The fourth type of MLC is a redox non-innocent ligand, where the ligand undergoes structural changes during the change in its state

of oxidation (Scheme 5 d). A redox non-innocent ligand can function as an electron donator/acceptor to influence the oxidation state of the metal and/or take directly part in bond activation of the substrate. Redox non-innocent ligands which are not involved in bond formation or cleavage are not discussed at this point, as they have no direct relevance to this work. Combinations of each cooperation type are possible in activation and catalytic processes.

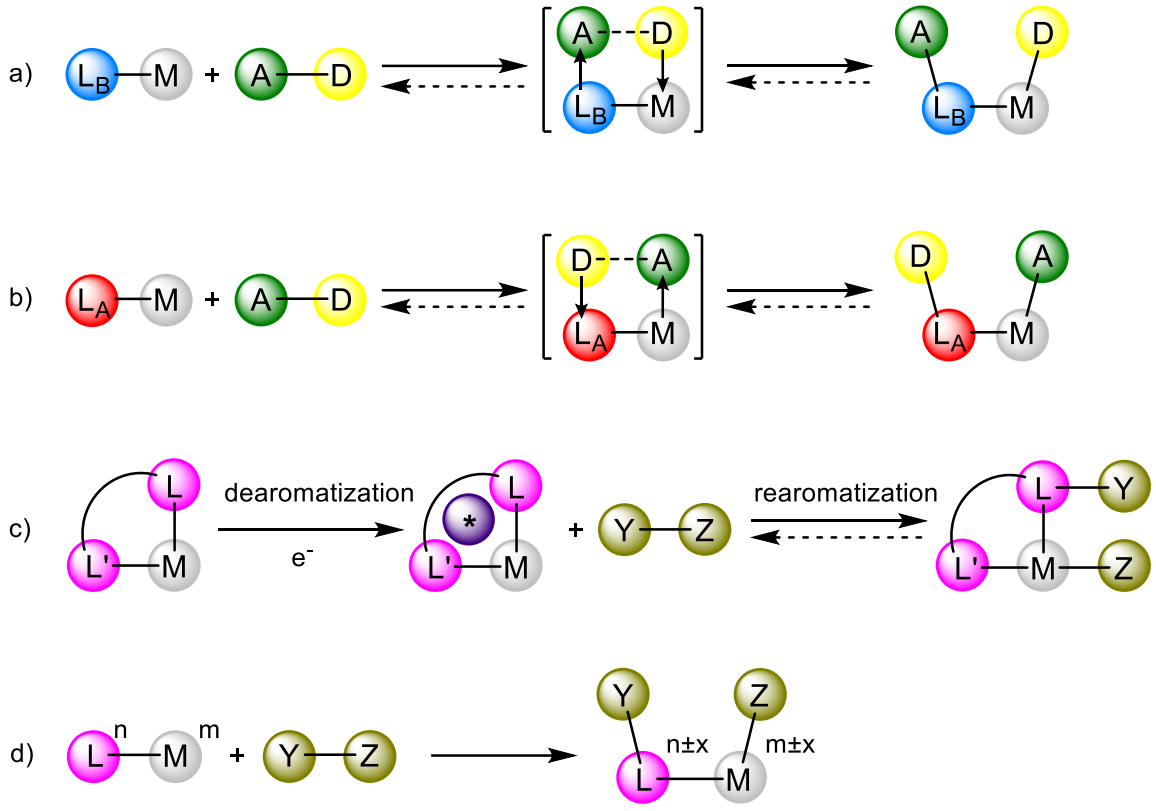

Scheme 5: Different modes of metal-ligand cooperation (MLC). a) Ligand L_B acting as Lewis base. b) Ligand L_A acting as Lewis acid. c) Substrate activation *via* dearomatization/rearomatization sequence (The asterisk indicates the dearomatized ligand). d) Redox non-innocent ligand substrate activation. (M = metal; A = acceptor, D = donor, Y—Z = substrate)

Additionally, more remote centers of activation can play a significant role. For instance, the amino group of the [FeFe]-hydrogenase (**1**) is not directly bound to the metal center. In this case, the cooperativity occurs in the 2nd coordination sphere of the metal complex.

1.1 Lewis Base MLC

Ligands that cooperatively operate as Lewis bases are more common than ligands that function as Lewis acids. Amido ligands in electron rich transition metal complexes are very suitable for MLC applications with ligands acting as Lewis base.[9; 26] Noyori *et al.* discovered that ruthenium catalysts, containing at least one primary amino group in the first coordination sphere, have a clearly improved reactivity in ketone hydrogenation.[27; 28] The cooperative interaction of the NH group was essential for the increasing reactivity of the catalyst.[29] Based on this research, they developed some very effective Ru-catalysts for ketone hydrogenation (Scheme 6).[28–31] The possibility of stereoselective hydrogenation of ketones was demonstrated in many cases with R-BINAP (**3**) and S-BINAP (**4**). Analogous complexes with tertiary amino groups like TMEDA not nearly reached the effectivity under the same conditions.

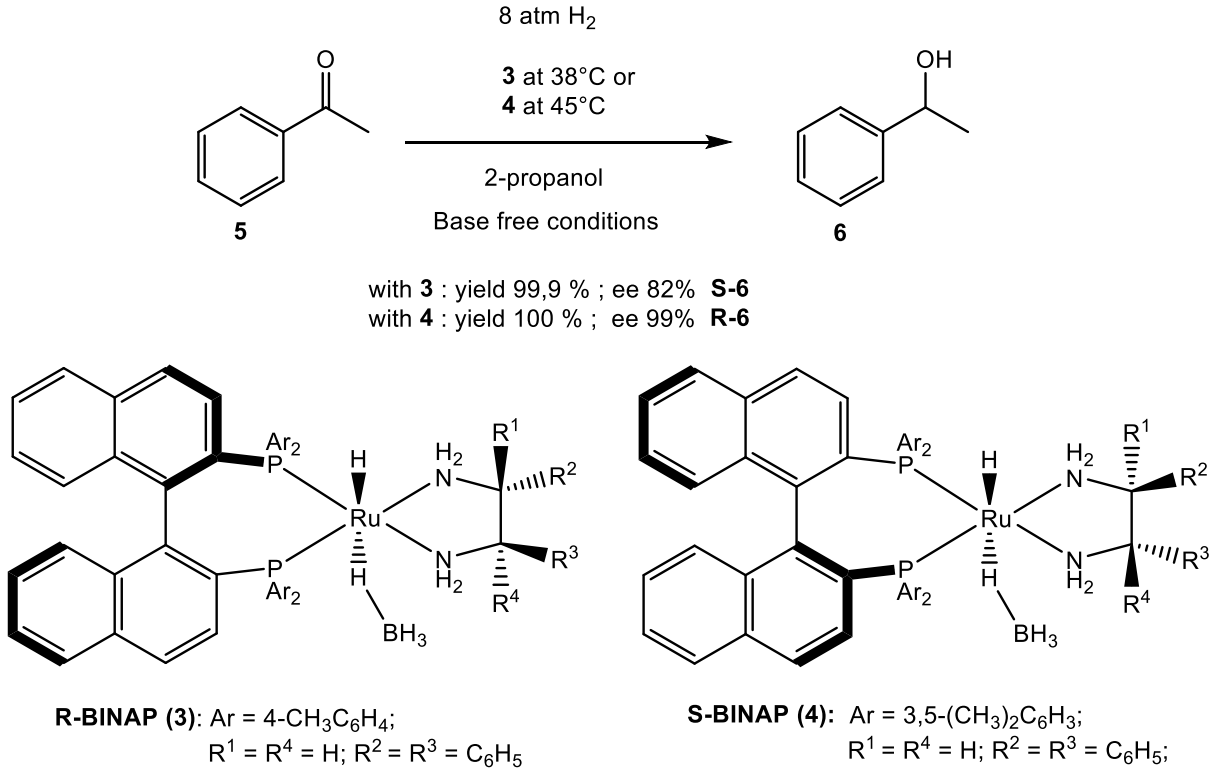

Scheme 6: Examples of efficient Ru-catalysts R-BINAP (**3**) and S-BINAP (**4**) for stereoselective ketone hydrogenation.[30] (ee = enantiomeric excess).

The proposed outer-sphere mechanisms of the hydrogenation of acetophenone (**5**) *via* MLC with a Ru-complex of S-BINAP (**4**) shows two cycles and three possible transition states (Scheme 7).[32]

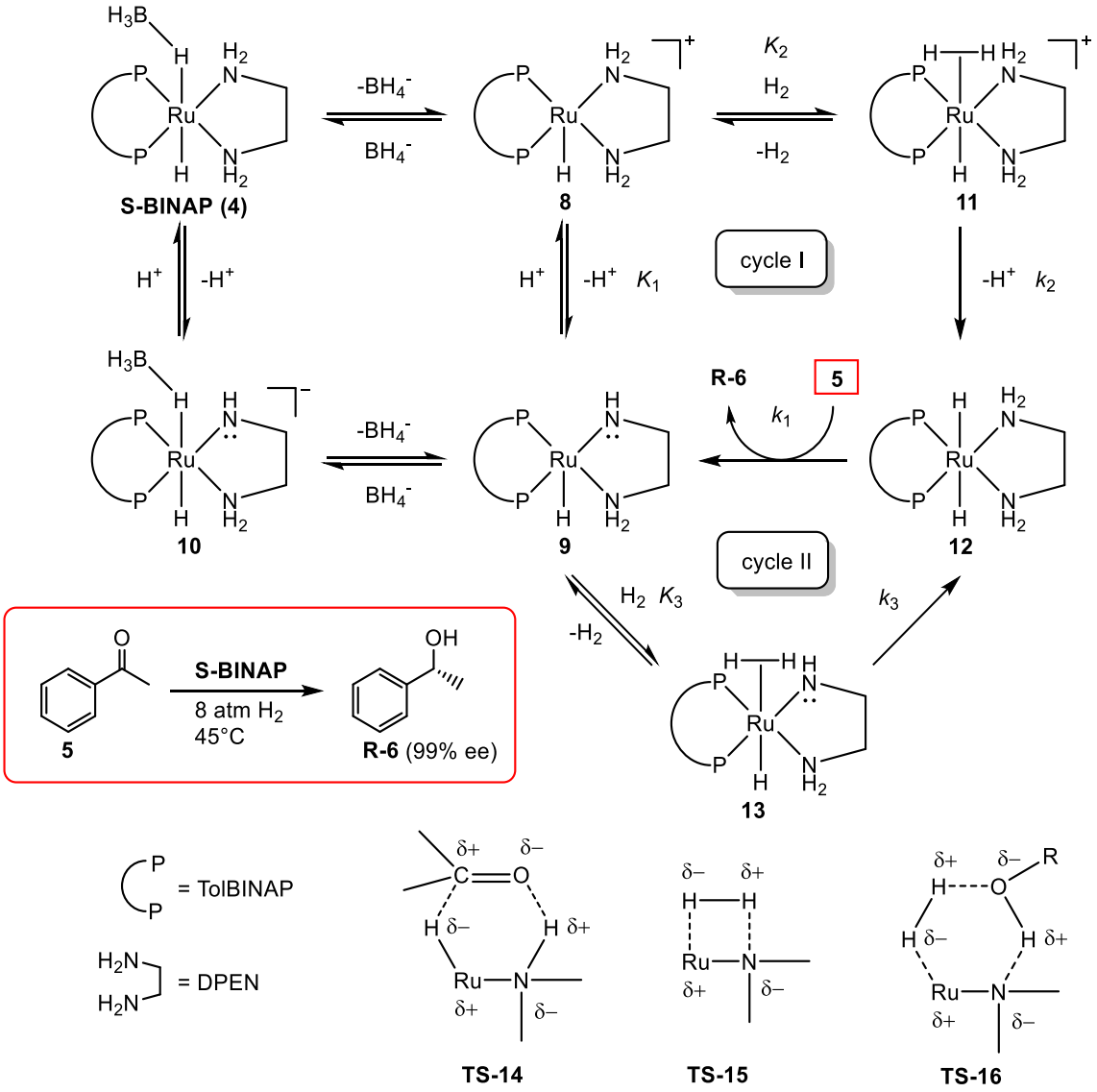

Scheme 7: Proposed mechanisms of ketone hydrogenation of acetophenone (**5**) by Ru-complex S-BINAP (**4**) in 2-propanol, to form (R)-1-phenylethanol (**R-6**) with 99% ee.[32] (DPEN = 1,2-diphenylethylene-diamine; ROH = 2-propanol; TolBINAP = 2,2'-bis(di-4-tolylphosphino)-1,1'-binaphthyl)

The active catalytic species **8** and **9** were generated from the pre-catalyst S-BINAP (**4**). In the transition state **TS-14** (cycle I), the mechanism occurs *via* a six-membered ring, where the hydrogen is transferred to the C=O group of the ketone contemporaneously. Transition states **TS-15** and **TS-16** (cycle II) proposed an activation of H_2 *via* a four-membered ring, or a six-membered ring in the presence of an alcohol as solvent. In both cycles, the interaction of a primary or a secondary amino group is essential for the presumed transition states. The activation of H_2 *via* MLC

leads to a large variety of highly effective hydrogenation catalysts for many functional groups over the course of the last years.[8; 33–35] The dehydrogenation of a variety of compound classes (e.g. alcohols, formic acid, aminoboranes, N-heterocycles) *via* MLC were also successfully realized.[33] Beller *et al*. observed efficient acceptorless dehydrogenation processes of alcohols under mild reaction conditions, using different pincer transition metal complexes.[36–38] Based on these results, Schneider *et al*. discovered that the Fe-PNP pincer complex **18** was active in catalytic acceptorless dehydrogenation of alcohols under base free conditions.[39] The activation mode of the alcohol was proposed to occur in a concerted way or stepwise (Scheme 8). The sustainable production of H_2 might be an important contribution to displace fossil fuels as source of energy.

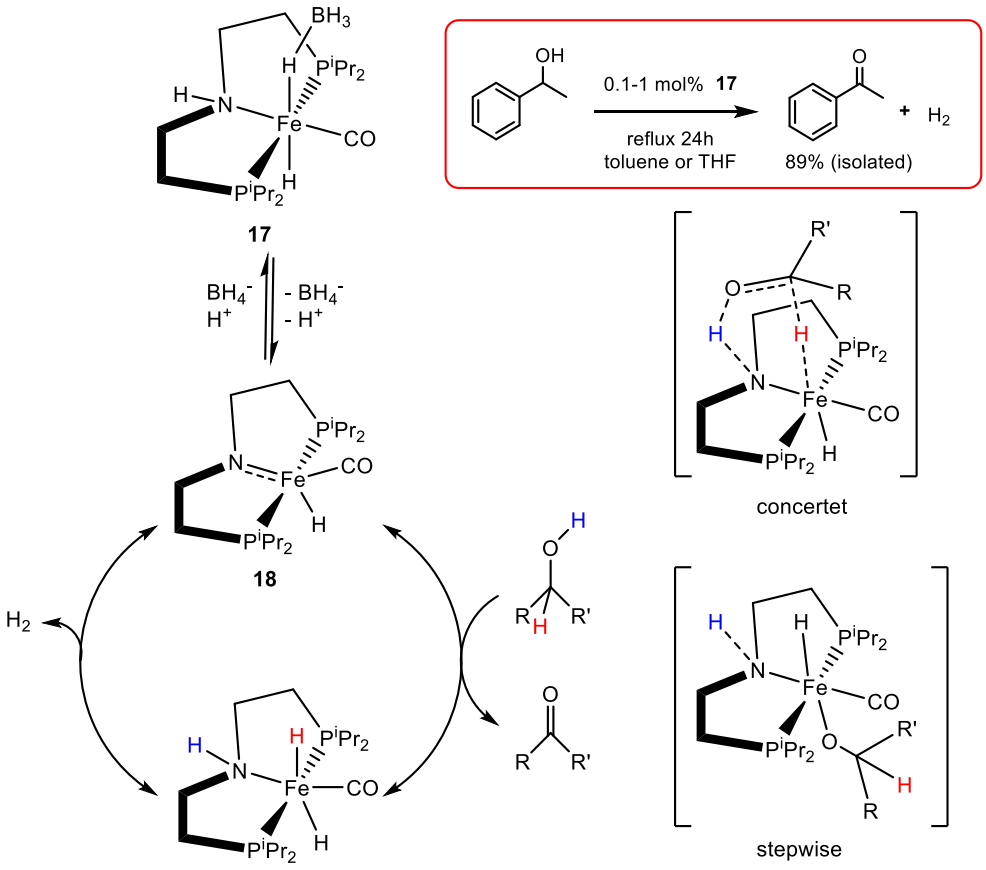

Scheme 8: Acceptorless dehydrogenation of alcohols using the Fe-PNP pincer complex **18** with proposed activation pathways.[39]

1.2 Lewis Acid MLC

Ligands acting as Lewis acid in MLC with base metals were first reported by Fontaine and Zargarian, using the nickel complex (1-Me-*Ind*)Ni(PPh_3)(Me) (**19**) in combination with $(Me_2PCH_2AlMe_2)_2$ (**20**) for the dehydrogenative coupling of phenylsilane (Scheme 9).[40] The result was a perceptible increase of the activity, with respect to the nickel complex with methylaluminoxane (MAO) as a co-catalyst. The species **21** was generated by addition of triethylamine to split the P-Al dimer **20** and displace the triphenylphosphine at the nickel atom. After the loss of NEt_3, and the formation of the active species **22**, a noticeable increase of catalytic activity was the result. It is proposed that the interaction of the R-$AlMe_2$ group and the Ni center with the substrate (**23**) is accelerating the Si-H bond activation and Si-Si bond formation.

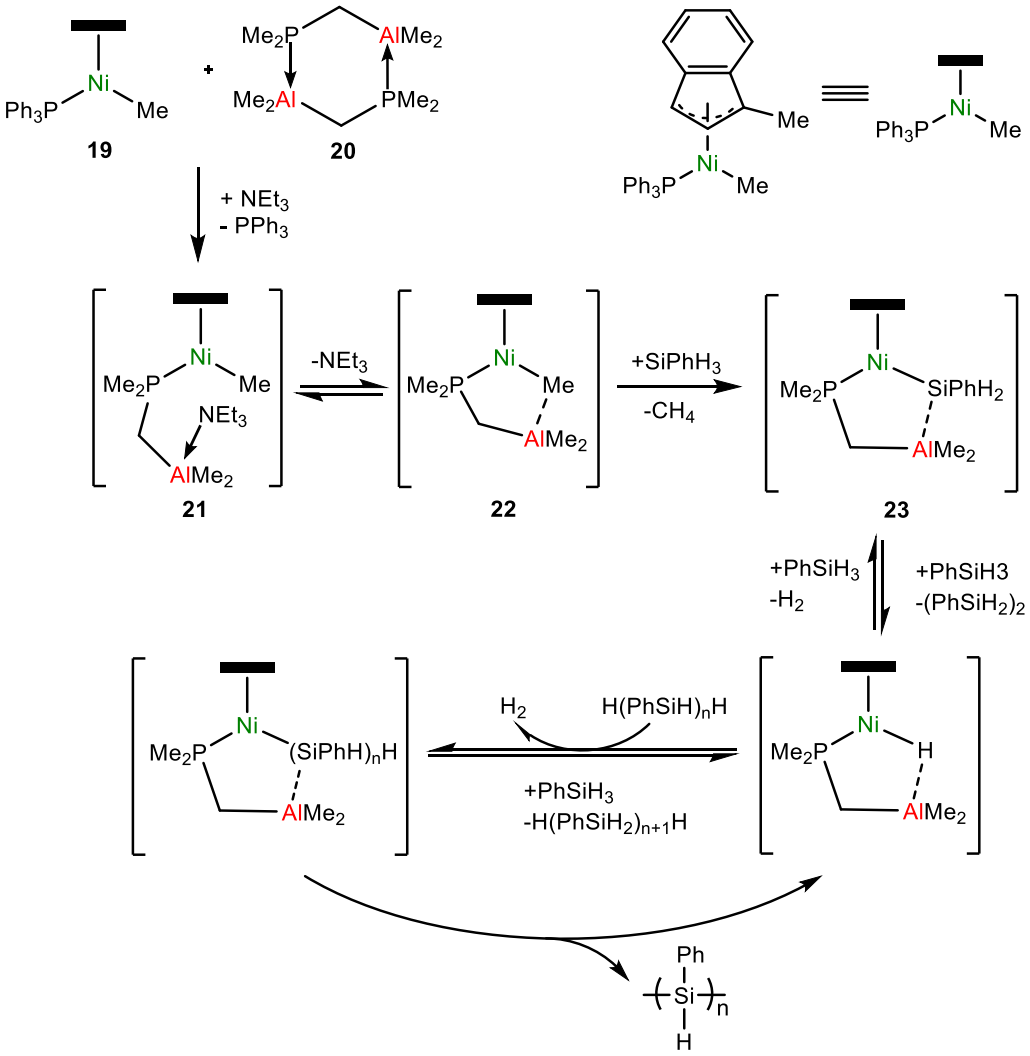

Scheme 9: Dehydrogenative coupling of $SiPhH_3$ with (1-Me-*Ind*)Ni(PPh_3)(Me) (**19**), enhanced with Lewis acidic Al-ligand (**22**).[40] (*Ind* = indenyl)

The most obvious approach for creating a Lewis acid based cooperating system is probably the installation of a borane in the ligand framework, that is able to interact with the substrate *via* MLC. Parkin *et al.* and Rabinovich *et al.* first reported Ni-, Fe- and Co-borane complexes which are showing the activation of several substrates *via* MLC.[41–43] In case of H_2, the activation differs significantly in comparison to Lewis basic ligands like amino groups, by forming a metal hydride and a boron hydride. With the nickel borane complex **26**, Peters *et al.* demonstrated a reversible oxidative activation of H_2, under formation of the Ni(II)-hydrido borohydrido complex **27**, which was capable for catalytic alkene hydrogenation (Scheme 10).[44]

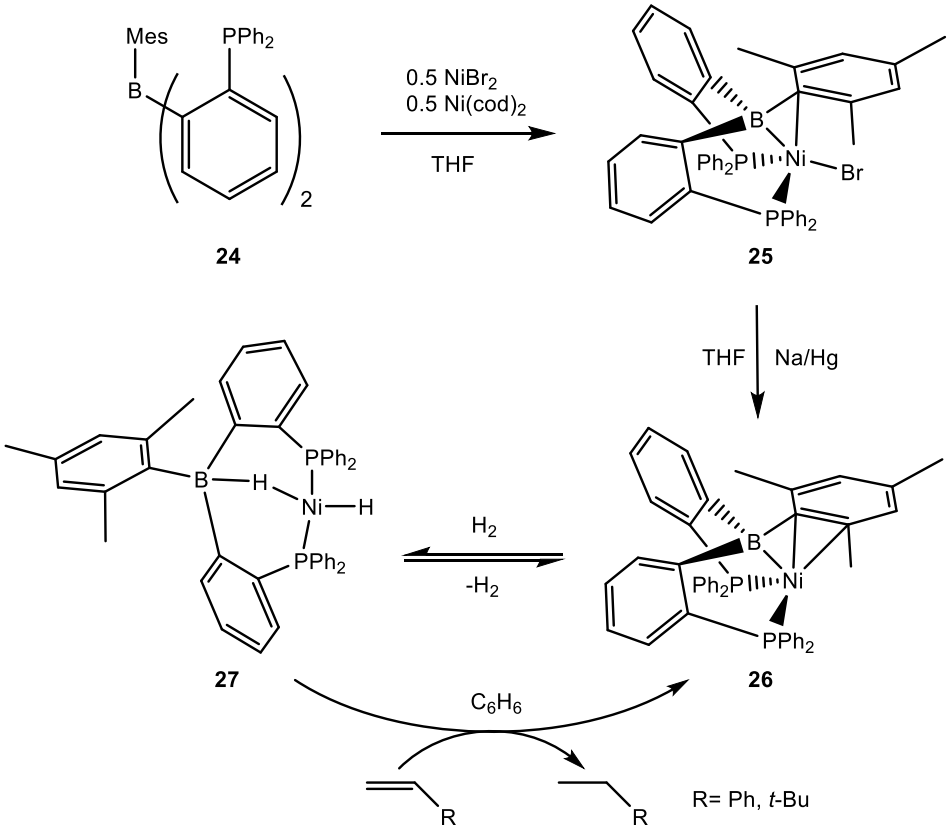

Scheme 10: Reversible activation of H_2 with the Ni-B-complex (^{Mes}DPB^{Ph})Ni (**26**) and catalytic alkene hydrogenation.[44] (DPB = diphosphine-borane)

1.3 Dearomatization/Rearomatization based MLC substrate activations

Many transition metal complexes[8; 9] and also element-ligand cooperativity with p-block elements[45] with different types of cooperating groups in the first and second coordination sphere, able to activate a variety of substrates in cooperative mode were described in the past. The first example of bifunctional substrate activation with a dearomatization/rearomatization sequence was reported in 1984 by Shvo *et al*..[46–48] Shvo's complex **28** is a dinuclear species potent as (pre)catalyst in transfer hydrogenation reactions of ketones (Scheme 11).[49]

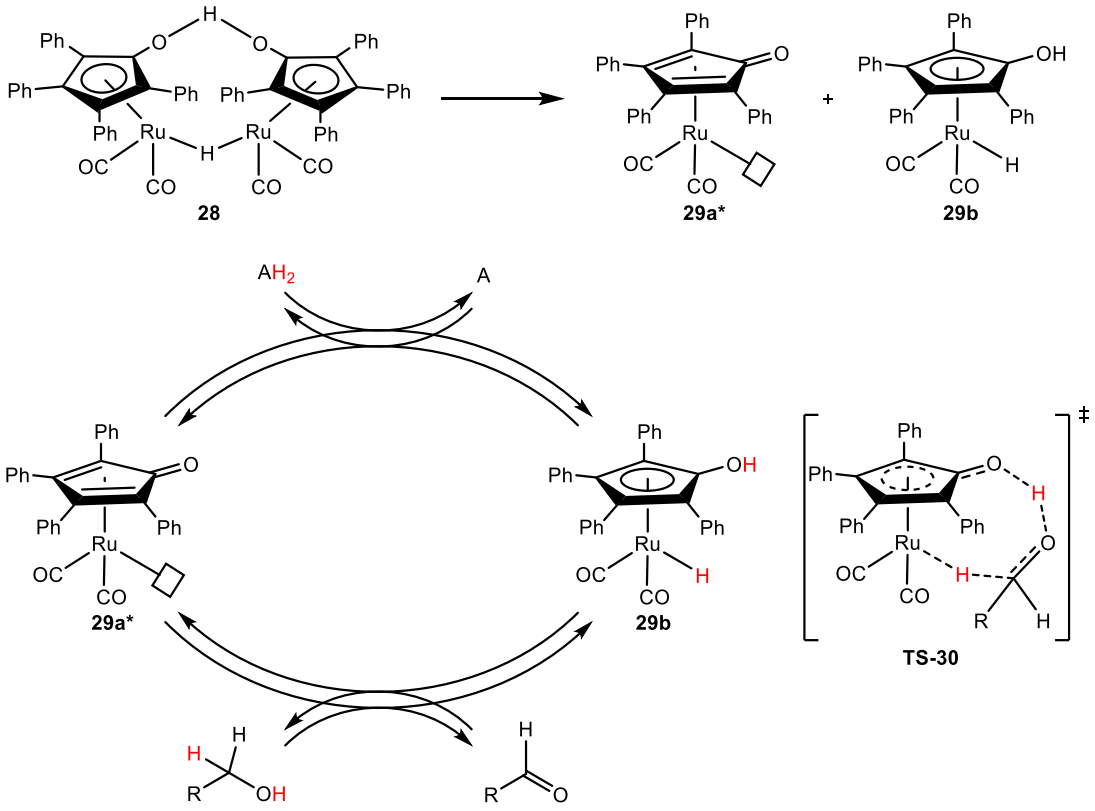

Scheme 11: Hydrogen transfer mechanism of alcohols with Shvo's complex **28** (A = hydrogen acceptor) and proposed outer-sphere transition state **TS-30**.[49]

The thermal dissociation of **28** led to two monomeric catalytically active species **29a*** (The asterisk indicates the dearomatized ligand) and **29b**. The unsaturated η^4-cyclopentadienone ligand in **29a*** reacts with alcohols as a proton acceptor and the Ru center as a hydride acceptor, under rearomatization and formation of the saturated

18e$^-$ valence electrons (VE) complex. Mechanistic studies recommend a concerted outer-sphere transition state **TS-30**.[50; 51] The species **29b** is able to transfer the hydrogen to an acceptor substrate under dearomatization to species **29a***. Further investigations indicated transfer hydrogenation to other functional groups e.g. alkenes, alkynes and aldehydes.[49; 52; 53] Analogous complexes for bifunctional catalysis with cyclopentadienone units were also developed by Knölker *et al*.[54] and Guan *et al*.[55]. Hydroxypyridine based ligands (**31**) were discovered to be well suited for MLC bond activation *via* dearomatization/rearomatization sequences (Scheme 12).[9; 56] The deprotonated species (**32a**) forms a dearomatized pyridonate resonance structure (**32b***), in which the nitrogen atom has a formally negative charge and acts as a strong π-donor. The dearomatized species is able to act *via* MLC in substrate activation reactions under rearomatization (**33**).

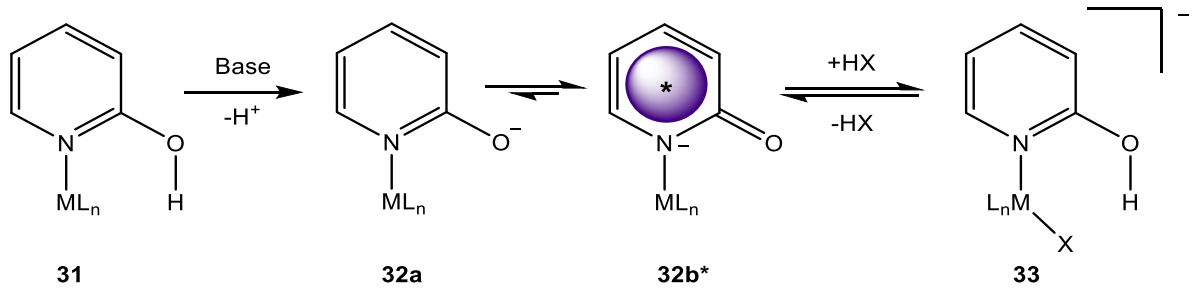

Scheme 12: MLC bond activation in hydroxypyridine complexes *via* dearomatization/ rearomatization sequence.

In 2004 Himeda *et al.* reported a significantly increased catalytic efficiency for hydrogenation reactions, after deprotonating the dihydroxy-phenanthroline Ir-complex [Cp*Ir(H_2L^1)Cl]Cl (**34**).[57; 58] The deprotonation of the OH-group was essential for the bifunctionality of the catalyst by forming the dearomatic moiety K[Cp*Ir(L^1)-Cl] (**35b***) **(**Scheme 13). Although there is no direct bond between the metal and the OH-group, there is a direct influence in the first coordination sphere of the metal, because of the formally negatively charged nitrogen atom. Based on this model additional catalysts have been developed and also the influence of the position of the OH-groups was examined.[58–60]

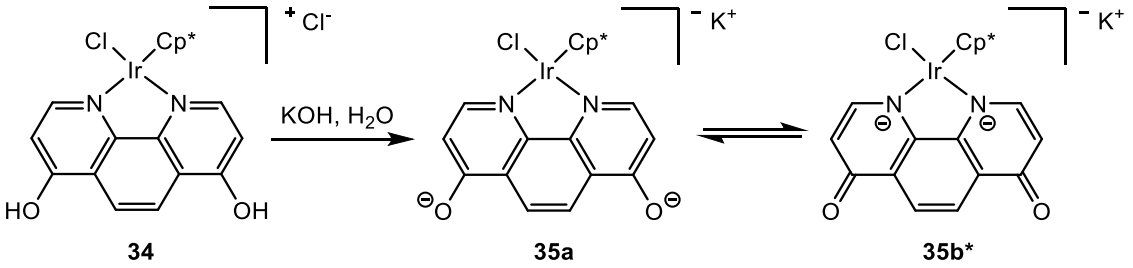

Scheme 13: Formation of the dearomatic species K[Cp*Ir(L^1)-Cl] (**35b***) by double deprotonation of the dihydroxy phenanthroline Ir-complex [Cp*Ir(H_2L^1)Cl]Cl (**34**).[57]

Yamaguchi *et al.* reported the water-soluble cationic dihydroxy bipyridine Ir-complex **36** for dehydrogenative oxidation of primary and secondary alcohols to aldehydes.[61] The catalytically active species **37*** were obtained by elimination of triflourmethanesulfonic acid (HOTf) and water from the di-cationic Ir-complex **36** (Scheme 14). The proposed reaction mechanism for secondary alcohol activation occurs *via* the alkoxo iridium species **38**. β-hydrogen elimination leads to the Ir-hydride species **39** and generation of the ketone. The regeneration of the catalyst was achieved by release of H_2 formed from the Ir-hydride and the hydroxyl hydrogen.

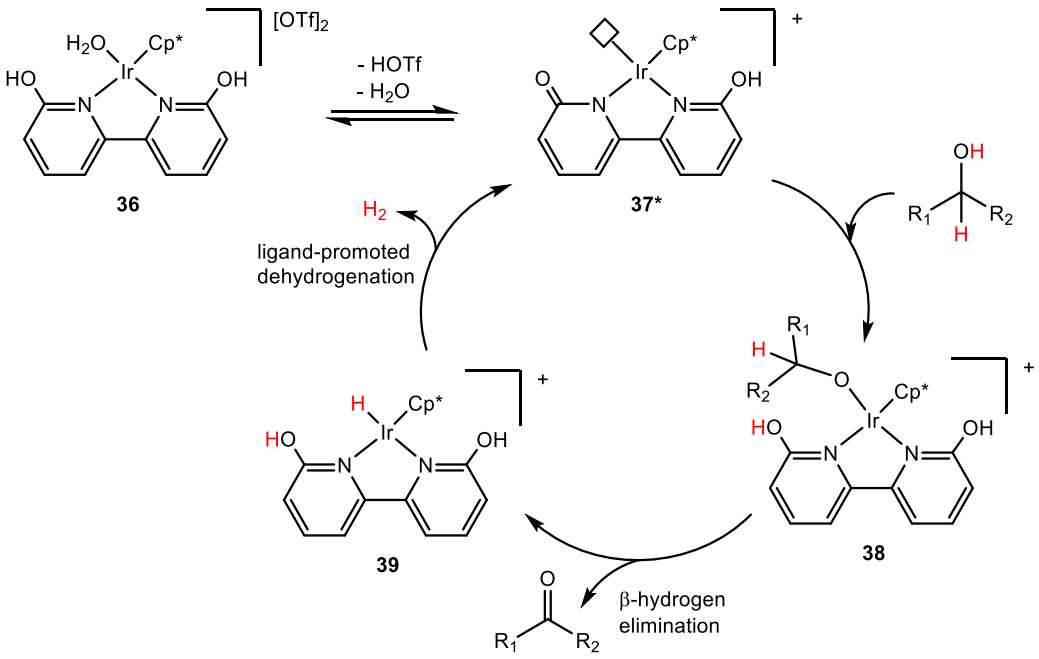

Scheme 14: Proposed dearomatization/rearomatization mechanism for the dehydrogenative oxidation of alcohols by Ir-complex **37***.[61]

1.4 Pyridine-based ligands in dearomatization/rearomatization reaction sequences for MLC substrate activations

Approximately at the same time the hydroxypyridine based system was reported, the pyridine-based pincer ligand motif (Scheme 15) took a key role in the development of high-performance catalysts for e.g. (de)hydrogenation reactions and dehydrogenative coupling reactions of alcohols.[8; 62; 63] The pincer motif shows advantages because of its accessibility for MLC activation, its chemical robustness and the good accessibility of the metal in homogeneous catalysis. Milstein *et al.* discovered a metal-ligand cooperating reactivity in pyridine-based PNN- and PNP-pincer ruthenium complexes utilizing a reversible dearomatization/rearomatization reaction sequences.[64–67] The deprotonation of the ligand 'arm' (i.e. the methylene group is converted to a methine moiety) causes the dearomatization of the pyridine unit under formation of an exocyclic double bond (**41***) (Scheme 15). Similar to the hydroxypyridine system, the amido character of the nitrogen atom in the pyridine unit directly influences the first coordination sphere of the metal.

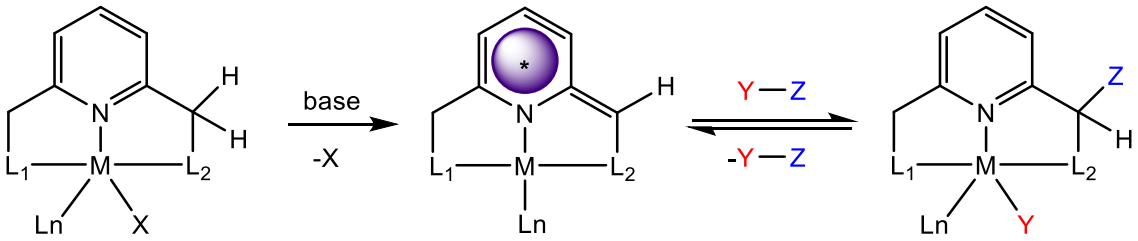

40 **41*** **42**

Scheme 15: MLC bond activation in pyridine-based pincer complexes *via a* dearomatization/rearomatization sequence. (Y—Z = substrate; L_1 and L_2 = amino or phosphine ligand)

The active species **41*** is capable to activate a chemical bond *via* 1,3-addition under rearomatization of the pyridine unit. The substrate is activated *via* bond formation to the metal center and the unsaturated aliphatic carbon atom of the 'pincer arm'. Pyridine based pincer ligands are especially adequate for this mode of MLC, because of the relatively low resonance energy of pyridine (28 kcal/mol) compared to benzene (36 kcal/mol), the acidity of the benzylic hydrogen atoms as well as the stabilization of the dearomatized ligand by the metal.[8] The driving force of the formation of the substrate activated species **42** is referred from rearomatization, C-Z bond formation

and reaching a saturated coordination sphere of the metal center *via* M-Y bond formation.[8; 68] The oxidation state of the metal normally remains unchanged. The first report of a catalytic reaction employing the concept of MLC in pyridine-based pincer complexes was reported by Milstein *et al.* 2005.[69] The dearomatized complex **44*** was obtained from the Ru-PNN pincer complex **43** by deprotonation with a strong base (Scheme 16).

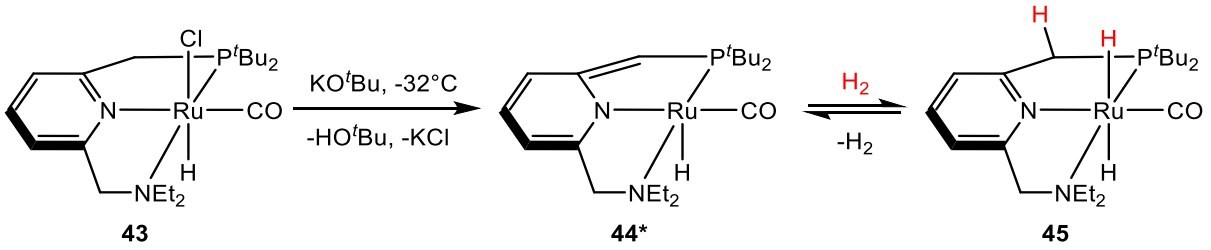

Scheme 16: Reversible activation of H_2 with the Ru-PNN pincer complex **44*** *via* dearomatization/rearomatization sequence.[69]

Reversible H_2 activation was observed, resulting in the aromatic *trans*-dihydride complex **45**, which could be isolated. Under base-free conditions complex **44*** turned out to be an effective catalyst for acceptorless dehydrogenative esterification of primary alcohols (Scheme 17).[64] NMR spectroscopic studies of complex **44*** corroborate the theory of a dearomatization/rearomatization mechanism. The ^{1}H NMR spectrum contains resonances of the pyridine unit shifted to lower frequencies after deprotonation. Deprotonation occurred at the P-arm, proven by the resulting ^{1}H NMR resonance associated with a methine CH. The mechanistic proposal was later reported by Wang *et al*.[70; 71] and Hall *et al*.[72] on the basis quantum chemical calculations using DFT (density functional theory). By calculations, in the case of H_2 activation, only a small energy difference of 1-4 kcal/mol between the dearomatized and the aromatized complex was determined.[8; 72] In later publications, dearomatized species and substrate activated species could be isolated and fully characterized in a PNP pincer Ir-complex.[73; 74] Single crystal X-ray diffraction experiments of the dearomatized species show significantly shorter C-C interatomic distances for the deprotonated 'arm', with respect to the aromatic complex.

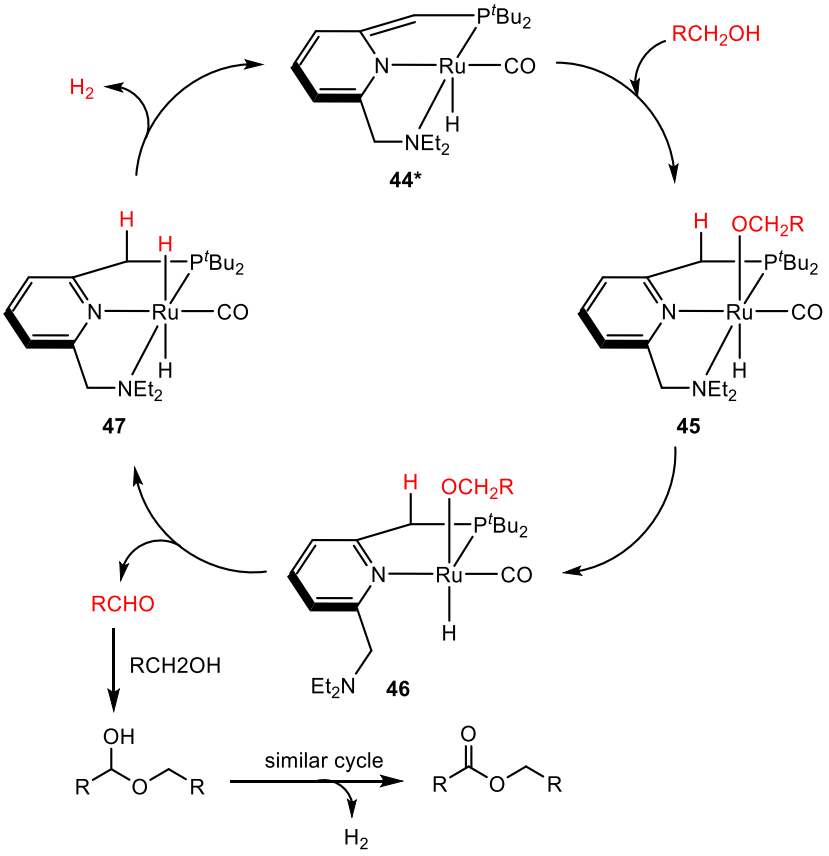

Scheme 17: Postulated mechanism for dehydrogenative coupling of alcohols to esters, catalyzed by the Ru-PNN pincer complex **44***.[64]

Many publications have appeared on this topic in recent years, describing hydrogenation reactions of aldehydes, ketones, esters, carboxylic acids, nitriles, azides and other functional groups, using the pincer platform with MLC activity rendering a dearomatization/rearomatization reaction mode.[9; 25] In contrast to the activation of the homogeneous σ-bond of H_2, the activation of polarized bonds is predestined for MLC, because of its bifunctional activation mode. An important example is the reversible activation of CO_2 *via* MLC which is also one focal point of this work. CO_2 is a very unreactive compound and because of its thermodynamic stability not easy to activate using conventional transition metal complexes. For the electrochemical reduction of CO_2, large overpotentials are needed.

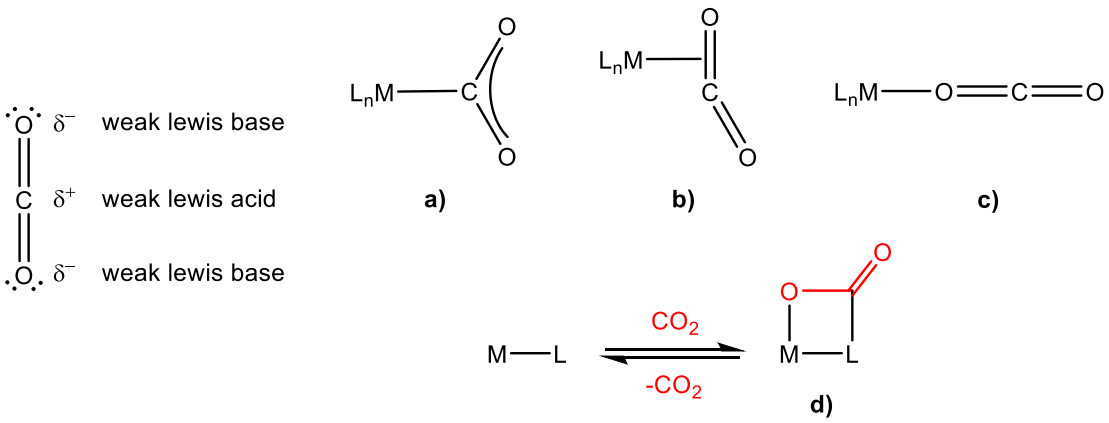

Scheme 18: Properties of CO_2 and different modes of CO_2 activation in metallic complexes. a): M-C σ-bond; b): π-coordination; c): M-O coordination; d): MLC under M-O and C-C bond formation. (M = metal; L = ligand)

After one-electron reduction the CO_2 molecule loses its low-energy linear structure. The highly energetic one electron reduction radical anion $CO_2^{\bullet-}$ can be circumvented by the use of effective catalysts which are able to induce direct multielectron transfer reactions to the CO_2 molecule.[75–79] CO_2 activation, to make the molecule accessible as a C_1 feedstock for renewable energy sources or chemical products, is an attractive goal.[80–82] For efficient catalytic conversion reactions, the interaction of the CO_2 molecule with the catalyst is essential. There are several coordination modes known for CO_2 in transition metal complexes. An important feature is the σ-bond between the metal center and the carbon atom (Scheme 18 a). π-coordination of one C=O double bond to the metal center (Scheme 18 b) is also observed. M-O coordination between the oxygen and the metal center (Scheme 18 c) has also been described, but it is only possible with highly sterically demanding ligands.[18] CO_2 is outwardly neutral, but has negative partial charges at the oxygen atoms and a positive partial charge at the carbon atom (Scheme 18). The carbon atom thus exhibits weak Lewis acidity and the oxygen atoms can act as weak Lewis bases. This characteristic makes CO_2 a promising substrate for MLC activation (Scheme 18 d). The first report of bifunctional reversible CO_2 activation was made by Floriani *et al.* in 1974[83], in an counterion cooperating mode, using the anionic Na[Co(I)(salen)] complex **48** (Scheme 19 a).[84] Interesting in this mode of activation is the role of the counterion, which in this case represents the bifunctionality of activation. The interaction of CO_2 with such anionic complexes depends primary on the counterion and the solvent. This circumstance also gains special importance in this work and is mainly discussed in **3.1**. In 1981

Braunstein *et al.* first reported a bifunctional reversible CO_2 activation with the Pd(II) complex **49** by insertion in a C-H bond under Pd-O and C-C bond formation (Scheme19 b).[85] Late transition metals (d^8-d^{10}) turned out to be very suitable for CO_2 insertion reactions in metal-element bonds, because of their Lewis basic character and their possibility to bind a weak ligand such as CO_2 *via* backbonding.[18]

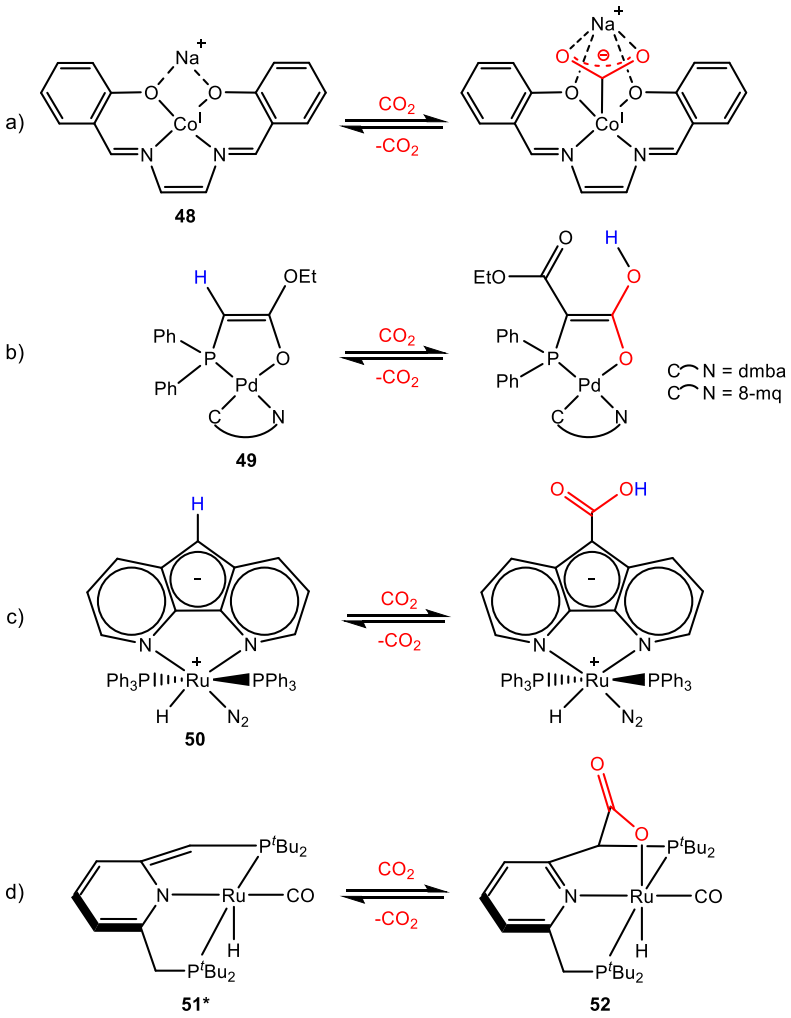

Scheme 19: Alternative variants of reversible CO_2 activation with transition metal complexes. a) bifunctional counterion activation by Floriani *et al.*[83]; b) bifunctional insertion under C-C and Pd-O bond formation by Braunstein *et al.*[85]; c) actor ligand activation under C-C bond formation by Song *et al.*[86]; d) bifunctional MLC activation *via* C-C and Ru-O bond formation and rearomatization by Milstein *et al.*[87]. (dmba-H = dimethylbenzylamine; 8-mq-H = 8-methylquinoline)

Another remarkable reversible CO_2 activation, reported by Song *et al.*, is an insertion of CO_2 into a C-H bond of a C-nucleophilic actor ligand in a zwitterionic Ru-diazafluorenide (daf^-) complex **50** (Scheme 19 c).[86] The insertion in the

“redox-active actor ligand” shows no cooperative mode, the metal center remains unmodified.[88] In an earlier publication they reported the reversible splitting of H_2 with the same complex in a cooperative mode under Ru-H and C-H bond formation.[89] A new mode of reversible CO_2 activation was published by Milstein *et al.* in 2012 *via* a dearomatization/rearomatization mode.[87] The Ru(II)-PNP pincer complex **51***, was capable to activate CO_2 *via* MLC under reversible C-C and Ru-O bond formation at ambient temperature. Under a pressure of 1 bar of CO_2, the dearomatized complex **51*** reacts rapidly with CO_2, forming the rearomatized 1,3-addition product **52** under [2+2]-cycloaddition. The unusual reversibility of the C-C bond could be demonstrated in NMR spectroscopic experiments, showing a fast exchange of labeled $^{13}CO_2$ at ambient temperature under 1 bar of non-isotopically labeled CO_2. The CO_2-complex **52** could be isolated and the obtained molecular structure from single crystal X-ray diffraction (scXRD) studies shows an (slightly) elongated C-C single bond between the benzylic carbon atom and the CO_2, compared to common carboxylic C-C single bonds (Figure 1). The Ru-O bond lengths is consistent with other similar complexes.[66; 90] Compared to single bond activation, leading to bond cleavage, a [2+2]-cycloaddition product is obtained by double bond MLC activation.

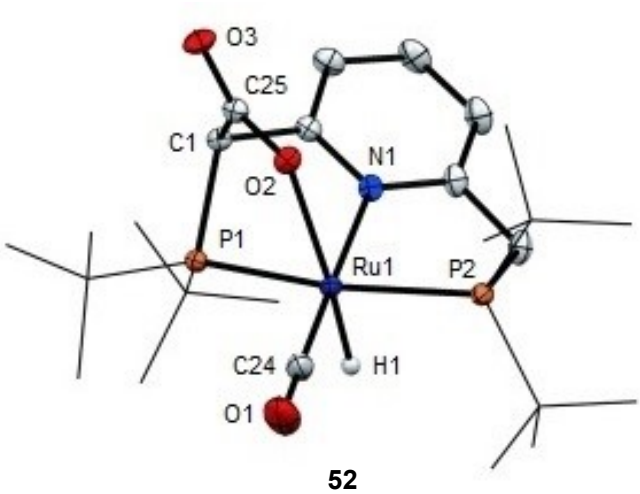

52

Ru1-O2	2.255(1)
C1-C25	1.562(2)
C25-O2	1.276(1)
C25-O3	1.237(1)
O3-C25-O2	126.4°

Figure 1: ORTEP plot of [Ru(PNP*t*Bu-COO)(CO)(H)] (**52**).[87] (Selected bond lengths in [Å] angle in [°]; Thermal ellipsoids at 50% probability, H atoms omitted for clarity, except for hydride Ru-H)

DFT calculations suggested a concerted addition of CO_2. Further transition metal pincer complexes were reported, activating CO_2 under MLC.[19; 91–93] The development of first-row transition metal catalysts (on the basis of e.g. Fe, Mn, Cu) and/or the

substitution in related precious metal complexes is desirable because of their natural abundance, their low cost and their potentially improved sustainability with respect to rare precious metals. Especially the development of Mn(I)-complexes has increased in recent years. The availability of air-stable and commercially available halogen pentacarbonyl complexes, or the simple preparation from $Mn_2(CO)_{10}$ with e.g., elemental bromine, has increased the significance of such complexes. A major advantage during the development of Mn(I) carbonyl complexes is their diamagnetic behavior (d^6-low-spin), which also makes them accessible for NMR spectroscopic analysis.[8; 94; 95] The Mn(I)-PNN pyridine pincer complex **53*** reacts with CO_2 *via* a dearomatization/rearomatization mode under 1,3-addition, forming Mn-complex **54**, similar to Ru-complex **52** (Scheme 19 d). With Mn(I)-PNN pyridine pincer complex **56**, an amido/amino mode was observed, under [1,2]-addition, forming the CO_2 complex **57** (Scheme 20 b). The amido group was obtained by deprotonating the secondary amine of the precatalyst **55**. Similar reactions were reported with molybdenum and tungsten pincer complexes, giving rise to a [1,2]-addition of CO_2 under N-C bond formation.[96; 97]

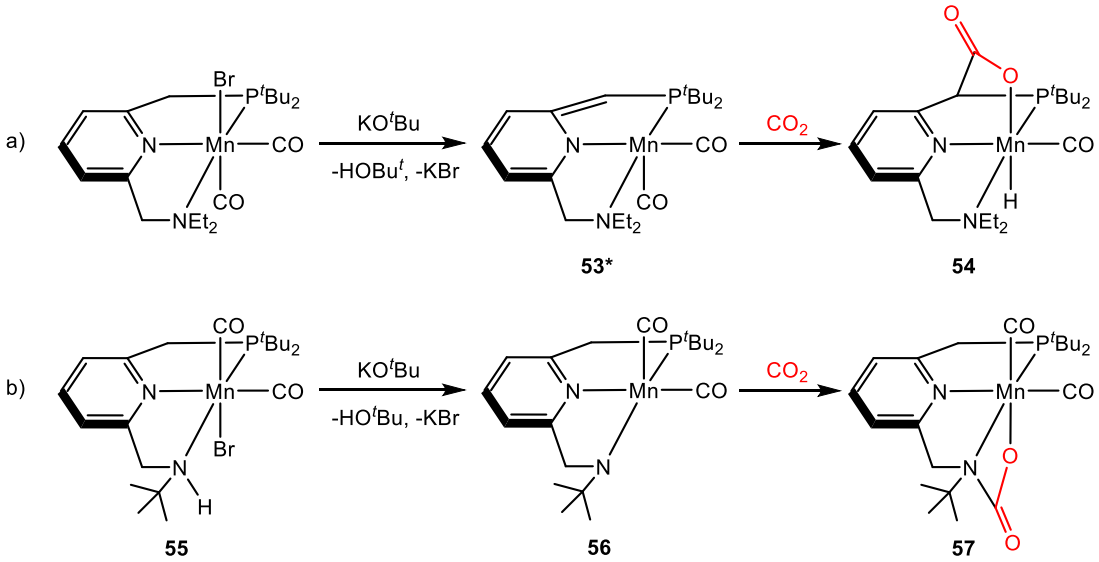

Scheme 20: Activation of CO_2 by the Mn PNN pincer complexes **53*** and **56**. a) dearomatization/rearomatization mode. b) amido/amino mode.[93]

Successful CO_2-hydrogenation reactions *via* MLC with different pincer complexes were reported by several groups in the past.[98; 99] Though, the CO_2-adduct has probably not played an active role so far. The hydrogenation of CO_2 probably always was followed after activation of H_2 by prior displacing of CO_2.[100] However, the MLC addition

products are observed during the hydrogenation reactions and can also lead to catalytically active species.[101]

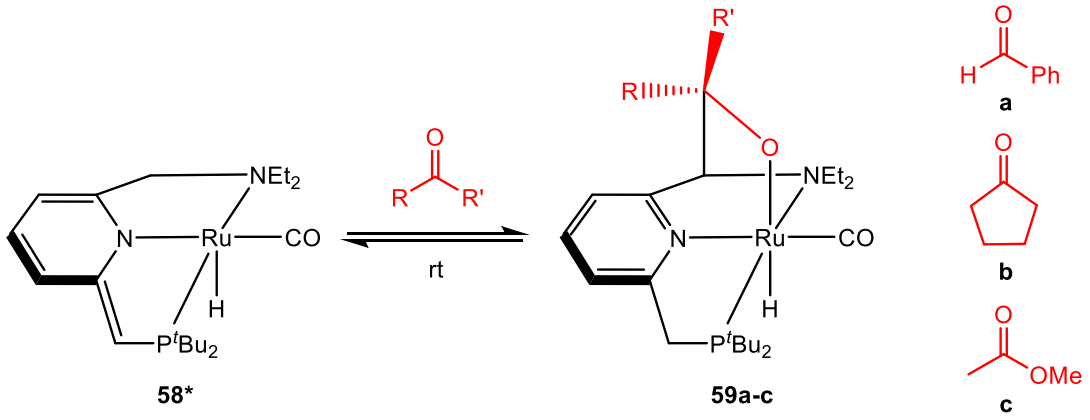

Scheme 21: Reversible activation of different carbonyl groups *via* MLC with the ruthenium PNN pincer complex **58***.[102]

Activations of other heterogeneous C-O bonds, such as alcohols, ketones, aldehydes or esters were also reported *via* a dearomatization/rearomatization reaction scheme, as already mentioned for the hydrogenation. Sandford *et al.* demonstrated the reversible activation of several carbonyl groups using the ruthenium pincer complex **58*** *via* a dearomatization/rearomatization sequence (Scheme 21).[102] The carbonyl carbon is diastereotopic when carrying different substituents R and R' as in **59a** and **59c**. As a result, a mixture of diastereomers was obtained. Not only single (H_2) and double bonds (carbonyl groups) can be activated, but also triple bonds e.g. in nitriles show remarkable reactivity with MLC-platforms. The first reported cooperative activation of the nitrile group *via a* dearomatization/rearomatization mode in pincer-type complexes was also published by Milstein *et al.*.[103] The dearomatized Re-PNP pincer-complex **60*** reacts readily with nitriles under C-C and Re-N bond formation. Two types of adducts could be verified depending on the used nitrile. The ketimino complexes **61** were obtained with nitriles, in the absence of hydrogen in α-position. The enamido complexes **62** were formed, using aliphatic nitriles (Scheme 22).

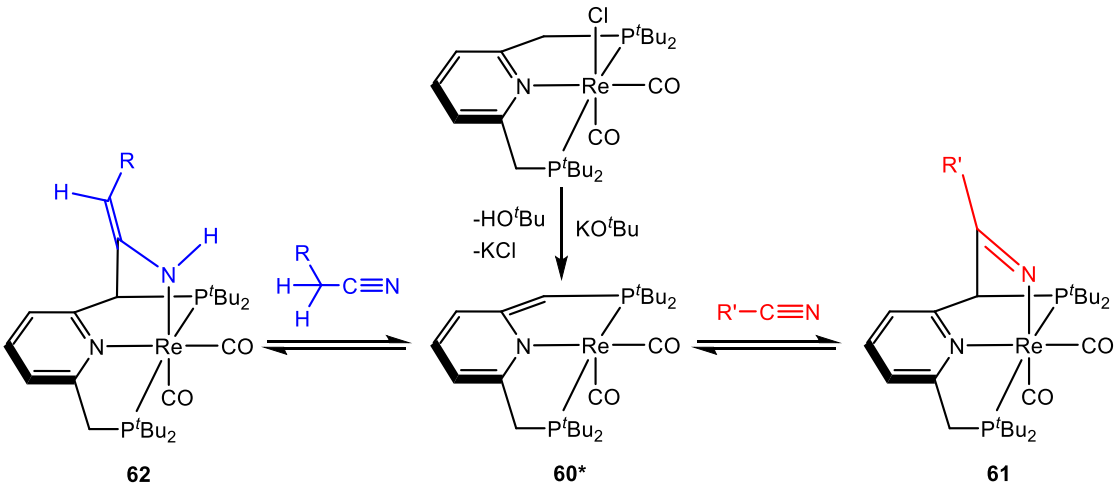

Scheme 22: Activation of nitriles with the Re-PNP pincer complex **60***.[103] (R = phenyl or methyl; R' = aryl or *t*-butyl)

Both types of nitrile activation reactions were shown to be reversible. Efficient catalytic addition reactions of nitriles with Michael acceptors could be successfully demonstrated with the Re(I)-complex **60**. In a later publication, Milstein *et al.* demonstrated the catalytic activity with the corresponding manganese PNP pincer complex **63***[104] (Scheme 23), which was also potent in hydrogenation reactions.[105]

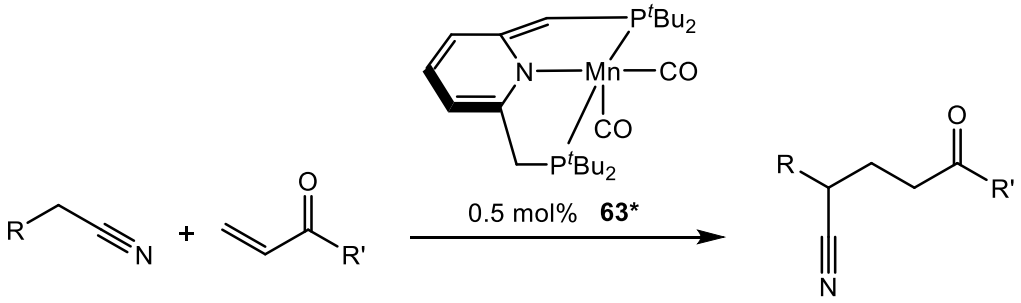

Scheme 23: Base-free Michael addition of aliphatic nitriles with ethyl acrylates, catalyzed by the Mn-PNP pincer complex **63***.[104]

Many review articles have been published in the last years, and the potential of MLC for activation in catalytic processes has only just begun.[8; 33; 56; 106; 107] The discovery of the influence of the dearomatization/rearomatization mode in catalytic mechanisms was an initial spark for the development of new efficient catalysts in the field of heterogeneous transition metal catalysis *via* MLC. Recent knowledge and a generally

newly accepted mechanism of many hydrogenation and dehydrogenation reactions in bifunctional catalysis using MLC was developed by Dub *et al.* on the basis of DFT calculations and is still being investigated.[108–113] The concerted reaction models of e.g. Shvo, Noyori[30] or Milstein[64] were reexamined in many computational mechanistic studies, using an alternative pathway by Dub *et al.*.[108; 109] In the "Dub mechanism" the ligand supports a stepwise catalytic reaction pathway only by hydrogen bonding interactions at the ligand without bond cleavage of hydrogen atoms (L-H) on the ligand (Scheme 24), while in the concerted mechanism the ligand undergoes a reversible H^+ transfer *via* bond formation and bond cleavage as seen before (e.g. Scheme 7 or Scheme 11). Bifunctional catalysis based on the Dub mechanism is therefore also referred as a metal ligand assisted (MLA) reaction pathway.

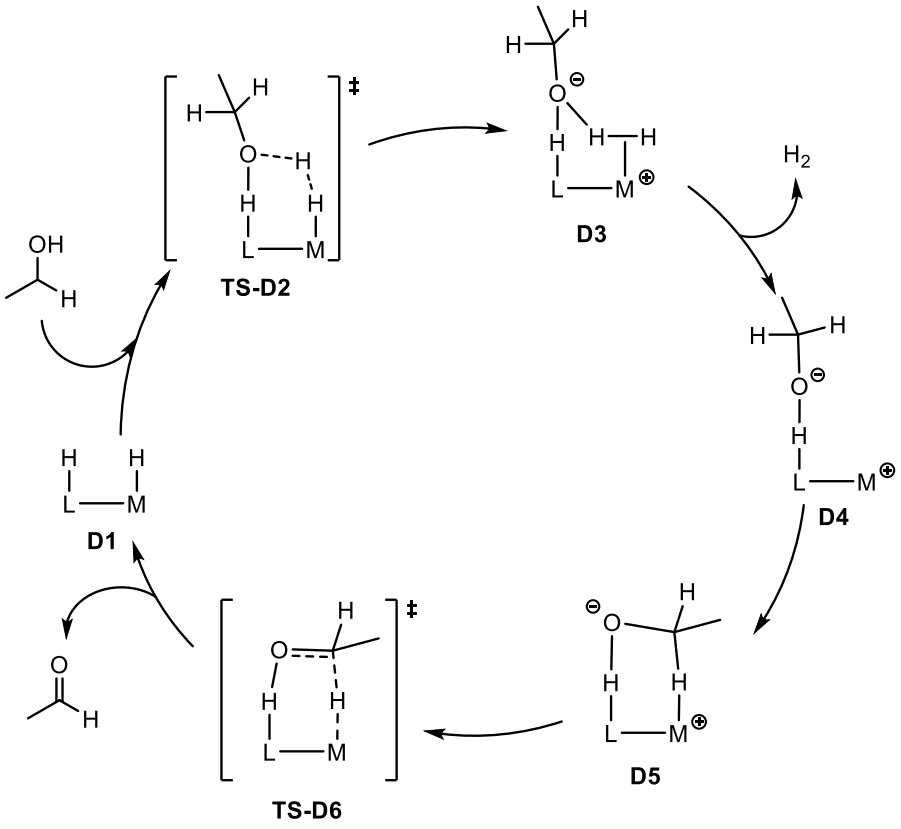

Scheme 24: Stepwise catalytic reaction pathway for the dehydrogenation of primary alcohols to aldehydes *via* MLA mechanism.[113]

In the MLA pathway for the catalytic dehydrogenation of primary alcohols to aldehydes, which is simplified in Scheme 24, the cycle starts with the dihydride complex **D1**. The transition state **TS-D2** shows the incorporation of the alcohol and a proton transfer from the alcohol leads to complex **D3,** which leads to complex **D4** under release of H_2. The

intramolecular hydride incorporation to the metal center in **D5** paves the way for the hydride transfer *via* **TS-D6**. In the last step the aldehyde is released under regeneration of the catalyst (**D1**). Although the reaction mechanism gets more complicated in many cases by the stepwise route, it leads to energetically more favorable and more plausible transition states.[108; 109; 113] This model has given a new look for many bifunctional catalytic mechanisms. However, this new mechanism still supports the essential presence of hydrogen on the ligand, as observed by Noyori[30], but calls for a critical consideration of many MLC-based catalytic processes. Due to the new results of the MLA studies and the better understanding of the transition states in the reaction cycles, even better bifunctional catalysts can be developed in the future, which should expand and improve the previously excellent results of the catalysts based on MLC. In addition to the diversification of the coordinated atoms and their bounding groups of the pyridine-based pincer ligand, a next logical step is the development of ligand scaffolds which are selective for the intended substrate, easy and inexpensive to synthesize and environmentally friendly. Huang *et al.* developed some new amino pyridine-based pincer ligand scaffolds for MLC substrate activation reactions.[114; 115] The benzylic CH_2-group was replaced by a NH-group (Scheme 25). With similar ligand scaffolds, Kirchner *et al.* were also able to show catalysts for the hydrogenation of aldehydes, cross-coupling reactions of C-C and C-N bonds or the alkylation of amines.[116–121]

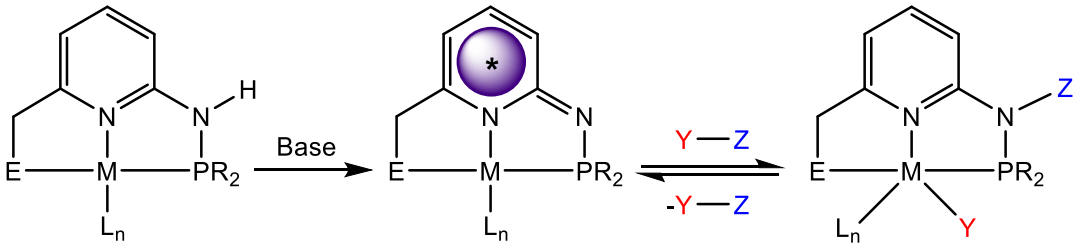

Scheme 25: Proposed bond activation *via* MLC with 2-amino-pyridine-based pincer complexes. Dearomatized active species in the middle. (E = N,P-donor ligands; Y—Z = substrate)

The deprotonation of the amino group causes the “dearomatization” of the pyridine unit. The benzylic N-H unit is more acidic, compared to the benzylic C-H in the Milstein system, which allows new possibilities in bond activations.[114; 115] A series of different bond activations was reported *via* MLC with reversible dearomatization/

rearomatization mode using the Huang system.[68; 122; 123] Huang *et al.* examined the potential role of the dearomatization/rearomatization mode in the activation process. They compared the system of Milstein with their own, by substitution of the bridging nitrogen atom by a carbon atom, and came to the conclusion that Milstein's system gains more energy from rearomatization than their amino-pyridine system (Scheme 26).[68; 123] The reason for this is that the dearomatized species of Huang keeps a much higher aromatic character than that of Milstein.[124] Common models for the determination of aromaticity are HOMA (Harmonic Oscillator Model of Aromaticity), NICS (Nucleus Independent Chemical Shifts), ASE (Aromatic Stabilization Energy) or VBSCF (Valence Bond Self-Consistent Field).[125–130]

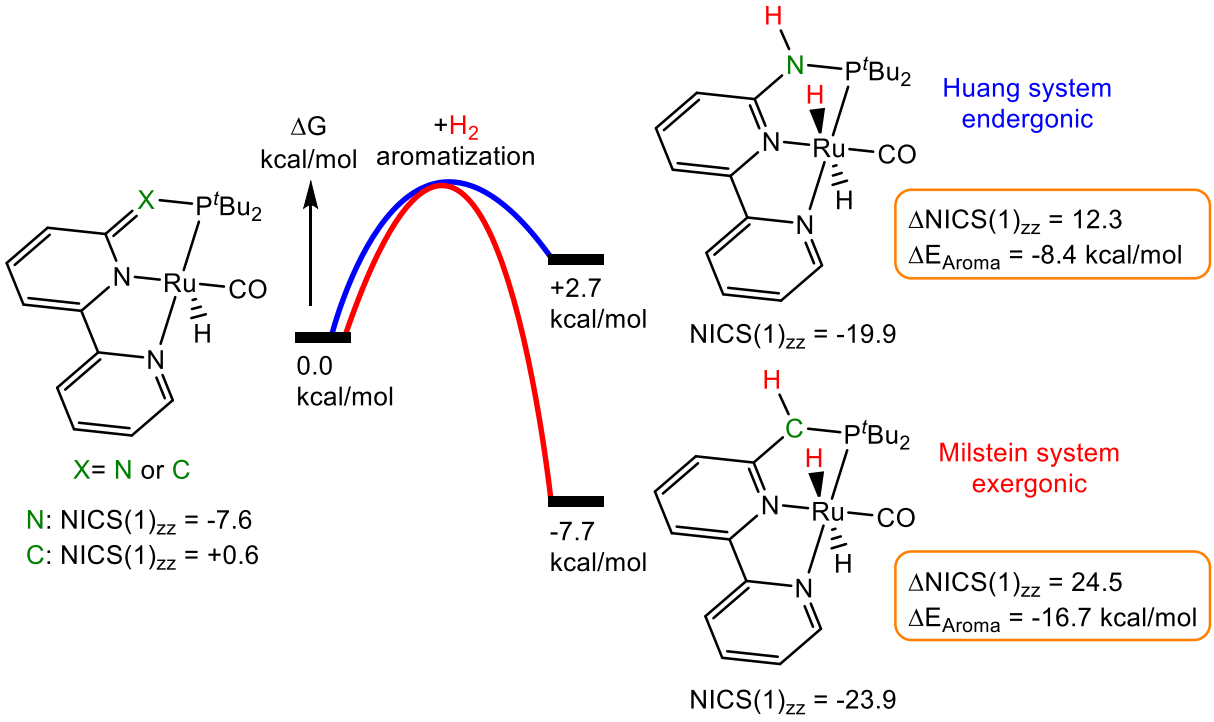

Scheme 26: Thermodynamic comparison of Huang's system and Milstein's system and calculated energy differences after reacting with H_2 under rearomatization. ΔE_{Aroma} from ASE calculations and $NICS(1)_{zz}$ from improved NICS calculations.[68; 123]

The determination of the degree of aromaticity is a challenging task and not directly scalable. Calculations with amino-triazin ligands have also been demonstrated, providing similar results.[131; 132] The exact influence of aromatization in bond activation reactions must be further investigated, in order to get a better understanding to develop catalysts customized to the substrate. Further interesting ligand scaffolds for MLC dearomatization/rearomatization modes were reported with different N-heterocyclic

ligands, 1,3-diketimine ligands or carbocyclic ligands and also summarized in several review articles.[8; 9; 33; 56] Considering the previous results, in the following the dearomatization also means a disruption of the π-system in the pyridine unit if the bonding conditions in the activated species are not unequivocally proven. Due to different resonance structures, electron density can be distributed to some extent over the ligand framework and also to the metal center, so that dearomatization cannot always be clearly proven.

2 Motivation

Many pyridine-based tridentate pincer ligands were reported over the last years, having the ability for bifunctional substrate activation.[8; 9; 33; 106; 122] In addition to the previously listed advantages of the PNP and PNN pyridine pincer ligands, the disadvantage is their elaborate synthesis, which also makes them relatively expensive, and the high reactivity of the alkylphosphane ligands. The production of these ligands is also not very sustainable due to the use of toxic substances e.g. white phosphorus or PCl_3. Along these lines, this work presents three different ligand systems suitable for substrate activation under metal ligand cooperativity *via* a dearomatization/ rearomatization reaction scheme. The synthesis of the ligands is compared to the PNN and PNP pincer ligands very simple or even available for purchase. The sustainability is additionally increased by omitting alkylphosphane ligands. In this project, MLC substrate activation with different bidentate and tridentate 2-picoline based transition metal complexes will be shown. A dearomatization/rearomatization mode as a driving force for substrate activation turned out to be very efficient for MLC. The activation of known substrates/bonds as well as the expansion of previously unknown substrates *via* dearomatization/rearomatization mode is a focal point of this work. Analytical studies of the activated species and - if possible - the isolation of the adduct-complexes is another main target of this work. The simplification of ligand systems and reduced expenditure are further targets, as well the combination of other activation properties like previously described. Furthermore, there is a focus on the transfer from electron-rich late transition metals to first-row transition metals. In addition to their different chemical properties, they are more available and usually mined in a more environmentally friendly manner.[133] In this work the transfer from the group 7 metal rhenium to manganese will be shown.

Introduction of the Developed Complexes

Redox-Active Bidentate Iminopyridine ligands give rise to anionic metal-ligand cooperative carbonyl complexes with Re and Mn metal centers. The complexes are characterized by the presence of counter cations, which can take an additional decisive role in substrate activation.

The first system is based on the bidentate ligand framework of 2-amino-/2-iminomethyl pyridine, in *fac*-tricarbonyl transition metal complexes of group 7 (Mn, Re) with oxidation state +I (Scheme 27).

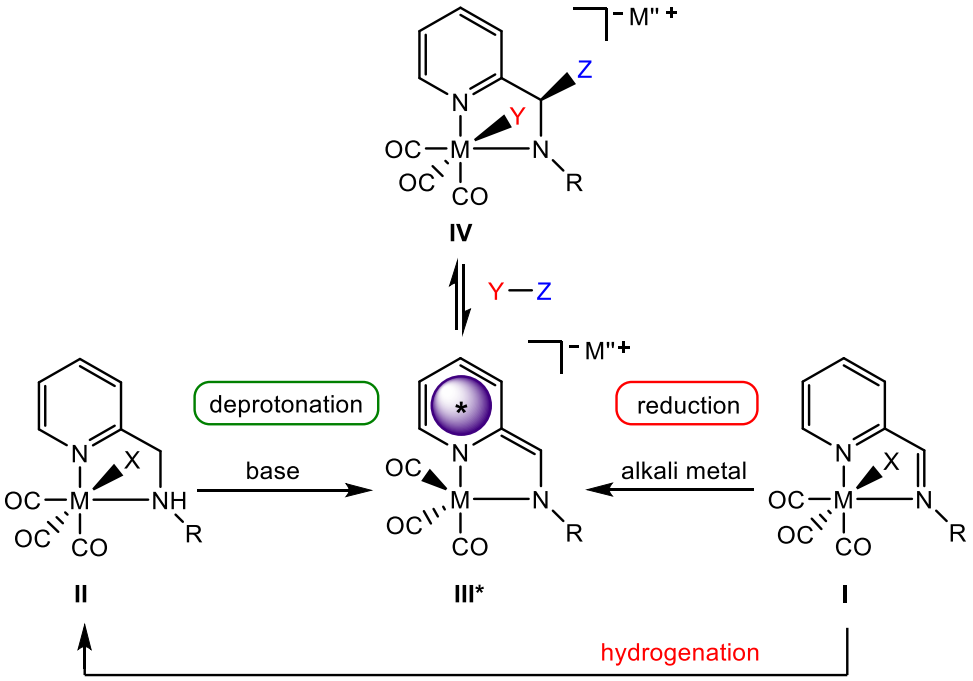

Scheme 27: Bidentate 2-amino-/2-iminomethyl pyridine system for MLC substrate activation. X = Cl, Br; M = Mn, Re; M" = Li, Na, K; R = Ph$^{p\text{-}Me}$; Y—Z = substrate.

The first target is to obtain the active "dearomatized" species **III*** *via* two different ways. That is, the reduction of the imin complex **I**, and the somewhat milder way of double deprotonation of the amin and methylene unit in complex **II**. Subsequently, the dearomatized anionic species **III*** can activate suitable substrates under rearomatization *via* MLC (**IV**). The redox active ligand operates as a Lewis base (nucleophilic methine carbon). As the resulting dearomatized complex **III*** is anionic, which is a significant difference to most pyridine-based PNN or PNP pincer complexes, the role of the counterion can play a significant role, as the e.g. alkali cation could

directly interact with the activated substrate (see work of Floriani[83; 84] above). That is, complexes of type **III*** bear an additional functionality next to the MLC as an additional feature for the regulation of a well-defined substrate environment. The influence of a coordinating alkali metal counterion for cooperative substrate activations has not been adequately studied yet and appears to be underdeveloped. This matter is addressed in the course of this work.

Cooperative Tridentate Ligand Design: Fusion of the Aminopyridine Unit with 5H-dibenzo[b,f] azepine as steering Ligand

The second system is a tridentate 2-aminomethyl pyridine ligand scaffold, which is expanded by a seven-membered ring, able to act as an olefinic unit as steering ligand for chelation (Scheme 28).

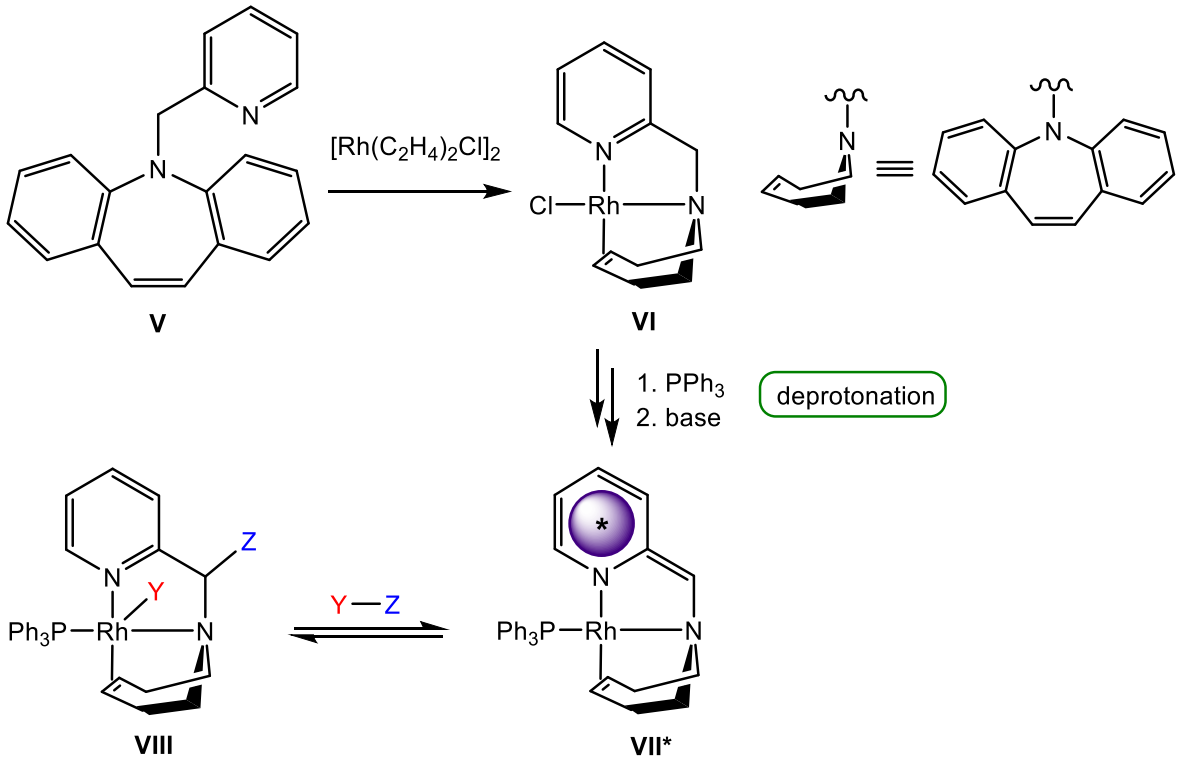

Scheme 28: Tridentate olefinic 2-aminomethyl pyridine system. (Y—Z = substrate, PPh_3 = triphenylphosphine)

Grützmacher *et al.* have extensively reported on the 5H-dibenzo[a,d]annulene scaffold (trop-ligand) in transition metal complexes and contributed publication with paramount importance with respect to aminyl radicals[134], methanol/water dehydrogenation[135] and ethanol as hydrogen donor for transfer hydrogenations[136], to only name a few.

The fused 2-aminomethyl pyridine unit allowing for potential MLC and the olefinic coordination[137; 138] site gives rise to an intriguing ligand platform for electron rich transition metals. In fact, the Rh(I)-complex **VI** was prepared by addition of the novel ligand **V** with $[Rh(C_2H_4)_2Cl]_2$. The dearomatized species **VII*** is obtained *via* addition of triphenylphosphine (PPh_3) and subsequent ligand deprotonation with a base. Rh(I)-complex **VII*** is able to activate carbonyl substrates under rearomatization *via* MLC (**VIII**). The olefinic entity remains coordinated to the rhodium center functioning as a steering ligand during substrate activation.

Further simplified bidentate pyridine-based ligands: Utilization of simple picoline-based alcohols and ketones as redox-active and cooperative N-O Chelates.

The third model is based on a 2-pyridinecarboxaldehyde/2-pyridinmethanol system with the group 7 transition metal Re(I) (Scheme 29).

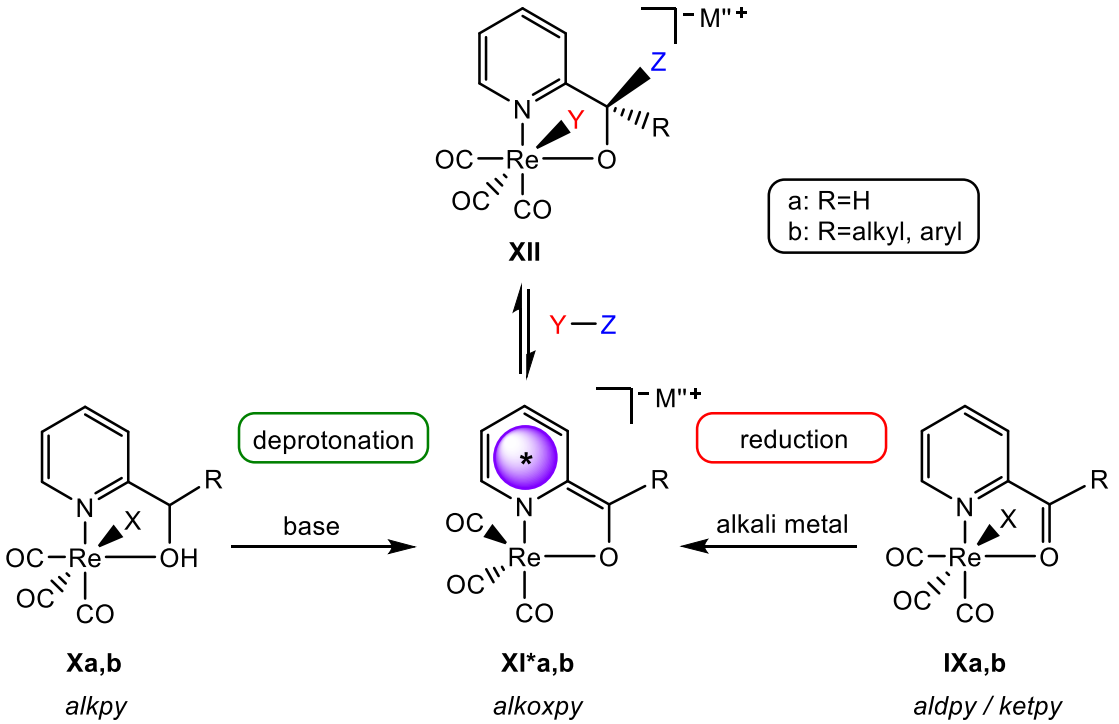

Scheme 29: Bidentate N,O-chelating pyridine Re(I)-complexes for substrate activation *via* MLC. (a: R = H (aldehyde/alcohol system); b: R = alkyl, aryl (ketone/alcohol system)) (X = Br; M" = Li, Na, K; R = H, alkyl or aryl; Y—Z = substrate)

Replacing one benzylic hydrogen atom by an alkyl or aryl group provides the corresponding secondary-alcohol/ketone system. Instead of the amino/imino system of the N,N-chelating Schiff base ligands, the use of aldehydes and ketones with their related alcohols as ligand results in the bidentate N,O-complexes **IXa** (*aldpy*), **IXb** (*ketpy*) or **Xa,b** (*alkpy*), forming an primary-alcohol/aldehyde system or a secondary-alcohol/ketone system showing reactivity similar to **I,II,III***. Two-electron reduction of *aldpy* or *ketpy* with alkali metals should lead to the "dearomatized" alkoxide-species **XIa*** (a-*alkoxpy*)* or **XIb*** (b-*alkoxpy**), capable of MLC substrate activation (**XIIa** or **XIIb)**. The formal oxidation state of the metal should remain unchanged as the ligand shows redox-noninnocent behavior. Oxygen atoms as a hemilabile ligand to the metal center have often shown some unexpected reaction pathways.[139–141] For the reaction pathway of deprotonation, the associated alcohol N,O-chelated complexes **Xa** (a-*alkpy*) or **Xb** (b-*alkpy*) is used. The simplicity of this system is a notable advantage compared to previous already simplified bidentate N,N-ligands, as the ligands are for instant commercially available.

3 Results

3.1 Bidentate Anionic 2-Amino-/2-Iminomethyl Pyridine Complexes

3.1.1 Overview

Inspired by the tridentate pincer scaffold and the previous work with bipyridine ligands[142–144] and at the beginning of this research work, Kubiak *et al.* studied the capability of bidentate imino-pyridine transition metal complexes for CO_2 reduction (Scheme 30 a).[145–147] The redox non innocent properties of this type of complexes were shown before in several publications.[148–151] The molybdenum tetracarbonyl complex **64** decorated with a pyridine mono-imino chelate was found to react with CO_2, after previous two-electron reduction, *via* C-C and Mo-O bond formation (Scheme 30 b).

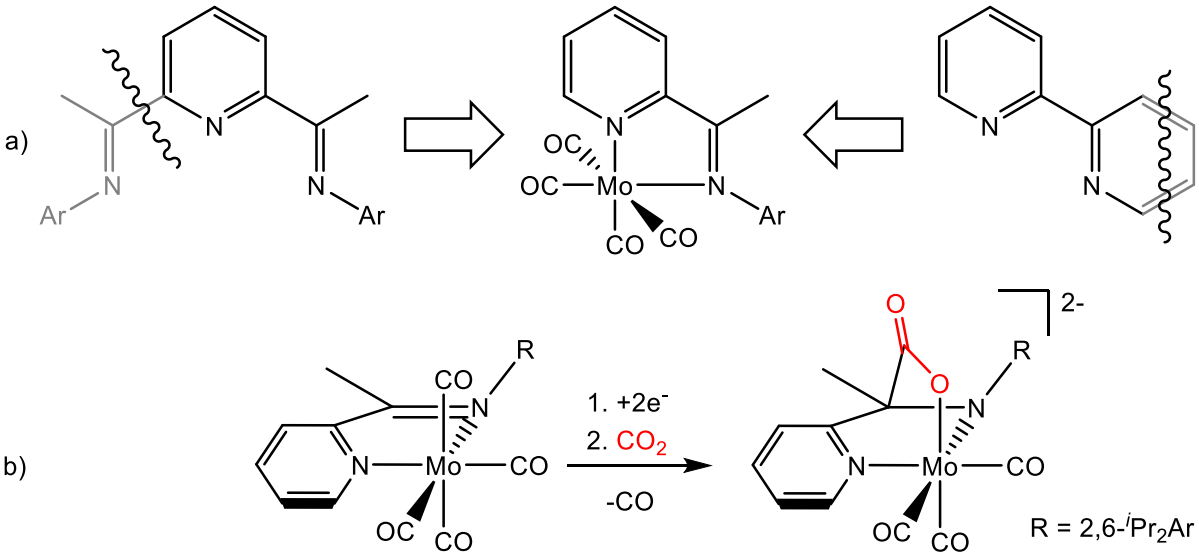

64

Scheme 30: a) Bidentate iminopyridine complex, inspired by pincer and bipyridine ligands. b) Proposed activation of CO_2, prepared *via* prior two-electron reduction, with the pyridine-based N,N-Mo complex **64**.[145]

Coupled UV/Vis spectroscopic cyclic voltammetric investigations, as well NMR spectroscopic studies of the monoanionic (first one e^- reduction step) and dianionic (second one e^- reduction step) species of **64**, suggest a fully separated ligand-based reduction. The first one-electron reduction step, which is proposed to form a ligand

centered anion radical, showed a reversibility in cyclic voltammetry (CV) analysis. The second one-electron reduction step indicated the dearomatization of the pyridine unit by ^{1}H NMR spectroscopic analysis, but was irreversible under loss of CO. The dianionic species could also be obtained by reduction with potassium graphite (KC_8). Broad signals in NMR spectra were attributed to a fluxional K^+ coordination/ decoordination. Isolation of the double reduced species was not successful. The state of dearomatization was not further analyzed. It was assumed that the electrons were distributed over the ligand scaffold. A molecular structure was obtained for the putative protonated dianionic CO_2-adduct, by scXRD, showing only one potassium counterion, interacting with the CO_2 unit. The CO_2 complex shows an angle of 125.8°, a sp^2-hybridized C atom and a delocalized C=O double bond with small preference to the not coordinated O-atom. The observed C-C single bond between the CO_2 and the ligand was considered to be deleterious for catalytic turnover for CO_2 reduction.[145] Kubiak *et al.* demonstrated the redox active behavior of bipyridine-ligands in *fac*-tricarbonyl group 7 transition metal complexes and showed several successful applications for CO_2 reduction in various publications.[142–144; 152–155] The redox-active properties could then also be shown for the pyridine monoimino rhenium complexes **65**.[147]

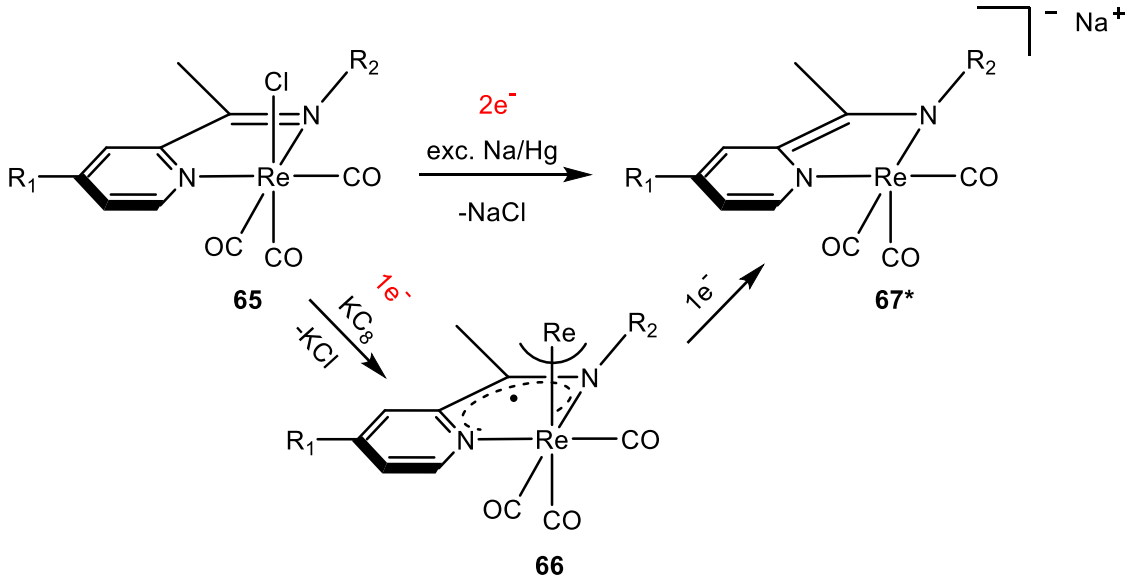

Scheme 31: One-electron reduction of pyridine monoimino Re-complex **65** with KC_8 under formation of the Re-Re dimer complex **66** and two-electron reduction with sodium amalgam under formation of the anionic complex **67***.[147] (R_1 = (H, Me); R_2 = (Me, Ph, 4-ClAr, Mes, 2,6-di^{i}PrAr))

They studied the single (**66**) and double reduced species (**67***) of several pyridine monoimino Re(I) *fac*-triscarbonyl complexes (Scheme 31) and additionally demonstrated the activation of CO_2.[146] Compared to the molybdenum tetracarbonyl monoamine pyridine complex **64** both one-electron reduction steps are reversible which is suggested by CV analysis. One- and two-electron reduction products could be isolated and fully characterized after preparative reduction. The one electron reduction product gave a dimeric structure under Re-Re bond formation (**66**). NMR spectroscopic analysis and the molecular structure of the two-electron reduced anionic species indicating the dearomatization of the pyridine unit. The authors were not able to isolate the CO_2-adduct. A three-step electrochemical reduction under CO_2-atmosphere yielded, due to a disproportionation reaction, free CO and a carbonate species, which suppresses the catalytic activity of CO_2 reduction. The reduction of CO_2 to CO, published before with bipyridine-based Re-complexes could not be transferred to the pyridine monoimine Re-complex[143; 156], allegedly because of the competitive ligand-based reactivity. During the course of this work, Weinstein *et al.* reported electrocatalytic CO_2 reduction, using a series of manganese tricarbonyl complexes **68a-e** with asymmetric 2-iminopyridine ligands (Scheme 32).[157]

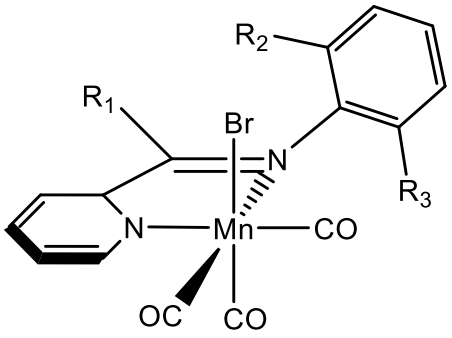

68

	R_1	R_2	R_3
68a	H	H	H
68b	H	^{i}Pr	H
68c	H	^{i}Pr	^{i}Pr
68d	H	^{i}Bu	H
68e	CH_3	^{i}Bu	H

Scheme 32: Varieties of the *fac*-triscarbonyl 2-iminopyridine manganese complex **68** for electrocatalytic reduction of CO_2 to CO.

The reduction of CO_2 to CO with all complexes (**68a-e**) has been confirmed under CO_2-atmosphere (Scheme 33). The increase of CO in the spectro-electrochemical cell causes an exchange of the ligand, forming $Mn[CO]_5^-$. The most sterically demanding ligand **68c**, however, showed a higher stability against ligand displacement by CO. In contrast, the least sterically hindered ligand **68a** showed the highest activity. Also, this group did not report CO_2-adduct isolation. It was shown that the substitution on the

ligand frame work has direct influence on the catalytic activity. While the groups R_2 and R_3 have primarily a steric effect, group R_1 has a strong influence on the electrochemical properties of the complex. The relatively independent tuning of steric and electronic properties is an interesting attribute of these types of ligands.

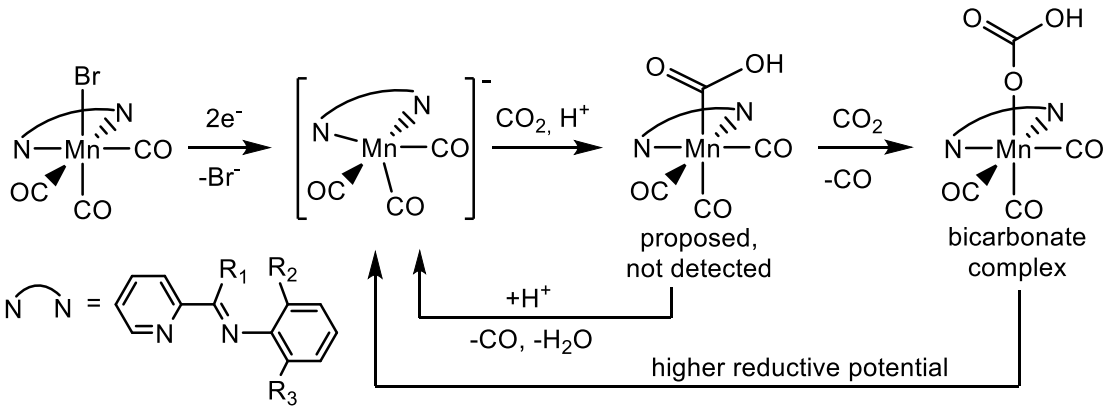

Scheme 33: Proposed CO_2 reduction pathway with the Mn(I) 2-iminopyridine complex **68** under CO_2 atmosphere.[157]

The usage of 2-aminomethyl pyridine complexes as precatalyst has not been studied until now. The possibility for a milder reaction pathway could make these types of complexes more interesting for future catalytic applications.

3.1.2 Precursor Chemistry

The first project is based on simple-to-use 2-iminomethyl-pyridine and 2-aminomethyl pyridine ligands in rhenium(I) and manganese(I) *fac*-triscarbonyl complexes. The imino ligand **71** (*impy)* is easily prepared by the condensation reaction of pyridine-2-carbaldehyde **69** with *p*-toluidine **70** (Scheme 34).[158] The amino ligand **72** (*ampy)* is obtained by hydrogenation of the azomethine **71**. The hydrogenation reaction can also be done in good yield after complexation. In comparison to tridentate pyridine-based pincer ligands, the synthesis of these bidentate ligands is prepared in higher yield and the starting materials are less expensive.

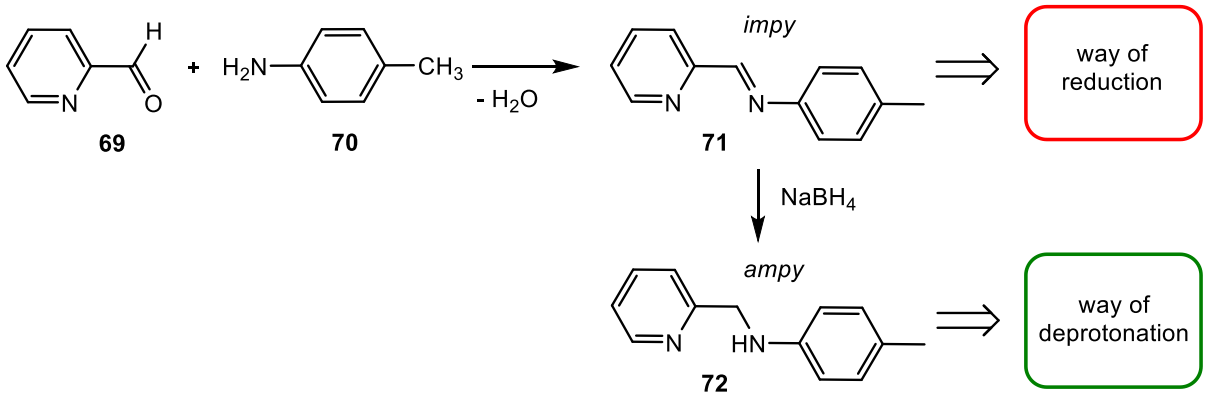

Scheme 34: Condensation reaction of pyridine-2-carbaldehyde (**69**) with *p*-toluidine (**70**), forming the Schiff base **71** (*impy*) and the hydrogenation product **72** (*ampy*) by subsequent reduction with $NaBH_4$.

The complexes *fac*-[M(I)(*impy*)$(CO)_3$Br] **73** (M = Mn, Re) and *fac*-[M(I)(*ampy*)$(CO)_3$Br] **74** were prepared by stirring *impy* or *ampy* with $M(CO)_5Br$ (M = Mn, Re), under replacement of two equivalents of CO, in good yields (Scheme 34). Alternatively, the *impy* complexes can also be prepared in a one-pot synthesis. The anionic dearomatized amido complexes M''[M(*amidopy**)$(CO)_3$] **75*** (M'' = Li, Na, K and M = Re, Mn) (the asterisk indicates the dearomatized pyridine unit) were obtained by two-electron reduction of the *impy*-complex **73** with alkali metals or by deprotonation of the *ampy*-complex **74** with the corresponding bis(trimethylsilyl)amide salt (M''HMDS). The possibility of obtaining the dearomatized species **75*** by deprotonation, allows a milder reaction pathway, instead of the reduction by strong reductants. The dearomatized anionic *amidopy**-complex **75*** is highly reactive and able to activate different polarized multiple bonds (such as C=O, S=O or C≡N) depending on the metal center and the counterion *via* 1,3-addition and under rearomatization of the pyridine unit. The possible activation of heterogeneous double bonds *via* [2+2]-cycloaddition (**76**) is shown in Scheme 35.

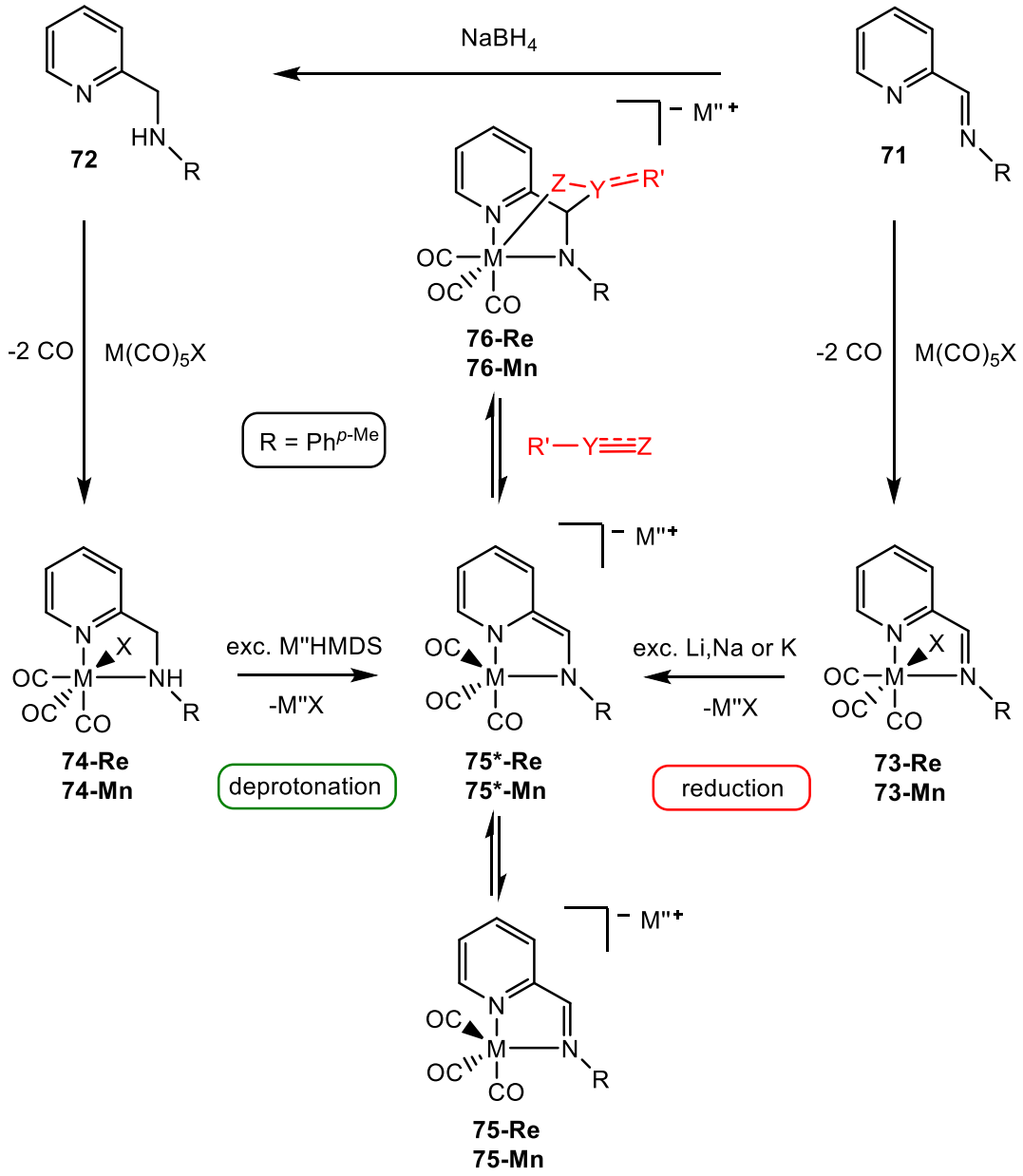

Scheme 35: Synthesis scheme of the rhenium and manganese complexes **73**, **74** and **75*** with possible substrate activation *via* MLC (**76**). (Y = C,S; Z = N,O; X = Br; M = Mn, Re; M" = Li, Na, K; R = Ph$^{p\text{-}Me}$; R' = organic substituent)

Formally there is an additional active center by the coordinated amido group, that might also be able to activate substrates *via* [1,2]-addition. The 2-iminomethyl-pyridine system demonstrates the activation of CO_2, SO_2, ketones, aldehydes and nitriles *via* MLC 1,3-addition, depending on the metal center and the counterion.

3.1.3 Rhenium(I) Triscarbonyl Complexes with Redox-Active Amino- and Iminopyridine Ligands: Metal-Ligand Cooperation as Trigger for the Reversible Binding of CO_2 *via* a Dearomatization/ Rearomatization Reaction Sequence[159]

This work shows the reversible binding of CO_2 *via* MLC, starting from redox-active amino- and iminopyridine Re(I) triscarbonyl complexes **73-Re** and **74-Re**. The reported reactions demonstrate the activation of CO_2 *via* MLC with the anionic complexes M"[Re(I)(*amidopy**)$(CO)_3$] (M" = Li, K) (**75*-Re**) and show the formation of the dearomatized reactive species **75*** by reduction of **73** as well as by deprotonation of **74** (Scheme 36).

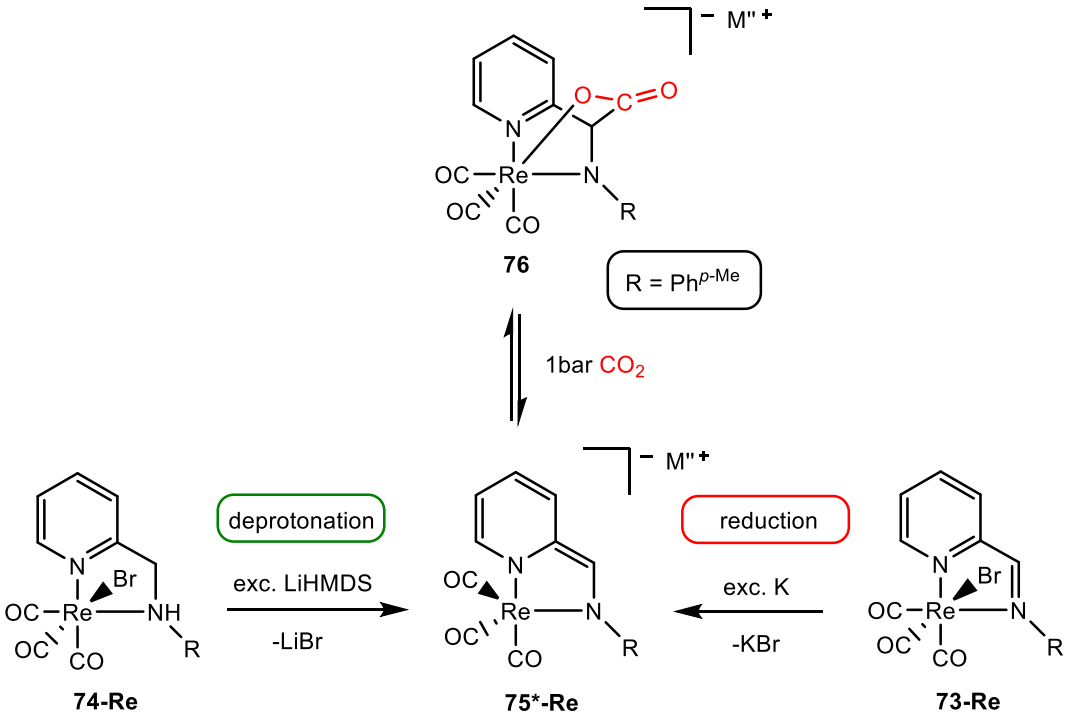

Scheme 36: Reversible binding of CO_2 with the dearomatized bidentate complex M"[Re(*amidopy**)$(CO)_3$] (**75*-Re**), obtained from reduction or deprotonation pathway. (M" = Li, K; R = $Ph^{p\text{-}Me}$)

Previous works by Arne Helmers and Jennifer Bremer evaluated the chemistry of these ligand-types. I conducted the major part of the experiments along with a large part of the characterization and the experimental section. Markus Rohdenburg and André Wark supported the implementation of the syntheses during their research internship. Single crystal X-ray diffraction (scXRD) analysis was measured and evaluated by Dr. Enno Lork.

The obtained results were published in the following journal:

R. Stichauer[#], A. Helmers[#], J. Bremer[#], M. Rohdenburg, A. Wark, E. Lork, M. Vogt, *Organometallics* **2017,** *36*, 839-848. ([#] = these authors contributed equally)
DOI: 10.1021/acs.organomet.6b00897

My percentage contribution of this publication in categories: experimental concept and design: ca. 40%, experimental work and acquisition of experimental data: 30%, data analysis and interpretation: 75%, preparation of Figures and Tables: ca. 30%, drafting of the manuscript: ca. 50%.

ORGANOMETALLICS

Article

pubs.acs.org/Organometallics

Rhenium(I) Triscarbonyl Complexes with Redox-Active Amino- and Iminopyridine Ligands: Metal–Ligand Cooperation as Trigger for the Reversible Binding of CO_2 via a Dearmomatization/Rearomatization Reaction Sequence

Rasmus Stichauer,[#] Arne Helmers,[#] Jennifer Bremer,[#] Markus Rohdenburg, André Wark, Enno Lork, and Matthias Vogt*

Institut für Anorganische Chemie und Kristallographie, Universität Bremen, Leobener Strasse NW2 – C Block, 28359 Bremen, Germany

Supporting Information

ABSTRACT: We describe rhenium(I) triscarbonyl compounds (**3** and **4**) decorated with simple-to-use 2-iminomethyl-pyridine (**1**, *impy*) and 2-aminomethyl-pyridine (**2**, *ampy*) ligands, respectively, which can serve as cooperative ligand scaffolds enabling CO_2 binding via a formal [1,3] addition under Re–O and C–C bond formation. *fac*-[Re(*impy*)$(CO)_3$Br] (**3**) is readily prepared by stirring (1-(pyridin-2-yl)-*N*-(*p*-tolyl)methanimine (*impy*, **1**) and [$Re(CO)_5$Br] in refluxing THF. Alternatively, complex **3** can be readily obtained when a mixture of [$Re(CO)_5$Br], *p*-toluidine, and picolinaldehyde is refluxed in ethanol. Complex **3** is reduced with excess potassium metal in THF (two-electron reduction) to give the anionic amido complex K[Re(*amidopy**)$(CO)_3$] (**5b**, the asterisk indicates the dearomatized ligand). Analysis of the ^{1}H and $^{13}C\{^1H\}$ NMR spectra of **5b** suggest the dearomatization of the pyridine unit. Complex **5b** is highly reactive and gives rise to the facile [1,3] addition of CO_2. The addition of the CO_2 and thus the formation of K[Re(*amidopy*-COO)$(CO)_3$] (**6**) is characterized by the concomitant formation of a Re–O and a C–C bond. The addition is triggered by the rearomatization of the pyridine unit in **6**. Remarkably, isotopic labeling experiments involving $^{13}CO_2$ suggest a reversible binding of CO_2 to the complex. The related amine complex *fac*-[Re(*ampy*)$(CO)_3$Br] (**4**) is similarly prepared by stirring (4-methyl-*N*-(pyridin-2-ylmethyl)aniline (**2**) and [$Re(CO)_5$Br] in THF at 60 °C. Upon addition of excess base (LiHMDS), complex **3** is readily deprotonated twice to give likewise the anionic amido complex Li[Re(*amidopy**)$(CO)_3$] (**5a**). The latter reaction gives rise to a facile access to the reactive dearomatized anionic fragment [Re(*amidopy**)$(CO)_3]^-$ with no need for the application of strong reducing agents. The ion pair M^+/[Re(*amidopy**)$(CO)_3]^-$ is highly reactive and combines MLC (metal–ligand cooperation) via a dearomatization/rearomatization scheme and bifunctional reactivity enabled by the nucleophilic nature of the Re complex and the Lewis acidic counter alkali cation.

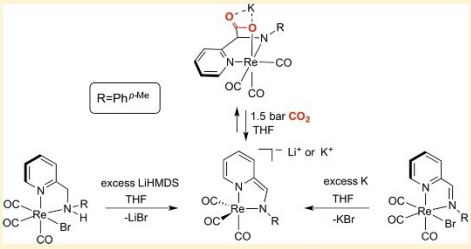

INTRODUCTION

Chelating α-iminopyridine ligands are frequently used in coordination chemistry and entail valuable redox-properties qualifying such ligands as electron reservoirs in transition metal complexes.[1,2] Their redox-noninnocent properties,[3−5] especially in complexes of transition metals of the first row, was explored by Wieghardt, Lu, van Gastel, and co-workers.[6−9] Tridentate bis(α-diimino)pyridine ligands (PDI) also show remarkable redox-noninnocent properties.[10−13] The ligand-centered reactivity in PDI-type complexes was summarized by Budzelaar et al.[14] Transition metal complexes involving such bidentate or tridentate motifs find versatile applications, especially in catalysts for olefin polymerization.[15] Among those, cobalt-and iron-based PDI complexes, initially reported by Brookhart and Gibson, are probably the most prominent examples.[16−20] The hydrosilylation of ketones catalyzed by manganese-based (PDI) compounds was recently reported by Trovitch and co-workers.[21] The importance of redox-active PDI ligands in an iron-based catalyst was illuminated for the [2 + 2]-cycloaddition reaction of α,ω-dienes.[22] Kubiak and co-workers investigated bidentate amino-pyridine ligands as suitable ligand platform for catalytic species involved in the electrochemical reduction of CO_2.[23] Concerning this matter, the (reductive) transformation of CO_2 into a valuable C_1 feedstock for the production of chemical commodities or liquid fuel is an attractive goal with growing importance.[24−27] Commonly, the catalytic conversion of CO_2 in homogeneous solution requires the initial activation of CO_2 at the metal center. The binding of CO_2 to a single metal center generally

Received: December 3, 2016
Published: February 7, 2017

DOI: 10.1021/acs.organomet.6b00897
Organometallics 2017, 36, 839–848

Scheme 1. Alternative Reversible Binding Modes of CO_2 in Complexes with a Single Metal Center

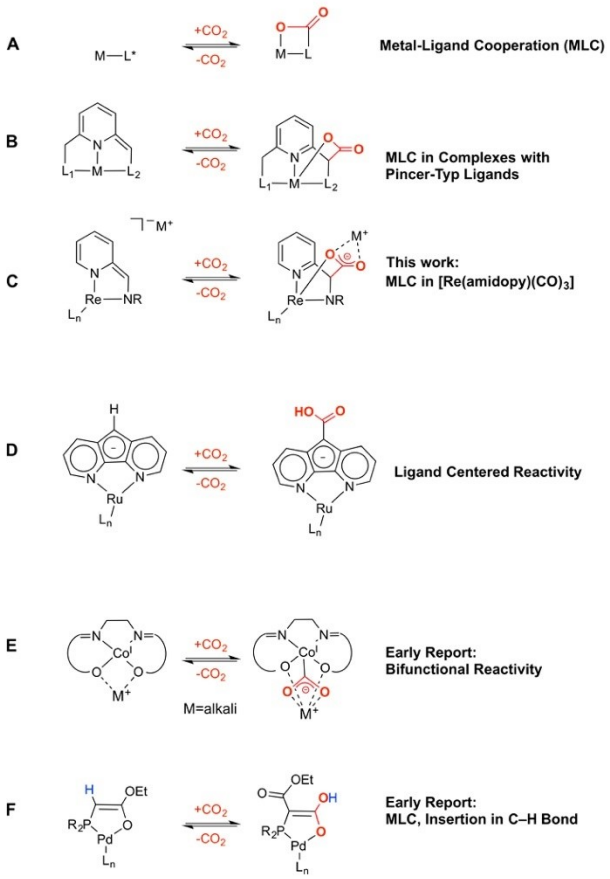

proceeds via π-coordination of a C=O bond (η^2-CO coordination, analogous to the Dewar−Chatt−Duncanson binding scheme for olefins) or formation of a σ-bond to the η^1-bonded carbon atom. In contrast, η^1-coordination via the oxygen atom is rare.[28,29] Alternative binding modes, where CO_2 binds a coordination entity reversibly became an active field of research only recently (Scheme 1). Milstein and co-workers have demonstrated the activation of CO_2 in rhenium[30] and ruthenium[31] PNP-pincer-type compounds (PNP = 2,6-bis(di-*tert*-butylphosphinomethyl)pyridine), in which a dearomatization/rearomatization reaction scheme plays a key role in course of the CO_2 addition. Similar observations were reported by Sanford and co-workers in a ruthenium PNN-pincer-type compound (PNN = 6-(di-*tert*-butylphosphinomethylene)-2-(*N*,*N*-diethylaminomethyl)pyridine).[32] Pidko and co-workers investigated the catalytic hydrogenation of CO_2 using a Ru(PNP) species as catalyst and describe the addition of CO_2 via MLC (metal−ligand cooperation) to the dearomatized Ru(PNP)complex as deactivation pathway of the catalyst.[33]

The general MLC reaction sequence is depicted in Scheme 1A,B. The same principle reaction scheme not only allows for the [1,3]-addition of the C=O double bond of CO_2 but also allows for the activation of C=O bonds of carbonyl compounds[34−36] and CN-triple bonds of nitriles.[37−40] Song and co-workers reported a reversible insertion of CO_2 into a C−H bond of the ligand remotely located from the Ru(II) center (Scheme 1D).[41−43] However, the bifunctional, reversible addition of CO_2 reach back to earlier reports. Floriani and co-workers describe the bifunctional activation of CO_2 in anionic low-valent cobalt salen compounds. Floriani details this variant of a η^1-CO_2 coordination as a result stemming from a concerted attack of the nucleophilic Co center on the electrophilic CO_2 carbon and stabilization of the basic oxygen by a Lewis acidic alkali metal (Scheme 1E).[44−47] Notably, such anionic system can reversibly bind CO_2, strongly depending on the solvent and the nature of the employed Lewis acidic alkali countercation. A further early report by Braunstein and co-workers described the fully reversible addition of CO_2 in a Pd(II) phosphino-enolate

DOI: 10.1021/acs.organomet.6b00897
Organometallics 2017, 36, 839−848

Scheme 2. Syntheses Scheme of the Rhenium Complexes 3−6 with R = Ph−*p*-Me

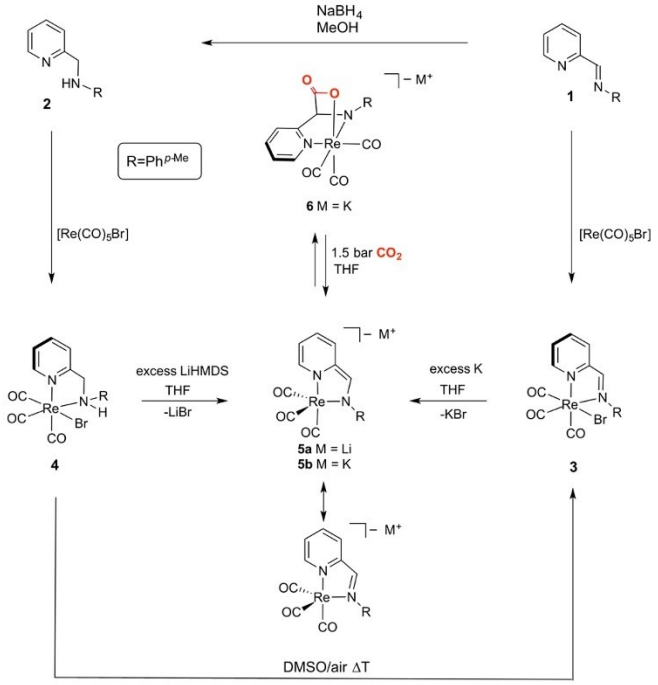

complex under Pd−O and C−C bond formation with the CO_2 formally inserting into a C−H bond of the chelating phosphino-enolate ligand (Scheme 1F).[48] Dearomatization/rearomatization reaction schemes are very successfully exploited in transition metal complexes with pincer-type ligands. Such sequences are frequently observed in single and multiple bond activation processes and became a powerful tool in catalysis.[49,50] Such multidentate ligands can be used as versatile (cooperative) actor ligands in small molecule activation and catalysis.[51] In general, metal−ligand cooperative reaction pathways became a powerful tool in chemical bond activation and gave rise to remarkable catalytic transformations.[49,50,52−57] With this background, we now describe rhenium(I) triscarbonyl compounds (**3** and **4**) decorated with simple-to-use 2-iminomethyl-pyridin (**1**, *impy*) and 2-aminomethyl-pyridine (**2**, *ampy*) ligands, which can serve as bifunctional and metal−ligand cooperative scaffolds enabling reversible CO_2 binding. MLC, where both the rhenium center and the amidopyridine ligand undergo Re−O and C−C bond formation, gives rise to the reversible [1,3]-addition of CO_2 in simple systems as illustrated in Scheme 1C.

■ RESULTS AND DISCUSSION

The ligands (1-(pyridin-2-yl)-*N*-(*p*-tolyl)methanimine (*impy*, **1**) and (1-(pyridin-2-yl)-*N*-(*p*-tolyl)methanamine (*ampy*, **2**) were prepared as previously described by Cuevas and coworkers:[58] Imino-ligand **1** is obtained by simple Schiff base formation via condensation of *p*-toluidine and picolinaldehyde. Compound **1** is reduced using $NaBH_4$ in methanol solution to give amino-ligand **2** in quantitative yield. *fac*-[Re(*impy*)$(CO)_3$Br] (**3**) is prepared via the reaction of *impy* and [$Re(CO)_5$Br] in toluene at 80 °C for 24 h under concomitant release of CO gas (Scheme 2). The product is isolated as a red microcrystalline solid in 89% yield. Alternatively, complex **3** can readily be obtained when a mixture of [$Re(CO)_5$Br], *p*-toluidine, and picolinaldehyde is heated in refluxing ethanol. The ^{1}H NMR spectrum of **3** in THF-d_8 (298 K, 360 MHz) shows four resonances for the pyridine protons in the aromatic region (d, 9.10 ppm $^3J_{HH}$ = 5.4 Hz Py(6); m 8.33−8.07 ppm overlap Py(4) and Py(3); m, 7.70 ppm Py(5)). The characteristic singlet resonance at 9.03 ppm corresponds to the *exo*-cyclic methine group of the imino moiety Py−*H*C = N−Ph$^{p\text{-Me}}$. The ^{13}C{^{1}H} NMR spectrum (THF-d_8, 298 K, 91.0 MHz) shows three distinct resonances for the CO ligands at 198.7, 197.4, and 187.7 ppm signaling a mutual *facial* arrangement. The imino ^{13}C nucleus gives rise to a characteristic singlet resonance at 168.5 ppm. The *para*-methyl group gives rise to a singlet resonance at 21.3 ppm. The corresponding amino complex *fac*-[Re(*ampy*)$(CO)_3$Br] (**4**) is similarly prepared via heating a THF solution of *ampy* and [$Re(CO)_5$Br] at 50 °C for 24 h. Subsequent recrystallization from methylene chloride and *n*-hexane at 4 °C gives complex **4** as an off-white crystalline solid in 63% yield (Scheme 2). The corresponding ^{1}H NMR spectrum of **4** in THF-d_8 has four characteristic resonances for the pyridine unit, which are well-resolved (d, 8.84 ppm $^3J_{HH}$ = 7.2 Hz, Py(6); td 8.0 ppm J_{HH} =

DOI: 10.1021/acs.organomet.6b00897
Organometallics 2017, 36, 839−848

7.7 and 1.5 Hz Py(4); d, 7.68 ppm, J_{HH} = 7.9 Hz Py(3); t, 7.46 ppm $^3J_{HH}$ = 7.9 Hz Py(5)). The *exo*-cyclic methylene moiety gives rise to two characteristic doublets of doublets resonances (4.99 and 4.89 ppm) with a large germinal coupling constant $^2J_{HH}$ = 15.3 Hz and two corresponding smaller vicinal (CH_2–N*H*) coupling constants of $^3J_{HH}$ = 4.9 and 8.7 Hz, respectively. The corresponding resonance of the N*H* proton is observed as broad dd at 6.70 ppm ($^3J_{HH}$ = 8.1 and 4.8 Hz). In general, all aromatic ^{1}H NMR signals of **4** are observed slightly high-field-shifted with respect to those of iminopyridine complex **3**. This might be addressed to the increased shielding in complex **4** due to the increased electron density in the reduced amino-pyridine ligand. The $^{13}C\{^1H\}$ NMR spectrum (THF-d_8, 298 K, 91.0 MHz) shows, analogous to complex **3**, three distinct resonances for the CO ligands (197.7, 197.5, and 192.9 ppm) indicating a mutual *facial* arrangement. Characteristically, the resonance corresponding to the *exo*-cyclic methylene moiety is observed as singlet resonance at 60.6 ppm. The *para*-methyl Ph–*p*-CH_3 group gives rise to a typical singlet resonance at 17.7 ppm. Remarkably, amino complex **4** can be transformed into imino complex **3** by heating a solution of **4** in DMSO in air (85 °C, 11 h, 30% yield; for spectral details see Figure S16). It should be noted that the usage of DMSO is crucial for the transformation. No reaction occurs when the analogous reaction is performed in chloroform or acetone.

Single crystals of compound **3** suitable for X-ray diffraction analysis were obtained from a *n*-hexane layered methylene chloride solution. The DIAMOND plot of the molecular structure is shown in Figure 1 (top). The rhenium center resides in a distorted octahedral coordination sphere with three CO ligands in mutual *facial* arrangement. The *impy* ligand coordinates the Re center in a bidentate fashion via both N-donors. The bromide moiety resides in mutual *cis* position with respect to the pyridine ring. The observed structural features are typical for this class of Re(+I) triscarbonyl compounds bearing iminopyridine ligand sets.[59,60] The short C6–N2 interatomic distance of 1.288(3) Å indicates an imino C=N double bond. Crystal structures of a related free iminopyridine ligand show very similar C–N interatomic distances for the imino group.[61] The molecular structure of a closely related rhenium tris-carbonyl compound [Re(*impy*^{Ph})(CO)$_3$Cl] exhibits a comparable C–N distance (1.296(8)).[59] Likewise, slow diffusion of *n*-hexane into a methylene chloride solution of **4** gave single crystals suitable for X-ray diffraction analysis. The molecular structure (Figure 1, bottom) is closely related to complex **3**. The rhenium center resides in a distorted octahedral coordination sphere shaped by three CO ligands in mutual *facial* arrangement and the bidentate *ampy* ligand. The bromide ligand in apical position completes the octahedron around the Re(+I) center. The coordination of the amine moiety gives rise to a pyramidalized substitution pattern around nitrogen atom N2. The bromide ligand resides in mutual *syn* position with respect to the calculated N2–H hydrogen atom. The interatomic distance between C6 and N2 amount to 1.491(7) Å indicating an amino C–N single bond. Similar bond lengths have been previously reported, for instance, for a molecular structure of a related free aminopyridine ligand carrying a protonated amine (1.50(2) Å),[62] for a corresponding rhenium tris-carbonyl complex (1.488(9) Å),[62] and for aminopyridine complexes of other transition metals, e.g., group 11 (average 1.48 Å)[63] and group 10 (average 1.48 Å).[64] Comparing both structures **3** and **4** it becomes evident that the imino moiety (N2–Re1) exhibits a significant shorter bond length (2.186(2) Å) with respect to the corresponding amino moiety in **4** (2.230(5) Å). The N1–Re1 distance related to the coordination of the pyridine unit to rhenium is approximately 2.17 Å in both compounds.

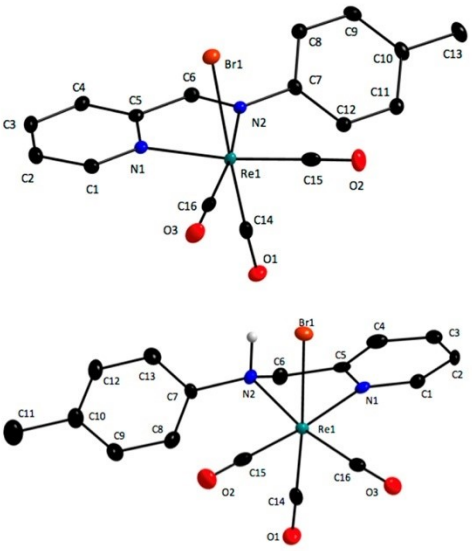

Figure 1. DIAMOND plot (thermal ellipsoids at 50% probability) of complex **3** (top) and **4** (bottom). H atoms neglected for clarity (except N2–H in complex **4**). Selected bond lengths [Å] for complex **3**: Re1–N1 = 2.172(2) Å, Re1–N2 = 2.186(2) Å, C6–N2 = 1.288(3) Å, C1–N1 = 1.337(3) Å, C1–C2 = 1.391(4) Å, C2–C3 = 1.382(4) Å, C3–C4 = 1.389(4) Å, C4–C5 = 1.390(3) Å, C5–C6 = 1.449(3) Å, C5–N1 = 1.357(3) Å, C7–N2 = 1.436(3) Å, Re1–Br1 = 2.625(2) Å, Re1–C16 1.915(3) Å, Re1–C14 = 1.933(3) Å, Re1–C15 = 1.936(3) Å, C14–O1 = 1.111(3) Å, C15–O2 = 1.143(3) Å, C16– O3 = 1.153(3) Å. For complex **4**: Re1–N1 = 2.176(5) Å, Re1–N2 = 2.230(5) Å, C6–N2 = 1.491(7) Å, N1–C1 = 1.337(7) Å, C1–C2 = 1.375(8) Å, C2–C3 = 1.376(8) Å, C3–C4 = 1.381(9) Å, C4–C5 = 1.386(8) Å, C5–N1 = 1.360(7) Å, C7–N2 = 1.452(7) Å, C5–C6 = 1.498(8) Å, Re1–C16 = 1.912(6) Å, Re1–C15 = 1.930(6) Å, Re1–C14 = 1.932(6) Å, Re1–Br1 = 2.618(1) Å, O1–C14 = 1.086(7) Å, O2–C15 = 1.153(7) Å, O3–C16 = 1.150(7) Å.

Complex **3** reacts with excess of potassium metal in THF to give the anionic amido-complex K[Re(*amidopy**)(CO)$_3$] (**5b**, the asterisk indicates a doubly reduced ligand and thus dearomatization of the pyridine unit) as a deep red solution in THF. Complex **5b** is highly reactive. Multiple attempts to isolate the anionic compound did not lead to the desired pure material. A cyclic voltammetry study in THF of complex **3** (voltammogram depicted in Figure 2) showed two quasi-reversible redox waves with half-potentials (referenced to the Fc/Fc$^+$ redox couple) at $E^1_{1/2}$ = −1.51 V and $E^2_{1/2}$ = −1.89 V, respectively, indicating two one-electron redox steps. In this study, we restricted our attention to doubly reduced species **5b**. The singly reduced species is not discussed in this work.

The reduction reaction with excess potassium was monitored in THF-d_8 via ^{1}H and $^{13}C\{^1H\}$ NMR spectroscopy. The obtained spectra revealed the quantitative formation of diamagnetic complex **5b**. A representative section of the ^{1}H

DOI: 10.1021/acs.organomet.6b00897
Organometallics 2017, 36, 839–848

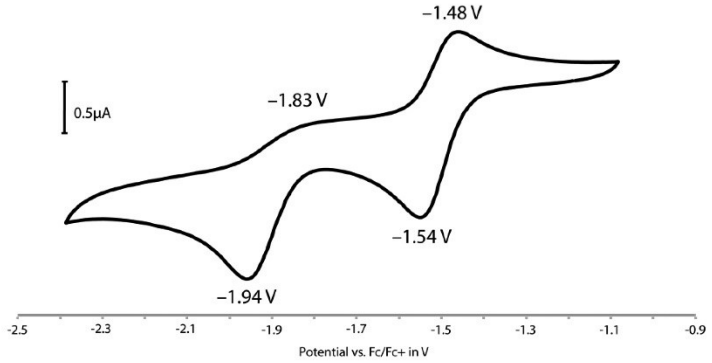

Figure 2. Cyclic voltammogram of complex **3** in THF with $[TBA]PF_6$ electrolyte (0.1 M), 100 mV/s scan rate, referenced against freccocene/ferrocenium redox couple. Half potentials: $E^1_{1/2} = -1.51$ V and $E^2_{1/2} = -1.89$ V.

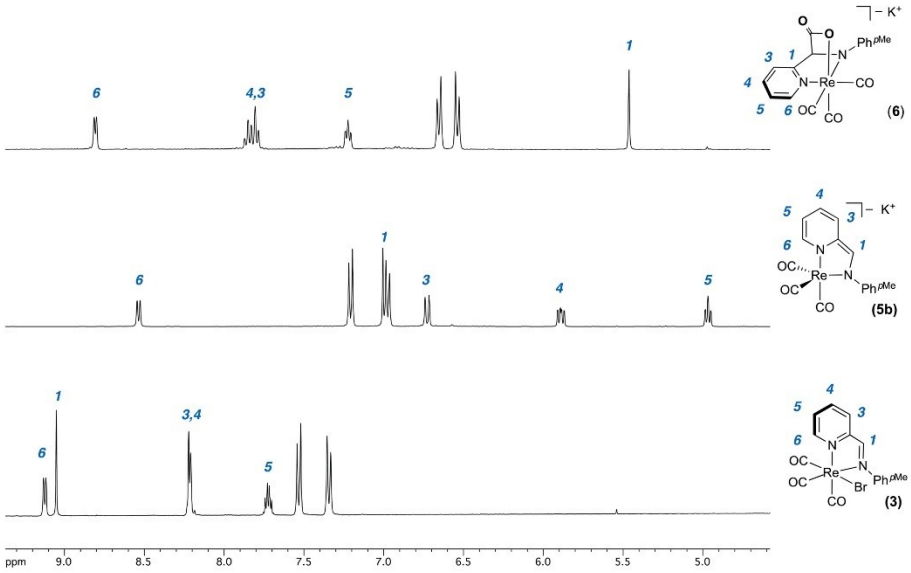

Figure 3. Sections of the ^{1}H NMR (360 MHz, THF-d_8, 298 K) spectra of complex **3** (bottom), **5b** (middle), and **6** (top).

NMR spectrum of **5b** is shown in Figure 3 (middle). The two-electron reduction of compound **3** gives rise to a drastic shift to lower frequencies of all four resonances associated with the pyridine protons in compound **5b** (d, 8.51 ppm $^3J_{HH}$ = 6.4 Hz Py(6); d 6.70 ppm $^3J_{HH}$ = 7.2 Hz Py(3); br t 5.86 ppm $^3J_{HH}$ = 7.2 Hz Py(4); br t, 4.94 ppm $^3J_{HH}$ = 6.0 Hz Py(5)). A similar drastic shift upfield is observed for the *exo*-cyclic methine proton (s, 6.98 ppm in compound **5b**; $\Delta\partial$ = 2.05 ppm, with respect to **3**). Analysis of the $^{13}C\{^1H\}$ NMR (91.0 MHz, THF-d_8, 298 K) spectrum reveals a gain in symmetry for complex **5b** with respect to starting material **3**. Only a single resonance associated with all three carbonyl moieties are observed at 210.6 ppm, suggesting the loss of the octahedral coordination sphere (and presumably the formation of a trigonal bipyramidal geometry) as well as a rapid exchange of the three CO ligands in solution with respect to the NMR time scale. Structural data from single X-ray diffraction analysis of a closely related anionic rhenium tris-carbonyl compound was very recently reported by Kubiak and co-workers, revealing indeed a trigonal bipyramidal structure in the solid state.[65] The high-field-shifted ^{1}H resonances of the pyridine unit accompanied by a drastic high-field shift of the ^{1}H resonance corresponding to the *HC*=N imino methine moiety, as well as the high-field-shifted resonance of the ^{13}C nucleus of the *exo*-cyclic carbon (121.5, $\Delta\partial$ = 47.5 ppm with respect to **3**), and the ^{13}C resonances associated with all pyridine *CH* moieties suggest a dearomatiza-

DOI: 10.1021/acs.organomet.6b00897
Organometallics 2017, 36, 839−848

tion of the pyridine unit in compound **5b** as similarly observed in rhenium(+I) bis-carbonyl complexes with PNP and PNN pincer-type ligands.[37,66,67] Such pincer complexes proved to be readily deprotonated at the *exo*-cyclic methylene moiety to give rise to highly reactive dearomatized species. A dearomatization/rearomatization sequence is key to metal−ligand cooperative bond activations and is frequently observed for transition metal complexes decorated with pyridine-based pincer-type ligands.[68] We now found that the related amine complex *fac*-[Re(*ampy*)-$(CO)_3$Br] (**4**) reacts upon addition of excess base (LiHMDS) via double deprotonation to give likewise the anionic amido complex Li[Re(*amidopy**)$(CO)_3$] (**5a**, the asterisk indicates the double deprotonation and thus denotes the dearomatized ligand). Hence, dearomatized anionic species **5** is not only accessible via the reaction with strong reductants of **3** but also via simple deprotonation of **4** with a moderate base as illustrated in Scheme 2. However, other resonance forms may contribute to the overall electronic structure, for instance, a resonance structure with the rhenium center in the formal oxidation state −I and an intact aromatic pyridine unit as shown Scheme 2. However, the ^{1}H and ^{13}C{^{1}H} NMR spectroscopic data suggest a principal contribution of the dearomatized resonance structure, in which the rhenium center resides in the oxidation state +I and the reduction is ligand-centered.

Remarkably, a THF solution of complex **5b** reacts instantaneously with CO_2 (1.5 bar, at ambient temperature) to form the [1,3]-addition product K[Re(*amidopy-COO*)-$(CO)_3$] (**6**, Scheme 2). The ^{1}H NMR spectroscopic data suggest the rearomatization of complex **6**: All signals associated with the pyridine ring are shifted back to higher frequencies (d, 8.77 ppm $^3J_{HH}$ = 5.3 Hz Py(6); m, 7.80 ppm overlap Py(3) and Py(4); ddd 7.19 ppm J_{HH} = 7.2, 5.6, 1.5 Hz Py(5)). The *exo*-cyclic C*H* moiety is drastically shifted upfield and has a characteristic singlet resonance at 5.43 ppm in agreement with an alpha-C*H* adjacent to a carboxylic group (Figure 3, top). The ^{13}C{^{1}H} NMR spectrum shows a new signal at 181.3 ppm consistent with a carbon nucleus of the new formed carboxylic HC−*C*OO−Re group[67] and shares a significant cross-peak in the ^{13}C−^{1}H multiple bond coherence spectrum (HMBC NMR) with the ^{1}H resonance related to the *exo*-cyclic C*H*−COO moiety (s, 5.43 ppm). The vibrational spectrum of **6** shows a typical absorption band at 1653 cm^{-1} for the carboxylate moiety accompanied by absorptions at 1902 cm^{-1} (broad, very strong) and 2027 cm^{-1} (sharp, strong) associated with the three CO ligands in mutual *facial* arrangement. Single crystals of the anionic compound K[Re(*amidopy-COO*)$(CO)_3$] suitable for single crystal X-ray diffraction analysis are obtained when a solution of **5b** and 18-*crown*-6 in THF is subjected to CO_2 gas (1 bar). The mixture was layered with *n*-hexane to give orange-brown crystals of [K(18-*crown*-6)][Re(*amidopy-COO*)-$(CO)_3$] (**6**-(*crown*)). The obtained molecular structure of **6**-(*crown*) is depicted in Figure 4. The Re center resides in a distorted octahedral coordination sphere consisting of the bidentate amidopyridine ligand and three CO ligands in mutual *facial* arrangement. The octahedral coordination sphere is completed by the carboxylate moiety stemming from the incorporation of the CO_2 into the *amidopy* ligand via C−C bond formation. The negative charge of the anionic [Re-(*amidopy-COO*)$(CO)_3$]$^-$ fragment is balanced by the potassium countercation. The K^+ ion is chelated by 18-*crown*-6 and resides in an apical position with short contacts to the oxygen atoms of the carboxylate unit (K1−O4 = 2.885(4) Å and K1−O5 = 2.769(4) Å). An interesting structural feature is the close contact of the potassium ion K1 and the *para*-methyl group (C13) of a neighboring [Re(*amidopy-COO*)$(CO)_3$]$^-$ fragment. The contact is established on the opposite side of the central molecular plane of the [K(18-*crown*-6)] chelate, with respect to the COO moiety, which gives rise to a chain motive within the crystal lattice. The formed C−C bond between the *exo*-cyclic carbon moiety of the *amidopy** ligand and CO_2 (C6−C17 = 1.530(7) Å) is slightly shorter with respect to a recently reported Mo tris-carbonyl compound by Kubiak and co-workers exhibiting a similar CO_2 binding pattern (1.572(5) Å).[23] The carboxylic unit in **6**-(*crown*) is characterized by an O4−C17−O5 angle of 124.6(5)° and O4−C17 and O5−C17 interatomic distances of 1.284(6) and 1.231(6) Å, respectively. The C6−N2 interatomic distance of 1.468(6) Å suggest the formation of a C−N single bond, which is in line with an rearomatization of the pyridine ring, which has four almost equidistant C−C bonds (average 1.39 Å). The Re1−N2 bond distance of 2.130(4) Å is significantly shorter compared to its counterpart in complex **4** (2.230(5) Å) indicating a stronger Re−N(amido) interaction.

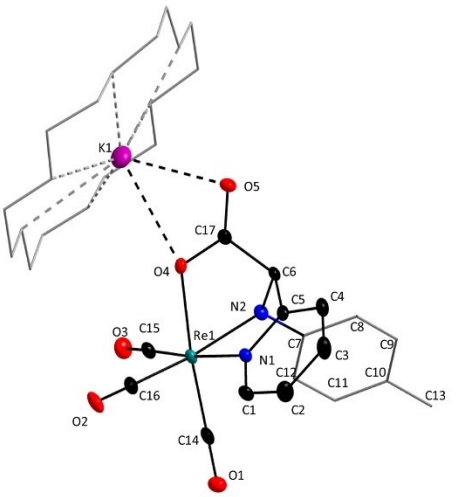

Figure 4. DIAMOND plot (thermal ellipsoids at 50% probability) of complex 6-(*crown*). H atoms neglected for clarity. Php-Me and 18-*crown*-6 depicted as wireframe. Selected bond lengths [Å] and angles [°]: Re1−O4 = 2.157(3) Å, Re1−N1 = 2.205(4) Å, Re1−N2 = 2.130(4) Å, C6−C17 = 1.530(7) Å, O5−C17 = 1.231(6) Å, O4−C17 = 1.284(6) Å, K1−O4 = 2.885(4) Å, K1−O5 = 2.769(4) Å, K1−C17 = 3.165(5) Å, Re1−C15 = 1.907(6) Å, Re1−C16 = 1.916(5) Å, Re1−C14 = 1.904(6) Å, O1−C14 = 1.158(6) Å, O2−C15 = 1.158(7) Å, O3−C16 = 1.153(6) Å, N1−C1 = 1.340(6) Å, C1−C2 = 1.386(8) Å, C2−C3 = 1.386(8) Å, C3−C4 = 1.386(8) Å, C4−C5 = 1.384(7) Å, N1−C5 = 1.339(6) Å, C6−C5 = 1.520(7) Å, N2−C6 = 1.468(6) Å, N2−C7 = 1.395(7) Å; O4−C17−O5 = 124.6(5)°.

Significantly, the [1,3]-addition of CO_2 to complex **5b** is fully reversible. This is best demonstrated when a THF-d_8 solution of **5b** is reacted in a J. Young NMR tube with isotopically labeled $^{13}CO_2$ gas to give K[Re(*amidopy*-^{13}*COO*)$(CO)_3$] (**6**-$^{13}CO_2$). The C−C bond is reversibly cleaved and formed: When the NMR tube is purged with nonlabeled CO_2 gas and a

DOI: 10.1021/acs.organomet.6b00897
Organometallics 2017, 36, 839−848

final pressure of two bars is applied, nonlabeled complex **6** is obtained. The slow exchange reaction **6**-$^{13}CO_2$ + CO_2 → **6** + $^{13}CO_2$ can be conveniently monitored via $^{13}C\{^1H\}$ NMR spectroscopy. The relevant section of the $^{13}C\{^1H\}$ NMR spectrum associated with the *exo*-cyclic carbon moiety are shown in Figure 5 (∂ = 75.7 ppm, HC−^{13}COO). The *exo*-cyclic

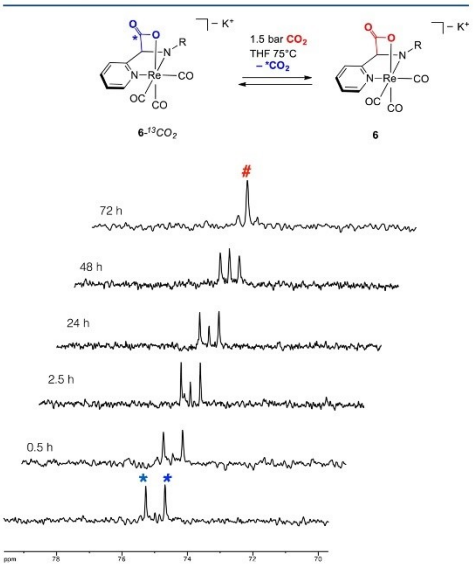

Figure 5. Stacked sections of the $^{13}C\{^1H\}$ NMR spectra (91 MHz, THF-d_8, 298 K) of the *exo*-cyclic HC−COO moiety of complex **6**-$^{13}CO_2$ (associated resonance is marked with *) and complex **6** (associated resonance is marked with #). Initial spectrum of the labeled complex **6**-$^{13}CO_2$ (bottom) and successively recorded spectra after addition of CO_2 and heating at 75 °C after 0.5, 2.5, 24, 48, and 72 h.

carbon resonance of complex **6**-$^{13}CO_2$ shows initially a large C−C coupling constant of $^1J_{CC}$ = 53.1 Hz due to the vicinal ^{13}C-enriched carbon of the carboxylate moiety (Figure 5, bottom spectrum). After pressurizing with nonlabeled CO_2 gas, the mixture was kept at 75 °C and $^{13}C\{^1H\}$ NMR spectra were consecutively recorded. The stacked spectra of the relevant section are shown in Figure 5. The exchange reaction occurs slowly. The singlet resonance associated with the *exo*-cyclic carbon of the nonlabeled complex **6** could be detected after 2.5 h in small amount. The conversion of **6**-$^{13}CO_2$ to complex **6** is completed after 72 h indicated by the absence of the $^1J_{CC}$ coupling and the sole presence of the singlet resonance at 75.7 ppm associated with complex **6** (Figure 5, top spectrum). Additionally, a continuously increasing resonance associated with free (dissolved) $^{13}CO_2$ gas is observed at 126.0 ppm in course of the reaction.

■ SUMMARY AND CONCLUSION

The redox noninnocence of the iminopyridine ligand *impy* present in compound **3** is exploited for the formation of reactive dearomatized compound **5b** upon reduction with potassium metal. Alternatively, dearomatized compound **5a** can be generated by deprotonation of **4** with base. Hence, we could show herein that the dearomatized anionic species **5**(**a**,**b**) are not only accessible via the reaction of **3** with strong reductants but moreover via simple deprotonation of **4** with a moderate base as illustrated in Scheme 2. Amino complex **4** is identified as a convenient precursor for the anionic motif [Re(*amidopy**)-$(CO)_3]^-$ since double deprotonation is facile and can be performed readily *in situ* in solution. This feature gains special importance as dearomatization/rearomatization sequences in pincer-type compounds have been proposed to be crucial for various bond-activation processes.[69] We found that anionic compound **5b** is highly reactive toward the C═O double bond of carbon dioxide giving rise to [1,3]-addition product K[Re(*amidopy-COO*)$(CO)_3$] (**6**). The *exo*-cyclic carbon in **5b** is nucleophilic in character to enable the C−C bond formation with the electrophilic carbon of CO_2. Consequently, the rhenium center with its vacant coordination site allows for the Re−O bond formation with the negatively polarized O of CO_2. Significantly, CO_2 is reversibly bound in complex **6**. This can be best demonstrated via the displacement experiment using isotopically labeled $^{13}CO_2$ gas. Complex **6**-$^{13}CO_2$ reacts under an atmosphere of nonlabeled CO_2 (1.5 bar) slowly to **6** + $^{13}CO_2$ at elevated temperature in THF. Thereby, the effect of the nature of the alkali countercation on the reversible binding of CO_2 is currently studied in our group and the results will be reported promptly. We conclude that complex **5** (**a** and **b**) has the potential of a multifunctional platform. The ion pair M^+/[Re(*amidopy**)$(CO)_3]^-$ combines metal−ligand cooperative reactivity involving a dearomatization/rearomatization scheme (similar to pyridine-based pincer-type complexes; Scheme 1B) and shows concurrently bifunctional reactivity enabled by the nucleophilic nature of the Re complex and the Lewis acidic counter alkali-cation useful in bond activation reactions described by Floriani (Scheme 1E). Under this aspect we are investigating cooperative bond activation processes across the Re−NR_2 (amido) bond and pursue the synergistic combination thereof and MLC, or accordingly bifunctional reactivity, in M^+/[Re(*amidopy**)$(CO)_3]^-$.

■ EXPERIMENTAL SECTION

General. Reagents were obtained commercially (Sigma-Aldrich, Germany) and were used as received. THF-d_8 was purchased from ABCR, degassed, and dried over molecular sieves. Isotopically labeled $^{13}CO_2$ was purchased from Westfalen Gas. Dry solvents were collected from a SPS800 mBraun solvent purification system and additionally dried over 4 Å molecular sieves prior to their use. [$Re(CO)_5Br$] was prepared according to literature procedure.[70] ^1H and $^{13}C\{^1H\}$ NMR spectra were recorded at 298 K on a Bruker Avance-NB360 spectrometer and are referenced to tetramethylsilane (^1H, ^{13}C). Chemical shifts are reported in parts per million (ppm), and coupling constants (*J*) are given in Hertz (Hz). Electron impact mass spectroscopy (EIMS) was carried out using a Finnigan MAT 95. The ESI MS spectra (ion spray ionization) were recorded on a Bruker Esquire-LC MS. Dichloromethane/acetonitrile solutions (or otherwise stated, $c = 1 \times 10^{-6}$ mol L^{-1}) were injected directly into the spectrometer at a flow rate of 3 μL min^{-1}. Nitrogen was used both as a drying gas and for nebulization with flow rates of approximately 5 L min^{-1} and a pressure of 5 psi. Pressure in the mass analyzer region was usually about 1×10^{-5} mbar. Spectra were collected for 1 min and averaged. The nozzle-skimmer voltage was adjusted individually for each measurement. IR spectra were recorded on an THERMONICOLET Avatar 370 FT-IR spectrometer. The samples were prepared as pellets in KBr matrix.

Crystallography. Intensity data were collected on a Bruker Venture D8 diffractometer with graphite-monochromated Mo Kα (0.7107 Å)

DOI: 10.1021/acs.organomet.6b00897
Organometallics 2017, 36, 839−848

radiation. All structures were solved by direct methods and refined based on F^2 by use of the SHELX program package as implemented in OLEX2. All non-hydrogen atoms were refined using anisotropic displacement parameters. Hydrogen atoms attached to carbon atoms were included in geometrically calculated positions using a riding model. Figures were created using DIAMOND2.

Cyclic Voltammetry. Experiments were performed with a Metrohm potentiostat running the NOVA 2.1 software package using a RHD Instruments electrochemical cell TSC 1600 closed, with THF as solvent, $[TBA]PF_6$ electrolyte at 298 K, Pt working electrode, Ag/AgCl pseudo reference electrode, and Pt counter electrode.

Bulk Purity of the Isolated Compounds. The purity of complex **3** and **4** was assessed via elemental analysis (CHN)of the bulk material using a CHN-Rapid of Heraeus. Compound **3** (yield 92%): calculated (found) [%] C = 35.17 (35.15); H = 2.21 (2.09); N: 5.13 (5.18). Complex **4** (yield 64%): calculated (found) [%] C = 35.04 (35.21); H = 2.57 (2.39); N: 5.11 (5.16). The air and moisture sensitivity of **6**/**6**-(*crown*) and the reversible binding of CO_2 to the complex precluded a precise elemental analysis. ^1H and $^{13}C\{^1H\}$ NMR spectra of high quality are provided for all reported compounds in the Supporting Information.

[Re(*impy*)(CO)$_3$Br] (3). *Method A.* Bromopentacarbonylrhenium(I) (500 mg, 1.23 mmol) and *impy* (**3**) (240 mg, 1.23 mmol) were stirred in a closed Schlenk vessel in 10 mL of toluene at 80 °C for 24 h. The reaction mixture was allowed to cool to ambient temperature. The obtained red solid was filtrated off and washed with a small amount of toluene and diethyl ether until the washing solution remains colorless. The red powder was dried *in vacuo* to give complex **3** as air-stable red powder. Yield: 620 mg, 92%.

Method B. Bromopentacarbonylrhenium(I) (256 mg, 0.63 mmol) was added to a stirred solution of *p*-toluidine (74 mg, 0.69 mmol, 1.1 equiv) and 2-pyridinecarboxaldehyde (84 mg, 0.69 mmol, 1.1 equiv) in 20 mL of ethanol. The reaction mixture was heated under reflux for 6 h. Subsequently, the mixture was stirred at ambient temperature overnight. The solvent was removed using a rotary evaporator, and the obtained red residue was recrystallized from dichloromethane and *n*-hexane. The formed red crystals were filtered off, washed with *n*-haxane, and dried under vacuum to give complex **3** (249 mg, 72% yield).

^1H NMR (360 MHz, THF-d_8, 298 K, δ) 9.10 (d, $^3J_{HH}$ = 5.4 Hz, 1H, $CH_{py\text{-}6}$). 9.03 (s, 1H, CH_{imine}), 8.33−8.07 (m, 2H, overlap $CH_{py3,4}$), 7.73−7.66 (m, 1H, $CH_{py\text{-}5}$), 7.50 (d, $^3J_{HH}$ = 8.2 Hz, 2H, CH_{Ar}), 7.32 (d, $^3J_{HH}$ = 8.2 Hz, 2H, CH_{Ar}), 2.41 (s, 3H, CH_3). $^{13}C\{^1H\}$ NMR (91 MHz, THF-d_8, 298 K, δ) 198.7 (s, 1C, Re−CO).), 197.4 (s, 1C, Re−CO), 187.7 (s, 1C, Re−CO), 168.5 (s, 1C, CH_{imine}), 156.9 (s, 1C, C_{quart}), 154.4 (s, 1C, CH_{py}), 150.3 (s, 1C, C_{quart}), 140.4 (s, 1C, CH_{py}), 140.3 (s, 1C_{quart}), 130.8 (s, 1C, CH_{Ar}), 130.4 (s, 1C, CH_{py}), 129.8 (1C, CH_{py}), 123.4 (s, 2C, CH_{Ar}), 21.3 (1C, CH_3). IR (KBR, pellet) ν/cm^{-1}: ν_{CO} = 2027 (s), 1911 (s), 1881 (s). EI MS m/z = 546.0 (Re(*impy*)$(CO)_3$Br); 518.1 (Re(*impy*)$(CO)_2$Br); 490.1 (Re(*impy*)-(CO)Br); 462.1 (Re(*impy*)Br).

[Re(*ampy*)(CO)$_3$Br] (4). A 25 mL Schlenk tube was charged with bromopentacarbonylrhenium(I) (300 mg, 0.74 mmol) and *ampy* (**2**, 145 mg, 0.73 mmol). Subsequently, 10 mL of THF was added. The mixture in the closed vessel was heated at 50 °C for 24 h. Subsequently, the solvent was removed *in vacuo*. The obtained residue was dissolved in dichloromethane and subsequently passed through a syringe filter (0.45 μm porosity, PTFE). The clear filtrate was transferred to a 25 mL vial and layered with *n*-hexane (no protective atmosphere necessary). The mixture was allowed to crystallize at 4 °C in a refrigerator. The formed voluminous crystals were decanted from the mother liquor, washed with *n*-hexane, and dried under reduced pressure. Yield: 256 mg, 64%. ^1H NMR (360 MHz, THF-d_8, 298 K, δ) 8.84 (d, $^3J_{HH}$ = 7.2 Hz, 1H, $CH_{py\text{-}6}$), 8.00 (td, J = 7.7, 1.5 Hz, 1H, $CH_{py\text{-}4}$), 7.68 (d, $^3J_{HH}$ = 7.9 Hz, 1H, $CH_{py\text{-}3}$), 7.46 (t, $^3J_{HH}$ = 7.9 Hz, 1H, $CH_{py\text{-}5}$), 7.25−7.14 (m, 4H, CH_{Ar}), 6.70 (dd, J = 8.1, 4.8 Hz, 1H, N*H*), 4.99 (dd, J = 15.3, 4.9 Hz, 1H, CH_2), 4.89 (dd, J = 15.3, 8.7 Hz, 1H, CH_2), 2.32 (s, 3H, CH_3). $^{13}C\{^1H\}$ NMR (91 MHz, THF-d_8, 298 K, δ) 197.7 (s, 1C, Re−CO), 197.5 (s, 1C, Re−CO), 192.9 (s, 1C, Re−CO), 161.5 (s, 1C, C_{quart}), 154.3 (s, 1C, $CH_{py\text{-}6}$), 147.9 (s, 1C, C_{quart}), 140.2 (s, 1C, $CH_{py\text{-}4}$), 136.0 (s, 1C, C_{quart}), 130.8 (s, 1C, CH_{Ar}), 126.1 (s, 1C, $CH_{py\text{-}5}$), 123.2 (s, 1C, $CH_{py\text{-}3}$), 119.8 (s, 1C, CH_{Ar}), 60.6 (s, 1C, CH_2), 17.7 (s, 1C, CH_3). IR (KBR, pellet) ν/cm^{-1}: ν_{CO} = 2026 (s), 1933 (s), 1846 (s). ESI MS (MeOH, positive mode) m/z = 469.2 (Re(*ampy*)$CO)_3$); (MeOH, negative mode) 546.9 (Re(*ampy*)-$CO)_3$)+Na$^+$.

K[Re(*amidopy)(CO)$_3$] (5b).** *Method A.* Complex **3** (52 mg, 0.10 mmol) was dissolved in 5 mL of dry THF. Potassium (16 mg, 0.40 mmol, 4 equiv) was added, and the suspension was mixed in an ultrasonic bath resulting in a color change to deep red. The reaction mixture was filtered through a PTFE syringe filter (0.45 μm porosity), and we attempted to crystallize product from the obtained solution in multiple experiments, varying concentrations (mixtures with *n*-hexanes) and crystallization temperatures. No crystalline material could be obtained.

Method B. Complex **3** (10 mg, 0.02 mmol) was dissolved in 0.5 mL of THF-d_8 in an J. Young NMR tube with Teflon valve. Potassium metal (3 mg, 0.08 mmol, 4 equiv) was added to the solution. After sonication for 2.5 h, a deep red solution of pure complex **5b** was obtained. The *in situ* recorded ^1H and $^{13}C\{^1H\}$ NMR spectra of the reaction mixture indicated the quantitative formation of complex **5b**. ^1H NMR (360 MHz, THF-d_8, 298 K, δ) 8.51 (d, $^3J_{HH}$ = 6.4 Hz, 1H, $CH_{py\text{-}6}$), 7.18 (d, $^3J_{HH}$ = 8.0 Hz, 2H, CH_{Ar}), 6.98 (s, 1H, CH_{HCN}), 6.95 (d, $^3J_{HH}$ = 8.0 Hz, 2H, CH_{Ar}), 6.70 (d, $^3J_{HH}$ = 7.2 Hz, 1H, $CH_{py\text{-}3}$), 5.86 (t, 1H, $^3J_{HH}$ = 7.2 Hz, $CH_{py\text{-}4}$), 4.94 (t, $^3J_{HH}$ = 6.0 Hz, 1H, $CH_{py\text{-}5}$), 2.29 (s, 3H, CH_3). $^{13}C\{^1H\}$ NMR (91 MHz, THF-d_8, 298 K, δ) 210.6 (s, 3C, Re−CO), 158.6 (s, 1C, C_{quart}), 152.9 (s, 1C, $CH_{py\text{-}6}$), 141.8 (s, 1C, C_{quart}), 131.3 (s, 1C, C_{quart}), 128.9 (s, 1C, CH_{Ar}), 126.4 (s, 1C, CH_{Ar}), 122.6 (s, 1C, $CH_{py\text{-}3}$), 121.5 (s, 1C, CH_{CHN}), 119.1 (s, 1C, $CH_{py\text{-}4}$), 102.8 (s, 1C, $CH_{py\text{-}5}$), 21.0 (s, 1C, CH_3).

Li[Re(*amidopy)(CO)$_3$] (5a).** Complex **4** (20 mg, 0.04 mmol) was dissolved in 1.5 mL of THF-d_8 in a J. Young NMR tube with Teflon valve. Lithium hexamethyldisilazane (LiHMDS) (33 mg, 0.2 mmol, 5 equiv) was added to the solution. A deep red solution was formed instantaneously. The *in situ* recorded ^1H and $^{13}C\{^1H\}$ NMR spectra of the reaction mixture indicated the quantitative formation of complex **5a**. Stoichiometric addition of one or two equivalents of LiHMDS gave complex reaction mixtures. Only the addition of excess LiHMDS gave rise to the clean formation of **5a**. ^1H NMR (200 MHz, THF-d_8, 298 K, δ) 8.49 (d, $^3J_{HH}$ = 6.7 Hz, 1H, $CH_{py\text{-}6}$), 7.19 (br d, $^3J_{HH}$ = 8.3 Hz, 2H, CH_{Ar}), 6.96 (s, 1H, CH_{HCN}, overlap CH_{Ar}), 6.94 (d, $^3J_{HH}$ = 8.2 Hz, 2H, CH_{Ar}), 6.67 (td, $^3J_{HH}$ = 8.9. Hz, J_{HH} = 1.3 Hz, 1H, $CH_{py\text{-}3}$), 5.82 (ddd, 1H, J_{HH} = 8.9, 5.9, 1.3 Hz, $CH_{py\text{-}4}$), 4.91 (ddd, J = 7.0, 5.9, 1.3 Hz, 1H, $CH_{py\text{-}5}$), 2.29 (s, 3H, CH_3). $^{13}C\{^1H\}$ NMR (91 MHz, THF-d_8, 298 K, δ) 210.0 (s, 1C, Re−CO), 158.6 (s, 1C, C_{quart}), 153.0 (s, 1C, $CH_{py\text{-}6}$), 141.8 (s, 1C, C_{quart}), 131.0 (s, 1C, C_{quart}), 128.9 (s, 1C, CH_{Ar}), 126.3 (s, 1C, CH_{Ar}), 122.5 (s, 1C, $CH_{py\text{-}3}$), 121.0 (s, 1C, CH_{CHN}), 118.9 (s, 1C, $CH_{py\text{-}4}$), 102.5 (s, 1C, $CH_{py\text{-}5}$), 21.02 (s, 1C, CH_3).

K[Re(amidopy-COO)(CO)$_3$] (6). *Method A.* A 25 mL Schlenk tube fitted with a Teflon valve was charged with complex **3** (56 mg, 0.10 mmol) and dissolved in a minimum of THF. Potassium metal (16 mg, 0.40 mmol, 4 equiv) was added to the red solution. The reaction mixture was sonicated until a deep red solution was obtained. Subsequently, an overpressure of CO_2. gas (1.5 bar) was applied to the reaction vessel. The color of the suspension turns instantaneously from deep red to brownish yellow. The suspension was subsequently filtered via a syringe filter (PTFE, 0.45 μm porosity), and all volatiles were removed *in vacuo*. The obtained brownish solid was spectroscopically analyzed. Multiple attempts of recrystallization did not give single crystals suitable for X-ray diffraction analysis.

Method B. A J. Young NMR tube fitted with Kontes Teflon valve was charged with complex **3** (15 mg, 0.03 mmol) dissolved in 0.5 mL of THF-d_8. Potassium metal (5 mg, 0.15 mmol, 4 equiv) was added to the solution, and the mixture was sonicated in an ultrasonic bath. The obtained deep red solution was analyzed by ^1H NMR spectroscopy to verify the quantitative formation of **5b**. The solution of **5b** was subsequently subjected to CO_2 gas (1.5 bar), and the resulting brown solution was analyzed by means of ^1H and $^{13}C\{^1H\}$ NMR spectroscopy indicating the quantitative formation of K[Re(*amidopy*-COO)$(CO)_3$] (**6**). ^1H NMR (360 MHz, THF-d_8, 298 K, δ) 8.77 (d,

DOI: 10.1021/acs.organomet.6b00897
Organometallics 2017, 36, 839−848

$^3J_{HH}$ = 5.3 Hz, 1H, $CH_{py\text{-}6}$), 7.80 (m, 2H, overlap $CH_{py\text{-}4}$ and $CH_{py\text{-}3}$), 7.19 (ddd, J_{HH} = 7.2, 5.6, 1.5 Hz, $CH_{py\text{-}5}$), 6.62 (d, $^3J_{HH}$ = 8.4 Hz, 2H, CH_{Ar}), 6.51 (d, $^3J_{HH}$ = 8.4. Hz, 2H, CH_{Ar}), 5.43 (s, 1H, HC(COO)N), 2.06 (s, 3H, CH_3). $^{13}C\{^1H\}$ NMR (91 MHz, THF-d_8, 298 K, δ) 203.2 (s, 1C, Re−CO), 202.3 (s, 1C, Re−CO), 202.1 (s, 1C, Re−CO), 181.3 (s, 1C, COO), 166.1 (s, 1C, $C_{py\text{-}quart}$), 157.4 (s, 1C, $C_{Ar\text{-}quart}$), 154.0 (s, 1C, $CH_{py\text{-}6}$), 139.7 (s, 1C, $CH_{py\text{-}4}$), 129.6 (s, 1C, CH_{Ar}), 123.6 (s, 1C, $CH_{py\text{-}5}$), 122.5 (s, 1C, $CH_{py\text{-}3}$), 120.6 (s, 1C, $C_{Ar\text{-}quart}$), 115.7 (s, 1C, CH_{Ar}), 75.8 (s, 1C, $CH_{HC(COO)N}$), 20.7 (s, 1C, CH_3). IR (KBR, pellet) ν/cm^{-1}: ν_{CO} = 2027(s), 1902 (br, vs), ν_{COO} 1653 (s).

K[Re(amidopy-^{13}COO)(CO)$_3$]. (6-$^{13}CO_2$) was prepared similarly: A J. Young NMR tube was charged with complex **3** (17 mg, 0.03 mmol) and 0.7 mL of THF-d_8. Potassium metal (5 mg, 0.12 mmol, 4 equiv) was added, and the solution was sonicated until the solution turned deep red. The solution was degassed (freeze−pump−thaw method), and the tube was pressurized with isotopically labeled $^{13}CO_2$ (1.2 bar). An immediate color change to brown was observed. ^1H NMR (360 MHz, THF-d_8, 298 K, δ) 8.78 (d, $^3J_{HH}$ = 5.2 Hz, 1H, $CH_{py\text{-}6}$), 7.78 (m, 2H, overlap $CH_{py\text{-}4}$ and $CH_{py\text{-}3}$), 7.19 (t, J_{HH} = 7.0 Hz, $CH_{py\text{-}5}$), 6.62 (d, $^3J_{HH}$ = 8.4 Hz, 2H, CH_{Ar}), 6.51 (d, $^3J_{HH}$ = 8.4. Hz, 2H, CH_{Ar}), 5.43 (d, $^2J_{HC}$ = 3.8 Hz 1H, $HC(^{13}COO)N$), 2.06 (s, 3H, CH_3). $^{13}C\{^1H\}$ NMR (91 MHz, THF-d_8, 298 K, δ) 203.1 (s, 1C, Re−CO), 202.2 (s, 1C, Re−CO), 202.1 (s, 1C, Re−CO), 181.1 (s, 1C, COO), 165.7 (s, 1C, $C_{py\text{-}quart}$), 157.2 (s, 1C, $C_{Ar\text{-}quart}$), 154.0 (s, 1C, $CH_{py\text{-}6}$), 139.7 (s, 1C, $CH_{py\text{-}4}$), 129.6 (s, 1C, CH_{Ar}), 123.6 (s, 1C, $CH_{py\text{-}5}$), 122.5 (s, 1C, $CH_{py\text{-}3}$), 120.7 (s, 1C, $C_{Ar\text{-}quart}$), 115.7 (s, 1C, CH_{Ar}), 75.7 (d, $^1J_{CC}$ = 53.1 Hz, 1C, $CH_{HC(COO)N}$), 20.7 (s, 1C, CH_3).

[K(18-*crown*-6][Re(*amidopy-COO*)(CO)$_3$] (6-(*crown*)). A 10 mL Schlenk tube fitted with a Teflon valve was charged with complex **3** (20 mg, 0.04 mmol) and dissolved in a minimum of THF (1.5 mL). Potassium metal (6 mg, 0.16 mmol, 4 equiv) was added to the red solution. The reaction mixture was sonicated until a deep red solution was obtained (2.5 h). The reaction mixture was filtered via a syringe filter (PTFE, 0.45 μm porosity). To the clear deep red filtrate, 18-*crown*-6-ether (11 mg, 0.04 mmol, 1 equiv) was added, and the reaction mixture was sonicated for additional 10 min. Subsequently, an overpressure of CO_2 gas (1.5 bar) was applied to the reaction vessel. The color of the solution turned instantaneously from deep red to brown. The clear solution was layered with *n*-hexane. The formed brownish orange crystals were suitable for X-ray diffraction analysis. The crystalline solid was collected, washed with *n*-hexanes, and dried under reduced pressure. Yield: 11 mg, 34%. ^1H NMR (360 MHz, THF-d_8, 298 K, δ) 8.76 (d, $^3J_{HH}$ = 5.3 Hz, 1H, $CH_{py\text{-}6}$), 7.80 (m, 2H, overlap $CH_{py\text{-}4}$ and $CH_{py\text{-}3}$), 7.18 (ddd, J_{HH} = 7.0, 5.4, 1.4 Hz, $CH_{py\text{-}5}$), 6.61 (d, $^3J_{HH}$ = 8.5 Hz, 2H, CH_{Ar}), 6.52 (d, $^3J_{HH}$ = 8.5 Hz, 2H, CH_{Ar}), 5.41 (s, 1H, HC(COO)N), 3.54 (br s, 24H, overlap THF-d_8, $CH_{2\text{-}crown}$), 2.06 (s, 3H, CH_3). $^{13}C\{^1H\}$ NMR (91 MHz, THF-d_8, 298 K, δ) 203.6 (s, 1C, Re−CO), 202.6 (s, 1C, Re−CO), 202.4 (s, 1C, Re−CO), 179.7 (s, 1C, COO), 166.7 (s, 1C, $C_{py\text{-}quart}$), 157.6 (s, 1C, $C_{Ar\text{-}quart}$), 153.8 (s, 1C, $CH_{py\text{-}6}$), 139.5 (s, 1C, $CH_{py\text{-}4}$), 126.1 (s, 1C, CH_{Ar}), 123.4 (s, 1C, $CH_{py\text{-}5}$), 122.4 (s, 1C, $CH_{py\text{-}3}$), 120.1 (s, 1C, $C_{Ar\text{-}quart}$), 115.7 (s, 1C, CH_{Ar}), 76.2 (s, 1C, $CH_{HC(COO)N}$), 71.3 (s, 12C, $CH_{2\text{-}crown}$), 20.7 (s, 1C, CH_3).

■ ASSOCIATED CONTENT

Supporting Information

The Supporting Information is available free of charge on the ACS Publications website at DOI: 10.1021/acs.organomet.6b00897.

NMR spectra (PDF)

X-ray crystallographic data for **3**, **4**, and **6**-*crown* (CIF)

■ AUTHOR INFORMATION

Corresponding Author

*E-mail: mavogt@uni-bremen.de.

ORCID

Matthias Vogt: 0000-0002-2636-2531

Author Contributions

#R.S., A.H., and J.B. contributed equally to this work.

Notes

The authors declare no competing financial interest.

■ ACKNOWLEDGMENTS

This research was funded by the Central Research Development Fund of the Universität Bremen. M.V. thanks the Fonds der Chemischen Industrie (FCI) for the generous support.

■ REFERENCES

(1) Chirik, P. J.; Wieghardt, K. *Science* **2010**, *327*, 794−795.

(2) Praneeth, V. K. K.; Ringenberg, M. R.; Ward, T. R. *Angew. Chem., Int. Ed.* **2012**, *51*, 10228−10234.

(3) Kaim, W. *Eur. J. Inorg. Chem.* **2012**, *2012*, 343−348.

(4) Kaim, W.; Schwederski, B. *Coord. Chem. Rev.* **2010**, *254*, 1580−1588.

(5) Kaim, W. *Inorg. Chem.* **2011**, *50*, 9752−9765.

(6) Lu, C. C.; DeBeer George, S.; Weyhermüller, T.; Bill, E.; Bothe, E.; Wieghardt, K. *Angew. Chem., Int. Ed.* **2008**, *47*, 6384−6387.

(7) van Gastel, M.; Lu, C. C.; Wieghardt, K.; Lubitz, W. *Inorg. Chem.* **2009**, *48*, 2626−2632.

(8) Lu, C. C.; Weyhermüller, T.; Bill, E.; Wieghardt, K. *Inorg. Chem.* **2009**, *48*, 6055−6064.

(9) Lu, C. C.; Bill, E.; Weyhermüller, T.; Bothe, E.; Wieghardt, K. *J. Am. Chem. Soc.* **2008**, *130*, 3181−3197.

(10) Russell, S. K.; Bowman, A. C.; Lobkovsky, E.; Wieghardt, K.; Chirik, P. J. *Eur. J. Inorg. Chem.* **2012**, *2012*, 535−545.

(11) Russell, S. K.; Hoyt, J. M.; Bart, S. C.; Milsmann, C.; Stieber, S. C. E.; Semproni, S. P.; DeBeer, S.; Chirik, P. J. *Chem. Sci.* **2014**, *5*, 1168−1174.

(12) Bart, S. C.; Chlopek, K.; Bill, E.; Bouwkamp, M. W.; Lobkovsky, E.; Neese, F.; Wieghardt, K.; Chirik, P. J. *J. Am. Chem. Soc.* **2006**, *128*, 13901−13912.

(13) Tondreau, A. M.; Milsmann, C.; Patrick, A. D.; Hoyt, H. M.; Lobkovsky, E.; Wieghardt, K.; Chirik, P. J. *J. Am. Chem. Soc.* **2010**, *132*, 15046−15059.

(14) Knijnenburg, Q. Q.; Gambarotta, S. S.; Budzelaar, P. H. M. P. *Dalton Trans.* **2006**, 5442−5448.

(15) Ma, J.; Feng, C.; Wang, S.; Zhao, K.-Q.; Sun, W.-H.; Redshaw, C.; Solan, G. A. *Inorg. Chem. Front.* **2014**, *1*, 14−34.

(16) Small, B. L.; Brookhart, M.; Bennett, A. M. A. *J. Am. Chem. Soc.* **1998**, *120*, 4049−4050.

(17) Britovsek, G. J. P.; Gibson, V. C.; McTavish, S. J.; Solan, G. A.; White, A. J. P.; Williams, D. J.; Britovsek, G. J. P.; Kimberley, B. S.; Maddox, P. J. *Chem. Commun.* **1998**, 849−850.

(18) Britovsek, G. J. P.; Bruce, M.; Gibson, V. C.; Kimberley, B. S.; Maddox, P. J.; Mastroianni, S.; McTavish, S. J.; Redshaw, C.; Solan, G. A.; Strömberg, S.; White, A. J. P.; Williams, D. J. *J. Am. Chem. Soc.* **1999**, *121*, 8728−8740.

(19) Gibson, V. C.; Spitzmesser, S. K. *Chem. Rev.* **2003**, *103*, 283−316.

(20) Gibson, V. C.; Redshaw, C.; Solan, G. A. *Chem. Rev.* **2007**, *107*, 1745−1776.

(21) Mukhopadhyay, T. K.; Flores, M.; Groy, T. L.; Trovitch, R. J. *J. Am. Chem. Soc.* **2014**, *136*, 882−885.

(22) Bouwkamp, M. W.; Bowman, A. C.; Lobkovsky, E.; Chirik, P. J. *J. Am. Chem. Soc.* **2006**, *128*, 13340−13341.

(23) Sieh, D.; Lacy, D. C.; Peters, J. C.; Kubiak, C. P. *Chem. - Eur. J.* **2015**, *21*, 8497−8503.

(24) Behr, A. *Angew. Chem., Int. Ed. Engl.* **1988**, *27*, 661−678.

(25) Schaub, T.; Paciello, R. A. *Angew. Chem., Int. Ed.* **2011**, *50*, 7278−7282.

(26) Quadrelli, E. A.; Centi, G.; Duplan, J.-L.; Perathoner, S. *ChemSusChem* **2011**, *4*, 1194−1215.

(27) He, M.; Sun, Y.; Han, B. *Angew. Chem., Int. Ed.* **2013**, *52*, 9620−9633.

(28) Paparo, A.; Okuda, J. *Coord. Chem. Rev.* **2016**, DOI: 10.1016/j.ccr.2016.06.005.
(29) Castro-Rodriguez, I.; Nakai, H.; Zakharov, L. N.; Rheingold, A. L.; Meyer, K. *Science* **2004**, *305*, 1757−1759.
(30) Vogt, M.; Nerush, A.; Diskin-Posner, Y.; Ben-David, Y.; Milstein, D. *Chem. Sci.* **2014**, *5*, 2043−2051.
(31) Vogt, M.; Gargir, M.; Iron, M. A.; Diskin-Posner, Y.; Ben-David, Y.; Milstein, D. *Chem. - Eur. J.* **2012**, *18*, 9194−9197.
(32) Huff, C. A.; Kampf, J. W.; Sanford, M. S. *Organometallics* **2012**, *31*, 4643−4645.
(33) Filonenko, G. A.; Conley, M. P.; Copéret, C.; Lutz, M.; Hensen, E. J. M.; Pidko, E. A. *ACS Catal.* **2013**, *3*, 2522−2526.
(34) Perdriau, S.; Zijlstra, D. S.; Heeres, H. J.; de Vries, J. G.; Otten, E. *Angew. Chem.* **2015**, *127*, 4310−4314.
(35) Montag, M.; Zhang, J.; Milstein, D. *J. Am. Chem. Soc.* **2012**, *134*, 10325−10328.
(36) Huff, C. A.; Kampf, J. W.; Sanford, M. S. *Chem. Commun.* **2013**, *49*, 7147−7149.
(37) Vogt, M.; Nerush, A.; Iron, M. A.; Leitus, G.; Diskin-Posner, Y.; Shimon, L. J. W.; Ben-David, Y.; Milstein, D. *J. Am. Chem. Soc.* **2013**, *135*, 17004−17018.
(38) Nerush, A.; Vogt, M.; Gellrich, U.; Leitus, G.; Ben-David, Y.; Milstein, D. *J. Am. Chem. Soc.* **2016**, *138*, 6985−6997.
(39) Filonenko, G. A.; Cosimi, E.; Lefort, L.; Conley, M. P.; Copéret, C.; Lutz, M.; Hensen, E. J. M.; Pidko, E. A. *ACS Catal.* **2014**, *4*, 2667−2671.
(40) Eijsink, L. E.; Perdriau, S. C. P.; de Vries, J. G.; Otten, E. *Dalton Trans.* **2016**, *45*, 16033−16039.
(41) Annibale, V. T.; Song, D. *Organometallics* **2014**, *33*, 2776−2783.
(42) Annibale, V. T.; Song, D. *Chem. Commun.* **2012**, *48*, 5416−5418.
(43) Annibale, V. T.; Dalessandro, D. A.; Song, D. *J. Am. Chem. Soc.* **2013**, *135*, 16175−16183.
(44) Floriani, C.; Fachinetti, G. *J. Chem. Soc., Chem. Commun.* **1974**, 615−616.
(45) Fachinetti, G.; Floriani, C.; Zanazzi, P. F. *J. Am. Chem. Soc.* **1978**, *100*, 7405−7407.
(46) Fachinetti, G.; Floriani, C.; Zanazzi, P. F.; Zanzari, A. R. *Inorg. Chem.* **1979**, *18*, 3469−3475.
(47) Gambarotta, S.; Arena, F.; Floriani, C.; Zanazzi, P. F. *J. Am. Chem. Soc.* **1982**, *104*, 5082−5092.
(48) Braunstein, P.; Matt, D.; Dusausoy, Y.; Fischer, J.; Mitschler, A.; Ricard, L. *J. Am. Chem. Soc.* **1981**, *103*, 5115−5125.
(49) Gunanathan, C.; Milstein, D. *Top. Organomet. Chem.* **2011**, *37*, 55−84.
(50) Khusnutdinova, J. R.; Milstein, D. *Angew. Chem., Int. Ed.* **2015**, *54*, 12236−12273.
(51) Annibale, V. T.; Song, D. *RSC Adv.* **2013**, *3*, 11432.
(52) Grützmacher, H. *Angew. Chem., Int. Ed.* **2008**, *47*, 1814−1818.
(53) Ikariya, T., Shibasaki, M., Vol. Eds.; *Bifunctional Molecular Catalysis*; Springer: Berlin, 2011; Vol. 37.
(54) van der Vlugt, J. I. *Eur. J. Inorg. Chem.* **2012**, *2012*, 363−375.
(55) Gunanathan, C.; Milstein, D. *Science* **2013**, *341*, 1229712.
(56) Albrecht, M.; Lindner, M. M. *Dalton Trans.* **2011**, *40*, 8733.
(57) Ikariya, T.; Blacker, A. J. *Acc. Chem. Res.* **2007**, *40*, 1300−1308.
(58) Diez, V.; Cuevas, J. V.; García-Herbosa, G.; Aullón, G.; Charmant, J. P. H.; Carbayo, A.; Muñoz, A. *Inorg. Chem.* **2007**, *46*, 568−577.
(59) Dominey, R. N.; Hauser, B.; Hubbard, J.; Dunham, J. *Inorg. Chem.* **1991**, *30*, 4754−4758.
(60) Sieh, D.; Kubiak, C. P. *Chem. - Eur. J.* **2016**, *22*, 10638−10650.
(61) Wiebcke, M.; Mootz, D. IUCr. *Acta Crystallogr., Sect. B: Struct. Crystallogr. Cryst. Chem.* **1982**, *38*, 2008−2013.
(62) Song, X.; Lim, M. H.; Mohamed, D. K. B.; Wong, S. M.; Zhao, J.; Hor, T. S. A. *J. Organomet. Chem.* **2016**, *814*, 1−7.
(63) Braymer, J. J.; Merrill, N. M.; Lim, M. H. *Inorg. Chim. Acta* **2012**, *380*, 261−268.
(64) Lin, Y.-C.; Yu, K.-H.; Huang, S.-L.; Liu, Y.-H.; Wang, Y.; Liu, S.-T.; Chen, J.-T. *Dalton Trans.* **2009**, 9058−9067.
(65) Sieh, D.; Kubiak, C. P. *Chem. - Eur. J.* **2016**, *22*, 10638−10650.
(66) Pichaandi, K. R.; Mazzotta, M. G.; Harwood, J. S.; Fanwick, P. E.; Abu-Omar, M. M. *Organometallics* **2014**, *33*, 1672−1677.
(67) Vogt, M.; Nerush, A.; Diskin-Posner, Y.; Ben-David, Y.; Milstein, D. *Chem.l Sci.* **2014**, *5*, 2043−2051.
(68) Milstein, D. *Philos. Trans. R. Soc., A* **2015**, *373*, 20140189−20140189.
(69) Note that dearomatization/rearomatization reaction sequences were proposed to play significant roles for bond activation processes in dehydrogenative coupling and hydrogenation reactions catalyzed by transition metal compounds with PNN or PNP pincer ligands. However, computational studies have also proposed alternative reaction steps in which dearomatization/re-armomatization sequences are not necessarily involved in the lowest energy pathways. For a computational review concerning this matter see Li, H.; Hall, M. B. *ACS Catal.* **2015**, *5*, 1895−1913.
(70) Schmidt, S. P.; Trogler, W. C.; Basolo, F.; Urbancic, M. A.; Shapley, J. R. *Inorg. Synth.* **1990**, *28*, 160−165.

DOI: 10.1021/acs.organomet.6b00897
Organometallics 2017, 36, 839−848

3.1.4 Cooperative Binding of SO_2 under M-O and C-S Bond Formation in a Rhenium(I) Complex with Activated Amino- or Iminopyridine Ligand[160]

This work shows the activation of SO_2 *via* MLC using the dearomatized Re(I)-complex **75*-Re**. The expansion of MLC activations *via* a dearomatization/rearomatization sequence to the unprecedented substrate SO_2 was the motivation of this research. The activation of S=O bonds *via* MLC had not been reported in the literature at the time of publication. The reaction of **75*-Re** with DABSO (1,4-diazabicyclo[2.2.2]octane-bis(sulfur dioxide) adduct) as a convenient SO_2 source, leads to the 1,3-addition product *fac*-[K(18-*crown*-6][Re(*amidopy*-OSO)$(CO)_3$] (**77-crown**) under [2+2]-cycloaddition.

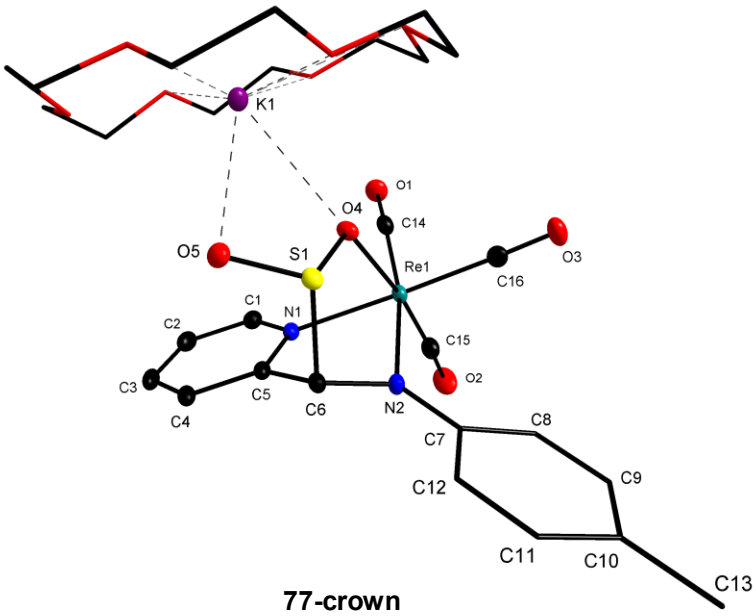

77-crown

C5-C6	1.484(2)
C6-S1	1.907(2)
S1-O4	1.560(1)
S1-O5	1.490(1)
C6-N2	1.431(2)
Re1-N2	2.131(2)
Re1-N1	2.162(2)
Re1-O4	2.222(1)
K1-O4	2.852(1)
K1-O5	2.774(1)
K1-S1	3.304(1)

Figure 2: Diamond plot of the 1,3-addition product *fac*-[K(18-*crown*-6)][Re(*amidopy*-OSO)$(CO)_3$] (**77-crown**) from reaction of K[Re(*amidopy**)$(CO)_3$] (**75*-Re**) with DABSO and crown ether (18-*crown*-6). Selected bond lengths in [Å]. (Thermal ellipsoids at 50% probability, H atoms omitted for clarity)

I was responsible for all experimental work, all analytical characterizations and the evaluation of the ^{1}H NMR spectral line shape analysis. scXRD analyses were measured and evaluated by Dr. Enno Lork.

The obtained results were published in the following journal:

R. Stichauer, M. Vogt, *Organometallics* **2018,** *37*, 3639-3643.
DOI: 10.1021/acs.organomet.8b00485

My percentage contribution of this publication in categories: experimental concept and design: ca. 60%, experimental work and acquisition of experimental data: 99%, data analysis and interpretation: 100%, preparation of Figures and Tables: ca. 100%, drafting of the manuscript: ca. 55%.

ORGANOMETALLICS
Cite This: Organometallics 2018, 37, 3639−3643
Communication
pubs.acs.org/Organometallics

Cooperative Binding of SO_2 under M−O and C−S Bond Formation in a Rhenium(I) Complex with Activated Amino- or Iminopyridine Ligand

Rasmus Stichauer and Matthias Vogt*

Universität Bremen, Institut für Anorganische Chemie und Kristallographie, Leobener Straße 7, NW2 C2060, 28359 Bremen, Germany

Supporting Information

ABSTRACT: Metal−ligand cooperative activation of C=O and CN multiple bonds in transition metal complexes with pyridine-based ligands is a currently active field of research. We herein expand the substrate scope to S=O bonds. The anionic complex K [Re(*amidopy*)$(CO)_3$] readily reacts with a SO_2 source to give the sulfinate *fac*-K[Re(*amidopy-OSO*)-$(CO)_3$] under Re−O and C−S bond formation as a diastereomeric mixture, which shows mutual dynamic interconversion even at ambient temperature. The chemical exchange was studied by 2D ^{1}H ^{1}H EXSY NMR spectroscopy. Activation parameters are obtained via VT ^{1}H NMR and spectral line shape analysis.

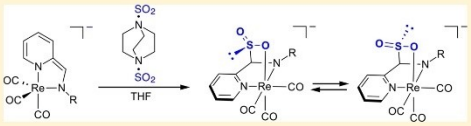

Sulfur dioxide takes a pivotal role as a commodity[1] with versatile applications.[2] Beyond its industrial relevance, SO_2 is recognized as an intriguing ligand in the field of coordination chemistry, showing a great variety of bonding motifs[3−8] with reports dating back to the late 1930s.[9] Specifically, SO_2 can act as an ambiphilic ligand: The η^1-*S* coordination mode to a metal center can be governed by electron donor (L-type) or electron acceptor (Z-type ligand) properties through the same sulfur atom. Each scenario is characterized by a distinct geometry, that is, a coplanar or pyramidal arrangement, respectively (Scheme 1, (I) A,B).[10,11] In addition, the η^1-*O* (C)[12,13] and η^2-*S,O* coordination modes are observed (D).[14−16] Stephan, Erker, Grimm, and co-workers reported the activation of SO_2 by frustrated Lewis acid/base pairs (FLPs) under concomitant P−S and B−O bond formation (Scheme 1, (II)).[17,18] Recent reports concerning the activation of SO_2 include uranium(III) compounds, which allow for the formation of sulfite and dithionite complexes[19] as well as the reaction of SO_2 and decamethylmetallocenes.[20,21] Herein, we report on an unusual binding mode of SO_2 triggered by metal−ligand cooperation (MLC), where both the transition metal center and a iminopyridine-based C-nucleophilic actor ligand participate in the activation of SO_2 via M−O and C−S bond formation (Scheme 1, (III)). MLC in transition metal complexes involving pyridine-based ligands was developed into an important tool in bond-activation chemistry.[22−26] Along these lines, we recently described an anionic Re(I) triscarbonyl complex, which includes a redox active bidentate amidopyridine ligand (K[Re(*amidopy*)$(CO)_3$] (Scheme 2, **1**). Complex **1** is prepared by two-electron reduction of the iminopyridine ligand in *fac*-[Re(*impy*)$(CO)_3$Br] (i) using potassium metal or, alternatively, via a milder route, by double deprotonation of the related aminopyridine complex *fac*-[Re(*ampy*)$(CO)_3$Br] (ii).[27] Both strategies give rise to the activated complex **1**, which is characterized by an increased nucleophilicity of the benzylic carbon atom (dearomatization of the pyridine unit). As a result, **1** reacts reversibly with CO_2 via a MLC pathway

Scheme 1. Binding Motifs of SO_2: (I) to a Single Metal Center, (II) in FLPs, and (III) via MLC

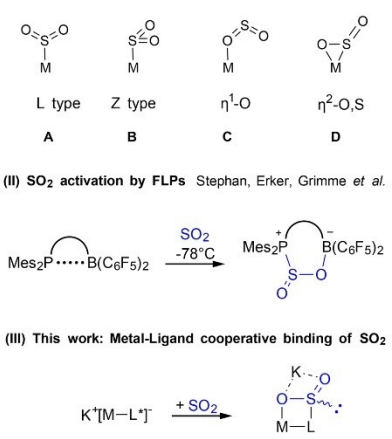

Received: July 17, 2018
Published: October 1, 2018

DOI: 10.1021/acs.organomet.8b00485
Organometallics 2018, 37, 3639−3643

Scheme 2. Synthesis of Complexes 1 and 2ab

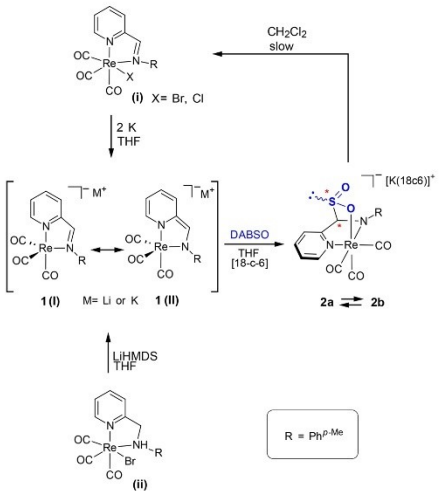

under Re−O and C−C bond formation and concomitant rearrangement of the ligand π-system (rearomatization).[27] Kubiak and co-workers observed a similar reaction scheme in a molybdenum compound.[28] The activation of CO_2 involving C-nucleophilic actor ligands has attracted increased attention and was recently reviewed by Song and co-workers.[29] In this regard, the role of MLC-triggered activation/binding of CO_2 was discussed for various complexes.[30−39] Recent studies also concern the MLC-triggered activation of multiple bonds such as carbonyls[40] and CN-multiple bonds[41−45] in complexes with pyridine-based pincer ligands. Against this background, we herein report the extension of the substrate scope to S=O bonds, as complex **1** readily reacts with the adduct of 1,4-diazabicyclo[2.2.2]octane and sulfur dioxide (DABSO),[46] which is a convenient source of SO_2, to give the sulfinate compound *fac*-K[Re(*amidopy-OSO*)(CO)$_3$] (**2ab**) under Re−O and C−S bond formation (Scheme 2, **2ab**). The reaction is characterized by a color change from deep purple to brownish-orange. Compound **2** was isolated as a diastereomeric mixture (**2ab**) via slow diffusion of *n*-hexanes into a concentrated THF solution in the presence of 18-*crown*-6 in 59% yield. Note, the representation of **1** as a mesomeric resonance structure featuring a bis-amido ligand with reduced aromaticity of the pyridine unit (Scheme 2, **1 II**) appears advantageous as it reflects the NMR spectroscopic findings[27] and C-centered nucleophilic reactivity toward SO_2. The benzylic sp^2-carbon atom in **1** (C6, as indicated in Figure 2) is prochiral. Owing to the binding of SO_2 and the resulting C−S bond, complex **2** encompasses a chiral carbon center as well as a pyramidal sulfur-center of chirality. Consequently, a diastereomeric mixture is formed. This is best observed in the ^{1}H NMR spectrum of **2ab** in CD_2Cl_2: The spectrum indicates very similar resonances associated with both diastereomeric pairs **2a** and **2b** in an approximate 1:1 ratio. FLPs with chiral carbon centers in their backbone have been previously described to give rise to diastereomeric mixtures upon binding of SO_2.[18] The ^{1}H NMR spectrum of **2ab** in CD_2Cl_2 at 268 K reveals a shift of the pyridine resonances of both diastereomers back to higher frequencies, signifying a redistribution of the π-system to form a pyridine-amido chelate in **2ab**.[47] The ^{1}H resonance of the benzylic (O_2S)*CH* proton is shifted further upfield (6.68 (s, 1H$_b$, O_2S−*CH*−N; 6.17 (s, 1H$_a$, O_2S−*CH*−N with respect to **1**. The corresponding resonances of the benzylic ^{13}C nuclei in **2ab** are observed as characteristic singlets at 97.8 ppm (1C$_b$, *C*(SOO)) and 94.4 ppm (1C$_a$, *C*(SOO)), suggesting the formation of an sp^3-carbon moiety in the vicinal position between the sulfinato and amido moiety. Remarkably, at ambient temperature, the ^{1}H NMR spectrum shows broad resonance suggesting a rapid interconversion of both diastereomers with respect to the NMR time scale. Upon cooling to 268 K, the signals become sharp and well separated. Conversely, raising the temperature gives rise to a broadening of the lines until they coalesce at 308 K (see Figure S6). The interconversion of both diastereomers can be best observed by ^{1}H^{1}H EXSY NMR exchange spectroscopy. The spectrum shows significant cross-peaks between the resonances of both diastereomers **2a** and **2b**, indicating a chemical exchange process (Figure 1). Standard line shape analysis[48] at various

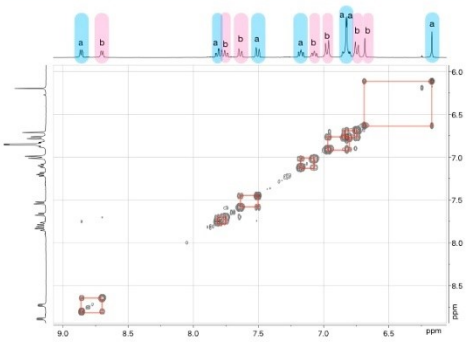

Figure 1. ^{1}H ^{1}H EXSY NMR spectrum of compound **2** in CD_2Cl_2 at 268 K. Cross-peaks indicate ^{1}H nuclei experiencing mutual chemical exchange between the diastereomers **2a** and **2b**.

temperatures (253−308 K in CD_2Cl_2) allowed for the determination of the activation parameters via Eyring plot analysis ($\Delta G^{\#}_{298}$ = 14.8 ± 2.0 kcal/mol, $\Delta H^{\#}$ = 19.8 ± 1.4 kcal/mol, $\Delta S^{\#}$ = 16.9 ± 4.8 cal/mol K). Reversible equilibration with similar activation barriers were also observed for FLP−SO_2 adducts for epimerization at sulfur.[18] In comparison, chiral inversion at trisubstituted pyramidal sulfur centers, which is not associated with the presence of additional auxiliaries, usually proceeds with higher inversion barriers with respect to **2**, as demonstrated mainly for sulfoxides.[49−53] In this regard, a rather small entropy of activation ($\Delta S^{\#} \approx 0$) can be indicative of a nondissociative inversion about the S atom (pyramidal inversion).[49] A few sulfinate esters were reported to rearrange via a reversible dissociation-recombination process. This rearrangement can either lead to sulfones or result in racemization; both pathways can proceed via an ion-pair intermediate.[54,55] In that context, the positive value of $\Delta S^{\#}$ for the interconversion of **2a**/**2b** may hint toward a process different from simple pyramidal inversion. Single crystals suitable for X-ray diffraction analysis were obtained via

DOI: 10.1021/acs.organomet.8b00485
Organometallics 2018, 37, 3639−3643

recrystallization of **2ab** from CH_2Cl_2/*n*-hexanes. The obtained structure is shown in Figure 2. The Re center resides in a

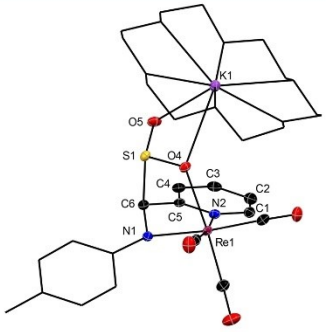

Figure 2. Mercury plot of the molecular structure of **2** with thermal ellipsoids drawn at 50% probability, $Ph^{P\text{-}Me}$, and 18-crown-6 plotted as wireframe. Hydrogen atoms and CH_2Cl_2 solvent molecule are neglected for clarity. Selected bond lengths [Å] and angles [°]: Re1−N1 = 2.131(2), Re1−N2 = 2.162(2), Re1−O4 = 2.222(1), N1−C6 = 1.431(2), C6−C5 = 1.484(2), C6−S1 = 1.907(2), S1−O4 = 1.560(1), S1−O5 = 1.490(1), K1−O5 = 2.774(1), K1−O4 = 2.852(1), K1−S1 = 3.3044(6), O5−S1−O4 = 108.49(8).

distorted octahedral coordination sphere involving three CO ligands in mutual *fac*-arrangement and the bidentate amidopyridine unit. The SO_2 moiety is incorporated into the ligand scaffold. The formation of the C−S bond between C6 and S1 allows for completion of the octahedral coordination sphere via sulfinate η^1-*O* coordination to the rhenium center in apical position (O4−Re1 = 2.222(1) Å). The C6−S1 interatomic distance of 1.907(2) Å is elongated with respect to previously reported transition metal sulfinate complexes, which show C−S bond lengths typically ranging from 1.81 to 1.89 Å for η^1-*O* bound sulfinates.[56−58] The overall negative charge of the anionic complex is balanced by a K^+ countercation chelated by the crown ether. K1 has close contacts to the oxygen atoms O4 and O5 of the SO_2 moiety (K1−O4 = 2.852(1) Å and K1−O5 = 2.774(1) Å). The angles about the sulfur center sum to 311.6°, indicating a distorted pyramidal geometry. The C6−C5 interatomic distance of 1.484(2) Å indicates a C−C single bond. Conversely, the C6−N1 distance of 1.431(2) Å suggests a C−N single bond as well, which is in line with the observed four almost equidistant C−C bonds of the pyridine unit (~1.39 Å), indicating a delocalized π-system (rearomatization) in the pyridine ring. We showed previously that complex **1** reversibly binds CO_2 via formal [1,3] addition triggered by MLC. In this aspect, we were intrigued to investigate the reversible binding/activation of SO_2 in complex **2ab**. Non-cooperative reversible SO_2 binding to a metal center is known, e.g., in lanthanide complexes,[59] and Albrecht and van Koten reported on fully reversible SO_2 binding (η^1-*S*) of gaseous SO_2 in a Pt pincer complex even in a crystalline-state reaction.[60] However, although we found dynamic inversion at the sulfinate moiety, our experiments have not suggested a fully reversible binding of SO_2 in **2ab** so far. However, we found that complex **2ab** in CH_2Cl_2 undergoes slow oxidation under concomitant loss of the sulfinate moiety. Heating, sonication, or merely prolonged reaction times at ambient temperature gave rise to the reformation of the imino complex [fac-Re(*impy*)$(CO)_3$Cl] (Scheme 2, **i-*Cl***). Further experiments included the reaction of complex **2ab** in a THF suspension with excess CO_2. Extended heating did not lead to the exchange of SO_2. The reaction of **2ab** in CH_2Cl_2 solution, either in the presence or absence of CO_2, gave rise to the formation of the imino complex *fac*-[Re(*impy*)$(CO)_3$Cl] (**i-*Cl***).

■ ASSOCIATED CONTENT

Supporting Information

The Supporting Information is available free of charge on the ACS Publications website at DOI: 10.1021/acs.organomet.8b00485.

Compound **2** and experimental details (PDF)

Accession Codes

CCDC 1856368 contains the supplementary crystallographic data for this paper. These data can be obtained free of charge via www.ccdc.cam.ac.uk/data_request/cif, or by emailing data_request@ccdc.cam.ac.uk, or by contacting The Cambridge Crystallographic Data Centre, 12 Union Road, Cambridge CB2 1EZ, UK; fax: +44 1223 336033.

■ AUTHOR INFORMATION

Corresponding Author

*E-mail: mavogt@uni-bremen.de.

ORCID

Matthias Vogt: 0000-0002-2636-2531

Notes

The authors declare no competing financial interest.

■ ACKNOWLEDGMENTS

We are grateful to Enno Lork for supporting the crystallographic analysis and to Johannes Stelten for supporting the VT NMR measurements. Generous financial support from Verband der Chemischen Industrie (VCI) and the Central Research and Development Fund (CRDF) of the University of Bremen is greatly acknowledged.

■ REFERENCES

(1) Bisseret, P.; Blanchard, N. Taming Sulfur Dioxide: A Breakthrough for Its Wide Utilization in Chemistry and Biology. *Org. Biomol. Chem.* **2013**, *11*, 5393−5398.

(2) Müller, H. *Sulfur Dioxide*, 3rd ed.; Wiley-VCH Verlag GmbH & Co. KGaA: Weinheim, Germany, 2000; Vol. *81*.

(3) Schenk, W. A. Sulfur Oxides as Ligands in Coordination Compounds. *Angew. Chem., Int. Ed. Engl.* **1987**, *26*, 98−109.

(4) Schenk, W. A. The Coordination Chemistry of Small Sulfur-Containing Molecules: A Personal Perspective. *Dalton Trans.* **2011**, *40*, 1209−1219.

(5) Phillips, A. E.; Cole, J. M.; d'Almeida, T.; Low, K. S. Ru−OSO Coordination Photogenerated at 100 K in Tetraammineaqua(Sulfur Dioxide)Ruthenium(II) (±)-Camphorsulfonate. *Inorg. Chem.* **2012**, *51*, 1204−1206.

(6) Bowes, K. F.; Cole, J. M.; Husheer, S. L. G.; Raithby, P. R.; Savarese, T. L.; Sparkes, H. A.; Teat, S. J.; Warren, J. E. Photocrystallographic Structure Determination of a New Geometric Isomer of $[Ru(NH_3)_4(H_2O)(H_1\text{-}OSO)][MeC_6H_4SO_3]_2$. *Chem. Commun.* **2006**, 2448−2450.

(7) Kovalevsky, A. Y.; Bagley, K. A.; Coppens, P. The First Photocrystallographic Evidence for Light-Induced Metastable Linkage Isomers of Ruthenium Sulfur Dioxide Complexes. *J. Am. Chem. Soc.* **2002**, *124*, 9241−9248.

DOI: 10.1021/acs.organomet.8b00485
Organometallics 2018, 37, 3639−3643

(8) Cole, J. M.; Velazquez-Garcia, J. de J.; Gosztola, D. J.; Wang, S. G.; Chen. eta^2-SO_2 Linkage Photoisomer of an Osmium Coordination Complex. *Inorg. Chem.* **2018**, *57*, 2673.
(9) Gleu, K.; Breuel, W.; Rehm, K. Sulfito-Ammine Des Zweiwertigen Rutheniums Tetrammino-Reihe (Ruthen-Ammine. II.). *Z. anorg. allg. Chem.* **1938**, *235*, 201−210.
(10) Li, J.; Rogachev, A. Y. SO_2− Yet Another Two-Faced Ligand. *Phys. Chem. Chem. Phys.* **2015**, *17*, 1987−2000.
(11) Mingos, D. M. P. A Review of Complexes of Ambivalent and Ambiphilic Lewis Acid/Bases with Symmetry Signatures and an Alternative Notation for These Non-Innocent Ligands. *J. Organomet. Chem.* **2014**, *751*, 153−173.
(12) Lork, E.; Petersen, J.; Mews, R. Synthesis and Structure of $[Ni(SO_2)_6](AsF_6)_2$ and $[Fe(SO_2)_4(FAsF_5)_2]$. *Angew. Chem., Int. Ed. Engl.* **1994**, *33*, 1663−1665.
(13) Gott, G. A.; Fawcett, J.; McAuliffe, C. A.; Russell, D. R. The X-Ray Crystal Structure of Trans-Bis(Sulphur Dioxide)Tetrakis-(Triphenylphosphineoxide)Manganese(II) Di-Iodide, a Compound Which Undergoes Demi-Reversible Binding of Sulphur Dioxide: the First Crystallographically Characterised Example of O-Bonded Sulphur Dioxide in a Transition Metal Complex. *J. Chem. Soc., Chem. Commun.* **1984**, 1283−1284.
(14) Baumann, F.-E.; Burschka, C.; Schenk, W. A. Ligand Substitution at Cis-$Mo(CO)_2(PPh_3)_2(MeCN)$(eta^2-SO_2) Crystal and Molecular Structure of Cis-$Mo(CO)_2(PMe_3)_3$(eta^2-SO_2). *Z. für Naturforsch. B* **1986**, *41*, 1211−1218.
(15) Cotton, F. A.; Schmid, G. Mononuclear Molybdenum(IV) Complexes with Two Multiply Bonded Chalcogen Ligands in Trans Configuration and Chelating Biphosphine Ligands. *Inorg. Chem.* **1997**, *36*, 2267−2278.
(16) Lang, R. F.; Ju, T. D.; Hoff, C. D.; Bryan, J. C.; Kubas, G. J. Synthesis and Structure of W(CO)(Phen)$(SPh)_2$(eta^2-SO_2): A Tungsten(II) Sulfur Dioxide Complex That Spontaneously Extrudes Sulfur to Form the Tungsten(VI) Dioxo Complex W(Phen)-$(SPh)_2(O)_2$. *J. Am. Chem. Soc.* **1994**, *116*, 9747−9748.
(17) Stephan, D. W.; Erker, G. Frustrated Lewis Pair Chemistry of Carbon, Nitrogen and Sulfur Oxides. *Chem. Sci.* **2014**, *5*, 2625−2641.
(18) Sajid, M.; Klose, A.; Birkmann, B.; Liang, L.; Schirmer, B.; Wiegand, T.; Eckert, H.; Lough, A. J.; Fröhlich, R.; Daniliuc, C. G.; et al. Reactions of Phosphorus/Boron Frustrated Lewis Pairs with SO_2. *Chem. Sci.* **2013**, *4*, 213−219.
(19) Schmidt, A.-C.; Heinemann, F. W.; Kefalidis, C. E.; Maron, L.; Roesky, P. W.; Meyer, K. Activation of SO_2 and CO_2 by Trivalent Uranium Leading to Sulfite/Dithionite and Carbonate/Oxalate Complexes. *Chem. - Eur. J.* **2014**, *20*, 13501−13506.
(20) Klementyeva, S. V.; Gamer, M. T.; Schmidt, A.-C.; Meyer, K.; Konchenko, S. N.; Roesky, P. W. Activation of SO_2 with $[(eta^5\text{-}C_5Me_5)_2Ln(THF)_2]$ (Ln = Eu, Yb) Leading to Dithionite and Sulfinate Complexes. *Chem. - Eur. J.* **2014**, *20*, 13497−13500.
(21) Klementyeva, S. V.; Arleth, N.; Meyer, K.; Konchenko, S. N.; Roesky, P. W. Dithionite and Sulfinate Complexes From the Reaction of SO_2 with Decamethylsamarocene. *New J. Chem.* **2015**, *39*, 7589−7594.
(22) Milstein, D. Metal-Ligand Cooperation by Aromatization-Dearomatization as a Tool in Single Bond Activation. *Philos. Trans. R. Soc., A* **2015**, *373*, 20140189−20140189.
(23) Khusnutdinova, J. R.; Milstein, D. Metal-Ligand Cooperation. *Angew. Chem., Int. Ed.* **2015**, *54*, 12236−12273.
(24) Gunanathan, C.; Milstein, D. Bond Activation by Metal-Ligand Cooperation: Design of "Green" Catalytic Reactions Based on Aromatization-Dearomatization of Pincer Complexes. *Top. Organomet. Chem.* **2011**, *37*, 55−84.
(25) Milstein, D. Discovery of Environmentally Benign Catalytic Reactions of Alcohols Catalyzed by Pyridine-Based Pincer Ru Complexes, Based on Metal−Ligand Cooperation. *Top. Catal.* **2010**, *53*, 915−923.
(26) van der Vlugt, J. I.; Reek, J. N. H. Neutral Tridentate PNP Ligands and Their Hybrid Analogues: Versatile Non-Innocent Scaffolds for Homogeneous Catalysis. *Angew. Chem., Int. Ed.* **2009**, *48*, 8832−8846.
(27) Stichauer, R.; Helmers, A.; Bremer, J.; Rohdenburg, M.; Wark, A.; Lork, E.; Vogt, M. Rhenium(I) Triscarbonyl Complexes with Redox-Active Amino- and Iminopyridine Ligands: Metal−Ligand Cooperation as Trigger for the Reversible Binding of CO_2 via a Dearmomatization/Rearomatization Reaction Sequence. *Organometallics* **2017**, *36*, 839−848.
(28) Sieh, D.; Lacy, D. C.; Peters, J. C.; Kubiak, C. P. Reduction of CO 2by Pyridine Monoimine Molybdenum Carbonyl Complexes: Cooperative Metal-Ligand Binding of CO_2. *Chem. - Eur. J.* **2015**, *21*, 8497−8503.
(29) Janes, T.; Yang, Y.; Song, D. Chemical Reduction of CO_2 facilitated by C-Nucleophiles. *Chem. Commun.* **2017**, *53*, 11390−11398.
(30) Vogt, M.; Nerush, A.; Diskin-Posner, Y.; Ben-David, Y.; Milstein, D. Reversible CO_2 Binding Triggered by Metal-Ligand Cooperation in a Rhenium(I) PNP Pincer-Type Complex and the Reaction with Dihydrogen. *Chem. Sci.* **2014**, *5*, 2043−2051.
(31) Filonenko, G. A.; Conley, M. P.; Copéret, C.; Lutz, M.; Hensen, E. J. M.; Pidko, E. A. The Impact of Metal−Ligand Cooperation in Hydrogenation of Carbon Dioxide Catalyzed by Ruthenium PNP Pincer. *ACS Catal.* **2013**, *3*, 2522−2526.
(32) Filonenko, G. A.; Hensen, E. J. M.; Pidko, E. A. Mechanism of CO 2hydrogenation to Formates by Homogeneous Ru-PNP Pincer Catalyst: From a Theoretical Description to Performance Optimization. *Catal. Sci. Technol.* **2014**, *4*, 3474−3485.
(33) Feller, M.; Gellrich, U.; Anaby, A.; Diskin-Posner, Y.; Milstein, D. Reductive Cleavage of CO_2 by Metal-Ligand-Cooperation Mediated by an Iridium Pincer Complex. *J. Am. Chem. Soc.* **2016**, *138*, 6445−6454.
(34) Rivada-Wheelaghan, O.; Dauth, A.; Leitus, G.; Diskin-Posner, Y.; Milstein, D. Synthesis and Reactivity of Iron Complexes with a New Pyrazine-Based Pincer Ligand, and Application in Catalytic Low-Pressure Hydrogenation of Carbon Dioxide. *Inorg. Chem.* **2015**, *54*, 4526−4538.
(35) Huff, C. A.; Kampf, J. W.; Sanford, M. S. Role of a Noninnocent Pincer Ligand in the Activation of CO_2 at (PNN)Ru-(H)(CO). *Organometallics* **2012**, *31*, 4643−4645.
(36) Vogt, M.; Rivada-Wheelaghan, O.; Iron, M. A.; Leitus, G.; Diskin-Posner, Y.; Shimon, L. J. W.; Ben-David, Y.; Milstein, D. Anionic Nickel(II) Complexes with Doubly Deprotonated PNP Pincer-Type Ligands and Their Reactivity Toward CO_2. *Organometallics* **2013**, *32*, 300−308.
(37) Feller, M.; Ben-Ari, E.; Diskin-Posner, Y.; Milstein, D. CO2 Activation by Metal−Ligand-Cooperation Mediated by Iridium Pincer Complexes. *J. Coord. Chem.* **2018**, 1−11.
(38) Oren, D.; Diskin-Posner, Y.; Avram, L.; Feller, M.; Milstein, D. Metal−Ligand Cooperation as Key in Formation of Dearomatized Ni^{II}−H Pincer Complexes and in Their Reactivity Toward CO and CO_2. *Organometallics* **2018**, *37*, 2217.
(39) Rivada-Wheelaghan, O.; Dauth, A.; Leitus, G.; Diskin-Posner, Y.; Milstein, D. Synthesis and Reactivity of Iron Complexes with a New Pyrazine-Based Pincer Ligand, and Application in Catalytic Low-Pressure Hydrogenation of Carbon Dioxide. *Inorg. Chem.* **2015**, *54*, 4526−4538.
(40) Montag, M.; Zhang, J.; Milstein, D. Aldehyde Binding Through Reversible C−C Coupling with the Pincer Ligand Upon Alcohol Dehydrogenation by a PNP−Ruthenium Catalyst. *J. Am. Chem. Soc.* **2012**, *134*, 10325−10328.
(41) Vogt, M.; Nerush, A.; Iron, M. A.; Leitus, G.; Diskin-Posner, Y.; Shimon, L. J. W.; Ben-David, Y.; Milstein, D. Activation of Nitriles by Metal Ligand Cooperation. Reversible Formation of Ketimido- and Enamido-Rhenium PNP Pincer Complexes and Relevance to Catalytic Design. *J. Am. Chem. Soc.* **2013**, *135*, 17004−17018.
(42) Filonenko, G. A.; Cosimi, E.; Lefort, L.; Conley, M. P.; Copéret, C.; Lutz, M.; Hensen, E. J. M.; Pidko, E. A. Lutidine-Derived Ru-CNC Hydrogenation Pincer Catalysts with Versatile Coordination Properties. *ACS Catal.* **2014**, *4*, 2667−2671.

DOI: 10.1021/acs.organomet.8b00485
Organometallics 2018, 37, 3639−3643

(43) Perdriau, S.; Zijlstra, D. S.; Heeres, H. J.; de Vries, J. G.; Otten, E. A Metal–Ligand Cooperative Pathway for Intermolecular Oxa-Michael Additions to Unsaturated Nitriles. *Angew. Chem.* **2015**, *127*, 4310–4314.
(44) Hernández-Juárez, M.; López-Serrano, J.; Lara, P.; Morales-Cerón, J. P.; Vaquero, M.; Álvarez, E.; Salazar, V.; Suárez, A. Ruthenium(II) Complexes Containing Lutidine-Derived Pincer CNC Ligands: Synthesis, Structure, and Catalytic Hydrogenation of C-N Bonds. *Chem. - Eur. J.* **2015**, *21*, 7540–7555.
(45) Eijsink, L. E.; Perdriau, S. C. P.; de Vries, J. G.; Otten, E. Metal-Ligand Cooperative Activation of Nitriles by a Ruthenium Complex with a De-Aromatized PNN Pincer Ligand. *Dalton Trans.* **2016**, *45*, 16033–16039.
(46) Woolven, H.; González-Rodríguez, C.; Marco, I.; Thompson, A. L.; Willis, M. C. DABCO-Bis(Sulfur Dioxide), DABSO, as a Convenient Source of Sulfur Dioxide for Organic Synthesis: Utility in Sulfonamide and Sulfamide Preparation. *Org. Lett.* **2011**, *13*, 4876–4878.
(47) ^{1}H NMR spectrum of **2ab**, 360 MHz, 268 K in CD_2Cl_2: 8.86 (d, $^{3}J_{HH}$ = 5.3 Hz, $1H_a$, $CH_{py\text{-}6}$), 8.70 (d, $^{3}J_{HH}$ = 5.3 Hz, $1H_b$, $CH_{py\text{-}6}$), 7.78 (m, J = 9.0, 7.7, 1.5 Hz, $1H_a$ and $1H_b$, overlap $CH_{py\text{-}4}$), 7.64 (d, $^{3}J_{HH}$ = 7.7 Hz, $1H_b$, $CH_{py\text{-}3}$), 7.51 (d, $^{3}J_{HH}$ = 7.8 Hz, $1H_a$, $CH_{py\text{-}3}$), 7.22–7.13 (m, $1H_a$, $CH_{py\text{-}5}$), 7.12 – 7.05 (m, $1H_b$, $CH_{py\text{-}5}$).
(48) Chemical exchange rate parameters were determined via spectral fitting and line shape analysis (253–308 K) using the dynamic NMR module (DNMR 1.1) implemented in BRUKER TOPSPIN 4.0.3. Subsequent Eyring-Polanyi plot analysis gave the activation parameters (see Supporting Information).
(49) Toyota, S. Mechanisms of Inversion at Pyramidal Sulfur Atoms in Three-Coordinate Sulfur Compounds. *Rev. Heteroatom Chem.* **1999**, *21*, 139–162.
(50) Rayner, D. R.; Miller, E. G.; Bickart, P.; Gordon, A. J.; Mislow, K. Mechanisms of Thermal Racemization of Sulfoxides1. *J. Am. Chem. Soc.* **1966**, *88*, 3138–3139.
(51) Marom, H.; Biedermann, P. U.; Agranat, I. Pyramidal Inversion Mechanism of Simple Chiral and Achiral Sulfoxides: A Theoretical Study. *Chirality* **2007**, *19*, 559–569.
(52) Kimura, T.; Tsuru, T.; Momochi, H.; Satoh, T. Configurational Stability of Optically Active Dichloromethyl *p*-Tolyl Sulfoxide and Its Anionic Species: Experimental and Theoretical Study. *Heteroat. Chem.* **2013**, *24*, 131–137.
(53) Rayner, D. R.; Gordon, A. J.; Mislow, K. Thermal Racemization of Diaryl, Alkyl Aryl, and Dialkyl Sulfoxides by Pyramidal Inversion. *J. Am. Chem. Soc.* **1968**, *90*, 4854–4860.
(54) Ciuffarin, E.; Isola, M.; Fava, A. Ion-Pair Return in Racemization and Isomerization of Sulfinate Esters. *J. Am. Chem. Soc.* **1968**, *90*, 3594–3595.
(55) Kirmse, W.; Herpers, E. Recombination of Carbocation–Sulfinate Ion Pairs. *Angew. Chem., Int. Ed. Engl.* **1991**, *30*, 1018–1020.
(56) McDonald, A. R.; Bukowski, M. R.; Farquhar, E. R.; Jackson, T. A.; Koehntop, K. D.; Seo, M. S.; De Hont, R. F.; Stubna, A.; Halfen, J. A.; Muenck, E.; et al. Sulfur Versus Iron Oxidation in an Iron-Thiolate Model Complex. *J. Am. Chem. Soc.* **2010**, *132*, 17118–17129.
(57) Ibrahim, M. M.; Vahrenkamp, H. Ungewöhnliche Bildung Und Struktur Eines O-Sulfinato-Zinkkomplexes. *Z. Anorg. Allg. Chem.* **2006**, *632*, 1083–1085.
(58) Kelly, R. P.; Kazeminejad, N.; Lamsfus, C. A.; Maron, L.; Roesky, P. W. Activation of SO_2 by $[Zn(Cp^*)_2]$ and $[(Cp^*)Zn^{I}–Zn^{I}(Cp^*)]$. *Chem. Commun.* **2016**, *52*, 13090–13093.
(59) Benndorf, P.; Schmitt, S.; Köppe, R.; Oña-Burgos, P.; Scheurer, A.; Meyer, K.; Roesky, P. W. Catching Gaseous SO_2 In Cone-Type Lanthanide Complexes: An Unexpected Coordination Mode for SO_2 In F-Element Chemistry. *Angew. Chem., Int. Ed.* **2012**, *51*, 5006–5010.
(60) Albrecht, M.; Lutz, M.; Spek, A. L.; van Koten, G. Organoplatinum Crystals for Gas-Triggered Switches. *Nature* **2000**, *406*, 970–974.

DOI: 10.1021/acs.organomet.8b00485
Organometallics 2018, 37, 3639–3643

3.1.5 Manganese(I) Tricarbonyle Complexes with Bidentate Pyridine-Based Actor Ligands: Reversible Binding of CO_2 and Benzaldehyde *via* Cooperative C-C and Mn-O Bond Formation at Ambient Temperature[161]

In this work, the metal center was altered from rhenium to the base metal pendant manganese. Additionally, the influence of the counter ion (M'' = Li, Na, K) was investigated. MLC was demonstrated under reversible Mn-O and C-C bond formation, represented by the reaction of CO_2 and benzaldehyde at ambient temperature. The Mn(I)-complex **75*-Mn** reacts readily with CO_2 and also with benzaldehyde, forming the 1,3-addition products **78** and **79** (Scheme 37). The counter ion takes a decisive role in CO_2 activation, revealed by varying the counterion of the Mn(I)-CO_2 adduct complex **78** by K^+ (**78-K**), Na^+ (**78-Na**) and Li^+ (**78-Li**) in exchange reactions and additionally in quantum chemical calculations using DFT (Density functional theory).

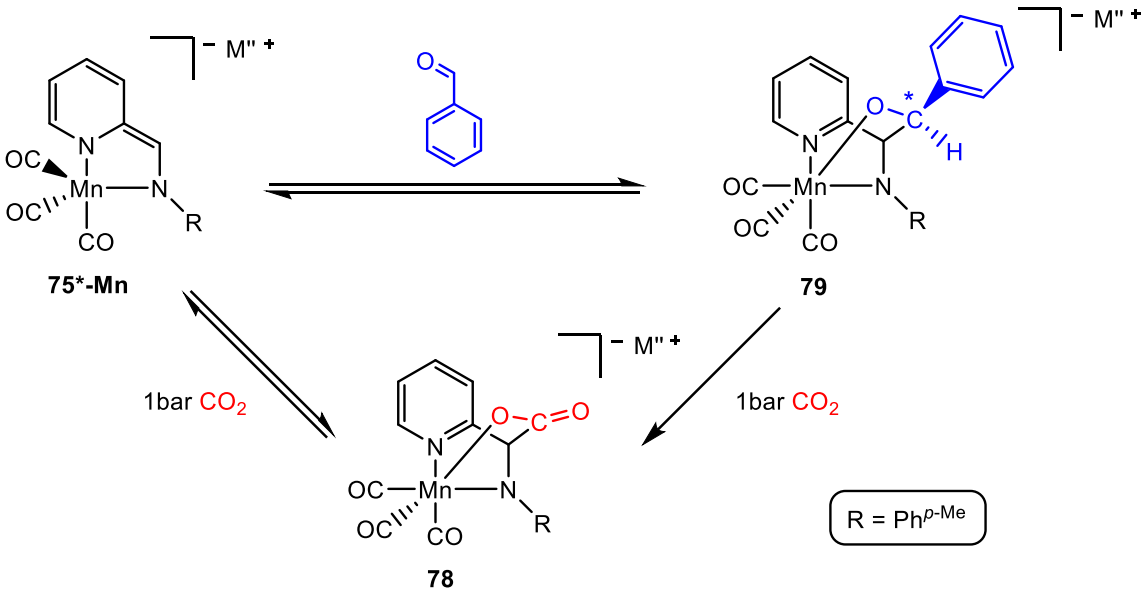

Scheme 37: Reversible binding of CO_2 in *fac*-M''[Mn(I)(*amidopy*-CO_2)$(CO)_3$] (**78**) and benzaldehyde in *fac*-M''[Mn(I)(*amidopy-ba*)$(CO)_3$] (**79**) with the dearomatized bidentate Mn(I)-complex M''[Mn(I)(*amidopy**)$(CO)_3$] (**75*-Mn**). (M'' = Li, Na, K)

I was responsible for the conception and all experimental work, all analytical characterizations and created the experimental section as well the major part of the supporting information, except the computational details. Computational calculations were accomplished by Prof. Dr. Robert Langer at the Martin-Luther-Universität Halle-Wittenberg. scXRD analysis was measured and evaluated by Daniel Duvinage.

The obtained results were published in the following journal:

R. Stichauer, D. Duvinage, R. Langer, M. Vogt, *Organometallics* **2022,** *41*, 2798-2809.
DOI: 10.1021/acs.organomet.2c00387

My percentage contribution of this publication in categories: experimental concept and design: ca. 60%, experimental work and acquisition of experimental data: 90%, data analysis and interpretation: 70 %, preparation of Figures and Tables: ca. 90%, drafting of the manuscript: ca. 55%.

ORGANOMETALLICS

pubs.acs.org/Organometallics Article

Manganese(I) Tricarbonyl Complexes with Bidentate Pyridine-Based Actor Ligands: Reversible Binding of CO_2 and Benzaldehyde via Cooperative C−C and Mn−O Bond Formation at Ambient Temperature

Rasmus Stichauer, Daniel Duvinage, Robert Langer, and Matthias Vogt*

Cite This: *Organometallics* 2022, 41, 2798−2809 Read Online

ACCESS | Metrics & More | Article Recommendations | Supporting Information

ABSTRACT: We report manganese(I) tricarbonyl complexes decorated with imino- and amino-pyridine ligands [Mn(*impy*)$(CO)_3$Br] and [Mn(*ampy*)$(CO)_3$Br], respectively. Both compounds can be transformed either via two-electron reduction for the former or double deprotonation for the latter into anionic species with a disturbed ("dearomatized") π-electron system of the pyridine ring M[Mn(*amidopy**)$(CO)_3$] (M = alkali metal). The newly formed five-coordinated complex is anionic and encompasses a nucleophilic carbon center within its metalla cycle. This leads to noteworthy reactivity: [Mn(*amidopy**)$(CO)_3]^-$ readily reacts with C=O double bonds. Specifically, CO_2 and benzaldehyde can bind to the complex via a metal−ligand cooperative [1,3]-addition under C−C and Mn−O bond formation and concomitant rearomatization of the pyridine ring. Remarkably, we found that this addition is reversible. Exchange reactions using isotopically labeled $^{13}CO_2$ indicate reversible C−C and Mn−O bond formation at ambient temperature. Likewise, bonded benzaldehyde is exchanged from the complex under a CO_2 atmosphere. Density functional theory calculations suggest a significant role for the cationic counter ion in the bond activation reactions that can make this bond activation feasible.

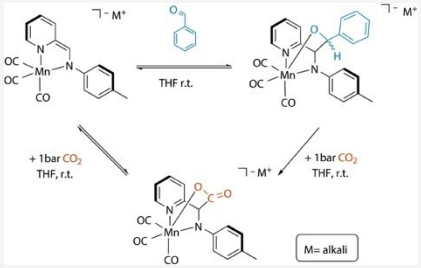

1. INTRODUCTION

Great efforts are spent to develop robust and potent catalysts based on abundant first-row transition metals enabling reactions relevant to a sustainable energy and natural resource management. In this regard, manganese(I) carbonyl complexes have attracted increased attention during the last decade owing to their utilization, for instance, in homogeneous catalysis with relevance to (atom economic) environmentally benign reaction schemes addressing fundamental chemical[1−14] and electrocatalytic transformations.[15−18] They have been explored as homogeneous catalysts facilitating C−C bond formations[19−22] and have been also discussed in photo-therapeutic applications.[23−25] Against this background, the concept of metal−ligand cooperation (MLC) is a central feature for substrate/small molecule activation in first-row transition metal complexes.[26] Examples for MLC processes in Mn(I) tricarbonyls with bidentate actor ligands were given, e.g., by Khusnutdinova and co-workers for a Mn(I) tricarbonyl complex carrying a pyridine-based P,N-donor ligand. The authors reported the catalytic hydrogenation of nonactivated alkenes and gathered evidence for an MLC-assisted activation of H_2 in course of the catalytic hydrogenation.[27] Valyaev, Lugan, Canac, Sortais, and co-workers described a Mn(I) triscarbonyl complex with a bidentate N-heterocyclic carbene (NHC)-based C,P-donor ligand. Upon activation with a base, NHC-phosphinomethanide species is formed, capable of activating H_2 and binding CO_2 triggered by an MLC pathway.[28] Specifically with respect to unusual CO_2 bonding situations, ligand-centered C-nucleophiles have been identified as a key feature for (reversible) binding/activation schemes.[29] For instance, Song and co-workers reported a reversibly formed C−C bond between CO_2 and a remote nucleophilic C-center in zwitterionic species.[30] CO_2 uptake involving MLC under concomitant C−C (ligand−substrate) and M−O (metal−substrate) bond formation was described by several research groups, for instance, by Kubiak and co-workers in an imino-pyridine Mo complex[31] or in a Pd complex with a functional phosphine ligand described by Braunstein and co-workers.[32] Selected further examples are depicted in Figure 1: Milstein and co-workers reported on Ru(II) and Re(I) PNP pyridine-based pincer-type complexes capable of reversibly

Received: July 30, 2022
Published: September 20, 2022

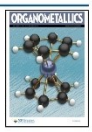

https://doi.org/10.1021/acs.organomet.2c00387
Organometallics 2022, 41, 2798−2809

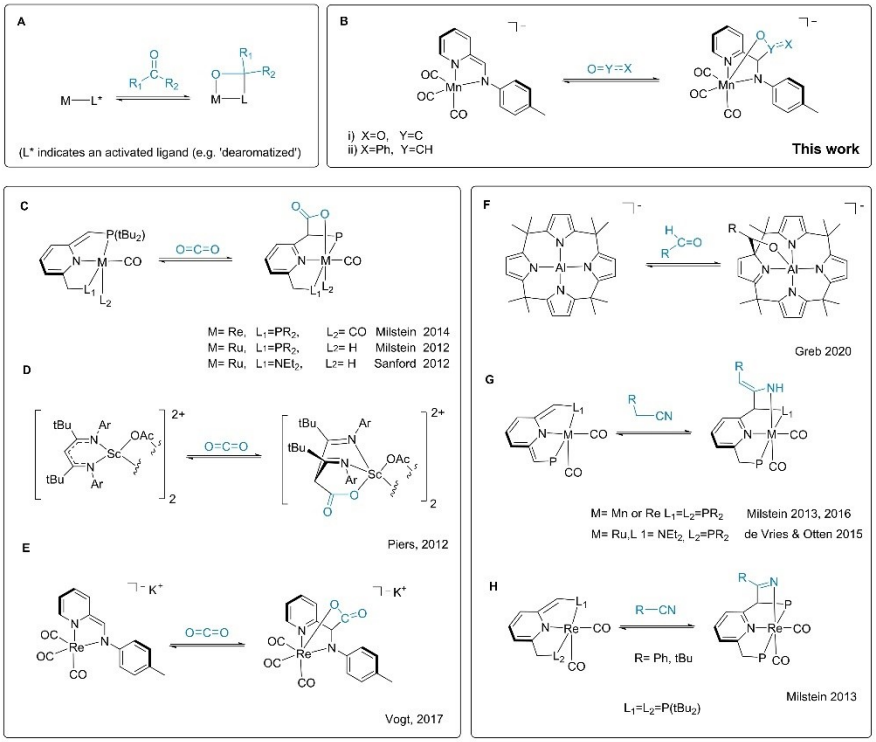

Figure 1. (A) Metal−ligand cooperative activation of the C=O double bond in a reversible bonding scheme. (B) MLC binding of CO_2/benzaldehyde presented in this work. (C−H) Overview of selected examples of reversible substrate (CO and CN) binding via MLC.

binding CO_2 via an MLC reaction (**C**).[33,34] Sanford and co-workers reported similar reactivity in a Ru(II) PNN pincer-type complex (**C**).[35] Pidko and co-workers investigated the hydrogenation of CO_2 to formic acid catalyzed by a Ru PNP-type pincer complex and showed that the ML-cooperative uptake of CO_2 can also lead to inhibition of the catalysts.[36] Piers and co-workers describe a scandium complex decorated with a diketiminate ligand, which cooperatively binds CO_2 (**D**).[37] Our group reported cooperative CO_2 binding in a Re(I) tricarbonyl complex decorated with an redox-active imino-pyridine ligand set (**E**).[38] An intriguing reaction pathway was proposed by Gessner and co-workers, where reversible addition of CO_2 to a ligand-centered C-nucleophile gives rise to transient carboxylate species, which directs a subsequent C−H activation of an adjacent phenyl group. The authors propose that owing to the reversible MLC bonding, CO_2 serves as a catalyst and gives rise to the high selectivity of this reaction demonstrating the catalytic utilization of such a reversible binding mode.[39] Beyond the cooperative activation of the C=O double bond of CO_2, the reversible bonding scheme (**A**) was extended to other multiple bonds involving carbonyl[40,41] (**F**) and nitrile moieties (**G,H**) and has been exploited in catalyzed conjugate addition reactions encompassing, for instance, C−C[20,42] and C−O[43,44] couplings. A recent example of great elegance was reported by Greb and co-workers where the reversible ML-cooperative addition of CO_2 and carbonyl moieties was transferred to a p-block element, specifically to a constrained, square-planarly coordinated, aluminum(III) complex with a *meso*-octamethylcalix[4]pyrrolato ligand (**F**).[41]

We now report the extension of our previous work on the cooperative activation of CO_2 in Re(I) triscabonyl complexes with bidentate pyridine-based actor ligands (**B**) to related Mn(I) triscarbonyl complexes and their reactivity with CO_2 and extend the reactivity study to C=O double bonds of aldehyde groups.

2. RESULTS AND DISCUSSION

The triscarbonyl manganese(I) complex *fac*-[Mn(*impy*)-$(CO)_3$Br] (**1**, *impy* = (1-(pyridin-2-yl)-*N*-(*p*-tolyl)-methanimine, Scheme 1) has been previously mentioned in the literature but was not fully characterized.[45] We have prepared **1** in excellent yield (96%) as a red powder via a modified synthesis reacting [$Mn(CO)_5$Br] and the corresponding imino-pyridine *impy* in THF at 60 °C. The related complex decorated with the bidentate amino-pyridine *ampy*-ligand *fac*-[Mn(*ampy*)$(CO)_3$Br] (**2**, *ampy* = (1-(pyridin-2-yl)-N-(p-tolyl)methanamine, Scheme 1) was obtained as a yellow powder under similar reaction conditions and yield. The ^{1}H NMR spectrum of complex **1** dissolved in THF-d_8 has the characteristic singlet resonance associated with the C*H*=N imine moiety at 8.61 ppm. Resonances corresponding to the

https://doi.org/10.1021/acs.organomet.2c00387
Organometallics 2022, 41, 2798−2809

Scheme 1. Synthesis and Reactivity Pathways for Compounds 1−5

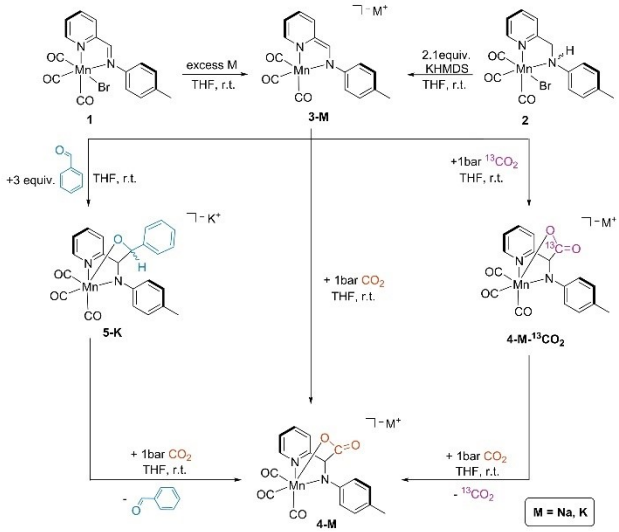

Scheme 2. Relevant Sections of the ^{1}H NMR Spectra of Complexes 1 and (3K—5K) and Assignment of the Specific Resonances (Numbering Scheme in Blue)

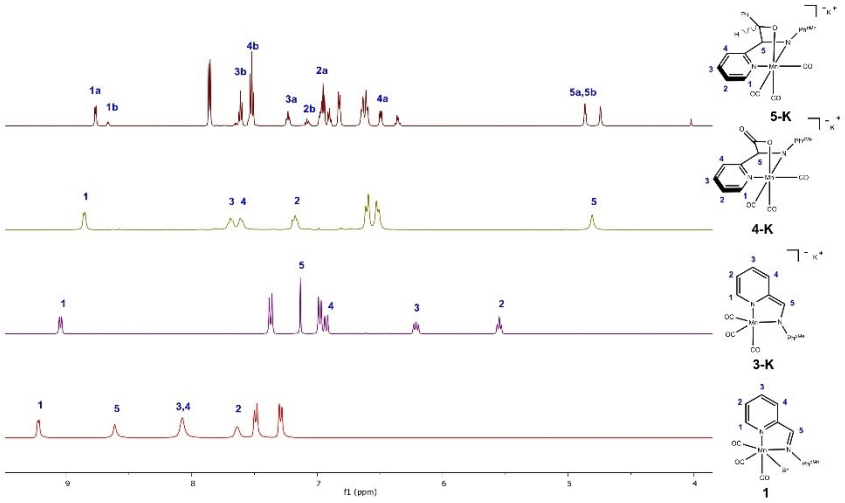

pyridine unit are at 9.22, 8.07, and 7.64 ppm. The spectral section with a numbering scheme is shown in Scheme 2. For full spectral characterization of all compounds reported, see the Experimental Section and Supporting Information. The corresponding $^{13}C\{^1H\}$ NMR spectrum has typical resonances located at higher frequencies at 224.2, 222.4, and 219.9 ppm consistent with the three CO ligands in mutual *facial* arrangement. The ^{13}C-nucleus of the imine moiety gives rise to a resonance at 166.9 ppm. The IR spectrum (ATR) has characteristic absorbances associated with the CO carbonyl ligands. Typical CO stretching vibrations were recorded at $\tilde{\nu}_{CO}$ = 2024 (s), 1935 (s), and 1912 (s) cm^{-1}. The closely related amino complex **2** has similar NMR and IR spectral features ($\tilde{\nu}_{CO}$ = 2021 (s), ν_{CO} = 1926 (s), and ν_{CO} = 1894 (s) cm^{-1}). However, the most characteristic features with respect to **1** are linked to the amino moiety: The ^{1}H NMR spectrum exhibits a broad singlet at 6.29 ppm associated with the N−H moiety, and the CH_2 methylene group is observed as two doublets of doublets at 4.81 and 4.68 ppm displaying a large geminal coupling of $^2J_{HH}$ = 15 Hz and respective smaller vicinal

https://doi.org/10.1021/acs.organomet.2c00387
Organometallics 2022, 41, 2798−2809

couplings (to N−H group) of $^{3}J_{HH}$ = 9 Hz and $^{3}J_{HH}$ = 4 Hz, respectively. Accordingly, the $^{13}C\{^{1}H\}$ NMR spectrum has a resonance at 59.4 ppm associated with the CH_2 methylene unit.

Complexes **1** and **2** were crystallized via slow diffusion of *n*-hexane into solutions of the according complex in dichloromethane (DCM) for the former and tetrahydrofuran (THF) for the latter. Suitable single crystals were subjected to X-ray diffraction (XRD) analysis. The obtained molecular structures are shown in Figure 2. In both compounds, the manganese

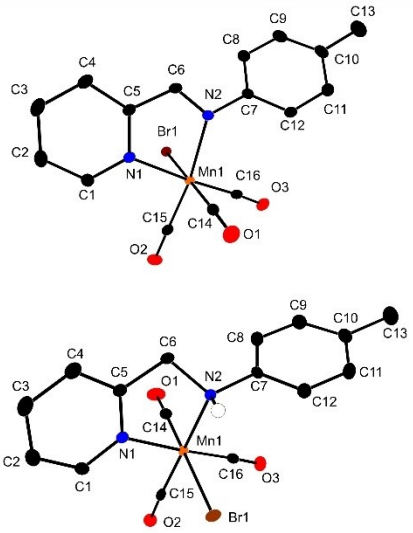

Figure 2. Diamond plots (thermal ellipsoids at 50% probability, H atoms neglected for clarity, except N−H) of complex **1** (top) and **2** (bottom). Selected bond lengths [Å] for **1**: C1−C2 = 1.393(2), C2−C3 = 1.383(2), C3−C4 = 1.389(2), C4−C5 = 1.390(2), C5−C6 = 1.447(2), C6−N2 = 1.288(2), C5−N1 = 1.358(2), Mn1−N1 = 2.052(1), Mn1−N2 = 2.058(1). For **2**: C1−C2 = 1.383(2), C2−C3 = 1.390(2), C3−C4 = 1.384(2), C4−C5 = 1.384(2), C5−C6 = 1.503(2), C6−N2 = 1.486(2), C5−N1 = 1.354(2), Mn1−N1 = 2.051(1), Mn1−N2 = 2.102(1).

center resides in an octahedral coordination sphere encompassing three CO ligands in mutual *facial* configuration. The *impy* ligand (in **1**) or respective *ampy* ligand (in **2**) chelates the Mn center via both N-donors. The bromido ligand completes the respective coordination sphere giving rise to a neutral complex. Complex **1** has a characteristic short C6−N2 interatomic distance (1.288(2) Å) for the C=N double bond of the imine group. In accordance, complex **2** exhibits an elongated C6−N2 distance of 1.486(2) Å for the respective amine moiety. Noteworthy, also the Mn1−N2 interatomic distance in the imino complex **1** is significantly shorter with respect to the amino analogue **2**. The difference accounts to Δ 0.044 Å (2.058(1) Å in **1** and 2.102(1) in **2**). The pyridine rings in both complexes show almost equidistant C−C and C−N bonds indicating a delocalized π-system. Overall, the determined structures compare well to the previously reported Re(I) complexes with an analogous coordination sphere.[38,46]

The reduction of complex **1** using an excess of potassium metal results in a change of color from red to deep purple. A diamagnetic species is formed, which is very reactive and was not isolated, but could be well studied in solution by means of ^{1}H- and $^{13}C\{^{1}H\}$ NMR spectroscopy. We assign the quantitatively formed species to the two-electron reduced anionic manganate complex K[Mn(*amidopy**)$(CO)_3$] (**3**, the asterisk indicates the two-electron-reduced ligand resulting in the disturbed π-delocalization within the pyridine unit). The reduced ligand gives rise to a substantial upfield shift of the ^{1}H NMR resonances of the pyridine ring 9.05 (d, $^{3}J_{HH}$ = 6.3 Hz, 1H, $CH_{Py\text{-}1}$), 6.93 (d, $^{3}J_{HH}$ = 8.6 Hz, 1H, $CH_{Py\text{-}4}$), 6.21 (dd, $^{3}J_{HH}$ = 7.8, 6.6 Hz, 1H, $CH_{Py\text{-}3}$), and 5.55 (t, $^{3}J_{HH}$ = 6.0 Hz, 1H, $CH_{Py\text{-}2}$). Respectively, also the methine CH resonance at 7.13 (s, 1H, NCH) exhibits an upfield shift of Δδ 1.48 ppm. Relevant sections of the ^{1}H NMR spectra of **2** and **3** are displayed in Scheme 2. The carbonyl ligands give rise to a single broad resonance in the $^{13}C\{^{1}H\}$ NMR spectrum at 235.1 ppm suggesting the loss of the Br ligand and a rather dynamic structure with fast exchange of the CO ligands, likewise previously observed for the related Re(I) species.[38,47] The resonance for the ^{13}C nucleus associated with the methine C(H)N moiety experiences a drastic upfield-shift of Δδ 39.1 ppm with respect to **1**. The ^{13}C resonances of the pyridine carbons are shifted upfield as well, which is most pronounced for the positions Py-2 and Py-3 (for details, see the Supporting Information). Overall, the two-electron reduction of **1** gives rise to upfield shifts of ^{1}H and ^{13}C resonances associated with the pyridine ring as well as the imine moiety. This effect is frequently observed upon deprotonation of a methylene "arm" in pyridine-based pincer-type complexes[48] also with Mn(I) carbonyl motifs[20,42,49] allowing for MLC substrate activation via a "dearomatization−rearomatization" sequence. With respect to the observed reactivity (see below), this prompts us to consider complexes **1** and **3** as a structurally related diamagnetic aromatized−dearomatized redox couple (ligand centered) with a Mn metal center in the formal oxidation state +I, although, naturally, other possible resonance structures may contribute to the overall electronic structure. Along these lines, it is remarkable that amino complex **2** can be converted into the "dearomatized" complex **3** via reaction with two equivalents of base KHMDS (Scheme 1; KOtBu and NaOEt are also suitable bases; however, utilization thereof requires a slight excess).

2.1. Reactivity Study of 3-M. Complex **3-K** reacts readily with CO_2 gas to form the [1,3]-addition product (with respect to the addition to the complex). The reaction proceeds via C−C and Mn−O bond formation under concomitant rearomatization of the pyridine unit. Crystallization via slow diffusion of *n*-hexane into a THF solution at −16 °C in the presence of 18-*crown*-6 ether allows for the isolation of the anionic carboxylate species *fac*-[K(18-crown-6)][Mn(*amidopy-COO*)$(CO)_3$] (**4-K-*crown***, Figure 3) as red brown crystals. The analogous compound bearing a Na^+ counter cation can be obtained via the same reaction sequence starting from complex **1** and sodium metal utilizing the suitable 15-*crown*-5 ether to give *fac*-[Na(15-crown-5)][Mn(*amidopy-COO*)$(CO)_3$] (**4-Na-*crown***). For NMR spectroscopic and structural details from single-crystal XRD, see the Experimental Section and Supporting Information. In accordance with a "rearomatization", the ^{1}H NMR resonances of **4-K** in the pyridine ring characteristically shift (back) down-field (8.84 (d, $^{3}J_{HH}$ = 2.8 Hz, 1H, $CH_{Py\text{-}1}$), 7.67 (s, 1H, $CH_{Py\text{-}3}$), 7.60 (s, 1H, $CH_{Py\text{-}4}$),

https://doi.org/10.1021/acs.organomet.2c00387
Organometallics 2022, 41, 2798−2809

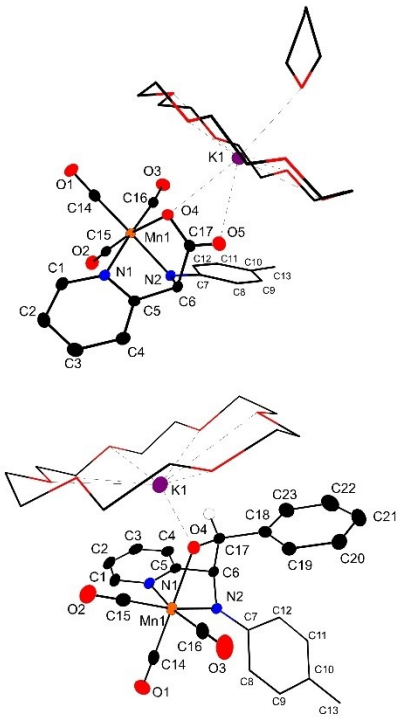

Figure 3. Diamond plots (thermal ellipsoids at 50% probability, H atoms neglected for clarity, except for benzylic C−H of complex **4-K-*crown*** (top) and **5-K-*crown*** (bottom). Selected bond lengths [Å] for **4-K-*crown***: C1−C2 = 1.380(2), C2−C3 = 1.390(3), C3−C4 = 1.391(3), C4−C5 = 1.386(2), C5−C6 = 1.511(2), C6−C17 = 1.544(2), C17−O4 = 1.291(2), C17−O5 = 1.237(2), C6−N2 = 1.467(2), C5−N1 = 1.350(2), Mn1−N1 = 2.046(1), Mn1−N2 = 2.026(2), Mn1−O4 = 2.084(1), K1−O4 = 2.920(1), K1−O5 = 2.797(1). For **5-K-*crown***: C1−C2 = 1.379(3), C2−C3 = 1.385(3), C3−C4 = 1.382(3), C4−C5 = 1.390(3), C5−C6 = 1.507(3), C6−C17 = 1.571(2), C17−O4 = 1.393(2), C6−N2 = 1.452(3), C5−N1 = 1.344(3), Mn1−N1 = 2.055(2), Mn1−N2 = 2.003(2), Mn1−O4 = 2.065(1), K1−O4 = 2.613(1).

and 7.14 (s, 1H, $CH_{Py\text{-}2}$)), and most noticeably, the NCH(COO) proton, residing in the α-position between the amido-nitrogen and carboxylate carbon, gives rise to a strongly upfield-shifted singlet resonance at 4.80 ppm (Scheme 2, green trace, no 18-*crown*-6 present). The ^{13}C nucleus of the carboxylate group gives rise to a new singlet at 180.7 ppm in the $^{13}C\{^1H\}$ NMR spectrum. As a result of the newly formed C−C bond upon CO_2 incorporation into the ligand scaffold, the two-dimensional $^1H-^{13}C$ HMBC NMR spectrum has a significant cross peak of the latter ^{13}C resonance and the proton resonance at 4.80 ppm (NCH(COO) moiety). For spectral details, see the Supporting Information. The IR spectrum shows the corresponding absorption at 1644 cm^{-1} for the carboxylate group. Single crystals suitable for XRD analysis were grown from THF solutions in the presence of 18-*crown*-6 ether. The molecular structure of **4-K-*crown*** is shown in Figure 3.

The Mn center resides in a distorted octahedral coordination sphere with three CO ligands in *facial* arrangement. Upon incorporation of CO_2 into the *amidopy* ligand scaffold, a tridentate N,N,O coordination mode is established, which completes the octahedral coordination sphere. The pyridine C−C interatomic distances are all similar (1.39 Å) suggesting a rearomatization. Correspondingly, the N2−C6 and C5−C6 interatomic distances of 1.467(2) Å and 1.511(2) Å, respectively, suggest the formation of single bonds. The charge of the anionic complex is balanced by a potassium cation chelated within the *18-crown-6* ether, and a THF solvent molecule coordinates the potassium in the apical position. Close contacts are observed between K1 and the two carboxylate oxygen atoms O4 and O5 (2.920(1) and 2.797(1) Å, respectively). Although the carboxylic C−C bond in the *amidopy-COO* ligand is not unusually elongated[31,38] within the XRD structure (C6−C17 = 1.544(2)), the CO_2 binds reversibly in complex **4-K** in THF solution. This matter was investigated via the utilization of isotopically labeled $^{13}CO_2$. Complex **3-K** was dissolved in THF-d_8 and reacted with $^{13}CO_2$ gas to give K[Mn(amidopy-^{13}COO)-$(CO)_3$] (**4-K-$^{13}CO_2$**). The reaction was monitored via $^{13}C\{^1H\}$ NMR spectroscopy. Formation of **4-K-$^{13}CO_2$** gives rise to an intense singlet at 182.4 ppm for the ^{13}COO carboxylic carbon nucleus. A doublet resonance associated with the neighboring carbon nucleus (C6, N(H)C-^{13}COO) appears at 76.0 ppm with a $^1J_{CC}$ coupling constant of 53.6 Hz, which agrees well with the previously observed related Re(1) compound.[38] Upon purging of the NMR tube and pressurizing it with 1 bar of nonlabeled CO_2 gas, an exchange of the ^{13}COO moiety was observed. While in the related Re-complex K[Re(amidopy-^{13}COO)$(CO)_3$],[38] the exchange reaction occurred relatively slow at elevated temperatures (72 h at 75 °C), this process occurs more rapidly in complex **4-K-$^{13}CO_2$** even at ambient temperature. Figure 4 includes $^{13}C\{^1H\}$ NMR spectral sections relevant to the exchange process: Section I contains the doublet resonance (76.0 ppm, $^1J_{CC}$ = 53.6 Hz)

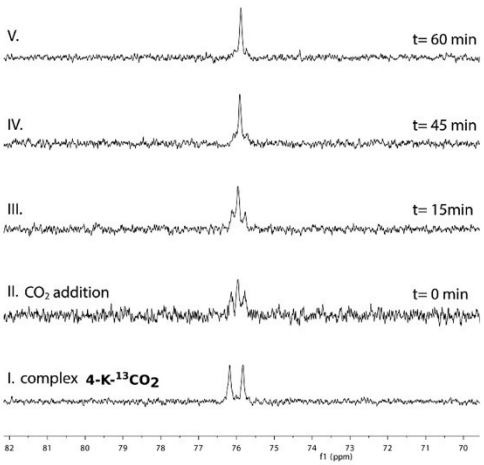

Figure 4. Sections of the $^{13}C\{^1H\}$ NMR spectra relevant to the carboxylic carbon nucleus in **4-K**/**4-K-$^{13}CO_2$**.

https://doi.org/10.1021/acs.organomet.2c00387
Organometallics 2022, 41, 2798−2809

associated with the carbon nucleus in C6 significant for the $^{13}CO_2$ incorporation in complex **4-K-$^{13}CO_2$**. Upon addition of nonlabeled CO_2 at ambient temperature, an additional singlet resonance can be instantly observed for C6. The absence of the $^1J_{CC}$ coupling is indicative for the formation of the nonlabeled complex **4-K** (Section 2). Over time (1 h), the intensity of the doublet resonance gradually reduces, indicating the exchange reaction at ambient temperature. Under analogous reaction conditions, the exchange reaction in *fac*-Na[Mn(*amidopy-*^{13}*COO*)(CO)$_3$] (**4-Na-$^{13}CO_2$**) appears noticeable hampered with respect to **4-K-$^{13}CO_2$** as the formation of **4-Na** requires longer reaction times (see SI Figure 49S).

Complex **3-K** shows further significant reactivity: When a THF-d_8 solution of **3-K** is reacted in an NMR tube with three equivalents of benzaldehyde, an adduct is readily and quantitatively formed at ambient temperature. The cooperative [1,3]-addition of the C=O double bond of the aldehyde across the Mn center and the ligand scaffold results in an alkoxy moiety under concomitant formation of new Mn−O and C−C bonds, similarly to the carboxylate formation in the reaction between **3-K** and CO_2. In contrast, the addition of the prochiral benzaldehyde to **3-K** gives rise to a diastereomeric mixture of K[Mn(*amidopy-ba*)(CO)$_3$] (**5-K**) in a ratio of 85:15 (5a/5b). Consistently, two sets of NMR resonances are observed as a result of the formed diastereomeric mixture. The rearomatization of the pyridine unit is indicated by the downfield shift of the associated ^{1}H NMR resonances in the range between 8.77 and 6.49 ppm. In accordance, the NCH proton resonances are observed as singlets at 4.87 and 4.86 ppm for the respective diastereomer. The former aldehyde C(H) = O ^{1}H NMR resonance drastically shifts from 9.96 ppm (free benzaldehyde) to lower frequencies, due to bond order reduction caused by the concomitant formation of the C−C and Mn−O bonds. Accordingly, the formed alkoxy ligand gives rise to the HC−O singlet resonances at 4.74 and 4.02 ppm, for the respective diastereomer. For a relevant ^{1}H NMR spectral section, see Scheme 2 (brown trace). Consequently, the ^{13}C{^{1}H} NMR resonances of the formed alkoxy carbon nuclei experience a similar drastic shift and are observed at 77.0 and 78.1 ppm, respectively (192.2 ppm in free benzaldehyde).

Crystals of [K(*18-crown-6*)][Mn(*amidopy-ba*)(CO)$_3$] (**5-K-*crown***) were obtained from concentrated THF/*n*-hexane layered solutions at −16 °C in the presence of *18-crown-6* ether in 48% yield. The crystals were suitable for XRD analysis and gave rise to the molecular structure depicted in Figure 3. The obtained structure outlines a Mn(I) center in a distorted octahedral coordination environment. All three CO ligands are located on one face of the octahedron. The amido-pyridine ligand is C−C coupled with benzaldehyde to give the tridentate pyridine-amido-alkoxide ligand, consistently in *fac* arrangement coordinating the Mn(I) center. The overall negative charge of the complex is compensated by a potassium cation chelated by the crown ether. A close contact between K1 and O4 of the alkoxide is observed (2.613(1)). The newly formed C6−C17 bond gives rise to an interatomic distance of = 1.571(2)Å. The C−C distances in the pyridine ring are almost equidistant (1.38−1.39 Å) suggesting the rearomatization.

The C5−C6, C6−17, C6-N2, and C17−O4 interatomic distances within the five-membered metalla cycles fall all in the range of single bonds indicating the formation of the alkoxide moiety similarly observed in a related adduct of benzaldehyde and a Ru PNN pincer complex.[40] The addition of benzaldehyde to **4-K** appears to be reversible. Similar reactivity was previously observed for Ru pincer-type complexes via an MLC route when reacted with aldehydes.[40,50] A mixture of **3-K** and three equivalents of benzaldehyde gives rise to **5-K**. Subjection of the mixture to 1 bar of CO_2 gas results in the formation of the carboxylate complex **4-K** suggesting aldehyde bonding under reversible C−C and Mn−O bond formation at ambient temperature.

Quantum chemical investigations using density functional theory (DFT) on the B97D3/def2-SVP level of theory were performed to gain further insight into the ligand-centered activation of benzaldehyde and CO_2. The molecular structures of the anionic complexes in [**4**]$^-$ and [**5**]$^-$ in the solid state are well reproduced by the DFT-optimized geometries, which were confirmed to be energetic minima via frequency calculations by the absence of imaginary frequencies. The formation of **4** and **5** from complex **3** and benzaldehyde or CO_2 was calculated to be exothermic, ranging from $\Delta H = -1.7$ kcal/mol for [**4**]$^-$ to $\Delta H = -11.0$ kcal/mol for [**5**]$^-$. However, the corresponding Gibbs energy for both reactions remained positive ($\Delta G \approx 3.6-10.9$ kcal/mol, Table 1), suggesting a

Table 1. Calculated Results Based on DFT (B97D3/def2-TZVP)

formation of	TS ($\Delta H/\Delta G$ in kcal/mol)	$\Delta H/\Delta G$ in kcal/mol
[**4**]$^-$	−0.7/11.1	−1.7/10.9
[**4**][**K(18-*crown*-6)(thf)**]		−5.3/5.2
4-K	−10.4/2.2	−16.6/−2.8
4-Na	−10.3/1.2	−15.7/−3.4
4-Li	−9.1/1.5	−18.7/−6.4
[**5**]$^-$	−10.6/4.7	−11.0/3.6

dominating entropy contribution and a strong temperature dependence for these reaction steps. For the activation of benzaldehyde, the transition state **TS$_{3/5}$**, connecting **3** and **5** (Figure 5), was calculated to be 4.7 kcal/mol higher in Gibbs energy than the starting materials. The C···C distance between the ligand carbon atom and the carbonyl carbon atom of benzaldehyde in **TS$_{3/5}$** was found to be 1.947 Å, in line with a significant degree of pyramidalization for both carbon atoms with respect to **3** (345.6−348.1° vs 332.6−335.5° in **5**).

Similar findings were obtained for the activation of CO_2 by complex **3**, which is uphill in Gibbs energy by 10.9 kcal/mol with respect to the starting materials. The corresponding transition state **TS$_{3/4}$** for the CO_2 activation by **3** was calculated to be 11.1 kcal/mol higher in Gibbs energy than the starting materials. In a similar manner to the benzaldehyde activation, one oxygen atom of the CO_2 molecule binds to the central manganese atom, while the C−C bond is being formed with a $d_{C\cdots C}$ of 1.885 Å in **TS$_{3/4}$**. The CO_2 molecule in the transition state displays a significant degree of bending ($\angle_{OCO}$ = 141°).

As both activation products, **4-K** and **5-K**, crystalize with a [K(18-*crown*-6)(thf)$_n$]$^+$ counter ion (n = 0, 1) and the O → Mn coordination in the product complexes and in the transitions seem to be relevant for the activation step, we investigated the role of the counter ion in these reactions. The CO_2-activation step in the presence of [K(18-*crown*-6)(thf)]$^+$ turns out to be less endergonic with ΔG = 5.2 kcal/mol and more exothermic (ΔH = −5.2 kcal/mol).

https://doi.org/10.1021/acs.organomet.2c00387
Organometallics 2022, 41, 2798−2809

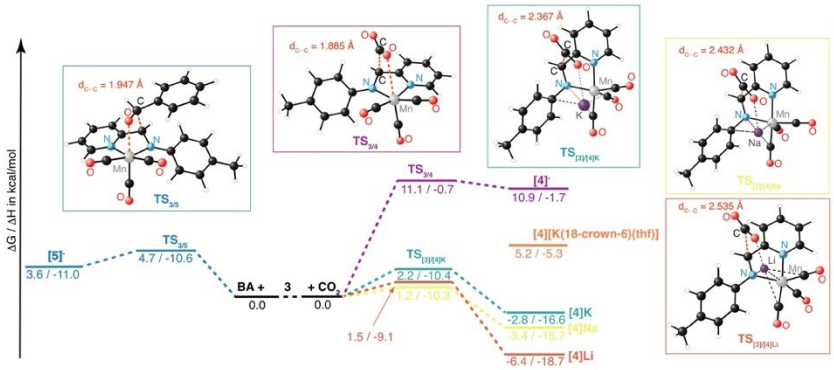

Figure 5. Calculated reaction pathways for the activation of benzaldehyde (BA) and CO_2 by complex **3** with different alkali metal counter ions 298.15 K (G16, B97D3/def2-SVP/SMD(THF)).

Using a potassium counter ion with an implicit solvation model based on density (SMD) for THF, the reaction with CO_2 becomes more exothermic with −16.6 kcal/mol and exergonic with ΔG = −2.8 kcal/mol. The reaction barrier in the presence of an implicitly solvated potassium ion ($\mathbf{T_{3/[4]K}}$) is significantly reduced too (ΔG = 2.2 kcal/mol). The C···C distance in the transition $\mathbf{T_{3/[4]K}}$ ($d_{C\cdots C}$ = 2.367 Å) is considerably elongated with respect to $\mathbf{TS_{3/4}}$, and the $\angle_{OCO}$ is with 153° larger than without counter ions. With the lighter homologue sodium, similar observations are made: the CO_2-activation step is approx. equally exothermic in enthalpy (ΔH = −15.7 kcal/mol) and slightly more exergonic than with potassium. The reaction barrier $\mathbf{T_{3/[4]Na}}$ (ΔG = 1.2 kcal/mol) is reduced with respect to $\mathbf{T_{3/[4]K}}$, and an increased elongation of the C···C distance is observed in this transition state ($d_{C\cdots C}$ = 2.432 Å). This trend is in part continued for the lightest homologue, lithium, investigated in this series: a transition state ($\mathbf{T_{3/[4]Li}}$) was located with a C···C distance of 2.535 Å, which was found to be slightly higher in Gibbs energy than with sodium (ΔG = 1.5 kcal/mol), whereas the CO_2-activation step itself becomes more favorable (ΔG = −6.4 kcal/mol). From the calculated reaction profiles, it becomes evident that the barriers for reversible CO_2 binding to complex **3** in the presence of K^+ and Na^+ counter ions are in a similar range, whereas **[4]Li** is expected to show decreased reversibility of the CO_2 activation. In this regard, we have experimentally observed that $^{13}CO_2/CO_2$ exchange in **4-Na-$^{13}CO_2$** and **4-K-^{13}CO2** occurs in the range of minutes to hours (for details, see Figure 46S and 49S), whereas, unfortunately, **4-Li** was not sufficiently stable to allow for the investigation of such exchange reactions. Considering the impact of the alkaline metal counter ion and its solvation on ΔH and ΔG, as well as on the structure of the connecting transition states for this reaction step, the cationic counter ion plays a decisive role in the bond activation reactions that can make this bond activation feasible.

3. SUMMARY AND CONCLUSIONS

The iminopyridine (*impy*) ligand in complex **1** is readily reduced by potassium metal to give the anionic "dearomatized" complex **3-K**, which can serve as an MLC platform. Likewise, complex **3-K** can be formed via the double deprotonation of the related amino-pyridine ligand in complex **2** (Scheme 1). The latter reaction is reminiscent to the often-reported "aromatization−dearomatization" sequence in pyridine-based pincer complexes with relevance to atom-economic cooperative catalysis.[48,51] Against this background, complex **3-K** exhibits similar reactivity as it features a C-nucleophilic carbon moiety within the metalla cycle, which can prompt the reversible addition of a C═O (carbonyl) bond in CO_2 and benzaldehyde under concomitant C−C and Mn−O bond formation to give rise to complex **4-K** and **5-K**, respectively. Similar to our previously reported triscarbonyl complex K[Re(*impy*](CO)$_3$][38,46] utilizing the heavier homologue rhenium, the addition of the substrates is reversible: Pressurizing a THF solution of the $^{13}CO_2$ adduct **4-M-$^{13}CO_2$** (M = Na, K) or the benzaldehyde adduct **5-K** with 1 bar of CO_2 results in an exchange reaction to form complex **4-M**. This process occurs already fast at ambient temperature and does not require elevated temperatures as previously observed for the analogous rhenium complex. Quantum chemical investigations using DFT reveal the impact of the particular alkali counter ion upon cooperative C═O activation. The counter ion, as well as its mode of solvation, impacts ΔH and ΔG, as well as the structure of the connecting transition states for the specific substrate activation of CO_2 or benzaldehyde, respectively. In summary our investigations show that the counter ion has a significant impact on the MLC bond activation reactions in such an anionic MLC cooperative platform.

4. EXPERIMENTAL SECTION

The synthetic work was performed using standard Schlenk- and glove-box techniques under an argon protective atmosphere. All reagents were purchased from commercial sources (Sigma-Aldrich, ABCR) and were used as received. THF-d_8 (ABCR) was degassed and dried over molecular sieves prior use. $^{13}CO_2$ was purchased from Westfalen Gas, Germany. All solvents were collected from the solvent purification system SPS800 by MBraun and stored over 4 Å molecular sieves. Both ligands (1-(pyridin-2-yl)-N-(p-tolyl)methanimine (*impy*) and 1-(pyridin-2-yl)-N-(p-tolyl)methanamine (*ampy*)) were prepared as previously described in the literature.[38,52] Compound **1** has been previously reported.[45] NMR spectra were recorded

https://doi.org/10.1021/acs.organomet.2c00387
Organometallics 2022, 41, 2798−2809

on a Bruker Avance Neo 600 MHz and Bruker Avance 360NB spectrometer at 23 °C unless otherwise described. Chemical shifts for ^{1}H-NMR spectra were reported as δ with respect to tetramethylsilane (parts per million) referenced to the residual signal of THF at 1.72 ppm. Chemical shifts for $^{13}C\{^1H\}$ NMR spectra were reported as δ with respect to tetrametylsilan (parts per million) referenced to the signal of THF at 25.3 ppm. HR-ESI mass spectra were recorded on a Thermo Fisher Scientific LTQ Orbitrap XL hybrid ion trap mass spectrometer.

4.1. [Mn(*impy*)(CO)$_3$Br] (1). Bromopentacarbonylmanganese(I) (250 mg, 0.91 mmol) and 1.1 equiv of *impy* (196 mg, 1.00 mmol) dissolved in 10 mL of THF were stirred at 60 °C in an occasionally ventilated Schlenk vessel for 8 h. Subsequently, the mixture was stirred over night at ambient temperature. *n*-Hexane was added to the formed red solution upon which the product precipitated. The obtained red powder was decanted from the mother liquor, subsequently washed with *n*-hexane, and finally dried in a vacuum. Yield: 362 mg (0.87 mmol, 96%). Solution of complex **1** in DCM layered with *n*-hexane gave rise to red single crystals suitable for XRD analysis. ^{1}H NMR (360 MHz, THF-d8) δ 9.22 (d, $^3J_{HH}$ = 4.5 Hz, 1H, $CH_{Py\text{-}1}$), 8.61 (s, 1H, NCH), 8.07 (s, 2H, $CH_{Py\text{-}3,4}$), 7.64 (s, 1H, $CH_{Py\text{-}2}$), 7.49 (d, $^3J_{HH}$ = 7.7 Hz, 2H, $CH_{Ar\text{-}6,9}$), 7.29 (d, $^3J_{HH}$ = 7.6 Hz, 2H, $CH_{Ar\text{-}7,8}$), 2.39 (s, 3H, CH_3). $^{13}C\{^1H\}$ NMR (91 MHz, THF-d8) δ 224.18 (s, 1C, Mn−CO), 222.39 (s, 1C, Mn−CO), 219.88 (s, 1C, Mn−CO), 166.89 (s, 1C, NCH), 156.53 (s, 1C, $C_{Py\text{-}quart}$), 154.73 (s, 1C, $CH_{Py\text{-}1}$), 151.34 (s, 1C, $NC_{Ar\text{-}quart}$), 139.23 (s, 1C, $C_{Ar\text{-}10\text{-}quart}$), 139.21 (s, 1C, $CH_{Py\text{-}3}$), 130.40 (s, 2C, $CH_{Ar\text{-}9,11}$), 129.37 (s, 1C, $CH_{Py\text{-}4}$), 128.18 (s, 1C, $CH_{Py\text{-}2}$), 122.58 (s, 2C, $CH_{Ar\text{-}8,12}$), 21.11 (s, 1C, CH_3). IR (ATR) ν/cm^{-1}: $\tilde{\nu}_{CO}$ = 2024 (s), $\tilde{\nu}_{CO}$ = 1935 (s), $\tilde{\nu}_{CO}$ = 1912 (s). HRMS-ESI CH_3CH_2OH/CH_2Cl_2 (m/z): $[M + Na]^+$ calcd for $C_{16}H_{12}N_2O_3{}^{79}BrMnNa^+$ 436.93040; found 436.93082 (0.9 ppm), $[M + Na]^+$ calcd for $C_{16}H_{12}N_2O_3{}^{81}BrMnNa^+$ 438.92852; found 438.92871 (0.43 ppm), $[M\text{-}(3CO) + Na]^+$ calcd for $C_{13}H_{12}N_2{}^{79}BrMnNa^+$ 352.94566; found 352.94601 (1.0 ppm), $[M\text{-}(3CO) + Na]^+$ calcd for $C_{13}H_{12}N_2{}^{81}BrMnNa^+$ 354.94370; found 354.94394 (0.68 ppm), $[M\text{-}(3CO,Br,Mn) + Na]^+$ calcd for $C_{13}H_{12}N_2Na^+$ 219.08927; found 219.08952 (1.1 ppm).

4.2. [Mn(*ampy*)(CO)$_3$Br] (2). Bromopentacarbonylmanganese(I) (247 mg, 0.90 mmol) and 1.1 equiv of *ampy* (196 mg, 0.99 mmol) were dissolved in 10 mL of THF and heated at 60 °C for 8 h under constant stirring in an occasionally ventilated Schlenk vessel. Subsequently, the mixture was stirred over night at ambient temperature. To the obtained yellow solution, *n*-hexane was added, causing the product to precipitate. The yellow powder was decanted from the mother liquor, subsequently washed with *n*-hexane, and finally dried in a vacuum. Yield: 352.1 mg (0.84 mmol, 94%). A solution of **2** in THF layered with *n*-hexane allows for the growth of yellow crystals suitable for single-crystal X-ray diffraction analysis.^{1}H NMR (360 MHz, THF-d8) δ 8.96 (d, $^3J_{HH}$ = 5.2 Hz, 1H,$CH_{Py\text{-}1}$), 7.90 (t, $^3J_{HH}$ = 7.2 Hz, 1H, $CH_{Py\text{-}3}$), 7.54 (d, $^3J_{HH}$ = 7.5 Hz, 1H, $CH_{Py\text{-}4}$), 7.45 (t, $^3J_{HH}$ = 6.4 Hz, 1H, $CH_{Py\text{-}2}$), 7.23 (t, $^3J_{HH}$ = 8.6 Hz, 2H, $CH_{Ar\text{-}8/11}$), 7.16 (d, $^3J_{HH}$ = 8.2 Hz, 2H, $CH_{Ar\text{-}9/10}$), 6.29 (s, 1H, NH), 4.81 (dd, J_{HH} = 14.9, 8.9 Hz, 1H, CH_2), 4.68 (dd, J_{HH} = 15.5, 4.5 Hz, 1H, CH_2), 2.30 (s, 3H, CH_3). $^{13}C\{^1H\}$ NMR (91 MHz, THF-d8) δ 224.12 (s, 1C, Mn−CO), 222.87 (s, 1C, Mn−CO), 221.73 (s, 1C, Mn−CO), 161.04 (s, 1C, $C_{Py\text{-}quart}$), 154.48 (s, 1C, $CH_{Py\text{-}1}$), 148.49 (s, 1C, $NC_{Ar\text{-}quart}$), 139.26 (s, 1C, $CH_{Py\text{-}3}$), 135.28 (s, 1C, $C_{Ar\text{-}quart}$), 130.57 (s, 2C, $CH_{Ar\text{-}9,11}$), 125.36 (s, 1C, $CH_{Py\text{-}2}$), 122.27 (s, 1C, $CH_{Py\text{-}4}$), 119.21 (s, 2C, $CH_{Ar\text{-}8,12}$), 59.36 (s, 1C, CH_2), 20.76 (s, 1C, CH_3). IR (ATR) ν/cm^{-1}: $\tilde{\nu}_{CO}$ = 2021 (s), $\tilde{\nu}_{CO}$ = 1926 (s), $\tilde{\nu}_{CO}$ = 1894 (s). HRMS-ESI CH_3CH_2OH/CH_2Cl_2 (m/z): $[M + Na]^+$ calcd for $C_{16}H_{14}{}^{79}BrMnN_2O_3Na^+$ 438.94605; found 438.94578 (0.6 ppm), $[M + Na]^+$ calcd for C16H14^{81}BrMnN$_2$O$_3$Na$^+$ 440.94417; found 440.94373 (1.0 ppm), $[M\text{-}Br]^+$ calcd for $C_{16}H_{14}MnN_2O_3^+$ 337.03794; found 337.03781 (0.4 ppm), $[M\text{-}Br\text{-}3CO]^+$ calcd for $C_{13}H_{14}MnN_2^+$ 253.0532; found 253.05309 (0.4 ppm).

4.3. K[Mn(*amidopy)(CO)$_3$Br] (3-K).** Method **A** reduction using potassium metal: 17.7 mg of [Mn(*impy*)(CO)$_3$Br] (**1**) (0.043 mmol) was dissolved in 0.8 mL of THF-d$_8$ in a J. Young-NMR tube. Excess potassium metal (6.7 mg, 0.17 mmol, 4.0 equiv) was added to the red solution, and the mixture was sonicated until the color changed to deep purple, and ^{1}H NMR-spectral monitoring indicated the quantitative formation of **3**. ^{1}H NMR (360 MHz, THF-d$_8$) δ 9.05 (d, $^3J_{HH}$ = 6.3 Hz, 1H, $CH_{Py\text{-}1}$), 7.37 (d, $^3J_{HH}$ = 8.0 Hz, 2H, $CH_{Ar\text{-}6,9}$), 7.13 (s, 1H, NCH), 6.98 (d, $^3J_{HH}$ = 7.9 Hz, 2H, $CH_{Ar\text{-}7,8}$), 6.93 (d, $^3J_{HH}$ = 8.6 Hz, 1H, $CH_{Py\text{-}4}$), 6.21 (dd, $^3J_{HH}$ = 7.8, 6.6 Hz, 1H, $CH_{Py\text{-}3}$), 5.55 (t, $^3J_{HH}$ = 6.0 Hz, 1H, $CH_{Py\text{-}2}$), 2.29 (s, 3H, CH_3). $^{13}C\{^1H\}$ NMR (91 MHz, THF-d8) δ 235.1 (s, 3C, Mn−CO), 159.5 (s, 1C, $NC_{Ar\text{-}quart}$), 154.3 (s, 1C, $CH_{py\text{-}1}$), 145.0 (s, 1C, $C_{Py\text{-}quart}$), 131.3 (s, 1C, $C_{Ar\text{-}quart}$), 128.7 (s, 2C, $CH_{Ar\text{-}9,11}$), 127.8 (s, 1C, NCH), 125.5 (s, 2C, $C_{Ar\text{-}8,12}$), 122.8 (s, 1C, $CH_{Py\text{-}4}$), 120.5 (s, 1C, $CH_{Py\text{-}3}$), 105.1 (s, 1C, $CH_{Py\text{-}2}$), 21.0 (s, 1C, CH_3).

*4.3.1. Method **B** Deprotonation Using KHMDS.* First, 19.8 mg of [Mn(*ampy*)(CO)$_3$Br] (**2**) (0.047 mmol) was transferred into a *J. Young*-NMR tube and dissolved in 1.2 mL of THF-d$_8$. Upon addition of 19.7 mg of KHMDS (2.1 equiv), an immediate color change occurred from yellow to violet. ^{1}H NMR-spectral monitoring indicated the quantitative formation of **3-K**. ^{1}H NMR (600 MHz, THF-d$_8$) δ 9.04 (s, 1H, $CH_{Py\text{-}1}$), 7.37 (s, 2H, $CH_{Ar\text{-}6,9}$), 7.13 (s, 1H, NCH), 6.98 (s, 2H, $CH_{Ar\text{-}7,8}$), 6.93 (s, 1H, $CH_{Py\text{-}4}$), 6.21 (s, 1H, $CH_{Py\text{-}3}$), 5.55 (s, 1H, $CH_{Py\text{-}2}$), 2.29 (s, 3H, CH_3). $^{13}C\{^1H\}$ NMR (151 MHz, THF-d$_8$) δ 235.2 (s, 3C, Mn−CO), 159.5 (s, 1C, $NC_{Ar\text{-}quart}$), 154.3 (s, 1C, $CH_{py\text{-}1}$), 145.0 (s, 1C, $C_{Py\text{-}quart}$), 131.3 (s, 1C, $C_{Ar\text{-}quart}$), 128.7 (s, 2C, $CH_{Ar\text{-}9,11}$), 127.8 (s, 1C, NCH), 125.5 (s, 2C, $C_{Ar\text{-}8,12}$), 122.8 (s, 1C, $CH_{Py\text{-}4}$), 120.5 (s, 1C, $CH_{Py\text{-}3}$), 105.1 (s, 1C, $CH_{Py\text{-}2}$), 21.0 (s, 1C, CH_3).

*4.3.2. Method **C** Deprotonation Using KOtBu.* First, 8.2 mg of [Mn(*ampy*)(CO)$_3$Br] (**2**) (0.022 mmol) in a *J. Young*-NMR tube was dissolved in 0.5 mL of THF-d$_8$, and 3.0 equiv (7.4 mg, 0.066 mmol) of KOtBu was added. An immediate color change from yellow to violet was visible. ^{1}H NMR-spectral monitoring indicated the quantitative formation of **3**. ^{1}H NMR (600 MHz, THF-d$_8$) δ 9.04 (d, $^3J_{HH}$ = 6.4 Hz, 1H, $CH_{Py\text{-}1}$), 7.37 (d, $^3J_{HH}$ = 8.1 Hz, 2H, $CH_{Ar\text{-}6,9}$), 7.13 (s, 1H, NCH), 6.98 (d, $^3J_{HH}$ = 8.0 Hz, 2H, $CH_{Ar\text{-}7,8}$), 6.93 (d, $^3J_{HH}$ = 8.6 Hz, 1H, $CH_{Py\text{-}4}$), 6.21 (t, $^3J_{HH}$ = 7.1 Hz, 1H, $CH_{Py\text{-}3}$), 5.55 (t, $^3J_{HH}$ = 5.8 Hz, 1H, $CH_{Py\text{-}2}$), 2.29 (s, 3H, CH_3). $^{13}C\{^1H\}$ NMR (151 MHz, THF-d$_8$) δ 235.2 (s, 3C, Mn−CO), 159.5 (s, 1C, $NC_{Ar\text{-}quart}$), 154.3 (s, 1C, $CH_{py\text{-}1}$), 145.0 (s, 1C, $C_{Py\text{-}quart}$), 131.3 (s, 1C, $C_{Ar\text{-}quart}$), 128.7 (s, 2C, $CH_{Ar\text{-}9,11}$), 127.8 (s, 1C, NCH), 125.5 (s, 2C, $C_{Ar\text{-}8,12}$), 122.8 (s, 1C, $CH_{Py\text{-}4}$), 120.5 (s, 1C, $CH_{Py\text{-}3}$), 105.1 (s, 1C, $CH_{Py\text{-}2}$), 21.0 (s, 1C, CH_3).

4.4. Preparation of Na[Mn(*amidopy)(CO)$_3$] (3-Na).** Preparation of Na[Mn(*amidopy**)(CO)$_3$] (**3-Na**) in THF-d$_8$ solution: 20.0 mg of complex **1** (0.048 mmol) was dissolved in 0.8 mL of THF-d$_8$ in a *J. Young*-NMR tube. Then, 8.0 equiv of

https://doi.org/10.1021/acs.organomet.2c00387
Organometallics 2022, 41, 2798−2809

sodium metal (8.7 mg, 0.384 mmol) was added to the red solution, the mixture was sonicated until the color changed to deep purple (6 h), and the ^{1}H NMR-spectral monitoring indicated the quantitative formation of **3-Na**. ^{1}H NMR (600 MHz, THF-d_8) δ 9.04 (d, $^3J_{HH}$ = 3.9 Hz, 1H, $CH_{Py\text{-}1}$), 7.36 (d, $^3J_{HH}$ = 7.7 Hz, 2H, $CH_{Ar\text{-}6,9}$), 7.13 (s, 1H, NCH), 6.97 (d, $^3J_{HH}$ = 7.6 Hz, 2H, $CH_{Ar\text{-}7,8}$), 6.92 (d, $^3J_{HH}$ = 8.8 Hz, 1H, $CH_{Py\text{-}4}$), 6.21 (s, 1H, $CH_{Py\text{-}3}$), 5.54 (s, 1H, $CH_{Py\text{-}2}$), 2.29 (s, 3H, CH_3). ^{13}C NMR (91 MHz, THF-d_8) δ 235.44 (s, 3C, Mn−CO), 159.60 (s, 1C, $NC_{Ar\text{-}quart}$), 154.29 (s, 1C, $CH_{py\text{-}1}$), 145.03 (s, 1C, $C_{Py\text{-}quart}$), 131.25 (s, 1C, $C_{Ar\text{-}quart}$), 128.69 (s, 2C, $CH_{Ar\text{-}9,11}$), 127.96 (s, 1C, NCH), 125.48 (s, 2C, $C_{Ar\text{-}8,12}$), 122.86 (s, 1C, $CH_{Py\text{-}4}$), 120.40 (s, 1C, $CH_{Py\text{-}3}$), 105.12 (s, 1C, $CH_{Py\text{-}2}$), 20.98 (s, 1C, CH_3).

4.5. *fac*-[K(18-*crown*-6)][Mn(*amidopy*-*COO*)(CO)$_3$] (4-K-*crown*). First, 50.2 mg (0.12 mmol) of complex **1** was dissolved in 2 mL of THF in a 10 mL Schlenk tube with a Teflon valve. Then, 4.0 equiv of potassium metal (18.9 mg, 0.48 mmol) was added to the red solution, and the mixture was sonicated until the color changed to deep purple (4 h). To the deep purple solution, 1 bar of CO_2 gas was added and the color changed to brown. The reaction mixture was filtered through a syringe filter (PTFE, 0.45 μm porosity), and 1.0 equiv of 18-*crown*-6 ether (32.0 mg, 0.12 mmol) was added. Subsequently, the brown solution was layered with *n*-hexane and allowed to crystallize at −16 °C in a freezer to obtain brown crystals suitable for X-ray diffraction analysis. Yield 64.3 mg (0.094 mmol, 78%) ^{1}H NMR (360 MHz, THF) δ 8.84 (d, $^3J_{HH}$ = 2.8 Hz, 1H, $CH_{Py\text{-}1}$), 7.67 (s, 1H, $CH_{Py\text{-}3}$), 7.60 (s, 1H, $CH_{Py\text{-}4}$), 7.14 (s, 1H, $CH_{Py\text{-}2}$), 6.59 (d, $^3J_{HH}$ = 8.2 Hz, 2H, $CH_{Ar\text{-}7,8}$), 6.53 (d, $^3J_{HH}$ = 8.1 Hz, 2H, $CH_{Ar\text{-}6,9}$), 4.80 (s, 1H, NCH), 3.52 (s, 24H, $CH_{2\text{-}Crown}$), 2.04 (s, 3H, CH_3). ^{13}C{^{1}H} NMR (91 MHz, THF) was recorded under an atmosphere of CO_2 δ 227.7 (s, 1C, Mn−CO), 227.5 (s, 1C, Mn−CO), 221.5 (s, 1C, Mn−CO), 180.7 (s, 1C, OCO), 167.6 (s, 1C, $C_{Py\text{-}quart}$), 159.9 (s, 1C, $NC_{Ar\text{-}quart}$), 152.9 (s, 1C, $CH_{Py\text{-}1}$), 137.7 (s, 1C, $CH_{Py\text{-}3}$), 129.3 (s, 2C, $CH_{Ar\text{-}9,11}$), 125.9 (s, free CO_2), 121.9 (s, 1C, $CH_{Py\text{-}2}$), 121.9 (s, s, 1C, $CH_{Py\text{-}4}$), 118.9 (s, 1C, $C_{Ar\text{-}quart}$), 115.6 (s, 2C, $CH_{Ar\text{-}8,12}$), 76.5 (s, 1C, NCH), 71.1 (s, 12C, $CH_{2\text{-}Crown}$), 20.7 (s, 1C, CH_3). IR (ATR) $\tilde{\nu}$ cm^{-1}: $\tilde{\nu}_{CO}$ = 2025 (m), $\tilde{\nu}_{CO}$ = 2000 (m), $\tilde{\nu}_{CO}$ = 1886 (s), ν_{COO} = 1644 (m). HRMS-ESI CH_3CH_2OH/CH_2Cl_2 (*m*/*z*): neg. $[M]^-$ calcd for $C_{17}H_{12}N_2O_5Mn^-$ 379.01322; found 379.01395 (1.9 ppm). The intensity of the molecular ion peak of [Mn(*amidopy*-*COO*)(CO)$_3$]$^-$ is low. [M-(CO$_2$)]$^-$ calcd for $C_{16}H_{12}N_2O_3Mn^-$ 335.02339; found 335.02368 (0.9 ppm), pos:[18*c*6 + K]$^+$ calcd for $C_{12}H_{24}KO_6^+$ 303.12045; found 303.12042 (0.1 ppm) HRMS-ESI CH3OH (0.1% formic acid)/CH_2Cl_2 (*m*/*z*): [MH + Na]$^+$ calcd for $C_{17}H_{13}N_2O_5MnNa^+$ 403.00972; found 403.00955 (0.3 ppm), [MH + H]$^+$ calcd for $C_{17}H_{14}N_2O_5Mn^+$ 381.02777; found 381.02744 (0.9 ppm).

4.6. Synthesis of Na[Mn(*amidopy*-COO)(CO)$_3$] (4-Na) in THF-d$_8$ Solution. First, 20.0 mg (0.048 mmol) of complex **1** was dissolved in 0.8 mL of THF-d_8 in a *J. Young*-NMR tube. Then, 8.0 equiv of sodium metal (8.7 mg, 0.38 mmol) was added to the red solution and the mixture was sonicated until the color changed to deep purple (6 h). Subsequently, 1 bar of CO_2 was added and the color changed to brown. ^{1}H - and ^{13}C{^{1}H} NMR-spectral monitoring indicated the quantitative formation of **4-Na**. ^{1}H NMR (600 MHz, THF-d_8) δ 8.88 (s, 1H, $CH_{Py\text{-}1}$), 7.72 (s, 1H, $CH_{Py\text{-}3}$), 7.64 (s, 1H, $CH_{Py\text{-}4}$), 7.20 (s, 1H, $CH_{Py\text{-}2}$), 6.60 (s, 2H, $CH_{Ar\text{-}7,8}$), 6.53 (s, 2H, $CH_{Ar\text{-}6,9}$), 4.87 (s, 1H, NCH), 2.05 (s, 3H, CH_3). ^{13}C{^{1}H} NMR (151 MHz, THF-d_8) δ 227.71 (s, 1C, Mn−CO), 226.85 (s, 1C, Mn−CO), 221.27 (s, 1C, Mn−CO), 183.31 (s, 1C, OCO), 166.68 (s, 1C, $C_{Py\text{-}quart}$), 159.46 (s, 1C, $NC_{Ar\text{-}quart}$), 153.22 (s, 1C, $CH_{Py\text{-}1}$), 138.12 (s, 1C, $CH_{Py\text{-}3}$), 129.33 (s, 2C, $CH_{Ar\text{-}9,11}$), 125.86 (s, free CO_2), 122.47 (s, 1C, $CH_{Py\text{-}2}$), 122.12 (s, 1C, $CH_{Py\text{-}4}$), 119.99 (s, 1C, $C_{Ar\text{-}quart\text{-}10}$), 115.63 (s, 2C, $CH_{Ar\text{-}8,12}$), 75.30 (s, 1C, NCH), 20.59 (s, 1C, CH_3).

4.7. Synthesis of *fac*-[K(15-*crown*-5)]Mn(*amidopy*-COO)(CO)$_3$] (4-Na-*crown*). First, 20.0 mg (0.048 mmol) of complex **1** was dissolved in 0.8 mL of THF-d_8 in a Young-NMR tube. Then, 8.0 equiv of sodium metal (8.7 mg, 0.38 mmol) was added to the red solution and the mixture was sonicated until the color changed to deep purple (6 h). To the deep purple solution, 1 bar of CO_2 gas was added and the color changed to brown. The reaction mixture was filtered through a syringe filter (PTFE, 0.45 μm porosity), and 1.0 equiv of 15-*crown*-5 ether (10.6 mg, 0.048 mmol) was added. The brown solution was layered with *n*-hexane at −16 °C, upon which brown crystals were obtained suitable for diffraction analysis. Yield 20.9 mg (0.034 mmol, 71%). ^{1}H NMR (600 MHz, THF-d_8) δ 8.85 (s, 1H, $CH_{Py\text{-}1}$), 7.69 (s, 1H, $CH_{Py\text{-}3}$), 7.62 (s, 1H, $CH_{Py\text{-}4}$), 7.17 (s, 1H, $CH_{Py\text{-}2}$), 6.61 (s, 2H, $CH_{Ar\text{-}7,8}$), 6.55 (s, 2H, $CH_{Ar\text{-}6,9}$), 4.81 (s, 1H, NCH), 3.57 (s, 20H, $CH_{2\text{-}crown}$), 2.05 (s, 3H, CH_3) ^{13}C{^{1}H} NMR (151 MHz, THF-d_8) δ 227.53 (s, 1C, Mn−CO), 226.98 (s, 1C, Mn−CO), 221.50 (s, 1C, Mn−CO), 181.90 (s, 1C, OCO), 166.90 (s, 1C, $C_{Py\text{-}quart}$), 159.34 (s, 1C, $NC_{Ar\text{-}quart}$), 153.06 (s, 1C, $CH_{Py\text{-}1}$), 137.90 (s, 1C, $CH_{Py\text{-}3}$), 129.30 (s, 2C, $CH_{Ar\text{-}9,11}$), 125.85 (s, free CO_2), 122.22 (s, 1C, $CH_{Py\text{-}2}$), 122.08 (s, 1C, $CH_{Py\text{-}4}$), 119.95 (s, 1C, $C_{Ar\text{-}quart\text{-}10}$), 115.82 (s, 2C, $CH_{Ar\text{-}8,12}$), 75.52 (s, 1C, NCH), 70.08 (s, 10C, 15-*crown*-5), 20.65 (s, 1C, CH_3). IR (ATR) $\tilde{\nu}$/cm^{-1}: $\tilde{\nu}_{CO}$ = 2005 (m), $\tilde{\nu}_{CO}$ = 1911 (s), $\tilde{\nu}_{CO}$ = 1879 (s), $\tilde{\nu}_{COO}$ = 1625 (s). MS: HRMS-ESI $CH3CH_2OH/CH_2Cl_2$ (*m*/*z*): neg: $[M^-]$ calcd for $C_{17}H_{12}N_2O_5Mn^-$ 379.01322; found 379.01324 (0.05 ppm), [M-(CO$_2$)]$^-$ calcd for $C_{16}H_{12}O_3N_2Mn^-$ 335.02339; found 335.02338 (0.03 ppm), [M-(3CO)]$^-$ calcd for C14H12O2N2Mn$^-$ 295.02848; found 295.02878 (1,0 ppm). pos: [15-c-5 + Na]$^+$ calcd for $C_{10}H_{20}NaO_5$ 243.12029; found 243.12042 (0.5 ppm).

4.8. *fac*-K[Mn(*amidopy*-^{13}COO)(CO)$_3$] (4-K-^{13}CO$_2$). First, 14.3 mg (0.034 mmol) of complex **1** was dissolved in 0.7 mL of THF-d_8 in a *J. Young*-NMR tube. Then, 4.0 equiv of potassium metal (5.4 mg, 0.138 mmol) was added to the red solution and the mixture was sonicated until the color changed to deep purple (4 h). The reaction mixture was filtered through a syringe filter (PTFE, 0.45 μm porosity) into a *J. Young*-NMR tube. The deep purple solution was subsequently pressurized with 1 bar of isotopically labeled $^{13}CO_2$ gas, and the color changed to brown. ^{1}H NMR spectral monitoring indicated the quantitative formation of **4-^{13}CO$_2$**. ^{1}H NMR (360 MHz, THF-d_8) δ 8.86 (s, 1H, $CH_{Py\text{-}1}$), 7.69 (s, 1H, $CH_{Py\text{-}3}$), 7.60 (s, 1H, $CH_{Py\text{-}4}$), 7.17 (s, 1H, $CH_{Py\text{-}2}$), 6.59 (s, 2H, $CH_{Ar\text{-}7,8}$), 6.51 (s, 2H, $CH_{Ar\text{-}6,9}$), 4.81 (s, 1H, NCH), 2.04 (s, 3H, CH_3). ^{13}C{^{1}H} NMR (91 MHz, THF-d_8) δ 227.6 (s, 1C, Mn−CO), 227.2 (s, 1C, Mn−CO), 221.3 (s, 1C, Mn−CO), 182.4 (s, 1C, O^{13}CO), 167.1 (s, 1C, $C_{Py\text{-}quart}$), 159.7 (s, 1C, $NC_{Ar\text{-}quart}$), 153.1 (s, 1C, $CH_{Py\text{-}1}$), 137.9 (s, 1C, $CH_{Py\text{-}3}$), 129.3 (s, 2C, $CH_{Ar\text{-}9,11}$), 125.9 (s, free $^{13}CO_2$), 122.2 (s, 1C, $CH_{Py\text{-}2}$), 121.9 (s, 1C, $CH_{Py\text{-}4}$), 119.5 (s, 1C, $C_{Ar\text{-}quart\text{-}10}$), 115.5 (s, 2C, $CH_{Ar\text{-}8,12}$), 76.0 (d, $^1J_{CC}$ = 53.6 Hz, 1C, NCH), 20.6 (s, 1C, CH_3). The corresponding complex bearing a Na$^+$ counter cation *fac*-Na[Mn(*amidopy*-^{13}COO)(CO)$_3$] (**4-Na-^{13}CO$_2$**)

https://doi.org/10.1021/acs.organomet.2c00387
Organometallics 2022, 41, 2798−2809

was analogously prepared starting from 11.6 mg (0.028 mmol) of complex **1** and 8.0 equiv of sodium metal (5.1 mg, 0.224 mmol). ^{1}H NMR (360 MHz, THF-d_8) δ 8.89 (s, 1H, $CH_{Py\text{-}1}$), 7.73 (s, 1H, $CH_{Py\text{-}3}$), 7.65 (s, 1H, $CH_{Py\text{-}4}$), 7.21 (s, 1H, $CH_{Py\text{-}2}$), 6.61 (s, 2H, $CH_{Ar\text{-}7,8}$), 6.55 (s, 2H, $CH_{Ar\text{-}6,9}$), 4.87 (s, 1H, NCH), 2.06 (s, 3H, CH_3). ^{13}C{^{1}H} NMR (151 MHz, THF-d_8) δ 227.62 (s, 1C, Mn−CO), 226.70 (s, 1C, Mn−CO), 221.31 (s, 1C, Mn−CO), 183.02 (s, 1C, OCO), 166.59 (s, 1C, $C_{Py\text{-}quart}$), 159.20 (s, 1C, $NC_{Ar\text{-}quart}$), 153.23 (s, 1C, $CH_{Py\text{-}1}$), 138.18 (s, 1C, $CH_{Py\text{-}3}$), 129.36 (s, 2C, $CH_{Ar\text{-}9,11}$), 125.86 (s, free CO_2), 122.52 (s, 1C, $CH_{Py\text{-}2}$), 122.19 (s, 1C, $CH_{Py\text{-}4}$), 120.35 (s, 1C, $C_{Ar\text{-}quart\text{-}10}$), 115.77 (s, 2C, $CH_{Ar\text{-}8,12}$), 75.20 (d, $^1J_{CC}$ = 43.9 Hz, 1C, NCH), 20.59 (s, 1C, CH_3).

4.93.1.10. *fac*-[K][Mn(*amidopy-ba*)(CO)$_3$] (5-K). First, 15.0 mg (0.036 mmol) of complex **1** was dissolved in 1.0 mL of THF-d_8 in a *J. Young*-NMR tube. Then, 4.0 equiv. of potassium metal (5.7 mg, 0.144 mmol) was added to the red solution and the mixture was sonicated until the color changed to deep purple (4 h). The reaction mixture was filtered through a syringe filter (PTFE, 0.45 μm porosity). Subsequently, 3.0 equiv of fresh distilled benzaldehyde was added (11.5 mg), upon which the color changed from purple to brown. ^{1}H NMR-spectral monitoring indicated the quantitative conversion of **3-K** and the formation of two diastereomeric compounds (85:15 ratio 5a/5b). ^{1}H NMR (601 MHz, THF-d_8, sharp resonances are only observed in the presence of benzaldehyde δ 9.96 (s, $1H_{BA}$, CHO), 8.77 (d, J = 5.2 Hz, $1H_a$, $CH_{Py\text{-}1}$), 8.67 (d, J = 5.2 Hz, $1H_b$, $CH_{Py\text{-}1}$), 7.86 (d, J = 6.6 Hz, $2H_{BA}$, $CH_{Ar\text{-}14,18}$), 7.65 (t, J = 7.2 Hz, $1H_b$, $CH_{Py\text{-}3}$), 7.61 (t, J = 7.4 Hz, $1H_{BA}$, $CH_{Ar\text{-}16}$), 7.56 − 7.50 (m, $2H_{BA}$, $CH_{Ar\text{-}15,17}$; $3H_b$, $CH_{Py\text{-}4}$, $CH_{Ar\text{-}14,18}$), 7.23 (t, J = 7.5 Hz, $1H_a$, $CH_{Py\text{-}3}$), 7.10 − 7.05 (m, $3H_b$,$CH_{Py\text{-}2}$, $CH_{Ar\text{-}15,17}$), 7.00 − 6.93 (m, $3H_a$, $CH_{Py\text{-}2}$, $CH_{Ar\text{-}15,17}$; $1H_b$, $CH_{Ar\text{-}16}$), 6.90 (t, J = 7.1 Hz, $1H_a$, $CH_{Ar\text{-}16}$), 6.82 (d, J = 7.2 Hz, $2H_a$, $CH_{Ar\text{-}14,18}$), 6.64 (d, J = 8.2 Hz, $2H_a$, $CH_{Ar\text{-}6,9}$), 6.60 (d, J = 8.2 Hz, $2H_a$, $CH_{Ar\text{-}7,8}$), 6.49 (d, J = 7.7 Hz, $1H_a$, $CH_{Py\text{-}4}$), 6.39−6.33 (m, $4H_b$, $CH_{Ar\text{-}6,7,8,9}$), 4.87 (s, $1H_a$, NC*H*), 4.86 (s, $1H_b$, NC*H*), 4.74 (s, $1H_a$, OC*H*), 4.02 (s, $1H_b$, OC*H*), 2.07 (s, $3H_a$, CH_3), 1.93 (s, $3H_b$, CH_3). ^{13}C{^{1}H} NMR (151 MHz, THF-d_8) δ 229.5 (s, $1C_a$, Mn−CO), 226.5 (s, $1C_a$, Mn−CO), 223.2 (s, $1C_a$, Mn−CO), (Mn−CO of 5b not detectable due to low concentrations), 192.2 (s, $1C_{BA}$, CO), 170.3 (s, $1C_b$, $C_{Py\text{-}5}$), 165.3 s, $1C_a$, $C_{Py\text{-}5}$), 159.4 (s, $1C_b$, $C_{Ar\text{-}7}$), 159.1 (s, $1C_a$, $C_{Ar\text{-}7}$), 152.2 (s, $1C_b$, $C_{Ar\text{-}18}$), 151.3 (s, $1C_a$, $C_{Ar\text{-}18}$), 151.2 (s, $1C_b$, $CH_{Py\text{-}1}$), 150.8 (s, $1C_a$, $CH_{Py\text{-}1}$), 138.0 (s, $1C_{BA}$, $CH_{Ar\text{-}18}$), 137.3 (s, $1C_b$, $CH_{Py\text{-}3}$), 135.4 (s, $1C_a$, $CH_{Py\text{-}3}$), 134.8 (s, $1C_{BA}$, $CH_{Ar\text{-}21}$), 130.2 (s, $2C_{BA}$, $CH_{Ar\text{-}19,23}$), 129.7 (s, $2C_{BA}$, $CH_{Ar\text{-}20,22}$), 129.4 (s, $2C_a$, $CH_{Ar\text{-}9,11}$), 129.0 (s, $2C_b$, $CH_{Ar\text{-}9,11}$), 128.0(s, $2C_b$, $CH_{Ar\text{-}19,23}$), 127.8 (s, $2C_b$, $CH_{Ar\text{-}20,22}$), 127.6 (s, $2C_a$, $CH_{Ar\text{-}20,22}$), 127.0 (s, $2C_a$, $CH_{Ar\text{-}19,23}$), 125.8 (s, $1C_b$, $CH_{Ar\text{-}21}$), 125.7 (s, $1C_a$, $CH_{Ar\text{-}21}$), 122.7 (s, $1C_a$, $CH_{Py\text{-}4}$), 121.0 (s, $1C_b$, $CH_{Py\text{-}2}$), 120.6 (s, $1C_a$, $CH_{Py\text{-}2}$), 119.8 (s, $1C_a$, $CH_{Py\text{-}4}$), 117.3 (s, $1C_a$, $C_{Ar\text{-}10}$), 117.2 (s, $1C_b$, $C_{Ar\text{-}10}$), 114.2 (s, $2C_b$, $C_{Ar\text{-}8,12}$), 114.0 (s, $2C_a$, $C_{Ar\text{-}8,12}$), 78.1 (s, $1C_b$, HCO), 77.8 (s, $1C_a$, NCH), 77.0 (s, $1C_a$, HCO), 76.7 (s, $1C_b$, NCH), 20.7 (s, $1C_b$, CH_3), 20.6 (s, $1C_b$, CH_3). IR (ATR) $\tilde{\nu}$ cm^{-1}: $\tilde{\nu}_{CO}$= 2020 (m), $\tilde{\nu}_{CO}$ = 1897 (m), $\tilde{\nu}_{CCO}$ = 1595 (m), $\tilde{\nu}$ = 1551 (s), $\tilde{\nu}$ = 1386 (s). HRMS-ESI CH_3OH/CH_2Cl_2 (m/z): neg: [M-(BA)] $^-$ calcd for $C_{16}H_{12}N_2O_3Mn^-$ 335.02339; found 335.02344 (0.15 ppm). [M] $^-$ detectable only with a very low signal intensity. HRMS-ESI CH_3OH (0.1% FA)/CH_2Cl_2 (m/z): pos: [MH+H]$^+$ calcd for $C_{23}H_{20}N_2O_4Mn^+$ 443.07981; found 443.07980 (0.02 ppm).

4.10. *fac*-[K(18-*crown*-6)][Mn(*amidopy-ba*)(CO)$_3$] (5-K-*crown*). First, 28.0 mg (0.067 mmol) of complex **3-K** was dissolved in 1.5 mL of THF in a *J. Young*-NMR tube. Then, 4.0 equiv of potassium metal (10.5 mg, 0.270 mmol) was added to the red solution and the mixture was sonicated until the color changed to deep purple (4 h). The reaction mixture was filtered through a syringe filter (PTFE, 0.45 μm porosity) and added to 3.0 equiv of freshly distilled benzaldehyde (21.3 mg). The color changed from purple to brown. To the mixture, 1 equiv of 18-crown-6 was added (17.7 mg). Subsequently, the solution was layered with *n*-hexane and kept at −16 °C in a freezer. An oily dark brown product precipitated. The supernatant solvent was carefully removed, and the oil was washed with *n*-hexane. After 3 days at ambient temperature, compound **5-K-*crown*** formed as orange crystals also suitable for XRD analysis. Then, 23.8 mg (0.0032 mmol, 48% yield). IR (ATR) $\tilde{\nu}$ cm^{-1}: $\tilde{\nu}_{CO}$ = 1984 (m), $\tilde{\nu}_{CO}$ = 1857 (s), $\tilde{\nu}$ = 1604(m), $\tilde{\nu}$ = 1350 (m), and $\tilde{\nu}_{crown}$ = 1106 (s). HRMS-ESI CH_3OH/CH_2Cl_2 (m/z): neg: [M-(BA)]$^-$ calcd for $C_{16}H_{12}N_2O_3Mn^-$ 335.02339; found 335.02338 (0.03 ppm). [M]$^-$ detectable only with a very low signal intensity. HRMS-ESI CH_3OH (0.1% FA)/CH_2Cl_2 (m/z): pos: [MH + H]$^+$ calcd for $C_{23}H_{20}N_2O_4Mn^+$ 443.07981; found 443.07944 (0.84 ppm), [(MH-(3CO) + H]$^+$ calcd for $C_{20}H_{20}N_3OMn^+$ 359.09506; found 359.09479 (0.75 ppm) [18-*c*-6 + K]$^+$ calcd for $C_{12}H_{24}O_6K^+$ 303.12045; found 303.12024 (0.69 ppm).

■ ASSOCIATED CONTENT

Supporting Information

The Supporting Information is available free of charge at https://pubs.acs.org/doi/10.1021/acs.organomet.2c00387.

DFT-optimized geometries (XYZ)
NMR, IR, and HR-MS spectra (PDF)

Accession Codes

CCDC 2193730−2193734 contain the supplementary crystallographic data for this paper. These data can be obtained free of charge via www.ccdc.cam.ac.uk/data_request/cif, or by emailing data_request@ccdc.cam.ac.uk, or by contacting The Cambridge Crystallographic Data Centre, 12 Union Road, Cambridge CB2 1EZ, UK; fax: +44 1223 336033.

■ AUTHOR INFORMATION

Corresponding Author

Matthias Vogt − *Institut für Anorganische Chemie und Kristallographie, Universität Bremen, 28359 Bremen, Germany; Institut für Chemie, Naturwissenschaftliche Fakultät II, Martin-Luther-Universität Halle-Wittenberg, 06120 Halle (Saale), Germany*; orcid.org/0000-0002-2636-2531; Email: matthias.vogt@chemie.uni-halle.de

Authors

Rasmus Stichauer − *Institut für Anorganische Chemie und Kristallographie, Universität Bremen, 28359 Bremen, Germany*

Daniel Duvinage − *Institut für Anorganische Chemie und Kristallographie, Universität Bremen, 28359 Bremen, Germany*; orcid.org/0000-0002-9387-7172

Robert Langer − *Institut für Chemie, Naturwissenschaftliche Fakultät II, Martin-Luther-Universität Halle-Wittenberg, 06120 Halle (Saale), Germany*

Complete contact information is available at: https://pubs.acs.org/10.1021/acs.organomet.2c00387

Notes

The authors declare no competing financial interest.

■ ACKNOWLEDGMENTS

M.V. wants to acknowledge the generous financial support by the *Fonds der Chemischen Industrie (FCI)* and the Central Research and Development Fund (CRDF) of the University of Bremen.

■ DEDICATION

This article is dedicated to Professor David Milstein on the occasion of his 75th birthday.

■ REFERENCES

(1) Mastalir, M.; Glatz, M.; Pittenauer, E.; Allmaier, G.; Kirchner, K. Sustainable Synthesis of Quinolines and Pyrimidines Catalyzed by Manganese PNP Pincer Complexes. *J. Am. Chem. Soc.* **2016**, *138*, 15543−15546.

(2) Perez, M.; Elangovan, S.; Spannenberg, A.; Junge, K.; Beller, M. Molecularly Defined Manganese Pincer Complexes for Selective Transfer Hydrogenation of Ketones. *ChemSusChem* **2017**, *10*, 83−86.

(3) Kumar, A.; Espinosa-Jalapa, N. A.; Leitus, G.; Diskin-Posner, Y.; Avram, L.; Milstein, D. Direct Synthesis of Amides by Dehydrogenative Coupling of Amines with Either Alcohols or Esters: Manganese Pincer Complex as Catalyst. *Angew. Chem., Int. Ed.* **2017**, *56*, 14992−14996.

(4) Yang, W.; Chernyshov, I. Y.; van Schendel, R. K. A.; Weber, M.; Müller, C.; Filonenko, G. A.; Pidko, E. A. Robust and Efficient Hydrogenation of Carbonyl Compounds Catalysed by Mixed Donor Mn(I) Pincer Complexes. *Nat. Commun.* **2021**, *12*, 12.

(5) Wei, D.; Bruneau-Voisine, A.; Valyaev, D. A.; Lugan, N.; Sortais, J.-B. Manganese Catalyzed Reductive Amination of Aldehydes Using Hydrogen as a Reductant. *Chem. Commun.* **2018**, *54*, 4302−4305.

(6) Pal, D.; Mondal, A.; Srimani, D. Well-Defined Manganese Complex Catalyzed Dehydrogenative Synthesis of Quinazolin-4(3 H)-Ones and 3,4-Dihydro-2 H-1,2,4-Benzothiadiazine 1,1-Dioxides. *Catal. Sci. Technol.* **2022**, *12*, 3202−3208.

(7) Neumann, J.; Elangovan, S.; Spannenberg, A.; Junge, K.; Beller, M. Improved and General Manganese-Catalyzed N-Methylation of Aromatic Amines Using Methanol. *Chem. − A Eur. J.* **2017**, *23*, 5410−5413.

(8) Espinosa-Jalapa, N. A.; Nerush, A.; Shimon, L. J. W.; Leitus, G.; Avram, L.; Ben-David, Y.; Milstein, D. Manganese-Catalyzed Hydrogenation of Esters to Alcohols. *Chem. − A Eur. J.* **2017**, *23*, 5934−5938.

(9) Elangovan, S.; Garbe, M.; Jiao, H.; Spannenberg, A.; Junge, K.; Beller, M. Hydrogenation of Esters to Alcohols Catalyzed by Defined Manganese Pincer Complexes. *Angew. Chem., Int. Ed.* **2016**, *55*, 15364−15368.

(10) Zell, T.; Langer, R. From Ruthenium to Iron and Manganese—A Mechanistic View on Challenges and Design Principles of Base-Metal Hydrogenation Catalysts. *ChemCatChem* **2018**, *10*, 1930−1940.

(11) van Putten, R.; Uslamin, E. A.; Garbe, M.; Liu, C.; Gonzalez-de-Castro, A.; Lutz, M.; Junge, K.; Hensen, E. J. M.; Beller, M.; Lefort, L.; Pidko, E. A. Non-Pincer-Type Manganese Complexes as Efficient Catalysts for the Hydrogenation of Esters. *Angew. Chem., Int. Ed.* **2017**, *56*, 7531−7534.

(12) Kallmeier, F.; Dudziec, B.; Irrgang, T.; Kempe, R. Manganese-Catalyzed Sustainable Synthesis of Pyrroles from Alcohols and Amino Alcohols. *Angew. Chem., Int. Ed.* **2017**, *56*, 7261−7265.

(13) Widegren, M. B.; Harkness, G. J.; Slawin, A. M. Z.; Cordes, D. B.; Clarke, M. L. A Highly Active Manganese Catalyst for Enantioselective Ketone and Ester Hydrogenation. *Angew. Chem., Int. Ed.* **2017**, *56*, 5825−5828.

(14) Das, U. K.; Ben-David, Y.; Leitus, G.; Diskin-Posner, Y.; Milstein, D. Dehydrogenative Cross-Coupling of Primary Alcohols To Form Cross-Esters Catalyzed by a Manganese Pincer Complex. *ACS Catal.* **2019**, *9*, 479−484.

(15) Sampson, M. D.; Kubiak, C. P. Manganese Electrocatalysts with Bulky Bipyridine Ligands: Utilizing Lewis Acids To Promote Carbon Dioxide Reduction at Low Overpotentials. *J. Am. Chem. Soc.* **2016**, *138*, 1386−1393.

(16) Machan, C. W.; Kubiak, C. P. Electrocatalytic Reduction of Carbon Dioxide with Mn(Terpyridine) Carbonyl Complexes. *Daltons Trans.* **2016**, *45*, 17179−17186.

(17) Yang, J.; He, S.; Wu, Q.; Zhang, P.; Chen, L.; Huang, F.; Li, F. A Bio-Inspired Mononuclear Manganese Catalyst for High-Rate Electrochemical Hydrogen Production. *Daltons Trans.* **2021**, *50*, 4783−4788.

(18) Srinivasan, A.; Campos, J.; Giraud, N.; Robert, M.; Rivada-Wheelaghan, O. MnI Complex Redox Potential Tunability by Remote Lewis Acid Interaction. *Daltons Trans.* **2020**, *49*, 16623−16626.

(19) Rana, J.; Gupta, V.; Balaraman, E. Manganese-Catalyzed Direct C−C Coupling of α-C−H Bonds of Amides and Esters with Alcohols via Hydrogen Autotransfer. *Daltons Trans.* **2019**, *48*, 7094−7099.

(20) Nerush, A.; Vogt, M.; Gellrich, U.; Leitus, G.; Ben-David, Y.; Milstein, D. Template Catalysis by Metal−Ligand Cooperation. C−C Bond Formation via Conjugate Addition of Non-Activated Nitriles under Mild, Base-Free Conditions Catalyzed by a Manganese Pincer Complex. *J. Am. Chem. Soc.* **2016**, *138*, 6985−6997.

(21) Chakraborty, S.; Das, U. K.; Ben-David, Y.; Milstein, D. Manganese Catalyzed α-Olefination of Nitriles by Primary Alcohols. *J. Am. Chem. Soc.* **2017**, *139*, 11710−11713.

(22) Peña-López, M.; Piehl, P.; Elangovan, S.; Neumann, H.; Beller, M. Manganese-Catalyzed Hydrogen-Autotransfer C−C Bond Formation: α-Alkylation of Ketones with Primary Alcohols. *Angew. Chem., Int. Ed.* **2016**, *55*, 14967−14971.

(23) Niesel, J.; Pinto, A.; Peindy N'Dongo, H. W.; Merz, K.; Ott, I.; Gust, R.; Schatzschneider, U. Photoinduced CO Release, Cellular Uptake and Cytotoxicity of a Tris(Pyrazolyl)Methane (Tpm) Manganese Tricarbonyl Complex. *Chem. Commun.* **2008**, *15*, 1798.

(24) Üstün, E.; Özgür, A.; Coşkun, K. A.; Demir Düşünceli, S.; Özdemir, İ.; Tutar, Y. Anticancer Activities of Manganese-Based Photoactivatable CO-Releasing Complexes (PhotoCORMs) with Benzimidazole Derivative Ligands. *Transition Met. Chem.* **2017**, *42*, 331−337.

(25) Khaled, R. M.; Friedrich, A.; Ragheb, M. A.; Abdel-Ghani, N. T.; Mansour, A. M. Cytotoxicity of Photoactivatable Bromo Tricarbonyl Manganese(1) Compounds against Human Liver Carcinoma Cells. *Daltons Trans.* **2020**, *49*, 9294−9305.

(26) Elsby, M. R.; Baker, R. T. Strategies and Mechanisms of Metal−Ligand Cooperativity in First-Row Transition Metal Complex Catalysts. *Chem. Soc. Rev.* **2020**, *49*, 8933−8987.

(27) Rahaman, S. M. W.; Pandey, D. K.; Rivada-Wheelaghan, O.; Dubey, A.; Fayzullin, R. R.; Khusnutdinova, J. R. Hydrogenation of Alkenes Catalyzed by a Non-pincer Mn Complex. *ChemCatChem* **2020**, *12*, 5912−5918.

(28) Buhaibeh, R.; Filippov, O. A.; Bruneau-Voisine, A.; Willot, J.; Duhayon, C.; Valyaev, D. A.; Lugan, N.; Canac, Y.; Sortais, J.-B. Phosphine-NHC Manganese Hydrogenation Catalyst Exhibiting a Non-Classical Metal-Ligand Cooperative H 2 Activation Mode. *Angew. Chem., Int. Ed.* **2019**, *58*, 6727−6731.

(29) Janes, T.; Yang, Y.; Song, D. Chemical Reduction of CO 2 Facilitated by C-Nucleophiles. *Chem. Commun.* **2017**, *53*, 11390−11398.

(30) Yang, Y.; Yan, L.; Xie, Q.; Liang, Q.; Song, D. Zwitterionic Indenylammonium with Carbon-Centred Reactivity towards Reversible CO 2 Binding and Catalytic Reduction. *Org. Biomol. Chem.* **2017**, *15*, 2240−2245.

(31) Sieh, D.; Lacy, D. C.; Peters, J. C.; Kubiak, C. P. Reduction of CO 2 by Pyridine Monoimine Molybdenum Carbonyl Complexes: Cooperative Metal−Ligand Binding of CO2. *Chem. − A Eur. J.* **2015**, *21*, 8497−8503.

(32) Braunstein, P.; Matt, D.; Dusausoy, Y.; Fischer, J.; Mitschler, A.; Ricard, L. Complexes of Functional Phosphines. 4. Coordination

Properties of (Diphenylphosphino)Acetonitrile, Ethyl (Diphenylphosphino)Acetate and Corresponding Carbanions. Characterization of a New Facile Reversible Carbon Dioxide Insertion into Palladium(II) Complexes. *J. Am. Chem. Soc.* **1981**, *103*, 5115−5125.
(33) Vogt, M.; Gargir, M.; Iron, M. A.; Diskin-Posner, Y.; Ben-David, Y.; Milstein, D. A New Mode of Activation of CO2 by Metal-Ligand Cooperation with Reversible C−C and M−O Bond Formation at Ambient Temperature. *Chem. − A Eur. J.* **2012**, *18*, 9194−9197.
(34) Vogt, M.; Nerush, A.; Diskin-Posner, Y.; Ben-David, Y.; Milstein, D. Reversible CO2 Binding Triggered by Metal-Ligand Cooperation in a Rhenium(i) PNP Pincer-Type Complex and the Reaction with Dihydrogen. *Chem. Sci.* **2014**, *5*, 2043−2051.
(35) Huff, C. A.; Kampf, J. W.; Sanford, M. S. Role of a Noninnocent Pincer Ligand in the Activation of CO 2 at (PNN)Ru(H)(CO). *Organometallics* **2012**, *31*, 4643−4645.
(36) Filonenko, G. A.; Conley, M. P.; Copéret, C.; Lutz, M.; Hensen, E. J. M.; Pidko, E. A. The Impact of Metal-Ligand Cooperation in Hydrogenation of Carbon Dioxide Catalyzed by Ruthenium PNP Pincer. *ACS Catal.* **2013**, *3*, 2522−2526.
(37) LeBlanc, F. A.; Berkefeld, A.; Piers, W. E.; Parvez, M. Reactivity of Scandium β-Diketiminate Alkyl Complexes with Carbon Dioxide. *Organometallics* **2012**, *31*, 810−818.
(38) Stichauer, R.; Helmers, A.; Bremer, J.; Rohdenburg, M.; Wark, A.; Lork, E.; Vogt, M. Rhenium(I) Triscarbonyl Complexes with Redox-Active Amino- and Iminopyridine Ligands: Metal−Ligand Cooperation as Trigger for the Reversible Binding of CO2 via a Dearmomatization/Rearomatization Reaction Sequence. *Organometallics* **2017**, *36*, 839−848.
(39) Scharf, L. T.; Feichtner, K.-S.; Gessner, V. H. Carbon Dioxide Catalyzed Cyclometallation of a Carbene Complex: Synthesis and Mechanism. *Eur. J. Inorg. Chem.* **2019**, *2019*, 2990−2995.
(40) Huff, C. A.; Kampf, J. W.; Sanford, M. S. Reversible Carbon-Carbon Bond Formation between Carbonyl Compounds and a Ruthenium Pincer Complex. *Chem. Commun.* **2013**, *49*, 7147−7149.
(41) Ebner, F.; Sigmund, L. M.; Greb, L. Metal−Ligand Cooperativity of the Calix[4]Pyrrolato Aluminate: Triggerable C−C Bond Formation and Rate Control in Catalysis. *Angew. Chem., Int. Ed.* **2020**, *59*, 17118−17124.
(42) Vogt, M.; Nerush, A.; Iron, M. A.; Leitus, G.; Diskin-Posner, Y.; Shimon, L. J. W.; Ben-David, Y.; Milstein, D. Activation of Nitriles by Metal Ligand Cooperation. Reversible Formation of Ketimido- and Enamido-Rhenium PNP Pincer Complexes and Relevance to Catalytic Design. *J. Am. Chem. Soc.* **2013**, *135*, 17004−17018.
(43) Perdriau, S.; Zijlstra, D. S.; Heeres, H. J.; De Vries, J. G.; Otten, E. A Metal-Ligand Cooperative Pathway for Intermolecular Oxa-Michael Additions to Unsaturated Nitriles. *Angew. Chem., Int. Ed.* **2015**, *54*, 4236−4240.
(44) Guo, B.; Zijlstra, D. S.; de Vries, J. G.; Otten, E. Oxa-Michael Addition to α,β-Unsaturated Nitriles: An Expedient Route to γ-Amino Alcohols and Derivatives. *ChemCatChem* **2018**, *10*, 2868−2872.
(45) Stor, G. J.; Morrison, S. L.; Stufkens, D. J.; Oskam, A. The Remarkable Photochemistry of Fac-XMn(CO)3(.Alpha.-Diimine) (X = Halide): Formation of Mn2(CO)6(.Alpha.-Diimine)2 via the Mer Isomer and Photocatalytic Substitution of X- in the Presence of PR3. *Organometallics* **1994**, *13*, 2641−2650.
(46) Stichauer, R.; Vogt, M. Cooperative Binding of SO2 under M-O and C-S Bond Formation in a Rhenium(I) Complex with Activated Amino- or Iminopyridine Ligand. *Organometallics* **2018**, *37*, 3639−3643.
(47) Sieh, D.; Kubiak, C. P. A Series of Diamagnetic Pyridine Monoimine Rhenium Complexes with Different Degrees of Metal-to-Ligand Charge Transfer: Correlating13C NMR Chemical Shifts with Bond Lengths in Redox-Active Ligands. *Chem. − A Eur. J.* **2016**, *22*, 10638−10650.
(48) Kumar, A.; Milstein, D. Recent Advances in the Applications of Metal-Ligand Cooperation via Dearomatization and Aromatization of Pincer Complexes. *Top. Organomet. Chem.* **2021**, *68*, 1−23.
(49) Kumar, A.; Daw, P.; Espinosa-Jalapa, N. A.; Leitus, G.; Shimon, L. J. W.; Ben-David, Y.; Milstein, D. CO2 Activation by Manganese Pincer Complexes through Different Modes of Metal-Ligand Cooperation. *Daltons Trans.* **2019**, *48*, 14580−14584.
(50) Montag, M.; Zhang, J.; Milstein, D. Aldehyde Binding through Reversible C-C Coupling with the Pincer Ligand upon Alcohol Dehydrogenation by a PNP-Ruthenium Catalyst. *J. Am. Chem. Soc.* **2012**, *134*, 10325−10328.
(51) Gonçalves, T. P.; Dutta, I.; Huang, K. W. Aromaticity in Catalysis: Metal Ligand Cooperation via Ligand Dearomatization and Rearomatization. *Chem. Commun.* **2021**, *57*, 3070−3082.
(52) Gómez, J.; García-Herbosa, G.; Cuevas, J. V.; Arnáiz, A.; Carbayo, A.; Muñoz, A.; Falvello, L.; Fanwick, P. E. Diastereospecific and Diastereoselective Syntheses of Ruthenium(II) Complexes Using N,N′ Bidentate Ligands Aryl-Pyridin-2-Ylmethyl-Amine ArNH-CH_2−2-C_5H_4N and Their Oxidation to Imine Ligands. *Inorg. Chem.* **2006**, *45*, 2483−2493.

https://doi.org/10.1021/acs.organomet.2c00387
Organometallics 2022, 41, 2798−2809

3.1.6 Reversible Binding of Benzaldehyde and Benzophenone *via* Cooperative C-C and Re-O Bond Formation with Bidentate Pyridine-Based Rhenium(I) Triscarbonyl Complexes

This chapter describes further investigations entailing K[Re(*amidopy**)(CO)$_3$] **75*-Re** and the MLC activity to activate aldehydes, represented by benzaldehyde. Furthermore, C=O double bond activations are extended to ketones, represented by benzophenone.

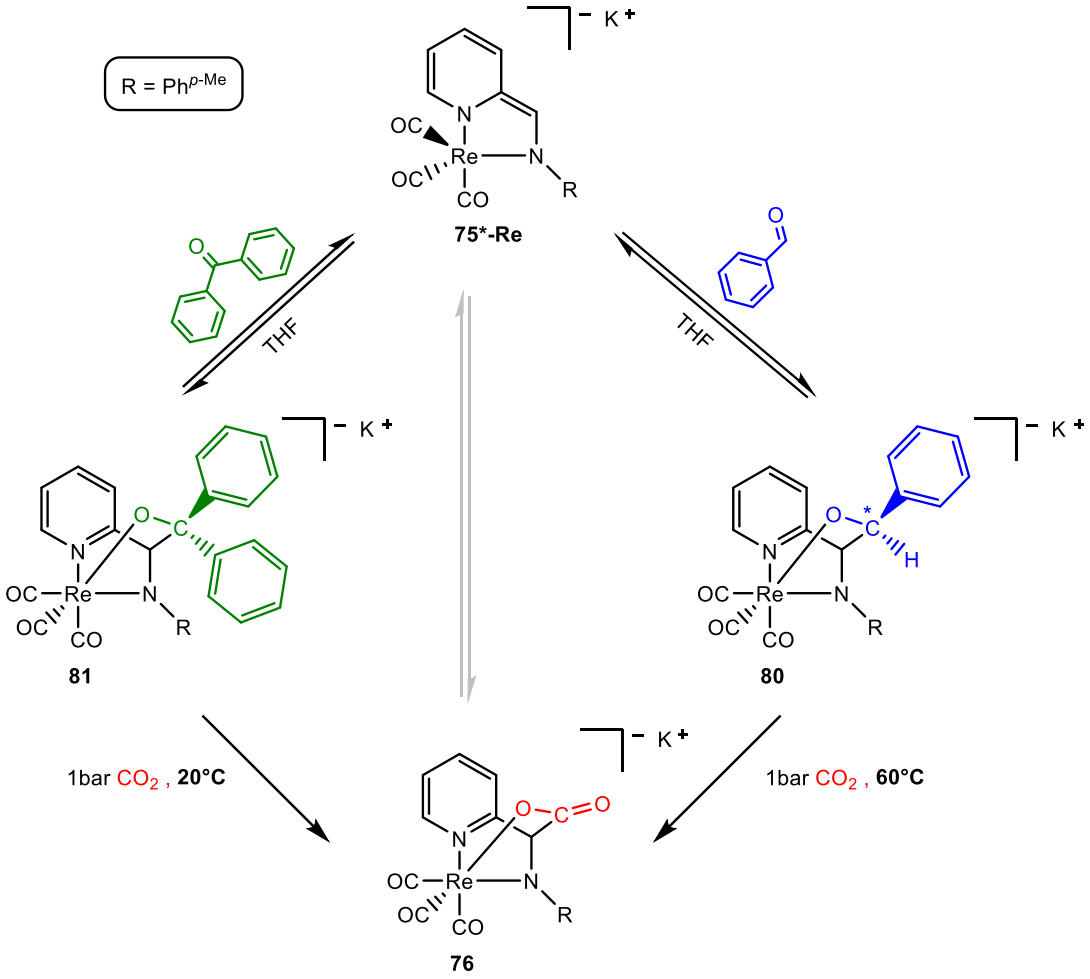

Scheme 38: Synthesis of the aldehyde adduct complex *fac*-K[Re(*amidopy-ba*)(CO)$_3$] (**80**) and the ketone adduct complex *fac*-K[Re(*amidopy-bph*)(CO)$_3$] (**81**) and exchange reactions with CO_2.

Substrate activation *via* MLC of the C=O double bond in CO_2 by K[Re(*amidopy**)(CO)$_3$] (**75*-Re**) was shown in a previous publication[159], presented in the context of this work.

The reversible binding of benzaldehyde by C=O double bond activation using K[Mn(*amidopy**)(CO)$_3$] (**75*-Mn**) *via* MLC was demonstrated in another previous work.[161] The activation of different carbonyl groups, using the ruthenium PNN pincer complex **58*** was already mentioned before.[102] The resulting aldehyde-complex *fac*-K[Re(*amidopy-ba*)(CO)$_3$] (**80**) and the ketone-complex *fac*-K[Re(*amidopy-bph*)(CO)$_3$] (**81**) were formed *via* MLC 1,3-addition under C-C and Re-O bond formation (Scheme 38). The ^{1}H NMR spectrum of complex **80** in THF-d$_8$ shows a diastereomeric mixture like previously described for the similar Mn(I)-complex **78** and the ruthenium pincer complex **59a**.[102; 161] In contrast to **78**, the usage of K[Re(*amidopy**)(CO)$_3$] **75*-Re** does not require an excess of benzaldehyde for a quantitative turnover. The ratio of the diastereomeric mixture is similar to the Mn(I)-complex **79**, at 82:18 (**80a/80b**). The downfield shift of the ^{1}H NMR signals associated with the pyridine unit from 8.51-4.94 ppm to 8.70-6.59 ppm indicates the rearomatization. The ^{1}H NMR resonances of the NCH protons are shifted upfield from 6.98 ppm to 5.17 ppm (**80a**) and 5.12 ppm (**80b**). While the ^{1}H NMR resonance of the NC*H* proton of **80b** is a singlet, the corresponding NC*H* signal in **80a** at 5.17 ppm is detected as a doublet with a coupling constant of $^3J_{HH}$ = 2.6 Hz. The C(*H*)=O proton of the benzaldehyde (9.96 ppm) experiences a strong upfield shift to 4.86 ppm (**80a**) and 4.27 ppm (**80b**) in the adduct-complex. This is in good agreement with the similar reaction involving the Mn(I)-complex **79**. The previous reported doublet signal of the NC*H* proton in **80a** results from coupling with the *H*C-O proton from the formed alkoxy group. Therefore, it is accurate to acquire a doublet signal ($^3J_{HH}$ = 2.6 Hz) for **80a** in the ^{1}H NMR spectrum as well, whereas **80b** shows again a singlet signal. The coupling of both benzylic H atoms is clearly visible in the ^{1}H^{1}H COSY NMR spectrum. In the ^{13}C NMR spectrum of **80**, the ^{13}C NMR resonance associated with the carbon atom of the alkoxy group is observed at 78.26 ppm in **80b** and at 77.61 ppm in **80a**, respectively. For full spectral characterization of **80**, see the experimental section and the supporting information (**7.4**). In the negative HRMS ESI spectrum of **80**, only the molecular ion without benzaldehyde [M-ba]$^-$ was found, showing the most abundant isotopic mass of m/z = 467.04086 for $C_{16}H_{12}O_3N_2Re$. In the positive HRMS ESI spectrum of **80** the double protonated molecule ion [MH+H]$^+$ was found, showing the most abundant isotopic mass of m/z = 575.09741 for $C_{23}H_{20}O_4N_2Re$ with its typically isotopic pattern. Collision induced dissociation (cid) of [MH+H]$^+$ (m/z = 575.10) from **80** shows exemplary the subsequent loss of each CO ligand and

benzaldehyde in the positive HRMS^2 ESI spectrum. For full spectral characterization of **80**, see the experimental section and the supporting information. Single crystals of *fac*-K[Re(*amidopy-ba*)(CO)$_3$] (**80**) suitable for scXRD analysis could be obtained from concentrated THF solution, layered with *n*-hexane at -16 °C in 68% yield (Figure 3). Noteworthy, addition of 18-*crown*-6 ether for crystal growing was not necessary, in contrast to the Mn-complex **79**.

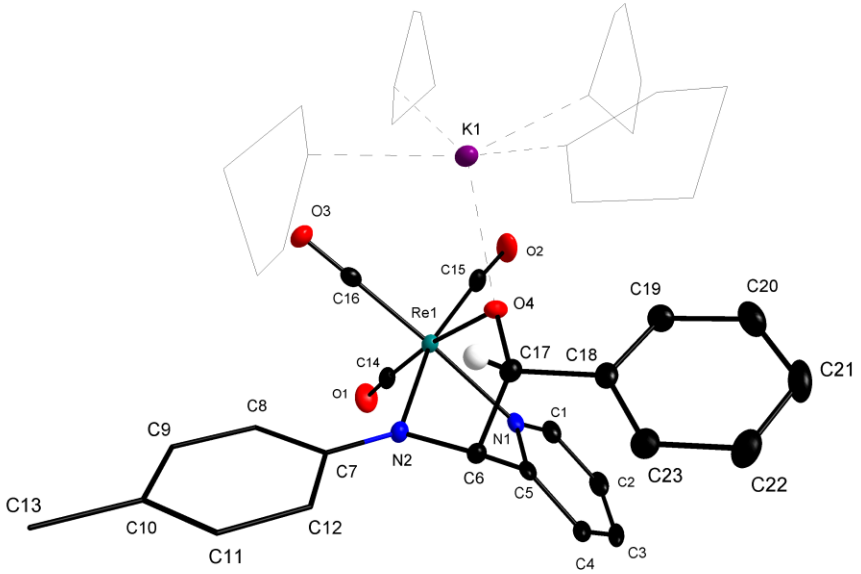

80

C1-C2	1.381(3)
C2-C3	1.385(3)
C3-C4	1.385(3)
C4-C5	1.393(3)
C1-N1	1.348(2)
C5-N1	1.348(2)
C5-C6	1.500(2)
C6-C17	1.568(3)
C17-O4	1.394(2)
C6-N2	1.462(2)
Re1-N1	2.186(2)
Re1-N2	2.135(2)
Re1-O4	2.125(1)
K1-O4	2.609(2)

Figure 3: Diamond plot of *fac*-K[Re(*amidopy-ba*)(CO)$_3$] (**80**) with potassium surrounded by four molecules of THF (stick model with 50% transparency for clarity) and selected bond lengths [Å]. (Thermal ellipsoids at 50% probability, H atoms omitted for clarity, except for benzylic C-H)

In contrast to the obtained molecular structure of the Mn(I)-benzaldehyde complex **79-crown**, in *fac*-K[Re(*amidopy-ba*)(CO)$_3$] (**80**) the phenyl group of the benzaldehyde points into the direction of the pyridine unit, whereas in the manganese complex the benzylic H atom from the benzaldehyde occupies this position. Multiple scXRD measurements of single crystals of **80** gave exclusively the structure of the same diastereomer. The potassium counter cation is surrounded by four THF molecules and compensates the negative charge of the Re(I)-complex. The octahedral coordination sphere of the potassium cation is completed by the interaction of a carbonyl group (C16-O3) with a neighboring molecule. The obtained molecular structure otherwise has a quite similar arrangement and bond lengths compared to the Mn(I)-complex

79-crown. The Re(I) center has a distorted octahedral coordination environment. The three CO ligands reside in facial arrangement. The pyridine-amido-alkoxide ligand chelates the Re center in a tridentate fashion giving rise to the 18 VE Re(I)-complex **80**. Upon MLC activation, the sp^2-carbon atom from the aldehyde group in free benzaldehyde changes to a sp^3-hybridization state in the adduct-complex. The formed C-C bond between C6 and C17 has a length of 1.568(3) Å and is in good agreement with **79-crown** (1.571(2) Å), but slightly elongated compared to the ruthenium benzaldehyde complexes **59a-i** and **59a-ii** (1.534(3) Å and 1.558(3) Å). The interatomic distance of 1.394(2) Å between C17 and O4 corresponds to a C-O single bond and indicates the alkoxide formation and is also slightly elongated with respect to the Ru pincer complexes **59a-i** and **59a-ii** (1.374(3) Å and 1.377(2) Å). The nearly equivalent bond lengths in the pyridine unit infer the rearomatization. Despite the absence of the crown ether, the interatomic distance between O4 and K1 of 2.609(2) Å is similar to that of the corresponding manganese complex **79-crown**. While K[Mn(*amidopy**)$(CO)_3$] (**75*-Mn**) shows no reaction towards ketones, K[Re(*amidopy**)$(CO)_3$] (**75*-Re**) reacts quantitatively with benzophenone. Due to the homogeneous substitution of the carbonyl C, the ^{1}H NMR spectrum of *fac*-K[Re(*amidopy-bph*)$(CO)_3$] (**81**) shows no diastereomeric mixture. The signals of the pyridine unit indicate again the rearomatization by a downfield shift. The NC*H* hydrogen gives rise to a singlet at 5.74 ppm, which experienced a slightly stronger downfield shift compared to *fac*-K[Re(*amidopy-ba*)$(CO)_3$] (**79**). The ^{13}C NMR resonance of the carbonyl carbon atom of the benzophenone (195.8 ppm), which forms the new C-C bond, undergoes a drastic upfield shift (83.2 ppm), as already seen in **80** for benzaldehyde, as well as in **76** and **78** for CO_2.[159; 161] Due to the presumably dynamic bond formation and cleavage, a definite assignment of the signals was only possible with small excess of benzophenone in solution, as this was the only way to obtain sharp and defined resonances in NMR spectroscopic measurements. A clear cross peak in the ^{1}H^{13}C HMBC NMR spectrum between the NC*H* proton resonance at 5.74 ppm and the quaternary carbon of the newly formed alkoxy group at 83.21 ppm is recognizable. A cross peak in the ^{1}H^{1}H NOESY NMR spectrum between the hydrogen atoms of the aryl group of the ligand at 6.60 ppm and the hydrogen atoms of only one aryl group of the bonded benzophenone at 7.40 ppm allows for a precise assignment. The obtained single crystals of *fac*-[K(18-*crown*-6)][Re(*amidopy-bph*)$(CO)_3$] **81-crown** (Figure 4) from concentrated

THF solution layered with *n*-hexane at -40 °C in 58% yield, were very unstable at ambient temperature and also at lower temperature with common settings and conditions of the scXRD set up. It was necessary to increase the temperature of measurement to -20 °C to prevent the crystal from cracking. As with almost every adduct-complex in this work, it was not possible to produce single crystals of the Re(I)-complex **81** suitable for scXRD analysis without a crown ether. The significant difference to all other adduct structures is that the potassium atom is clearly separated from the oxygen atom in the formed alkoxy group due to formation of an ion pair and is surrounded by two THF molecules.

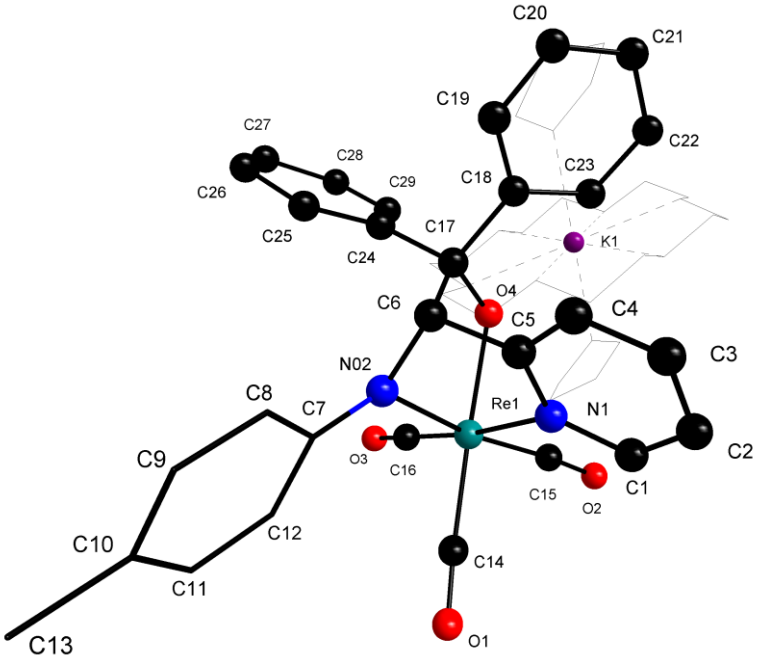

C1-C2	1.359(15)
C2-C3	1.434(17)
C3-C4	1.338(16)
C4-C5	1.395(11)
C1-N1	1.345(10)
C5-N1	1.338(9)
C5-C6	1.502(10)
C6-C17	1.560(9)
C17-O4	1.370(8)
C6-N2	1.459(8)
Re1-N1	2.198(7)
Re1-N2	2.120(5)
Re1-O4	2.105(4)
K1-O4	6.482(1)

81-crown

Figure 4: Diamond plot of *fac*-[K(18-*crown*-6)][Re(*amidopy-bph*)(CO)$_3$] (**81-crown**) with a separated potassium ion coordinated by 18-*crown*-6 and two THF molecules (stick model with 50% transparency for clarity) Selected bond lengths in [Å] listed in the table. (Atoms with 0.25 Å diameter as standard ("Ball-and-Stick" design of Diamond plot), H-atoms omitted for clarity)

The increased steric bulk of the two phenyl groups presumably plays an important role for the separation. The Re(I) center resides in a distorted octahedral coordination sphere and the three CO ligands are located in mutual facial arrangement. The pyridine-amido-alkoxide ligand completes the octahedral sphere in the Re(I)-complex **81-crown**. The newly formed C6-C17 bond exhibits an interatomic distance of

1.560(9) Å and is slightly shorter than in the Re(I)-benzaldehyde complexes **80**. Measuring at elevated temperatures may causes these inaccuracies. The atomic distance of 6.482(1) Å clearly shows the separation of O4 and K1. The corresponding interatomic distance of 1.370(8) Å between C17 and O4 indicates the alkoxide formation (C-O single bond). Both adduct complexes (**80** and **81**) show reversible binding of the substrate. This is best demonstrated *via* the exchange reaction under an atmosphere of 1 bar of CO_2.

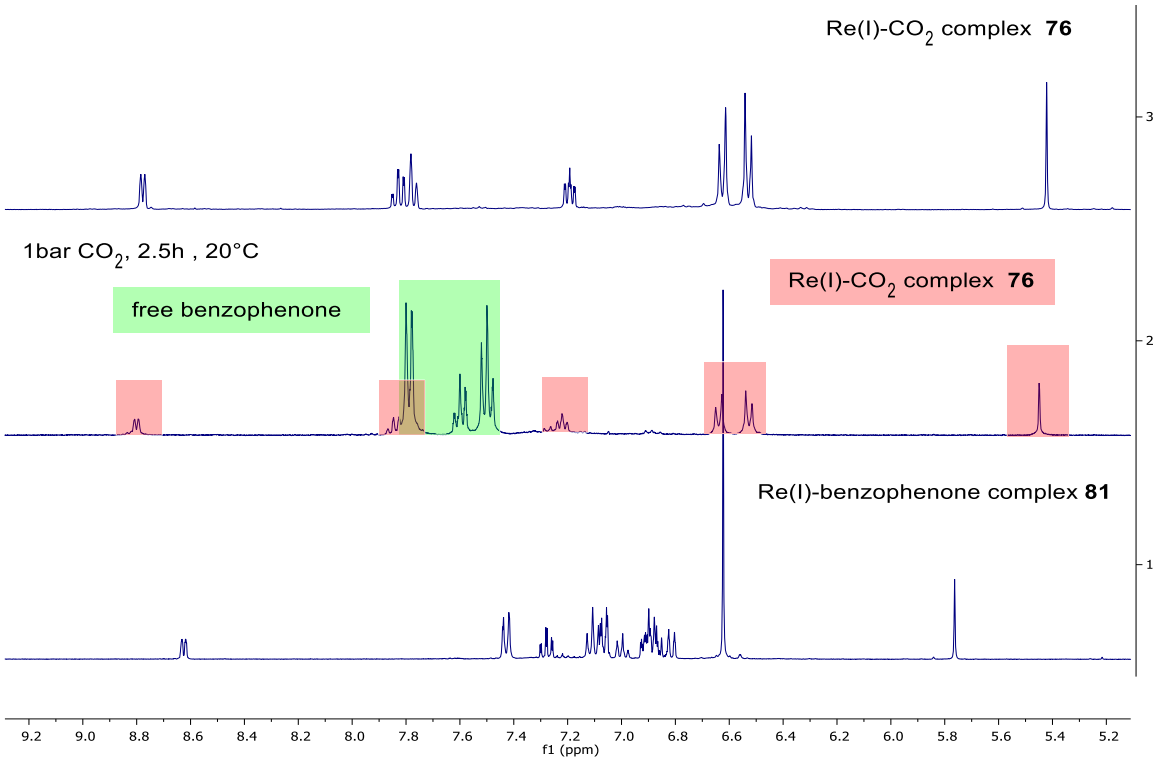

Figure 5: Relevant sections of the ^{1}H NMR spectra for the reaction of benzophenone in *fac*-K[Re(*amidopy-bph*)(CO)$_3$] (**81**) (bottom) with CO_2 under 1 bar of CO_2 atmosphere at ambient temperature (middle). For comparison the spectrum of *fac*-K[Re(*amidopy*-CO_2)(CO)$_3$] (**76**) is shown on top.

Whereas the exchange of benzophenone with CO_2 (Figure 5) takes place at ambient temperature with an almost quantitative conversion after 2.5 h, the exchange of the benzaldehyde (Figure 6) requires an increase in the temperature to 60 °C and a significantly longer reaction time of 12 h. A big discrepancy can be noticed with respect to the exchange reaction of CO_2 with the Re(I)-benzaldehyde complex **80** and the corresponding Mn(I)-complex **79**.[161] While **80** requires elevated temperature with 12 h

reaction time, **79** reacts instantaneously with CO_2 at ambient temperature. Exchange reactions with SO_2, using DABSO as an SO_2 source, were not successful.

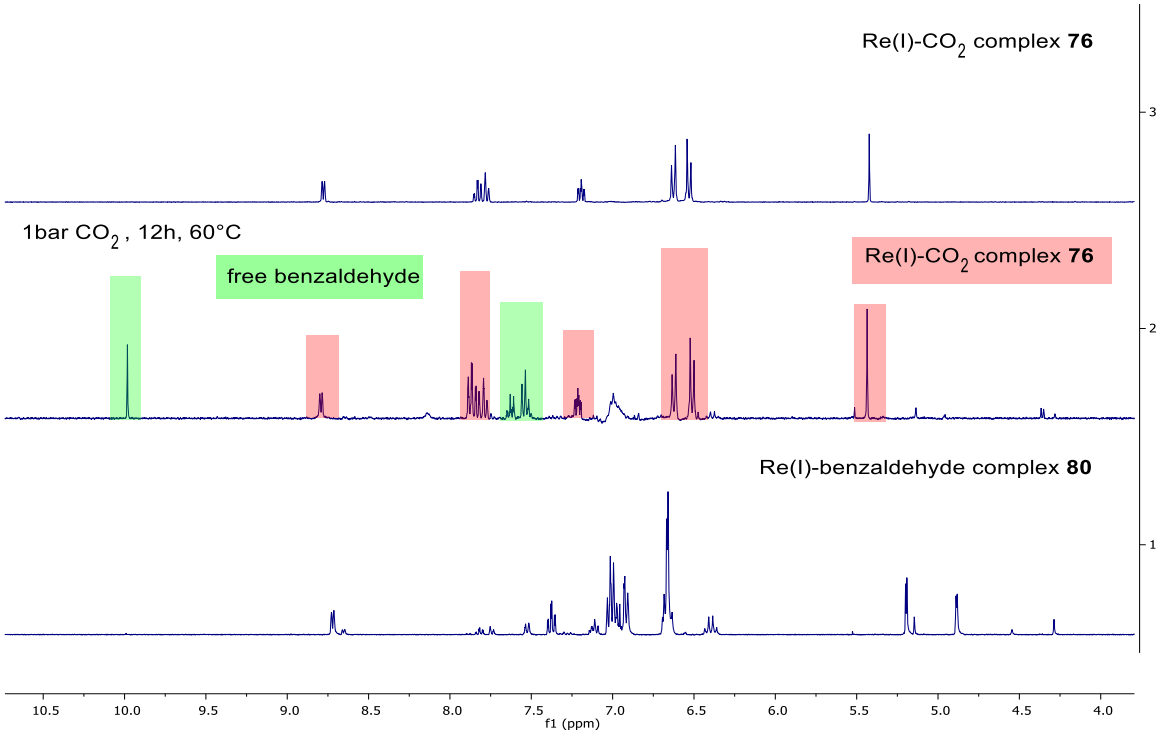

Figure 6: Relevant sections of the ^{1}H NMR spectra for the exchange reaction of benzaldehyde in *fac*-K[Re(*amidopy-ba*)(CO)$_3$] (**80**) (bottom) with CO_2 under 1 bar of CO_2 atmosphere at 60 °C (middle). For comparison the spectrum of *fac*-K[Re(*amidopy*-CO_2)(CO)$_3$] (**76**) is shown on top.

In the negative HRMS ESI spectrum of *fac*-[K(18-*crown*-6)][Re(*amidopy-bph*)(CO)$_3$] (**81-crown**), only the molecule ion without benzophenone $[M\text{-bph}]^-$ was detectable (m/z = 467.04096). In positive HRMS ESI mode, the double protonated molecule ion $(MH+H]^+$) with molecular formula $C_{29}H_{24}O_4N_2Re$ was found (m/z = 575.09741), as well as the 18-*crown*-6 chelated potassium ion (m/z = 303.12048). The cid HRMS^2 ESI spectrum of $[MH+H]^+$ by m/z = 651.13 shows the loss of the CO ligands and benzophenone and additionally the loss of H_2O can be suspected.

Summary and conclusion

The dearomatized bidentate 2-iminomethyl pyridine Re(I)-complex **75*-Re** could be successfully reacted with ketones and aldehydes *via* an MLC reaction pattern under reversible C-C and Re-O bond formation. Compared to the corresponding dearomatized bidentate 2-iminomethyl pyridine Mn(I)-complex **75*-Mn**, the Re(I)-complex **75*-Re** reacts readily with benzophenone in a quantitative way. The reversibility of the bonded substrates could be successfully demonstrated by exchange reactions with CO_2, similar to the previously published Mn(I)-complex **79**. The Re(I)-complex **75*-Re** indicates an increased affinity towards the C=O double bond of benzaldehyde with respect to benzophenone, as the exchange reaction with CO_2 requires harsher conditions for the Re(I)-benzaldehyde complex (**80**). It is noteworthy that the exchange of benzaldehyde with CO_2 in the corresponding Mn(I) complex **79** occurs immediately at room temperature.[161]

Experimental section

Synthetic works were performed using standard Schlenk techniques or executed in a glove box under argon atmosphere. Reagents were purchased from commercial sources (Sigma-Aldrich, ABCR) and used as received. THF-d_8 (ABCR) was degassed and dried over molecular sieves (4 Å). All solvents were collected from the solvent purification system SPS800 by MBraun. NMR spectra were recorded on a Bruker Avance Neo 600 MHz or Bruker Avance 360NB spectrometer at 23 °C. Chemical shifts for ^{1}H NMR spectra were reported as δ with correlation to tetramethylsilane (ppm), referenced to the signal of THF at 1.72 ppm. Chemical shifts for $^{13}C\{^1H\}$ NMR spectra were reported as δ with correlation to tetramethylsilane (ppm), referenced to the signal of THF at 25.31 ppm. HRMS-ESI mass spectra were recorded on a Thermo Fisher Scientific LTQ Orbitrap XL hybrid ion trap mass spectrometer. Crystallographic data were recorded on a Bruker Venture D8 diffractometer with graphite-monochromated Mo Kα (0.7107 Å) radiation. IR spectra were recorded with a Thermo Scientific Nicolet iS10 spectrometer.

Synthetic procedures

***fac*-K[Re(*amidopy-ba*)(CO)$_3$] (80)**

26.7 mg (0.05 mmol) of *fac*-[Re(*impy*)(CO)$_3$Br] (**73-Re**) was dissolved in 3 mL THF in a Schlenk tube. 4 eqiv. of potassium metal (7.8 mg, 0.20 mmol) were added to the red solution and the mixture was sonicated until the color changed to deep purple (4 h). The reaction mixture was filtered through a syringe filter (PTFE, 0.45 µm porosity) and added to 1 eqiv. (0.05 mmol, 5.3 mg) fresh distilled benzaldehyde. The color changed from purple to brown. ^{1}H NMR and ^{13}C NMR spectra indicated a quantitative turnover of benzaldehyde and the formation of a diastereomeric mixture (82:18 ratio **80a/80b**). The solution was layered with *n*-hexane at -16 °C, to obtain orange crystals suitable for X-ray diffraction analysis. Yield: 20.9 mg (0.03 mmol, 68%). ^{1}H NMR (360 MHz, THF) δ = 8.70 (d, , *J* = 5.2 Hz, 1H$_a$, CH$_{Py-1}$), 8.63 (d, *J* = 5.4 Hz, 1H$_b$, CH$_{Py-1}$), 7.80 (t, *J* = 7.5 Hz, 1H$_b$, CH$_{Py-3}$), 7.72 (d, *J* = 7.4 Hz, 1H$_b$, CH$_{Py-4}$), 7.50 (d, *J* = 7.6 Hz, 2H$_b$, CH$_{Ar-14,18}$), 7.35 (t, *J* = 7.6 Hz, 1H$_a$, CH$_{Py-3}$), 7.14-7.05 (m, 3H$_b$, CH$_{Py-2,}$ CH$_{Ar-15,17}$), 7.02-6.93 (m, 4H$_a$, CH$_{Py-2,}$ CH$_{Ar-15,17}$, CH$_{Ar-16}$; 1H$_b$ CH$_{Ar-16}$), 6.89 (d, *J* = 7.1 Hz, 2H$_a$, CH$_{Ar-14,18}$), 6.71-6.59 (m, 5H$_a$, CH$_{Py-4}$, CH$_{Ar-6,7,8,9}$), 6.43-6.32 (m, 4H$_b$, CH$_{Ar-6,7,8,9}$), 5.17 (d, *J* = 2.6 Hz, 1H$_a$, NCH), 5.12 (s, 1H$_b$, NCH), 4.86 (d, *J* = 2.6 Hz, 1H$_a$, OCH), 4.27 (s, 1H$_b$, OCH), 2.07 (s, 3H$_a$, CH$_3$), 1.94 ppm (s, 3H$_b$, CH$_3$). ^{13}C{^{1}H} NMR (91 MHz, THF-*d*$_8$) δ = 205.33 (s, 1C$_a$, CO), 205.20 (s, 1C$_b$, CO), 204.92 (s, 1C$_b$, CO), 203.75 (s, 1C$_a$, CO), 201.91 (s, 1C$_a$, CO), 201.79 (s, 1C$_b$, CO), 169.86 (s, 1C$_b$, C$_{q-5}$), 165.03 (s, 1C$_a$, C$_{q-5}$), 157.76 (s, 1C$_b$, C$_{q-7}$), 157.35 (s, 1C$_a$, C$_{q-7}$), 152.04 (s, 1C$_b$, C$_{Py-1}$), 151.47 (s, 1C$_a$, C$_{Py-1}$), 150.73 (s, 1C$_b$, C$_{q-18}$), 149.70 (s, 1C$_a$, C$_{q-18}$), 138.99 (s, 1C$_b$, C$_{Py-3}$), 137.13 (s, 1C$_a$, C$_{Py-3}$), 129.42 (s, 2C$_a$, C$_{Ar-9,11}$), 129.10 (s, 2C$_b$, C$_{Ar-9,11}$), 128.02 (s, 2C$_b$, C$_{Ar-19,23}$), 127.92 (s, 2C$_b$, C$_{Ar-20,22}$), 127.79 (s, 2C$_a$, C$_{Ar-20,22}$), 127.04 (s, 2C$_a$, C$_{Ar-19,23}$), 126.24 (s, 1C$_b$, C$_{Ar-21}$), 126.11 (s, 1C$_a$, C$_{Ar-21}$), 122.99 (s, 1C$_a$, C$_{Py-4}$), 122.18 (s, 1C$_b$, C$_{Py-2}$), 121.90 (s, 1C$_a$, C$_{Py-2}$), 120.07 (s, 1C$_b$, C$_{Py-4}$), 119.00 (s, 1C$_a$, C$_{q-10}$), 118.77 (s, 1C$_b$, C$_{q-10}$), 115.05 (s, 2C$_b$, C$_{Ar-8,12}$), 114.66 (s, 2C$_a$, C$_{Ar-8,12}$), 78.72 (s, 1C$_a$, NCH), 78.26 (s, 2C$_b$, NCH, OCH), 77.61 (s, 1C$_a$, OCH), 20.57 (s, 1C$_a$, CH$_3$), 20.50 ppm (s, 1C$_b$, CH$_3$). HRMS-ESI [CH$_2$Cl$_2$/CH$_3$OH] (m/z): neg: [M-ba]$^-$ calcd for C$_{16}$H$_{12}$N$_2$O$_3$Re$^-$: 467.04113; found 467.04086 (0.58 ppm). HRMS-ESI [CH$_2$Cl$_2$/CH$_3$OH(0.1% FA)] (m/z): pos [MH+H]$^+$ calcd for C$_{23}$H$_{20}$N$_2$O$_4$Re$^+$: 575.09758; found 575.09741 (0.3 ppm). IR (ATR) $\tilde{\nu}$ [cm^{-1}]: $\tilde{\nu}_{CO}$ = 1988 (m), $\tilde{\nu}_{CO}$ = 1859 (m), $\tilde{\nu}$ = 1595 (m), $\tilde{\nu}$ = 1551 (s), $\tilde{\nu}$ = 1389 (s). Selected bond lengths in Å from Diamond plot scXRD analysis: C1-C2 = 1.381(3), C2-C3 = 1.385(3), C3-C4 = 1.385(3), C4-C5 = 1.393(3), C5-C6 = 1.500(2), C7-C8 =

1.416(3), C8-C9 = 1.385(3), C9-C10 = 1.396(3), C10-C11 = 1.388(3), C11-C12 = 1.392(3), C7-C12 = 1.415(3), C10-C13 = 1.514(3), N1-C1 = 1.348(2), N1-C5 = 1.348(2), N1-Re1 = 2.186(2), N2-C6 = 1.462(2), N2-C7 = 1.376(2), N2-Re1 = 2.1347(15), Re1-C14 = 1.910(2), Re1-C15 = 1.920(2), Re1-C16 = 1.910(2), C14-O1 = 1.161(2), C15-O2 = 1.158(2), C16-O3 = 1.161(2), C17-C6 = 1.568(3), C17-O4 = 1.394(2), C17-C18 = 1.518(3), O4-Re1 = 2.125(1), O4-K1 = 2.609(1), C18-C19 = 1.389(3), C19-C20 = 1.392(3), C20-C21 = 1.384(3), C21-C22 = 1.385(3), C22-C23 = 1.388(3), C18-C23 = 1.396(3).

***fac*-K[Re(*amidopy-bph*)(CO)$_3$] (81)**

10.4 mg (0.02 mmol) of *fac*-[Re(*impy*)(CO)$_3$Br] (**73-Re**) was dissolved in 1 mL THF-d$_8$ in a Schlenk tube. 4 eqiv. of potassium metal (3 mg, 0.08 mmol) were added to the red solution and the mixture was sonicated until the color changed to deep purple (4 h). The reaction mixture was filtered through a syringe filter (PTFE, 0.45 µm porosity) to 1 eqiv. of benzophenone (3.5 mg, 0.02 mmol). The color changed from purple to brown. The NMR spectra indicated a quantitative yield of **81**. ^{1}H NMR (360 MHz, THF-d$_8$) δ = 8.60 (d, *J* = 4.8 Hz, 1H, CH$_{Py-1}$), 7.40 (dd, *J* = 8.2, 1.1 Hz, 2H, CH$_{Ar-18,22}$), 7.25 (td, *J* = 7.6, 1.6 Hz, 1H, CH$_{Py-3}$), 7.08 (t, *J* = 7.5 Hz, 2H, CH$_{Ar-19,21}$), 7.04 (dd, *J* = 8.1, 1.6 Hz, 2H, CH$_{Ar-13,17}$), 6.97 (t, $^3J_{HH}$ = 7.3 Hz, 1H, CH$_{Ar-20}$), 6.91-6.82 (m, 4H, CH$_{Ar-14,15,16}$, CH$_{Py-2}$), 6.79 (d, *J* = 7.7 Hz, 1H, CH$_{Py-4}$), 6.60 (s, 4H, CH$_{Ar-6,7,8,9}$), 5.74 (s, 1H, NCH), 2.04 ppm (s, 3H, CH$_3$). ^{13}C{^{1}H} NMR (91 MHz, THF-d$_8$) δ = 205.65 (s, 1C, CO), 203.60 (s, 1C, CO), 201.21 (s, 1C, CO), 167.29 (s, 1C, C$_{Py-q-5}$), 157.00 (s, 1C, C$_{q-7}$), 153.26 (s, 1C, C$_{q-18}$), 153.06 (s, 1C, C$_{q-24}$), 151.53 (s, 1C, CH$_{Py-1}$), 136.93 (s, 1C, CH$_{Py-3}$), 129.57 (s, 2C, CH$_{Ar-9,11}$), 128.53 (s, 2C, CH$_{Ar-25,29}$), 128.04 (s,2C, CH$_{Ar-26,28}$), 127.99 (s, 2C, CH$_{Ar-19,23}$), 127.25 (s, 2C, CH$_{Ar-20,22}$), 125.53 (s, 2C, CH$_{Ar-21,27}$), 123.51 (s, 1C, CH$_{Py-4}$), 121.68 (s, 1C, CH$_{Py-2}$), 119.81 (s, 1C, C$_{q-10}$), 115.29 (s, 2C, C$_{Ar-8,12}$), 83.21 (s, 1C, C$_{q-17}$), 78.45 (s, 1C, NCH), 20.54 ppm (s, 1C , CH$_3$).

***fac*-[K(18-*crown*-6)][Re(*amidopy-bph*)(CO)$_3$] (81-crown)**

22.7 mg (0.04 mmol) of *fac*-[Re(*impy*)(CO)$_3$Br] (**73-Re**) was dissolved in 3 mL THF in a Schlenk tube. 4 eqiv. of potassium metal (6.5 mg, 0.16 mmol) were added to the red solution and the mixture was sonicated until the color changed to deep purple (4 h). The reaction mixture was filtered through a syringe filter (PTFE, 0.45 µm porosity) to 1 eqiv. of benzophenone (7.3 mg, 0.04 mmol). The color changed from purple to

brown. 1 eqiv. (10.6 mg, 0.04 mmol) of 18-*crown*-6 was added and the solution was layered with *n*-hexane at -40 °C to obtaining yellow crystals suitable for X-ray diffraction analysis. Yield: 22.3 mg (0.02 mmol, 57.5%). HRMS-ESI [CH_2Cl_2/CH_3OH] (m/z): neg: $[M\text{-bph}]^-$ calcd for $C_{16}H_{12}N_2O_3Re^-$: 467.04113; found 467.04096 (0.36 ppm). HRMS-ESI [CH_3OH(0.1% FA)/CH_2Cl_2] (m/z): pos: $[MH+H]^+$ calcd for $C_{29}H_{24}N_2O_4Re^+$: 651.12892; found 651.12861 (0.48 ppm), $[18K6+K]^+$ calcd for $C_{12}H_{24}O_6K^+$: 303.12045; found 303.12048 (0.10 ppm). IR (ATR) $\tilde{\nu}$ [cm^{-1}]: $\tilde{\nu}_{CO}$ = 1973 (m), $\tilde{\nu}_{CO}$ = 1836 (s), $\tilde{\nu}$ = 1604 (m), $\tilde{\nu}$ = 1498 (m), $\tilde{\nu}$ = 1350 (m), $\tilde{\nu}_{crown}$ = 1102 (s). After addition of 1 eqiv. of 18-*crown*-6, signals in the ^{1}H NMR spectrum became very broad and a clear assignment was no longer possible. Selected bond lengths in Å from Olex report scXRD analysis (temperature of measurement at 253K): C1-C2 = 1.359(15), C2-C3 = 1.434(17), C3-C4 = 1.338(16), C4-C5 = 1.395(11), 5-C6 = 1.502(10), C7-C8 = 1.426(9), C8-C9 = 1.358(10), C9-C10 = 1.407(12), C10-C11 = 1.359(12), C11-C12 = 1.376(11), C7-C12 = 1.409(9) , C10-C13 = 1.511(11), N1-C1 = 1.345(10), N1-C5 = 1.338(9), N1-Re1 = 2.198(7), N2-C6 = 1.459(8), N2-C7 = 1.382(8) , N2-Re1 = 2.120(5), Re1-C14 = 1.892(8), Re1-C15 = 1.900(10), Re1-C16 = 1.892(8), C14-O1 = 1.175(9), C15-O2 = 1.168(10), C16-O3 = 1.161(9), C17-C6 = 1.560(9), C17-O4 = 1.370(8), C17-C18 = 1.527(9), O4-Re1 = 2.105(4), O4-K1 = 6.4826(2), C18-C19 = 1.402(11), C19-C20 = 1.387(13), C20-C21 = 1.361(18), C21-C22 = 1.392(18), C22-C23 = 1.390(13), C18-C23 = 1.375(12), C17-C24 = 1.527(11), C24-C25 = 1.335(11), C25-C26 = 1.397(12), C26-C27 = 1.333(16), C27-C28 = 1.365(16),C28-C29 = 1.417(13), C24-C29 = 1.404(11).

3.1.7 Nitrile Activation *via* Cooperative C-C and Re-N Bond Formation with Bidentate Pyridine-Based Rhenium(I) Triscarbonyle Complex

Similar to the previously reported Re-pincer complexes **60***[103] and **63***[104], the bidentate complex K[Re(*amidopy**)(CO)$_3$] (**75*-Re**) also reacts readily with nitriles. The reaction with aliphatic phenylacetonitrile, with a CH_2 in α-position to the nitrile group, leads to the quantitative formation of the enamido complex *fac*-K[Re(*amidopy-phacn*)(CO)$_3$] (**82**), under C-C and Re-N bond formation. Thereby an [1,3]-tautomeric H-shift from the methylene CH_2 group to the nitrogen atom occurs giving rise to an en-amido motif rather than a C=N ketimido functional group (Scheme 39).

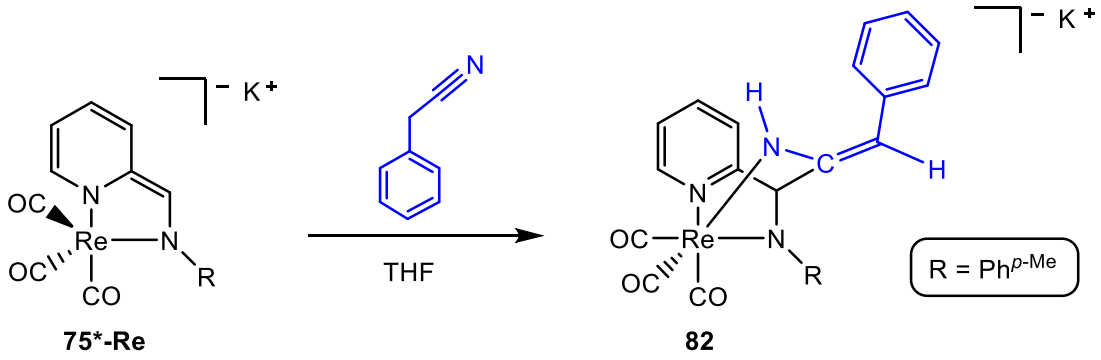

Scheme 39: Reaction of K[Re(*amidopy**)(CO)$_3$] (**75*-Re**) with phenylacetonitrile, forming the enamido complex *fac*-K[Re(*amidopy-phacn*)(CO)$_3$] (**82**).

The ^{1}H NMR spectrum of *fac*-K[Re(*amidopy-phacn*)(CO)$_3$] (**82**) clearly shows the three singlet resonances associated with NC*H* (5.42 ppm), C=C*H* (5.28 ppm) and N*H* (4.79 ppm) with an integral equal to one proton indicating the formation of the enamid group. The latter NH signal can be assigned due to the absence of a cross peak in the ^{1}H^{13}C HSQC NMR spectrum. The ^{1}H NMR resonance of the former CH_2 group of the phenylacetonitrile undergoes a downfield shift from 3.98 ppm to 5.28 ppm and the integral value is reduced to one proton. The rearomatization of the pyridine unit is indicated by a downfield shift of the respective resonances in the ^{1}H NMR spectrum (observed between 8.58 ppm and 7.07 ppm). Overall, these observations are consistent with the results obtained from the previously reported manganese and rhenium (**62**) pincer adduct complexes of **60***[103] and **63***[104] with phenylacetonitrile. In

the ^{13}C NMR spectrum of **82**, the signals of the two carbon atoms of the enamid group migrated also downfield from 117.9 ppm (*C*N) and 26.6 (*C*H_2) in free phenylacetonitrile to 157.19 ppm (*C*=NH) and 87.68 ppm (=*C*H). For full spectral characterization of **82**, see the experimental section and the supporting information (**7.5**). In the negative HRMS ESI spectrum of **82** the main signal is the molecule ion ($[M]^-$) peak of the adduct complex, showed the most abundant isotopic mass of m/z = 584.09863 for $C_{24}H_{19}O_3N_3Re$ and a small amount of the complex ($[M\text{-}phacn]^-$) where phenylacetonitrile is eliminated. The negative cid $HRMS^2$ ESI spectrum of $[M]^-$ results in the loss of phenylacetonitrile, showing the signal of $[M\text{-}phacn]^-$ with m/z = 467.04067 for $C_{16}H_{12}O_3N_2Re$. In the positive HRMS ESI of **82,** the double protonated molecule ion $[MH+H]^+$ was detected, with m/z = 586.11340 for $C_{24}H_{21}O_3N_3Re$ with its typical isotopic pattern. The positive cid $HRMS^2$ ESI spectrum of $[MH+H]^+$ results in the loss of all three CO ligands, but not the phenylacetonitrile. Single crystals of **82** (Figure 7) suitable for scXRD analysis could be obtained by washing the oily reaction product with *n*-hexane and subsequent addition of ten equivalents of phenylacetonitrile dissolved in *n*-hexane and resting for one day.

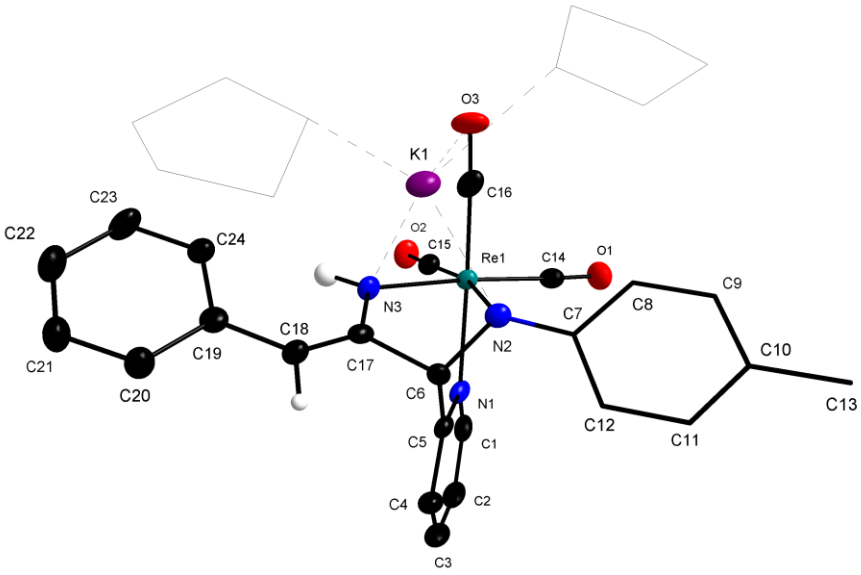

82

C1-C2	1.371(6)
C2-C3	1.388(7)
C3-C4	1.384(7)
C4-C5	1.382(6)
C1-N1	1.351(6)
C5-N1	1.364(5)
C5-C6	1.509(6)
C6-N2	1.472(5)
C6-C17	1.535(7)
C17-N3	1.354(5)
C17-C18	1.363(6)
Re1-N1	2.219(3)
Re1-N2	2.171(3)
Re1-N3	2.127(3)
K1-N2	2.824(3)
K1-N3	3.018(3)

Figure 7: Diamond plot of *fac*-K[Re(*amidopy-phacn*)$(CO)_3$] (**82**) with the potassium ion surrounded by two THF molecules (stick model with 50% transparency for clarity) and selected bond lengths [Å]. (Thermal ellipsoids at 50% probability, H atoms omitted for clarity except for enamido C-H and N-H)

The resulting molecular structure derived from scXRD analysis shows a distorted octahedral coordination sphere of the Re(I) center. The three CO ligands in **82** are arranged in a mutual facial position, the octahedral sphere is completed by the three coordinated nitrogen atoms of the ligand (N-pyridino, N-enamido, N-amido). The pyridine unit indicates the rearomatization by nearly equivalent C-C and C-N bond lengths. The newly formed C17-C6 bond, with a bond length of 1.535(7) Å, is in the range of the previously described phenylacetonitrile Re(I)-PNP[103] (1.55 Å) and Mn(I)-PNP[104] (1.54 Å) adduct-complexes. A [1,3]-tautomeric H shift gives rise to an enamido structural motif and the bond length of 1.363(6) Å indicates a C=C double bond in the enamido moiety. The C17-N3 single bond is characterized by a bond length of 1.354(5) Å and has a similar bond length to the corresponding bonds in the Re (**62**) and Mn phenylacetonitrile PNP pincer adduct complexes (1.35 Å) reported by Milstein. The generated bond of Re1-N3 has a length of 2.127(3) Å and is slightly shorter than in the phenylacetonitrile adduct Re(I) PNP-complex **62** (2.17 Å). The potassium counter ion, which is surrounded by two THF molecules, occupies a different position in the complex compared to the adduct complexes described previously.[159–161] The potassium ion, which compensates the negative charge of the complex, is coordinated by the two nitrogen atoms N2 and N3, indicated by similar bond lengths (N2-K1 = 2.824(3) Å and N3-K1 = 3.018(3) Å). This is in contrast to the previously shown complexes, in which it was only coordinated *via* the substrate's hetero atom (O). Some catalytic Michael addition reactions like described before by Milstein *et al.* were performed, but yields were far below values reported previously.[103; 104] Thus, the test conditions and the used substrates still need to be optimized. In addition, it could be observed that after a period of time with an excess of phenylacetonitrile, a formation of a cyclic C-C and C-N coupling product consisting of four phenylacetonitrile molecules was observed. The obtained product (**K-01)** is not discussed further in this work. However, the scXRD structural data and the mass spectrum can be found in the supporting information (**7.5**). Reactions with different nitriles without a hydrogen atom in α-position (benzonitrile) were also performed leading to a clean adduct, visible by ^{1}H NMR spectra in quantitative yield and suggesting the formation of the ketimino product. Unfortunately, the isolation of crystals for scXRD analysis was not successful. However, it is worth mentioning that, in contrast to rhenium complex **75*-Re**, the corresponding manganese complex **75*-Mn** reacts neither with nitriles with hydrogen

atom in α-position nor with nitriles without α-hydrogen atom by means of ^{1}H NMR spectroscopy *in-situ* reaction studies.

Summary and conclusion

Complex K[Re(*amidopy**)(CO)$_3$] (**75*-Re**), which has already shown effective activation reactions of CO_2 (**76**), SO_2 (**77-crown**) and various carbonyl groups (**80, 81**) was also capable of activating nitriles with a hydrogen atom in α-position under C-C and Re-N bond formation. The activated nitrile experienced an [1,3]-tautomeric H-shift from the CH_2 group to the former nitril nitrogen atom to give rise to an enamido moiety. The quantitative reaction of phenylacetonitrile led to the adduct complex *fac*-K[Re(*amidopy-phacn)(*CO)$_3$] (**82**), under rearomatization of the pyridine unit. Crystallographic data for the molecular structure of **82** is in accordance with previously reported pincer-type complexes incorporating a similar enamido group.[103; 104] The reversibility of the reaction shown before by Milstein *et al.* could not be confirmed yet. Attempted exchange reactions with CO_2 probably led to a new reaction product. ^{13}C labeled phenylacetonitrile could be used in reversibility studies similar to the ^{13}C labeled CO_2 studies in a previous publication.[159] Due to the tautomeric rearrangement of the α-hydrogen atom, the adduct complex **82** appeared to be less labile than the carbonyl complexes (**76**, **80**, **81**). The molecular ion $[M]^-$ was clearly visible in the negative HRMS ESI spectrum, which was usually only visible in traces in other adducts with **75*-Re**. Confirmation of MLC activity with nitriles without hydrogen in α-position has yet to be conclusively proven. The more diverse reactivity towards heterogeneous multiple bonds compared to the corresponding manganese complex **75*-Mn**, which has already been shown towards ketones, could also be shown with nitriles, since the manganese complex **75*-Mn** showed no reaction towards nitriles.

Experimental section

The experimental setup corresponds to the conditions as previous described in **3.1.6**. Phenylacetonitrile (Sigma-Aldrich) was dried and stored over molecular sieve (4 Å).

Synthetic procedures

***fac*-K[Re(*amidopy-phacn*)(CO)$_3$] (82)**

47.4 mg (0.09 mmol) of complex **86** were dissolved in 5.0 mL of THF in a Schlenk tube with Teflon valve. 4 eqiv. (13.6 mg, 0.35 mmol) of potassium metal were added to the

red solution and the mixture was sonicated until the color changed to deep purple (4 h). 1 eqiv. of phenylacetonitrile (10.2 mg, 0.09 mmol) was added and the color changed immediately to brown. The ^{1}H and ^{13}C NMR spectra showed a quantitative yield of complex **82**. The reaction mixture was filtered through a syringe filter (PTFE, 0.45 µm porosity) and the solution was layered with *n*-hexane, yielding a dark oily product. The *n*-hexane was separated from the oil by decantation and fresh *n*-hexane with 10 eqiv. of phenylacetonitrile added to the oily product and mixed up. Allowing the mixture to settle overnight led to orange crystals suitable for X-ray diffraction analysis. Yield of complex **82**: 49.0 mg 0.08 mmol, 90.7%). ^{1}H NMR (600 MHz, THF-d_8) δ = 8.58 (d, *J* = 5.0 Hz, 1H, CH_{Py-1}), 7.85 (d, *J* = 7.6 Hz, 1H, CH_{Py-4}), 7.75 (t, *J* = 7.3 Hz, 1H, CH_{Py-3}), 7.07 (t, *J* = 6.5 Hz, 1H, CH_{Py-2}), 7.03 (d, *J* = 7.8 Hz, 1H, $CH_{Ar-15,19}$), 6.99 (t, *J* = 7.6 Hz, 2H, $CH_{Ar-16,18}$), 6.65 (d, *J* = 8.0 Hz, 2H, $CH_{Ar-7,8}$), 6.60 (t, *J* = 7.2 Hz, 1H, CH_{Ar-17}), 6.57 (d, *J* = 8.1 Hz, 2H, $CH_{Ar-6,9}$), 5.42 (s, 1H, NCH), 5.28 (s, 1H, NC=CH), 4.79 (s, 1H, NH), 2.05 ppm (s, 2H, CH_3). $^{13}C\{^{1}H\}$ NMR (151 MHz, THF-d_8) δ = 205.30 (s, 1C, CO), 201.99 (s, 1C, CO), 201.36 (s, 1C, CO), 167.60 (s, 1C, $C_{quart-Py-5}$), 157.82 (s, 1C, $C_{quart-Ar-7}$), 157.19 (s, 1C, $C_{quart-17}$), 152.44 (s, 1C, CH_{Py-1}), 143.84 (s, 1C, $C_{quart-Ar-19}$), 138.77 (s, 1C, CH_{Py-3}), 129.65 (s, 2C, $CH_{Ar-9,11}$), 128.63 (s, 2C, $CH_{Ar-21,23}$), 124.41 (s, 2C, $CH_{Ar-20,24}$), 122.61 (s, 1C, CH_{Py-2}), 122.00 (s, 1C, CH_{Py-4}), 121.40 (s, 1C, $C_{quart-Ar-10}$), 120.26 (s, 1C, CH_{Ar-22}), 115.72 (s, 2C, $CH_{Ar-8,12}$), 87.68 (s, 1C, C_{18}), 80.34 (s, 1C, C_6), 20.45 ppm (s, 1C, CH_3). HRMS-ESI [CH_3OH(0.1% FA, 2mM AF (ammonium formiate))] (m/z): neg: $[M]^-$ calcd for $C_{24}H_{19}N_3O_3Re^-$: 584.09902; found 584.09863 (0.67 ppm). HRMS-ESI [CH_3OH(0.1% FA, 2mM AF)] (m/z): pos: $[MH+H]^+$ calcd for $C_{24}H_{21}N_3O_3Re^+$: 586.11357; found 586.11340 (0.29 ppm). IR (ATR) $\tilde{\nu}$ [cm^{-1}]: $\tilde{\nu}$ = 1984 (s), $\tilde{\nu}_{CO}$ = 1863 (s), $\tilde{\nu}_{CO}$ = 1815 (s). Selected bond lengths in Å from Diamond plot scXRD analysis: C1-C2 = 1.371(6), C2-C3 = 1.388(7), C3-C4 = 1.384(7), C4-C5 = 1.382(6), C5-C6 = 1.509(6), C7-C8 = 1.421(6), C8-C9 = 1.382(6), C9-C10 = 1.390(7), C10-C11 = 1.385(6), C11-C12 = 1.392(6), C7-C12 = 1.402(6), C10-C13 = 1.512(6), N1-C1 = 1.351(6), N1-C5 = 1.364(5), N1-Re1 = 2.219(3), N2-C6 = 1.472(5), N2-C7 = 1.379(5) = N2-Re1 = 2.171(3), Re1-C14 = 1.933(4), Re1-C15 = 1.914(5), Re1-C16 = 1.878(5), C14-O1 = 1.168(5), C15-O2 = 1.168(6), C16-O3 = 1.161(5), C17-C6 = 1.535(7), C17-N3 = 1.354(5), C17-C18 = 1.363(6), N3-Re1 = 2.127(3), N3-K1 = 3.018(3), N2-K1 = 2.824(3), O3-K1 = 3.451(4), C18-C19 = 1.460(6), C19-C20 = 1.399(6), C20-C21 = 1.391(6), C21-C22 = 1.370(7), C22-C23 = 1.380(7), C23-C24 = 1.394(6), C19-C24 = 1.403(6).

3.2 Tridentate Rh(I) π-Complexes for MLC Substrate Activation

3.2.1 Overview

Grützmacher *et al.* intensively explored the coordination chemistry of tethered *trop* (dibenzoa,d]cycloheptenyl) π-ligands, stabilizing electron-rich, low-valent transition metal complexes.[134; 162–164] The *trop* ligand exhibits a metal-alkene π-bonding unit with additional bulky aromatic groups. In the complexed concave structure, the olefinic group is electrically decoupled from the aromatic rings, which point away from the metal center (endo), having a strong steric influence (Scheme 40).[165] In addition, the ligand scaffold offers the possibility of an hemilabile olefinic ligand[166], through the possible exo or endo position of the seven-membered ring.

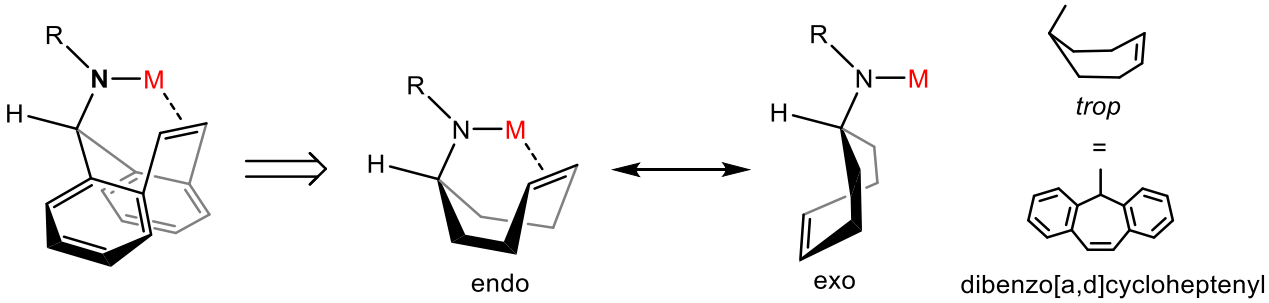

Scheme 40: Possible bonding modes (endo and exo) of the *trop* (dibenzo[a,d]cycloheptenyl) ligand in metal complexes.[165]

The strength of the metal-olefin bond is primarily determined by the intensity of the π-backbonding of the metal.[137; 138] The σ-donation to the metal center (Scheme 41 a) usually plays a subordinated role.

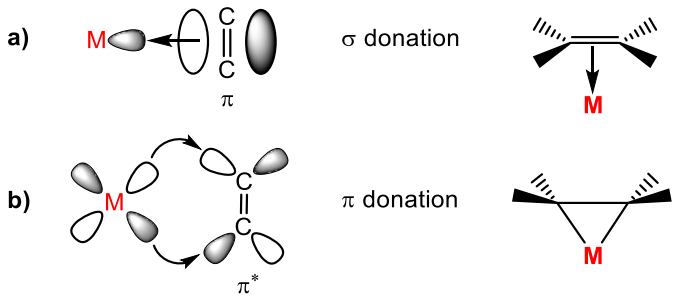

Scheme 41: Electronic interactions in a donor-acceptor model in metal-olefin complexes.

Metals of high oxidation states tend to have a rather weak π-bonding, resulting in a weaker binding mode. Strongly π-basic metals on the other hand, form a stronger π-backbonding to the olefin group and causes a significantly elongated C-C bond and the bonding situation is better represented as a metallacyclopropane structure (Scheme 41 b). Olefinic coordinated groups have the property of removing electron density from the metal center, especially from π-basic metals with strong π-backbonding. The nature of the metal center is significantly influenced by olefin chelation. A stabilizing effect of radical species and delocalization of the spin density over the *trop*-Ligand could also be demonstrated.[134; 162; 167]

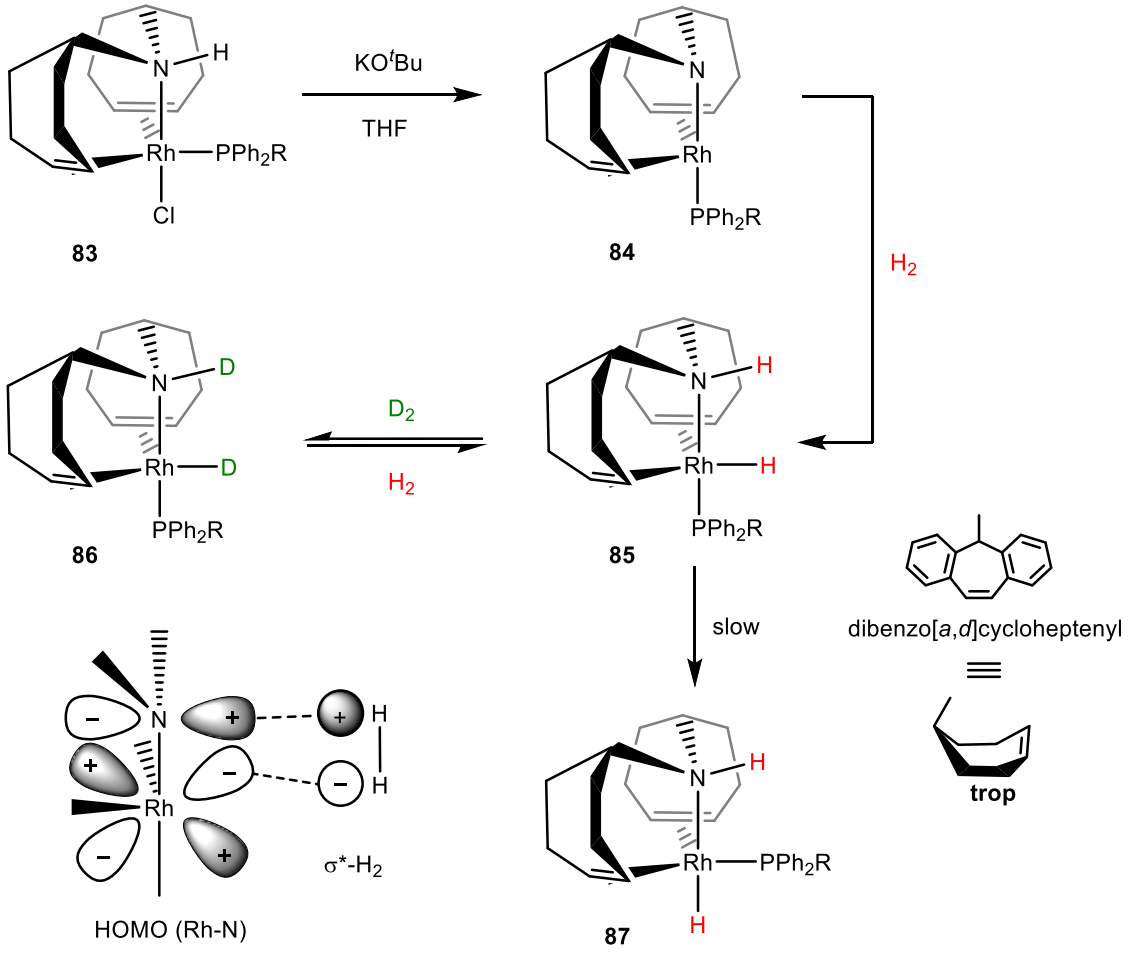

Scheme 42: Reversible heterolytic cleavage of H_2 with the *trop*$_2$NH Rh(I)-complex **83** and exchange reaction with D_2. The Catalytic inactive olefin complex **87** is formed after hydride isomerization.[6; 168] (R = p-tolyl)

With the *trop*$_2$NH Rh(I)-complex **96,** they could show a reversible heterolytic cleavage of H_2 across the Rh(I) center and the amido group under [1,2]-addition

(Scheme 42).[168] Later they showed the production of hydrogen from methanol-water mixtures.[135] The metal center has a well shielded backbone with an accessible front for substrate activation *via* MLC. The concerted addition of H_2 is an exothermic process. In contrast to this, the classical oxidative addition on the metal center is endothermic.[168] The preferred bifunctional activation is based on the fact, that the σ*-orbital of the H_2 molecule matches very well with the antibonding combination of the lone pair at the nitrogen atom and the filled d_{xz}-orbital at the Rh(I) center (Scheme 42).[6] Slow isomerization of the hydride to the axial position causes a conversion to the catalytically inactive olefin complex **87**. Additionally, successful hydrogenation reactions of ketones and imines with complex **84** with high catalytic turnovers could be demonstrated.[168]

3.2.2 Precursor Chemistry

The 2-aminomethyl pyridine scaffold has been extended to the multidentate olefinic actor ligand *dbap-py* (**90**). N-alkylation of dibenzazepine *dbap*-H **(88**) with 2-picolyl chloride (**89**) yielded the tridentate ligand *dbap-py* (**90**) (Scheme 43). The diamagnetic complex [Rh(I)(*dbap-py*)Cl] (**91**) was obtained by reaction of *dbap-py* (**90**) with chlorobis(ethylene)rhodium(I) dimer *via* pyridine-amine-olefin chelation. A strong binding of the olefinic group to the metal center is supposed because of an elongated C=C bond in the complexes, caused by a strong π-backbonding. This is in agreement with previous works with rhodium *trop*-olefin complexes.[169; 170] As a stabilizing ligand, triphenylphosphine is used to enable a later beneficial 18 VE environment and a more sterically hindered backbone to the metal center, to obtain complex [Rh(*dbap-py*)(PPh_3)Cl)] (**92**). The benzylic methylene group was readily deprotonated with base, giving rise to the dearomatized neutral square planar complex [Rh(*dbap-py**)PPh_3] (**93***) (the asterisk indicates the dearomatized pyridine unit), with a C-nucleophilic alkene moiety, suitable for MLC.

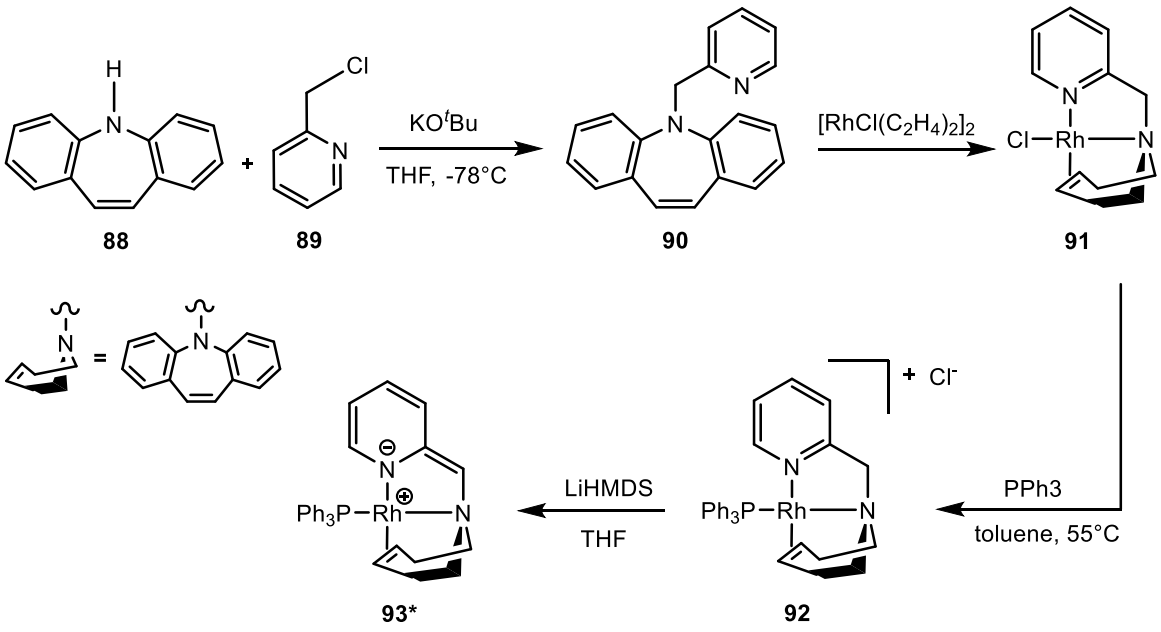

Scheme 43: Synthesis pathway for the square planar tridentate olefin complex [Rh(I)(*dbap-py**)PPh$_3$] (**93***), suitable for substrate activation *via* MLC.

The formal oxidation state of the metal center remains unchanged. In contrast to the *trop*$_2$NH ligand of Grützmacher[168], the complexed nitrogen atom is part of the seven-membered ring. Only a few examples of such ligand scaffolds with bidentate chelation over the seven-membered ring in a dibenzazepine unit have been described in the literature so far.[171–173] The nitrogen atom is not bound to a hydrogen atom, so it exhibits no cooperative properties for MLC. The iminostilbene scaffold solely serves as a bulky olefinic steering ligand giving rise to a somewhat unusual tridentate pincer-type ligand enabling a dearomatization/rearomatization reaction sequence.

3.2.3 Rh(I) Complex with a Tridentate Pyridine-Amino-Olefin Actor Ligand-Metal-Ligand Cooperative Activation of CO_2 and Phenylisocyanate under C-C and Rh-E (E = O,N) Bond Formation[174]

In this work, a fast reaction of **93*** with heterogeneous bonds (C=O, C=N), represented by CO_2 and phenylisocyanate, under C-C and Rh-E (E = O,N) bond formation *via* 1,3-addition under rearomatization of the pyridine unit was observed, giving rise to the penta-coordinated Rh(I) CO_2-complex [Rh(*dbap*-CO_2)(PPh_3)] (**94**) and Rh(I) phenylisocyanate complex [Rh(*dbap*-NCO)(PPh_3)] (**95**) (Scheme 44).

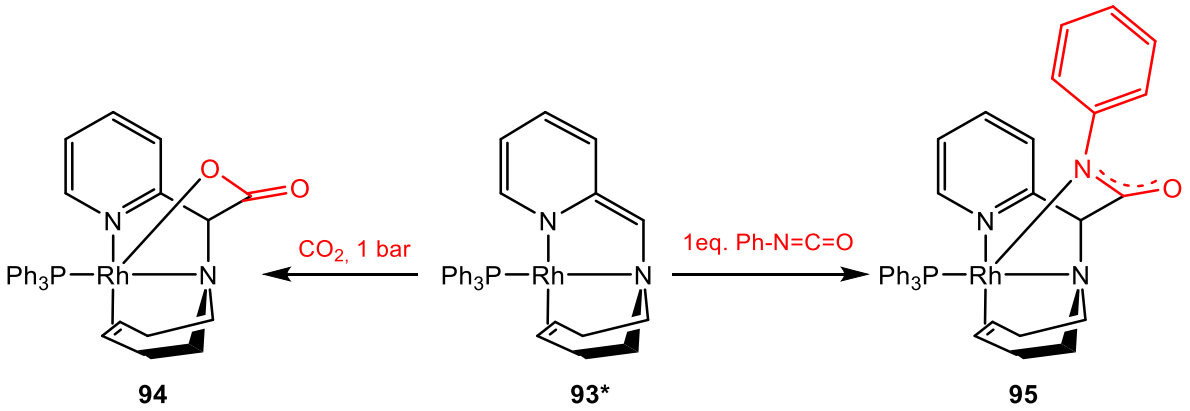

Scheme 44: Activation of CO_2 in [Rh(*dbap*-CO_2)(PPh_3)] (**94**) and phenylisocyanate in [Rh(*dbap*-NCO)(PPh_3)] (**95**) by the tridentate pyridine-amino-olefin complex **93*** *via* MLC under rearomatization and 1,3-addition.

I developed the synthesis of the ligand framework and achieved full characterization thereof. The synthesis of the Rh-complexes was carried out by Isabell Heuermann and Benjamin Heitmann. The synthesis of the adduct complexes and their characterization was carried out by Isabell Heuermann in the course of her master thesis. During the project I supported and supervised the work. scXRD analyses were measured and evaluated by Dr. Enno Lork and Daniel Duvinage.

The obtained results were published in the following journal:

I. Heuermann, B. Heitmann, R. Stichauer, D. Duvinage, M. Vogt, *Organometallics* **2019,** *38*, 1787-1799.
DOI: 10.1021/acs.organomet.9b00094

My percentage contribution of this publication in categories: experimental concept and design: ca. 50%, experimental work and acquisition of experimental data: 30%, data analysis and interpretation: 40%, preparation of Figures and Tables: ca. 30%, drafting of the manuscript: ca. 35%.

ORGANOMETALLICS
Article
Cite This: Organometallics 2019, 38, 1787−1799
pubs.acs.org/Organometallics

Rh(I) Complex with a Tridentate Pyridine−Amino−Olefin Actor Ligand−Metal−Ligand Cooperative Activation of CO_2 and Phenylisocyanate under C−C and Rh−E (E = O, N) Bond Formation

Isabell Heuermann,[†] Benjamin Heitmann,[†] Rasmus Stichauer, Daniel Duvinage, and Matthias Vogt*

FB 2 Biologie/Chemie, Institut für Anorganische Chemie und Kristallographie, Universität Bremen, Leobener Str. 7, NW2 C2060, 28359 Bremen, Germany

Supporting Information

ABSTRACT: We synthesized and characterized the novel olefinic multidentate actor ligand **dbap-py**. The ligand consists of a 2-methyl pyridine unit and an azepine component fused by an N-alkylation. The coordination chemistry to Rh(I) centers was explored and **dbap-py** revealed interesting tridentate chelation (pyridine−amine−olefin), which can suit square planar as well as distorted trigonal bipyramidal coordination spheres in Rh(I) complexes. Most notably, **dbap-py** in [Rh(dbap-py)(PPh_3)Cl] (**3**) entails an acidic benzylic methylene moiety, which is readily deprotonated allowing for the formation of the neutral square planar complex [Rh(dbap-py*)(PPh_3)] (**4**, the asterisk indicates the deprotonated ligand). As a result, the deprotonation disrupts the aromatic π-system of the pyridine unit in **4** and a C-nucleophilic methine moiety is formed. Complex **4** reacts in tetrahydrofuran solution at ambient temperature rapidly with C=O bonds present in CO_2 or the N=C bond of phenyl isocyanate (Ph-NCO) to give the penta-coordinated rhodium κ^1-*O* carboxylate [Rh(dbap-COO)(PPh_3)] (**5**) and the rhodium κ^1-*N* amidate [Rh(dbap-NCO)(PPh_3)] (**6**), respectively. Both reactions are characterized by a C−C and Rh−E (E = O (**5**); N (**6**)) bond formation under concomitant redistribution of the ligand's π-system of the pyridine unit ("rearomatization"). To the best of our knowledge, compound **6** gives precedence to Rh(I) complexes with a κ^1-*N* amidate ligand. Remarkably, metal−ligand cooperation is key to the uptake of Ph-NCO and allows for a convenient access to an amidate ligand motif.

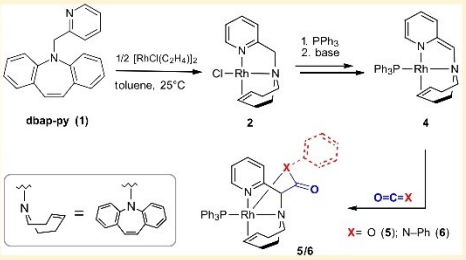

INTRODUCTION

The pioneering work by Zeise almost 200 years ago marked the starting point for the development of transition-metal complexes with olefinic ligands.[1] Overcoming their role as simple placeholders in metal precursors, as substrates, or additives, olefins were developed into important steering ligands[2,3] with applications, for instance, in asymmetric homogeneous catalysis.[4−8] In this regard, [5*H*]dibenzo[*b*,*f*]-azepine (**dbap-H**, Scheme 1I) is a tricyclic, nitrogen-containing heterocyclic compound, which can serve as building block for olefinic hybrid chelates. That is, the seven-membered heterocycle can form a bidentate concave ligand structure, which encompasses an olefinic binding site, as well as the N-donor moiety (Scheme 1I).[9] In this respect, **dbap-H** is an intriguing ligand precursor allowing not only for a facile N-functionalization and thus for the introduction of further binding sites, but also for the incorporation of substituents directly at the olefin.[10] Yet reports of **dbap** ligand motifs in the literature remain rather infrequent. However, the azepine motif is an important feature for a variety of pharmacologically active substances with importance for antiepileptic drugs,[11−13] which, as a result, makes **dbap-H** commercially available. Carreira and co-workers utilized **dbap-H** as precursor for the synthesis of chiral phosphoramidite−olefin motifs (Scheme 1, **C**) used as steering ligand in iridium complexes as catalysts for a variety of enatioselective bond formations, such as allylic[14−16] and allenylic substitutions,[17] allyl−allylsilanes cross-coupling,[18] or polyene cyclization.[19,20] Dorta and co-workers described chiral Rh complexes with phosphoramidite−olefin hybrid ligands as catalysts for [1,4]-additions to enones[21] and reported the development of a P-stereogenic **dbap**-based phosphoramidite ligand showing a variety of coordination modes in Ru(II) complexes.[22] The same group described s-block metal amide complexes employing dibenzoazepinate (**dbap**$^-$, **D**)[9] and very recently the development of (chiral) S(O)-dibenzazepine hybrid ligands (**E**) for Rh(I) complexation with application as catalysts for the Hayashi−Miyaura reaction.[10] Lammertsma, de Bruin, and co-workers reported related phosphane−olefin heterobidentate ligands with dibenzo[*b*,*f*]phosphepine backbone (e.g., **F**).[23] The coordination chemistry of the interrelated 5*H*-dibenzo[*a*,*d*]cycloheptene-5-yl motif ("trop" ligand, Scheme 1, **A** and **B**) was largely developed by Grützmacher and co-workers. The initial reports concerned phosphine−

Received: February 13, 2019
Published: April 9, 2019

DOI: 10.1021/acs.organomet.9b00094
Organometallics 2019, 38, 1787−1799

Scheme 1. Introduction to dbap and Trop Ligands (I and II); Double Deprotonation of Bis(2-picolyl)amine Coordinated to Olefin Complexes of Ir(I) and Rh(I) (III); Metal−Ligand Cooperation in Pyridine-Based Pincer Complexes, X−Y Single-Bond Activation (IV); Metal−Ligand Cooperative Activation in CO_2 in a Re Bis-amido Pyridine Complex (V)

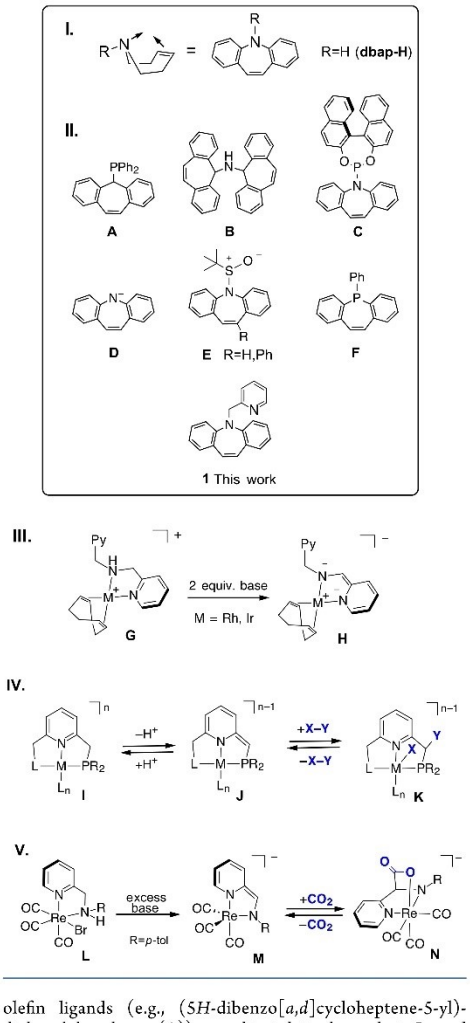

olefin ligands (e.g., (5*H*-dibenzo[*a*,*d*]cycloheptene-5-yl)-diphenylphosphane (**A**)) coordinated to low-valent Ir and Rh metal centers and date back to 1998.[24−26] Since then the trop-chemistry blossomed and a large variety of olefinic hybrid ligands were reported[27−32] giving rise to remarkable applications: For instance, trop ligands with N-donor moieties (e.g., "bistrop amine", **B**) in Rh(I) compounds allowing for catalytic transfer hydrogenation reactions using ethanol as sustainable hydrogen donor.[33,34] The transition-metal complexes with trop ligands were described as potent catalysts for the dehydrogenation of small molecules with implication for energy storage.[35−38] Rh complexes with bistrop-amine ligand **B** were employed as electrocatalysts deposited on a carbon anode for the electroreforming of renewable alcohols[39] and application in organometallic fuel cells.[40,41] Trop ligands gave rise to the stabilization and isolation of transient aminyl radicals in the coordination sphere of transition-metal complexes[42−44] and are suitable ligands for low-valent first-row transition-metal complexes.[45−47] We herein describe the new tridentate olefin ligand involving a **dbap** backbone fused with a 2-methyl pyridine unit via N-alkylation at the azepine unit to give (5-(pyridine-2-ylmethyl)5*H*-dibenzo[*b*,*f*]azepine, **dbap-py**, **1**). The scaffold allows for a three-dentate chelation of a metal center via the two N-donor moieties (pyridine and amine), as well as via the olefin of the azepine unit (N-N-ole chelating ligand). The [((2-pyridyl)methyl)amine] ligand motif in **1** is an intriguing structural feature, which can reveal noteworthy reactivity upon reaction with a strong base. A few reports describe the deprotonation of the methylene group to give rise to a methine moiety under concomitant rearrangement of the ligand's π-system ("dearomatization"). Specifically, Tejel, de Bruin, and co-workers reported the double deprotonation of bis(2-picolyl)amine coordinated to Ir(I) and Rh(I), allowing for the formation of ene−amido structures (**G** and **H**).[48−50] Redox noninnocent behavior was reported by Kojima and co-workers for a tris(2-pyridylmethyl)amine ligand induced by initial deprotonation at the methylene moiety in a Rh(III) complex.[51] Deprotonation of the CH_2 group of a picolyl-substituted N-heterocyclic carbene ligand in Ru(II) and Fe(II) piano−stool complexes was reported by Song and co-workers.[52] We have recently described the double deprotonation of an α-amino-pyridine ligand in a rhenium(I) triscarbonyl complex (**L**) allowing for the formation of the anionic ene−amido species (**M**).[53] Subsequent reaction with CO_2 gave rise to the carboxylate (**N**) via [1,3]-addition and Re−O and C−C bond formation. Similar reactivity was observed by Kubiak for an dianionic molybdenum complex.[54,55] Transition-metal complexes with substituted 2,6-lutidine ligands (e.g., PNN and PNP pincer-type ligands)[56−58] can undergo reversible deprotonation at the benzylic CH_2 moiety of the pincer-"arms" causing the disruption and reestablishment of the ligand's aromatic system (**I**−**J**).[59,60] Likewise, double deprotonation of two CH_2 groups of each pincer arm was reported.[61−63] Triggered by the reversible deprotonation, such "dearomatization/aromatization" sequence can be involved in remarkable metal−ligand cooperative (MLC) single- (Scheme 1IV) and multiple-bond activation reactions. The associated bond cleavage and bond formation proceed under participation of both the metal center and the pincer ligand (e.g., in reversible X−Y bond activation I−K). Recent advances have unveiled significant opportunities for pincer systems in homogeneous cooperative catalysis[64−68] and entail unusual templated catalytic C−C[69] and C−O[70] bond formations. The deprotonation of PNN-pincer ligands typically arises at the phosphine-arm rather than at the amine-arm (N-substituted picolyl group). However, Sanford and co-workers reported initial deprotonation of a [Ru(PNN)CO(H)] pincer-type complex (PNN = 6-(di-*tert*-butylphosphinomethylene)-2-(*N*,*N*-diethylaminometh-yl)-1,6-dihydropyridine) at the P-arm and subsequent metal−ligand cooperative uptake of CO_2 via C−C bond formation at the benzylic position of the P-arm. Yet, they observed the formation of the thermodynamic product, which

DOI: 10.1021/acs.organomet.9b00094
Organometallics 2019, 38, 1787−1799

Scheme 2. Synthesis of Ligand dbap-py (1) and Complexes 2−4

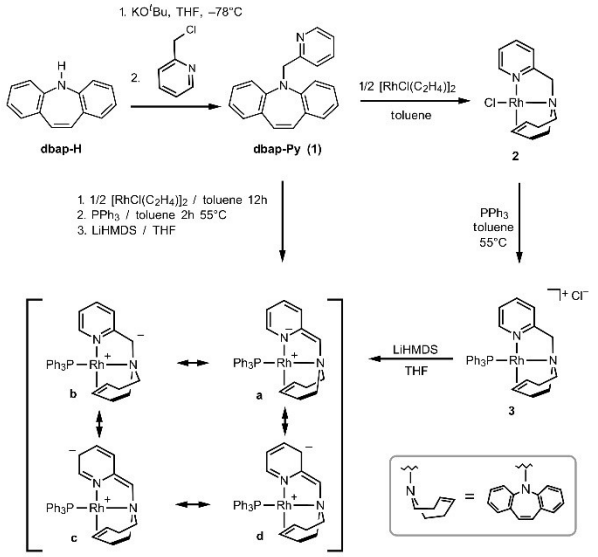

comprises C−C bond formation at the benzylic carbon moiety of the amine-arm.[71]

Against this background, this report concerns the synthesis of the **dbap-py** ligand and the examination of its properties as multidentate actor ligand in Rh(I) complexes. Our NMR spectroscopic investigations and single-crystal X-ray diffraction (XRD) analyses disclose the noteworthy metal−ligand cooperative activation of C=O bonds in CO_2, as well as of the C=N bond in phenyl isocyanate (Ph−N=C=O), via C−C and Rh−E (E = O, N) bond formation in a Rh(I) compound with deprotonated **dpab-py** ligand ([Rh(dbap-py*)PPh_3], **4**, the asterisk indicates the deprotonated ligand).

■ RESULTS AND DISCUSSION

Ligand **1** is readily obtained via a one-step synthesis strategy: iminostilbene (**dbap-H**) reacts with KO^{t}Bu in tetrahydrofuran (THF) at −78 °C. The subsequent addition of a solution of 2-chloromethyl pyridine hydrochloride in pyridine gives rise to the formation of **dbap-py** (Scheme 2, **1**) as an off-white crystalline solid. The ^{1}H NMR spectrum of **1** in $CDCl_3$ has characteristic resonances for the methylene group at 5.17 ppm (2H, s) and for both chemical equivalent olefinic protons at 6.86 ppm (2H, s). The resonances associated with the pyridine ring are observed at 8.50 ppm (1H, ddd, $^3J_{HH}$ = 5.0 Hz, J_{HH} = 1.7 Hz, J_{HH} = 1.0 Hz, py1), 7.59 ppm (1H, br d, $^3J_{HH}$ = 7.7 Hz, py4), 7.51 ppm (1H, td, $^3J_{HH}$ = 7.7 Hz, $^4J_{HH}$ = 1.7 Hz, py3), and 7.07 ppm (1H, br t, $^3J_{HH}$ = 5.00 Hz, C*H*, pyr2). The resonance for the benz-annulated rings of the azepine unit are centered at 7.22 ppm (2H, m, aze9), 7.11 ppm (4H, m, aze8,11), and 6.99 ppm (2H, td, $^3J_{HH}$ = 7.4 Hz, $^4J_{HH}$ = 1.1 Hz, aze10). The ^{13}C{^{1}H} NMR spectrum of **1** reveals the characteristic resonances associated with both ^{13}C nuclei of the olefin unit at 132.1 ppm (2C, s), and the benzylic CH_2 moiety at 56.9 ppm (1C, s). Detailed multidimensional NMR spectroscopic data can be found in the Supporting Information. Di-μ-chlorotetraethylene dirhodium(I) reacts readily with **1** in toluene at ambient temperature under concomitant release of ethene to give the pyridine−amino−olefin complex [Rh(dbap-py)Cl] (Scheme 2, **2**) in 89% yield. The ^{1}H NMR spectrum of **2** indicates the coordination of the olefin unit. The singlet resonance at 5.07 ppm associated with both chemically equivalent olefinic protons is significantly shifted by almost $\Delta\delta$ = 2 ppm to lower frequencies with respect to the free ligand. The absence of a mutual $^3J_{HH}$-coupling constant indicates a plane of symmetry and hints toward a rather square planar coordination sphere around the Rh(I) center with a central molecular mirror plane defined by the centroid of the olefin and both N-donor moieties. Consequently, a singlet ^{1}H resonance is observed at 4.94 ppm for both protons of the methylene group. Upon coordination of **1** to the Rh(I) center, the resonances associated with the C−H protons of the pyridine ring are shifted to higher frequencies (except for C−*H* in 4-position). The signals are observed at 8.93 ppm (1H, d, $^3J_{HH}$ 4.90 Hz, py1), 7.81 ppm (1H, t, $^3J_{HH}$ = 7.30 Hz, py3), 7.47 ppm (1H, d, $^3J_{HH}$ = 8.10 Hz, py4), and 7.34 ppm (1H, t, $^3J_{HH}$ = 6.30 Hz, py2). The ^{13}C{^{1}H} NMR spectrum of **2** corroborates the existence of a square planar coordination sphere, as only a single resonance is detected for both chemically equivalent olefinic carbon nuclei at 60.2 ppm. The resonance is shifted to lower frequencies by more than $\Delta\delta$ = 70 ppm, with respect to the free ligand **1**, and shows a significant coupling to the ^{103}Rh nuclei (d, $^1J_{CRh}$ = 15.8 Hz) indicating olefin coordination. The

DOI: 10.1021/acs.organomet.9b00094
Organometallics 2019, 38, 1787−1799

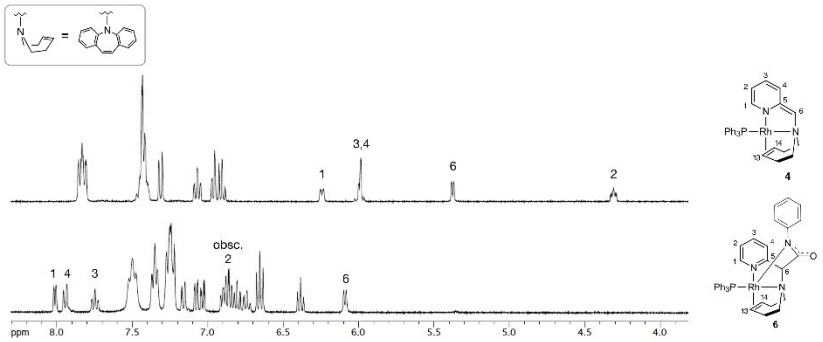

Figure 1. Sections of the ^{1}H NMR spectra (360 MHz, 298 K, THF-d_8) of the "dearomatized" complex **4** (top) and the "rearomatized" complex **6**.

resonance of the $^{13}CH_2$ nucleus of the methylene moiety is observed at a chemical shift of 61.6 ppm.

Complex **2** reacts with PPh_3 in toluene at 55 °C to give [Rh(dbap-py)PPh_3]Cl in 87% yield (Scheme 2, **3**). Upon coordination of the phosphine, the $^{31}P\{^{1}H\}$ NMR spectrum of **3** in $CDCl_3$ has a significant doublet resonance at 52.3 ppm with a $^{1}J_{PRh}$ coupling constant of 161 Hz. The ^{1}H NMR resonances associated with both olefinic protons in equal chemical environment are shifted further upfield, with respect to complex **2**. They are observed as doublet at 3.12 ppm with $^{3}J_{HP}$ = 2.7 Hz phosphorus coupling constant signaling the coordination of the double bond to the Rh center. The ^{1}H resonance of the methylene unit is centered at 5.44 ppm (2H, s). Hence, the ^{1}H NMR spectrum suggests a square planar coordination sphere for complex **3** in $CDCl_3$ solution, shaped by the tridentate py-N-olefin chelating motif and PPh_3 allowing for the formation of a cationic complex [Rh(dbap-py)PPh_3]$^{+}$ with Cl^{-} counteranion. The proton resonances for the C–*H* pyridine moieties are observed in the aromatic regime at 7.91 ppm (1H, d, $^{3}J_{HH}$ = 5.0 Hz, py1), 7.57 ppm (1H, t, $^{3}J_{HH}$ = 7.30 Hz, py3), 7.41 ppm (1H, py4, obscured by PPh_3), and 6.82 ppm (1H, t, $^{3}J_{HH}$ = 6.80 Hz, py2).

A suspension of complex **3** in THF reacts instantaneously with lithium bis(trimethylsilyl)amide (LiHMDS) under formation of a clear deep red solution. Layering the reaction mixture with *n*-hexane gives rise to the formation of large red crystals of the deprotonated compound [Rh(dbap-py*)-(PPh_3)] (Scheme 2, **4**, the asterisk indicates the deprotonated ligand) in good yield (86%). The $^{31}P\{^{1}H\}$ NMR spectrum of **4** in THF-d_8 exhibits a characteristic doublet at 55.7 ppm with a ^{103}Rh coupling constant of $^{1}J_{PRh}$ = 185.6 Hz. The ^{1}H NMR spectrum (360 MHz, THF-d_8, 298 K) indicates the deprotonation of the **dbap-py** ligand at the methylene moiety to give rise to a methine group: That is, a singlet resonance with an integral value associated with one proton is centered at 5.38 ppm. Complex **4** retains the plane of symmetry indicated by the doublet resonance ($^{3}J_{HP}$ = 2.7 Hz) correlated to both olefinic protons with a chemical shift of 3.51 ppm. Significantly, the deprotonation of compound **3** gives rise to a large upfield shift of the ^{1}H resonances linked to the C*H* pyridine moieties in **4** (see Figure 1, top): 6.24 ppm (1H, d, $^{3}J_{HH}$ = 6.4 Hz, py1), 5.99 ppm (2H, m, overlay, py3,4), and 4.31 ppm (1H, dt, $^{3}J_{HH}$ = 7.9 Hz, J_{HH} = 3.4 Hz, py2). Analysis of the $^{13}C\{^{1}H\}$ NMR spectrum of **4** recorded in THF-d_8 reveals the resonance for both olefinic ^{13}C nuclei as doublet of doublets at 59.7 ppm with a larger ^{103}Rh coupling constant ($^{1}J_{CRh}$ = 12.5 Hz) and smaller $^{2}J_{CP}$ = 1.7 Hz coupling constant, indicating the coordination of the double bond to the Rh center. The methine resonance falls at 91.4 ppm. In general, complex **4** can be described by several mesomeric structures (e.g., **4a–d**). The large upfield shift of the pyridine protons in the ^{1}H NMR spectrum and the chemical shift of 91.4 ppm of the ^{13}C methine resonance in the $^{13}C\{^{1}H\}$ NMR spectrum suggest a significant contribution of a resonance structure, which is characterized by an en-amine and the disruption of the pyridine π-system (dearomatization). Also, the nonequidistant C–C bond lengths of the pyridine unit, as well as the short C5–C6 interatomic distances in the planar ligand structure (torsion (N2–C6–C5–N1) = 2.1°), present in the molecular structure of **4** derived from our XRD study (see below), prompt us to describe the pyridine moiety in **dbap-py*** as a rather disrupted π-system. This is further corroborated by the reactivity of complex **4** allowing for C–C bond formation selectively at the benzylic carbon moiety via recovery of the pyridine π-system (see complexes **5** and **6**). Note, in addition to the stepwise synthesis approach, compound **4** can be conveniently obtained in high yield (83%) via a straightforward one-pot strategy avoiding time-consuming isolation of intermediates **2** and **3** (for details, see Experimental Section).

Reactivity of Compound 4. Complex 4 reacts in THF solution at ambient temperature rapidly with C=O bonds present in CO_2 or the N=C bond of phenyl isocyanate (Ph-NCO) to give the penta-coordinated rhodium κ^{1}-*O* carboxylate [Rh(dbap-COO)(PPh_3)] (**5**) and the rhodium κ^{1}-*N* amidate [Rh(dbap-NCO)(PPh_3)] (**6**), respectively (Scheme 3). Both reactions are characterized by a C–C and Rh–E (E = O (**5**); N (**6**)) bond formation under concomitant redistribution of the ligand's π-system of the pyridine unit ("rearomatization"). The reaction indicates the presence of a C-nucleophilic site in the benzylic position in the **dbap-py*** unit. In general, multidentate actor ligands have been identified as suitable platforms for small molecule activation[72] and specifically nucleophilic carbon sites within such ligands encompass interesting reactivity with respect to the reduction of CO_2.[73] Furthermore, amidate ligands show significant coordinative flexibility. The inherent hemilability of such heterofunctional multidentate ligands with small bite angles triggered increased

DOI: 10.1021/acs.organomet.9b00094
Organometallics 2019, 38, 1787–1799

Scheme 3. Reaction of the Deprotonated Complex 4 with CO_2, Ph-NCO, and H_2

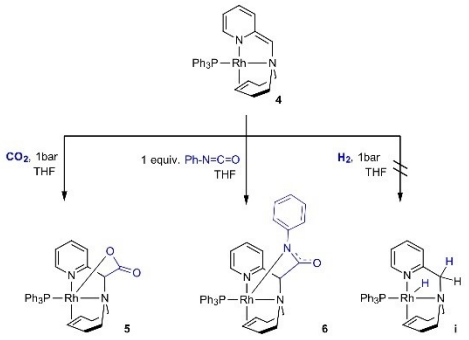

attention in the field of coordination chemistry.[74] However, Rh(I) complexes of such kind are sparsely reported and entail examples of μ_2-*N,O*, κ^2-*N,O*, and κ^1-*O* binding modes.[74,75] To the best of our knowledge, compound **6** gives precedence to Rh(I) complexes with a κ^1-*N* amidate feature. That is, MLC involving a dearomatization/rearomatization pathway is key to the unusual uptake of Ph-NCO and allows for an unconventional synthesis strategy to form amidates.

The ^{1}H NMR spectra of the formal [1,3]-addition products **5** and **6** show the characteristic downfield shift of the pyridine protons with respect to compound **4**, indicating the reestablishment of a rather aromatic pyridine π-system (resonances reside in the area 8.01−6.79 ppm; see Figure 1 and Table 1).

Additionally, the ^{1}H resonance of the benzylic proton shifts toward higher frequencies (br s, 6.18 ppm in **5** and d, 6.09 ppm in **6**) suggesting the formation of a sp^3-hybridized carbon moiety vicinal to the carboxylate and amidate moieties, respectively. The ^{1}H resonances associated with the olefin unit, observed at even lower frequencies with respect to **4** (see Table 1), indicating that the olefin remains tightly bonded to the Rh center. The presence of two chemical inequivalent olefinic protons in **5** gives rise to two distinct resonances at 2.91 ppm (1H, dd) and 3.19 ppm (1H, dd) with a large mutual $^3J_{HH}$ coupling constant of 6.50 Hz and smaller *J* coupling constants of 2.90 and 3.70 Hz, respectively. Similar to compound **5**, the ^{1}H NMR spectrum of **6** has two upfield-shifted olefinic resonances (each 1H, dd) at 3.23 and 3.41 ppm with a larger mutual H−H coupling constant ($^3J_{HH}$ = 6.70 Hz) and a smaller $^3J_{HP}$ coupling constant of 3.10 and 3.60 Hz, respectively. Hence, these spectral findings suggest a reduction in symmetry in **5**, as well as in **6**, due to the MLC-triggered uptake of CO_2 and Ph-NCO, respectively, into the ligand scaffold via C−C and concomitant Rh−E (E = O or N) bond formation. That is, the ^{1}H NMR spectra indicate the formation of a rather trigonal bipyramidal coordination sphere for compounds **5** and **6** in solution. The observed ^{31}P{^{1}H} NMR doublet resonance in THF-d_8 associated with compounds **5** and **6** are merely shifted (51.2 and 52.6 ppm, respectively) compared to compound **4** (55.7 ppm). However, the $^1J_{PRh}$ coupling constant significantly decreases to 167 Hz ($\Delta\partial$ = −19 Hz) for **5** and 159 Hz ($\Delta\partial$ = −27 Hz) for **6** with respect to **4** (186 Hz). The certainly interesting reaction of complex **4** with dihydrogen gas (1 atm, THF-d_8) did not yield the desired well-defined hydride species via an assumed H−H bond cleavage reaction under Rh−H and C−H bond formation (Scheme 3, i). Instead, a complex product mixture was observed in the ^{1}H NMR spectrum with multiple resonances associated to hydridic moieties.

Single-Crystal X-ray Diffraction Analysis. The molecular structures of the compounds **1**−**6** are shown in Figures

Table 1. Selected ^{1}H, ^{13}C{^{1}H}, and ^{31}P{^{1}H} NMR Chemical Shifts of the Compounds 1−6

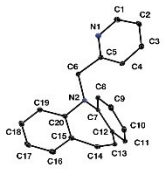

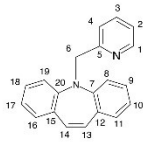

NMR chemical shifts (ppm)	1 $CDCl_3$	2 $CDCl_3$	3 THF-d_8	4 THF-d_8	5 THF-d_8	6 THF-d_8
$^1H_{olefin13/14}$	6.86	5.07	3.12	3.51	3.19; 2.91	3.41; 3.23
$^{13}C\{^1H\}_{olefin13/14}$	132.1	60.2	48.8	59.7[dS]	–[a]	49.6; 47.70
$^1H_{bzl}$	5.17	4.94	5.44	5.38	6.18	6.09
$^{13}C\{^1H\}_{bzl\text{-}6}$	56.9	61.6	57.5	91.4[dS]	–[a]	77.5
$^1H_{Py1}$	8.50	8.93	7.91	6.24	7.83	8.01
$^1H_{Py2}$	7.07	7.34	6.82	4.31	7.75−7.45[c]	6.90[b]
$^1H_{Py3}$	7.51	7.81	7.57	5.99	7.75−7.45[c]	7.75
$^1H_{Py4}$	7.59	7.47	7.41	5.99	7.75−7.45[c]	7.95
$^{31}P\{^1H\}$			52.3	55.7	51.2	52.6
			$^1J_{PRh}$ = 161 Hz	$^1J_{PRh}$ = 186 Hz	$^1J_{PRh}$ = 167 Hz	$^1J_{PRh}$ = 159 Hz

[a]Decomposition in polar chlorinated solvents and sparse solubility in THF-d_8 precluded acquisition of a ^{13}C{^{1}H} NMR spectrum. [b]Partly obscured in ^{1}H NMR spectrum, chemical shift extracted from ^{1}H−^{1}H correlation spectroscopy NMR spectrum. [c]Pyridine signals overlap partially with resonances of PPh_3. [dS]pectrum recorded in CD_2Cl_2.

DOI: 10.1021/acs.organomet.9b00094
Organometallics 2019, 38, 1787−1799

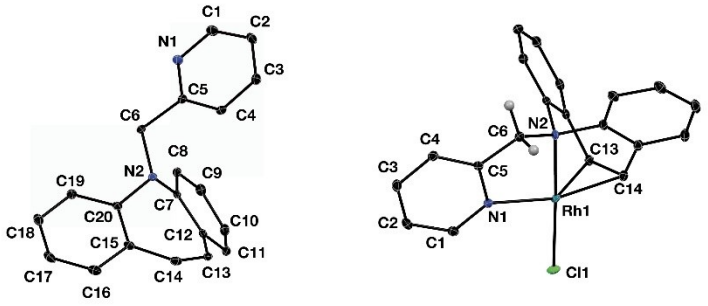

dbap-Py (**1**) [Rh(dbap-Py)Cl] (**2**)

Figure 2. Mercury plots of the molecular structures of compounds **1** and **2** derived from single-crystal X-ray diffraction analysis with thermal ellipsoids at 30% probability. Selected bond lengths (Å) and angles (deg). **1**: N1−C5 = 1.344(2), N1−C1 = 1.339(2), C1−C2 = 1.381(2), C2−C3 = 1.383(2), C3−C4 = 1.379(2), C4−C5 = 1.387(2), C5−C6 = 1.507(2), C13−C14 = 1.336(2), N2−C6 = 1.461(2); interplane angles ∂ = 87.0, α = 57.1, β = 29.9, γ = 54.4; **2**: Rh1−Cl1 = 2.337(1), Rh1−N1 = 2.088(1), Rh1−N2 = 2.058(1), Rh1−C13 = 2.056(1), Rh1−C14 = 2.106(1), N1−C5 = 1.359(1), N1−C1 = 1.341(1), C1−C2 = 1.385(2), C2−C3 = 1.386(2), C3−C4 = 1.392(2), C4−C5 = 1.387(1), C5−C6 = 1.502(1), C13−C14 = 1.433(2); ∂ = 67.6, α = 68.4, β = 44.0, γ = 75.7, torsion(N2−C6−C5−N1) = 35.4.

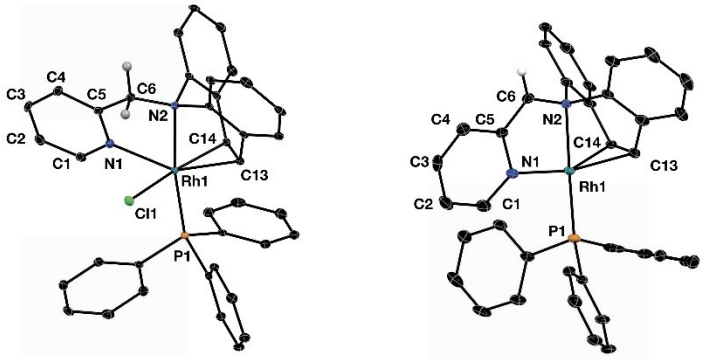

[Rh(dbap-Py)(PPh$_3$)Cl] (**3**) [Rh(dbap-Py*)(PPh$_3$)] (**4**)

Figure 3. Mercury plots of the molecular structures of compounds **3** and **4** derived from single-crystal X-ray diffraction analysis with thermal ellipsoids at 30% probability. Hydrogen atoms are omitted for clarity except for the exo-cyclic C(6)H$_2$ and C(6)H moiety. Selected bond lengths (Å) and angles (deg). **3**: Rh1−P1 = 2.2244(6), Rh1−N2 = 2.182(2), Rh1−N1 = 2.238(2), Rh1−C13 = 2.064(2), Rh1−C14 = 2.070(2), Rh1−ct(C13C14) = 1.934, N1−C5 = 1.353(3), N1−C1 = 1.344(3), C1−C2 = 1.386(3), C2−C3 = 1.382(4), C3−C4 = 1.386(3), C4−C5 = 1.391(3), C5−C6 = 1.509(3), C13−C14 = 1.461(3), N2−C6 = 1.476(3); ∂ = 68.3, α = 69.4, β = 42.3, γ = 75.7, torsion(N2−C6−C5−N1) = 30.7; **4**: Rh1−P1 = 2.221(1), Rh1−N2 = 2.149(4), Rh1−N1 = 2.045(4), Rh1−C14 = 2.113(5), Rh1−C13 = 2.110(5), Rh1−ct(C13C14) = 1.989, N1−C5 = 1.404(7), N1−C1 = 1.359(7), C1−C2 = 1.372(9), C2−C3 = 1.377(14), C3−C4 = 1.348(13), C4−C5 = 1.453(8), C5−C6 = 1.359(7), C13−C14 = 1.423(7), N2−C6 = 1.451(6); ∂ = 73.8, α = 67.9, β = 38.7, γ = 67.9, torsion(N2−C6−C5−N1) = 2.1.

2−4. Selected geometric features are given in the figure captions and summarized in Table 2. Crystallographic details are listed in Tables S1 and S2 in the Supporting Information. All structures reveal a nonplanar azepine unit, in which the N2 and C13═C14 moieties form a concave binding site, characterized by the interplane bite angle ∂. The corresponding interplane angles α and β define the deviation from planarity. The annulated six-membered rings form a butterfly-like motif on the opposite site of the azepine ring (boat shape). The six-membered rings point toward each other, which is characterized by the interplane angle γ. All characteristic angles are listed in Table 2 along with their graphic representation in the caption (Table 2, top).

Single crystals of the free ligand **1**, suitable for X-ray diffraction analysis, were grown from *n*-hexane layered ethyl acetate solution at 5 °C. The molecular structure is shown in Figure 2 (left). The aromatic π-system in the pyridine unit is signified by almost equidistant C−C interatomic distances (ca. 1.38−1.39 Å) and two equivalent N−C bonds (ca. 1.34 Å). The free olefinic binding site C13═C14 exhibits an interatomic distance of 1.336(2) Å, which is in line with previously reported azepinate structures.[9] The characteristic C5−C6 bond length is 1.507(2) Å, which indicates a C−C

DOI: 10.1021/acs.organomet.9b00094
Organometallics 2019, 38, 1787−1799

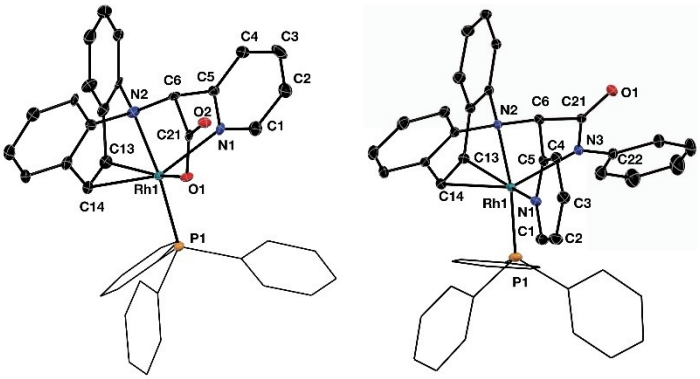

[Rh(dbap-COO)(PPh3)] (**5**) [Rh(dbap-NCO)(PPh3)] (**6**)

Figure 4. Mercury plots of the molecular structures of compounds **5** and **6** derived from single-crystal X-ray diffraction study with thermal ellipsoids at 30% probability. Selected bond lengths (Å) and angles (deg). **5**: Rh1−P1 = 2.217(2), Rh1−O1 = 2.258(5), Rh1−N2 = 2.109(5), Rh1−N1 = 2.210(6), Rh1−C13 = 2.066(7), Rh1−C14 = 2.084(7), Rh1−ct(C13C14) = 1.941, N1−C5 = 1.358(9), N1−C1 = 1.340(9), C1−C2 = 1.395(11), C2−C3 = 1.382(12), C3−C4 = 1.381(12), C4−C5 = 1.376(10), C5−C6 = 1.522(10), C13−C14 = 1.469(10), C21−C6 = 1.566(9), C21−O1 = 1.262(8), C21−O2 = 1.256(8), N2−C6 = 1.465(9); ∂ = 67.3, α = 70.0, β = 42.8, γ = 73.7, torsion(N2−C6−C5−N1) = 50.8; **6**: Rh1−P1 = 2.2393(7), Rh1−N3 = 2.271(2), Rh1−N2 = 2.113(2), Rh1−N1 = 2.216(2), Rh1−C13 = 2.082(3), Rh1−C14 = 2.077(2), Rh1−ct(C13C14) = 1.944, N1−C5 = 1.356(3), N1−C1 = 1.349(3), C1−C2 = 1.374(4), C2−C3 = 1.389(4), C3−C4 = 1.384(4), C4−C5 = 1.383(4), C5−C6 = 1.506(3), C13−C14 = 1.473(3), C21−C6 = 1.553(3), C21−N3 = 1.336(3), C21−O1 = 1.250(3), N2−C6 = 1.484(3); ∂ = 67.1, α = 70.0, β = 42.9, γ = 72.0, torsion(N2−C6−C5−N1) = 44.6.

Table 2. Selected Bond Lengths and Angles for Compounds 1−6 Derived from Single-Crystal X-ray Diffraction Analysis

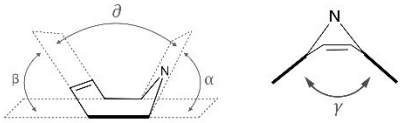

compound	1	2	3	4	5	6
Rh1−ct		1.954	1.934	1.989	1.941	1.944
C13−C14	1.336(2)	1.433(2)	1.461(3)	1.423(7)	1.469(10)	1.473(3)
interplane angles						
α (deg)	57.1	68.4	69.4	67.9	70.0	70.0
β (deg)	29.9	44.0	43.2	38.7	42.8	42.9
γ (deg)	54.4	78.5	75.7	67.5	73.7	72.0
∂ (deg)	87.0	67.6	68.3	73.8	67.3	67.1
Rh1−N1		2.088(1)	2.238(2)	2.045(4)	2.210(6)	2.216(2)
Rh1−N2		2.058(1)	2.182(2)	2.149(4)	2.109(5)	2.113(2)
C1−C2	1.381(2)	1.385(2)	1.386(3)	1.372(9)	1.395(11)	1.374(4)
C2−C3	1.383(2)	1.386(2)	1.382(4)	1.377(14)	1.382(12)	1.389(4)
C3−C4	1.379(2)	1.392(2)	1.386(3)	1.348(13)	1.381(12)	1.384(4)
C4−C5	1.387(2)	1.387(1)	1.391(3)	1.453(8)	1.376(10)	1.383(4)
N1−C1	1.339(2)	1.341(1)	1.344(3)	1.359(7)	1.340(9)	1.349(3)
N1−C5	1.344(2)	1.359(1)	1.353(3)	1.404(7)	1.358(9)	1.356(3)
C5−C6	1.507(2)	1.502(1)	1.509(3)	1.359(7)	1.522(10)	1.506(3)
tor(N2−C6−C5−N1) (deg)		35.4	30.7	2.1	50.8	44.6

single bond and thus reveals a methylene group in the benzylic position.

Single crystals of complex **2** were obtained from an *n*-hexane layered solution in dichloromethane. The obtained molecular structure (Figure 2, right) includes a Rh(I) center residing in a distorted square planar geometry, built by the tridentate **dbap-py** ligand via the two N-donors, as well as the olefinic binding site. The chloro ligand completes the coordination sphere and binds, due to the tridentate chelation mode of **dbap-py**, in mutual trans position with respect to the amine moiety. Upon coordination of **dbap-py** to the Rh center in **2**, the interplane angle ∂ contracts by ca. 20° with respect to the free ligand (∂ = 87.0°) due to the chelation of Rh(I) by the amine-olefin motif. The olefin bond C13═C14 is elongated (1.433(2) Å)

DOI: 10.1021/acs.organomet.9b00094
Organometallics 2019, 38, 1787−1799

compared to the free ligand (1.336(2) Å), suggesting efficient metal-to-ligand backdonation and tight binding, which is typically observed in the related rhodium complexes decorated with trop-olefin ligands.[34,76] In line with our observations, Dorta and co-workers reported a C−C interatomic distance of 1.423(2) Å for the coordinated olefin in a Rh(I) complex with dibenzazepin-based ligand.[10] The olefin binding in **2** is characterized by a corresponding Rh−ct distance of 1.989 Å (ct = centroid of the C13═C14 bond). The incorporation of **dbap-py** into a square planar coordination sphere results in a puckered structure with respect to the five-membered metallacycle Rh(−N1−C5−C6−N2−) with a torsion angle (N1−C5−C6−N2) of 35.4°. Single crystals of complex **3** were obtained from an *n*-hexane layered solution in dichloromethane. The mercury plot of complex **3** is shown in Figure 3 (left). Noteworthy, our ^{1}H NMR spectroscopic analysis of complex **3** suggests a rather square planar structure of $[Rh(dbap\text{-}py)PPh_3]^+$ with Cl^- counterion (see above).

Yet the structure in the solid state reveals the neutral compound $[Rh(dbap\text{-}py)PPh_3Cl]$, in which the Rh(I) center resides in a largely distorted trigonal bipyramidal coordination sphere. The Rh(I) center is chelated by the tridentate **dbap-py**. The amine donor of the azepine and PPh_3 bind in the axial positions (angle N2−Rh1−P1 = 171.68(5)°).

The olefin unit (Rh1−ct = 1.934 Å), the N-donor of the pyridine ring (Rh1−N2 = 2.182(2) Å), as well as the chloro ligand (Rh1−Cl = 2.552(1) Å) reside in the equatorial positions (relevant angles: N1−Rh1−Cl1 = 79.4°; N1−Rh1−ct = 133.6°; Cl1−Rh1−ct = 139.4°) The puckered five-membered ring Rh(−N1−C5−C6−N2−) is retained in the trigonal bipyramidal geometry of **3** with a slightly smaller torsion angle (N1−C5−C6−N2) of 30.7°. Coordination of the olefin to Rh(I) results in an elongated carbon−carbon interatomic distance C13−C14 = 1.461(3) Å, which is slightly longer than that observed in the corresponding complex **2**. The interplane angle ∂ (68.3°) is similar to the one observed in complex **2**. That is, the bite angle of the chelating azepine unit is only marginally affected by the change from a square planar to the distorted trigonal bipyramidal coordination sphere.

Deprotonation at the benzylic position of **3** gives rise to the neutral complex **4**. Deep red single crystals are obtained from an *n*-hexane layered solution in THF. The crystal structure is shown in Figure 3 (right). In agreement with our NMR spectroscopic findings in THF solution, complex **4** exhibits a square planar geometry, reflected by an angle of 2.1° (ideal 0°) between the mean planes defined by (N2−Rh1−ct) and (N1−Rh1−P1). The interplane angle ∂ of 73.8° indicates a slight flattening of the azepine ring, while the Rh1−ct distance lengthens (1.989 Å) and the Rh1−N1 bond length (2.045(4) Å) significantly contracts with respect to **3** (Rh1−ct = 1.934 Å; Rh1−N1 = 2.238(2) Å). The nonequidistant C−C bond length of the pyridine ring (see Table 2), the very short C5−C6 bond (1.359(7) Å), and elongated N1−C5 bond (1.404(7) Å) indicate a significant disturbance of the aromatic π-system (dearomatization) in the deprotonated **dbap-py*** ligand. Hence, the α-picolyl amine backbone in **dbap-py*** experiences a planarization upon deprotonation, resulting in a very small torsion angle of 2.1° (N1−C5−C6−N2) suggesting a rather planar en-amine motif for the −(C5═C6−N5)− unit.

Upon exposure of the deep red solution of **4** in THF to CO_2 gas (1 bar), the mixture turns yellow instantaneously. The color change is followed by the rapid precipitation of single crystals of complex **5**, which show an intense absorption band in the IR spectrum at $\nu_{C=O}$ = 1630 cm^{-1}, which was absent in complex **4** and is characteristic of a carboxylate moiety.[53] The molecular structure derived from XRD analysis is shown in Figure 4 (left). The significant bond formation between C21 of CO_2 and the benzylic carbon atom C6 gives rise to the tetradentate ligand (dbap-COO^-). The lengthened C6−C21 bond of 1.566(9) Å is in range of previously observed picolylcarboxylate compounds.[53,54] The concomitant formation of the Rh1−O1 bond (2.252(5) Å) indicates the cooperative CO_2 uptake in complex **5**. Significantly, upon CO_2 binding, the C−C interatomic distances within the pyridine ring are equidistant in the range of 1.38−1.39 Å and suggest a rearomatization of **5**. The interatomic distances N1−C1 (1.340(9) Å) and N1−C5 (1.358(9) Å) are very similar and indicate a reorganization of the aromatic π-system of the pyridine ring, as well. Conversely, the C5−C6 bond is elongated (1.522(10) Å) with respect to **4**, signifying a C−C single bond formation with a sp^3-hybridized C6 carbon atom. The Rh(I) center resides in a trigonal bipyramidal coordination sphere. That is, the azepine amine moiety (N2) resides in an axial position and the equatorial positions are occupied by the N-donor of the pyridine unit (N1), the olefin (C13═C14) unit, and the κ^1-carboxylate (O1). The phosphine donor (P1) of PPh_3 resides in mutual trans position with respect to the amine group (N2) completing the largely distorted trigonal bipyramidal coordination sphere. The torsion angle (N1−C5−C6−N2) of 50.8° indicates the pronounced puckered structure of the ligand backbone in **5**. Noteworthy, a Rh1−ct distance of 1.941 Å, as well as the C13═C14 interatomic distance of 1.469(10) Å indicates tight olefin bonding also for complex **5**.

Light yellow crystals of **6** suitable for single-crystal XRD analysis were obtained from an *n*-hexane layered solution in THF at −20 °C. The molecular structure is shown in Figure 4 (right). The metal−ligand cooperative activation of the C21═N3 bond results in the single-bond formation between C21 of the Ph−CNO substrate and the nucleophilic carbon C6 of the ligand (1.553(3) Å). Concomitantly, the Rh1−N3 bond is formed (2.271(2) Å) giving rise to the remarkable formation of the κ^1-*N* amidate motif in the tetradentate ligand **dbap-NCO**$^-$, which is, to the best of our knowledge, an unprecedented structural motif for Rh(I) complexes.

The angles about the amidate nitrogen N3 sum to 359.7°, indicating a planar geometry and hence C6, C21, O1, and N3 are located in-plane. The phenyl ring of the isocyanate moiety deviates from that plane by only 24.6°. Inherently, the κ^1-*N* amidate motif in complex **6** has an elongated N3−C21 = 1.336(3) Å and a shortened C21−O1 = 1.250(3) Å interatomic distance with respect to previously reported Rh(I) compounds bearing κ^2-*N*,*O*[75] and κ^1-*O*[77] amidate motifs. The Rh(I) center resides similar to complex **5**, in a distorted trigonal bipyramidal coordination sphere. The equatorial positions are occupied by the olefinic unit, the N donor of the pyridine ring, and the κ^1-*N* amidate moiety (relevant bond angels: N3−Rh1−ct = 130.0°, N1−Rh1−ct = 134.6°, N1−Rh1−N3 = 80.8°). The PPh_3 ligand and the N2 donor of the azepine moiety reside in axial position (angle N2−Rh1−P1 = 171.4°). The elongated olefinic C13−C14 distance (1.473(3) Å) indicates tight binding to the Rh(I) center. Similar to **5**, compound **6** shows almost equidistant C−C bond lengths in the pyridine ring (1.38−1.39 Å), as well as similar N1−C1 and N1−C5 interatomic distances. Consequently, the interatomic distance of C5−C6 is elongated and remains in a single-bond regime (1.506(3) Å). The latter

DOI: 10.1021/acs.organomet.9b00094
Organometallics 2019, 38, 1787−1799

findings suggest that the metal−ligand cooperative activation of phenyl isocyanate in complex **6** is associated with a reorganization of the aromatic π-system of the pyridine ring (rearomatization), as well.

CONCLUSIONS

We have synthesized and characterized the novel olefinic multidentate actor ligand **dbap-py**. The ligand consists of a 2-methyl pyridine unit and an azepine component fused by N-alkylation. The coordination chemistry to Rh(I) centers was explored and **dbap-py** revealed interesting tridentate chelation (pyridine−amine−olefin, N−N−(C=C)), which can suit square planar as well as distorted trigonal bipyramidal coordination spheres in Rh(I) complexes **2**−**6**. Most notably, the **dbap-py** ligand in [Rh(dbap-py)(PPh_3)Cl] (**3**) entails an acidic benzylic methylene moiety, which is readily deprotonated using LiHMDS. This allows for the formation of the neutral square planar complex [Rh(dbap-py*)(PPh_3)] (**4**), which encompasses a C-nucleophilic methine moiety (C6). The π-system of the pyridine fragment in **4** is significantly disturbed (dearomatization) as indicated by nonequidistant C−C interatomic distances of the pyridine ring and a short C5−C6 bond revealed in the crystal structure of **4**. The disturbance is also indicated by the upfield-shifted ^{1}H NMR resonances associated with the pyridine C*H* moieties. Complex **4** encompasses noteworthy metal−ligand cooperative reactivity, which is unveiled, inter alia, in the activation of C=O double bonds via a formal [1,3]-addition. This is best demonstrated when **4** reacts with CO_2 gas (1 atm). As a result, the carboxylate complex [Rh(dbap-COO)(PPh_3)] (**5**) is formed via C−C bond formation of the ligand's nucleophilic benzylic carbon and the electrophilic carbon center of CO_2. A Rh−O bond is concomitantly established and the disrupted π-system is restored (rearomatization) in complex **5**. Metal−ligand cooperative [1,3]-addition of CO_2 in transition-metal complexes with pyridine-based ligands was sporadically reported in recent years. However, this intriguing (reversible) addition remains still a rather unusual binding motif.[53,54,71,78−83] We showed very recently that this particular bond activation scheme can likewise be applied to SO_2.[84] This work further expands the substrate scope to the functional group of isocyanates: MLC triggers the reaction of complex **4** and Ph−N=C=O to give the κ^1-*N* amidate complex [Rh(dbap-NCO)(PPh_3)] (**6**). The activation of the C=N bond is characterized by the rearomatization of the pyridine moiety and C−C/Rh−N bond formation in **6**. In summary, MLC is demonstrated to allow for the formation of the unusual κ^1-*N* amidate ligand motif. While C=O and C=N bonds readily react with **4**, our studies involving the cooperative activation of the H−H bond in dihydrogen gas did not result in a well-defined product. Instead, the reaction of **4** in THF solution under an atmosphere of dihydrogen gas gave rise to complex product mixtures. The actor ligand **1** combines C-centered nucleophilic reactivity and a rigid concave olefinic binding site. Similar to the related trop ligands, **dbap-py** may allow for the stabilization of low-valent transition-metal centers. Along these lines, our current research focuses on bond activation pathways triggered by MLC in complexes with low-valent first-row transition-metal centers, decorated with ligands based on **dbap-py**.

EXPERIMENTAL SECTION

All air- and moisture-sensitive reactions were performed under an inert atmosphere of argon using standard Schlenk and glovebox techniques. Complex **2** and **3** are moderately air-stable and can be handled briefly in air. Complex **4**−**6** are highly air- and moisture-sensitive. All reagents were obtained commercially (Sigma-Aldrich, Germany) and used as received. Solvents were collected from an MBRAUN SPS-800 solvent purification system and additionally dried over 4 Å molecular sieves. ^{1}H, ^{13}C{^{1}H}, and ^{31}P{^{1}H} NMR spectra were recorded at 293 K with a Bruker Avance WB-360 spectrometer and referenced to tetramethylsilane (^{1}H, ^{13}C) and phosphoric acid (85% in water) (^{31}P). Chemical shifts are reported in parts per million (ppm), and coupling constants (J) are given in hertz (Hz). The electrospray ionization mass spectrometry (ESI-MS) images were obtained on a Bruker Esquire-LC MS. Dichloromethane/acetonitrile solutions (or otherwise stated, $c = 1 \times 10^{-6}$ mol L^{-1}) were injected directly into the spectrometer at a flow rate of 3 μL min^{-1}. Nitrogen was used both as a drying gas and for nebulization. Electron impact mass spectra were recorded with a Finnigan MAT 95. IR spectra were recorded with a Thermo Scientific Nicolet iS10 attenuated total reflection (ATR)-IR spectrometer. Crystallography: intensity data were collected on a Bruker Venture D8 diffractometer with graphite-monochromated Mo Kα (0.7107 Å) radiation. Figures were created using Mercury 3.9 (Build RC1).

Ligand 1 dbap-py. Potassium *tert*-butoxide (KO^{t}Bu) (4.488 g, 40 mmol) in 40 mL of THF was added at −78 °C to a solution of iminostilbene (1.932 g, 10 mmol) and 20 mL of THF. The mixture was stirred for 30 min at this temperature. Subsequently, the formed deep blue solution was warmed to room temperature and stirred for additional 30 min. 2-Picolyl chloride hydrochloride (2.461 g, 15 mmol) was dissolved in 100 mL of pyridine and added dropwise to the deep blue solution, which was beforehand cooled to −78 °C. After the color of the solution turned from green to red-yellow, the reaction mixture was warmed to room temperature and stirred for 8 h. The solvent was removed in vacuo, and the obtained brown residue was poured into water for extraction with dichloromethane. The organic extracts were filtered through water-absorbent cotton. The volatiles were removed in vacuo, and the compound was purified by column chromatography (eluent: ethyl acetate/*n*-hexane 5:2, R_f = 0.52). An off-white crystalline solid was isolated (48% yield, nonoptimized procedure). ^{1}H NMR (360 MHz, $CDCl_3$, 298 K): δ = 8.50 (1H, ddd, $^3J_{HH}$ = 5.0 Hz, J_{HH} = 1.7 Hz, J_{HH} = 1.0 Hz, py1), 7.59 (1H, br d, $^3J_{HH}$ = 7.7 Hz, py4), 7.51 (1H, td, $^3J_{HH}$ = 7.7 Hz, $^4J_{HH}$ = 1.7 Hz, py3), 7.22 (2H, m, C*H*, aze9), 7.11 (4H, m, C*H*, aze8/11), 7.07 (1H, br t, $^3J_{HH}$ = 5.00 Hz, C*H*, pyr2), 6.99 (2H, td, $^3J_{HH}$ = 7.4 Hz, $^4J_{HH}$ = 1.1 Hz, aze10), 6.86 (2H, s, C*H*, ole13), 5.17 (2H, s, CH_2, bzl6) ppm. ^{13}C{^{1}H} NMR (91 MHz, $CDCl_3$, 298 K): δ = 158.1 (1C, py-C5), 150.4 (2C, s, C_{quart} aze-C7), 148.4 (1C, s, CH py-C1), 136.3 (1C, s, CH py-C3), 133.4 (2C, s, C_{quart}, aze-C12), 132.1 (2C, s, CH ole-C13), 128.8 (2C, s, CH aze-C9), 128.7 (2C, s, CH aze-C11), 123.3 (2C, s, CH aze-C10), 121.9 (1C, s, CH py-C4), 121.6 (1C, s, CH py-C2), 120.2 (2C, s, CH aze-C8), 56.9 (1C, s, CH_2 bzl-C6) ppm. High-resolution mass spectrometry (HRMS)-ESI (70 eV) m/z = calcd [M$^+$] for $C_{20}H_{16}N_2$ 284.13080; found 284.13107.

Complex 2 [Rh(dbap-py)Cl]. 5-(Pyridine-2-ylmethyl)-5*H*-dibenzo[*b*,*f*]azepine (241 mg, 0.849 mmol) was added to a solution of di-μ-chlorotetraethylene dirhodium(I) (150 mg, 0.386 mmol) in 5 mL of toluene. The reaction mixture was subsequently stirred at room temperature for 12 h. After filtration, the crude product was washed with toluene (3 × 3 mL) and all volatiles were removed in vacuo. Extraction into dichloromethane and recrystallization by slow diffusion of *n*-hexane into a concentrated dichloromethane solution yielded red single crystals (290 mg, 0.686 mmol, 89%). ^{1}H NMR (360 MHz, $CDCl_3$, 298 K): δ = 8.93 (1H, d, $^3J_{HH}$ = 4.90 Hz, py1), 7.81 (1H, t, $^3J_{HH}$ = 7.30 Hz, py3), 7.47 (1H, d, $^3J_{HH}$ = 8.10 Hz, py4), 7.43 (2H, m, aze), 7.34 (1H, t, $^3J_{HH}$ = 6.30 Hz, py2), 7.00 (6H, m, aze), 5.07 (2H, s, C*H*, ole6), 4.94 (s, CH_2, bzl6) ppm. ^{13}C{^{1}H} NMR (91 MHz, $CDCl_3$, 298 K): δ = 161.3 (1C, s, C_{quart} py-C5), 152.3 (2C, s, C_{quart} aze), 150.2 (1C, s, CH py-C1), 144.7 (2C, s, C_{quart} aze), 138.6

DOI: 10.1021/acs.organomet.9b00094
Organometallics 2019, 38, 1787−1799

(1C, s, CH py-C3), 126.6 (4C, s, CH aze), 125.7 (2C, d, J_{CRh} = 21.5 Hz, CH aze), 123.4 (1C, s, CH py-C2), 120.6 (1C, s, CH py-C4), 113.9 (2C, s, CH aze), 61.6 (1C, s, CH_2, bzl), 60.2 (2C, d, $^1J_{CRh}$ = 15.8 Hz, CH ole) ppm. HRMS-ESI CH_2Cl_2/CH_3CN (m/z): [M + CH_3CN−Cl]$^+$ calcd for $C_{22}H_{19}N_3Rh$ 428.06285; found 428.06269 (0.39 ppm).

Complex 3 [Rh(dbap-py)PPh$_3$Cl]. Triphenylphosphine (103 mg, 0.391 mmol) was added to a stirred solution of chloro-5-(pyridine-2-ylmethyl)-5*H*-dibenzo[*b*,*f*]azepinrhodium(I) (150 mg, 0.355 mmol) in 5 mL toluene. After stirring at 55 °C for 2 h, the suspension was stirred at room temperature for another 12 h. Filtration and evaporation of solvent in vacuo left a light yellow solid. Extraction into chloroform and recrystallization by slow diffusion of *n*-hexane into a concentrated chloroform solution obtained beige single crystals (211 mg, 0.308 mmol, 87%). Note, compound **3** has limited solubility in THF and decomposes slowly in chlorinated solvents. ^{1}H NMR (360 MHz, $CDCl_3$, 298 K): δ = 7.91 (1H, d, $^3J_{HH}$ = 5.00 Hz, py1), 7.85 (6H, m, PPh_3), 7.57 (1H, t, py3), 7.41 (10H, m, PPh_3/1H py4), 7.07 (4H, m, C*H* aze), 6.97 (2H, t, $^3J_{HH}$ = 7.10 Hz, C*H* aze), 6.92 (2H, t, $^3J_{HH}$ = 7.20 Hz, C*H* aze), 6.82 (1H, t, $^3J_{HH}$ = 6.80 Hz, py2), 5.44 (2H, s, CH_2 bzl), 3.12 (2H, d, $^3J_{PH}$ = 2.70 Hz, ole) ppm. ^{13}C{^{1}H} NMR (91 MHz, CD_2Cl_2, 298 K): δ = 158.4 (1C, s, py-C5), 151.8 (1C, s, py-C1), 150.3 (2C, d, *J* = 3.6 Hz, C_{quart}), 146.2 (2C, s, C_{quart}), 136.9 (1C, s, py), 135.2 (6C, d, *J* = 10.4 Hz, CH PPh_3), 132.5 (3C, d, *J* = 47.3 Hz, 1C$_{quart}$ PPh_3), 130.5 (3C, d, *J* = 1.6 Hz, CH PPh_3), 128.5 (6C, d, *J* = 10.0 Hz, CH PPh_3), 127.5 (2C, s, CH aze), 125.2 (2C, s, CH aze), 125.1 (2C, s, CH aze), 124.6 (1C, s, CH py), 122.9 (1C, s, CH py), 116.6 (2C, s, CH aze), 57.5 (1C, s, CH bzl), 48.8 (2C, d, *J* = 17.1 Hz, CH ole). ^{31}P{^{1}H} NMR (81 MHz, $CDCl_3$, 298 K): δ = 52.3 (d, $^1J_{PRh}$ = 160.6 Hz) ppm. HRMS-ESI CH_2Cl_2/CH_3CN (m/z): [M − Cl]$^+$ calcd for $C_{38}H_{31}N_2PRh$ 649.12744; found 649.12725 (0.29 ppm).

Complex 4 [Rh(dbap-py*)PPh$_3$]. Method A: Lithium-bis-(trimethylsilyl)amide (49 mg, 0.292 mmol, 2 equiv) was added to a solution of complex **3** (100 mg, 0.146 mmol) in 5 mL of THF. Stirring the suspension for a few minutes gave rise to a deep red solution. Recrystallization by slow diffusion of *n*-hexane into a concentrated THF solution yielded deep red single crystals (82 mg, 0.126 mmol, 86%). Method B: Alternatively, complex **4** was obtained via a simplified "one-pot" synthesis: 5-(pyridine-2-ylmethyl)-5*H*-dibenzo[*b*,*f*]azepine (1, 293 mg, 1.028 mmol) was added to a solution of di-μ-chlorotetraethylene dirhodium(I) (200 mg, 0.514 mmol) in 10 mL of toluene. The suspension was stirred at room temperature for 12 h. Subsequently, triphenylphosphine (270 mg, 1.028 mmol) was added and the mixture was stirred for 2 h at 55 °C. The suspension was allowed to cool down and stirred for additional 12 h at ambient temperature. Subsequently, all volatiles were removed in vacuo and the solid was washed with toluene (3 × 3 mL). The obtained solid was dissolved in 10 mL of THF and lithium bis(trimethylsilyl)amide (301 mg, 1.802 mmol, 1.75 equiv) was added to the stirred solution. After a few minutes, the light yellow solution changed its color to deep red. The clear solution was layered with *n*-hexane, which gave rise to large deep red crystals of complex **4** (554 mg, 0.853 mmol, 83%). ^{1}H NMR (360 MHz, THF-d_8, 298 K): δ = 7.83 (6H, m, PPh_3), 7.43 (9H, m, PPh_3), 7.31 (2H, d, $^3J_{HH}$ = 7.90 Hz, aze8), 7.07 (2H, t, $^3J_{HH}$ = 7.50 Hz, C*H* aze), 6.96 (2H, d, $^3J_{HH}$ = 6.30 Hz, C*H* aze), 6.91 (2H, t, $^3J_{HH}$ = 7.3 Hz, C*H* aze), 6.24 (1H, d, $^3J_{HH}$ = 6.40 Hz, py1), 5.99 (2H, m, py3/4), 5.38 (1H, d, *J* = 5.00 Hz, C*H*, bzl), 4.31 ppm (1H, dt, $^3J_{HH}$ = 7.9 Hz, J_{HH} = 3.4 Hz, py2), 3.51 (2H, d, $^3J_{PH}$ = 2.70 Hz, C*H* ole) ppm. ^{13}C{^{1}H} NMR (91 MHz, THF-d_8, 298 K): δ = 157.7 (1C, s, C_{quart} py-C5), 149.5 (1C, s, CH py-C1), 147.4 (2C, s, C_{quart} aze), 142.3 (2C, s, C_{quart} aze), 134.4 (6C, d, $^2J_{CP}$ = 11.9 Hz, CH PPh_3), 132.4 (3C, d, $^1J_{CP}$ = 43.9 Hz, C_{quart} PPh_3), 129.7 (3C, d, $^4J_{CP}$ = 1.70 Hz, CH PPh_3), 128.4 (1C, s, CH py-C3), 127.8 (6C, d, $^3J_{PH}$ = 9.90 Hz, CH PPh_3), 125.6 (2C, s, CH aze), 124.9 (2C, s, CH aze), 122.9 (2C, s, CH aze), 117.2 (2C, s, CH aze), 112.3 (1C, s, CH py-C4), 96.7 (1C, s, CH py-C2), 91.4 (1C, d, ^2J = 2.7 Hz, CH bzl), 59.7 (2C, d, $^1J_{CRh}$ = 12.5 Hz, CH ole) ppm. ^{31}P{^{1}H} NMR (81 MHz, THF-d_8, 298 K): δ = 55.7 (d, $^1J_{PRh}$ = 185.6 Hz) ppm. HRMS-ESI CH_2Cl_2/CH_3CN (m/z): [M + H]$^+$ calcd for $C_{38}H_{31}N_2PRh$ 649.12744; found 649.12661 (1.2 ppm).

Complex 5 [Rh(dbap-COO)PPh$_3$]. Complex **4** (30 mg, 0.046 mmol) was dissolved in 5 mL of THF in a Schlenk tube with Teflon valve. The deep red solution was subjected to CO_2 gas (1 bar), which gave rise to an instantaneous color change to yellow. After a few minutes, compound **5** precipitates as a yellow single crystalline material. After 24 h, the crystals were decanted from the supernatant solution and washed with *n*-hexane. Subsequently, the product was dried under reduced pressure to give complex **5** in high yield (31 mg, 97%). ^{1}H NMR (360 MHz, THF-d_8, 298 K): δ = 7.83 (1H, d, $^3J_{HH}$ = 5.00 Hz, py1), 7.75 (7H, m, PPh_3/py), 7.65 (1H, dd, $^3J_{HH}$ = 7.90 Hz $^3J_{HH}$ = 6.60 Hz, py), 7.45 (1H, m, py), 7.37 (9H, m, PPh_3), 7.12 (2H, m, C*H* aze), 6.98 (2H, m, C*H* aze), 6.83 (2H, m, C*H* aze), 6.68 (2H, m, C*H* aze), 6.18 (1H, s, C*H*(COO), bzl), 3.19 (1H, dd, $^3J_{HH}$ = 6.50 Hz, $^3J_{HP}$ = 3.70 Hz, C*H*, ole), 2.91 (1H, dd, $^3J_{HH}$ = 6.50 Hz, $^3J_{HP}$ = 2.90 Hz, C*H*, ole) ppm. ^{31}P{^{1}H} NMR (81 MHz, $C_6H_4F_2$, 298 K, locked on external THF-d_8): δ = 51.2 (d, $^1J_{PRh}$ = 166.9 Hz) ppm. Note compound **5** crystallizes rapidly from THF solution (within minutes). The crystals are sparsely soluble in THF and decompose in polar chlorinated solvents. Therefore, we could not obtain a solution of sufficient concentration and stability allowing for the acquisition of a ^{13}C{^{1}H} NMR spectrum. HRMS-ESI CH_2Cl_2/CH_3CN (m/z): [M + Na]$^+$ calcd for $C_{39}H_{30}N_2O_2PRhNa$ 715.09921; found 715.09850 (1.0 ppm). IR (ATR) ν_{COO}1630 (very strong) cm^{-1}.

Complex 6 [Rh(dbap-NCO)PPh$_3$]. Phenyl isocyanate (9 mg, 0.077 mmol) was added to a stirred solution of complex **4** (50 mg, 0.077 mmol) in 5 mL of THF. Characteristically, the deep red solution instantaneously changed its color to light yellow. The product crystallizes slowly from the THF solution. The mixture was layered with *n*-hexane and allowed to crystallize for 4 days at ambient temperature. Subsequently, the mother liquor was decanted from the yellow solid, washed with *n*-hexanes, and dried at high vacuum to give the product as yellow microcrystalline material in quantitative yield. Crystals suitable for single-crystal X-ray diffraction crystallography were obtained by recrystallization from THF/*n*-hexane at −20 °C. ^{1}H NMR (360 MHz, THF-d_8, 298 K): δ = 8.01 (1H, d, $^3J_{HH}$ = 5.1 Hz, py1), 7.95 (1H, d, $^3J_{HH}$ = 7.7 Hz, py4), 7.75 (1H, t, $^3J_{HH}$ = 6.6 Hz, py3), 7.50 (6H, t, $^3J_{HH}$ = 8.5 Hz, P*Ph*$_3$), 7.35 (4H, br t, $^3J_{HH}$ = 6.6 Hz, 3H P*Ph*$_3$ + 1H C*H*aze obsc.), 7.27−7.22 (8H, m, 6H P*Ph*$_3$ + 2H C*H* i-cya), 7.13 (1H, d, *J* = 7.2, C*H*aze), 7.08 (1H, d, $^3J_{HH}$ = 7.3 Hz, C*H*aze), 7.03 (1H, dd, *J* = 7.0, 1.6 Hz, C*H*aze), 6.91−6.79 (4H, m, overlap 3H C*H*aze + 1H py2), 6.74 (1H, t, $^3J_{HH}$ = 7.4 Hz, C*H*aze), 6.66 (2H, t, $^3J_{HH}$ = 7.8 Hz, CH i-cya), 6.38 (1H, t, $^3J_{HH}$ = 7.3 Hz, CH i-cya *para*), 6.09 (1H, d, *J* = 6.0 Hz, C*H* bzl), 3.41 (1H, dd, $^3J_{HH}$ = 6.7 Hz, $^3J_{HP}$ = 3.6 Hz, C*H* ole), 3.23 (1H, dd, $^3J_{HH}$ = 6.7 Hz, $^3J_{HP}$ = 3.1 Hz, C*H* ole). ^{13}C{^{1}H} NMR (91 MHz, THF-d_8, 298 K): δ = 168.2 (1C, br s, C_{quart} N−C(O)−C), 160.0 (1C, s, C_{quart} py-C5), 152.1 (1C, s, C_{quart}), 151.7 (1C, s, CH py-C1), 151.0 (1C, d, *J* = 2.5 Hz, C_{quart}), 149.9 (1C, d, *J* = 4.0 Hz, C_{quart}), 147.8 (1C, s, C_{quart}), 147.4 (1C, s, C_{quart}), 137.8 (1C, s, CH py-C3), 135.1 (6C, d, J_{CP} = 10.7 Hz, CH PPh_3), 133.3 (3C, d, $^1J_{CP}$ = 46.2 Hz, C_{quart} PPh_3), 130.8 (3C, s, CH PPh_3 *para*), 128.9 (6C, d, J_{CP} = 9.9 Hz, CH PPh_3), 127.8 (1C, s, CH aze), 127.6 (1C, s, CH aze), 127.5 (2C, s, CH i-cya *ortho*), 127.2 (2C, s, CH i-cya *meta*), 125.7 (1C, br t, *J* = 6.1 Hz, CH aze), 125.6 (1C, s, CH aze), 125.2 (1C, s, CH aze), 124.9 (1C, s, CH aze), 124.4 (1C, s, CH aze), 123.2 (1C, s, CH py-C2), 120.7 (1C, s, CH i-cya *para*), 118.7 (2C, s, CH aze), 77.5 (1C, s, CH bzl), 49.6 (1C, dd, *J* = 18.2, 2.7 Hz, CH ole), 47.7 (1C, dd, *J* = 17.0, 4.8 Hz, CH ole). ^{31}P{^{1}H} NMR (81 MHz, THF-d_8, 298 K): δ = 52.6 (d, $^1J_{PRh}$ = 159 Hz) ppm. HRMS-ESI CH_2Cl_2/CH_3CN (m/z): [M + H]$^+$ calcd for $C_{45}H_{36}N_3OPRh$ 768.16455; found, 768.16398 (−0.8 ppm).

■ ASSOCIATED CONTENT

Supporting Information

The Supporting Information is available free of charge on the ACS Publications website at DOI: 10.1021/acs.organomet.9b00094.

DOI: 10.1021/acs.organomet.9b00094
Organometallics 2019, 38, 1787−1799

NMR spectra and crystallographic details of compounds **1**–**6** (PDF)

Accession Codes

CCDC 1894393–1894398 contain the supplementary crystallographic data for this paper. These data can be obtained free of charge via www.ccdc.cam.ac.uk/data_request/cif, or by emailing data_request@ccdc.cam.ac.uk, or by contacting The Cambridge Crystallographic Data Centre, 12 Union Road, Cambridge CB2 1EZ, UK; fax: +44 1223 336033.

AUTHOR INFORMATION

Corresponding Author

*E-mail: mavogt@uni-bremen.de.

ORCID

Matthias Vogt: 0000-0002-2636-2531

Author Contributions

†I.H. and B.H. contributed equally to this work.

Funding

This work was funded by the Central Research and Development Fund (CRDF) of the University of Bremen.

Notes

The authors declare no competing financial interest.

ACKNOWLEDGMENTS

The authors are grateful to Enno Lork for supporting the single-crystal X-ray diffraction analysis. The generous financial support from Verband der Chemischen Industrie (VCI) is greatly acknowledged. Dedicated to Professor Hansjörg Grützmacher on the occasion of his 60th birthday.

REFERENCES

(1) Zeise, W. C. Von Der Wirkung Zwischen Platinchlorid Und Alkohol, Und Von Den Dabei Entstehenden Neuen Substanzen. *Ann. Phys. Chem.* **1831**, *97*, 497–541.

(2) Johnson, J. B.; Rovis, T. More Than Bystanders: The Effect of Olefins on Transition-Metal-Catalyzed Cross-Coupling Reactions. *Angew. Chem., Int. Ed.* **2008**, *47*, 840–871.

(3) Verhoeven, D. G. A.; Moret, M.-E. Metal–Ligand Cooperation at Tethered Π-Ligands. *Dalton Trans.* **2016**, *45*, 15762–15778.

(4) Defieber, C.; Grützmacher, H.; Carreira, E. M. Chiral Olefins as Steering Ligands in Asymmetric Catalysis. *Angew. Chem., Int. Ed.* **2008**, *47*, 4482–4502.

(5) Krautwald, S.; David, S.; Schafroth, M. A.; Carreira, E. M. Enantio- and Diastereodivergent Dual Catalysis: A-Allylation of Branched Aldehydes. *Science* **2013**, *340*, 1065–1068.

(6) Krautwald, S.; Carreira, E. M. Stereodivergence in Asymmetric Catalysis. *J. Am. Chem. Soc.* **2017**, *139*, 5627–5639.

(7) Maire, P.; Deblon, S.; Breher, F.; Geier, J.; Böhler, C.; Rüegger, H.; Schönberg, H.; Grützmacher, H. Olefins as Steering Ligands for Homogeneously Catalyzed Hydrogenations. *Chem. – Eur. J.* **2004**, *10*, 4198–4205.

(8) Piras, E.; Läng, F.; Rüegger, H.; Stein, D.; Wörle, M.; Grützmacher, H. Chiral Phosphane Alkenes (PALs): Simple Synthesis, Applications in Catalysis, and Functional Hemilability. *Chem. – Eur. J.* **2006**, *12*, 5849–5858.

(9) Freitag, B.; Elsen, H.; Pahl, J.; Ballmann, G.; Herrera, A.; Dorta, R.; Harder, S. S-Block Metal Dibenzoazepinate Complexes: Evidence for Mg–Alkene Encapsulation. *Organometallics* **2017**, *36*, 1860–1866.

(10) Chelouan, A.; Bao, S.; Frieß, S.; Herrera, A.; Heinemann, F. W.; Escalona, A.; Grasruck, A.; Dorta, R. Developing Chiral Dibenzazepine-Based S(O)-Alkene Hybrid Ligands for Rh(I) Complexation: Catalysts for the Base-Free Hayashi–Miyaura Reaction. *Organometallics* **2018**, *37*, 3983–3992.

(11) Brodie, M. J. Sodium Channel Blockers in the Treatment of Epilepsy. *CNS Drugs* **2017**, *31*, 527–534.

(12) Schmidt, D.; Elger, C. E. What Is the Evidence That Oxcarbazepine and Carbamazepine Are Distinctly Different Antiepileptic Drugs? *Epilepsy Behav.* **2004**, *5*, 627–635.

(13) Gierbolini, J.; Giarratano, M.; Benbadis, S. R. Carbamazepine-Related Antiepileptic Drugs for the Treatment of Epilepsy - a Comparative Review. *Expert Opin. Pharmacother.* **2016**, *17*, 885–888.

(14) Rössler, S. L.; Krautwald, S.; Carreira, E. M. Study of Intermediates in Iridium–(Phosphoramidite,Olefin)-Catalyzed Enantioselective Allylic Substitution. *J. Am. Chem. Soc.* **2017**, *139*, 3603–3606.

(15) Hamilton, J. Y.; Sarlah, D.; Carreira, E. M. Iridium-Catalyzed Enantioselective Allylic Vinylation. *J. Am. Chem. Soc.* **2013**, *135*, 994–997.

(16) Defieber, C.; Ariger, M. A.; Moriel, P.; Carreira, E. M. Iridium-Catalyzed Synthesis of Primary Allylic Amines from Allylic Alcohols: Sulfamic Acid as Ammonia Equivalent. *Angew. Chem., Int. Ed.* **2007**, *46*, 3139–3143.

(17) Petrone, D. A.; Isomura, M.; Franzoni, I.; Rössler, S. L.; Carreira, E. M. Allenylic Carbonates in Enantioselective Iridium-Catalyzed Alkylations. *J. Am. Chem. Soc.* **2018**, *140*, 4697–4704.

(18) Hamilton, J. Y.; Hauser, N.; Sarlah, D.; Carreira, E. M. Iridium-Catalyzed Enantioselective Allyl-Allylsilane Cross-Coupling. *Angew. Chem., Int. Ed.* **2014**, *53*, 10759–10762.

(19) Schafroth, M. A.; Sarlah, D.; Krautwald, S.; Carreira, E. M. Iridium-Catalyzed Enantioselective Polyene Cyclization. *J. Am. Chem. Soc.* **2012**, *134*, 20276–20278.

(20) Sandmeier, T.; Krautwald, S.; Carreira, E. M. Stereoselective Synthesis of Piperidines by Iridium-Catalyzed Cyclocondensation. *Angew. Chem., Int. Ed.* **2017**, *56*, 11515–11519.

(21) Mariz, R.; Briceño, A.; Dorta, R.; Dorta, R. Chiral Dibenzazepine-Based P-Alkene Ligands and Their Rhodium Complexes: Catalytic Asymmetric 1,4 Additions to Enones. *Organometallics* **2008**, *27*, 6605–6613.

(22) Herrera, A.; Grasruck, A.; Heinemann, F. W.; Scheurer, A.; Chelouan, A.; Frieß, S.; Seidel, F.; Dorta, R. Developing P-Stereogenic, Planar–Chiral P-Alkene Ligands: Monodentate, Bidentate, and Double Agostic Coordination Modes on Ru(II). *Organometallics* **2017**, *36*, 714–720.

(23) Lyaskovskyy, V.; van Dijk-Moes, R. J. A.; Burck, S.; Dzik, W. I.; Lutz, M.; Ehlers, A. W.; Slootweg, J. C.; de Bruin, B.; Lammertsma, K. Dibenzo[b,f]Phosphepines: Novel Phosphane–Olefin Ligands for Transition Metals. *Organometallics* **2013**, *32*, 363–373.

(24) Schönberg, H.; Boulmaâz, S.; Wörle, M.; Liesum, L.; Schweiger, A.; Grützmacher, H. A Monomeric D9-Rhodium(0) Complex. *Angew. Chem., Int. Ed.* **1998**, *37*, 1423–1426.

(25) Thomaier, J.; Boulmaâz, S.; Schönberg, H.; Rüegger, H.; Currao, A.; Grützmacher, H.; Hillebrecht, H.; Pritzkow, H. Dibenzotropylidene Phosphanes (TROPPs): Synthesis and Coinage Metal Complexes. *New J. Chem.* **1998**, *22*, 947–958.

(26) Boulmaâz, S.; Loss, S.; Schönberg, H.; Deblon, S.; Wörle, M.; Nesper, R.; Grützmacher, H.; Mlakar, M. Synthesis of Stable Monomeric Iridium(0) and Iridium(−1) Complexes. *Chem. Commun.* **1998**, 2623–2624.

(27) Brill, M.; Collado, A.; Cordes, D. B.; Slawin, A. M. Z.; Vogt, M.; Grützmacher, H.; Nolan, S. P. Synthesis and Characterization of Gold(I) Complexes of Dibenzotropylidene-Functionalized NHC Ligands (Trop-NHCs). *Organometallics* **2015**, *34*, 263–274.

(28) Lichtenberg, C.; Bloch, J.; Gianetti, T. L.; Buettner, T.; Geier, J.; Gruetzmacher, H. Diolefins with an Ether/Thioether Functionality as Ligands in the Coordination Sphere of Ni and Rh. *Dalton Trans.* **2015**, *44*, 20056–20066.

(29) Puschmann, F. F.; Harmer, J.; Stein, D.; Rüegger, H.; de Bruin, B.; Grützmacher, H. Electromeric Rhodium Radical Complexes. *Angew. Chem.* **2010**, *122*, 395–399.

(30) Fischbach, U.; Rüegger, H.; Grützmacher, H. Tris(Dibenzo-[a,D]Cycloheptenyl)Phosphane: a Bulky Monodentate or Tetrapodal Ligand. *Eur. J. Inorg. Chem.* **2007**, *2007*, 2654–2667.

DOI: 10.1021/acs.organomet.9b00094
Organometallics 2019, 38, 1787–1799

(31) Breher, F.; Böhler, C.; Frison, G.; Harmer, J.; Liesum, L.; Schweiger, A.; Grützmacher, H. TROPDAD: a New Ligand for the Synthesis of Water-Stable Paramagnetic[16 + 1]-Electron Rhodium and Iridium Complexes. *Chem. – Eur. J.* **2003**, *9*, 3859–3866.
(32) Maire, P.; Königsmann, M.; Sreekanth, A.; Harmer, J.; Schweiger, A.; Grützmacher, H. A Tetracoordinated Rhodium Aminyl Radical Complex. *J. Am. Chem. Soc.* **2006**, *128*, 6578–6580.
(33) Zweifel, T.; Naubron, J.-V.; Büttner, T.; Ott, T.; Grützmacher, H. Ethanol as Hydrogen Donor: Highly Efficient Transfer Hydrogenations with Rhodium(I) Amides. *Angew. Chem., Int. Ed.* **2008**, *47*, 3245–3249.
(34) Zweifel, T.; Scheschkewitz, D.; Ott, T.; Vogt, M.; Grützmacher, H. Chiral [Bis(Olefin)Amine]Rhodium(I) Complexes – Transfer Hydrogenation in Ethanol. *Eur. J. Inorg. Chem.* **2009**, *2009*, 5561–5576.
(35) Trincado, M.; Sinha, V.; Rodríguez-Lugo, R. E.; Pribanic, B.; de Bruin, B.; Grützmacher, H. Homogeneously Catalysed Conversion of Aqueous Formaldehyde to H_2 and Carbonate. *Nat. Commun.* **2017**, *8*, No. 14990.
(36) Rodríguez-Lugo, R. E.; Trincado, M.; Vogt, M.; Tewes, F.; Santiso-Quinones, G.; Grützmacher, H. A Homogeneous Transition Metal Complex for Clean Hydrogen Production from Methanol–Water Mixtures. *Nat. Chem.* **2013**, *5*, 342–347.
(37) Vogt, M.; de Bruin, B.; Berke, H.; Trincado, M.; Grützmacher, H. Amino Olefin Nickel(I) and Nickel(0) Complexes as Dehydrogenation Catalysts for Amine Boranes. *Chem. Sci.* **2011**, *2*, 723–727.
(38) Trincado, M.; Vogt, M. CO_2-Based Hydrogen Storage – Hydrogen Liberation from Methanol/Water Mixtures and from Anhydrous Methanol. *Phys. Sci. Rev.* **2018**, *3*, No. 20170014.
(39) Bellini, M.; Filippi, J.; Miller, H. A.; Oberhauser, W.; Vizza, F.; He, Q.; Grützmacher, H. Hydrogen and Chemicals from Renewable Alcohols by Organometallic Electroreforming. *ChemCatChem* **2017**, *9*, 746–750.
(40) Bevilacqua, M.; Bianchini, C.; Marchionni, A.; Filippi, J.; Lavacchi, A.; Miller, H.; Oberhauser, W.; Vizza, F.; Granozzi, G.; Artiglia, L.; et al. Improvement in the Efficiency of an OrganoMetallic Fuel Cell by Tuning the Molecular Architecture of the Anode Electrocatalyst and the Nature of the Carbon Support. *Energy Environ. Sci.* **2012**, *5*, 8608–8620.
(41) Bellini, M.; Bevilacqua, M.; Filippi, J.; Lavacchi, A.; Marchionni, A.; Miller, H. A.; Oberhauser, W.; Vizza, F.; Annen, S. P.; Grützmacher, H. Energy and Chemicals from the Selective Electrooxidation of Renewable Diols by Organometallic Fuel Cells. *ChemSusChem* **2014**, *7*, 2432–2435.
(42) Rodríguez-Lugo, R. E.; de Bruin, B.; Trincado, M.; Grützmacher, H. A Stable Aminyl Radical Coordinated to Cobalt. *Chem. – Eur. J.* **2017**, *23*, 6795–6802.
(43) Büttner, T.; Geier, J.; Frison, G.; Harmer, J.; Calle, C.; Schweiger, A.; Schönberg, H.; Grützmacher, H. A Stable Aminyl Radical Metal Complex. *Science* **2005**, *307*, 235–238.
(44) Rosenthal, A. J.; Vogt, M.; de Bruin, B.; Grützmacher, H. A Diolefin Diamide Rhodium(I) Complex and Its One-Electron Oxidation Resulting in a Two-Center, Three-Electron Rh–N Bond. *Eur. J. Inorg. Chem.* **2013**, *2013*, 5831–5835.
(45) Lichtenberg, C.; Viciu, L.; Vogt, M.; Rodríguez-Lugo, R. E.; Adelhardt, M.; Sutter, J.; Khusniyarov, M. M.; Meyer, K.; de Bruin, B.; Bill, E.; et al. Low-Valent Iron: an Fe(I) Ate Compound as a Building Block for a Linear Trinuclear Fe Cluster. *Chem. Commun.* **2015**, *51*, 13890–13893.
(46) Gianetti, T. L.; Rodríguez-Lugo, R. E.; Harmer, J. R.; Trincado, M.; Vogt, M.; Santiso-Quinones, G.; Grützmacher, H. Zero-Valent Amino-Olefin Cobalt Complexes as Catalysts for Oxygen Atom Transfer Reactions from Nitrous Oxide. *Angew. Chem.* **2016**, *128*, 15549–15554.
(47) Trincado, M.; Rosenthal, A. J.; Vogt, M.; Grützmacher, H. η2-Coordination of a Phosphaalkyne to an Amino Olefin Nickel Complex and Regioselective Catalyzed Cyclooligomerization to Dewar 1,3,5-Triphosphabenzene. *Eur. J. Inorg. Chem.* **2014**, *2014*, 1599–1604.
(48) Tejel, C.; del Río, M. P.; Asensio, L.; van den Bruele, F. J.; Ciriano, M. A.; Tsichlis i Spithas, N.; Hetterscheid, D. G. H.; de Bruin, B. Cooperative Double Deprotonation of Bis(2-Picolyl)Amine Leading to Unexpected Bimetallic Mixed Valence (M –I, M I) Rhodium and Iridium Complexes. *Inorg. Chem.* **2011**, *50*, 7524–7534.
(49) Tejel, C.; del Río, M. P.; Ciriano, M. A.; Reijerse, E. J.; Hartl, F.; Záliš, S.; Hetterscheid, D. G. H.; Tsichlis i Spithas, N.; de Bruin, B. Ligand-Centred Reactivity of Bis(Picolyl)Amine Iridium: Sequential Deprotonation, Oxidation and Oxygenation of a "Non-Innocent" Ligand. *Chem. – Eur. J.* **2009**, *15*, 11878–11889.
(50) Tejel, C.; Asensio, L.; Pilar del Río, M.; de Bruin, B.; López, J. A.; Ciriano, M. A. Snapshots of a Reversible Metal-Ligand Two-Electron Transfer Step Involving Compounds Related by Multiple Types of Isomerism. *Eur. J. Inorg. Chem.* **2012**, *2012*, 512–519.
(51) Kotani, H.; Sugiyama, T.; Ishizuka, T.; Shiota, Y.; Yoshizawa, K.; Kojima, T. Redox-Noninnocent Behavior of Tris(2-Pyridylmethyl)Amine Bound to a Lewis Acidic Rh(III) Ion Induced by C–H Deprotonation. *J. Am. Chem. Soc.* **2015**, *137*, 11222–11225.
(52) Liang, Q.; Song, D. Reactivity of Fe and Ru Complexes of Picolyl-Substituted N-Heterocyclic Carbene Ligand: Diverse Coordination Modes and Small Molecule Binding. *Inorg. Chem.* **2017**, *56*, 11956–11970.
(53) Stichauer, R.; Helmers, A.; Bremer, J.; Rohdenburg, M.; Wark, A.; Lork, E.; Vogt, M. Rhenium(I) Triscarbonyl Complexes with Redox-Active Amino- and Iminopyridine Ligands: Metal–Ligand Cooperation as Trigger for the Reversible Binding of CO_2 via a Dearmomatization/Rearomatization Reaction Sequence. *Organometallics* **2017**, *36*, 839–848.
(54) Sieh, D.; Lacy, D. C.; Peters, J. C.; Kubiak, C. P. Reduction of CO_2 by Pyridine Monoimine Molybdenum Carbonyl Complexes: Cooperative Metal-Ligand Binding of CO_2. *Chem. – Eur. J.* **2015**, *21*, 8497–8503.
(55) Sieh, D.; Kubiak, C. P. A Series of Diamagnetic Pyridine Monoimine Rhenium Complexes with Different Degrees of Metal-to-Ligand Charge Transfer: Correlating (CNMR)-C-13 Chemical Shifts with Bond Lengths in Redox-Active Ligands. *Chem. – Eur. J.* **2016**, *22*, 10638–10650.
(56) Morales-Morales, D., Jensen, C. M., Eds.; *The Chemistry of Pincer Compounds*; Elsevier, 2007; pp 1–467.
(57) Peris, E.; Crabtree, R. H. Key Factors in Pincer Ligand Design. *Chem. Soc. Rev.* **2018**, *47*, 1959–1968.
(58) Valdés, H.; García-Eleno, M. A.; Canseco-Gonzalez, D.; Morales-Morales, D. Recent Advances in Catalysis with Transition-Metal Pincer Compounds. *ChemCatChem* **2018**, *10*, 3136.
(59) Gunanathan, C.; Milstein, D. Metal–Ligand Cooperation by Aromatization–Dearomatization: A New Paradigm in Bond Activation and "Green" Catalysis. *Acc. Chem. Res.* **2011**, *44*, 588–602.
(60) Milstein, D. Metal-Ligand Cooperation by Aromatization-Dearomatization as a Tool in Single Bond Activation. *Philos. Trans. R. Soc., A* **2015**, *373*, No. 20140189.
(61) Vogt, M.; Rivada-Wheelaghan, O.; Iron, M. A.; Leitus, G.; Diskin-Posner, Y.; Shimon, L. J. W.; Ben-David, Y.; Milstein, D. Anionic Nickel(II) Complexes with Doubly Deprotonated PNP Pincer-Type Ligands and Their Reactivity Toward CO_2. *Organometallics* **2013**, *32*, 300–308.
(62) Bailey, W. D.; Kaminsky, W.; Kemp, R. A.; Goldberg, K. I. Synthesis and Characterization of Anionic, Neutral, and Cationic PNP Pincer Pd II and Pt II Hydrides. *Organometallics* **2014**, *33*, 2503–2509.
(63) Feller, M.; Ben-Ari, E.; Iron, M. A.; Diskin-Posner, Y.; Leitus, G.; Shimon, L. J. W.; Konstantinovski, L.; Milstein, D. Cationic, Neutral, and Anionic PNP Pd II and Pt II Complexes: Dearomatization by Deprotonation and Double-Deprotonation of Pincer Systems. *Inorg. Chem.* **2010**, *49*, 1615–1625.
(64) Khusnutdinova, J. R.; Milstein, D. Metal-Ligand Cooperation. *Angew. Chem., Int. Ed.* **2015**, *54*, 12236–12273.
(65) van der Vlugt, J. I. Cooperative Catalysis with First-Row Late Transition Metals. *Eur. J. Inorg. Chem.* **2012**, *2012*, 363–375.

DOI: 10.1021/acs.organomet.9b00094
Organometallics 2019, 38, 1787–1799

(66) Grützmacher, H. Cooperating Ligands in Catalysis. *Angew. Chem., Int. Ed.* **2008**, *47*, 1814−1818.
(67) van der Vlugt, J. I.; Reek, J. N. H. Neutral Tridentate PNP Ligands and Their Hybrid Analogues: Versatile Non-Innocent Scaffolds for Homogeneous Catalysis. *Angew. Chem., Int. Ed.* **2009**, *48*, 8832−8846.
(68) Gunanathan, C.; Milstein, D. Bond Activation by Metal-Ligand Cooperation: Design of "Green" Catalytic Reactions Based on Aromatization-Dearomatization of Pincer Complexes. In *Bifunctional Molecular Catalysis*; Ikariya, T., Shibasaki, M., Eds.; Topics in Organometallic Chemistry; Springer: Berlin, Heidelberg, 2011; Vol. *37*, pp 55−84.
(69) Nerush, A.; Vogt, M.; Gellrich, U.; Leitus, G.; Ben-David, Y.; Milstein, D. Template Catalysis by Metal−Ligand Cooperation. C−C Bond Formation via Conjugate Addition of Non-Activated Nitriles Under Mild, Base-Free Conditions Catalyzed by a Manganese Pincer Complex. *J. Am. Chem. Soc.* **2016**, *138*, 6985−6997.
(70) Perdriau, S.; Zijlstra, D. S.; Heeres, H. J.; de Vries, J. G.; Otten, E. A Metal−Ligand Cooperative Pathway for Intermolecular Oxa-Michael Additions to Unsaturated Nitriles. *Angew. Chem.* **2015**, *127*, 4310−4314.
(71) Huff, C. A.; Kampf, J. W.; Sanford, M. S. Role of a Noninnocent Pincer Ligand in the Activation of CO_2 at (PNN)Ru-(H)(CO). *Organometallics* **2012**, *31*, 4643−4645.
(72) Annibale, V. T.; Song, D. Multidentate Actor Ligands as Versatile Platforms for Small Molecule Activation and Catalysis. *RSC Adv.* **2013**, *3*, 11432.
(73) Janes, T.; Yang, Y.; Song, D. Chemical Reduction of CO_2 Facilitated by C-Nucleophiles. *Chem. Commun.* **2017**, *53*, 11390−11398.
(74) Drover, M. W.; Love, J. A.; Schafer, L. L. 1,3-N,O-Complexes of Late Transition Metals. Ligands with Flexible Bonding Modes and Reaction Profiles. *Chem. Soc. Rev.* **2017**, *46*, 2913−2940.
(75) Drover, M. W.; Schafer, L. L.; Love, J. A. Amidate-Ligated Complexes of Rhodium(I): a Showcase of Coordination Flexibility. *Organometallics* **2015**, *34*, 1783−1786.
(76) Donati, N.; Stein, D.; Büttner, T.; Schönberg, H.; Harmer, J.; Anadaram, S.; Grützmacher, H. Rhodium and Iridium Amino, Amido, and Aminyl Radical Complexes. *Eur. J. Inorg. Chem.* **2008**, *2008*, 4691−4703.
(77) Drover, M. W.; Schafer, L. L.; Love, J. A. Isocyanate Deinsertion from K 1-O Amidates: Facile Access to Perfluoroaryl Rhodium(I) Complexes. *Dalton Trans.* **2015**, *44*, 19487−19493.
(78) Filonenko, G. A.; Smykowski, D.; Szyja, B. M.; Li, G.; Szczygieł, J.; Hensen, E. J. M.; Pidko, E. A. Catalytic Hydrogenation of CO_2 to Formates by a Lutidine-Derived Ru−CNC Pincer Complex: Theoretical Insight into the Unrealized Potential. *ACS Catal.* **2015**, *5*, 1145−1154.
(79) Rivada-Wheelaghan, O.; Dauth, A.; Leitus, G.; Diskin-Posner, Y.; Milstein, D. Synthesis and Reactivity of Iron Complexes with a New Pyrazine-Based Pincer Ligand, and Application in Catalytic Low-Pressure Hydrogenation of Carbon Dioxide. *Inorg. Chem.* **2015**, *54*, 4526−4538.
(80) Feller, M.; Ben-Ari, E.; Diskin-Posner, Y.; Milstein, D. CO_2 Activation by Metal−Ligand-Cooperation Mediated by Iridium Pincer Complexes. *J. Coord. Chem.* **2018**, 1679−1689.
(81) Vogt, M.; Gargir, M.; Iron, M. A.; Diskin-Posner, Y.; Ben-David, Y.; Milstein, D. A New Mode of Activation of CO_2 by Metal−Ligand Cooperation with Reversible C−C and M−O Bond Formation at Ambient Temperature. *Chem. − Eur. J.* **2012**, *18*, 9194−9197.
(82) Vogt, M.; Nerush, A.; Diskin-Posner, Y.; Ben-David, Y.; Milstein, D. Reversible CO_2 Binding Triggered by Metal-Ligand Cooperation in a Rhenium(I) PNP Pincer-Type Complex and the Reaction with Dihydrogen. *Chem. Sci.* **2014**, *5*, 2043−2051.
(83) Feller, M.; Gellrich, U.; Anaby, A.; Diskin-Posner, Y.; Milstein, D. Reductive Cleavage of CO_2 by Metal-Ligand-Cooperation Mediated by an Iridium Pincer Complex. *J. Am. Chem. Soc.* **2016**, *138*, 6445−6454.
(84) Stichauer, R.; Vogt, M. Cooperative Binding of SO_2 under M−O and C−S Bond Formation in a Rhenium(I) Complex with Activated Amino- or Iminopyridine Ligand. *Organometallics* **2018**, *37*, 3639−3643.

DOI: 10.1021/acs.organomet.9b00094
Organometallics 2019, 38, 1787−1799

3.3 Rhenium(I) Triscarbonyl Complexes with Pyridine-Based N,O-Chelating Ligands as MLC Platforms for CO_2 Activation

3.3.1 Overview M-O Complexes in MLC

Transition metal-oxygen (M-O) complexes for MLC substrate activation are less common because of the greater lability of oxygen compared to e.g. nitrogen or phosphorus. Gelman *et al.* reported the C_{sp^3}-metalated Ir-PCP-pincer complex **96**, based on a dibenzobarrelene scaffold.[175] The postulated inner sphere mechanism renders a hemi-labile alkoxide group in **97** ('arm-closed') allowing for initial deprotonation of the alcohol substrate and alcoholate coordination (**98**, 'arm-open'). Subsequent β-hydride elimination furnishes the hydrido complex **96**, which can release hydrogen under reformation of complex **96**. Gelman's system represents a catalyst for acceptorless dehydrogenation of alcohols to ketones and esters (Scheme 45).

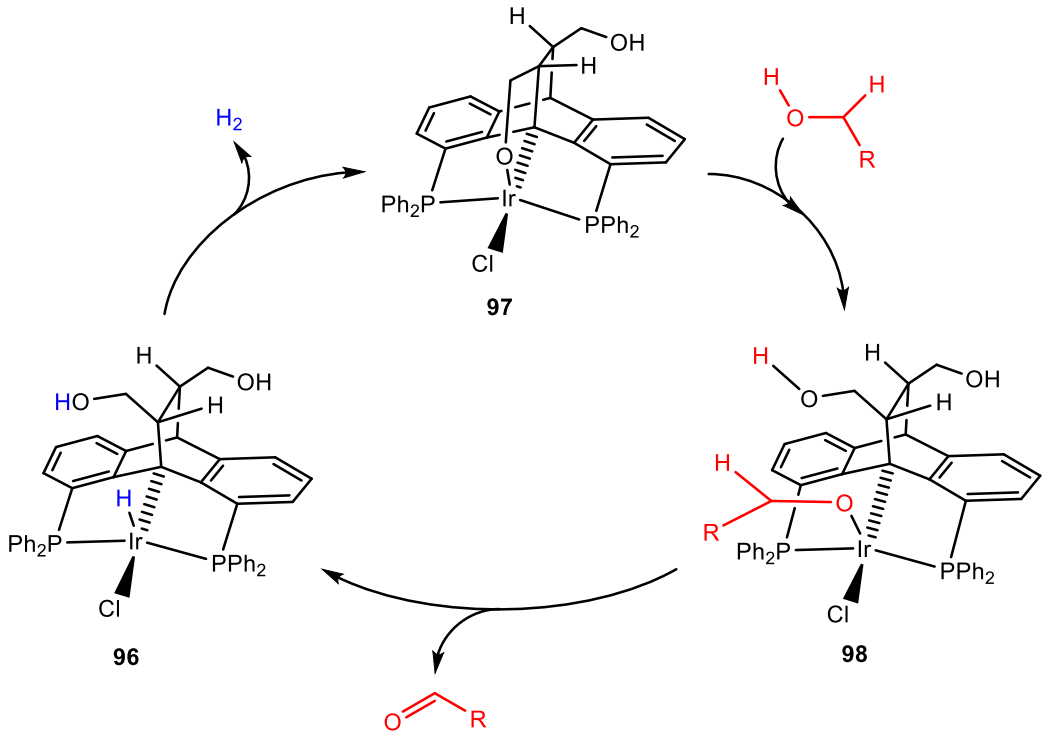

Scheme 45: Loss of H_2 in the iridium dibenzobarrelene PCP-pincer complex **96**, resulting in the Ir-PCP alkoxide complex **97** and postulated mechanism for acceptorless dehydrogenation of alcohols to ketones.[175]

Only a few more examples of M-O complexes were described for bifunctional catalysis.[176–179] Postulated mechanisms were mainly supposed *via* ligand-oxygen

substitution steps with oxygen as a placeholder of a vacant coordination site by displacing of the substrate molecule from the metal center. The lower basicity and the higher lability of the alkoxide ligand, in comparison to a coordinated nitrogen atom, permitted an inner-sphere mechanism *via* β-hydride elimination. A transition metal alkoxide pyridine complex for MLC activation *via* a dearomatization/rearomatization sequence could not be found in the literature so far. Yamagucchi *et al.* reported the dehydrogenation of alcohols catalyzed by an iridium 2-hydroxypyridine complex which indicates the dearomatization of the pyridine unit, like described before in the pyridonate resonance structure **32b***, under formation of a complexing ketone unit.[180; 181]

3.3.2 Precursor Chemistry

The herein discussed chelating system is, from the perspective of the ligands, a simplification of the first bidentate amino-/imino-pyridine system (**3.1**). Instead of a bidentate Schiff base (N,N-ligand) complex (**71**, **72**), a pyridine based N,O-ligand serves as an MLC platform for CO_2 activation. Pyridine-2-carbaldehyd (*aldpy*), pyridine-2-yl-methanol (H-*alkpy*), 2-benzoyl-pyridine (*ketpy*) and phenyl-pyridine-2-yl-methanol (Ph-*alkpy*) can serve as ligand scaffold for the Re(I) triscarbonyl complex synthesis (Scheme 46). The precursor for Re(I)-complex synthesis is again $Re(I)(CO)_5Br$. The Re(I)-complexes *fac*-[Re(I)(*aldpy*)$(CO)_3$Br] (**99a**) and *fac*-[Re(I)(*ketpy*)$(CO)_3$Br] (**99b**) are obtained by chelation under loss of two equivalents of CO. The derived compounds **99a** and **99b** should be readily reduced by potassium metal and give rise to the dearomatized anionic complexes K[Re(I)(H-*alkoxpy**)$(CO)_3$] (**101*a**) and K[Re(I)(Ph-*alkoxpy**)$(CO)_3$] (**101*b**) (the asterisk indicates the dearomatized pyridine unit). An alternative route entails the reaction of the Re(I)-complexes *fac*-[Re(I)(H-*alkpy*)$(CO)_3$Br] (**100a**) and *fac*-[Re(I)(Ph-*alkpy*)$(CO)_3$Br] (**100b**) with a strong base (LiHMDS) to yield the Re(I)(*alkoxpy**) species **101*a** and **101*b** as well, which are potent for the MLC activation of CO_2 giving rise to the 1,3-addition products **102a** and **102b**. The precursor complexes **99a** and **100a** of this system have been previously described in the literature.[182–187] The precursor *fac*-[Re(I)(*ketpy*)$(CO)_3$Br] (**99b**) has only been described with chloride instead of bromide in the literature so far.[182] The obtained molecular structure of **99b** from scXRD analysis is shown in the supporting information (**7.7**). ^{1}H and ^{13}C NMR analyses of **99b** show almost identical spectra to the pendant

chloride complex.[182] The synthesis of complex *fac*-[Re(I)(Ph-*alkpy*)(CO)$_3$Br] (**100b**) was developed in the course of this work.

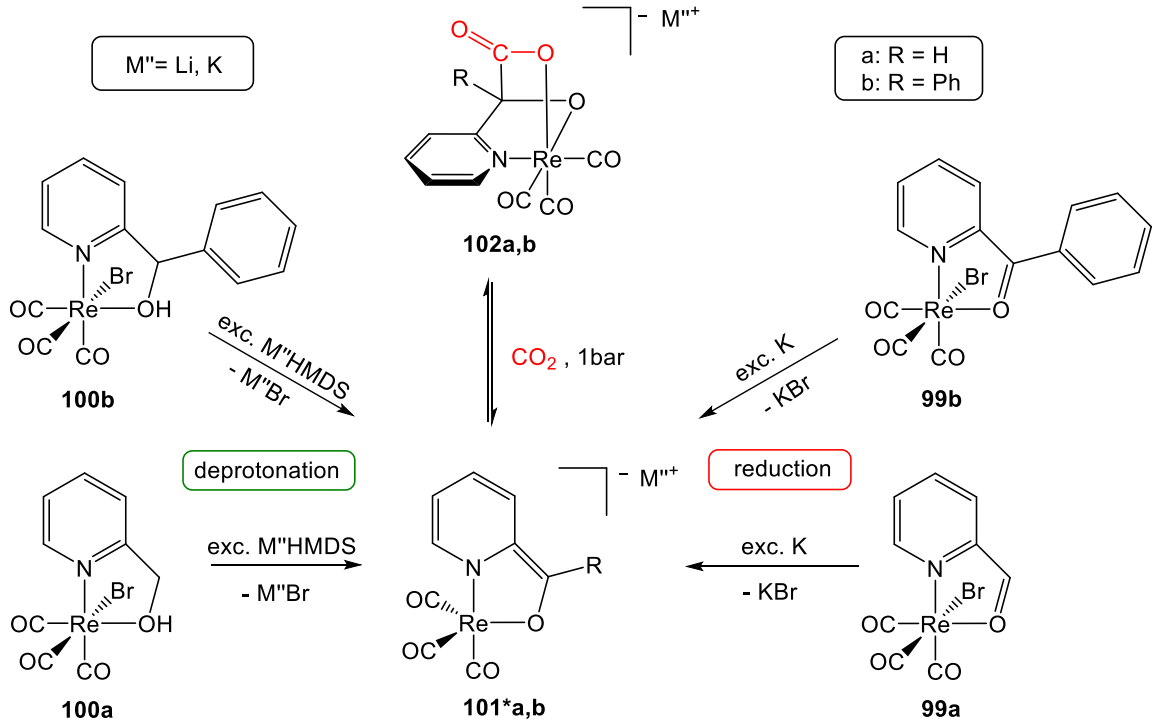

Scheme 46: Possible reaction pathways to reach the active species **101*a,b** from the used starting complexes Re(I)(*alkpy*) **100a,b** and Re(I)(*aldpy*) **99a**/ Re(I)(*ketpy*) **99b** and subsequent reaction with CO_2, obtaining the adduct complexes **102a,b**.

Sudbrake and Vahrenkamp used phenyl-pyridine-1-yl-methanol (Ph-*alkpy*) and 2-benzoyl-pyridine (*ketpy*) as ligands in chelate-stabilized zinc complexes and observed the greater lability of the alcohol in comparison to 2-benzoyl-pyridine as ligand.[188] Yumata *et al.* studied rhenium complexes of di-2-pyridinyl ketone, 2-benzoylpyridine and 2-hydroxybenzophenone.[182] They already described complex **99b** with a chloride substituent and the Ph-*alkpy* ligand in a neutral oxorhenium(V) complex with an oxygen atom and a hydroxy group in *trans* axial positions. The octahedral geometry of the oxorhenium(V) complex is completed by two bromide anions in *cis* position and PPh_3 in plane. Only one diastereomer was observed, probably due to the sterically demanding PPh_3 group. Upon coordination of the OH group to the rhenium in **100b**, a diastereotopic center is formed. The reaction of Ph-*alkpy* with Re(I)(CO)$_5$Br leads to a diastereomeric mixture (ratio 80:20) of

fac-[Re(I)(Ph-*alkpy*)(CO)$_3$Br] **100b**. Crystals of both diastereomeric complexes (**100b-R** and **100b-S**) could be isolated and their structure could be determined by means of scXRD analysis (Figure 8). The pair of diastereomers can be distinguished by the different configurations (R and S) of the C6 carbon atom.

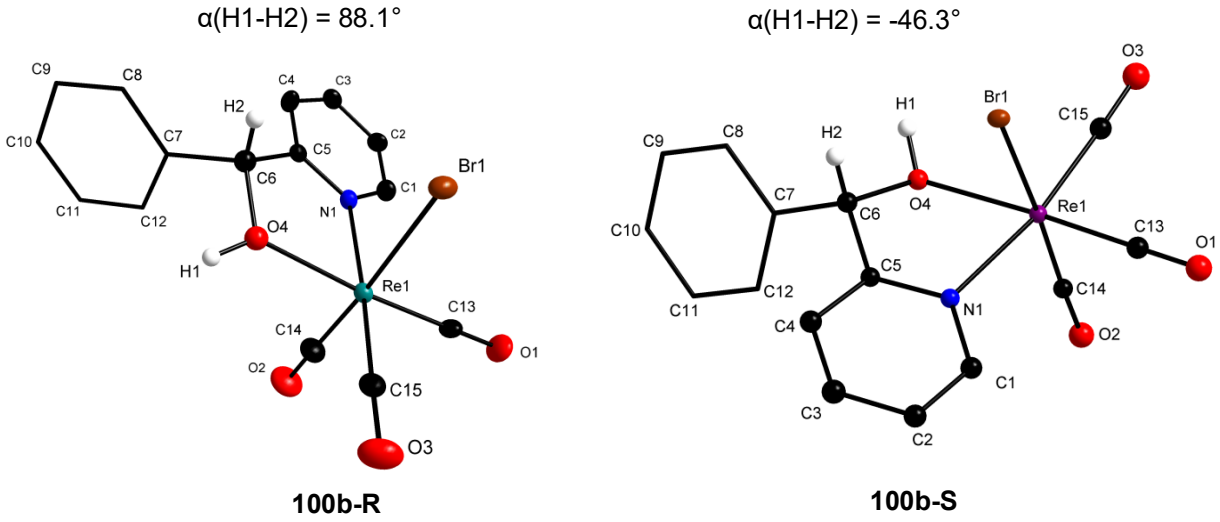

Figure 8: Diamond plot of the diastereomeric pair of *fac*-[Re(I)(Ph-*alkpy*)(CO)$_3$Br] (**100b-R** left and **100b-S** right) with selected torsion angles α [°] of H1-H2. (Thermal ellipsoids at 50% probability, H atoms omitted for clarity except for benzylic C-H and hydroxide O-H)

A torsion angle of 88.1° (**100b-R**) and -46.3° (**100b-S**) between H1 and H2 characterizes the two different coordination modes of the diastereomeric pair. The carbon atom C6 adopts R-configuration in **100b-R** and the respective S-configuration in **100b-S**. Similar to the above mentioned rhenium N,O-complexes (**99a,b** and **100a**) a disordered octahedral coordination mode was found for **100b-R** and **100b-S**. The coordinated pyridine units indicate an aromatic π-system and the carbon atom C6 shows sp^3-hybridization. For structural details from scXRD, see the experimental section and supporting information (**7.7**). In the ^{1}H NMR spectrum of **100b**, the pair of diastereomers are clearly visible by slightly staggered signals of each proton with a ratio of 80:20. The hydrogen signals of the pyridine unit between 8.90 ppm and 6.87 ppm are in the range of the previously described Re(I)-N,N complexes.[159] The ^{1}H NMR resonances of the hydroxy group are strongly shifted downfield to 10.00 ppm and 9.82 ppm compared to the free ligand (5.20 ppm). This is consistent with the previously reported ^{1}H NMR spectra of the Re(I)(H-*alkpy*) complex **100a**.[184] The

resonances associated with the benzylic proton have a chemical shift of 6.58 ppm and 6.21 ppm respectively, and also show a slight downfield shift with respect to the free ligand (5.78 ppm). The intact hydroxy group was identified by the absence of a cross peak in the 2D $^{1}H^{13}C$ HSQC NMR spectrum. The ^{13}C NMR spectrum exhibits the characteristic 80:20 ratio of the resonance pairs for **100b-R** and **100b-S**. The benzylic carbon signals were identified at 85.33 ppm and 82.31 ppm.

3.3.3 Activation of CO_2 *via* Dearomatization/Rearomatization Reaction Sequence – Investigation of the primary-Alcohol/Aldehyde vs. secondary-Alcohol/Keton Ligand System

As described before in the 2-amino-/2-iminomethyl pyridine system[159], the pyridine unit of the starting complexes (**99a,b** and **100a,b**) is dearomatized upon reduction or deprotonation, respectively. Crystals for scXRD analysis of the dearomatized species **101*a,b** could not be obtained. Typically, upfield shifted ^{1}H NMR signals of the pyridine units indicate again a disturbed π-system of **101*a,b** (Figure 9 and 10). In comparison to the 2-amino-/2-iminomethyl pyridine system, in which four equivalents of LiHMDS had to be used for complete deprotonation, ten equivalents of LiHMDS were necessary to obtain the dearomatized species **101*a** from **100a**. With five equivalents of base, the single deprotonated primary-alkoxide species could be observed in the ^{1}H NMR spectrum, in which the π-system of the pyridine unit appears to be still in intact (Figure 9). The reduction of Re(I)(*aldpy)* complex (**99a**) with potassium metal to obtain the dearomatized species **101*a** was not possible. Further reaction with CO_2 after previous deprotonation with LiHMDS did not lead to the desired CO_2 adduct. Possibly, the lithium as counterion plays a decisive role here, as it has already been shown with the Mn(I)-CO_2 adduct **78-Li**.[161] At this point, further investigations are needed to get a better understanding of the role of the counterion.

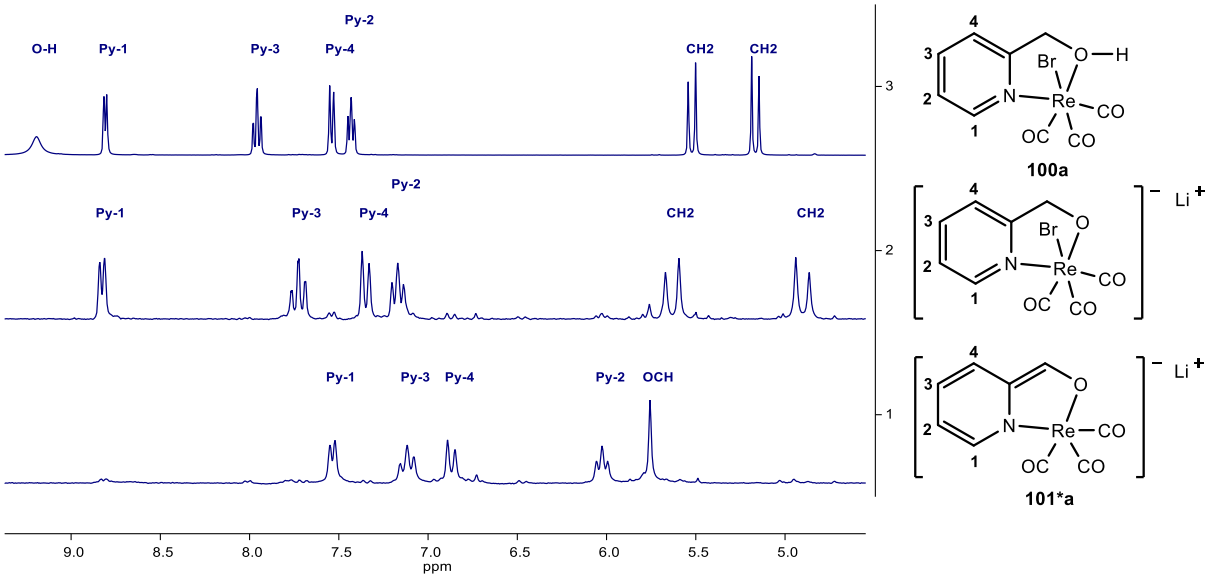

Figure 9: Sections of the ^{1}H NMR (THF-d_8, 298 K) spectra of Re(I)(H-*alkpy)* **100a** (top), the dearomatized species **101*a** (bottom) and the single deprotonated intermediate (middle).

It is also to mention that LiHMDS reacts with CO_2 as well, which complicates the characterization of the products, when an *in-situ* reaction was performed. In contrast to the primary-alcohol/aldehyde system, the secondary-alcohol/ketone system successfully reacts with CO_2 under Re-O and C-C bond formation and rearomatization (Figure 10). The dearomatized species **101*b**, can be obtained *via* both routes: two electron reduction of **99b** with potassium metal and deprotonation of **100b** with LiHMDS. Complex **101*b** reacts instantaneously in an atmosphere of CO_2 (1 bar) to the CO_2-adduct complex *fac*-K[Re(I)(Ph-*alkoxpy*-CO_2)$(CO)_3$] (**102b**). The ^{1}H NMR signals associated with the pyridine ring of **102b** indicate the rearomatization (typical downfield shift, see figure 10). In the ^{13}C NMR spectrum, the ^{13}C resonance associated with R-CO_2 carboxylate is observed at 182.03 ppm, which is consistent with the previously reported chemical shifts of the CO_2-adduct complexes **76** and **78**.[159; 161]

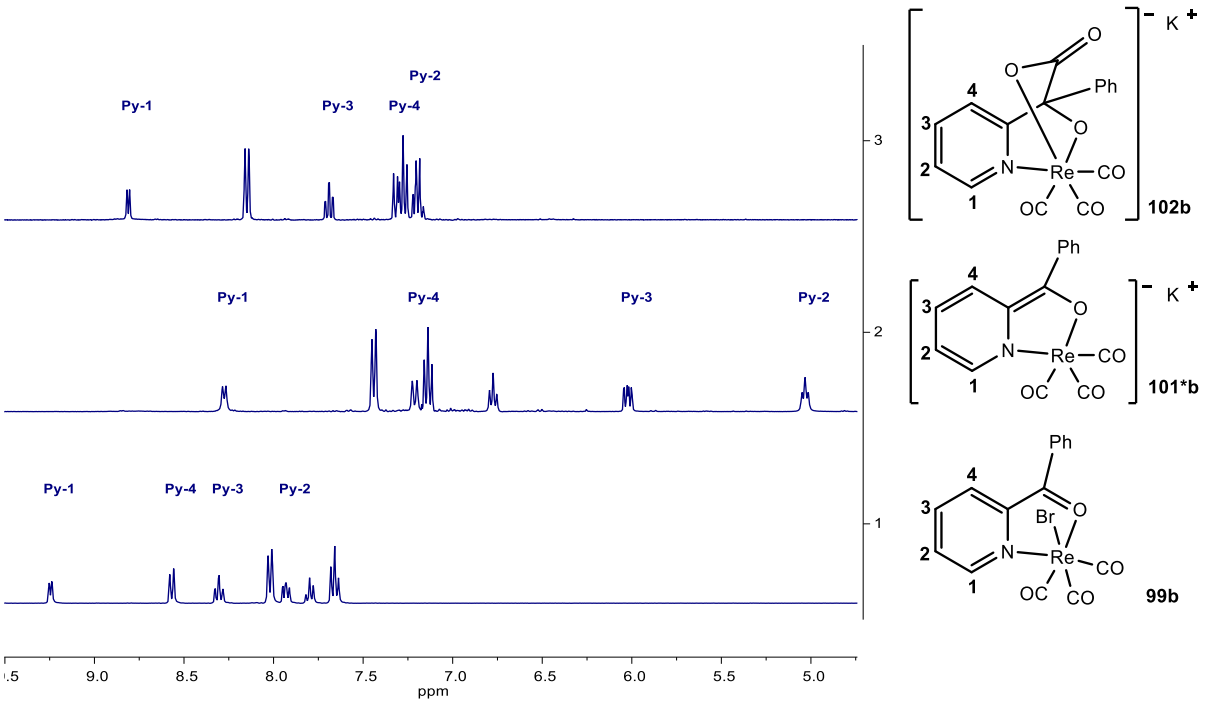

Figure 10: Sections of the ^{1}H NMR (THF-d_8, 298 K) spectra of Re(I)(*ketpy)* **99b** (bottom), the dearomatized species **101*b** (middle) and the CO_2 adduct complex **102b** (top).

The quaternary benzylic C atom exhibits a ^{13}C NMR chemical shift of 89.88 ppm similarly observed for the related complex Re(I)(Ph-*alkpy*) **100b**. The solubility of the CO_2 adduct in THF is significantly reduced compared to the precursor **101*b** and after addition of CO_2 it slowly precipitates. Crystals of *fac*-[K[18-*crown*)][Re(I)(Ph-*alkoxpy*-CO_2)$(CO)_3$] **102b-crown** suitable for scXRD analysis, could be obtained from a concentrated CH_2Cl_2 solution with one equivalents of 18-*crown*-6 by diffusion of *n*-hexane (Figure 11). The Re(I)-CO_2 adduct complex has a disordered octahedral geometry. The formed carboxylate interacts with the alkali metal counterion, as already shown in the Mn(*amidopy*-CO_2) (**78**) and Re(*amidopy*-CO_2) (**76**) complexes.[159; 161] The oxygen atom of the CO_2 which is not bonded to the rhenium center has an intramolecular interaction with the *ortho*-hydrogen atoms of the aryl group, showing an interatomic distance of 2.264(1) Å. This close proximity may be also reflected in the ^{1}H NMR spectrum of **102b** as the resonances associated with the *ortho*- and the *meta*-aryl hydrogen atoms are significantly separated. The newly formed C-C bond between CO_2 and the benzylic sp^3-C atom is slightly elongated with an interatomic distance of 1.577(8) Å and is in accordance with previously reported CO_2 adduct complexes **76**, **78** and **94**.[159; 161; 174]

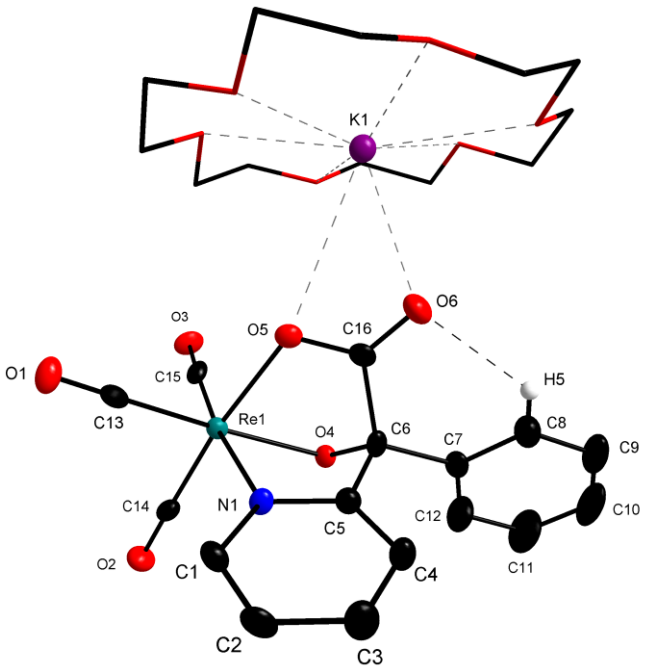

102b-crown

C1-C2	1.388(8)
C2-C3	1.380(9)
C3-C4	1.384(8)
C4-C5	1.382(8)
N1-C1	1.342(7)
N1-C5	1.358(7)
C5-C6	1.538(8)
C6-C7	1.520(8)
C6-O4	1.413(7)
C6-C16	1.577(8)
C16-O5	1.283(7)
C16-O6	1.229(7)
Re1-O4	2.078(4)
Re1-O5	2.155(4)
K1-O5	3.324(4)
K1-O6	2.769(5)
H5-O6	2.264(1)
O5-C16-O6	125°

Figure 11: Diamond plot of *fac*-[K(18-*crown*-6)][Re(I)(Ph-*alkoxpy*-CO_2)$(CO)_3$] (**102b-crown**) with selected bond lengths [Å] and angles [°]. (Thermal ellipsoids at 50% probability, solvent and H atoms omitted for clarity except for aryl C8-H5)

The bond length of Re1-O5 (2.155(4) Å) is also elongated, compared to Re1-O4 (2.078(4) Å), and indicates a weaker bonding. The interatomic distance of K1-O5 (3.324(4) Å) and K1-O6 (2.769(5) Å) show an interaction of the potassium with the CO_2 entity in the adduct complex. The formed carboxylate moiety shows an O-C-O angle of 125° in the adduct complex **102b-crown**. The negative ESI-MS spectrum of **102b-crown** in MeOH shows the main signal of the anionic molecule ion without CO_2 $[(M)\text{-}CO_2]^-$ at m/z = 454.0 for $C_{15}H_9NO_4Re^-$ with matching isotopic pattern. The molecule ion $[M]^-$ at m/z = 497.9 for $C_{16}H_9NO_6Re^-$ only has a very weak signal in the spectrum but still visible with associated ^{185}Re isotopic peak at m/z = 496.0. The MS^2 spectrum of m/z = 454.0 shows the loss of each CO ligand. The positive ESI-MS shows a strong signal at m/z = 303.3 for $[K(18\text{-}crown\text{-}6)]^+$ ($C_{12}H_{24}O_6K^+$). The reversibility of the C6-C16 bond by exchange reactions of CO_2 using labeled $^{13}CO_2$ or another substrate has not yet been confirmed and will be investigated in the future.

Summary and conclusion

The amin/imin system with pyridine-based Re(I)-complexes **73-Re** and **74-Re** could be successfully adapted to the secondary-alcohol/ketone system with pyridine-based Re(I)-complexes *fac*-[Re(I)(*ketpy*)$(CO)_3$Br] (**99b**) and *fac*-[Re(I)(Ph-*alkpy*)$(CO)_3$Br] (**100b**) for CO_2 activation *via* MLC under a dearomatization/rearomatization reaction sequence. The primary-alcohol/aldehyde system showed promising approaches for MLC activation *via* a dearomatization/rearomatization sequence, but they have not yet been successfully implemented. It was shown that the dearomatized species K[Re(I)(Ph-*alkoxpy**)$(CO)_3$] (**101*b**) could be obtained by reduction of **99b** or by deprotonation of **100b**. The activation of CO_2 led to the adduct complex *fac*-K[Re(I)(Ph-*alkoxpy*-CO_2)$(CO)_3$] (**102b**) under rearomatization of the pyridine unit. Crystallographic data of **102b** showed an intramolecular hydrogen bonding of the ortho-hydrogen atoms of the aryl-group with one carboxylate oxygen. This finding implies that ortho-substitution may have an influence on the reaction with CO_2 or related species and can, for instance, promote or hamper the 1,3-addition to the complex. The influence of this interaction is interesting for further work. By installation of a phenyl group to the bridging benzylic C atom by the substitution of hydrogen, this could also be applied to the previous 2-amino-/2-iminomethyl pyridine system.[159] The bonded CO_2 interacted with the potassium cation, which compensates the negative charge, as already shown in the Re(I)-*amidopy*-CO_2 complex **76**. Exchange reactions of CO_2 with labeled $^{13}CO_2$ or other substrates have not been performed yet.

Experimental section

Most of the experimental work was performed by Lennart Schmiedeken during a research internship. I supervised his work and helped partly with the implementation and the analytic evaluation. The experimental setup corresponds to the conditions as described previously in **3.1.6**. Additionally, NMR spectra were recorded also on a Bruker Avance DPX 200 spectrometer.

My percentage contribution of the workload in categories: experimental concept and design: ca. 90%, experimental work and acquisition of experimental data: 30%, data analysis and interpretation: 100%, preparation of Figures and Tables: ca. 100%, drafting of the manuscript: ca. 100%.

Synthetic procedures

***fac*-[Re(I)(*aldpy*)(CO)$_3$Br] (99a)**

250.1 mg Re(I)(CO)$_5$Br (0.62 mmol) and 1.2 eqiv. pyridine-2-carbaldehyd (79.8 mg, 0.75 mmol) were stirred in a ventilated Schlenk tube in 10 mL of THF at 60 °C for 8 h and subsequently overnight at room temperature. To the obtained solution, *n*-hexane was added and the product was precipitated. The red powder was washed with *n*-hexane and dried in vacuum. Yield: 263.1 mg, 0.58 mmol, 93%. ^{1}H NMR (200 MHz, THF-d_8) δ = 10.44 (s, 1H, C(H)=O), 9.14 (d, *J* = 4.9 Hz, 1H, CH$_{py-1}$), 8.59 (d, *J* = 7.6 Hz, 1H, CH$_{py-4}$), 8.36 (t, *J* = 7.6 Hz, 1H, CH$_{py-3}$), 7.93 ppm (t, *J* = 6.7 Hz, 1H, CH$_{py-2}$).

***fac*-[Re(I)(*ketpy*)(CO)$_3$Br] (99b)**

Re(I)(CO)$_5$Br (100.0 mg, 0.25 mmol) and 1.5 eqiv. 2-benzoyl-pyridine (70.0 mg, 0.38 mmol) were stirred in a ventilated Schlenk tube in 20 mL of toluene at 100 °C for 8 h and subsequently overnight at room temperature. The product precipitate during cooling to room temperature. The dark red powder was washed with *n*-hexane and dried in vacuum. Yield: 101.5 mg, 0.19 mmol, 76%. ^{1}H NMR (360 MHz, THF-d_8) δ = 9.25 (d, *J* = 5.1 Hz, 1H, CH$_{py-1}$), 8.57 (d, *J* = 7.9 Hz, 1H, CH$_{py-4}$), 8.31 (td, *J* = 7.9, 1.6 Hz, 1H, CH$_{py-3}$), 8.02 (d, *J* = 7.3 Hz, 2H, CH$_{aryl-5,9}$), 7.93 (ddd, *J* = 7.8, 5.3, 1.3 Hz, 1H, CH$_{py-2}$), 7.80 (t, *J* = 7.5 Hz, 1H, CH$_{aryl-7}$), 7.66 ppm (t, *J* = 7.8 Hz, 2H, CH$_{ayl-6,8}$). ^{13}C{^{1}H} NMR (91 MHz, THF-d$_8$) δ = 206.46, 198.55, 197.24, 188.56, 154.99, 151.86, 135.83, 135.62, 134.08, 131.98, 131.43, 129.90, 67.39, 25.31 ppm. Selected bond lengths of **99b** in Å from Olex report scXRD analysis: C1-C2 = 1.392(5), C2-C3 = 1.381(6), C3-C4 = 1.395(5), C5-C4 = 1.393(5), C6-C5 = 1.483(5), C6-C7 = 1.467(5), C8-C7 = 1.403(5), C8-C9 = 1.388(5), C10-C9 = 1.397(6) , C10-C11 = 1.390(6), C12-C11 = 1.397(6) , C7-C12 = 1.397(6), C1-N1 = 1.339(5), N1-C5 = 1.364(5), O4-C6 = 1.245(4), O1-C13 = 1.150(5), O2-C14 = 1.086(6), C15-O3 = 1.138(5), Re1-O4 = 2.162(3), Re1-N1 = 2.175(3), Re1-Br1 = 2.604(1), Re1-C13 = 1.904(4), Re1-C14 = 1.958(5), Re1-C15 = 1.939(4).

***fac*-[Re(I)(H-*alkpy*)(CO)$_3$Br] (100a)**

Re(I)(CO)$_5$Br (300.0 mg, 0.74 mmol) and 1.1 eqiv. pyridine-2-methanol (88.7 mg, 0.81 mmol) were stirred in a ventilated Schlenk tube in 10 mL of THF at 60 °C for 8 h and subsequently overnight at room temperature. To the obtained solution *n*-hexane was added and the product was precipitated. The brownish powder was washed with

n-hexane and dried in vacuum. Yield: 313.4 mg, 0.68 mmol, 92%. ^{1}H NMR (360 MHz, THF-d_8) δ = 9.19 (s, 1H, OH), 8.81 (d, *J* = 5.5 Hz, 1H, CH_{py-1}), 7.96 (td, *J* = 7.8, 1.6 Hz, 1H, CH_{py-3}), 7.54 (d, *J* = 7.9 Hz, 1H, CH_{py-4}), 7.43 (t, *J* = 6.5 Hz, 1H, CH_{py-2}), 5.52 (d, *J* = 14.8 Hz, 1H, CH_2), 5.17 ppm (d, *J* = 14.8 Hz, 1H, CH_2).

***fac*-[Re(I)(Ph-*alkpy*)(CO)$_3$Br] (100b)**

$Re(I)(CO)_5Br$ (100.4 mg, 0.25 mmol) and 1.5 eqiv. phenyl-pyridine-1-yl-methanol (70.4 mg, 0.38 mmol) were stirred in a ventilated Schlenk tube in 20 mL of toluene at 100 °C for 8 h and subsequently overnight at room temperature. By cooling down and adding *n*-hexane, the product precipitated. The dark red powder was washed with *n*-hexane and dried in vacuum. Yield: 110.5 mg, 0.21 mmol, 83%. Crystals for scXRD analysis could be obtained by dissolving the product in THF and slow diffusion of *n*-hexane. ^{1}H NMR (360 MHz, THF-d_8) δ = 10.00 (s, $1H_a$, OH), 9.82 (s, $1H_b$, OH), 8.90 (d, *J* = 5.3 Hz, $1H_a$, CH_{Py-1}), 8.86 (d, *J* = 5.4 Hz, $1H_b$, CH_{Py-1}), 7.86 (td, *J* = 7.9, 1.5 Hz, $1H_a$, CH_{Py-3}), 7.83 (td, *J* = 7.9, 1.6 Hz, $1H_b$, CH_{Py-3}), 7.71-7.65 (m, $2H_b$, $CH_{Aryl-6,10}$), 7.49-7.41 (m, $6H_a$, CH_{Py-2}, $CH_{Aryl-6-10}$; $4H_b$, CH_{Py-2}, $CH_{Aryl-7-9}$), 7.01 (d, *J* = 8.0 Hz, $1H_a$, CH_{Py-4}), 6.87 (d, *J* = 8.0 Hz, $1H_b$, CH_{Py-4}), 6.58 (s, $1H_a$, OCH), 6.21 ppm (s, $1H_b$, OCH). ^{13}C{^{1}H} NMR (91 MHz, THF-d$_8$) δ = 197.70 (s, $1C_a$, Re-CO), 197.23 (s, $1C_a$, Re-CO), 192.91 (s, $1C_a$, Re-CO), 161.79 (s, $1C_a$, $C_{Py-quart}$), 161.70 (s, $1C_b$, $C_{Py-quart}$), 152.90 (s, $1C_b$, C_{Py-1}), 152.70 (s, $1C_a$, C_{Py-1}), 140.63 (s, $1C_a$, $C_{Aryl-quart}$), 140.24 (s, $1C_b$, $C_{Aryl-quart}$), 139.88 (s, $1C_a$, C_{Py-3}), 139.71 (s, $1C_b$, C_{Py-3}), 130.84 (s, $2C_b$, $C_{Aryl-8,12}$), 130.57 (s, $1C_b$, $C_{Aryl-10}$), 130.39 (s, $1C_a$, $C_{Aryl-10}$), 130.02 (s, $2C_a$, C_{Aryl}), 129.89 (s, $2C_b$, $C_{Aryl-9,11}$), 129.43 (s, $2C_a$, C_{Aryl}), 125.72 (s, $1C_b$, C_{Py-2}), 125.55 (s, $1C_a$, C_{Py-2}), 124.72 (s, $1C_a$, C_{Py-4}), 124.25 (s, $1C_b$, C_{Py-4}), 85.33 (s, $1C_a$, OCH), 82.31 ppm (s, $1C_b$, OCH). The three carbon signals ($3C_b$) of Re-CO are not visible in the ^{13}C NMR spectrum due to the low concentration. Selected bond lengths of **100b-R** in Å from Olex report scXRD analysis: N1-C1 = 1.344(8), N1-C5 = 1.351(8), C1-C2 = 1.380(9), C2-C3 = 1.154(9), C3-C4 = 1.398(8), C4-C5 = 1.397(8) , C5-C6 = 1.515(8), C6-C7 = 1.526(9), C6-O4 = 1.444(8), C7-C8 = 1.386(10), C8-C9 = 1.394(10), C9-C10 = 1.382(12), C10-C11 = 1.411(13), C11-C12 = 1.375(12), C7-C12 = 1.396(10), Re1-N1 = 2.175(5), Re1-O4 = 2.149(5), Re1-Br1 = 2.6303(6), Re1-C13 = 1.897(7), Re1-C14 = 1.901(7), Re1-C15 = 1.906(6), C13-O1 = 1.154(9), C14-O2 = 1.160(9), C15-O3 = 1.167(8), C6-O4 = 1.444(8). Selected bond lengths of **100b-S** in Å from Olex report scXRD analysis: N1-C1 = 1.356(4), N1-C5 = 1.351(4), C1-C2 = 1.377(4), C2-C3 = 1.391(5), C3-C4 = 1.390(4),

C4-C5 = 1.389(4), C5-C6 = 1.506(4), C6-C7 = 1.513(4), C6-O4 = 1.462(4), C7-C8 = 1.387(4), C8-C9 = 1.401(4), C9-C10 = 1.382(5), C10-C11 = 1.377(5), C11-C12 = 1.388(5), C7-C12 = 1.397(4), Re1-N1 = 2.179(3), Re1-O4 = 2.178(2), Re1-Br1 = 2.6409(3), Re1-C13 = 1.890(3), Re1-C14 = 1.903(3), Re1-C15 = 1.928(3), C13-O1 = 1.160(4), C14-O2 = 1.153(4), C15-O3 = 1.142(4).

Li[Re(I)(H-*alkoxpy)(CO)$_3$] (101*a-Li)**

10.2 mg (20 µmol) of [Re(H-*alkpy*)(CO)$_3$Br] (**100a**) were dissolved in 1.5 mL THF-d$_8$ and 10 eqiv. LiHMDS (39.8 mg, 240 µmol) were added. A color change to dark red was visible. ^{1}H NMR spectra showed almost quantitative yield of Li[Re(H-*alkoxpy**-)(CO)$_3$] (**101*a**). ^{1}H NMR (200 MHz, THF-*d*$_8$) δ = 7.54 (d, *J* = 5.8 Hz, 1H, CH$_{py-1}$), 7.12 (t, *J* = 7.8 Hz, 1H, CH$_{Py-3}$), 6.87 (d, *J* = 8.3 Hz, 1H, CH$_{Py-4}$), 6.02 (t, *J* = 6.4 Hz, 1H, CH$_{Py-2}$), 5.76 ppm (s, 1H, OCH).

Li[Re(I)(Ph-*alkoxpy)(CO)$_3$] (101*b-Li)**

10.0 mg (19 µmol) of [Re(Ph-*alkpy*)(CO)$_3$Br] (**100b**) were dissolved in 1.5 mL THF-d$_8$ in a Young-NMR tube and 10 eqiv. LiHMDS (33.5 mg, 200 µmol) were added. A color change to deep red was visible. The ^{1}H NMR spectrum indicated a quantitative yield of Li[Re(Ph-*alkoxpy**)(CO)$_3$] (**101*b-Li**). ^{1}H NMR (360 MHz, THF-*d*$_8$) δ = 8.27 (d, *J* = 6.7 Hz, 1H, CH$_{Py-1}$), 7.46 (d, *J* = 7.8 Hz, 2H, CH$_{Aryl-5,9}$), 7.22 (d, *J* = 9.2 Hz, 1H, CH$_{Py-4}$), 7.09 (t, *J* = 7.7 Hz, 2H, CH$_{Aryl-6,8}$), 6.71 (t, *J* = 7.2 Hz, 1H, CH$_{Aryl-7}$), 6.01 (dd, *J* = 9.0, 6.0 Hz, 1H, CH$_{Py-3}$), 5.01 ppm (t, *J* = 4.9 Hz, 1H, CH$_{Py-2}$). ^{13}C{^{1}H} NMR (91 MHz, THF-*d*$_8$) δ = 207.89 (s, 3C, Re-CO), 152.10 (s, 1C, C$_{Py-1)}$, 141.73 (s, 1C, C$_q$), 141.22 (s, 1C, C$_q$), 136.22 (s, 1C, C$_q$), 127.98 (s, 2C, C$_{Aryl-9,11}$), 124.73 (s, 2C, C$_{Aryl-8,12}$), 122.60 (s, 1C, C$_{Py-3}$), 121.67 (s, 1C, C$_{Aryl-7}$), 119.90 (s, 1C, C$_{Py-4}$), 102.77 ppm (s, 1C, C$_{Py-2}$).

K[Re(I)(Ph-*alkoxpy)(CO)$_3$] (101*b)**

10.0 mg (19 µmol) of Re(I)(*ketpy)* (**99b**) were dissolved in 1.5 mL THF-d$_8$ in a Young-NMR tube. 5 eqiv. of potassium metal (3.9 mg, 0.10 mmol) were added and the mixture was sonicated until the color changed to deep red (5 h). ^{1}H and ^{13}C NMR spectra showed a quantitative yield of K[Re(Ph-*alkoxpy**)(CO)$_3$] (**101*b**). ^{1}H NMR (360 MHz, THF-*d*$_8$) δ = 8.28 (d, *J* = 6.6 Hz, 1H, CH$_{Py-1}$), 7.44 (d, *J* = 7.5 Hz, 2H, CH$_{Aryl-5,9}$), 7.21 (d, *J* = 9.3 Hz, 1H, CH$_{Py-4}$), 7.14 (t, *J* = 7.8 Hz, 2H, CH$_{Aryl-6,8}$), 6.77

(t, *J* = 7.3 Hz, 1H, CH_{Aryl-7}), 6.02 (ddd, *J* = 9.4, 5.9, 1.3 Hz, 1H, CH_{Py-3}), 5.03 ppm (t, *J* = 6.4 Hz, 1H, CH_{Py-2}). $^{13}C\{^1H\}$ NMR (91 MHz, THF-d_8) δ = 207.75 (s, 3C, Re-CO), 151.81 (s, 1C, C_{Py-1}), 141.53 (s, 1C, C_q), 141.00 (s, 1C, C_q), 136.36 (s, 1C, C_q), 128.36 (s, 2C, $C_{Aryl-9,11}$), 124.93 (s, 2C, $C_{Aryl-8,12}$), 122.80 (s, 1C, C_{Py-3}), 122.25 (s, 1C, C_{Aryl-7}), 119.97 (s, 1C, C_{Py-4}), 103.23 ppm (s, 1C, C_{Py-2}).

***fac*-K[Re(I)(Ph-*alkoxpy*-CO_2)$(CO)_3$] (102b)**

10.0 mg (19 µmol) of Re(I)(*ketpy)* (**99b**) were dissolved in 1.5 mL THF-d_8 in a Young-NMR tube. 5 eqiv. of potassium metal (3.9 mg, 100 µmol) were added and the mixture was sonicated until the color changes to deep red (5 h). 1 bar of CO_2 was added and the color changed to deep brown followed by partly precipitation. ^1H and ^{13}C NMR spectra showed a quantitative turnover to *fac*-K[Re(I)(Ph-*alkoxpy*-CO_2)$(CO)_3$] (**102b**). Addition of *n*-hexane caused precipitation of the product. Yield after drying *in vacuo*: 9.6 mg (18 µmol, 95%). ^1H NMR (360 MHz, THF-d_8) δ = 8.81 (d, *J* = 5.3 Hz, 1H, CH_{Py-1}), 8.15 (dd, *J* = 8.4, 1.4 Hz, 2H, $CH_{Ar-5,9}$), 7.69 (td, *J* = 7.7, 1.6 Hz, 1H, CH_{Py-3}), 7.35-7.25 (m, 3H, CH_{Py-4}, $CH_{Ar-6,8}$), 7.23-7.16 ppm (m, 2H, CH_{Py-2}, CH_{Ar-7}). $^{13}C\{^1H\}$ NMR (91 MHz,THF-d_8) δ = 203.29 (s, 1C, Re-CO), 203.08 (s, 1C, Re-CO), 201.95 (s, 1C, Re-CO), 182.03 (s, 1C, OCO), 169.48 (s, 1C, C_{py-5}), 153.12 (s, 1C, C_{Py-1}), 144.84 (s, 1C, C_{Ar-7}), 139.12 (s, 1C, C_{Py-3}), 129.74 (s, 2C, $C_{Ar-5,9}$), 127.13 (s, 2C, $C_{Ar-6,8}$), 127.01 (s, 1C, C_{Ar-7}), 125.86 (free CO_2), 123.21 (s, 1C, C_{Py-2}), 121.89 (s, 1C, C_{Py-4}), 89.88 ppm (s, 1C, C_{q-6}).

***fac*-[K(18-*crown*-6)][Re(I)(Ph-*alkoxpy*-CO_2)$(CO)_3$] (102b-crown)**

10.2 mg (19 µmol) of *fac*-K[Re(Ph-*alkoxpy*-CO_2)$(CO)_3$] (**102b**) were dissolved in CH_2Cl_2 and 1 eqiv. of 18-*crown*-6 (5.3 mg, 20 µmol) was added. The brown solution was layered with *n*-hexane at -16 °C to obtain brown crystals suitable for X-ray diffraction analysis. Yield: 13.6 mg (0.017 mmol, 89%). ^1H NMR (360 MHz, Aceton-d_6) δ = 8.85 (d, *J* = 5.1 Hz, 1H, CH_{Py-1}), 8.21 (d, *J* = 7.1 Hz, 2H, $CH_{Ar-5,9}$), 7.82 (td, *J* = 7.8, 1.5 Hz, 1H, CH_{Py-3}), 7.38-7.28 (m, 4H, $CH_{Ar-6,8}$, $CH_{Py-4,2}$), 7.22 (t, *J* = 7.3 Hz, 1H, CH_{Ar-7}), 3.63 ppm (s, 24H, 18-*crown*-6). For appropriate ^{13}C NMR analysis, the solution of **102b-crown** in THF could not be prepared with a sufficient concentration. MS-ESI [CH_3OH] (m/z) neg: $[M]^-$ calcd for $C_{16}H_9NO_6Re^-$: 498.0; found 497.9 (detectable only with low signal intensity), $[(M)-CO_2]^-$ calcd for $C_{15}H_9NO_4Re^-$: 554.0; found 554.0, MS-ESI [CH_3OH] (m/z) pos: $[K(18\text{-}crown\text{-}6)]^+$ calcd for $C_{12}H_{24}O_6K^+$: 303.1; found

303.3. Selected bond lengths in Å from Olex report scXRD analysis: C1-C2 = 1.388(8), C2-C3 = 1.380(9), C3-C4 = 1.384(8), C4-C5 = 1.382(8), C5-C6 = 1.538(8), C6-C7 = 1.520(8), C7-C8 = 1.382(10), C8-C9 = 1.391(10), C9-C10 = 1.357(13), C10-C11 = 1.366(13), C11-C12 = 1.386(10), C7-C12 = 1.387(9), N1-C1 = 1.342(7), N1-C5 = 1.358(7), C6-C16 = 1.577(8), C6-O4 = 1.413(7), C16-O5 = 1.283(7) , C16-O6 = 1.229(7), Re1-C13 = 1.919(6), Re1-C14 = 1.891(6), Re1-C15 = 1.916(6), Re1-O4 = 2.078(4), Re1-05 = 2.155(4), Re1-N1 = 2.179(4), K1-O5 = 3.324(4), K1-O6 = 2.769(5), O1-C13 = 1.154(7), O2-C14 = 1.165(7), O3-C15 = 1.157(7), H5-O6 = 2.2641(1).

4 Summary

This work demonstrates three different ligand systems suitable for substrate activation *via* metal ligand cooperativity (MLC) under a dearomatization/rearomatization sequence of the pyridine unit (Scheme 47). The ligand frameworks are accessible *via* simple syntheses and still encompass a great potential for the design of suitable environments enabling substrate activations. All systems showed the possibility of activating polarized multiple bonds *via* MLC.

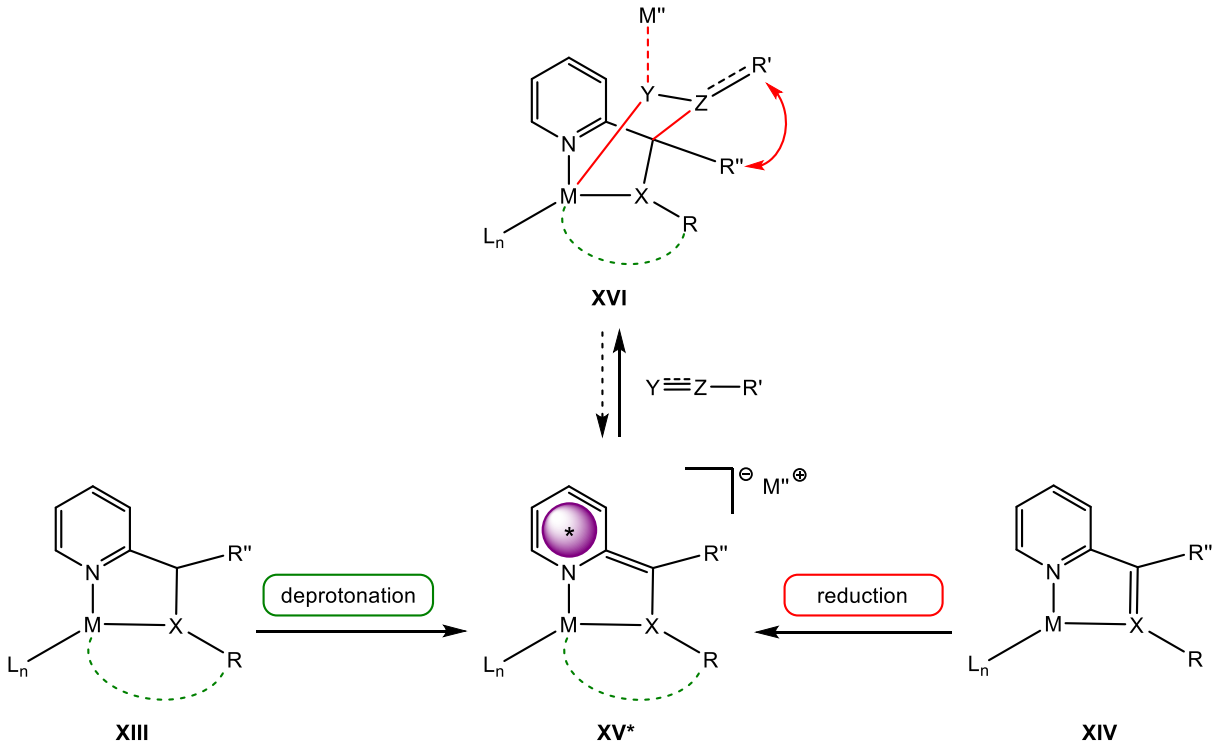

Scheme 47: Preparation of the dearomatized active species **XV*** *via* deprotonation (**XIII**) or reduction (**XIV**). Substrate activation *via* rearomatization of the pyridine unit and possible interactions (red lines) of the activated substrate (Y—Z—R') in the previously presented adduct complexes (**XVI**). 1) M—Y and C—Z bond formation *via* MLC. 2.) Electrostatic interaction of the counterion (Y- - -M"). 3.) Intramolecular hydrogen bonding (R'↔R"). (M = Mn, Re, Rh; M" = Li, Na, K; X = N, O; #Y = N, O; #Z = C, S; R = lone pair, $Ph^{p\text{-}Me}$, *dbap* (green line); #R' = O, (H, Ph), Ph_2, CH_2-Ph, N-Ph; R" = H, Ph; L = CO, PPh_3) (# = free substrate)

In particular, carbonyl groups in CO_2, aldehydes and ketones, C≡N triple bonds in nitriles, S=O double bonds in SO_2, and N=C double bonds in phenylisocyanate could be cooperatively activated. Especially CO_2 showed a high reactivity and the MLC activation was demonstrated with complexes encompassing each ligand system. In many cases a reversible bonding of the activated substrates could be demonstrated. Primarily, three different substrate interactions could be observed in the adduct complexes. That is specifically, in addition to the binding *via* MLC under M-Y and C-Z bond formation, the electrostatic interaction (M''- - -Y) of the substrate with the counterion could be shown in the anionic complexes (**3.1** and **3.3**) was observed to have significant impact. Furthermore, an intramolecular interaction *via* hydrogen bonding (R'↔R'') in the CO_2 complex **102b** (**3.3**) could be demonstrated by means of scXRD analysis and ^{1}H NMR spectroscopy. The dearomatized active species **XV*** (the asterisk indicates the dearomatized pyridine unit) was readily obtained *via* deprotonation of **XIII** (**3.1**, **3.2** and **3.3**) or *via* two-electron reduction of **XIV** (**3.1** and **3.3**). The activation of the substrate led to the rearomatized adduct-complexes **XVI**.

Table 1: 2-amino-/2-iminomethyl pyridine system (**3.1**): Overview of the complexes and substrates used in this work for activation reactions *via* MLC.

metal center	Substrate	Y—Z	exchange /substrate	notable properties	M''	adduct-complex
Re(I)	CO_2	C=O	✓ $^{13}CO_2$	very slow exchange	K^+	**76**
Mn(I)	CO_2	C=O	✓ $^{13}CO_2$	slow exchange	K^+	**78-K**
Mn(I)	CO_2	C=O	✓ $^{13}CO_2$	fast exchange	Na^+	**78-Na**
Mn(I)	CO_2	✗	-	decomposition	Li^+	-
Re(I)	SO_2 (DABSO)	S=O	✗ CO_2	diastereomeric interconversion of SO_2	K^+	**77**
Mn(I)	SO_2 (DABSO)	✗	-	no reaction	K^+	-
Re(I)	Benzaldehyde	C=O	✓ CO_2	exchange at 60 °C	K^+	**80**
Mn(I)	Benzaldehyde	C=O	✓ CO_2	exchange at RT	K^+	**79**
Re(I)	Benzophenone	C=O	✓ CO_2	exchange at RT	K^+	**81**
Mn(I)	Benzophenone	✗	-	no reaction	-	-
Re(I)	Phenylacetonitrile	C≡N	✗ CO_2	new compound	K^+	**82**
Mn(I)	Phenylacetonitrile	✗	-	no reaction	-	-
Re(I)	Phenylisocyanate	✗	-	mixture	K^+	-
Mn(I)	Phenylisocyanate	✗	-	no reaction	-	-
Re(I)	H_2	✗	-	no reaction	-	-
Mn(I)	H_2	✗	-	no reaction	-	-

The bidentate anionic 2-amino-/2-iminomethyl pyridine system **3.1**, with the group 7 transition metals in the formal oxidation state +I (Re(I) and Mn(I)), demonstrated the affinity to various hetero multiple bonds *via* MLC under cycloadditions (Table 1). The successful substitution of the metal center from rhenium to manganese gave rise to the corresponding complexes with the first-row congener allowing for a comparable study their (different) reactivity. Furthermore, it could be shown that the counterion in anionic adduct complexes plays a crucial role in substrate activation reactions by varying the alkali metal of the counter ion (Li, Na, K) in CO_2 exchange reactions. This matter was also evaluated in a computational study by means of DFT calculations (**3.1.5**). In conclusion the Re(I) complex **75*-Re** showed a larger scope of substrates, including a variety of different multiple bond type activations in comparison to the analogue Mn(I) complex **75*-Mn**, as well as stronger substrate bonding in case of CO_2 and benzaldehyde with respect to the performed exchange reactions. In general, regarding the activation of carbonyl groups, both complexes (**75*-Re** and **75*-Mn**) indicated a high selectivity for CO_2 in the performed exchange reactions. For the Re(I) complex **75*-Re**, the variety of bond types suitable for MLC binding could be extended to nitriles (**3.1.7**) and SO_2 (**3.1.4**). Importantly the 1,3-cycloaddition of SO_2 *via* MLC was not known to date of our publication and expanded the reported binding modes of SO_2 in the literature (demonstrated in *fac*-K[Re(*amidopy*-OSO)$(CO)_3$] (**77**)). MLC uptake and activation of nitriles could be effectively shown for phenylacetonitrile, having a hydrogen atom in α-position, under formation of an enamido group *via* C-C and Re-N bond formation, demonstrated in *fac*-K[Re(*amidopy-phacn*)$(CO)_3$] (**82**). Evidence was gathered for the MLC activation for nitriles without an α-hydrogen (such as benzonitrile), but could not be fully characterized. With the Mn(I) complex **78**, the influence of the counter ion to the activated substrate (CO_2) was successfully demonstrated. While lithium as a counterion induced the decomposition of the CO_2 adduct complex, the sodium and potassium complexes reacted reversibly with CO_2, but with very different exchange rates at ambient temperature. Computational DFT calculations supported the experimental results and showed also a significant influence of the counter cations on the CO_2 activation reactions. That is, the additional influence of the counterion remarkably opens another option to control the substrate uptake. The influence of the counterion in anionic complexes for MLC activation reactions has not been extensively studied so far. In general, all carbonyl adducts complexes showed reversible substrate exchange reactions (C-C and M-O reversible bond cleavage).

In the SO_2 adduct complex **77**, a dynamic bonding of the substrate as a diastereomeric interconversion could be shown *via* $^1H^1H$ EXSY NMR exchange spectroscopy. The phenylacetonitrile adduct complex provided a new compound in a CO_2 exchange reaction. It is remarkable that both complexes (**75*-Re** and **75*-Mn**) do not react with H_2 in experiments under similar conditions.

Table 2: Tridentate pyridine-amino-olefin system (**3.2**): Overview of the complexes and substrates used in this work for activation reactions *via* MLC.

Metal center	Substrate	Y—Z	exchange/ substrate	notable properties	adduct-complex
Rh(I)	CO_2	C=O	✘ $^{13}CO_2$	"fixation"	**94**
Rh(I)	Phenylisocyanate	C=N	✘ CO_2	"fixation"	**95**
Rh(I)	H_2	✘	-	mixture	-

The tridentate pyridine-amino-olefin system (**3.2**), with group 9 transition metal Rh(I), cooperatively react with hetero multiple bonds (C=O and C=N), represented by CO_2 and phenylisocyanate, *via* an MLC reaction sequence (Table 2). The azepine unit of the tridentate *dbap*-ligand allows for a rigid concave N-olefine binding site, giving rise to a sterically well-shielded backbone of the metal center. The olefin unit of the azepine moiety can stabilize low valent transition metal centers due to strong backbonding into the π*-orbitals of the olefin. The disturbed π-system of the pyridine unit in the dearomatized active species **93*** could additionally be proven by scXRD analysis, observable by the not equivalent bond lengths in the pyridine unit. Compared to the bidentate 2-amino-/2-iminomethyl pyridine system (**3.1**), the reactivity turned out to be significantly different: Complex **93*** gives rise to strongly bonded adduct complexes of CO_2 in [Rh(*dbap*-CO_2)(PPh_3)] (**94**) and phenylisocyanate in [Rh(*dbap*-NCO)(PPh_3)] (**95**), which showed no reversibility of the bonded substrates. The reaction with phenylisocyanate expanded the scope of functional groups to isocyanates under formation of an amidate moiety. A reaction with H_2 could be observed but did not lead to a defined compound.

Table 3: Bidentate anionic Re(I)-N,O primary-alcohol/ketone and secondary-alcohol/aldehyde system (**3.3**): Overview of the complexes used in this work for CO_2 activation.

metal center	system	Substrate	exchange/ substrate	notable properties	M"	adduct-complex
Re(I)	primary-alcohol/aldehyde	✘	-	-	Li^+	-
Re(I)	secondary-alcohol/ketone	CO_2	?	intramolecular CO_2 hydrogen bonding	K^+	**102b**

The anionic secondary-alcohol/ketone system (**3.3**) with bidentate N,O-ligands in Re(I)-tricarbonyl complexes successfully showed the activity towards CO_2 *via* the MLC reaction sequence (Table 3), similar to the bidentate N,N-ligand system (**3.1**). The dearomatized species (**101*b**), suitable for substrate activation *via* MLC, could be obtained by deprotonation with LiHMDS of the alcohol complex or *via* reduction of the ketone complex with potassium metal. Except of the alkoxide moiety, the CO_2 adduct complex (**102b**) resembles that of the 2-amino-/2-iminomethyl pyridine system, by 1,3-addition under Re-O and C-C bond formation and the additional interaction of the alkali metal counter ion with CO_2, proven by scXRD analysis. A major difference was an intramolecular interaction of the CO_2 oxygen with the *ortho*-hydrogen atoms of the aryl group *via* hydrogen bonding. This feature may be interesting with respect to ligand tuning, as alterations of the adjacent phenyl group can be investigated to adapt the environment for the substrate enabling or hampering specific MLC-substrate interactions. This interesting feature could also be transferred to the 2-amino-/2-iminomethyl pyridine system (**3.1**) or the tridentate pyridine-amino-olefin system (**3.2**) by replacement of a benzylic hydrogen atom. The investigations on the reversibility of CO_2 complexation and the activity towards other substrates and the influence of the counterion are still pending. In contrast, the corresponding anionic primary-alcohol/aldehyde system (**3.3**) showed that the active species (**101*a**) was only accessible *via* deprotonation with LiHMDS of the primary-alcohol complex **100a** but not by two-electron reduction with potassium metal of the aldehyde-complex **99a**. Further reaction of **101*a** with CO_2 showed no successful conversion. Further investigations involving the substitution of the counterion with Li^+, Na^+ or K^+ have to be done in the future to get a better understanding of the role of the counterion in the

activation of CO_2 in this system. The successful exchange of the nitrogen atom in the bidentate N,N-complexes (**3.1**) to oxygen in the bidentate N,O-complexes (**3.3**) may suggest further investigations with other elements (e.g. sulfur).

Overall, this work presented three different pyridine-based ligand designs, all successfully showing the activation of CO_2 and other different heterogeneous double bonds *via* MLC. The described ligand systems showed significant potential for optimizing the MLC-substrate environment by simple straight forward alterations of commercially available starting materials for ligand synthesis. In addition to the MLC interaction of the substrate, which has been well investigated in the last years, the additional interaction of the counterion, which has been barely explored so far, could be better described. Furthermore, it could be shown that the ligand environment also exerts an influence on the activated substrate, in this case of CO_2, due to an intramolecular hydrogen bonding. The simple synthesis and adaptation of the ligand scaffold ensures an easy access to develop an environment adapted to the substrate of interest.

5 Zusammenfassung

Diese Arbeit zeigt drei verschiedene Ligandensysteme mit der Fähigkeit der Substrataktivierung über Metallligandenkooperation (MLC), unter Dearomatisierungs-/Rearomatisierungssequenz der Pyridineinheit (Schema 48). Die Ligandengerüste sind über einfache Synthesen zugänglich und bieten dennoch ein großes Potential für die Gestaltung einer geeigneten Umgebung zur Aktivierung potentieller Substrate. Alle Systeme zeigten dabei die Möglichkeit polarisierte Mehrfachbindungen durch MLC zu aktivieren.

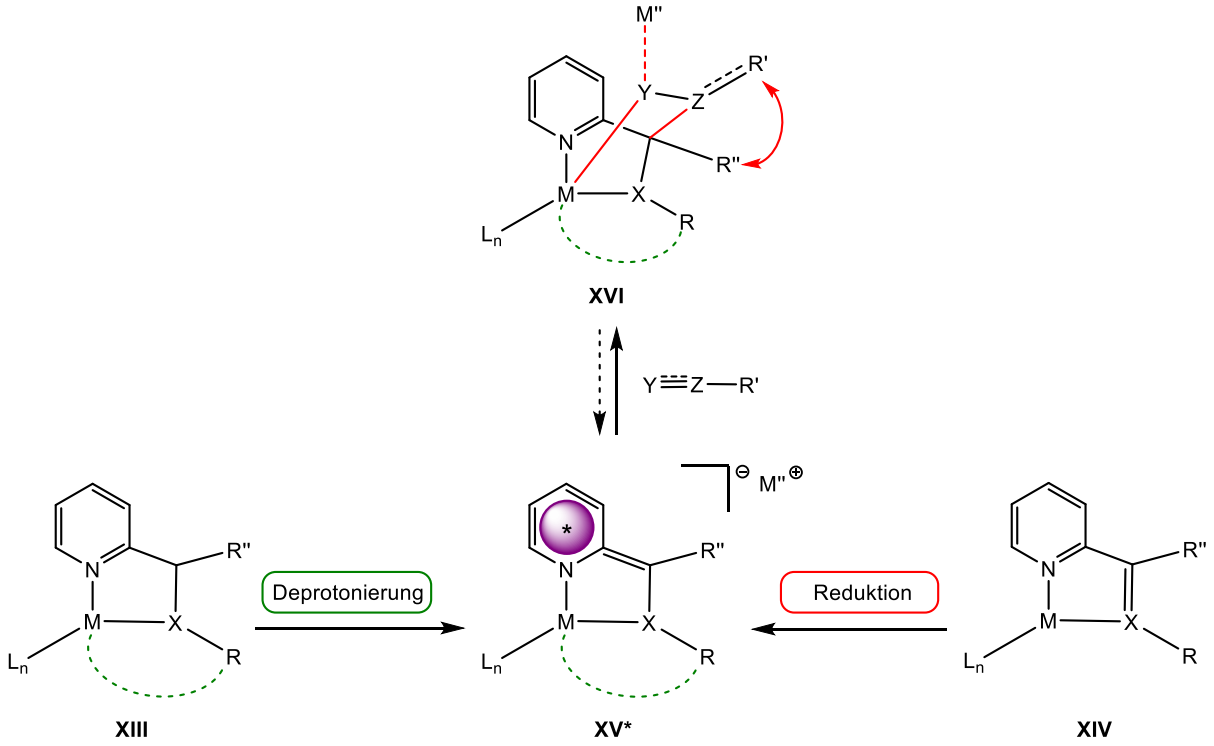

Schema 48: Erzeugung der dearomatisierten aktiven Spezies **XV*** durch Deprotonierung (**XIII**) oder Reduktion (**XIV**). Substrataktivierung unter Rearomatisierung der Pyridineinheit und mögliche Interaktionen (rote Linien) des aktivierten Substrates (Y—Z—R') in den hier präsentierten Adduktkomplexen (**XVI**). 1) M—Y und C—Z Bindungsbildung durch MLC. 2.) Elektrostatische Wechselwirkung mit dem Gegenion (Y- - -M"). 3.) Intramolekulare Wasserstoffbrückenbindung (R'↔R"). (M = Mn, Re, Rh; M" = Li, Na, K; X = N, O; #Y = N, O; #Z = C, S; R = freies Elektronenpaar, $Ph^{p\text{-}Me}$, *dbap* (grüne Linie); #R' = O, (H, Ph), Ph_2, CH_2-Ph, N-Ph; R" = H, Ph; L = CO, PPh_3) (# = freies Substrat)

Insbesondere konnten Carbonylgruppen in CO_2, Aldehyden und Ketonen, C≡N Dreifachbindungen in Nitrilen, S=O Doppelbindungen in SO_2 und N=C Doppelbindungen in Phenylisocyanat aktiviert werden. Vor allem CO_2 zeigte eine hohe Reaktivität und eine Aktivierung mittels MLC konnte mit jedem Ligandensystem nachgewiesen werden. In vielen Fällen konnte eine reversible Bindung der aktivierten Substrate nachgewiesen werden. In den beschriebenen Adduktkomplexen konnten insbesondere drei verschiedene Substratwechselwirkungen beobachtet werden. Zusätzlich zur Bindung über MLC unter M-Y und C-Z Bindungsbildung hatte die elektrostatische Wechselwirkung des Substrats mit dem Gegenion in den anionischen Komplexen (**3.1** und **3.3**) einen signifikanten Einfluss. Darüber hinaus konnte mittels scXRD-Analyse und NMR-Spektroskopie eine intramolekulare Wechselwirkung über Wasserstoffbrückenbindung (R'↔R") im CO_2-Komplex **102b** (**3.3**) gezeigt werden. Die dearomatisierte aktive Spezies **XV*** konnte leicht durch Deprotonierung von **XIII** (**3.1**, **3.2**, **3.3**) erhalten werden oder durch Zwei-Elektronenreduktion aus **XIV** (**3.1**, **3.3**). Die Aktivierung des Substrats führte zu den rearomatisierten Adduktkomplexen **XVI**.

Tabelle 4: 2-Amino-/2-Iminomethyl Pyridin-System (**3.1**): Übersicht der in dieser Arbeit verwendeten Komplexe und Substrate für Aktivierungsreaktionen mittels MLC.

Zentral-Atom	Substrat	Y—Z	Austausch/ Substrat	erwähnenswerte Eigenschaften	M''	Addukt-Komplex
Re(I)	CO_2	C=O	✓ $^{13}CO_2$	sehr langsamer Austausch	K^+	**76**
Mn(I)	CO_2	C=O	✓ $^{13}CO_2$	langsamer Austausch	K^+	**78-K**
Mn(I)	CO_2	C=O	✓ $^{13}CO_2$	schneller Austausch	Na^+	**78-Na**
Mn(I)	CO_2	✗	-	Zersetzung	Li^+	-
Re(I)	SO_2 (DABSO)	S=O	✗ CO_2	diastereomere Interkonversion von SO_2	K^+	**77**
Mn(I)	SO_2 (DABSO)	✗	-	keine Reaktion	K^+	-
Re(I)	Benzaldehyd	C=O	✓ CO_2	Austausch bei 60 °C	K^+	**80**
Mn(I)	Benzaldehyd	C=O	✓ CO_2	Austausch bei RT	K^+	**79**
Re(I)	Benzophenon	C=O	✓ CO_2	Austausch bei RT	K^+	**81**
Mn(I)	Benzophenon	✗	-	keine Reaktion	-	-
Re(I)	Phenylacetonitril	C≡N	✗ CO_2	neue Verbindung	K^+	**82**
Mn(I)	Phenylacetonitril	✗	-	keine Reaktion	-	-
Re(I)	Phenylisocyanat	✗	-	Mischung	K^+	-
Mn(I)	Phenylisocyanat	✗	-	keine Reaktion	-	-
Re(I)	H_2	✗	-	keine Reaktion	-	-
Mn(I)	H_2	✗	-	keine Reaktion	-	-

Das zweizähnige anionische 2-Amino-/2-Iminomethylpyridin System (**3.1**) mit den Übergangsmetallen der Gruppe 7 in der formalen Oxidationsstufe +I (Re(I) und Mn(I)), zeigte mittels MLC die Affinität zu verschiedenen heterogenen Mehrfachbindungen unter Cycloaddition (Tabelle 4). Die erfolgreiche Substitution des Metallzentrums von Rhenium durch Mangan führte in mehreren Fällen zu gleichartigen Komplexen der vierten Periode, welche es ermöglicht haben, Vergleichsstudien ihrer (unterschiedlichen) Reaktivitäten durchzuführen. Darüber hinaus konnte gezeigt werden, dass das Gegenion in den anionischen Adduktkomplexen eine entscheidende Rolle bei der Aktivierungsreaktion von Substraten spielt, indem bei CO_2-Austauschreaktionen das Alkalimetall des Gegenions (Li, Na, K) variiert wurde. Diese Eigenschaft wurde ebenfalls in einer rechnerischen Studie mittels DFT-Rechnungen (**3.1.5**) verdeutlicht. Zusammenfassend lässt sich sagen, dass der Re(I)-Komplex **75*-Re** im Vergleich zum analogen Mn(I)-Komplex **75*-Mn** eine größere Bandbreite an Substraten aufwies, einschließlich der Aktivierung einer Vielzahl unterschiedlicher Mehrfachbindungen, so wie eine stärkere Substratbindung im Fall von CO_2 und Benzaldehyd im Hinblick auf die getätigten Austauschreaktionen. Hinsichtlich der Aktivierung von Carbonylgruppen zeigten beide Komplexe (**75*-Re** und **75*-Mn**) eine hohe Selektivität gegenüber CO_2 in den durchgeführten Austauschreaktionen. Für den Re(I)-Komplex **75*-Re** konnte die Vielfalt der für die MLC-Bindung geeigneten Bindungstypen auf Nitrile (**3.1.7**) und SO_2 (**3.1.4**) erweitert werden. Hervorzuheben ist, dass die 1,3-Cycloaddition von SO_2 mittels MLC zum Zeitpunkt der Veröffentlichung noch nicht bekannt war und die in der Literatur berichteten Bindungsmodifikationen von SO_2 erweitert hat (dargestellt in *fac*-K[Re(*amidopy*-OSO)$(CO)_3$] (**77**)). Die MLC-Aktivierung von Nitrilen konnte für Phenylacetonitril, mit einem Wasserstoffatom in α-Position, unter Ausbildung einer Enamid-gruppe über C-C und Re-N Bindungsbildung erfolgreich demonstriert werden (dargestellt in *fac*-K[Re(*amidopy-phacn*)$(CO)_3$] (**82**)). Belege für die MLC-Aktivierung für Nitrile ohne α-Wasserstoffatom (z.B. Benzonitril) wurden ebenfalls gesammelt, die erhaltenen Verbindungen konnten jedoch nicht eindeutig charakterisiert werden. Mit dem Mn(I)-Komplex **78** konnte der Einfluss des Gegenions auf das aktivierte Substrat (CO_2) erfolgreich experimentell nachgewiesen werden. Während Lithium als Gegenion die Zersetzung des CO_2-Adduktkomplexes induzierte, reagierten die Natrium- und Kaliumkomplexe beide reversibel mit CO_2, allerdings mit sehr unterschiedlichen Geschwindigkeiten in den Austauschreaktionen bei Umgebungstemperatur.

Computergestützte DFT-Rechnungen stützten die experimentellen Ergebnisse und zeigten ebenfalls einen signifikanten Einfluss der Gegenkationen auf die Aktivierungsreaktionen des CO_2-Moleküls. Das bedeutet, der zusätzliche Einfluss des Gegenions eröffnet eine weitere Möglichkeit die Substrataufnahme gezielt zu steuern. Der Einfluss des Gegenions in anionischen Komplexen auf MLC-Aktivierungsreaktionen wurde bisher nicht umfassend untersucht. Im Allgemeinen zeigten alle Carbonyl-Adduktkomplexe in Austauschreaktionen eine Reversibilität (reversible C-C und M-O Bindungsspaltung). Im SO_2-Adduktkomplex **77** konnte mittels $^1H^1H$ EXSY NMR-Austauschspektroskopie eine dynamische Bindung des Substrats in Form einer diastereomeren Interkonversion gezeigt werden. Der Phenylacetonitril-Adduktkomplex lieferte in einer Austauschreaktion mit CO_2 eine neue Verbindung. Bemerkenswert ist ebenfalls, dass beide Komplexe (**75*-Re** und **75*-Mn**) in Experimenten unter ähnlichen Bedingungen nicht mit H_2 reagieren.

Tabelle 5: Dreizähniges Pyridin-Amino-Olefin-System (**3.2**): Übersicht der in dieser Arbeit verwendeten Komplexe und Substrate für Aktivierungsreaktionen mittels MLC.

Zentral-Atom	Substrat	Y—Z	Austausch/ Substrat	Erwähnenswerte Eigenschaften	Addukt-Komplex
Rh(I)	CO_2	C=O	✘ $^{13}CO_2$	Fixierung	**94**
Rh(I)	Phenylisocyanat	C=N	✘ CO_2	Fixierung	**95**
Rh(I)	H_2	✘	-	Produkt-Mix	-

Das dreizähnige Pyridin-Amino-Olefin-System (**3.2**) mit dem Übergangsmetall Rh(I) der Gruppe 9 reagiert kooperativ mit heterogenen Mehrfachbindungen (C=O und C=N), dargestellt durch CO_2 und Phenylisocyanat, über eine MLC-Reaktionssequenz (Tabelle 5). Die Azepineinheit des dreizähnigen *dbap*-Liganden ermöglicht eine starre, konkave N-Olefin-Bindungsstelle, wodurch ein sterisch gut abgeschirmtes Rückgrat des Metallzentrums entsteht. Die Olefingruppe der Azepineinheit kann aufgrund der starken Rückbindung in die π*-Orbitale des Olefins niedervalente Übergangsmetallzentren stabilisieren. Das gestörte π-System der Pyridineinheit in der dearomatisierten aktiven Spezies **93*** konnte zusätzlich durch scXRD-Analyse nachgewiesen werden, erkennbar an den nicht äquivalenten Bindungslängen in der Pyridineinheit. Im Vergleich zum zweizähnigen 2-Amino-/2-Iminomethylpyridin-System

(**3.1**) stellte sich heraus, dass die Reaktivität deutlich anders war: Komplex **93*** führt zu stark gebundenen Adduktkomplexen von CO_2 in [Rh(*dbap*-CO_2)(PPh_3)] (**94**) und Phenylisocyanat in [Rh(*dbap*-NCO)(PPh_3)] (**95**), die keine Reversibilität der gebundenen Substrate zeigten. Die Reaktion mit Phenylisocyanat erweiterte den Umfang der funktionellen Gruppen zu Isocyanaten unter Bildung einer Amidateinheit. Eine Reaktion mit H_2 konnte beobachtet werden, führte jedoch zu keiner definierten Verbindung.

Tabelle 6: Zweizähniges anionisches Re(I)-N,O primär-Alkohol/Aldehyd und sekundär-Alkohol/Keton System (**3.3**): Übersicht der in dieser Arbeit verwendeten Komplexe und Substrate für Aktivierungsreaktionen mittels MLC.

Zentral-Atom	System	Substrat	Austausch	Erwähnenswerte Eigenschaften	M''	Addukt-Komplex
Re(I)	primär-Alkohol/Aldehyd	✘	-	-	Li^+	-
Re(I)	sekundär-Alkohol/Keton	CO_2	?	Intramolekulare Wasserstoffbrücken-bindung	K^+	**102b**

Das anionische sekundär-Alkohol/Keton-System (**3.3**) mit zweizähnigen N,O-Liganden in Re(I)-Tricarbonylkomplexen zeigte erfolgreich eine Aktivität gegenüber CO_2 mittels MLC-Reaktionssequenz (Tabelle 6), ähnlich dem zweizähnigen N,N-Liganden System (**3.1**). Die dearomatisierte Spezies (**101*b**), die für die Substrataktivierung mittels MLC geeignet ist, konnte durch Deprotonierung des Alkoholkomplexes (**100b**) mit LiHMDS oder durch Reduktion des Ketonkomplexes (**99b**) mit elementarem Kalium erhalten werden. Mit Ausnahme der Alkoxideinheit ähnelt der CO_2-Adduktkomplex (**102b**) dem des 2-Amino-/2-Iminomethylpyridinsystems (**3.1**) durch 1,3-Addition unter Re-O und C-C Bindungsbildung und der zusätzlichen Wechselwirkung des Alkalikations mit CO_2, nachgewiesen mittels scXRD-Analyse. Ein wesentlicher Unterschied war eine intramolekulare Wechselwirkung des CO_2-Sauerstoffs mit den *ortho*-Wasserstoffatomen der Arylgruppe durch Wasserstoffbrückenbindungen. Dieses Merkmal könnte im Hinblick auf das Ligandenumfeld interessant sein, da Veränderungen der benachbarten Phenylgruppe untersucht werden können, um die Umgebung für das gewünschte Substrat anzupassen und um spezifische

Substrat-Wechselwirkungen zu begünstigen oder zu unterdrücken. Dieses interessante Merkmal könnte durch Austausch eines benzylischen Wasserstoffatoms auch auf das 2-Amino-/2-Iminomethylpyridin-System (**3.1**) oder das dreizähnige Pyridin-Amino-Olefin-System (**3.2**) übertragen werden. Die Untersuchungen zur Reversibilität der CO_2-Komplexierung und der Aktivität gegenüber anderen Substraten sowie dem Einfluss des Gegenions stehen noch aus. Im Gegensatz dazu zeigte das entsprechende anionische primär-Alkohol/Aldehyd-System (**3.3**), dass die aktive Spezies (**101*a**) nur durch Deprotonierung des primären Alkoholkomplexes **100a** mit LiHMDS zugänglich war, nicht jedoch durch Zwei-Elektronen-Reduktion des Aldehyd-Komplexes **99a** mit elementarem Kalium. Eine weitere Reaktion von **101*a** mit CO_2 zeigte keine erfolgreiche Umsetzung. Weitere Untersuchungen zur Substitution des Gegenions durch Li^+, Na^+ oder K^+ müssen in Zukunft durchgeführt werden, um ein besseres Verständnis der Rolle des Gegenions bei der Aktivierung von CO_2 in diesem System zu erhalten. Der erfolgreiche Austausch des Stickstoffatoms in den zweizähnigen N,N-Komplexen (**3.1**) durch Sauerstoff in den zweizähnigen N,O-Komplexen (**3.3**) lässt weitere Untersuchungen mit anderen Elementen (z. B. Schwefel) naheliegend erscheinen.

Schlussendlich präsentierte diese Arbeit drei verschiedene pyridinbasierte Ligandendesigns, die alle erfolgreich die Aktivierung von CO_2 und anderen heterogenen Doppelbindungen über MLC zeigten. Die beschriebenen Ligandensysteme zeigten ein beträchtliches Potenzial zur Optimierung der Substratumgebung durch einfache, unkomplizierte Änderungen mit kommerziell verfügbarer Ausgangsmaterialien für die Synthese der Liganden. Neben der in den letzten Jahren gut untersuchten MLC-Wechselwirkung von Substraten konnte auch die bisher kaum erforschte zusätzliche Wechselwirkung des Gegenions besser beschrieben werden. Darüber hinaus konnte gezeigt werden, dass die Umgebung der Liganden aufgrund einer intramolekularen Wasserstoffbrückenbindung auch einen Einfluss auf das aktivierte Substrat, in diesem Fall CO_2, ausübt. Die einfache Synthese und Anpassung des Ligandengerüsts gewährleistet einen einfachen Zugang zur Entwicklung einer an das gewünschte Substrat angepassten Umgebung.

6 References

[1] R. A. Sheldon, I. Arends and U. Hanefeld, *Green chemistry and catalysis,* Wiley-VCH, **2008**.

[2] I. T. Horváth and P. T. Anastas, *Chem. Rev.* **2007**, *107,* 2169–2173, DOI: 10.1021/cr078380v.

[3] J. F. Hartwig, *Organotransition metal chemistry,* University Science Books, **2010**.

[4] A. Behr, *Angewandte homogene Katalyse,* Wiley-VCH, **2008**.

[5] N. Miyaura and A. Suzuki, *Chem. Rev.* **1995**, *95,* 2457–2483, DOI: 10.1021/cr00039a007.

[6] H. Grützmacher, *Angew. Chem. Int. Ed.* **2008**, *47,* 1814–1818, DOI: 10.1002/anie.200704654.

[7] R. J. Somerville, *Nat. Rev. Chem.* **2021**, *5,* 518–519, DOI: 10.1038/s41570-021-00295-0.

[8] G. van Koten, K. Kirchner and M.-E. Moret, *Metal-Ligand Co-Operativity,* Springer International Publishing AG, **2021**.

[9] J. R. Khusnutdinova and D. Milstein, *Angew. Chem. Int. Ed.* **2015**, *54,* 12236-12273, DOI: 10.1002/anie.201503873.

[10] M. D. Wodrich and X. Hu, *Nat. Rev. Chem.* **2018**, *2,* 12236, DOI: 10.1038/S41570-017-0099.

[11] W. Lubitz, H. Ogata, O. Rüdiger and E. Reijerse, *Chem. Rev.* **2014**, *114,* 4081-4148, DOI: 10.1021/cr4005814.

[12] N. S. Sickerman and Y. Hu, *Methods Mol. Biol.* **2019**, *1876,* 65–88, DOI: 10.1007/978-1-4939-8864-8_5.

[13] A. Adamska, A. Silakov, C. Lambertz, O. Rüdiger, T. Happe, E. Reijerse and W. Lubitz, *Angew. Chem. Int. Ed.* **2012**, *51,* 11458–11462, DOI: 10.1002/anie.201204800.

[14] C. Lorent, S. Katz, J. Duan, C. J. Kulka, G. Caserta, C. Teutloff, S. Yadav, U.-P. Apfel, M. Winkler, T. Happe, M. Horch and I. Zebger, *J. Am. Chem. Soc.* **2020**, *142,* 5493–5497, DOI: 10.1021/jacs.9b13075.

[15] E. B. Hulley, K. D. Welch, A. M. Appel, D. L. DuBois and R. M. Bullock, *J. Am. Chem. Soc.* **2013**, *135,* 11736–11739, DOI: 10.1021/ja405755j.

[16] B. Milani, G. Licini, E. Clot and M. Albrecht, *Dalton Trans.* **2016**, *45,* 14419-14420, DOI: 10.1039/c6dt90140a.

[17] S. Yadav, S. Saha and S. S. Sen, *ChemCatChem* **2016**, *8,* 486–501, DOI: 10.1002/cctc.201501015.

[18] M. Cokoja, C. Bruckmeier, B. Rieger, W. A. Herrmann and F. E. Kühn, *Angew. Chem. Int. Ed.* **2011**, *50,* 8510–8537, DOI: 10.1002/anie.201102010.

[19] R. Ayyappan, I. Abdalghani, R. C. Da Costa and G. R. Owen, *Dalton Trans.* **2022**, *51,* 11582–11611, DOI: 10.1039/d2dt01609e.

[20] Y. Kan and Q. Zhang, in: *Nanostructured Materials for Next-Generation Energy Storage and Conversion* (Hrsg.: Y.-P. Chen, S. Bashir and J. L. Liu), Springer Berlin Heidelberg**,** 43–84, **2017**.

[21] X. Yang and M. B. Hall, *J. Am. Chem. Soc.* **2010**, *132,* 120–130, DOI: 10.1021/ja9041065.

[22] W. B. Tolman, *Angew. Chem. Int. Ed.* **2010**, *49,* 1018–1024, DOI: 10.1002/anie.200905364.

[23] A. Kumar, P. Daw and D. Milstein, *Chem. Rev.* **2022**, *122,* 385–441, DOI: 10.1021/acs.chemrev.1c00412.

[24] Y. Tang, Y. Li and F. Feng Tao, *Chem. Soc. Rev.* **2022**, *51,* 376–423, DOI: 10.1039/D1CS00783A.

[25] C. Gunanathan and D. Milstein, *Chem. Rev.* **2014**, *114,* 12024–12087, DOI: 10.1021/cr5002782.

[26] M. R. Elsby and R. T. Baker, *Chem. Soc. Rev.* **2020**, *49,* 8933–8987, DOI: 10.1039/d0cs00509f.

[27] T. Ohkuma, H. Ooka, S. Hashiguchi, T. Ikariya and R. Noyori, *J. Am. Chem. Soc.* **1995**, *117,* 2675–2676, DOI: 10.1021/ja00114a043.

[28] R. Noyori and T. Ohkuma, *Angew. Chem. Int. Ed.* **2001**, *40,* 40–73, DOI: 10.1002/1521-3773(20010105)40:1<40::AID-ANIE40>3.0.CO;2-5.

[29] R. Noyori and S. Hashiguchi, *Acc. Chem. Res.* **1997**, *30,* 97–102, DOI: 10.1021/ar9502341.

[30] T. Ohkuma, M. Koizumi, K. Muñiz, G. Hilt, C. Kabuto and R. Noyori, *J. Am. Chem. Soc.* **2002**, *124,* 6508–6509, DOI: 10.1021/ja026136+.

[31] R. Noyori, *Angew. Chem. Int. Ed.* **2002**, *41,* 2008, DOI: 10.1002/1521-3773(20020617)41:12<2008::AID-ANIE2008>3.0.CO;2-4.

[32] C. A. Sandoval, T. Ohkuma, K. Muñiz and R. Noyori, *J. Am. Chem. Soc.* **2003**, *125,* 13490–13503, DOI: 10.1021/ja030272c.

[33] L. Alig, M. Fritz and S. Schneider, *Chem. Rev.* **2019**, *119,* 2681–2751, DOI: 10.1021/acs.chemrev.8b00555.

[34] S. Werkmeister, K. Junge, B. Wendt, E. Alberico, H. Jiao, W. Baumann, H. Junge, F. Gallou and M. Beller, *Angew. Chem. Int. Ed.* **2014**, *53,* 8722–8726, DOI: 10.1002/anie.201402542.

[35] T. Zell and D. Milstein, *Acc. Chem. Res.* **2015**, *48,* 1979–1994, DOI: 10.1021/acs.accounts.5b00027.

[36] M. Nielsen, A. Kammer, D. Cozzula, H. Junge, S. Gladiali and M. Beller, *Angew. Chem. Int. Ed.* **2011**, *50,* 9593–9597, DOI: 10.1002/anie.201104722.

[37] M. Peña-López, H. Neumann and M. Beller, *ChemCatChem* **2015**, *7,* 865–871, DOI: 10.1002/cctc.201402967.

[38] E. Alberico, P. Sponholz, C. Cordes, M. Nielsen, H.-J. Drexler, W. Baumann, H. Junge and M. Beller, *Angew. Chem. Int. Ed.* **2013**, *52,* 14162–14166, DOI: 10.1002/anie.201307224.

[39] S. Chakraborty, P. O. Lagaditis, M. Förster, E. A. Bielinski, N. Hazari, M. C. Holthausen, W. D. Jones and S. Schneider, *ACS Catal.* **2014**, *4,* 3994–4003, DOI: 10.1021/cs5009656.

[40] F.-G. Fontaine and D. Zargarian, *J. Am. Chem. Soc.* **2004**, *126,* 8786–8794, DOI: 10.1021/ja048911m.

[41] D. J. Mihalcik, J. L. White, J. M. Tanski, L. N. Zakharov, G. P. A. Yap, C. D. Incarvito, A. L. Rheingold and D. Rabinovich, *Dalton Trans.* **2004,** 1626–1634, DOI: 10.1039/B401056F.

[42] J. S. Figueroa, J. G. Melnick and G. Parkin, *Inorg. Chem.* **2006**, *45,* 7056–7058, DOI: 10.1021/ic061353n.

[43] K. Pang, J. M. Tanski and G. Parkin, *Chem. Commun.* **2008,** 1008–1010, DOI: 10.1039/b714466k.

[44] W. H. Harman and J. C. Peters, *J. Am. Chem. Soc.* **2012**, *134,* 5080–5082, DOI: 10.1021/ja211419t.

[45] L. Greb, F. Ebner, Y. Ginzburg and L. M. Sigmund, *Eur. J. Inorg. Chem.* **2020**, *2020,* 3030–3047, DOI: 10.1002/ejic.202000449.

[46] Y. Blum and Y. Shvo, *Isr. J. Chem.* **1984**, *24,* 144–148, DOI: 10.1002/ijch.198400024.

[47] Y. Blum, D. Czarkie, Y. Rahamim and Y. Shvo, *Organometallics* **1985**, *4,* 1459-1461, DOI: 10.1021/om00127a027.

[48] Y. Shvo, D. Czarkie, Y. Rahamim and D. F. Chodosh, *J. Am. Chem. Soc.* **1986**, *108,* 7400–7402, DOI: 10.1021/ja00283a041.

[49] B. L. Conley, M. K. Pennington-Boggio, E. Boz and T. J. Williams, *Chem. Rev.* **2010**, *110,* 2294–2312, DOI: 10.1021/cr9003133.

[50] C. P. Casey, S. W. Singer, D. R. Powell, R. K. Hayashi and M. Kavana, *J. Am. Chem. Soc.* **2001**, *123,* 1090–1100, DOI: 10.1021/ja002177z.

[51] C. P. Casey and J. B. Johnson, *Can. J. Chem.* **2005**, *83,* 1339–1346, DOI: 10.1139/v05-140.

[52] R. Karvembu, R. Prabhakaran and K. Natarajan, *Coord. Chem. Rev.* **2005**, *249,* 911–918, DOI: 10.1016/j.ccr.2004.09.025.

[53] J. S. M. Samec, J.-E. Bäckvall, P. G. Andersson and P. Brandt, *Chem. Soc. Rev.* **2006**, *35,* 237–248, DOI: 10.1039/B515269K.

[54] H.-J. Knölker, E. Baum, H. Goesmann and R. Klauss, *Angew. Chem. Int. Ed.* **1999**, *38,* 2064–2066, DOI: 10.1002/(SICI)1521 3773(19990712)38:13/14<2064: :AID-ANIE2064>3.0.CO;2-W.

[55] C. P. Casey and H. Guan, *J. Am. Chem. Soc.* **2007**, *129,* 5816–5817, DOI: 10.1021/ja071159f.

[56] T. Shimbayashi and K.-i. Fujita, *Catalysts* **2020**, *10,* 635, DOI: 10.3390/catal10060635.

[57] Y. Himeda, N. Onozawa-Komatsuzaki, H. Sugihara, H. Arakawa and K. Kasuga, *Organometallics* **2004**, *23,* 1480–1483, DOI: 10.1021/om030382s.

[58] Y. Himeda, N. Onozawa-Komatsuzaki, H. Sugihara and K. Kasuga, *J. Am. Chem. Soc.* **2005**, *127,* 13118–13119, DOI: 10.1021/ja054236k.

[59] W.-H. Wang, J. T. Muckerman, E. Fujita and Y. Himeda, *ACS Catal.* **2013**, *3,* 856–860, DOI: 10.1021/cs400172j.

[60] Y. Suna, M. Z. Ertem, W.-H. Wang, H. Kambayashi, Y. Manaka, J. T. Muckerman, E. Fujita and Y. Himeda, *Organometallics* **2014**, *33,* 6519–6530, DOI: 10.1021/om500832d.

[61] R. Kawahara, K.-i. Fujita and R. Yamaguchi, *J. Am. Chem. Soc.* **2012**, *134,* 3643–3646, DOI: 10.1021/ja210857z.

[62] D. Morales-Morales and C. M. Jensen, *The chemistry of pincer compounds,* Elsevier, **2007**.

[63] D. Morales-Morales, *Pincer compounds*, Elsevier, **2018**.

[64] J. Zhang, G. Leitus, Y. Ben-David and D. Milstein, *Angew. Chem. Int. Ed.* **2006**, *45,* 1113–1115, DOI: 10.1002/anie.200503771.

[65] C. Gunanathan, Y. Ben-David and D. Milstein, *Science* **2007**, *317,* 790–792, DOI: 10.1126/science.1145295.

[66] S. W. Kohl, L. Weiner, L. Schwartsburd, L. Konstantinovski, L. J. W. Shimon, Y. Ben-David, M. A. Iron and D. Milstein, *Science* **2009**, *324,* 74–77, DOI: 10.1126/science.1168600.

[67] D. Milstein, *Top. Catal.* **2010**, *53,* 915–923, DOI: 10.1007/s11244-010-9523-7.

[68] T. P. Gonçalves, I. Dutta and K.-W. Huang, *Chem. Commun.* **2021**, *57,* 3070-3082, DOI: 10.1039/d1cc00528f.

[69] J. Zhang, G. Leitus, Y. Ben-David and D. Milstein, *J. Am. Chem. Soc.* **2005**, *127,* 10840–10841, DOI: 10.1021/ja052862b.

[70] H. Li, X. Wang, F. Huang, G. Lu, J. Jiang and Z.-X. Wang, *Organometallics* **2011**, *30,* 5233–5247, DOI: 10.1021/om200620n.

[71] H. Li, M. Wen and Z.-X. Wang, *Inorg. Chem.* **2012**, *51,* 5716–5727, DOI: 10.1021/ic300175b.

[72] H. Li and M. B. Hall, *ACS Catal.* **2015**, *5,* 1895–1913, DOI: 10.1021/cs501875z.

[73] E. Ben-Ari, G. Leitus, L. J. W. Shimon and D. Milstein, *J. Am. Chem. Soc.* **2006**, *128,* 15390–15391, DOI: 10.1021/ja066411i.

[74] L. Schwartsburd, M. A. Iron, L. Konstantinovski, Y. Diskin-Posner, G. Leitus, L. J. W. Shimon and D. Milstein, *Organometallics* **2010**, *29,* 3817–3827, DOI: 10.1021/om1004435.

[75] K. Talukdar, S. Sinha Roy, E. Amatya, E. A. Sleeper, P. Le Magueres and J. W. Jurss, *Inorg. Chem.* **2020**, *59,* 6087–6099, DOI: 10.1021/acs.inorgchem.0c00154.

[76] E. R. M. Habraken, A. R. Jupp, M. B. Brands, M. Nieger, A. W. Ehlers and J. C. Slootweg, *Eur. J. Inorg. Chem.* **2019**, *2019,* 2436–2442, DOI: 10.1002/ejic.201900169.

[77] K. C. Poon, W. Y. Wan, H. Su and H. Sato, *RSC Adv.* **2022**, *12,* 22703–22721, DOI: 10.1039/d2ra03341k.

[78] D. D. Zhu, J. L. Liu and S. Z. Qiao, *Adv. Mater.* **2016**, *28,* 3423–3452, DOI: 10.1002/adma.201504766.

[79] D. Schröder, C. A. Schalley, J. N. Harvey and H. Schwarz, *Int. J. Mass Spectrom.* **1999**, *185-187,* 25–35, DOI: 10.1016/S1387-3806(98)14042-3.

[80] E. A. Quadrelli, G. Centi, J.-L. Duplan and S. Perathoner, *ChemSusChem* **2011**, *4,* 1194–1215, DOI: 10.1002/cssc.201100473.

[81] M. He, Y. Sun and B. Han, *Angew. Chem. Int. Ed.* **2013**, *52,* 9620–9633, DOI: 10.1002/anie.201209384.

[82] A. Otto, T. Grube, S. Schiebahn and D. Stolten, *Energy Environ. Sci.* **2015**, *8,* 3283–3297, DOI: 10.1039/c5ee02591e.

[83] C. Floriani and G. Fachinetti, *J. Chem. Soc., Chem. Commun.* **1974,** 615–616, DOI: 10.1039/C39740000615.

[84] G. Fachinetti, C. Floriani and P. F. Zanazzi, *J. Am. Chem. Soc.* **1978**, *100,* 7405–7407, DOI: 10.1021/ja00491a045.

[85] P. Braunstein, D. Matt, Y. Dusausoy, J. Fischer, A. Mitschler and L. Ricard, *J. Am. Chem. Soc.* **1981**, *103,* 5115–5125, DOI: 10.1021/ja00407a028.

[86] V. T. Annibale and D. Song, *Chem. Commun.* **2012**, *48,* 5416–5418, DOI: 10.1039/c2cc17933d.

[87] M. Vogt, M. Gargir, M. A. Iron, Y. Diskin-Posner, Y. Ben-David and D. Milstein, *Chem. Eur. J.* **2012**, *18,* 9194–9197, DOI: 10.1002/chem.201201730.

[88] V. T. Annibale and D. Song, *RSC Adv.* **2013**, *3,* 11432, DOI: 10.1039/c3ra40618k.

[89] E. Stepowska, H. Jiang and D. Song, *Chem. Commun.* **2010**, *46,* 556–558, DOI: 10.1039/b919606d.

[90] J. Zhang, M. Gandelman, L. J. W. Shimon, H. Rozenberg and D. Milstein, *Organometallics* **2004**, *23,* 4026–4033, DOI: 10.1021/om049716j.

[91] M. Vogt, A. Nerush, Y. Diskin-Posner, Y. Ben-David and D. Milstein, *Chem. Sci.* **2014**, *5,* 2043–2051, DOI: 10.1039/C4SC00130C.

[92] O. Rivada-Wheelaghan, A. Dauth, G. Leitus, Y. Diskin-Posner and D. Milstein, *Inorg. Chem.* **2015**, *54,* 4526–4538, DOI: 10.1021/acs.inorgchem.5b00366.

[93] A. Kumar, P. Daw, N. A. Espinosa-Jalapa, G. Leitus, L. J. W. Shimon, Y. Ben-David and D. Milstein, *Dalton Trans.* **2019**, *48,* 14580–14584, DOI: 10.1039/C9DT03088C.

[94] A. Sinopoli, N. T. La Porte, J. F. Martinez, M. R. Wasielewski and M. Sohail, *Coord. Chem. Rev.* **2018**, *365,* 60–74, DOI: 10.1016/j.ccr.2018.03.011.

[95] P. Schlichter and C. Werlé, *Synthesis* **2022**, *54,* 517–534, DOI: 10.1055/a-1657-2634.

[96] S. Chakraborty, O. Blacque and H. Berke, *Dalton Trans.* **2015**, *44,* 6560–6570, DOI: 10.1039/C5DT00278H.

[97] Y. Zhang, A. D. MacIntosh, J. L. Wong, E. A. Bielinski, P. G. Williard, B. Q. Mercado, N. Hazari and W. H. Bernskoetter, *Chem. Sci.* **2015**, *6,* 4291–4299, DOI: 10.1039/C5SC01467K.

[98] R. Sen, A. Goeppert and G. K. Surya Prakash, *Angew. Chem. Int. Ed.* **2022**, *61,* e202207278, DOI: 10.1002/anie.202207278.

[99] K. Schlenker, E. G. Christensen, A. A. Zhanserkeev, G. R. McDonald, E. L. Yang, K. T. Lutz, R. P. Steele, R. T. VanderLinden and C. T. Saouma, *ACS Catal.* **2021**, *11,* 8358–8369, DOI: 10.1021/acscatal.1c01709.

[100] G. A. Filonenko, M. P. Conley, C. Copéret, M. Lutz, E. J. M. Hensen and E. A. Pidko, *ACS Catal.* **2013**, *3,* 2522–2526, DOI: 10.1021/cs4006869.

[101] C. A. Huff and M. S. Sanford, *ACS Catal.* **2013**, *3,* 2412–2416, DOI: 10.1021/cs400609u.

[102] C. A. Huff, J. W. Kampf and M. S. Sanford, *Chem. Commun.* **2013**, *49,* 7147-7149, DOI: 10.1039/c3cc43517b.

[103] M. Vogt, A. Nerush, M. A. Iron, G. Leitus, Y. Diskin-Posner, L. J. W. Shimon, Y. Ben-David and D. Milstein, *J. Am. Chem. Soc.* **2013**, *135,* 17004–17018, DOI: 10.1021/ja4071859.

[104] A. Nerush, M. Vogt, U. Gellrich, G. Leitus, Y. Ben-David and D. Milstein, *J. Am. Chem. Soc.* **2016**, *138,* 6985–6997, DOI: 10.1021/jacs.5b13208.

[105] Q.-Q. Zhou, Y.-Q. Zou, S. Kar, Y. Diskin-Posner, Y. Ben-David and D. Milstein, *ACS Catal.* **2021**, *11,* 10239–10245, DOI: 10.1021/acscatal.1c01748.

[106] C. Gunanathan and D. Milstein, *Acc. Chem. Res.* **2011**, *44,* 588–602, DOI: 10.1021/ar2000265.

[107] D. Milstein, *Philos. Trans. R. Soc. A* **2015**, *373, DOI:* 10.1098/rsta.2014.0189.

[108] P. A. Dub and J. C. Gordon, *Dalton Trans.* **2016**, *45,* 6756–6781, DOI: 10.1039/c6dt00476h.

[109] P. A. Dub and J. C. Gordon, *ACS Catal.* **2017**, *7,* 6635–6655, DOI: 10.1021/acscatal.7b01791.

[110] T. Otsuka, A. Ishii, P. A. Dub and T. Ikariya, *J. Am. Chem. Soc.* **2013**, *135,* 9600–9603, DOI: 10.1021/ja403852e.

[111] P. A. Dub, N. J. Henson, R. L. Martin and J. C. Gordon, *J. Am. Chem. Soc.* **2014**, *136,* 3505–3521, DOI: 10.1021/ja411374j.

[112] P. A. Dub, B. L. Scott and J. C. Gordon, *J. Am. Chem. Soc.* **2017**, *139,* 1245-1260, DOI: 10.1021/jacs.6b11666.

[113] D. J. Tindall, M. Menche, M. Schelwies, R. A. Paciello, A. Schäfer, P. Comba, F. Rominger, A. S. K. Hashmi and T. Schaub, *Inorg. Chem.* **2020**, *59,* 5099–5115, DOI: 10.1021/acs.inorgchem.0c00337.

[114] T. Chen, L.-P. He, D. Gong, L. Yang, X. Miao, J. Eppinger and K.-W. Huang, *Tetrahedron Lett.* **2012**, *53,* 4409–4412, DOI: 10.1016/j.tetlet.2012.06.041.

[115] L.-P. He, T. Chen, D.-X. Xue, M. Eddaoudi and K.-W. Huang, *J. Organomet. Chem.* **2012**, *700,* 202–206, DOI: 10.1016/j.jorganchem.2011.10.017.

[116] N. Gorgas, B. Stöger, L. F. Veiros and K. Kirchner, *ACS Catal.* **2016**, *6,* 2664-2672, DOI: 10.1021/acscatal.6b00436.

[117] D. Benito-Garagorri, E. Becker, J. Wiedermann, W. Lackner, M. Pollak, K. Mereiter, J. Kisala and K. Kirchner, *Organometallics* **2006**, *25,* 1900–1913, DOI: 10.1021/om0600644.

[118] M. Mastalir, E. Pittenauer, G. Allmaier and K. Kirchner, *J. Am. Chem. Soc.* **2017**, *139,* 8812–8815, DOI: 10.1021/jacs.7b05253.

[119] N. Gorgas, B. Stöger, L. F. Veiros and K. Kirchner, *ACS Catal.* **2018**, *8,* 7973-7982, DOI: 10.1021/acscatal.8b01942.

[120] M. Mastalir, G. Tomsu, E. Pittenauer, G. Allmaier and K. Kirchner, *Org. Lett.* **2016**, *18,* 3462–3465, DOI: 10.1021/acs.orglett.6b01647.

[121] M. Mastalir, E. Pittenauer, B. Stöger, G. Allmaier and K. Kirchner, *Org. Lett.* **2017**, *19,* 2178–2181, DOI: 10.1021/acs.orglett.7b00857.

[122] H. Li, B. Zheng and K.-W. Huang, *Coord. Chem. Rev.* **2015**, *293-294,* 116–138, DOI: 10.1016/j.ccr.2014.11.010.

[123] H. Li, T. P. Gonçalves, D. Lupp and K.-W. Huang, *ACS Catal.* **2019**, *9,* 1619-1629, DOI: 10.1021/acscatal.8b04495.

[124] T. P. Gonçalves and K.-W. Huang, *J. Am. Chem. Soc.* **2017**, *139,* 13442–13449, DOI: 10.1021/jacs.7b06305.

[125] J. Kruszewski and T. M. Krygowski, *Tetrahedron Lett.* **1972**, *13,* 3839–3842, DOI: 10.1016/S0040-4039(01)94175-9.

[126] Z. Chen, C. S. Wannere, C. Corminboeuf, R. Puchta and P. v. R. Schleyer, *Chem. Rev.* **2005**, *105,* 3842–3888, DOI: 10.1021/cr030088+.

[127] P. v. R. Schleyer, C. Maerker, A. Dransfeld, H. Jiao and N. J. R. van Eikema Hommes, *J. Am. Chem. Soc.* **1996**, *118,* 6317–6318, DOI: 10.1021/ja960582d.

[128] H. Fallah-Bagher-Shaidaei, C. S. Wannere, C. Corminboeuf, R. Puchta and P. v. R. Schleyer, *Org. Lett.* **2006**, *8,* 863–866, DOI: 10.1021/ol0529546.

[129] M. K. Cyrañski, T. M. Krygowski, A. R. Katritzky and P. v. R. Schleyer, *J. Org. Chem.* **2002**, *67,* 1333–1338, DOI: 10.1021/jo016255s.

[130] Z. Rashid, J. H. van Lenthe and R. W. A. Havenith, *J. Phys. Chem. A* **2012**, *116,* 4778–4788, DOI: 10.1021/jp211105t.

[131] R. Fertig, T. Irrgang, F. Freitag, J. Zander and R. Kempe, *ACS Catal.* **2018**, *8,* 8525–8530, DOI: 10.1021/acscatal.8b02530.

[132] D. Lupp and K.-W. Huang, *Organometallics* **2020**, *39,* 18–24, DOI: 10.1021/acs.organomet.9b00102.

[133] K. M. Smith, *Organometallics* **2005**, *24,* 778–784, DOI: 10.1021/om049196s.

[134] T. Büttner, J. Geier, G. Frison, J. Harmer, C. Calle, A. Schweiger, H. Schönberg and H. Grützmacher, *Science* **2005**, *307,* 235–238, DOI: 10.1126/science.1106070.

[135] R. E. Rodríguez-Lugo, M. Trincado, M. Vogt, F. Tewes, G. Santiso-Quinones and H. Grützmacher, *Nat. Chem.* **2013**, *5,* 342–347, DOI: 10.1038/NCHEM.1595.

[136] T. Zweifel, J.-V. Naubron, T. Büttner, T. Ott and H. Grützmacher, *Angew. Chem. Int. Ed.* **2008**, *47,* 3245–3249, DOI: 10.1002/anie.200704685.

[137] J. B. Johnson and T. Rovis, *Angew. Chem. Int. Ed.* **2008**, *47,* 840–871, DOI: 10.1002/anie.200700278.

[138] D. G. A. Verhoeven and M.-E. Moret, *Dalton Trans.* **2016**, *45,* 15762–15778, DOI: 10.1039/C6DT02184K.

[139] P. Braunstein and F. Naud, *Angew. Chem. Int. Ed.* **2001**, *40,* 680–699, DOI: 10.1002/1521-3773(20010216)40:4<680::AID-ANIE6800>3.0.CO;2-0.

[140] G. M. Adams and A. S. Weller, *Coord. Chem. Rev.* **2018**, *355,* 150–172, DOI: 10.1016/j.ccr.2017.08.004.

[141] C. S. Slone, D. A. Weinberger and C. A. Mirkin, in: *Progress in Inorganic Chemistry* (Editor D. Karlin), *48*, 233–350, **1999**.

[142] C. Riplinger, M. D. Sampson, A. M. Ritzmann, C. P. Kubiak and E. A. Carter, *J. Am. Chem. Soc.* **2014**, *136,* 16285–16298, DOI: 10.1021/ja508192y.

[143] J. M. Smieja and C. P. Kubiak, *Inorg. Chem.* **2010**, *49,* 9283–9289, DOI: 10.1021/ic1008363.

[144] S. A. Chabolla, E. A. Dellamary, C. W. Machan, F. A. Tezcan and C. P. Kubiak, *Inorg. Chim. Acta* **2014**, *422,* 109–113, DOI: 10.1016/j.ica.2014.07.007.

[145] D. Sieh, D. C. Lacy, J. C. Peters and C. P. Kubiak, *Chem. Eur. J.* **2015**, *21,* 8497–8503, DOI: 10.1002/chem.201500463.

[146] C. W. Machan, S. A. Chabolla and C. P. Kubiak, *Organometallics* **2015**, *34,* 4678–4683, DOI: 10.1021/acs.organomet.5b00406.

[147] D. Sieh and C. P. Kubiak, *Chem. Eur. J.* **2016**, *22,* 10638–10650, DOI: 10.1002/chem.201600679.

[148] C. C. Lu, S. DeBeer George, T. Weyhermüller, E. Bill, E. Bothe and K. Wieghardt, *Angew. Chem. Int. Ed.* **2008**, *47,* 6384–6387, DOI: 10.1002/anie.200800669.

[149] M. van Gastel, C. C. Lu, K. Wieghardt and W. Lubitz, *Inorg. Chem.* **2009**, *48,* 2626–2632, DOI: 10.1021/ic802131w.

[150] C. C. Lu, T. Weyhermüller, E. Bill and K. Wieghardt, *Inorg. Chem.* **2009**, *48,* 6055–6064, DOI: 10.1021/ic9004328.

[151] C. C. Lu, E. Bill, T. Weyhermüller, E. Bothe and K. Wieghardt, *J. Am. Chem. Soc.* **2008**, *130,* 3181–3197, DOI: 10.1021/ja710663n.

[152] J. A. Barrett, C. J. Miller and C. P. Kubiak, *Trends Chem.* **2021**, *3,* 176–187, DOI: 10.1016/j.trechm.2020.12.009.

[153] J. M. Smieja, M. D. Sampson, K. A. Grice, E. E. Benson, J. D. Froehlich and C. P. Kubiak, *Inorg. Chem.* **2013**, *52,* 2484–2491, DOI: 10.1021/ic302391u.

[154] M. D. Sampson, A. D. Nguyen, K. A. Grice, C. E. Moore, A. L. Rheingold and C. P. Kubiak, *J. Am. Chem. Soc.* **2014**, *136,* 5460–5471, DOI: 10.1021/ja501252f.

[155] M. L. Clark, P. L. Cheung, M. Lessio, E. A. Carter and C. P. Kubiak, *ACS Catal.* **2018**, *8,* 2021–2029, DOI: 10.1021/acscatal.7b03971.

[156] K. A. Grice, N. X. Gu, M. D. Sampson and C. P. Kubiak, *Dalton Trans.* **2013**, *42,* 8498–8503, DOI: 10.1039/c3dt50612f.

[157] S. J. P. Spall, T. Keane, J. Tory, D. C. Cocker, H. Adams, H. Fowler, A. J. H. M. Meijer, F. Hartl and J. A. Weinstein, *Inorg. Chem.* **2016**, *55,* 12568–12582, DOI: 10.1021/acs.inorgchem.6b01477.

[158] V. Diez, J. V. Cuevas, G. García-Herbosa, G. Aullón, J. P. H. Charmant, A. Carbayo and A. Muñoz, *Inorg. Chem.* **2007**, *46,* 568–577, DOI: 10.1021/ic061060u.

[159] R. Stichauer, A. Helmers, J. Bremer, M. Rohdenburg, A. Wark, E. Lork, M. Vogt, *Organometallics* **2017**, *36,* 839–848, DOI: 10.1021/acs.organomet.6b00897.

[160] R. Stichauer and M. Vogt, *Organometallics* **2018**, *37,* 3639–3643, DOI: 10.1021/acs.organomet.8b00485.

[161] R. Stichauer, D. Duvinage, R. Langer and M. Vogt, *Organometallics* **2022**, *41,* 2798–2809, DOI: 10.1021/acs.organomet.2c00387.

[162] F. F. Puschmann, J. Harmer, D. Stein, H. Rüegger, B. de Bruin and H. Grützmacher, *Angew. Chem. Int. Ed.* **2010**, *49,* 385–389, DOI: 10.1002/anie.200903201.

[163] F. F. Puschmann, H. Grützmacher and B. de Bruin, *J. Am. Chem. Soc.* **2010**, *132,* 73–75, DOI: 10.1021/ja909022p.

[164] V. Sinha, B. Pribanic, B. de Bruin, M. Trincado and H. Grützmacher, *Chem. Eur. J.* **2018**, *24,* 5513–5521, DOI: 10.1002/chem.201705957.

[165] J. Martin, J. Langer, M. Wiesinger, H. Elsen and S. Harder, *Eur. J. Inorg. Chem.* **2020**, *2020,* 2582–2595, DOI: 10.1002/ejic.202000524.

[166] E. Piras, F. Läng, H. Rüegger, D. Stein, M. Wörle and H. Grützmacher, *Chem. Eur. J.* **2006**, *12,* 5849–5858, DOI: 10.1002/chem.200501470.

[167] B. de Bruin, J. C. Russcher and H. Grützmacher, *J. Organomet. Chem.* **2007**, *692,* 3167–3173, DOI: 10.1016/j.jorganchem.2007.01.041.

[168] P. Maire, T. Büttner, F. Breher, P. Le Floch and H. Grützmacher, *Angew. Chem. Int. Ed.* **2005**, *44,* 6318–6323, DOI: 10.1002/anie.200500773.

[169] T. Zweifel, D. Scheschkewitz, T. Ott, M. Vogt and H. Grützmacher, *Eur. J. Inorg. Chem.* **2009**, *2009,* 5561–5576, DOI: 10.1002/ejic.200900875.

[170] N. Donati, D. Stein, T. Büttner, H. Schönberg, J. Harmer, S. Anadaram and H. Grützmacher, *Eur. J. Inorg. Chem.* **2008**, *2008,* 4691–4703, DOI: 10.1002/ejic.200800702.

[171] B. Freitag, H. Elsen, J. Pahl, G. Ballmann, A. Herrera, R. Dorta and S. Harder, *Organometallics* **2017**, *36,* 1860–1866, DOI: 10.1021/acs.organomet.7b00200.

[172] S. Farah, S. Ababsa, N. Benhamada and B. Zouchoune, *Polyhedron* **2010**, *29,* 2722–2730, DOI: 10.1016/j.poly.2010.06.020.

[173] V. Lyaskovskyy, R. J. A. van Dijk-Moes, S. Burck, W. I. Dzik, M. Lutz, A. W. Ehlers, J. C. Slootweg, B. de Bruin and K. Lammertsma, *Organometallics* **2013**, *32,* 363–373, DOI: 10.1021/om301012z.

[174] I. Heuermann, B. Heitmann, R. Stichauer, D. Duvinage and M. Vogt, *Organometallics* **2019**, *38,* 1787–1799, DOI: 10.1021/acs.organomet.9b00094.

[175] S. Musa, I. Shaposhnikov, S. Cohen and D. Gelman, *Angew. Chem. Int. Ed.* **2011**, *50,* 3533–3537, DOI: 10.1002/anie.201007367.

[176] S. Musa, S. Fronton, L. Vaccaro and D. Gelman, *Organometallics* **2013**, *32,* 3069–3073, DOI: 10.1021/om400285r.

[177] B. Saha, S. M. W. Rahaman, P. Daw, G. Sengupta and J. K. Bera, *Chem. Eur. J.* **2014**, *20,* 6542–6551, DOI: 10.1002/chem.201304403.

[178] A. Bartoszewicz, R. Marcos, S. Sahoo, A. K. Inge, X. Zou and B. Martín-Matute, *Chem. Eur. J.* **2012**, *18,* 14510–14519, DOI: 10.1002/chem.201201845.

[179] W.-Y. Chu, X. Zhou and T. B. Rauchfuss, *Organometallics* **2015**, *34,* 1619-1626, DOI: 10.1021/om501152h.

[180] K.-i. Fujita, N. Tanino and R. Yamaguchi, *Org. Lett.* **2007**, *9,* 109–111, DOI: 10.1021/ol062806v.

[181] A. M. Royer, T. B. Rauchfuss and D. L. Gray, *Organometallics* **2010**, *29,* 6763-6768, DOI: 10.1021/om100901b.

[182] N. C. Yumata, G. Habarurema, J. Mukiza, T.I.A. Gerber, E. Hosten, F. Taherkhani and M. Nahali, *Polyhedron* **2013**, *62,* 89–103, DOI: 10.1016/j.poly.2013.06.025.

[183] B. Machura and R. Kruszynski, *J. Organomet. Chem.* **2007**, *692,* 4161–4167, DOI: 10.1016/j.jorganchem.2007.06.036.

[184] C. M. Álvarez, R. Carrillo, R. García-Rodríguez and D. Miguel, *chem. comm.* **2012**, *48,* 7705–7707, DOI: 10.1039/c2cc33443g.

[185] R. Costa, K. Chanawanno, J. T. Engle, B. Baroody, R. S. Herrick and C. J. Ziegler, *J. Organomet. Chem.* **2013**, *734,* 25–31, DOI: 10.1016/j.jorganchem.2012.10.025.

[186] C. M. Alvarez, R. García-Rodríguez and D. Miguel, *Dalton Trans.* **2007,** 3546-3554, DOI: 10.1039/b702418e.

[187] C. M. Alvarez, R. García-Rodríguez and D. Miguel, *J. Org. Chem.* **2007**, *692,* 5717–5726, DOI: 10.1016/j.jorganchem.2007.09.025.

[188] C. Sudbrake and H. Vahrenkamp, *Inorg. Chim. Acta* **2001**, *318,* 23–30, DOI: 10.1016/S0020-1693(01)00395-4.

7 Supporting Information

7.1

Supporting Information for:

Rhenium(I) Triscarbonyl Complexes with Redox-Active Amino- and Iminopyridine Ligands – Metal-Ligand Cooperation as Trigger for the Reversible Binding of CO_2 via a Dearmomatization / Re-aromatization Reaction Sequence

*Rasmus Stichauer,# Arne Helmers,# Jennifer Bremer#, Markus Rohdenburg, André Wark, Enno Lork, and Matthias Vogt**

Institut für Anorganische Chemie und Kristallographie, Universität Bremen, Leobener Str. NW2 - C2061, 28359 Bremen, Germany

R. Stichauer, A. Helmers, J. Bremer, M. Rohdenburg, A. Wark, E. Lork, M. Vogt, *Organometallics* **2017,** *36*, 839-848.
DOI: 10.1021/acs.organomet.6b00897

Index

^{1}H and $^{13}C\{^{1}H\}$ NMR Spectra for compounds:

[Re(*impy*](CO)$_3$Br] (**3**)

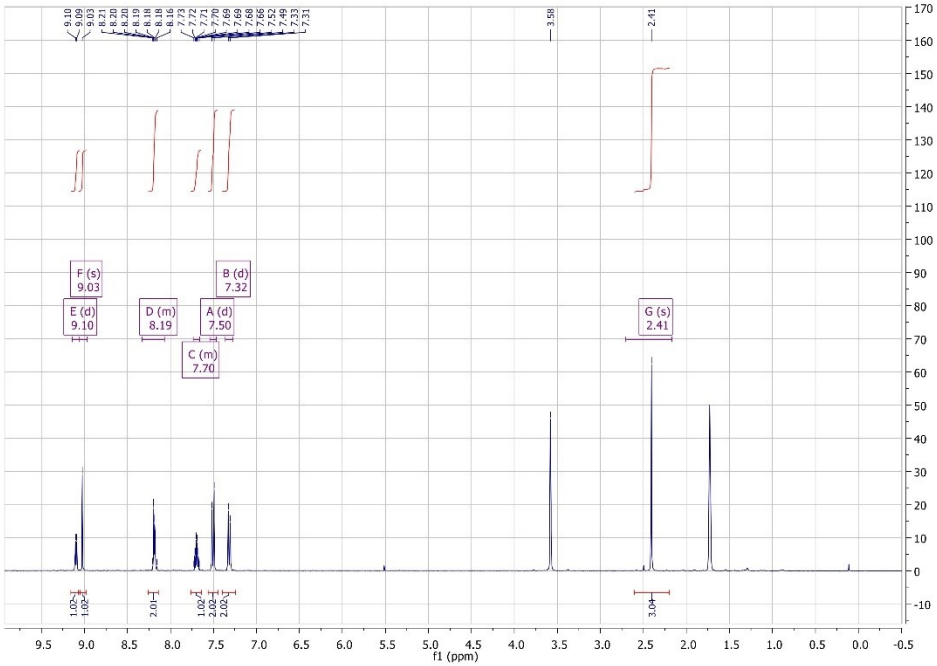

Figure S1. ^{1}H NMR (360 MHz, THF-d$_8$, 298 K) spectrum of [Re(*impy*](CO)$_3$Br] (**3**).

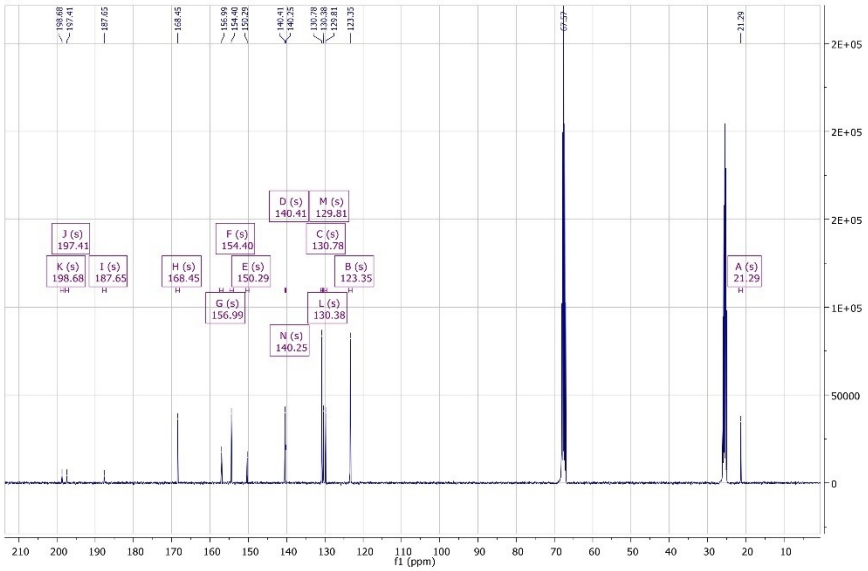

Figure S2. $^{13}C\{^{1}H\}$ NMR (91 MHz, THF-d_8, 298 K) spectrum of [Re(*impy*](CO)$_3$Br] (**3**).

[Re(*ampy*](CO)$_3$Br] (**4**)

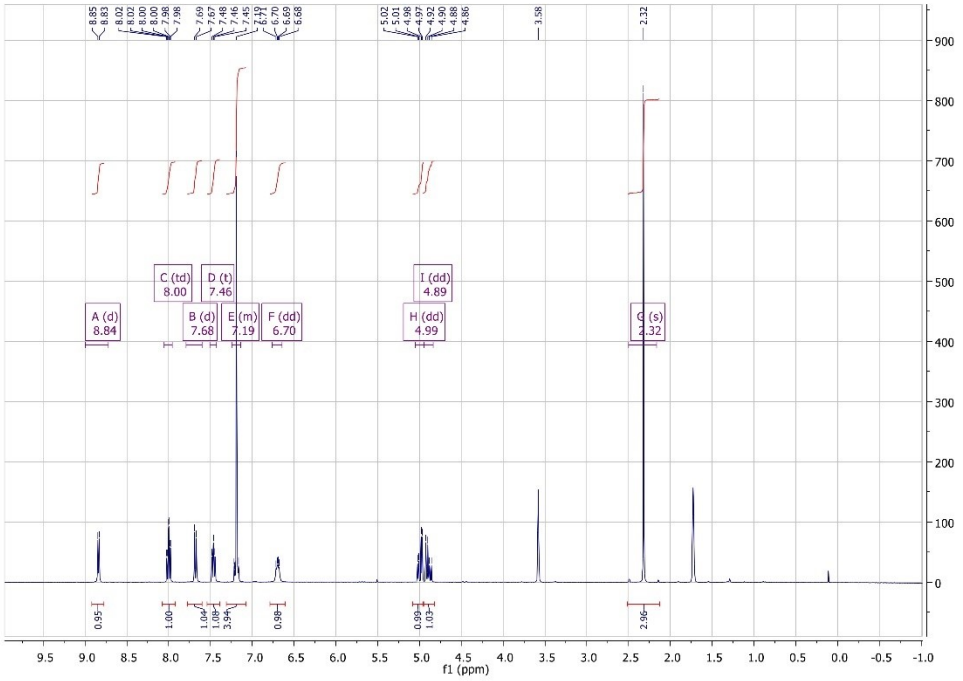

Figure S3. ^{1}H NMR (360 MHz, THF-d$_8$, 298 K) spectrum of [Re(*ampy*](CO)$_3$Br] (**4**).

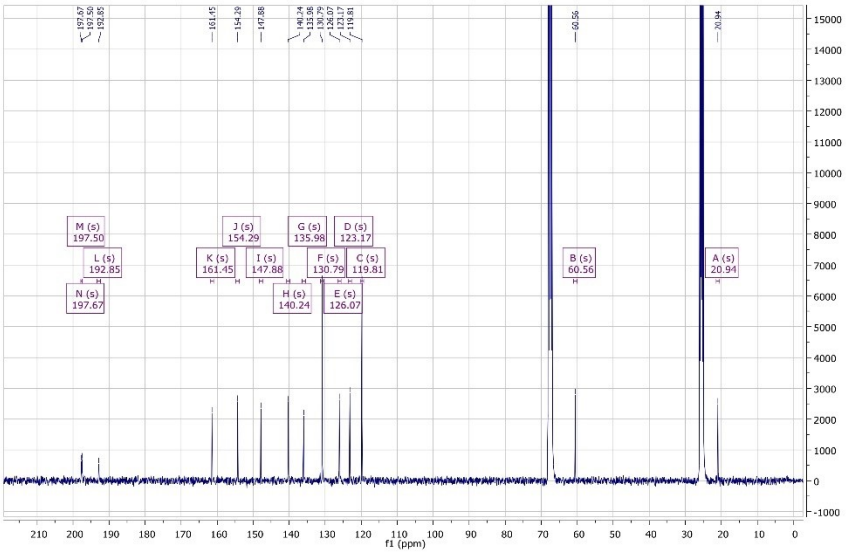

Figure S4. $^{13}C\{^{1}H\}$ NMR (91 MHz, THF-d_8, 298 K) spectrum of [Re(*ampy*](CO)$_3$Br] (**4**).

K[Re(*amidopy**](CO)$_3$] (**5b)**

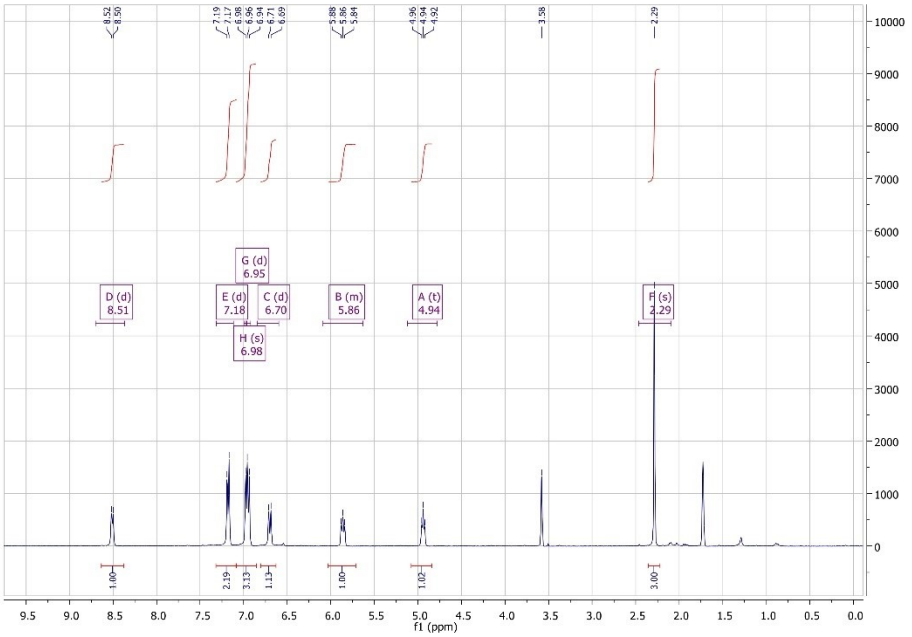

Figure S5. ^{1}H NMR (360 MHz, THF-d$_8$, 298 K) spectrum of K[Re(*amidopy**](CO)$_3$] (**5b**).

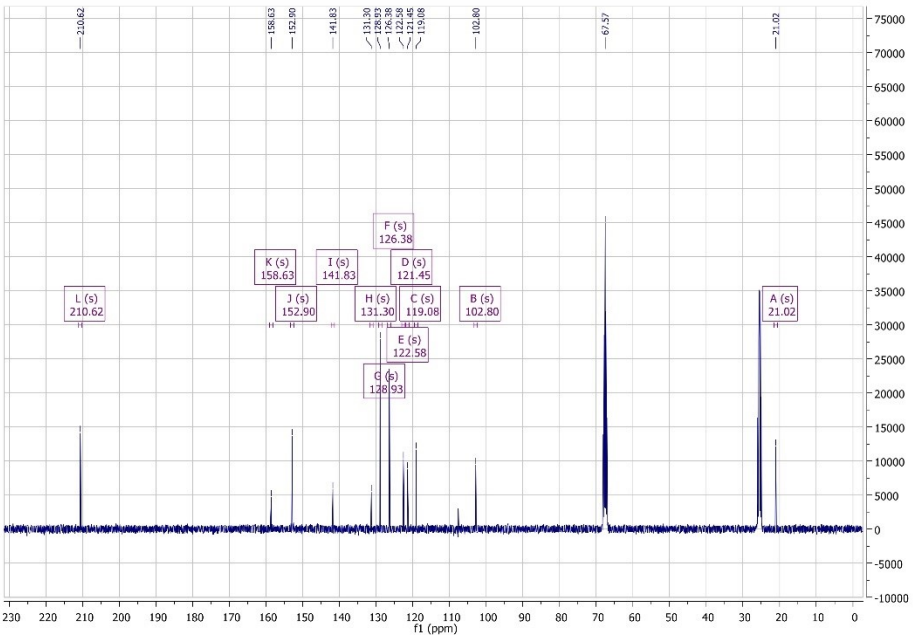

Figure S6. $^{13}C\{^{1}H\}$ NMR (91 MHz, THF-d_8, 298 K) spectrum of K[Re(*amidopy**](CO)$_3$] (**5b**).

Li[Re(*amidopy**](CO)$_3$] (**5a**)

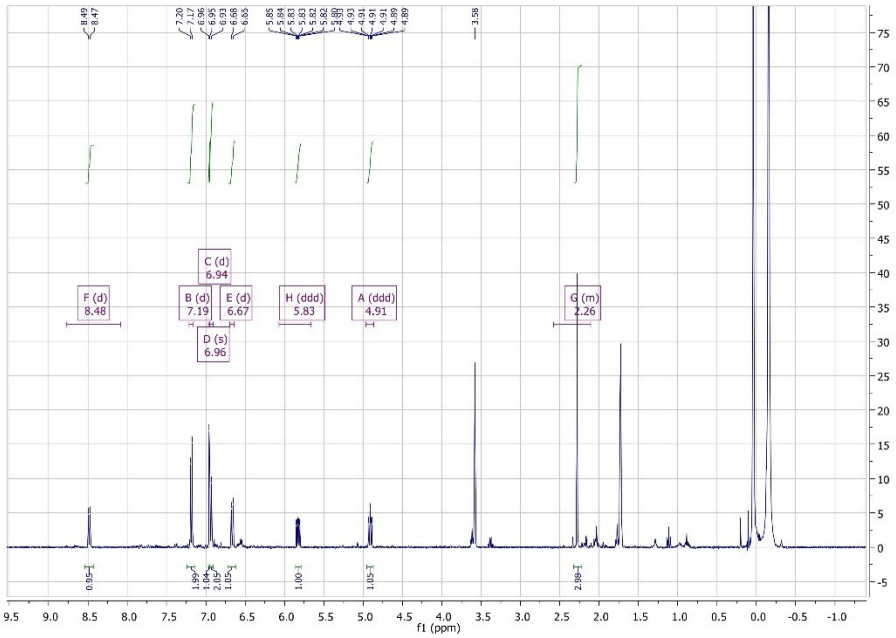

Figure S7. ^{1}H NMR (200 MHz, THF-d$_8$, 298 K) spectrum of Li[Re(*amidopy**](CO)$_3$] (**5a**).

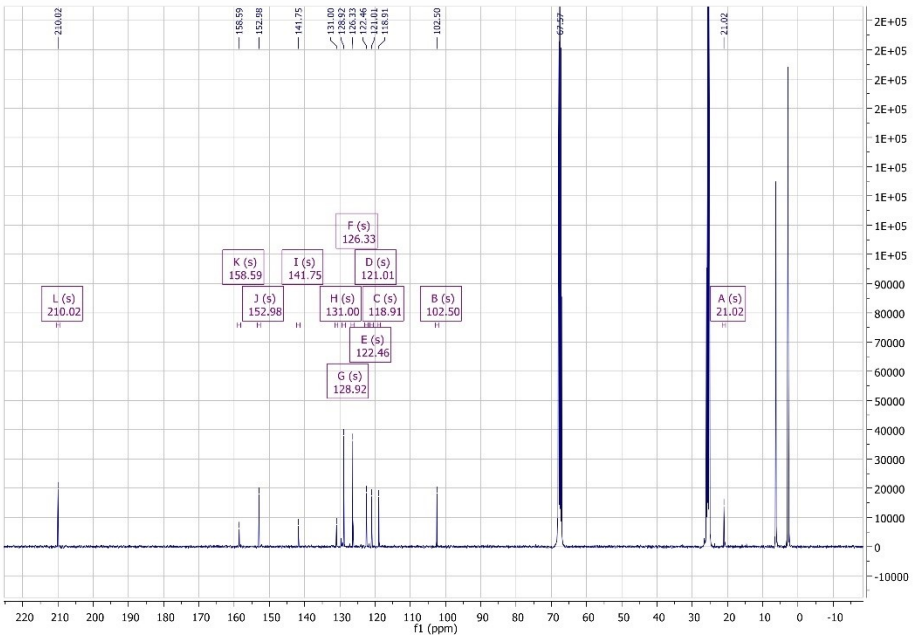

Figure S8. $^{13}C\{^{1}H\}$ NMR (91 MHz, THF-d_8, 298 K) spectrum of Li[Re(*amidopy**](CO)$_3$] (**5a**).

K[Re(*amidopy-COO*)$(CO)_3$] (**6**)

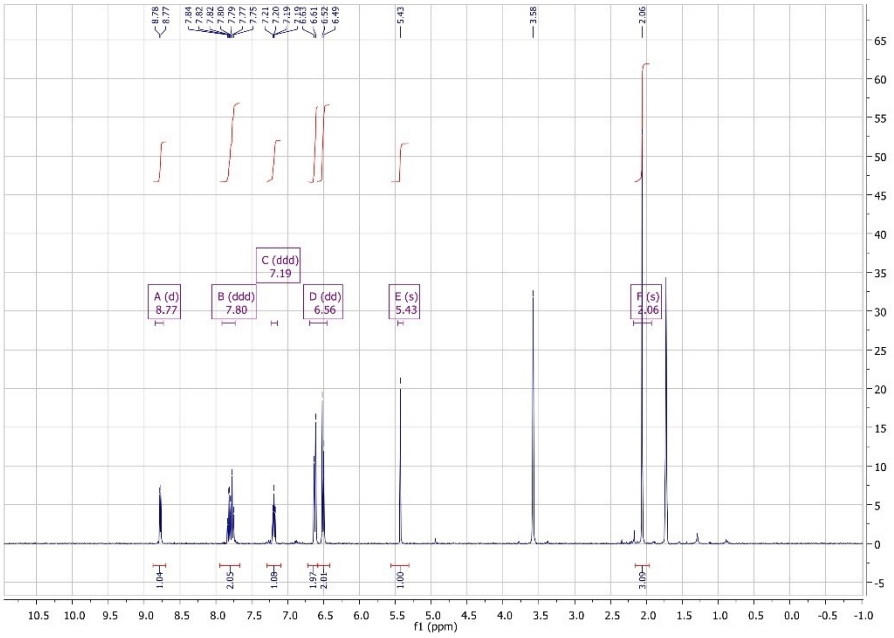

Figure S9. ^{1}H NMR (200 MHz, THF-d_8, 298 K) spectrum of K[Re(*amidopy-COO*](CO)$_3$] (**6**).

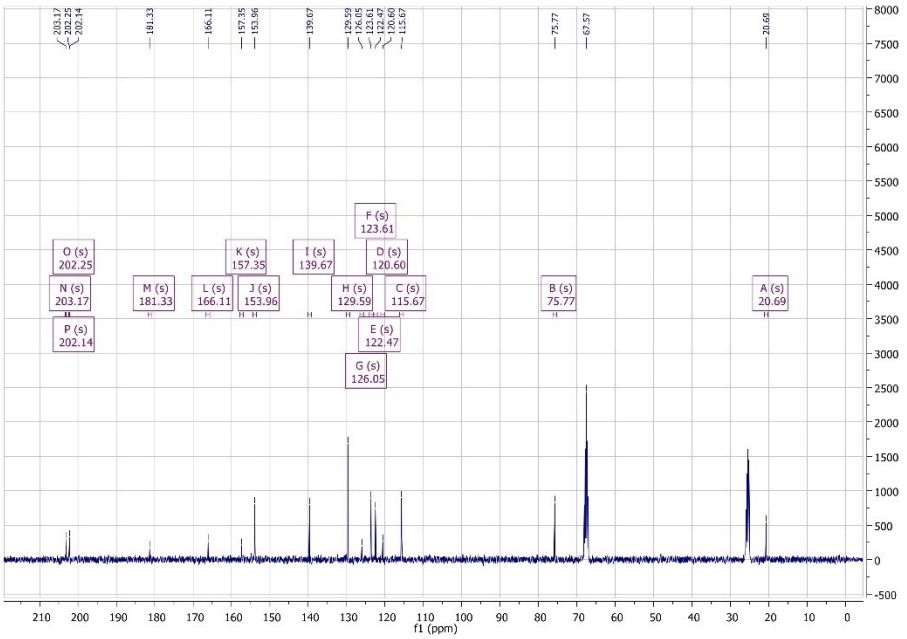

Figure S10. $^{13}C\{^{1}H\}$ NMR (91 MHz, THF-d_8, 298 K) spectrum of K[Re(*amidopy-COO*](CO)$_3$] (**6**).

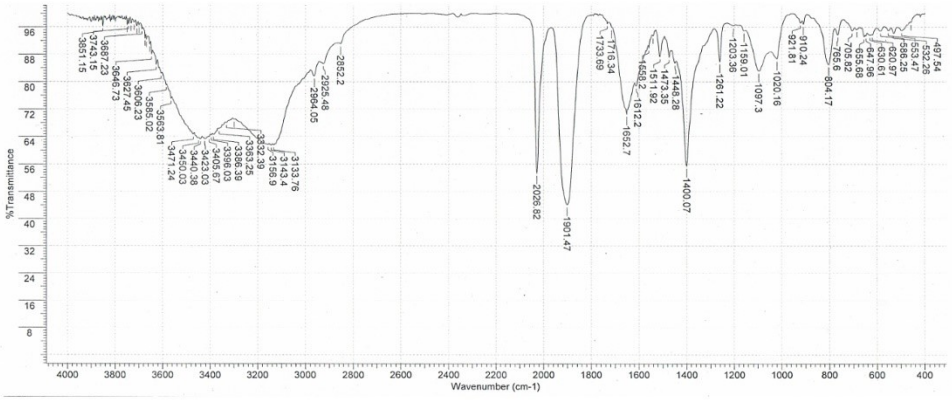

Figure S11. IR spectrum (KBr pellet) of K[Re(*amidopy-COO*](CO)$_3$] (**6**).

[K(18-crown-6)][Re(*amidopy-COO*)$(CO)_3$] (**6**-(*crown*))

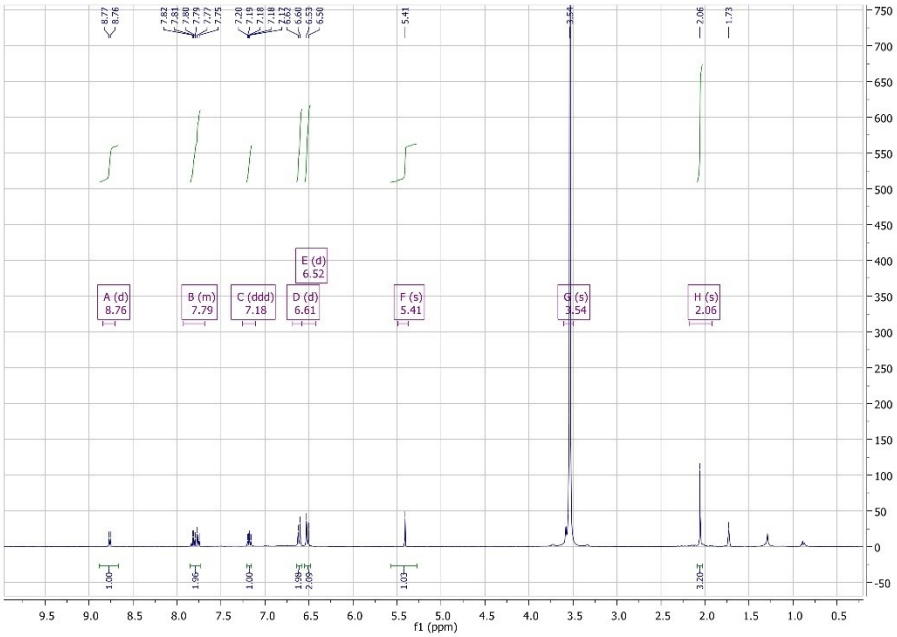

Figure S12. ^{1}H NMR (360 MHz, THF-d_8, 298 K) spectrum of [K(18-crown-6)][Re(*amidopy-COO*]$(CO)_3$] (**6**-(*crown*)).

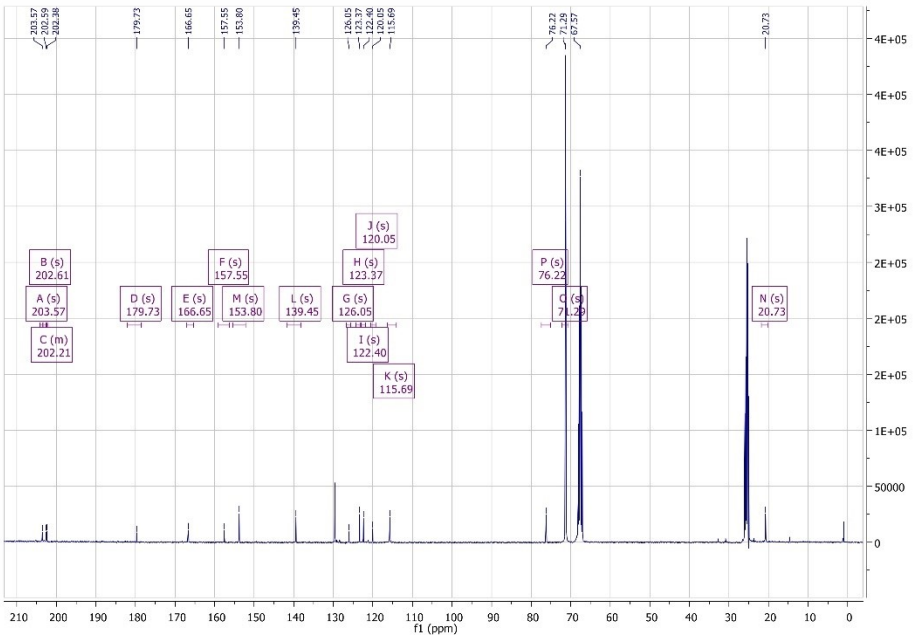

Figure S13. $^{13}C\{^{1}H\}$ NMR (91 MHz, THF-d_8, 298 K) spectrum of [K(18-crown-6)][Re(*amidopy-COO*](CO)$_3$] (**6**-(*crown*)).

K[Re(*amidopy-^{13}COO*)(CO)$_3$] (**6**-$^{13}CO_2$)

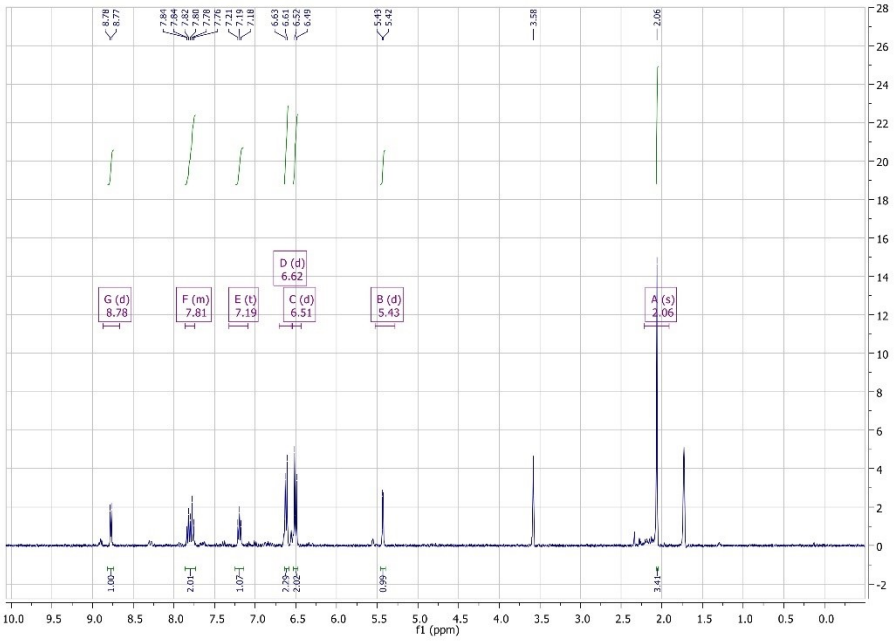

Figure S14. ^{1}H NMR (360 MHz, THF-d$_8$, 298 K) spectrum of K[Re(*amidopy-^{13}COO*](CO)$_3$] (**6**-$^{13}CO_2$).

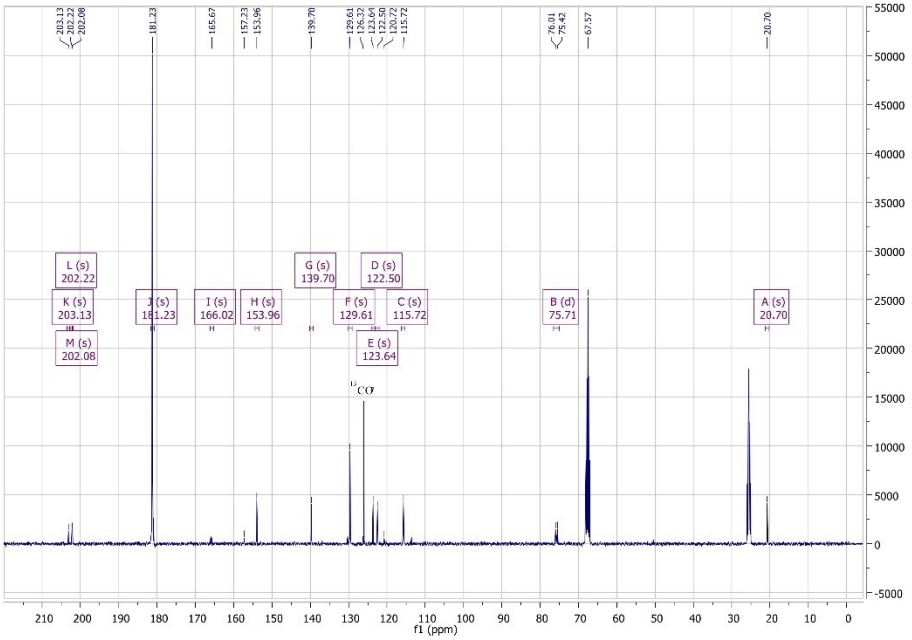

Figure S15. $^{13}C\{^{1}H\}$ NMR (91 MHz, THF-d_8, 298 K) spectrum of K[Re(*amidopy-*^{13}*COO*](CO)$_3$] (**6-**$^{13}CO_2$).

Heating complex **4** (10mg) in 0.6 mL DMSO-d_6)

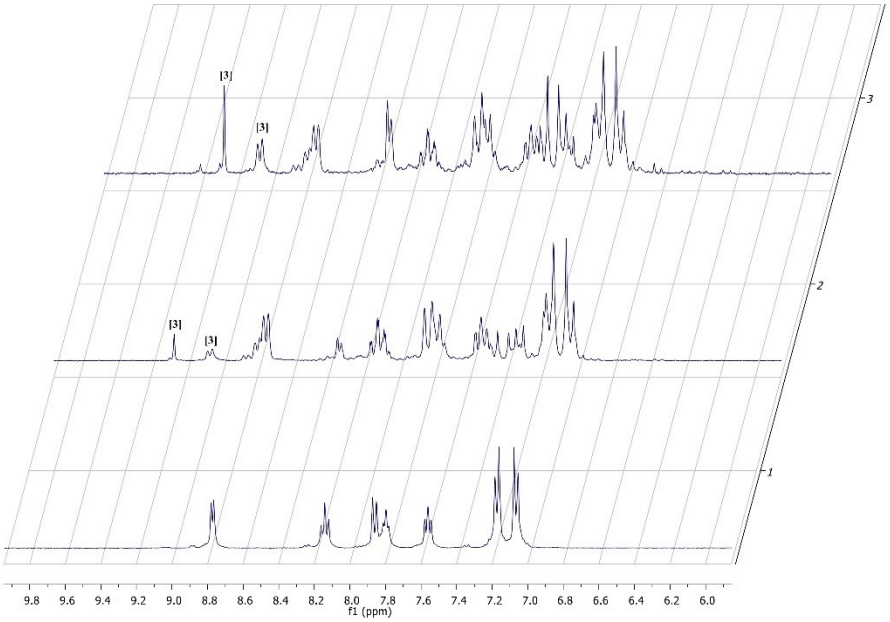

Figure S16. Stacked ^{1}H NMR spectra (360 MHz, 298 K) of complex **4** (10mg) in 0.6 mL DMSO-d_6 (bottom). Heating the sample for 80°C in air for 240 min (middle); Heating the sample for 670 min at 80°C (top). Resonances associated to complex **3** are labeled with [**3**].

7.2

Supporting Information for:

Cooperative Binding of SO_2 under M–O and C–S Bond Formation in a Rhenium(I) Complex with Activated Amino- or Iminopyridine Ligand

Rasmus Stichauer and Matthias Vogt*

Universität Bremen, FB 2 Biologie/Chemie, Institut für Anorganische Chemie und Kristallographie, Leobener Straße. 7, NW2 C2060, 28359 Bremen, Germany

R. Stichauer, M. Vogt, *Organometallics* **2018,** *37*, 3639-3643.

DOI: 10.1021/acs.organomet.8b00485

Index

Experimental

General: If not indicated otherwise, all manipulations were performed under inert conditions in a MBRAUN Labmaster glovebox or using standard Schlenk techniques. Reagents were obtained commercially (Sigma-Aldrich, Germany) and were used as received. THF-d_8 was purchased from EurIsotop, degassed, and dried over molecular sieves. Dry solvents were collected from a SPS800 MBRAUN solvent purification system and additionally dried over 4 Å molecular sieves prior to their use. [$Re(CO)_5Br$] was prepared according to literature procedure. [Schmidt, S. P.; Trogler, W. C.; Basolo, F.; Urbancic, M. A.; Shapley, J. R. Inorg. Synth. **1990**, 28, 160−165].

Spectroscopy: ^1H- and $^{13}C\{^1H\}$-, and 2D NMR spectra were recorded on a BRUKER Avance-NB360 spectrometer and are referenced to tetramethylsilane (^1H, ^{13}C). Chemical shifts are reported in parts per million (ppm), and coupling constants (J) are given in Hertz (Hz). IR spectra were recorded on an THERMO SCIENTIFIC Nicolet iS10 ATR FT-IR spectrometer.

Crystallography: Intensity data were collected on a BRUKER Venture D8 diffractometer with graphite-monochromated Mo Kα (0.7107 Å) The structure was solved by direct methods and refined based on F^2 by use of the SHELX program package as implemented in OLEX2. Figures were created using CCDC Mercury 3.9. Crystal Data for complex **2:** (M =1837.82 g/mol): monoclinic, space group P21/c (no. 14), a = 9.3525(3) Å, b = 16.0600(4) Å, c = 23.5208(6) Å, β = 96.0757(10)°, V = 3513.01(17) Å3, Z = 2, T = 100 K, μ(Mo Kα) = 3.848 mm-1, Dcalc = 1.7373 g/cm3, 239543 reflections measured (4.38° ≤ 2Θ ≤ 60.12°), 10287 unique (Rint = 0.0404, Rsigma = 0.0132) which were used in all calculations. The final R1 was 0.0197 (I>=2u(I)) and wR2 was 0.0445 (all data).

Bulk Purity of compound **2** was assessed via elemental analysis using a HERAEUS CHN-Rapid. Samples of **2** for combustion analysis were crystallized from CH_2Cl_2 and THF. Both solvents co-crystallize with compound **2** in a 1:1 ratio. Even prolonged drying under high vacuum does not yield in the removal of the solvent molecule.

Calculated (found) 2•THF: C = 42.42% (42.16), H = 4.89% (4.88), N = 3.09% (3.40) Combustion analysis for sulfur gave 3.54% (3.19).

Calculated (found) 2•CH_2Cl_2: C = 37.91% (38.20), H = 4.17% (4.41), N = 3.05% (3.28). Combustion analysis for sulfur gave 3.49% (2.92).

Synthesis of *fac*-[K(18-crown-6)][Re(*amidopy-OSO*)(CO)$_3$] (**2ab**)

62 mg (0.11mmol) of complex ***i-Br*** where dissolved in 6 mL dry THF in a 25 mL Schlenk tube with teflon valve. Four equivalents of potassium metal (0.46 mmol, 18 mg) where added and the red reaction mixture was sonicated for 3 h until the solution characteristically changed its color to deep violet. The reaction mixture was filtered via a syringe filter (PTFE 0.45 µm porosity). Subsequently, one equivalent of crown ether (18-crown-6) (0.11 mmol, 29 mg) and one equivalent of the adduct of 1,4-diazabicyclo[2.2.2]octane and two sulfur dioxide molecules (DABSO) (0.11 mmol, 26 mg) were added. Upon addition of the reagents, the color of the solution instantaneously changed to brownish-yellow. The solution was filtered once more through a syringe PTFE filter (0.45 µm porosity). The filtrate was layered with *n*-hexane to give **2ab** as orange crystals. The crystals where washed with a minimum of dry THF and *n*-hexane and dried under reduced pressure. Yield 54.2 mg (0.065 mmol, 59 %). Suitable crystals for X-ray diffraction analysis were obtained from slow diffusion of *n*-hexane into a CH_2Cl_2 solution of **2ab**.

^{1}H NMR (360 MHz, CD_2Cl_2) δ 8.86 (d, $^3J_{HH}$ = 5.3 Hz, 1H$_a$, CH$_{py\text{-}6}$), 8.70 (d, $^3J_{HH}$ = 5.3 Hz, 1H$_b$, CH$_{py\text{-}6}$), 7.78 (m, 1H$_a$ and 1H$_b$, overlap CH$_{py\text{-}4}$), 7.64 (d, $^3J_{HH}$ = 7.7 Hz, 1H$_b$, CH$_{py\text{-}3}$), 7.51 (d, $^3J_{HH}$ = 7.8 Hz, 1H$_a$, CH$_{py\text{-}3}$), 7.22 – 7.13 (m, 1H$_a$, CH$_{py\text{-}5}$), 7.12 – 7.05 (m, 1H$_b$, CH$_{py\text{-}5}$), 6.97 (d, $^3J_{HH}$ = 8.5 Hz, 2H$_b$, CH$_{Ar\text{-}8}$ and CH$_{Ar\text{-}12}$), 6.87 – 6.79 (m, 4H$_{Ar}$), 6.75 (d, $^3J_{HH}$ = 8.4 Hz, 2H$_b$, CH$_{Ar\text{-}9}$ and CH$_{Ar\text{-}12}$), 6.68 (s, 1H$_b$, HC(SOO)N), 6.17 (s, 1H$_a$, HC(SOO)N), 3.67 (m, 4H, CH$_{2\text{-}THF}$), 3.55 (br s, 48H, CH$_{2\text{-}crown}$), 2.17 (s, 3H$_a$, CH$_3$), 2.13 (s, 3H$_b$, CH$_3$), 1.80 (m, 4H, CH$_{2\text{-}THF}$).

^{13}C{^{1}H} NMR (91 MHz, CD_2Cl_2) δ 202.16 (s, 1C, Re–CO), 201.99 (s, 1C, Re–CO), 201.71 (s, 1C, Re–CO), 201.47 (s, 1C, Re–CO), 201.32 (s, 1C, Re–CO), 201.06 (s, 1C, Re–CO), 161.75 (s, 1C, C$_{quart}$), 156.96 (s, 1C, C$_{quart}$), 156.68 (s, 1C, C$_{quart}$), 155.24 (s, 1C, C$_{quart}$), 152.86 (s, 1C$_b$, CH$_{py\text{-}6}$), 152.12 (s, 1C$_a$, CH$_{py\text{-}6}$), 138.50 (s, 1C$_b$, CH$_{py\text{-}4}$), 137.10 (s, 1C$_a$, CH$_{py\text{-}4}$), 129.23 (s, 2C$_a$, CH$_{Ar\text{-}9,11}$), 128.99 (s, 2C$_b$, CH$_{Ar\text{-}9,11}$), 124.70 (s, 1C$_a$, CH$_{py\text{-}3}$) 122.60 (s, 1C, CH$_3$C$_{Ar\text{-}quart}$), 122.17 (s, 1C$_a$, CH$_{py\text{-}5}$), 122.11 (s, 1C$_b$, CH$_{py\text{-}5}$), 122.03 (s, 1C, CH$_3$C$_{Ar\text{-}quart}$), 121.17 (s, 1C$_b$, CH$_{py\text{-}3}$), 115.70 (s, 2C$_b$, CH$_{Ar\text{-}8,12}$), 114.21 (s, 2C$_a$, CH$_{Ar\text{-}8,12}$), 97.78 (s, 1C$_b$, C(SOO)), 94.43 (s, 1C$_a$, C(SOO)), 70.16 (s, 24C, CH$_{2\text{-}crown}$), 67.98 (s, 2C, CH$_{2\text{-}THF}$), 25.77 (s, 2C, CH$_{2\text{-}THF}$), 20.22 (s, 2C, CH$_3$).

IR ν/cm^{-1}: 2898 (br, w), ν_{CO} = 1991 (s), 1860 (br, s), 1606 (m), 1503 (m), 1472 (m), 1447 (w), 1350 (m), 1316 (m), 1276 (m), 1249 (w), 1104 (s), 1057 (s), 960 (m), 916 (w), 859 (m), 814 (w), 793 (w), 782 (w), 756 (m).

Sythesis of of *fac*-[Re(impy)$(CO)_3$Cl **i-*Cl***

Method A: was modified from a previously reported procedure starting from [$Re(CO)_5$Cl] instead of [$Re(CO)_5$Br]. [Stichauer, R.; Helmers, A.; Bremer, J.; Rohdenburg, M.; Wark, A.; Lork, E.; Vogt, M. *Organometallics* **2017**, *36*, 839–848.]

Method B: [K(18-crown-6)][Re(*amidopy-OSO*)$(CO)_3$] (**2ab**); 0,024 mmol, 20 mg) was dissolved in 0.6 mL dry CD_2Cl_2 in a J. *Young*-NMR-tube with teflon valve. The solution was sonicated at 323 K until the orange color of the solution changes to red. Subsequent layering with *n*-hexane gave red single crystals of *fac*-[Re(*impy*)$(CO)_3$Cl] (**i-*Cl***).

^{1}H NMR (360 MHz, CD_2Cl_2) δ 9.07 (d, $^3J_{HH}$ = 4.8 Hz, 1H, $CH_{py\text{-}6}$), 8.80 (s, 1H, CH_{imine}), 8.12 (t, $^3J_{HH}$ = 7.0 Hz, 1H, $CH_{py\text{-}4}$), 8.04 (d, $^3J_{HH}$ = 7.4 Hz, 1H, $CH_{py\text{-}3}$), 7.69 – 7.56 (m, 1H, $CH_{py\text{-}5}$), 7.42 (d, $^3J_{HH}$ = 8.4 Hz, 2H, $CH_{Ar\text{-}8,12}$), 7.34 (d, $^3J_{HH}$ = 8.1 Hz, 2H, $CH_{Ar\text{-}9,11}$), 2.44 (s, 3H, CH_3).

^{13}C {^{1}H} NMR (91 MHz, CD_2Cl_2) δ 197.99 (s, 1C, Re-CO), 196.69 (s, 1C, Re-CO), 187.25 (s, 1C, Re-CO), 166.04 (s, 1C, CH_{imine}), 155.69 (s, 1C, $C_{py\text{-}quart}$), 153.52 (s, 1C, $CH_{py\text{-}6}$), 148.71 (s, 1C, $C_{Ar\text{-}quart}$), 140.51 (s, 1C, $C_{Ar\text{-}quart}$), 139.86 (s, 1C, $CH_{py\text{-}4}$), 130.53 (s, 2C, CH_{Ar}), 129.39 (s, 1C, CH_{py}), 129.29 (s, 1C, CH_{py}), 122.37 (s, 2C, CH_{Ar}), 21.30 (s, 1C, CH_3).

IR ν/cm^{-1}: ν_{CO} = 2016 (s), 1875 (br,s)

*NMR Spectroscopic Data for fac-[K(18-crown-6)][Re(amidopy-OSO)(CO)$_3$] (**2ab**)*

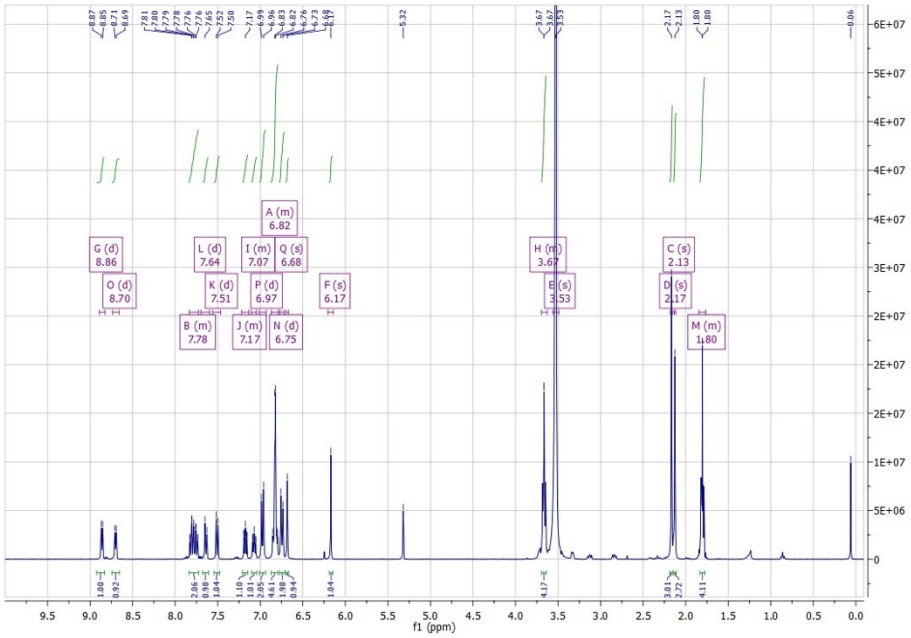

Figure S1. ^{1}H NMR (360 MHz, CD_2Cl_2, 268 K) spectrum of *fac*-[K(18-crown-6)][Re(*amidopy-OSO*)$(CO)_3$] (**2ab**).

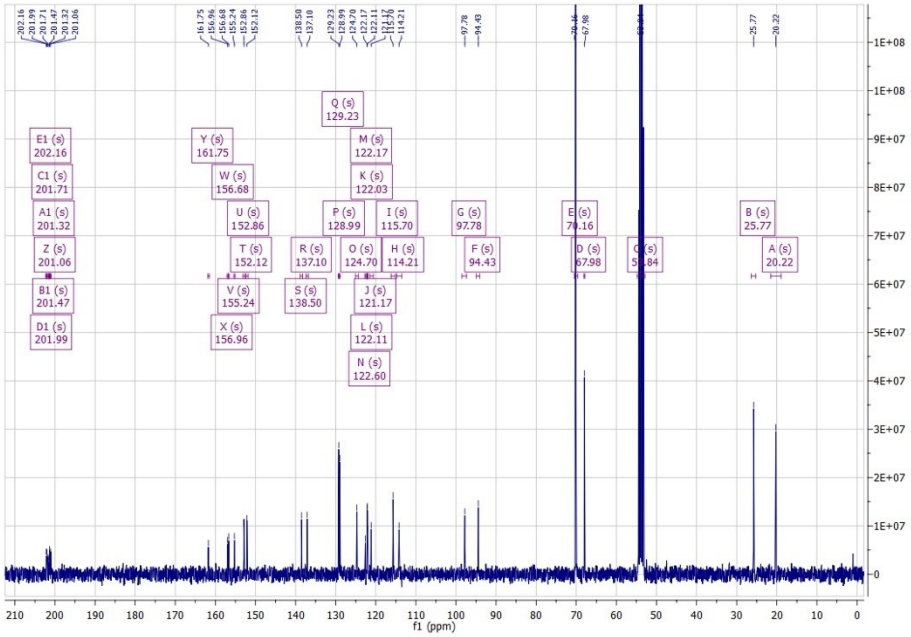

Figure S2. $^{13}C\{^{1}H\}$ NMR (91 MHz, CD_2Cl_2, 268 K) spectrum of *fac*-[K(18-crown-6)][Re(*amidopy-OSO*)$(CO)_3$] (**2ab**).

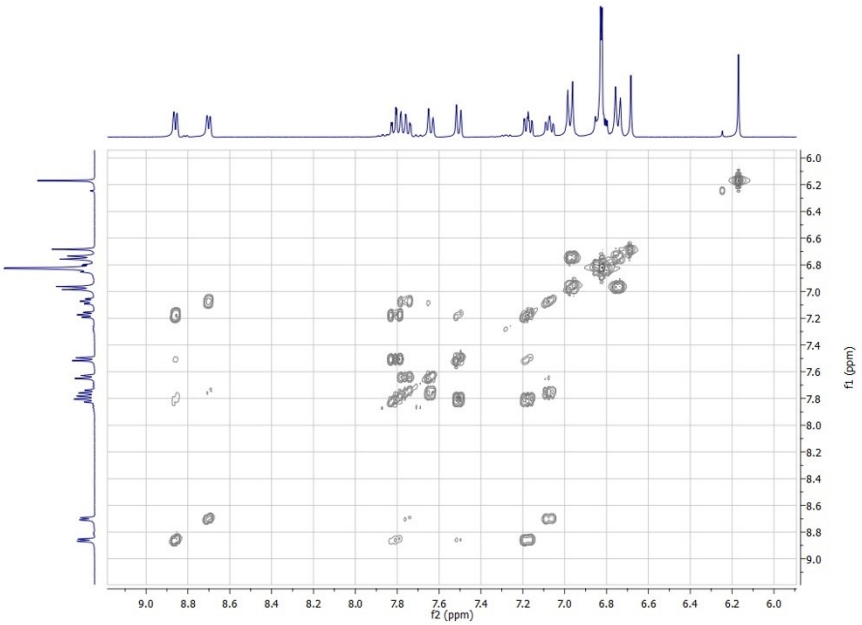

Figure S3. $^{1}H^{1}H$-COSY NMR (360 MHz, CD_2Cl_2, 268 K) spectrum of *fac*-[K(18-crown-6)][Re(*amidopy-OSO*)$(CO)_3$] (**2ab**).

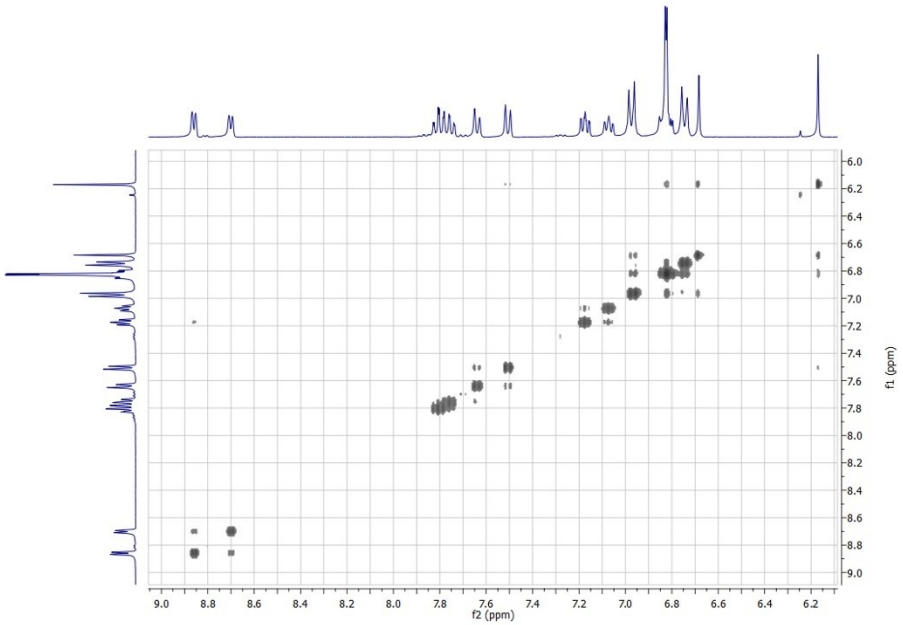

Figure S4. $^{1}H^{1}$HEXSY NMR (360 MHz, CD_2Cl_2, 268 K) spectrum of *fac*-[K(18-crown-6)][Re(*amidopy-OSO*)$(CO)_3$] (**2ab**).

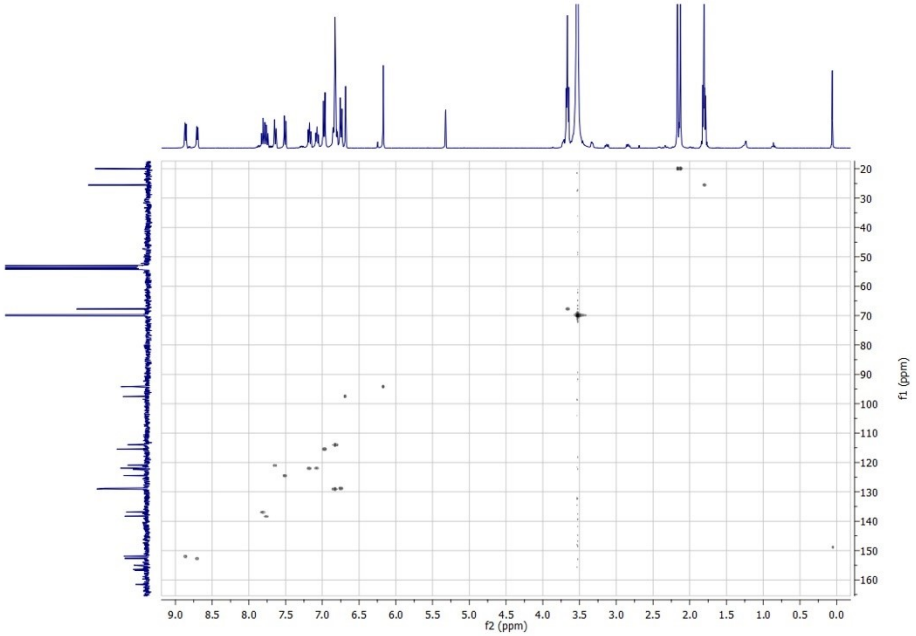

Figure S5. $^{1}H^{13}C$-HSQC NMR (360 MHz / 91 MHz, CD_2Cl_2, 268 K) spectrum of *fac*-[K(18-crown-6)][Re(*amidopy-OSO*)$(CO)_3$] (**2ab**).

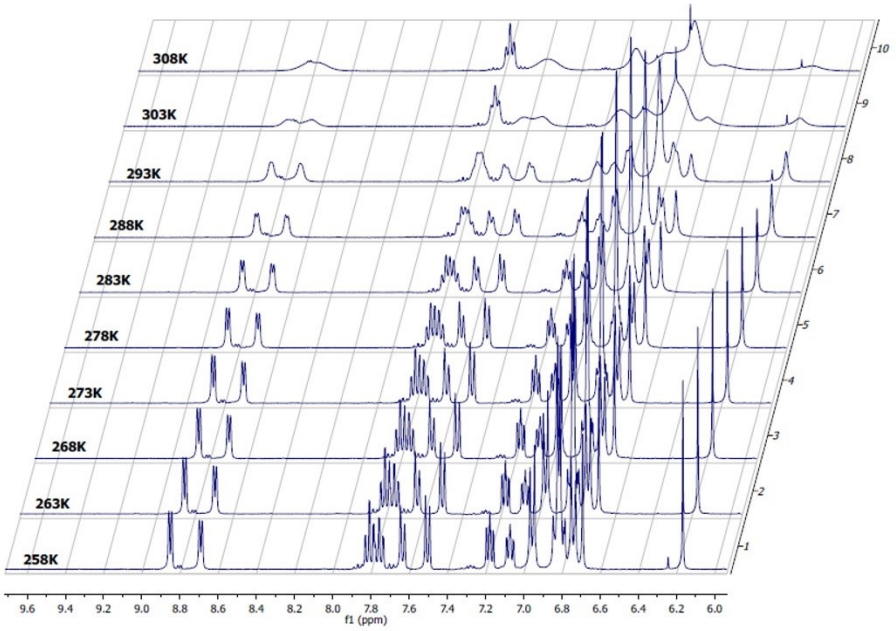

Figure S6. Section of the ^{1}H NMR (360 MHz, CD_2Cl_2) spectra of *fac*-[K(18-crown-6)][Re(*amidopy-OSO*)$(CO)_3$] (**2ab**) at at various temperatures (258-308 K).

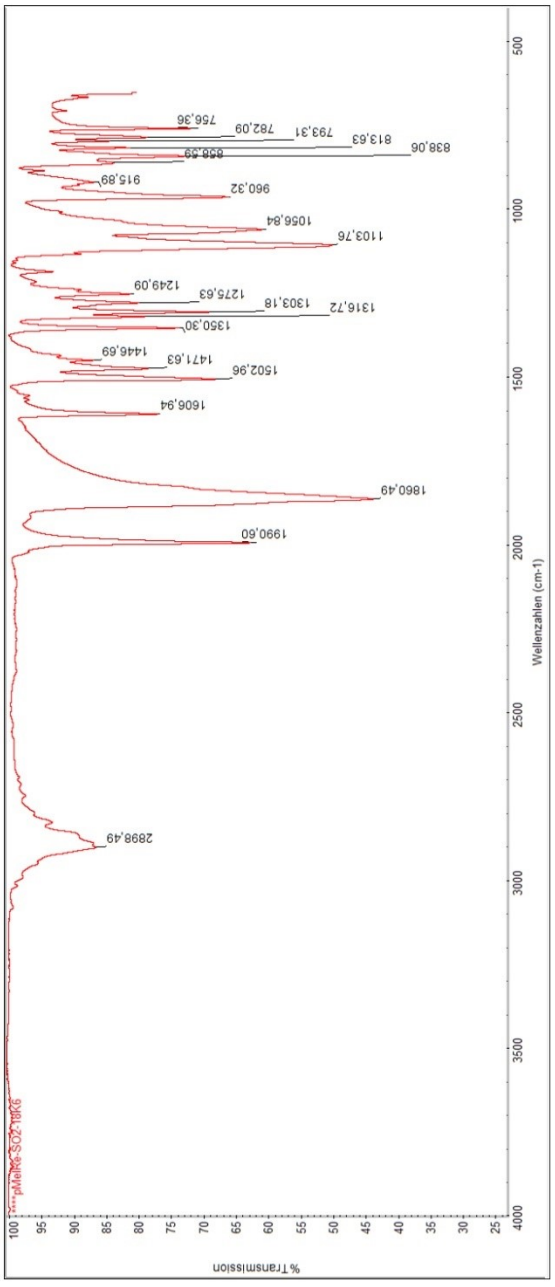

Figure S7. IR spectrum (FT-IR) of *fac*-[K(18-crown-6)][Re(*amidopy-OSO*)$(CO)_3$] (**2a**).

Determination of Activation Parameters for the interconversion of 2a and 2b

Chemical exchange rate parameters were determined via spectral fitting and line shape analysis (253-308 K) using the dynamic NMR module (DNMR 1.1) implemented in BRUKER TOPSPIN 4.0.3. (^{1}H well separated resonances used at ^{1}H NMR (360 MHz, CD_2Cl_2) δ 8.86 (d, $^3J_{HH}$ = 5.3 Hz, $1H_a$, $CH_{py\text{-}6}$), 8.70 (d, $^3J_{HH}$ = 5.3 Hz, $1H_b$, $CH_{py\text{-}6}$)). Subsequent Eyring-Polanyi plot analysis gave the activation parameter (see data below).

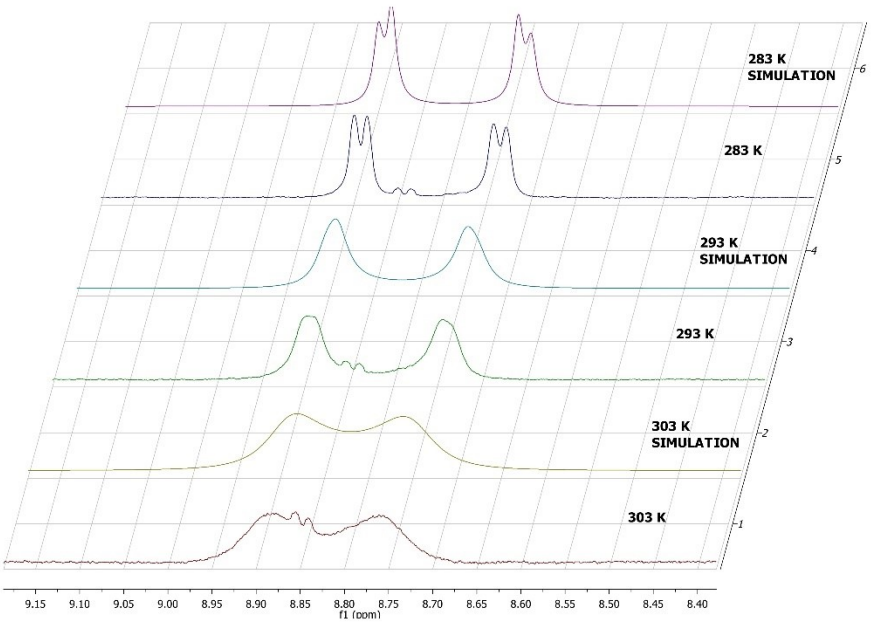

Figure S8. Examples for spectral fitting for line shape analysis using the dynamic NMR module (DNMR 1.1) implemented in BRUKER TOPSPIN 4.0.3; ^{1}H NMR (360 MHz, CD_2Cl_2) δ 8.86 (d, $^3J_{HH}$ = 5.3 Hz, $1H_a$, $CH_{py\text{-}6}$), 8.70 (d, $^3J_{HH}$ = 5.3 Hz, $1H_b$, $CH_{py\text{-}6}$).

Table S1. Data from dNMR line shape analysis tool implemented in Bruker TopSpin 4.0.3 software; resonances of [K(18-crown-6)][Re(*amidopy-SOO*)$(CO)_3$] (**2ab**) $1H_a$, $CH_{py\text{-}6}$ and $1H_b$, $CH_{py\text{-}6}$. Note, depending on the initial starting parameters, the fitting process derived slightly different overlap maxima. We therefore averaged runs with overlaps in an interval of ±0.2%.

T [K]	k [Hz]	1/T	ln(k/T)	Overlap of spectral simulation [%]
278	10,820	0,00359712	-3,246	92,297
278	10,293	0,00359712	-3,296	92,341
278	9,384	0,00359712	-3,389	92,385
278	8,953	0,00359712	-3,436	92,422
278	8,205	0,00359712	-3,523	92,46
278	7,598	0,00359712	-3,600	92,499
278	7,044	0,00359712	-3,675	92,535
278	6,062	0,00359712	-3,826	92,57
278	5,613	0,00359712	-3,903	92,607
278	5,022	0,00359712	-4,014	92,638
278	4,353	0,00359712	-4,157	92,677
283	19,29	0,00353357	-2,686	93,102
283	18,75	0,00353357	-2,714	93,138
283	18,21	0,00353357	-2,744	93,173
283	17,65	0,00353357	-2,775	93,206
283	17,07	0,00353357	-2,808	93,238
283	16,55	0,00353357	-2,839	93,269
283	15,92	0,00353357	-2,878	93,298
283	15,21	0,00353357	-2,924	93,326
283	14,57	0,00353357	-2,967	93,352
283	14,01	0,00353357	-3,006	93,377
283	13,37	0,00353357	-3,053	93,400
283	12,64	0,00353357	-3,109	93,421
283	11,91	0,00353357	-3,168	93,442
283	11,16	0,00353357	-3,233	93,462
283	10,48	0,00353357	-3,296	93,481
283	9,92	0,00353357	-3,351	93,499
283	9,33	0,00353357	-3,412	93,517
288	21,26	0,00347222	-2,606	94,755
288	23,14	0,00347222	-2,522	94,779
288	26,21	0,00347222	-2,397	94,781
288	26,84	0,00347222	-2,373	94,776
288	27,46	0,00347222	-2,350	94,769
288	29,23	0,00347222	-2,288	94,74

293	65,75180	0,00341297	-1,494	95,97600
293	60,60540	0,00341297	-1,576	96,05600
293	54,96960	0,00341297	-1,673	96,10400
293	53,32470	0,00341297	-1,704	96,11100
293	52,82570	0,00341297	-1,713	96,11300
293	52,56100	0,00341297	-1,718	96,11300
293	52,27980	0,00341297	-1,724	96,11300
293	51,70460	0,00341297	-1,735	96,11200
293	49,63310	0,00341297	-1,776	96,10800
293	49,07290	0,00341297	-1,787	96,10400
293	47,19590	0,00341297	-1,826	96,08800
293	44,51580	0,00341297	-1,884	96,06100
293	41,97380	0,00341297	-1,943	96,01800
293	39,56390	0,00341297	-2,002	95,95500
303	173,68	0,00330033	-0,556	97,38100
303	170,08	0,00330033	-0,577	97,39100
303	168,69	0,00330033	-0,586	97,39300
303	168,06	0,00330033	-0,589	97,39300
303	167,38	0,00330033	-0,593	97,39400
303	166,77	0,00330033	-0,597	97,39400
303	159,50	0,00330033	-0,642	97,38100
303	144,98	0,00330033	-0,737	97,27600
303	132,71	0,00330033	-0,826	97,06100
303	125,17	0,00330033	-0,884	96,91600
308	309,16	0,00324675	0,004	97,629
308	299,48	0,00324675	-0,028	97,634
308	288,37	0,00324675	-0,066	97,641
308	268,34	0,00324675	-0,138	97,653
308	247,66	0,00324675	-0,218	97,664
308	227,75	0,00324675	-0,302	97,674

Table S2. Estimation of error margins.

T [K]	ΔT	T+ΔT	k $\bar{x}$ [Hz]	k σ	1/T	ln(k/T)	1/(T+ΔT)	Δ (1/T)	k+σ	k-σ	ln(k+σ/T)	ln(k-σ/T)	Δ ln(k/T) pos	Δ ln(k/T) neg
278	1	279	7,58	2,16	0,00360	-3,60	0,00358	0,000013	9,74	5,41	-3,351	-3,939	0,251	0,336
283	1	284	14,47	3,21	0,00353	-2,97	0,00352	0,000012	17,68	11,26	-2,773	-3,224	0,200	0,251
288	1	289	25,69	2,94	0,00347	-2,42	0,00346	0,000012	28,64	22,75	-2,308	-2,539	0,109	0,122
293	1	294	51,14	6,87	0,00341	-1,75	0,00340	0,000012	58,01	44,27	-1,620	-1,890	0,126	0,144
303	1	304	157,70	17,19	0,00330	-0,65	0,00329	0,000011	174,90	140,51	-0,550	-0,768	0,103	0,115
308	1	309	273,46	31,48	0,00325	-0,12	0,00324	0,000011	304,94	241,98	-0,010	-0,241	0,109	0,122

.

Table S3. Activation Parameters for the mutual interconversion of **2a** and **2b.** $\Delta H^{\#}$ derived from slope, $\Delta S^{\#}$ derived from intercept

70,8	J/mol*K	$\Delta S^{\#}$
16,9	cal/mol*K	$\Delta S^{\#}$
82940,9	J/mol	$\Delta H^{\#}$
82,9	kJ/mol	$\Delta H^{\#}$
19,8	kcal/mol	$\Delta H^{\#}$
61,8	kJ/mol	$\Delta G^{\#}_{298}$
14,8	kcal/mol	$\Delta G^{\#}_{298}$

.

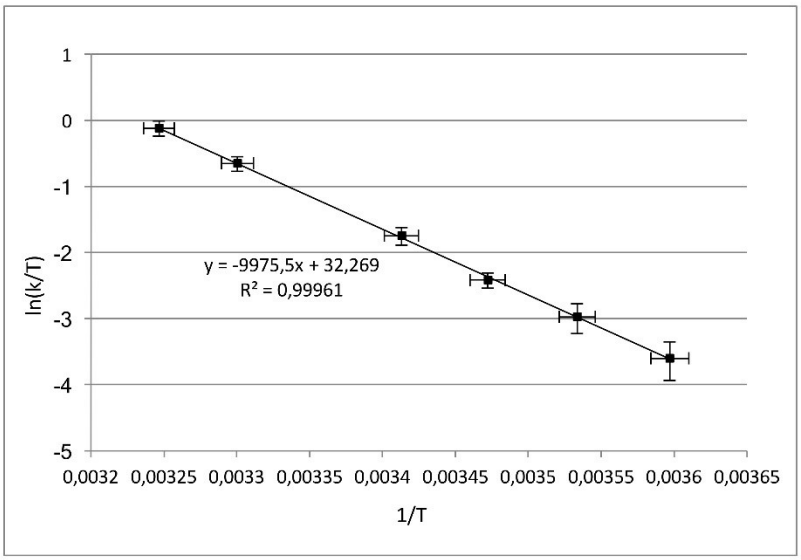

Figure S9 Eyring-Polanyi plot for the mutual interconversion between **2a** and **2b**.

Table S4 Estimation of error margins for activation parameters.

maximum										
T	1/T	ln(k/T)							error max	
278	0,00360	-3,47	29,90	Interc.	$\Delta S^{\#}$	51,0	J/molK	$\Delta\Delta S^{\#}$	19,7	J/molK
308	0,00325	-0,22	-9275,93	slope	$\Delta H^{\#}$	77124,4	J/mol	$\Delta\Delta H^{\#}$	5816,6	J/mol
					$\Delta H^{\#}$	77,1	kJ/mol	$\Delta\Delta H^{\#}$	5,8	kJ/mol
					$\Delta H^{\#}$	18,4	kcal/mol	$\Delta\Delta H^{\#}$	1,4	kcal/mol
									errorr min	
minimum					$\Delta S^{\#}$	91,0	J/molK	$\Delta\Delta S^{\#}$	20,2	J/mol*K
T	1/T	ln(k/T)			$\Delta H^{\#}$	88989,7	J/mol	$\Delta\Delta H^{\#}$	6048,7	J/mol
278	0,00360	-3,8	34,70	Interc.	$\Delta H^{\#}$	89,0	kJ/mol	$\Delta\Delta H^{\#}$	6,0	kJ/mol
308	0,00325	-0,05	-10703,00	slope	$\Delta H^{\#}$	21,3	kcal/mol	$\Delta\Delta H^{\#}$	1,4	kcal/mol

.

Table S5. Error margins for activation parameters.

$\Delta\Delta S^{\#}$	± 20,0	J/mol*K
$\Delta\Delta S^{\#}$	± 4.8	cal/mol*K
$\Delta\Delta H^{\#}$	± 5,9	kJ/mol
$\Delta\Delta H^{\#}$	± 1,4	kcal/mol
ΔT	± 1	K
$\Delta\Delta G^{\#}_{298}$	± 8.4	kJ/mol
$\Delta\Delta G^{\#}_{298}$	± 2.0	kcal/mol

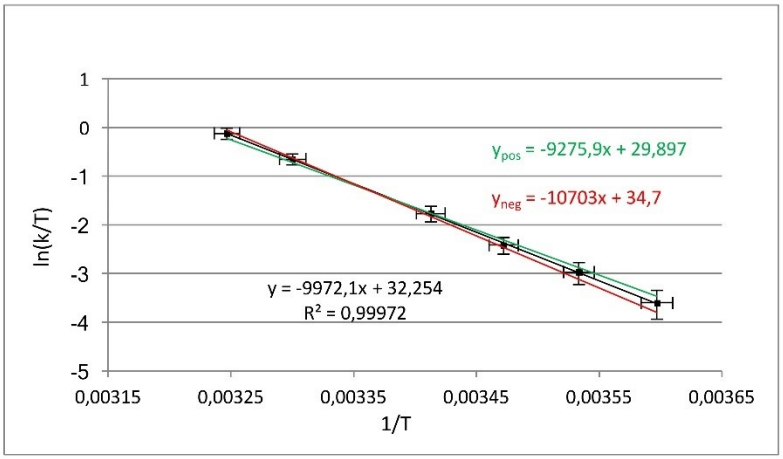

Figure S10 Error estimation for activation parameters from Eyring-Polanyi plot.

NMR spectroscopic data for *fac*-[Re(*impy*](CO)$_3$Cl] (**i-Cl**)

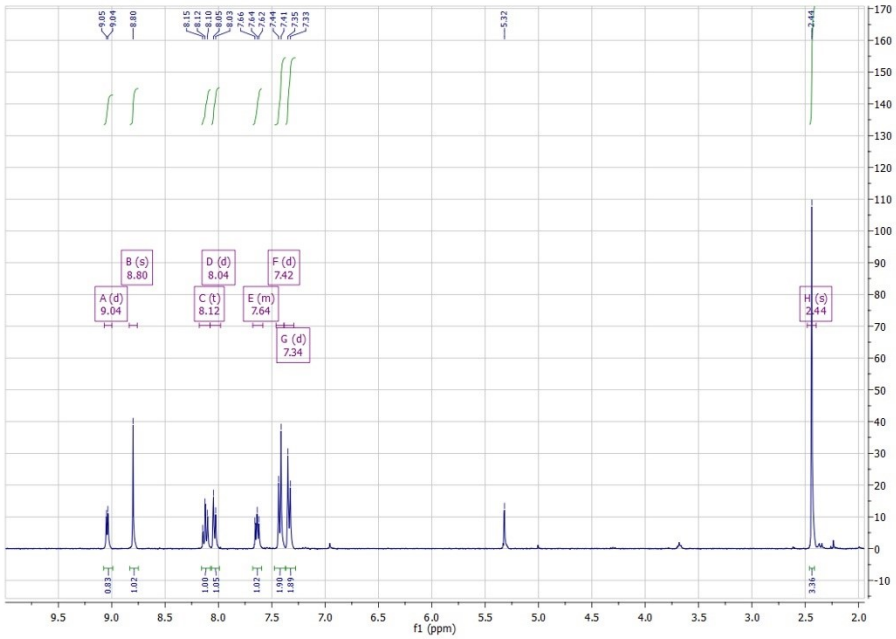

Figure S11. ^{1}H NMR (360 MHz, CD_2Cl_2, 293 K) spectrum of *fac*-[Re(*impy*](CO)$_3$Cl] (**i-*Cl***).

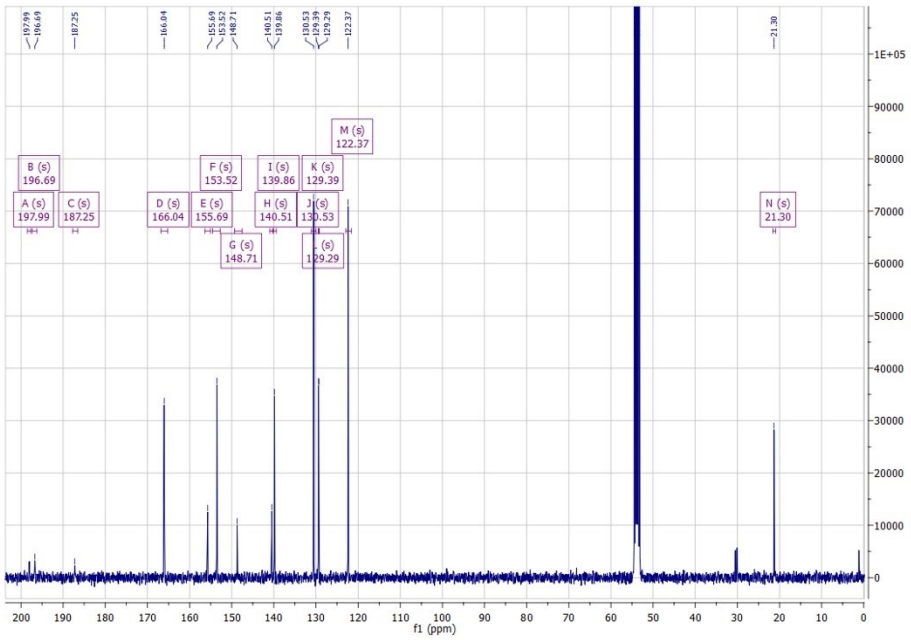

Figure S12. $^{13}C\{^{1}H\}$ NMR (91 MHz, CD_2Cl_2, 293 K) spectrum of *fac*-[Re(*impy*](CO)$_3$Cl] (**i-*Cl***).

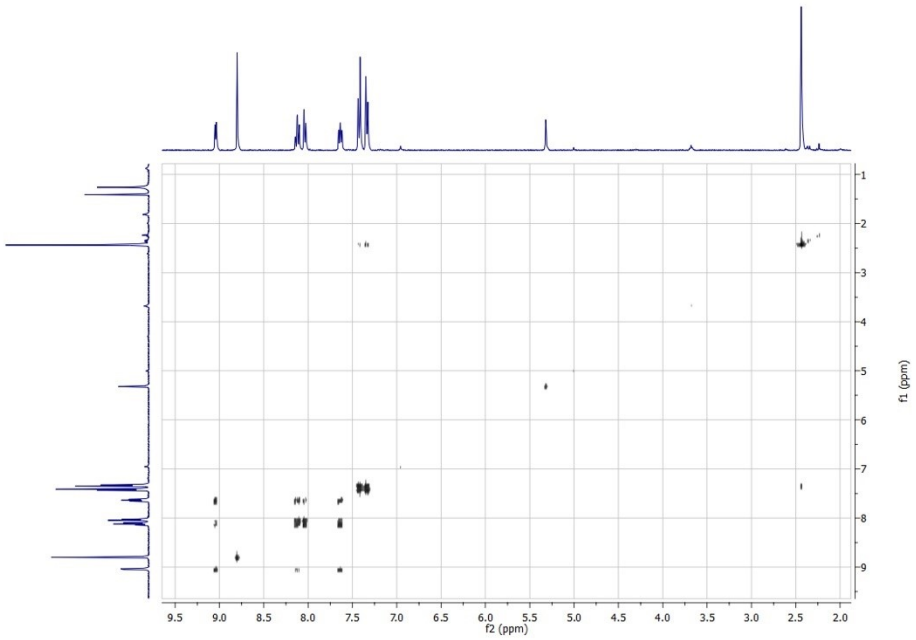

Figure S13. $^{1}H^{1}H$-COSY NMR (360 MHz, CD_2Cl_2, 293 K) spectrum of *fac*-[Re(*impy*](CO)$_3$Cl] (**i-*Cl***).

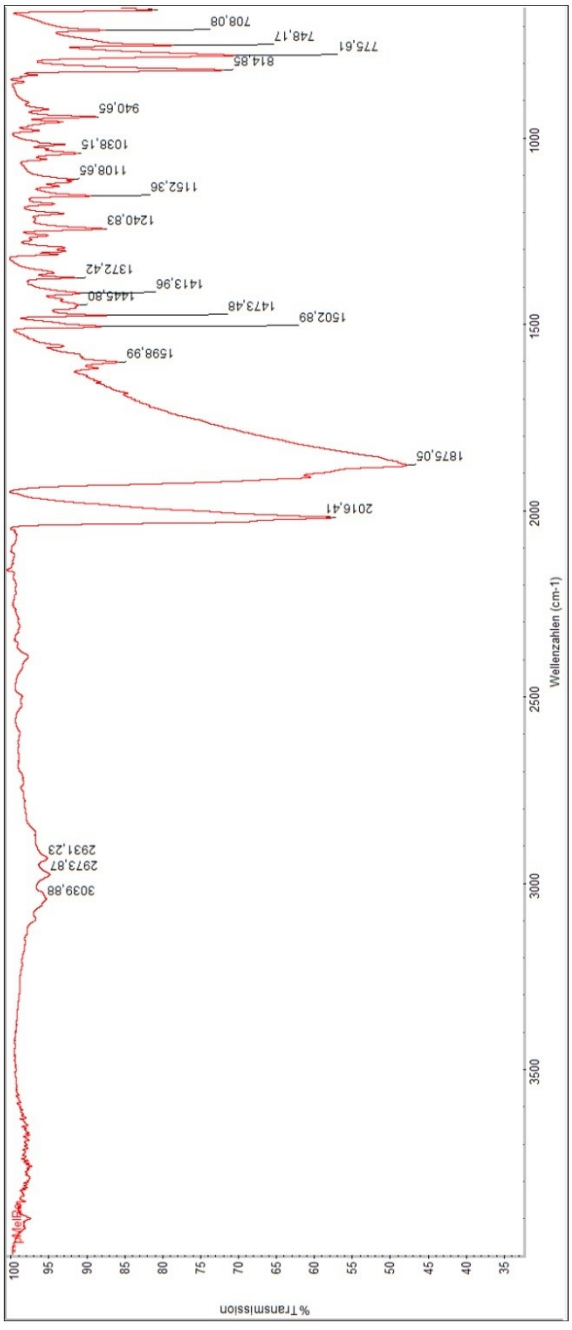

Figure S14. IR spectrum (FT-IR) of *fac*-[Re(*impy*](CO)$_3$Cl] (**i-*Cl***).

7.3

Supporting Information for:

Manganese(I) Tricarbonyl Complexes with Bidentate Pyridine-Based Actor Ligands – Reversible Binding of CO_2 and Benzaldehyde via Cooperative C–C and Mn–O Bond Formation at Ambient Temperature

Rasmus Stichauer[a], Daniel Duvinage[a], Robert Langer[b] and Matthias Vogt*[a,b]

[a]*Institut für Anorganische Chemie und Kristallographie, Universität Bremen, Leobener Str. NW2, 28359 Bremen, Germany*

[b]*Institut für Chemie, Naturwissenschaftliche Fakultät II, Martin-Luther-Universität Halle-Wittenberg, Kurt-Mothes-Str. 2, 06120 Halle (Saale), Germany. Email:* matthias.vogt@chemie.uni-halle.de

R. Stichauer, D. Duvinage, R. Langer, M. Vogt, *Organometallics* **2022,** *41*, 2798-2809.
DOI: 10.1021/acs.organomet.2c00387

Index

Spectroscopic, XRD structural, and MS spectrometric Data for compound:

Complex [Mn(*impy*)$(CO)_3$Br] (**1**)

^{1}H NMR (360 MHz, THF) δ 9.22 (d, *J* = 4.5 Hz, 1H), 8.61 (s, 1H), 8.07 (s, 2H), 7.64 (s, 1H), 7.49 (d, *J* = 7.7 Hz, 2H), 7.29 (d, *J* = 7.6 Hz, 2H), 2.39 (s, 3H).

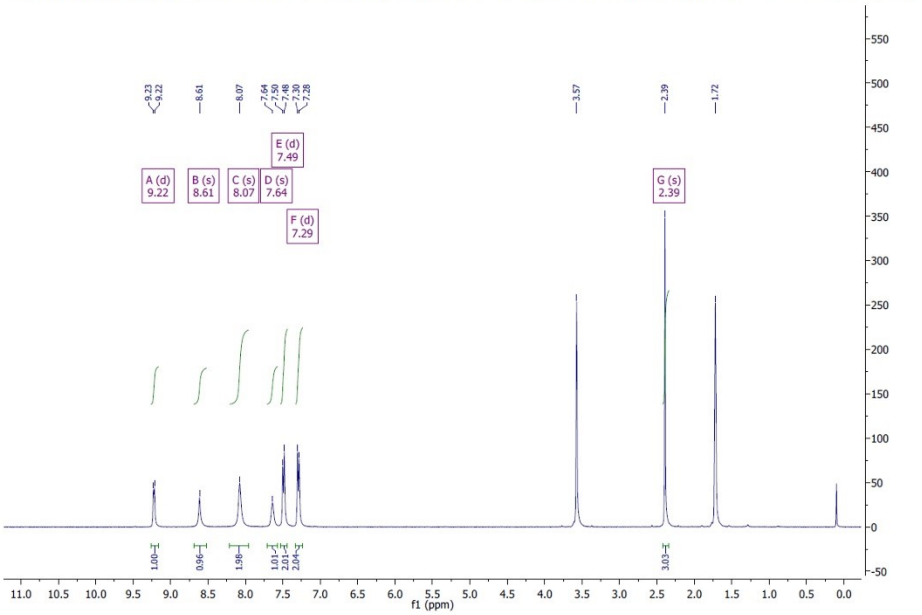

Figure 1S. ^{1}H NMR [360 MHz, THF-d_8, 298 K] spectrum of [Mn(*impy*)$(CO)_3$Br] (**1**).

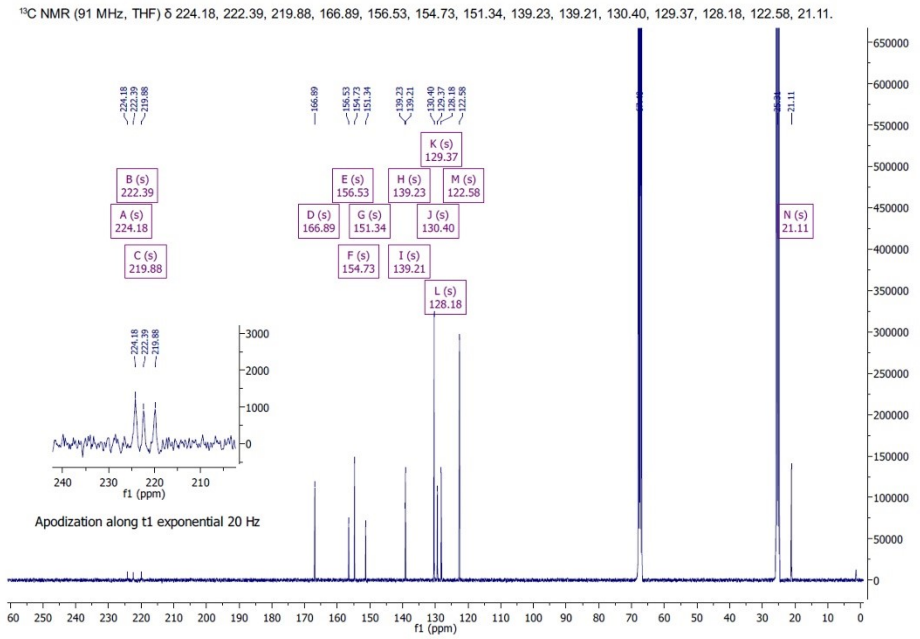

Figure 2S. $^{13}C\{^{1}H\}$ NMR [91 MHz, THF-d_8, 298 K] spectrum of [Mn(*impy*)$(CO)_3$Br] (**1**).

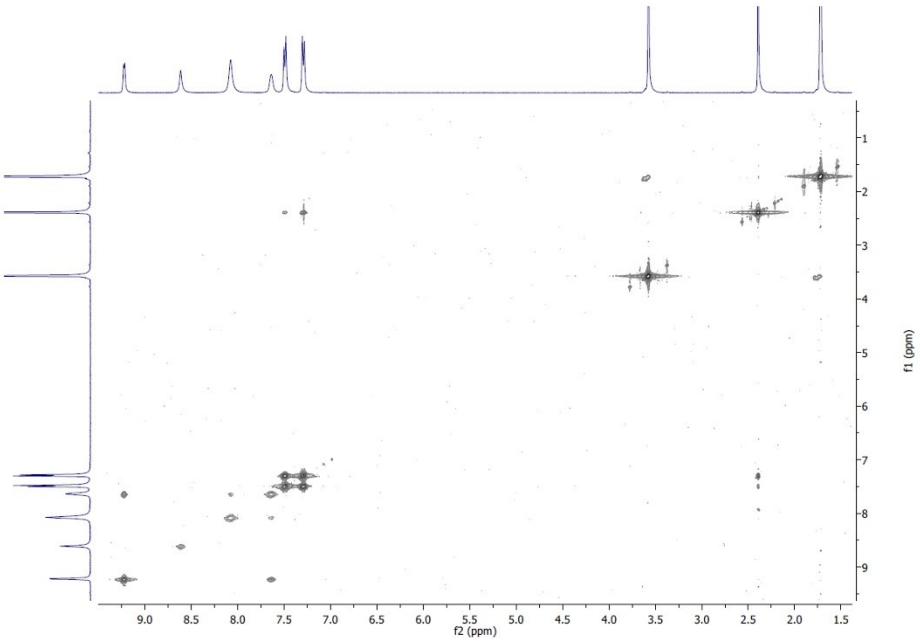

Figure 3S. $^{1}H^{1}H$ COSY NMR [360 MHz, THF-d_8, 298 K] spectrum of [Mn(*impy*)$(CO)_3$Br] (**1**).

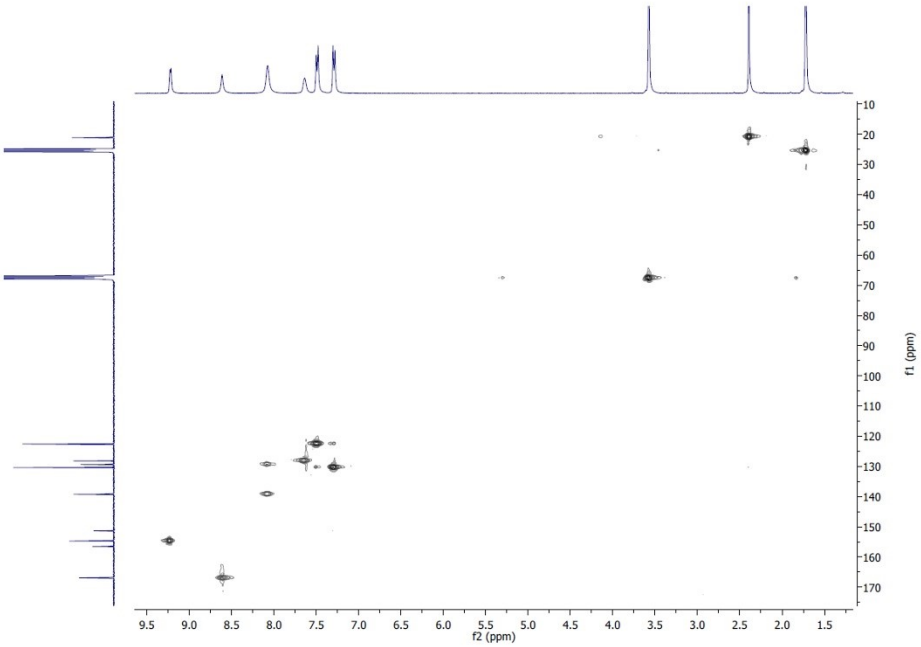

Figure 4S. $^{1}H^{13}C$ HSQC NMR [360 MHz/91 MHz, THF-d_8, 298 K] spectrum of [Mn(*impy*)$(CO)_3$Br] (**1**).

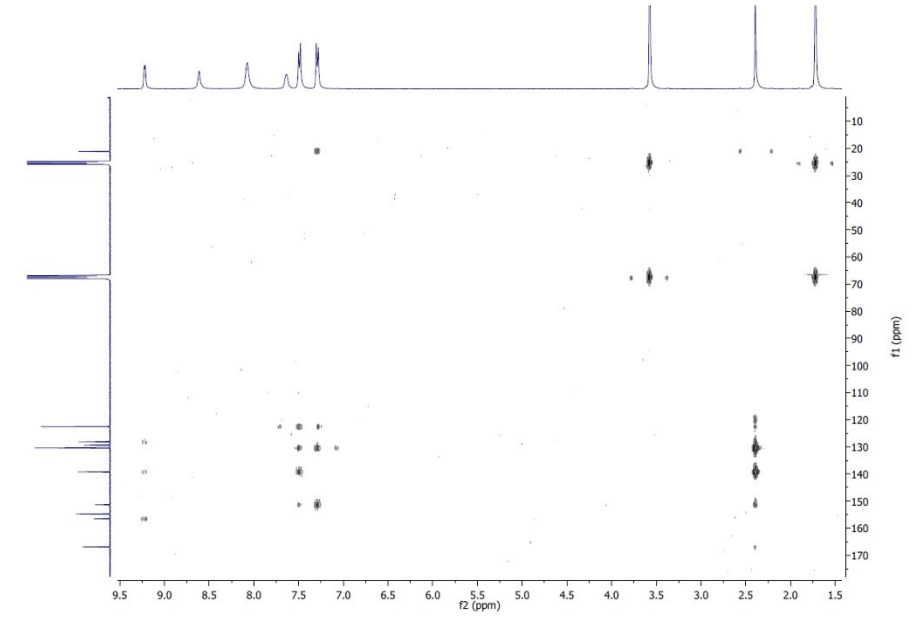

Figure 5S. $^{1}H^{13}C$ HMBC NMR [360 MHz/91 MHz, THF-d_8, 298 K] spectrum of [Mn(*impy*)$(CO)_3$Br] (**1**).

pMeIMnBr_DCM_EtOH_1#206 RT: 1.64
T: FTMS + c ESI Full ms [150.00-500.00]

m/z	Intensity	Relative	Composition
169.12000	5965691.0	59.02	
170.15401	2450561.3	24.24	
219.08952	10107658.0	100.00	$C_{13}H_{12}N_2Na$
220.09280	1374379.8	13.60	$C_{12}H_{14}O_3N$
221.10509	4415730.0	43.69	$C_{13}H_{14}N_2Na$
231.10254	1898031.8	18.78	$C_{15}H_{14}NNa$
253.05344	4482000.5	44.34	$C_{13}H_{14}N_2Mn$
267.03268	8207379.0	81.20	$C_{13}H_{12}ON_2Mn$
283.02768	6520795.0	64.51	$C_{13}H_{12}O_2N_2Mn$
285.04327	4639849.5	45.90	$C_{13}H_{14}O_2N_2Mn$
304.26135	2487110.8	24.61	
352.94601	1390160.0	13.75	$C_{13}H_{12}N_2BrMnNa$
354.94394	1387262.8	13.72	$C_{13}H_{12}N_2{}^{81}BrMnNa$
436.93082	2395795.0	23.70	$C_{16}H_{12}O_3N_2BrMnNa$
438.92871	2381201.3	23.56	$C_{16}H_{12}O_3N_2{}^{81}BrMnNa$

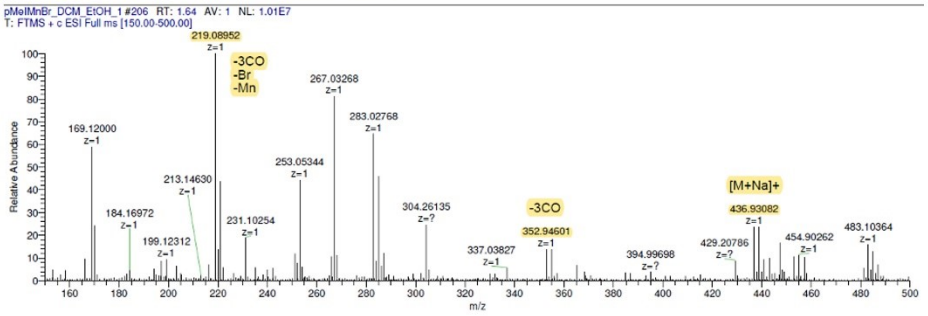

Figure 6S. HRMS-ESI pos CH_2Cl_2/C_2H_5OH spectrum of [Mn(*impy*)$(CO)_3$Br] (**1**).

pMeIMnBr_DCM_EtOH_1#364 RT: 2.94
T: FTMS + c ESI Full ms2 436.93@cid12.00 [120.00-450.00]

m/z	Intensity	Relative	Composition
219.08902	107671.3	8.84	$C_{13}H_{12}N_2Na$
352.94519	1217361.0	100.00	$C_{13}H_{12}N_2BrMnNa$

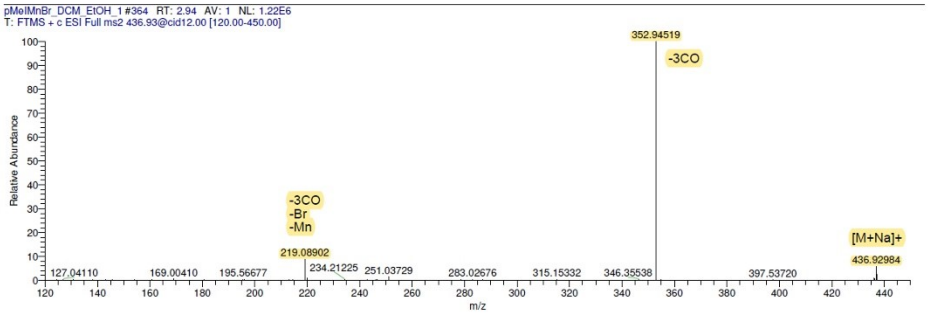

Figure 7S. HRMS^2-ESI pos CH_2Cl_2/C_2H_5OH spectrum of m/z 436.93@cid12.

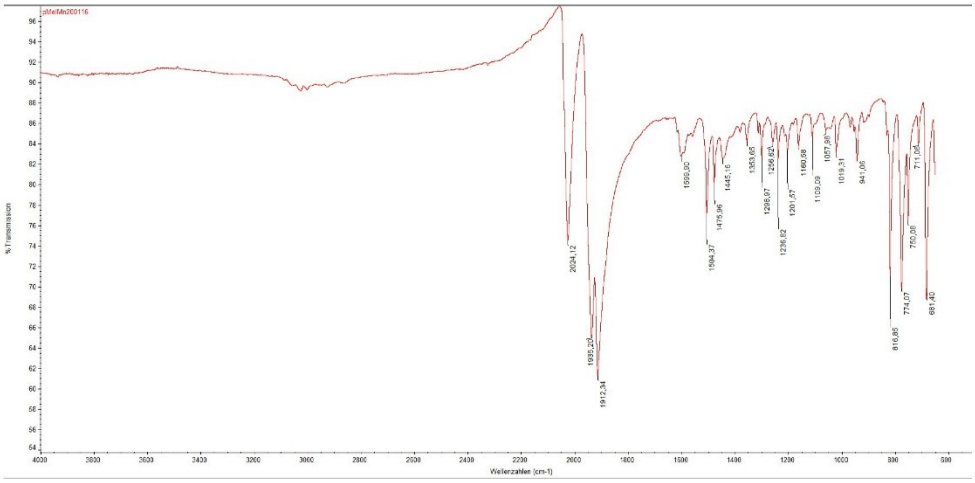

Figure 8S. IR spectrum (FT-IR) of [Mn(*impy*)$(CO)_3$Br] (**1**).

Complex [Mn(*ampy*)(CO)$_3$Br] (**2**)

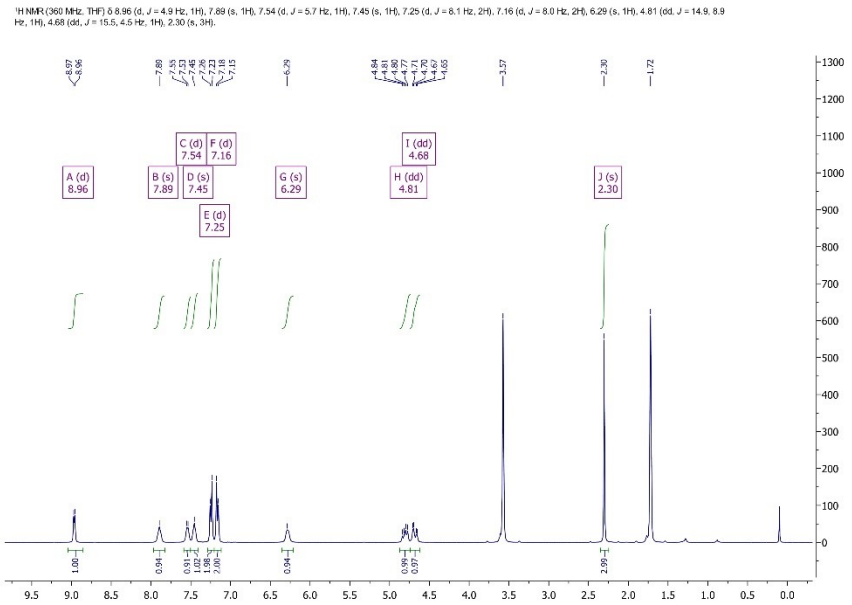

Figure 9S. ^{1}H NMR [360 MHz, THF-d$_8$, 298 K] spectrum of [Mn(*ampy*)(CO)$_3$Br] (**2**).

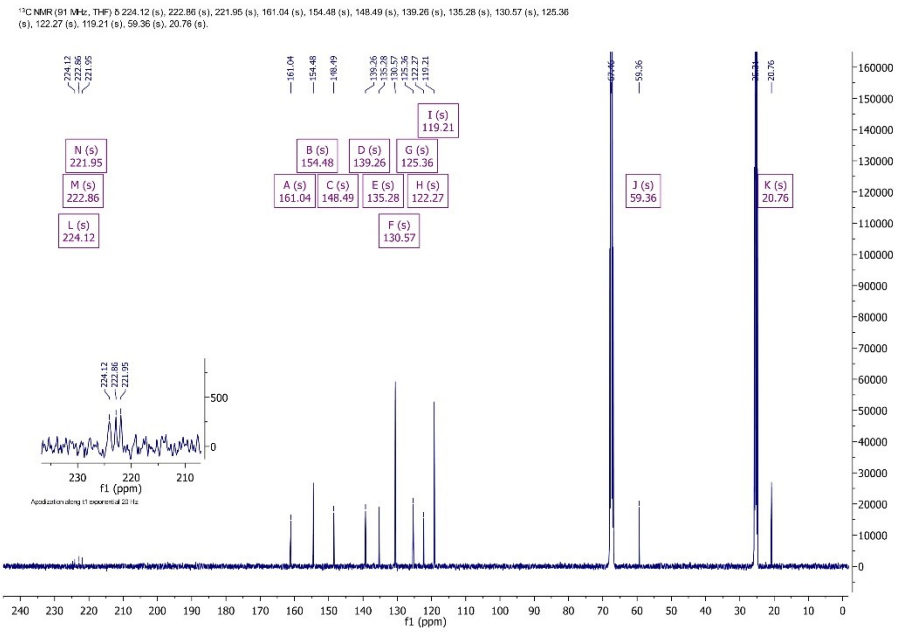

Figure 10S. ^{13}C{^{1}H} NMR [91 MHz, THF-d$_8$, 298 K] spectrum of [Mn(*ampy*)(CO)$_3$Br] (**2**).

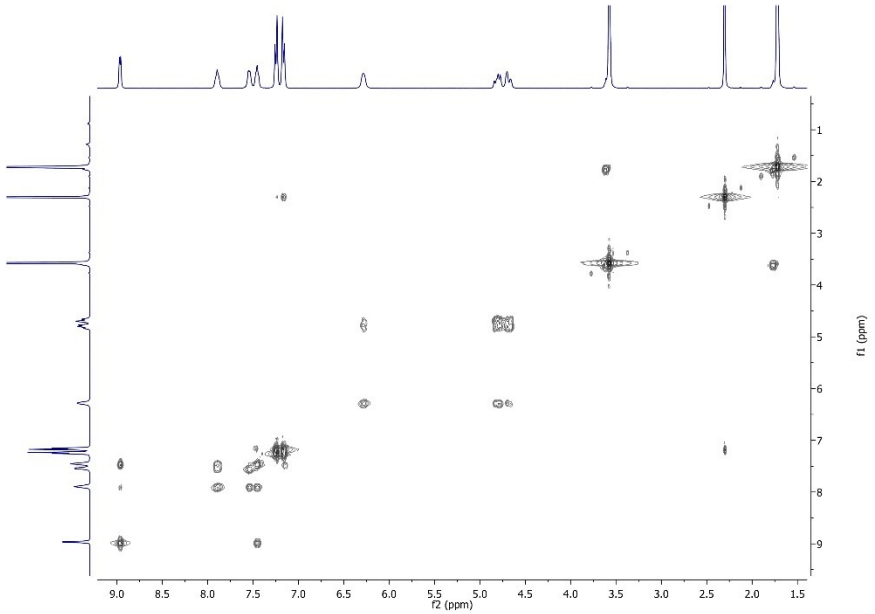

Figure 11S. $^{1}H^{1}H$ COSY NMR [360 MHz, THF-d_8, 298 K] spectrum of [Mn(*ampy*)$(CO)_3$Br] (**2**).

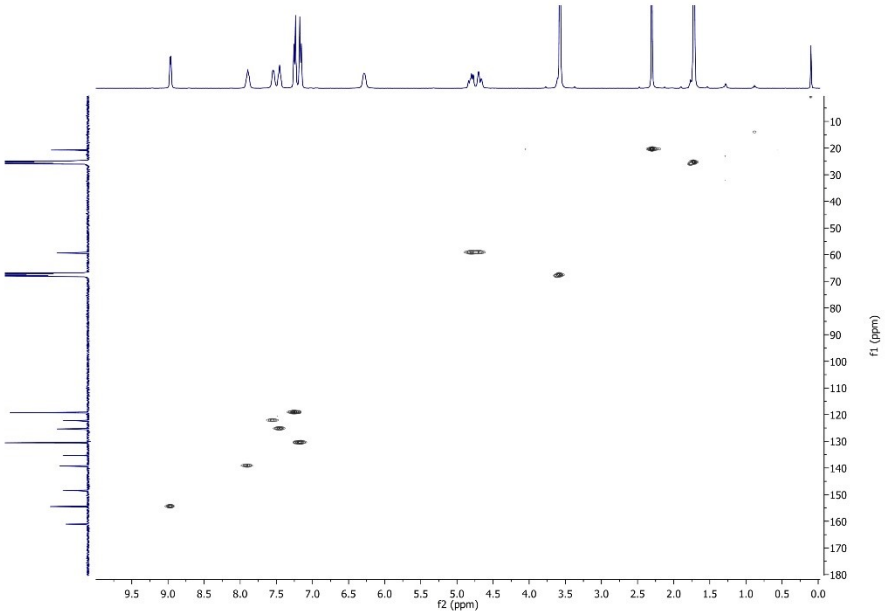

Figure 12S. $^{1}H^{13}C$ HSQC NMR [360 MHz/91 MHz, THF-d_8, 298 K] spectrum of [Mn(*ampy*)$(CO)_3$Br] (**2**).

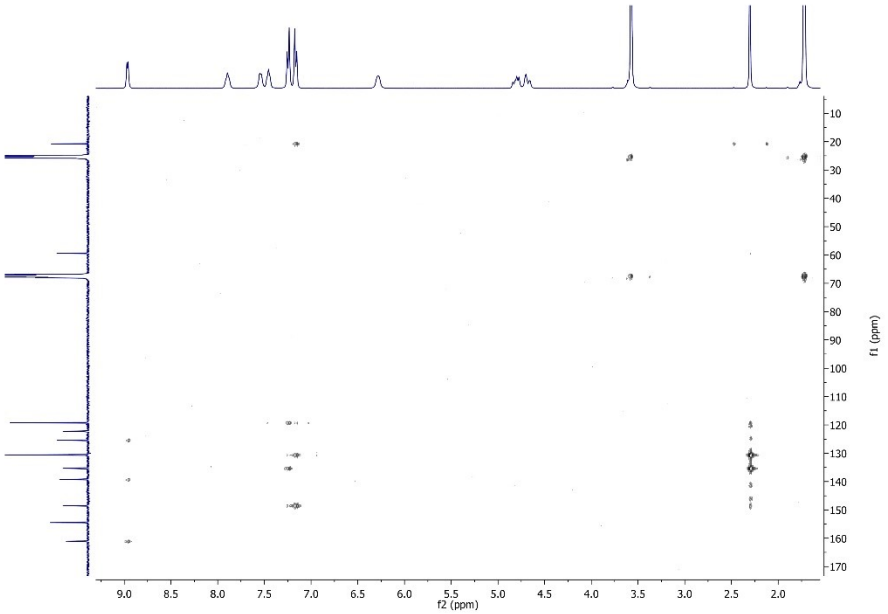

Figure 13S. $^{1}H^{13}C$ HMBC NMR [360 MHz/91 MHz, THF-d_8, 298 K] spectrum of [Mn(*ampy*)$(CO)_3$Br] (**2**).

pMeAMnBr_DCM_EtOH_5#52-72 RT: 0.41-0.57 AV: 21
T: FTMS + c ESI Full ms [150.00-1000.00]
m/z= 210.0000-480.0000

m/z	Intensity	Relative	Composition
219.08924	9858258.0	15.62	$C_{13}H_{12}N_2Na$
221.10483	17269042.0	27.36	$C_{13}H_{14}N_2Na$
252.00899	3329012.8	5.27	$C_{12}H_9ON_2Mn$
253.05309	63113680.0	100.00	$C_{13}H_{14}N_2Mn$
254.05634	8680236.0	13.75	$C_{16}H_9ONNa$
266.02452	4610783.5	7.31	$C_{13}H_{11}ON_2Mn$
267.03227	36146904.0	57.27	$C_{13}H_{12}ON_2Mn$
268.03553	4996351.0	7.92	$C_{16}H_7O_2NNa$
285.04287	31399888.0	49.75	$C_{13}H_{14}O_2N_2Mn$
286.04606	4301380.5	6.82	$C_{16}H_9O_3NNa$
337.03781	16001477.0	25.35	$C_{16}H_{14}O_3N_2Mn$
394.99642	10035292.0	15.90	
438.94578	3296287.0	5.22	$C_{16}H_{14}O_3N_2BrMnNa$
440.94373	3165667.0	5.02	$C_{16}H_{14}O_3N_2{}^{81}BrMnNa$

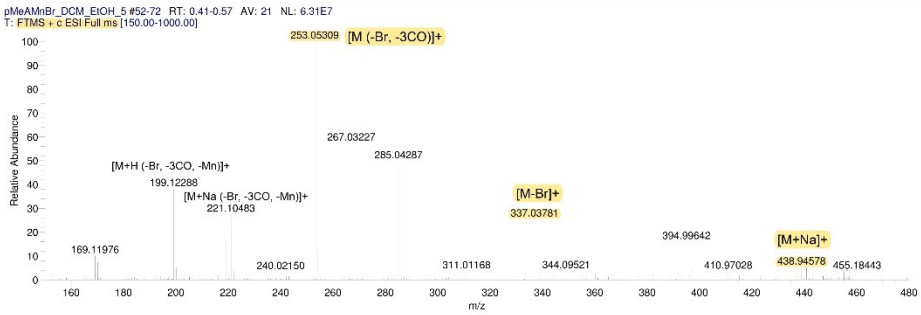

Figure 14S. HRMS-ESI pos CH_2Cl_2/C_2H_5OH spectrum of [Mn(*ampy*)$(CO)_3$Br] (**2**).

pMeAMnBr_DCM_EtOH_1#817 RT: 8.40
T: FTMS + c ESI Full ms2 438.95@cid12.00 [200.00-500.00]

m/z	Intensity	Relative	Composition
201.03342	11534.3	2.96	$C_{15}H_5O$
221.10545	195609.4	50.14	$C_{13}H_{14}N_2Na$
253.05377	245969.0	63.05	$C_{13}H_{14}N_2Mn$
253.56429	12540.3	3.21	
258.79724	9825.4	2.52	
265.89893	34030.2	8.72	$C_6H_7ONBrMnNa$
310.54031	9604.3	2.46	
337.03888	58673.1	15.04	$C_{16}H_{14}O_3N_2Mn$
345.33334	12682.4	3.25	
354.96213	390144.4	100.00	$C_{13}H_{14}N_2BrMnNa$
361.33020	9646.2	2.47	
366.37375	10961.4	2.81	
438.94690	75249.9	19.29	$C_{16}H_{14}O_3N_2BrMnNa$
440.85226	15598.6	4.00	

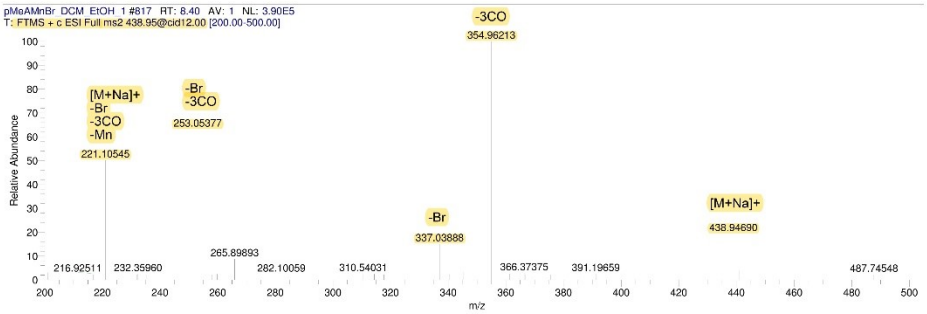

Figure 15S. HRMS^2-ESI pos CH_2Cl_2/C_2H_5OH spectrum of m/z 438.95@cid12.

pMeAMn_DCM_MeOH_FA#527 RT: 4.69
T: FTMS + c ESI Full ms2 337.04@cid2.00 [90.00-490.00]

m/z	Intensity	Relative	Composition
253.05267	40258.4	100.00	$C_{13}H_{14}N_2Mn$
337.03726	14649.1	36.39	$C_{16}H_{14}O_3N_2Mn$

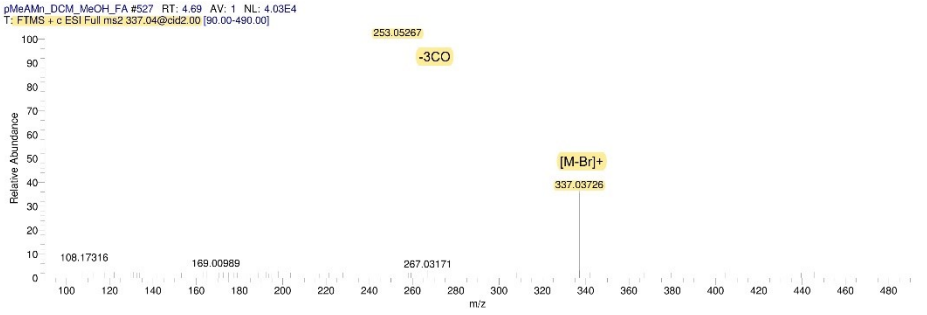

Figure 16S. HRMS^2-ESI pos CH_2Cl_2/CH_3OH spectrum of m/z 337.04@cid2.

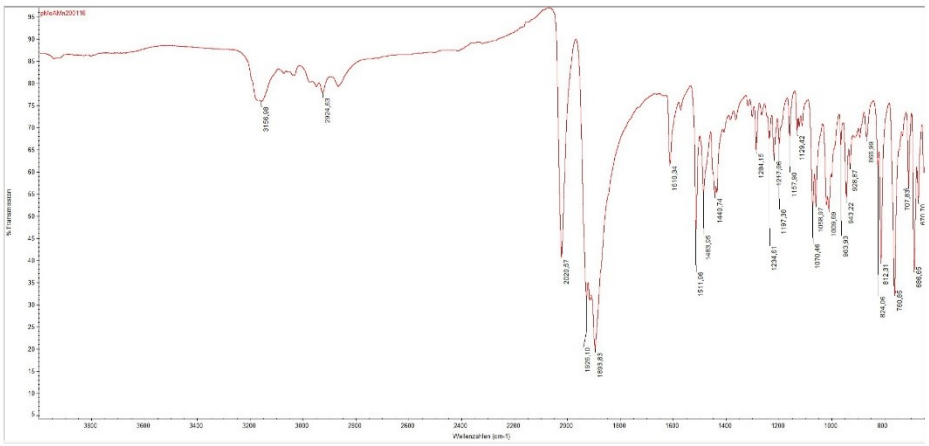

Figure 17S. IR spectrum (FT-IR) of [Mn(*ampy*)$(CO)_3$Br] (**2**).

Complex K[Mn(*amidopy**)$(CO)_3$Br] (**3-K**) (reduction with potassium)

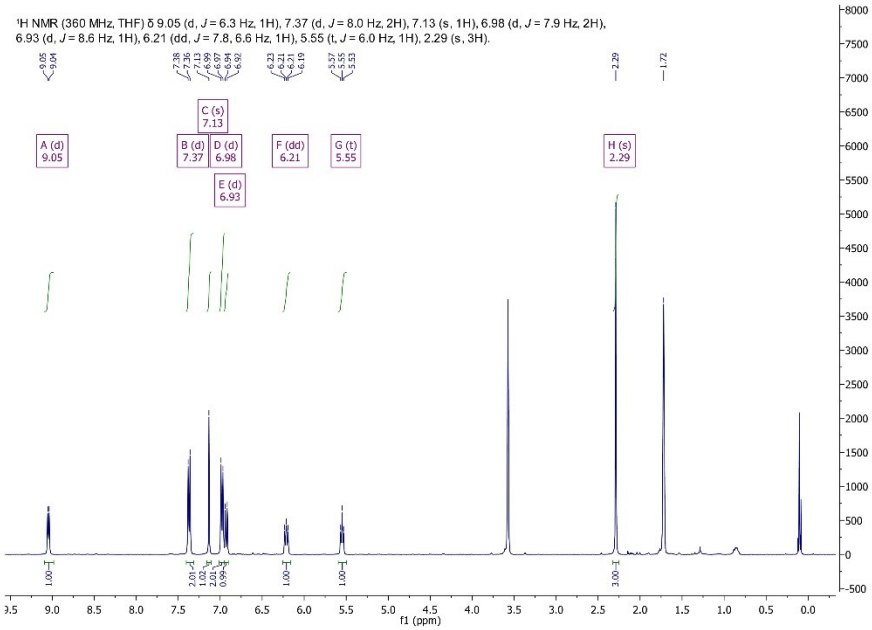

Figure 18S. ^{1}H NMR [360 MHz, THF-d_8, 298 K] spectrum of K[Mn(*amidopy**)$(CO)_3$Br] (**3-K**).

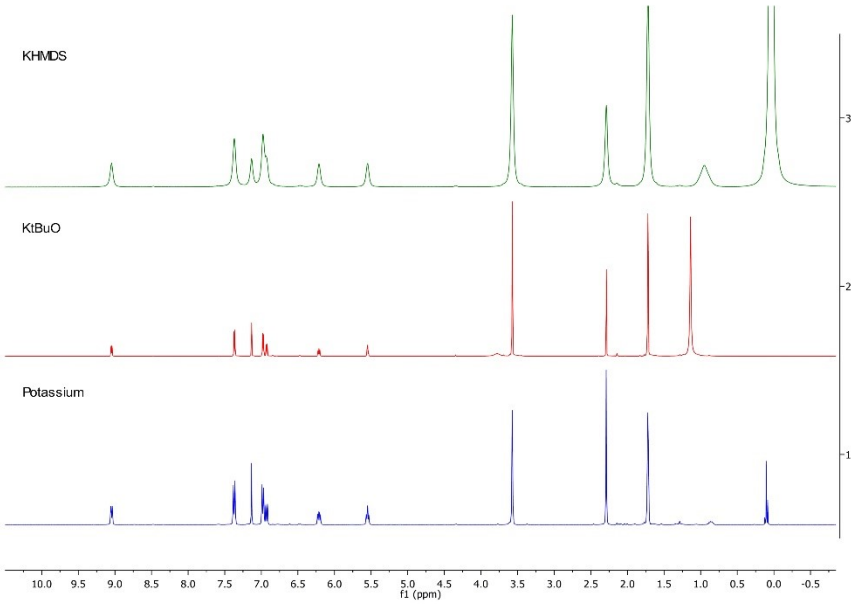

Figure 19S. ^{1}H NMR [360 MHz, THF-d_8, 298 K] spectrum of K[Mn(*amidopy**)$(CO)_3$Br] (**3-K**). Reduction with Potassium (blue), deprotonation with KtBuO (red) and KHMDS (green).

^{13}C NMR (91 MHz,THF-d_8) δ 235.14, 159.51, 154.34, 145.01, 131.33, 128.73, 127.76, 125.48, 122.81, 120.46, 105.10, 20.99.

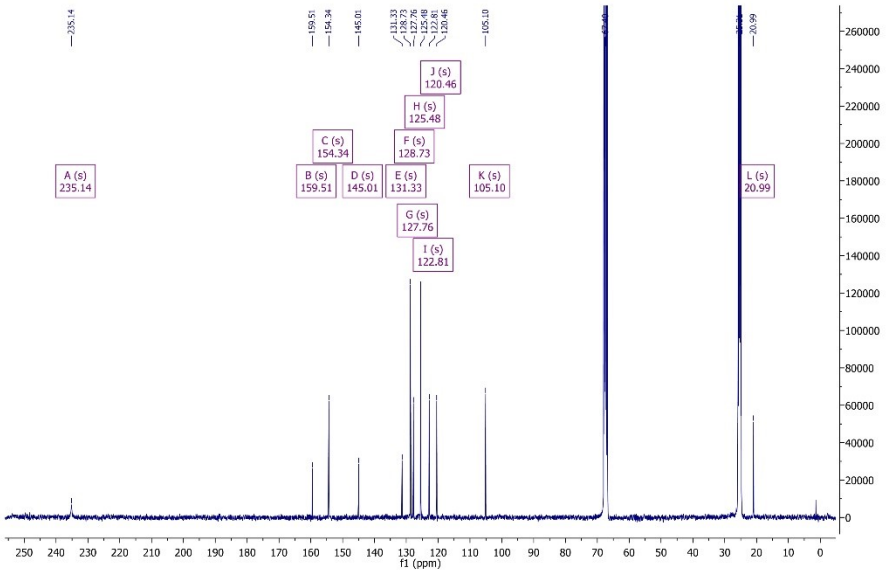

Figure 20S. $^{13}C\{^1H\}$ NMR [91 MHz, THF-d_8, 298 K] spectrum of K[Mn(*amidopy**)$(CO)_3$Br] (**3-K**).

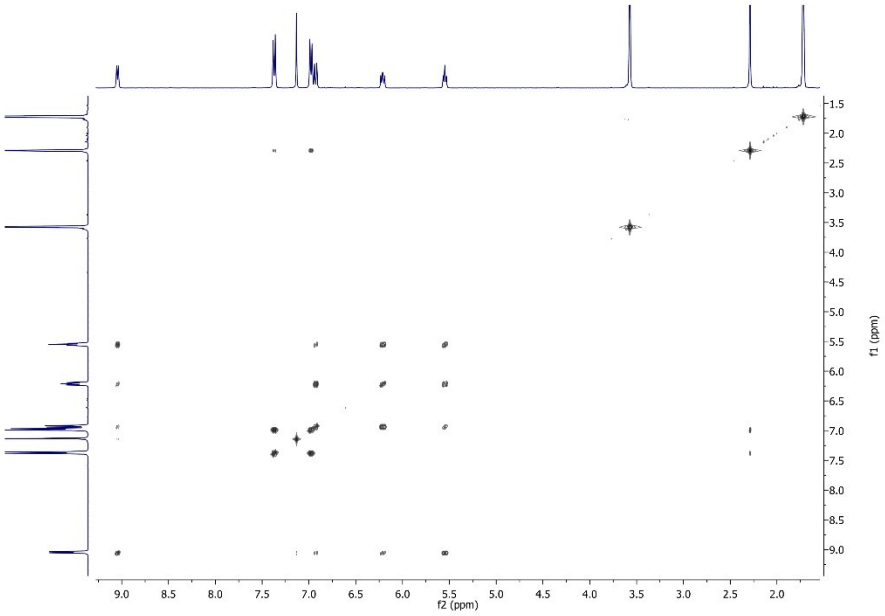

Figure 21S. $^1H^1H$ COSY NMR [360 MHz, THF-d_8, 298 K] spectrum of K[Mn(*amidopy**)$(CO)_3$Br] (**3-K**).

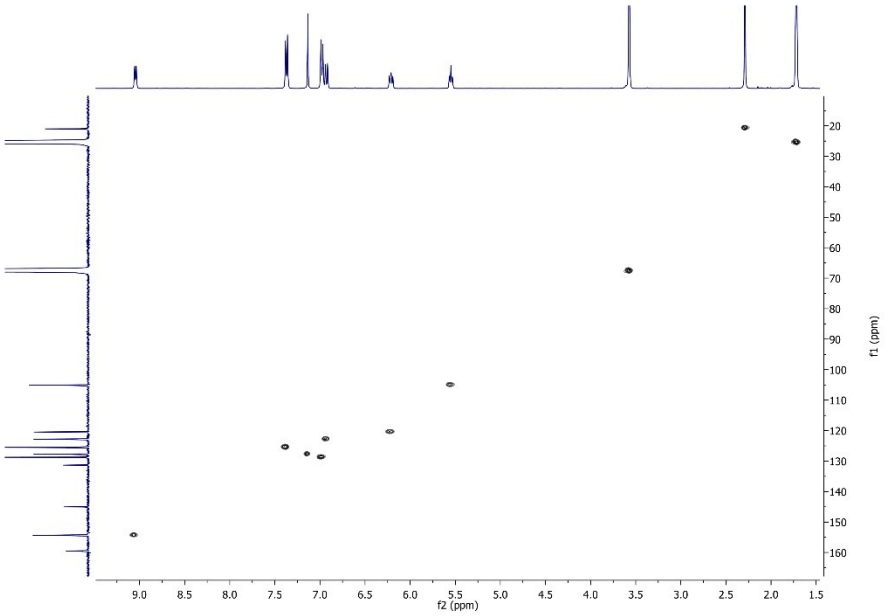

Figure 22S. $^{1}H^{13}C$ HSQC NMR [360 MHz/91 MHz, THF-d_8, 298 K] spectrum of K[Mn(*amidopy**)$(CO)_3$Br] (**3-K**).

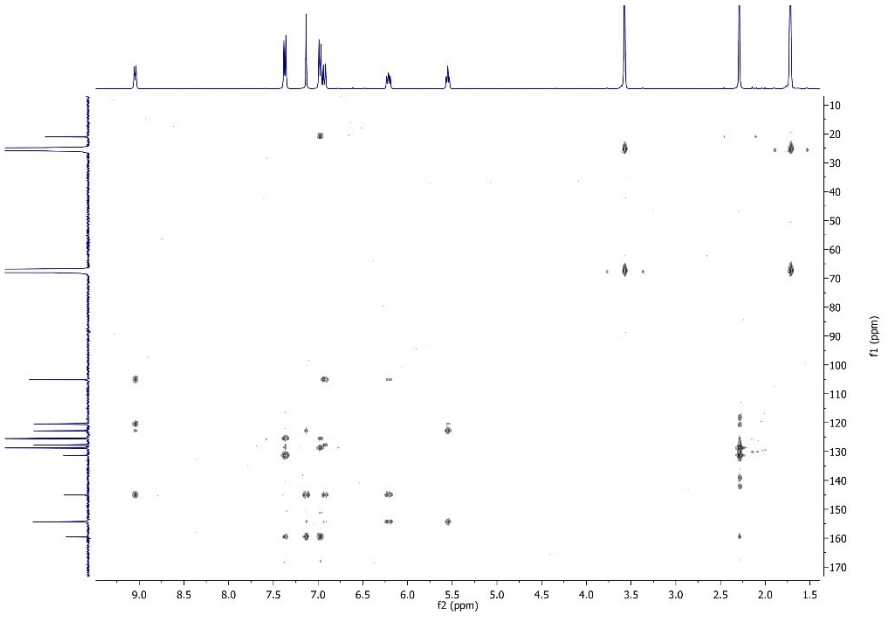

Figure 23S. $^{1}H^{13}C$ HMBC NMR [360 MHz/91 MHz, THF-d_8, 298 K] spectrum of K[Mn(*amidopy**)$(CO)_3$Br] (**3-K**).

Complex K[Mn(*amidopy**)$(CO)_3$Br] (**3-Na**) (reduction with sodium)

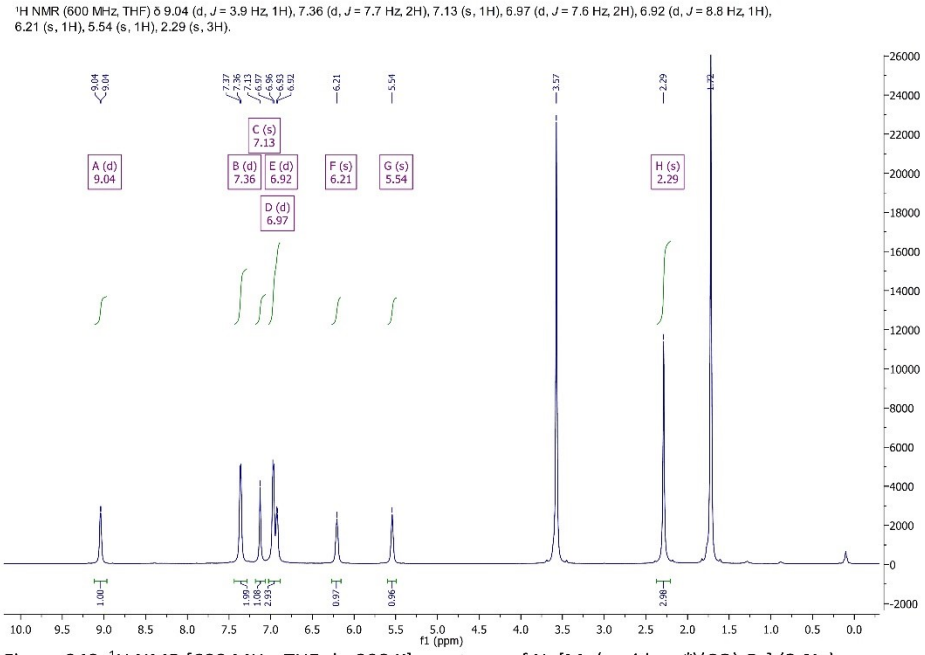

Figure 24S. ^{1}H NMR [600 MHz, THF-d_8, 298 K] spectrum of Na[Mn(*amidopy**)$(CO)_3$Br] (**3-Na**).

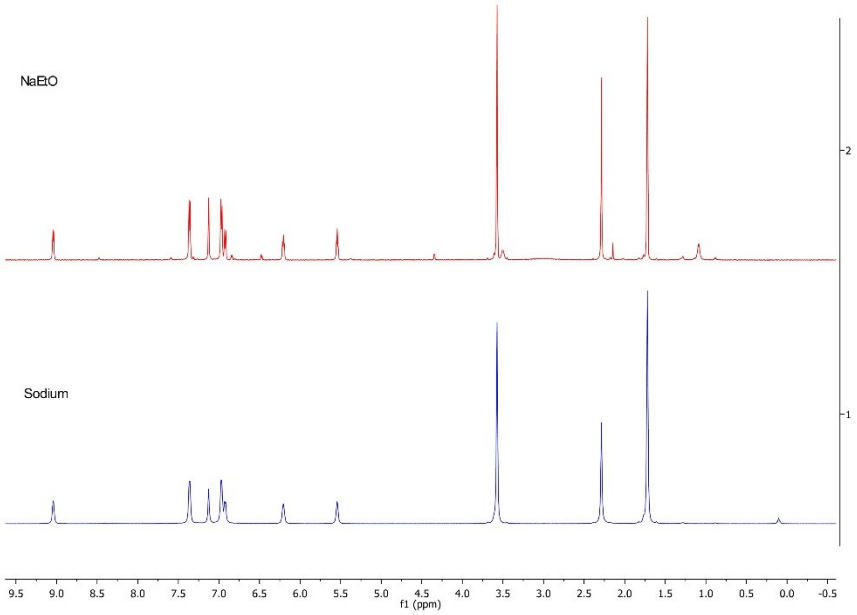

Figure 25S. ^{1}H NMR [360 MHz, THF-d_8, 298 K] spectrum of Na[Mn(*amidopy**)$(CO)_3$Br] (**3-Na**). Reduction with Sodium (blue) and deprotonation with NaEtO (red).

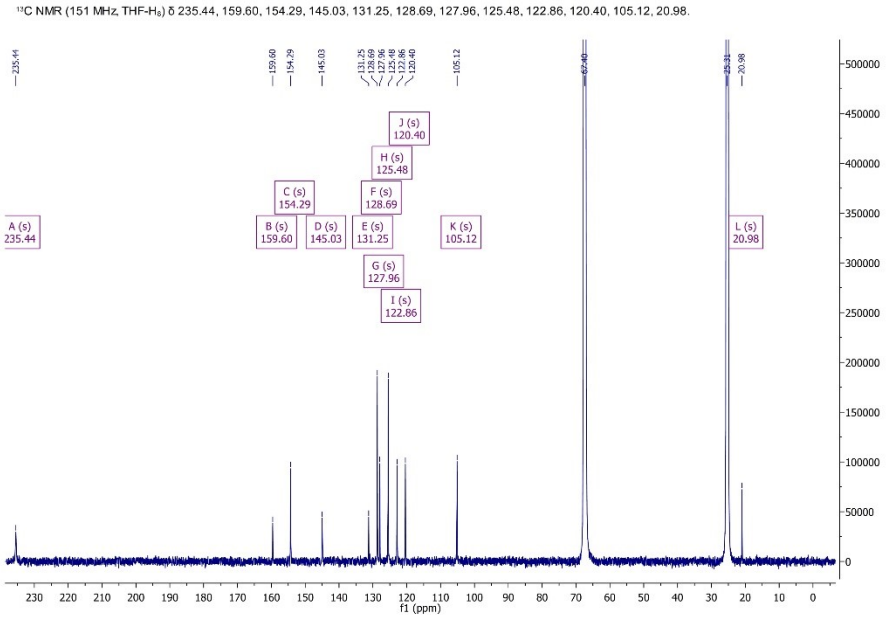

Figure 26S. $^{13}C\{^{1}H\}$ NMR [151 MHz, THF-d_8, 298 K] spectrum of Na[Mn(*amidopy**)$(CO)_3$Br] (**3-Na**).

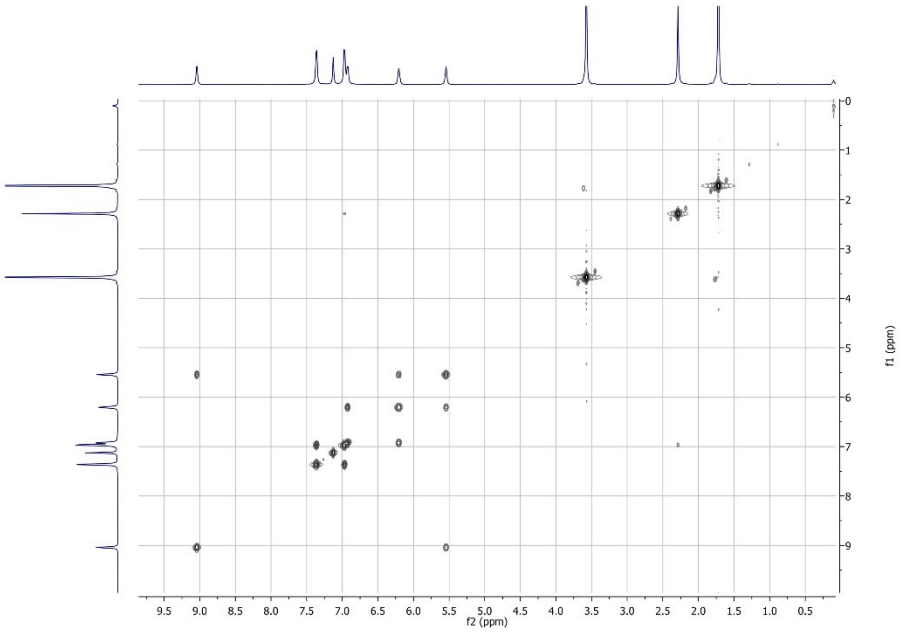

Figure 27S. $^{1}H^{1}H$ COSY NMR [600 MHz, THF-d_8, 298 K] spectrum of Na[Mn(*amidopy**)$(CO)_3$Br] (**3-Na**).

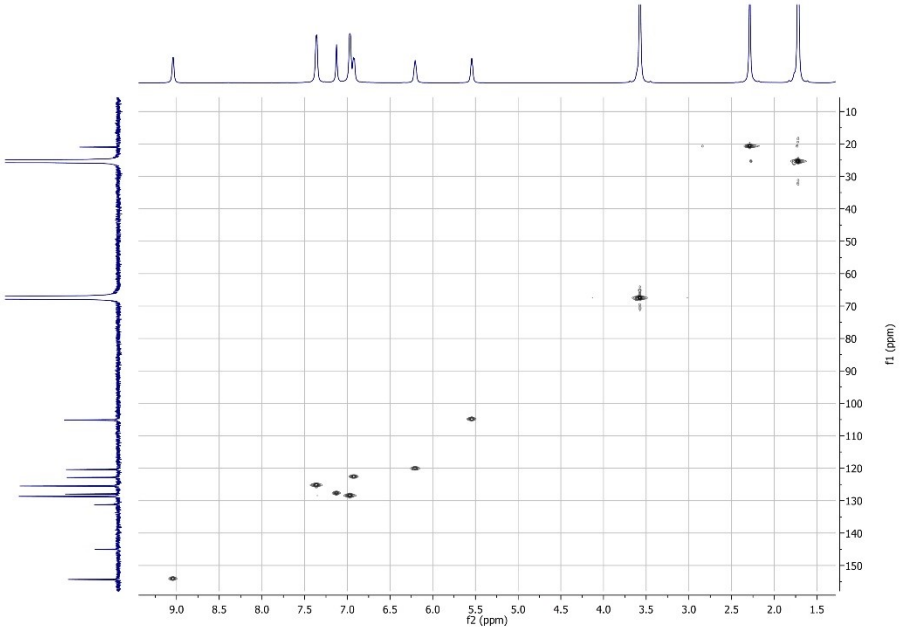

Figure 28S. $^{1}H^{13}C$ HSQC NMR [600 MHz/151 MHz, THF-d_8, 298 K] spectrum of Na[Mn(*amidopy**)$(CO)_3$Br] (**3-Na**).

Complex K[Mn(*amidopy**)(CO)$_3$Br] (**3-Li**) (deprotonation with LiHMDS)

^{1}H NMR (360 MHz, THF) δ 9.02 (d, *J* = 6.4 Hz, 1H), 7.38 (d, *J* = 8.0 Hz, 2H), 7.10 (s, 1H), 6.96 (d, *J* = 8.0 Hz, 2H), 6.88 (d, *J* = 8.6 Hz, 1H), 6.16 (dd, *J* = 7.6, 6.8 Hz, 1H), 5.50 (t, *J* = 6.1 Hz, 1H), 2.28 (s, 3H).

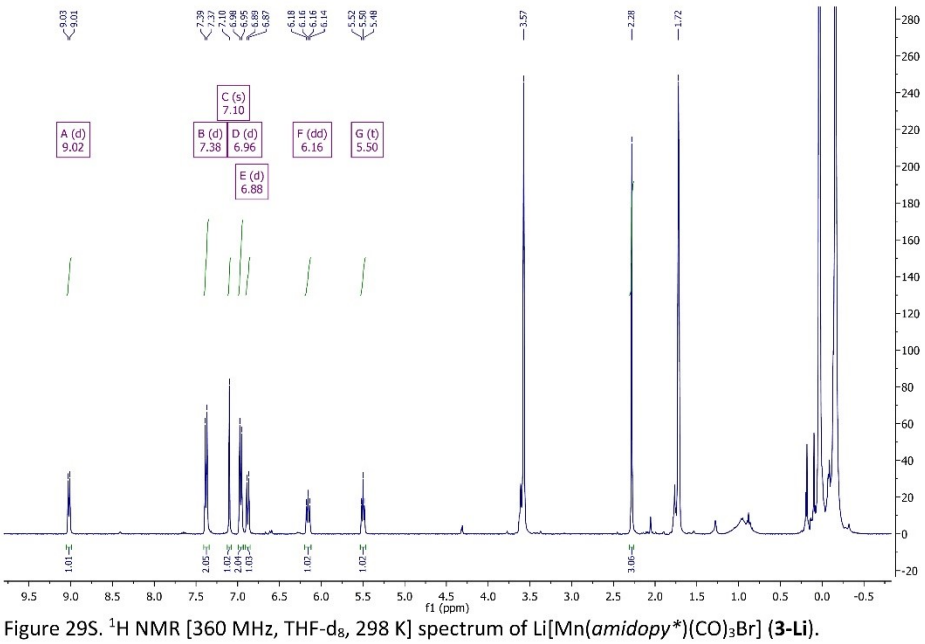

Figure 29S. ^{1}H NMR [360 MHz, THF-d$_8$, 298 K] spectrum of Li[Mn(*amidopy**)(CO)$_3$Br] (**3-Li**).

^{13}C NMR (91 MHz, THF) δ 234.75 (s), 159.56 (s), 154.40 (s), 144.80 (s), 131.01 (s), 128.70 (s), 127.09 (s), 125.51 (s), 122.65 (s), 120.10 (s), 104.68 (s), 21.01 (s).

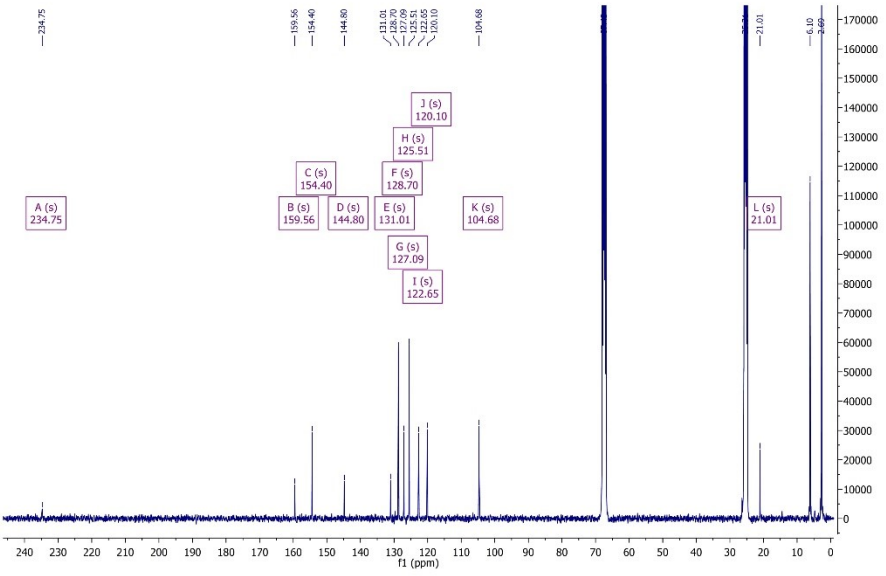

Figure 30S. ^{13}C{^{1}H} NMR [91 MHz, THF-d$_8$, 298 K] spectrum of Na[Mn(*amidopy**)(CO)$_3$Br] (**3-Li**).

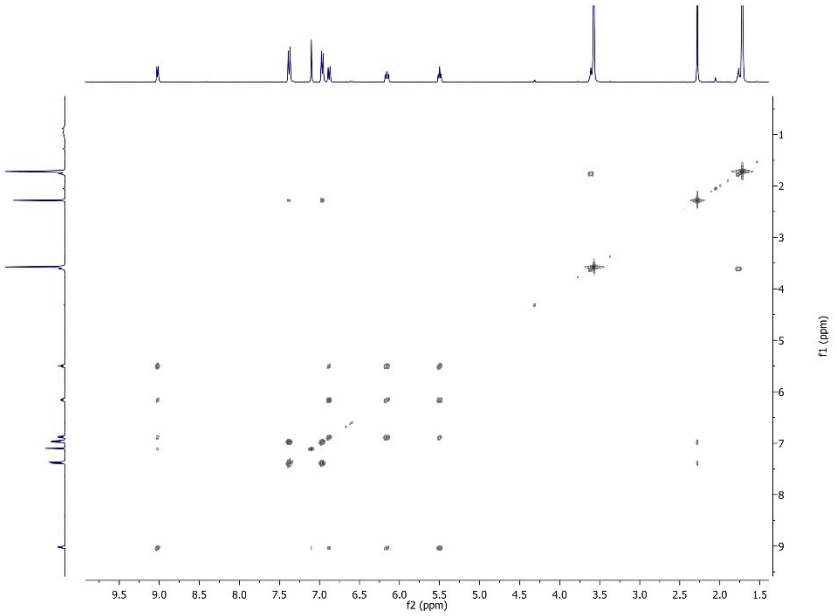

Figure 31S. $^{1}H^{1}H$ COSY NMR [360 MHz, THF-d_8, 298 K] spectrum of Li[Mn(*amidopy**)$(CO)_3$Br] (**3-Li**).

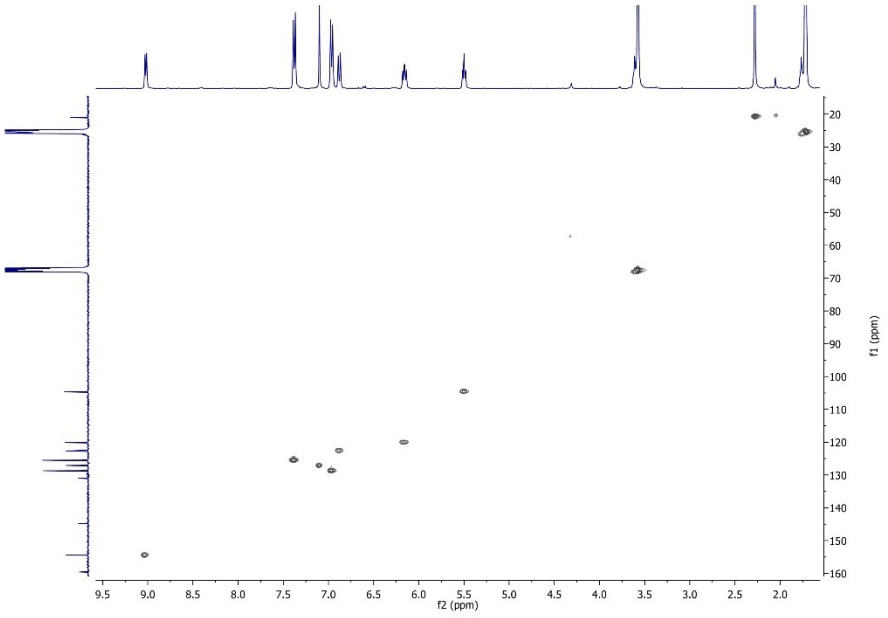

Figure 32S. $^{1}H^{13}C$ HSQC NMR [360 MHz/91 MHz, THF-d_8, 298 K] spectrum of Li[Mn(*amidopy**)$(CO)_3$Br] (**3-Li**).

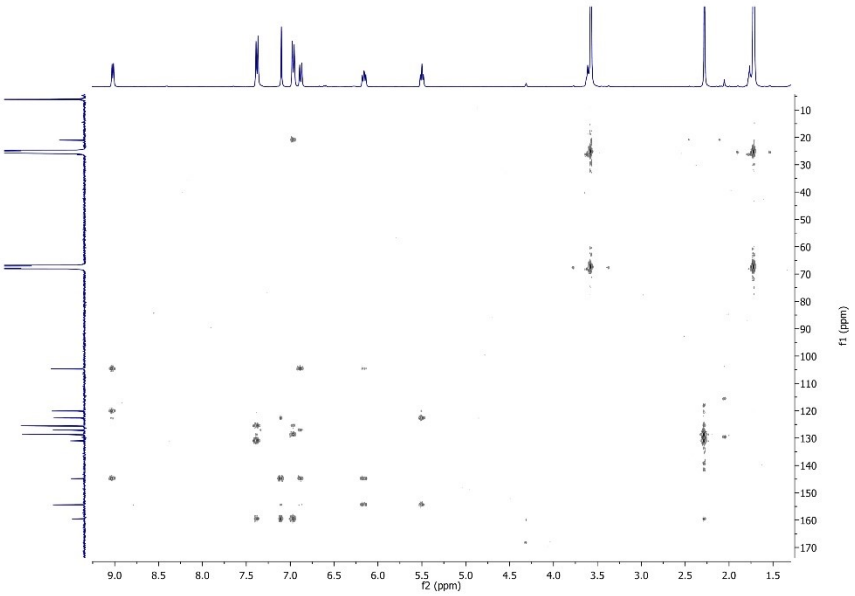

Figure 33S. $^{1}H^{13}C$ HMBC NMR [360 MHz/91 MHz, THF-d_8, 298 K] spectrum of Li[Mn(*amidopy**)$(CO)_3$Br] (**3-Li**).

Complex *fac*-K[Mn(*amidopy-COO*)(CO)$_3$] (**4-K**)

^{1}H NMR (360 MHz, THF-d_8) δ 8.86 (d, *J* = 4.5 Hz, 1H), 7.69 (t, *J* = 6.6 Hz, 1H), 7.60 (d, *J* = 7.6 Hz, 1H), 7.18 (t, *J* = 6.4 Hz, 1H), 6.60 (d, *J* = 7.8 Hz, 2H), 6.52 (d, *J* = 7.3 Hz, 2H), 4.81 (s, 1H), 2.05 (s, 3H).

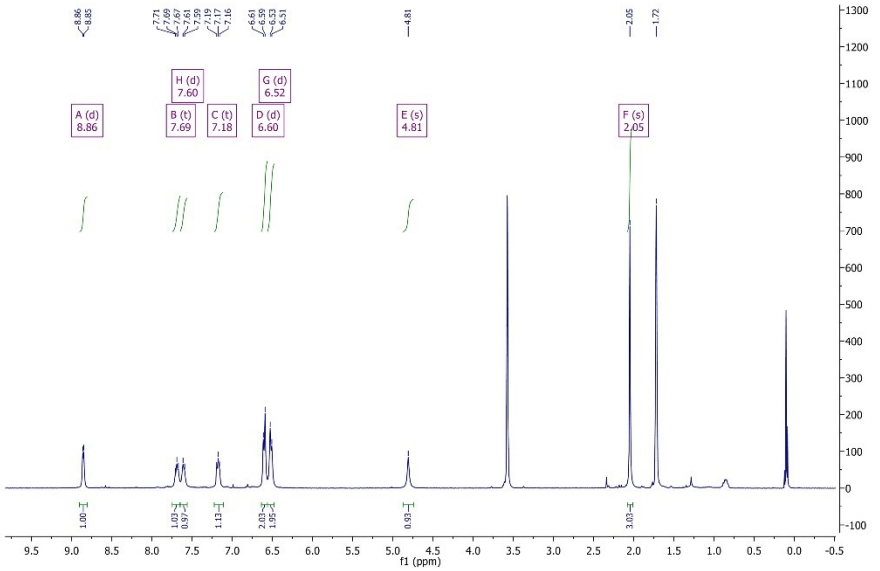

Figure 34S. ^{1}H NMR [360 MHz, THF-d_8, 298 K] spectrum of *fac*-K[Mn(*amidopy-COO*)(CO)$_3$] (**4-K**).

^{13}C NMR (91 MHz, THF-d_8) δ 227.52 (s), 227.14 (s), 221.35 (s), 182.38 (s), 166.91 (s), 159.41 (s), 153.13 (s), 137.96 (s), 129.35 (s), 125.88 (s), 122.29 (s), 122.00 (s), 119.81 (s), 115.52 (s), 75.95 (s), 20.61 (s).

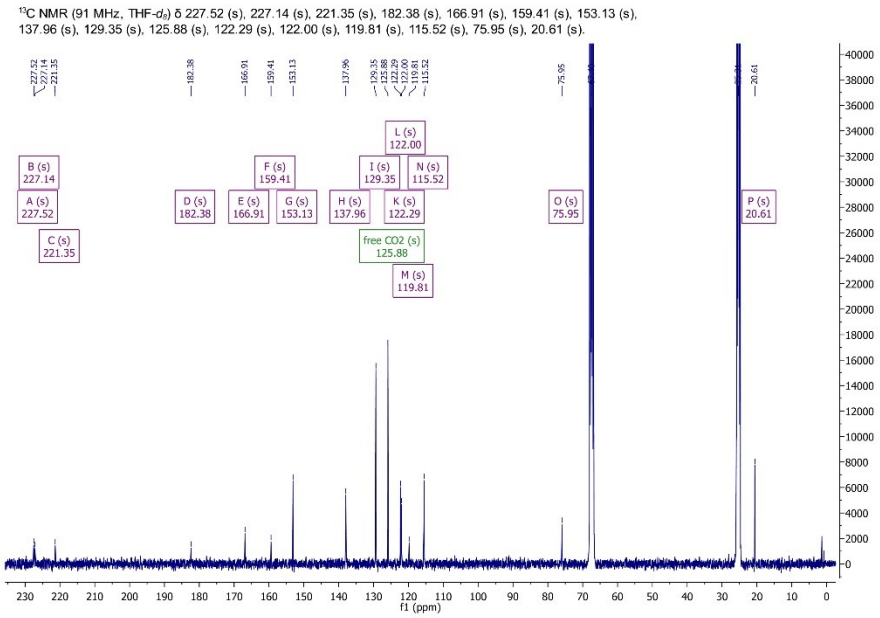

Figure 35S. ^{13}C{^{1}H} NMR [91 MHz, THF-d_8, 298 K] spectrum of *fac*-K[Mn(*amidopy-COO*)(CO)$_3$] (**4-K**).

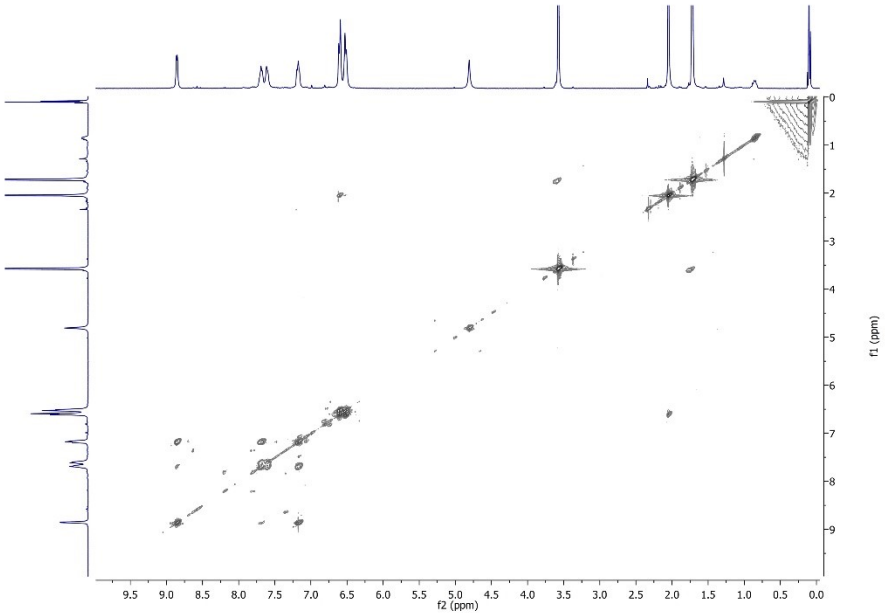

Figure 36S. $^{1}H^{1}H$ COSY NMR [360 MHz, THF-d_8, 298 K] spectrum of *fac*-K[Mn(*amidopy-COO*)$(CO)_3$] (**4-K**).

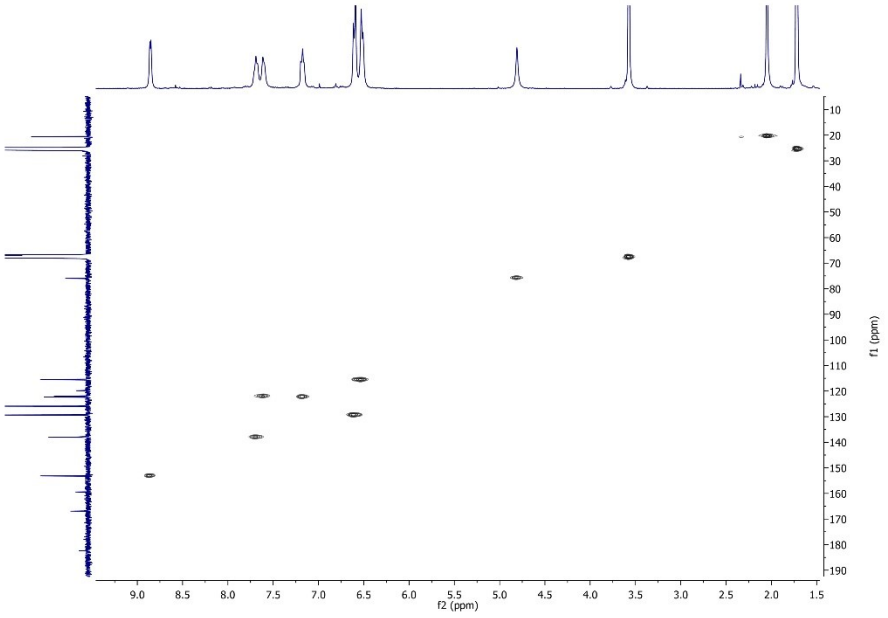

Figure 37S. $^{1}H^{13}C$ HSQC NMR [360 MHz/91 MHz, THF-d_8, 298 K] spectrum of *fac*-K[Mn(*amidopy-COO*)$(CO)_3$] (**4-K**).

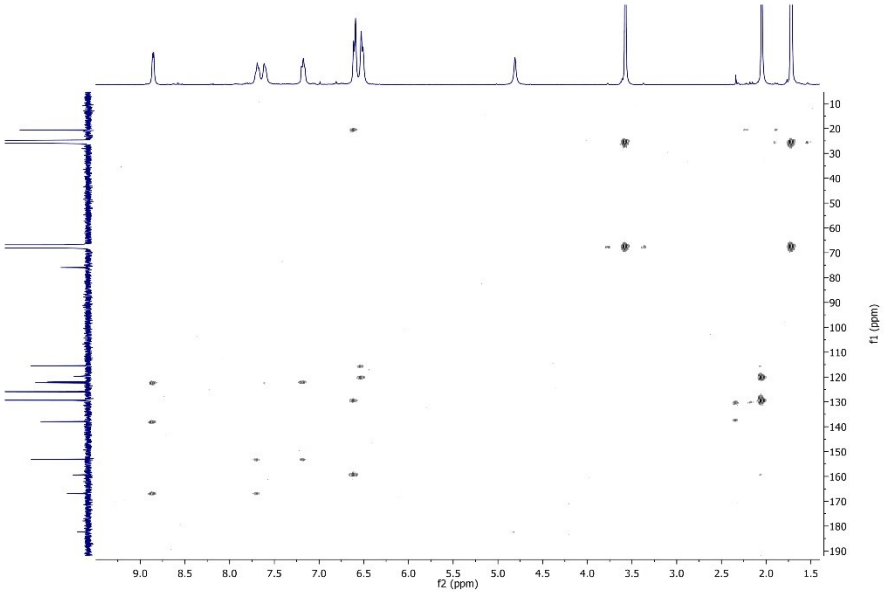

Figure 38S. $^{1}H^{13}C$ HMBC NMR [360 MHz/91 MHz, THF-d_8, 298 K] spectrum of *fac*-K[Mn(*amidopy-COO*)$(CO)_3$] (**4-K**).

Complex *fac*-Na[Mn(*amidopy-COO*)$(CO)_3$] (**4-Na**)

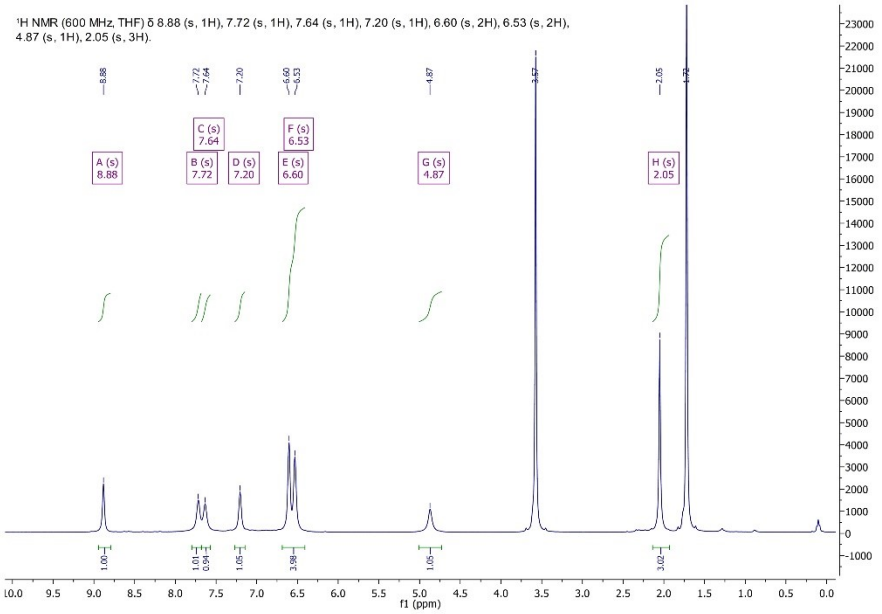

Figure 39S. ^{1}H NMR [600 MHz, THF-d_8, 298 K] spectrum of *fac*-Na[Mn(*amidopy-COO*)$(CO)_3$] (**4-Na**).

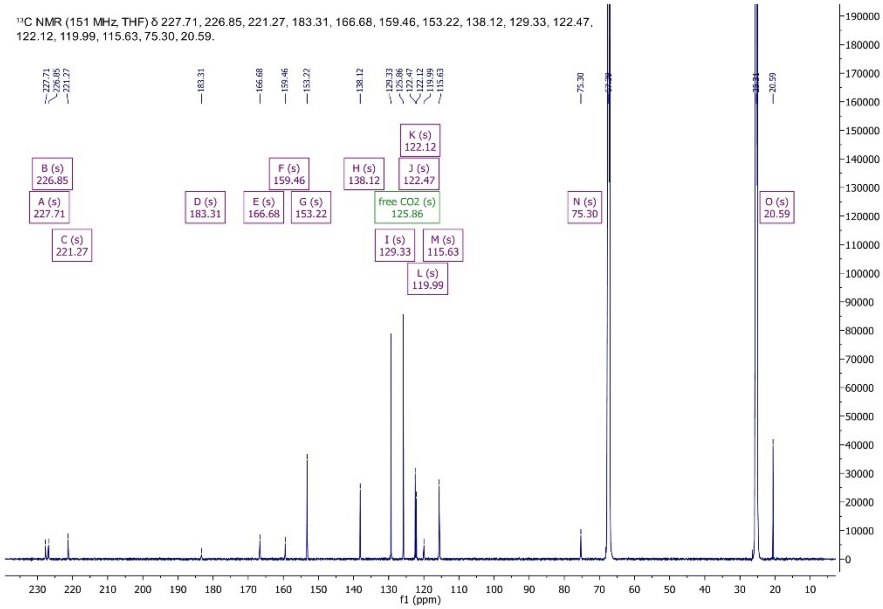

Figure 40S. $^{13}C\{^1H\}$ NMR [151 MHz, THF-d_8, 298 K] spectrum of *fac*-Na[Mn(*amidopy-COO*)$(CO)_3$] (**4-Na**).

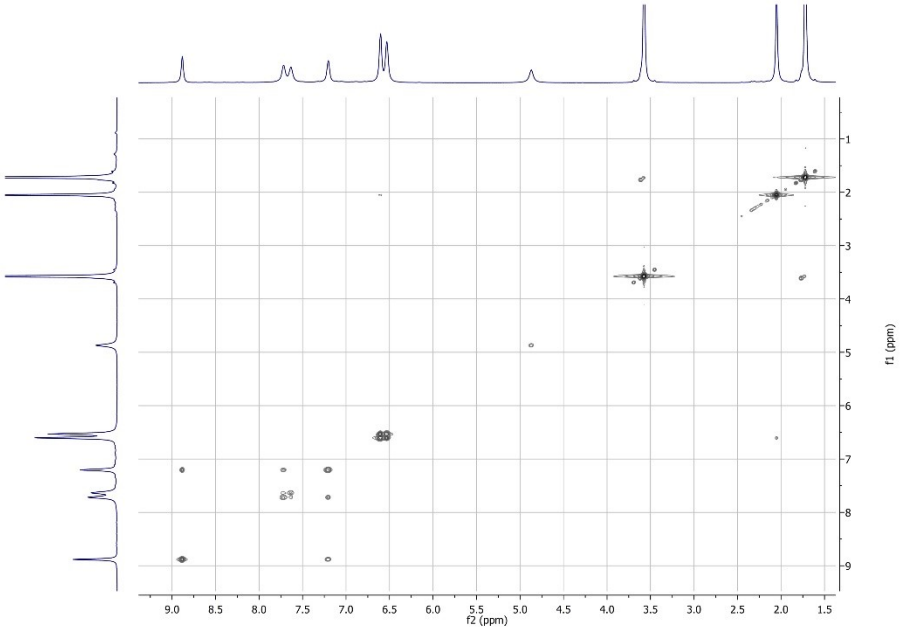

Figure 41S. $^{1}H^{1}H$ COSY NMR [600 MHz, THF-d_8, 298 K] spectrum of *fac*-Na[Mn(*amidopy-COO*)$(CO)_3$] (**4-Na**).

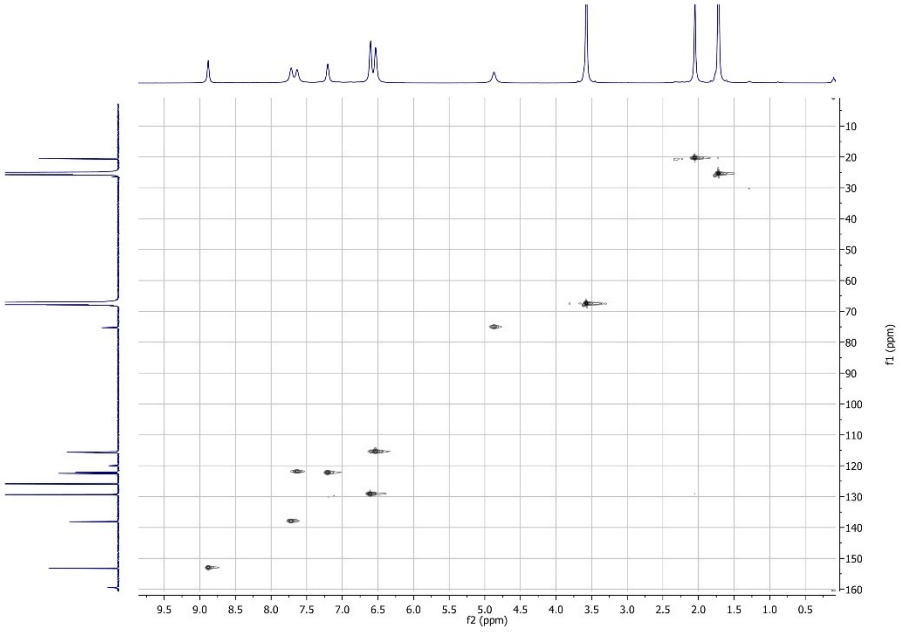

Figure 42S. $^{1}H^{13}C$ HSQC NMR [600 MHz/151 MHz, THF-d_8, 298 K] spectrum of *fac*-Na[Mn(*amidopy-COO*)$(CO)_3$] (**4-Na**).

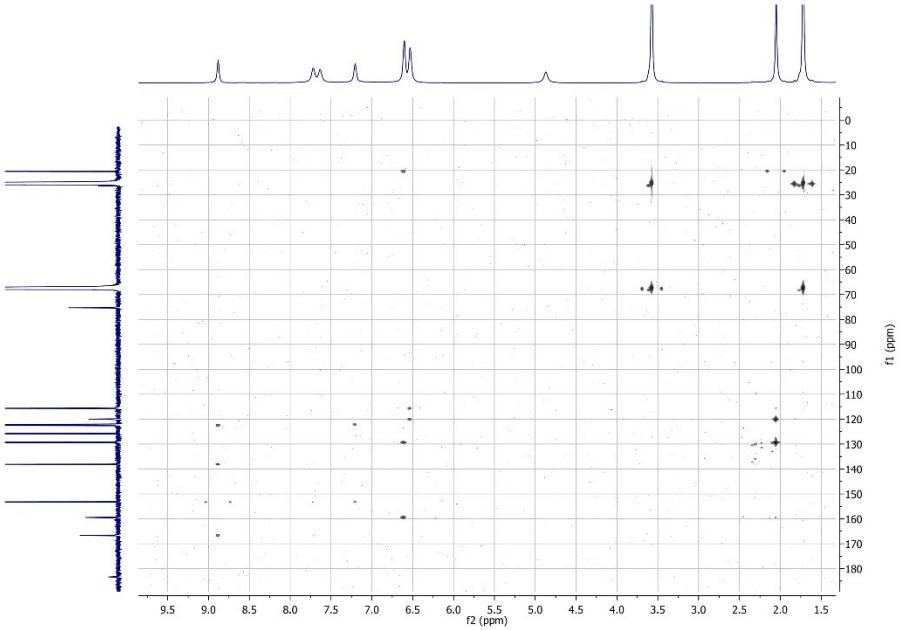

Figure 43S. $^{1}H^{13}C$ HMBC NMR [600 MHz/151 MHz, THF-d_8, 298 K] spectrum of *fac*-Na[Mn(*amidopy-COO*)$(CO)_3$] (**4-Na**).

Complex *fac*-K[Mn(*amidopy*-^{13}COO)(CO)$_3$] (**4-K-^{13}CO$_2$**)

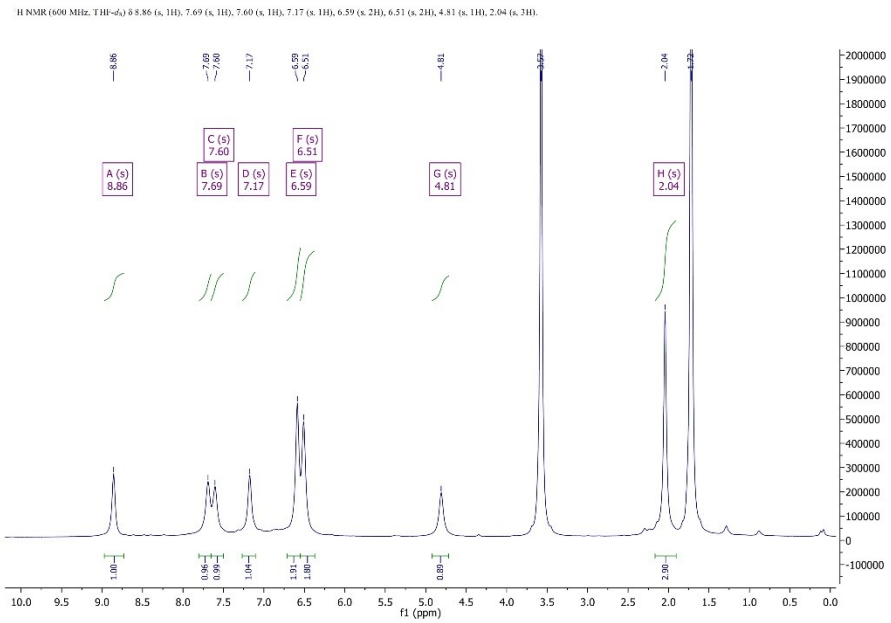

Figure 44S. ^{1}H NMR [600 MHz, THF-d$_8$, 298 K] spectrum of *fac*-K[Mn(*amidopy*-^{13}COO)(CO)$_3$] (**4-K-^{13}CO$_2$**).

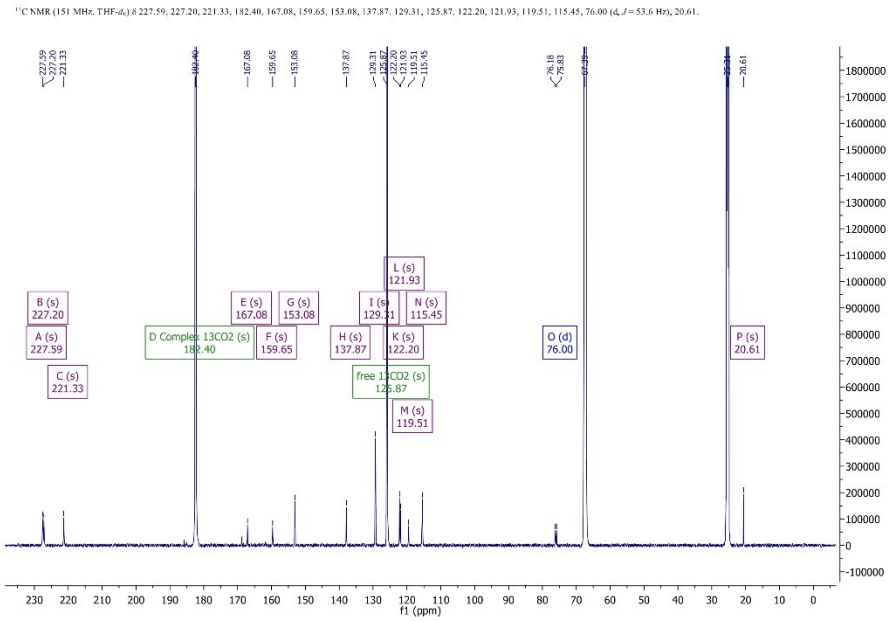

Figure 45S. ^{13}C{^{1}H} NMR [151 MHz, THF-d$_8$, 298 K] spectrum of *fac*-K[Mn(*amidopy*-^{13}COO)(CO)$_3$] (**4-K-^{13}CO$_2$**).

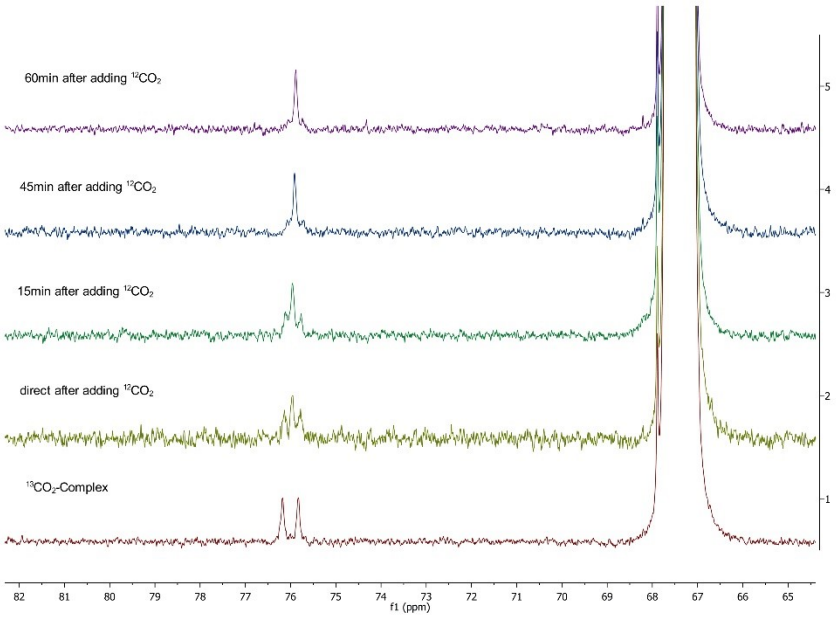

Figure 46S. $^{13}C\{^1H\}$ NMR [151 MHz, THF-d_8, 298 K] spectrum of *fac*-K[Mn(*amidopy*-^{13}COO)(CO)$_3$] (**4-K-$^{13}CO_2$**) with 1 bar CO_2 time lapse.

fac-Na[Mn(*amidopy*-^{13}COO)(CO)$_3$] (**4-Na-^{13}CO$_2$**)

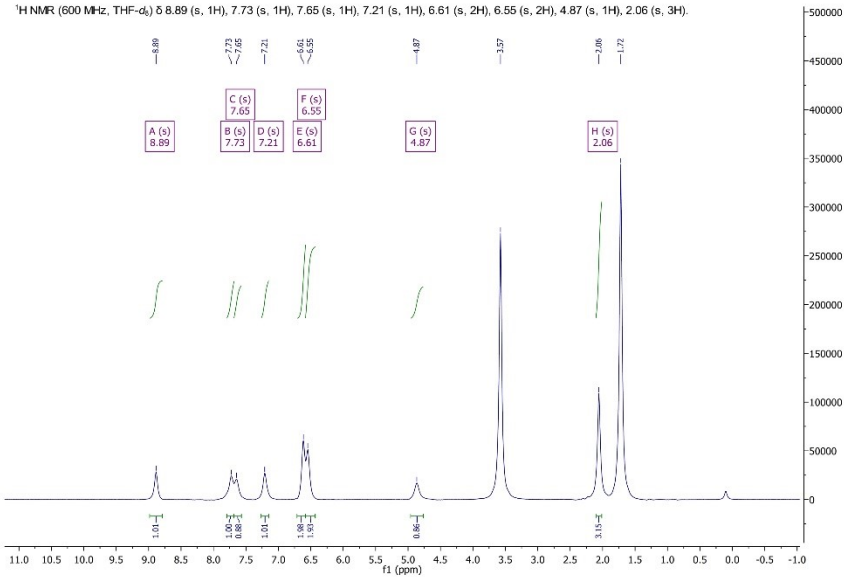

Figure 47S. ^{1}H NMR [600 MHz, THF-d_8, 298 K] spectrum of *fac*-Na[Mn(*amidopy*-^{13}COO)(CO)$_3$] (**4-Na-^{13}CO$_2$**).

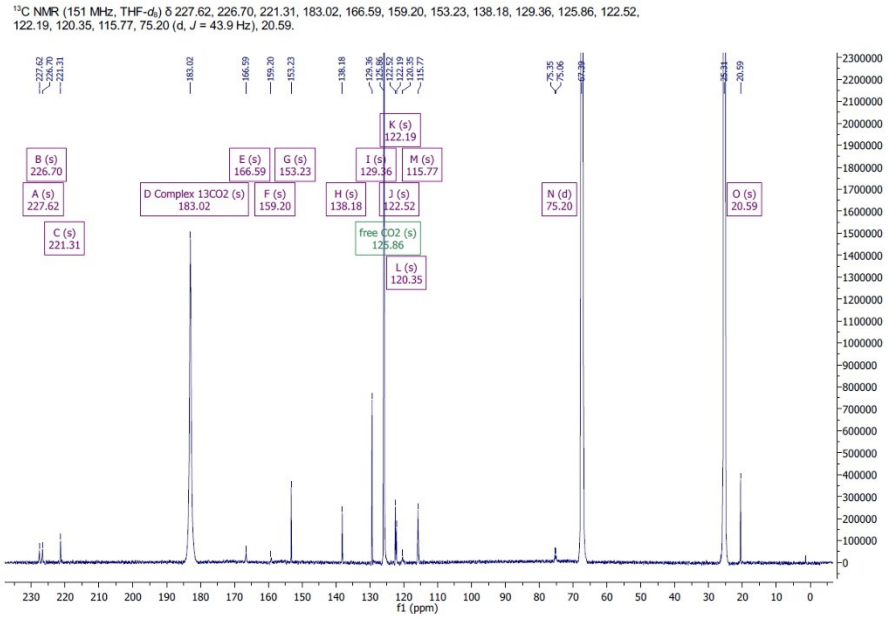

Figure 48S. ^{13}C{^{1}H} NMR [151 MHz, THF-d_8, 298 K] spectrum of *fac*-Na[Mn(*amidopy*-^{13}COO)(CO)$_3$] (**4-Na-^{13}CO$_2$**).

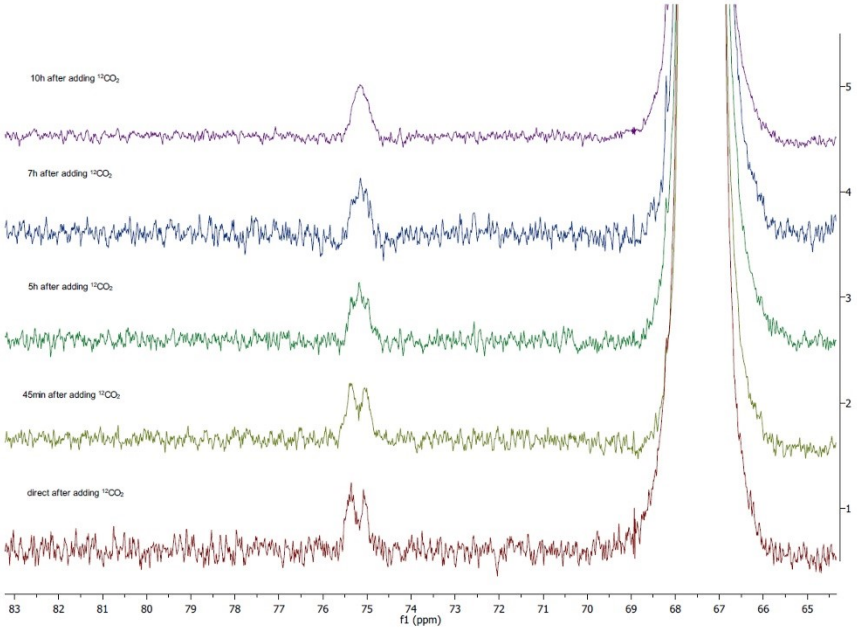

Figure 49S. $^{13}C\{^1H\}$ NMR [151 MHz, THF-d_8, 298 K] spectrum of *fac*-Na[Mn(*amidopy*-^{13}COO)(CO)$_3$] (**4-Na-$^{13}CO_2$**) with 1 bar CO_2 time lapse.

Complex *fac*-[K(18-crown-6)][Mn(*amidopy-COO*)(CO)$_3$] (**4-K-crown**)

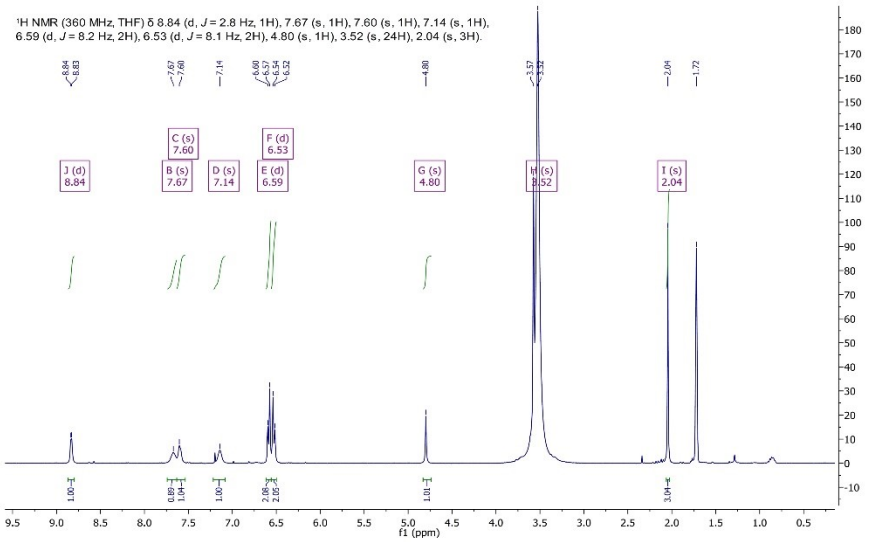

Figure 50S. ^{1}H NMR [360 MHz, THF-d$_8$, 298 K] spectrum of *fac*-[K(18-crown-6)][Mn(*amidopy-COO*)(CO)$_3$] (**4-K-crown**).

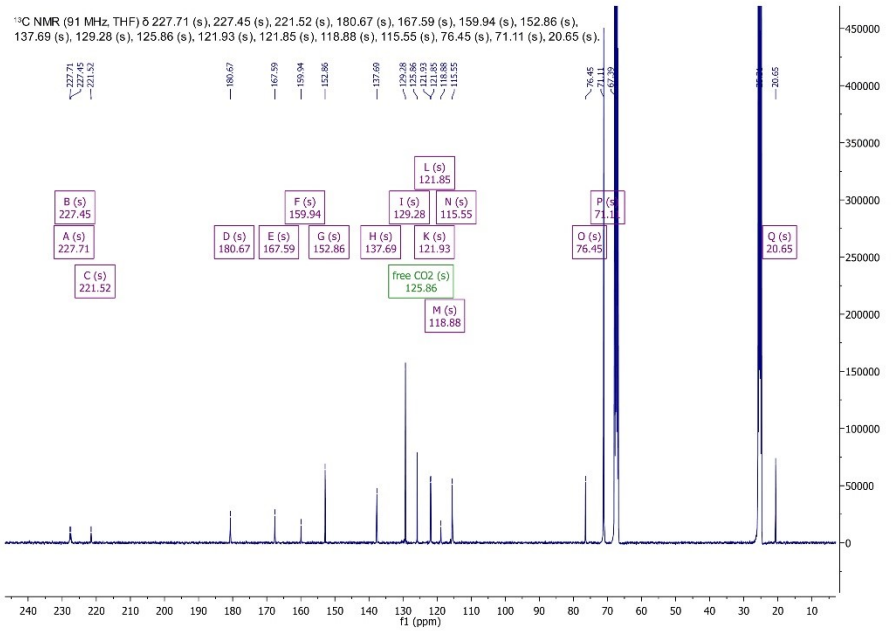

Figure 51S. ^{13}C{^{1}H} NMR [91 MHz, THF-d$_8$, 298 K] spectrum of *fac*-[K(18-crown-6)][Mn(*amidopy-COO*)(CO)$_3$] (**4-K-crown**).

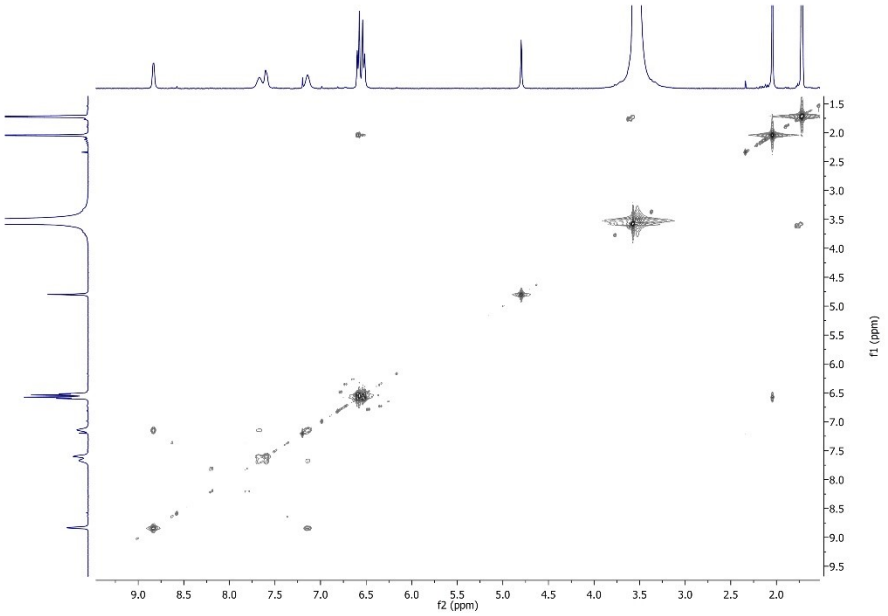

Figure 52S. $^{1}H^{1}H$ COSY NMR [360 MHz, THF-d_8, 298 K] spectrum of *fac*-[K(18-crown-6)][Mn(*amidopy-COO*)$(CO)_3$] (**4-K-crown**).

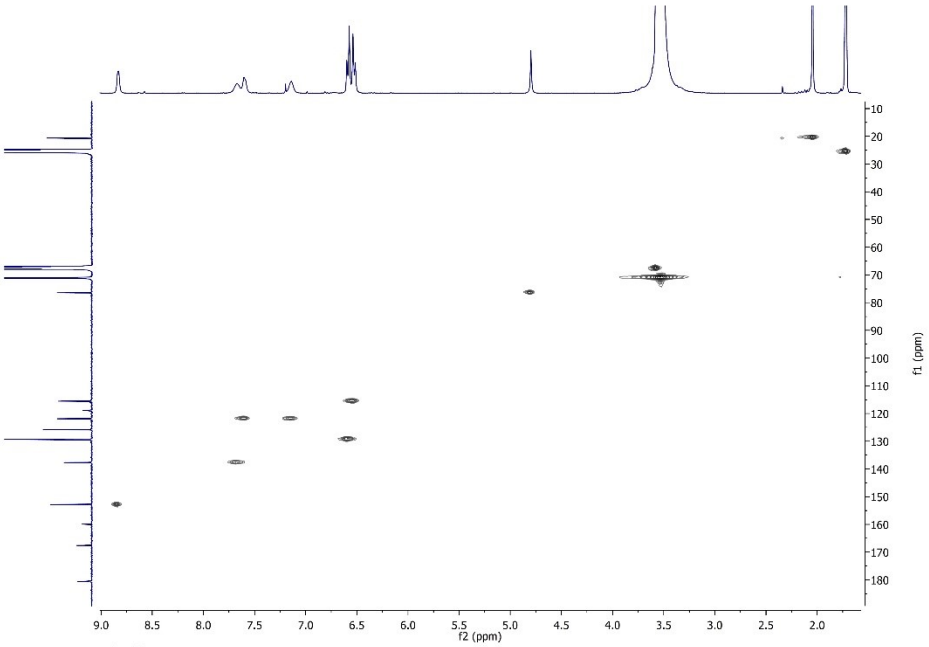

Figure 53S. $^{1}H^{13}C$ HSQC NMR [360 MHz/91 MHz, THF-d_8, 298 K] spectrum of *fac*-[K(18-crown-6)][Mn(*amidopy-COO*)$(CO)_3$] (**4-K-crown**).

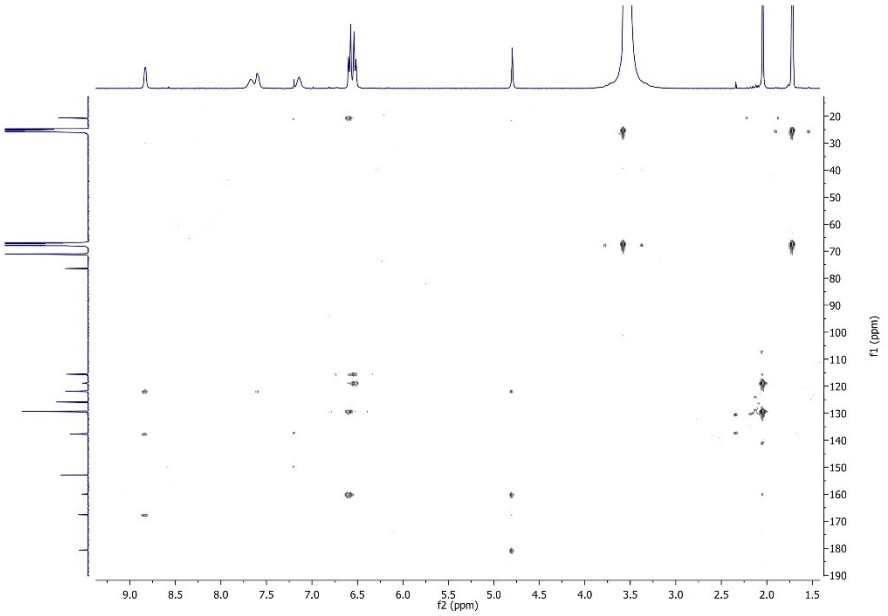

Figure 54S. $^{1}H^{13}C$ HMBC NMR [360 MHz/91 MHz, THF-d_8, 298 K] spectrum of *fac*-[K(18-crown-6)][Mn(*amidopy-COO*)$(CO)_3$] (**4-K-crown**).

pMeIMn-K-CO2-18K6_DCM_EtOH_1_20021915442l#255 RT: 2.45
T: FTMS - c ESI Full ms [320.00-500.00]

m/z	Intensity	Relative	Composition
332.98569	322756.4	2.06	
335.02368	15647588.0	100.00	$C_{16}H_{12}O_3N_2Mn$
336.02707	2582992.5	16.51	$C_{14}H_{14}O_3N_2MnNa$
365.03461	390267.3	2.49	$C_{17}H_{14}O_4N_2Mn$
377.03476	284987.4	1.82	$C_{13}H_{21}O_3N_3Mn_2$
379.01395	307924.0	1.97	$C_{15}H_{15}O_3N_3KMn$
384.98004	440099.7	2.81	$C_{14}H_{15}O_4N_2Mn_2$
403.02707	323326.3	2.07	$C_{15}H_{21}O_4N_2Mn_2$
414.99081	935653.5	5.98	$C_{13}H_{20}O_3N_3KMn_2$
419.04532	292922.0	1.87	$C_{15}H_{23}O_4N_3Mn_2$

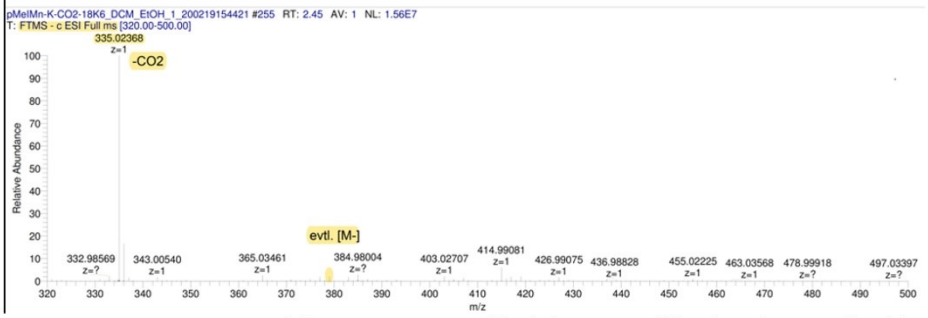

Figure 55S. HRMS-ESI neg CH_2Cl_2/C_2H_5OH spectrum of *fac*-[K(18-crown-6)][Mn(*amidopy-COO*)$(CO)_3$] (**4-K-crown**).

pMeIMn-K-CO2-18K6_DCM_EtOH_1_200219154421#357 RT: 4.31
T: FTMS - c ESI Full ms2 335.02@cid25.00 [90.00-500.00]
m/z= 100.0000-400.0000

m/z	Intensity	Relative	Composition
175.99152	4018.5	0.69	C_7H_7ONMn
251.03847	579438.7	100.00	$C_{13}H_{12}N_2Mn$
251.04765	4163.0	0.72	$C_9H_{14}O_2N_3Mn$
335.02307	216979.8	37.45	$C_{16}H_{12}O_3N_2Mn$
336.02625	4510.3	0.78	$C_{16}H_{13}O_3N_2Mn$

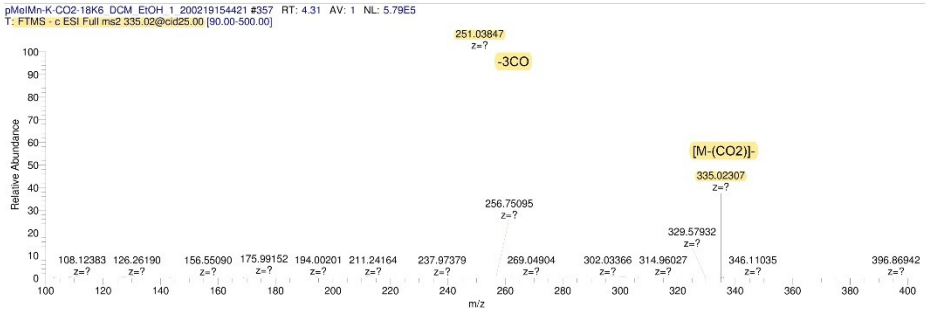

Figure 56S. HRMS^2-ESI neg CH_2Cl_2/C_2H_5OH spectrum of m/z 335.02@cid25.

pMeIMn-K-CO2-18K6_DCM_EtOH_1_200219154421#26 RT: 0.20
T: FTMS + c ESI Full ms [150.00-2000.00]
m/z= 150.0000-750.0000

m/z	Intensity	Relative	Composition
287.14664	53120408.0	5.45	$C_{14}H_{23}O_6$
288.14993	6670886.0	0.68	$C_{14}H_{24}O_6$
303.12042	975214080.0	100.00	$C_{12}H_{24}O_6K$
303.13226	6272455.5	0.64	$C_{10}H_{23}O_{10}$
304.12363	132249328.0	13.56	$C_{14}H_{26}O_2K_2$
305.11844	69101808.0	7.09	$C_{15}H_{22}O_4K$
306.12161	9489480.0	0.97	$C_{15}H_{23}O_4K$
533.13794	7987020.5	0.82	
641.21033	16131676.0	1.65	
643.20715	6580858.0	0.67	

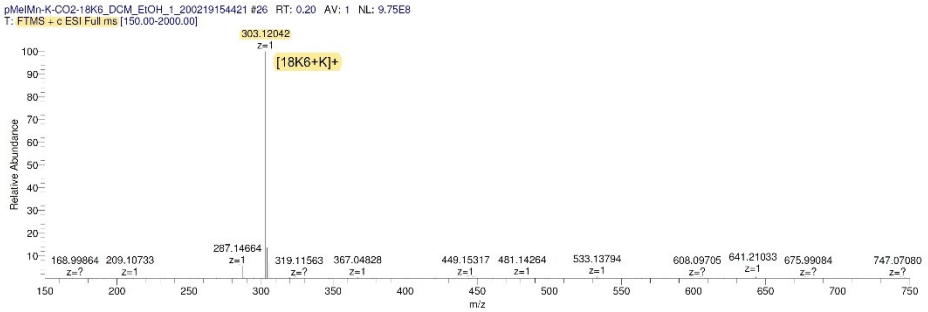

Figure 57S. HRMS-ESI pos CH_2Cl_2/C_2H_5OH spectrum of *fac*-[K(18-crown-6)][Mn(*amidopy-COO*)$(CO)_3$] (**4-K-crown**).

pMeIMn-K-CO2-18K6_DCM_MeOH_FA_1_200219160740#101 RT: 0.82
T: FTMS + c ESI Full ms [350.00-420.00]

m/z	Intensity	Relative	Composition
354.06372	422998.1	8.31	$C_{17}H_{14}O_2N_3KNa$
356.09540	1239968.3	24.37	$C_{18}H_{16}O_6N_2$
357.06421	367439.9	7.22	$C_{17}H_{15}O_3N_2KNa$
364.09241	2945821.3	57.90	$C_{17}H_{15}O_5N_3Na$
365.09637	359434.8	7.06	$C_{17}H_{16}O_5N_3Na$
367.04843	1692733.6	33.27	$C_{17}H_{16}O_4N_2Mn$
372.23785	5088153.0	100.00	
373.24121	1041001.3	20.46	
379.04825	376455.0	7.40	$C_{18}H_{16}O_4N_2Mn$
381.02744	845204.6	16.61	$C_{17}H_{14}O_5N_2Mn$
403.00955	1198094.3	23.55	$C_{17}H_{13}O_5N_2MnNa$
409.05887	700309.1	13.76	$C_{18}H_{16}O_6N_3K$
418.98343	1158244.6	22.76	$C_{17}H_{13}O_5N_2KMn$
419.22269	1273048.4	25.02	

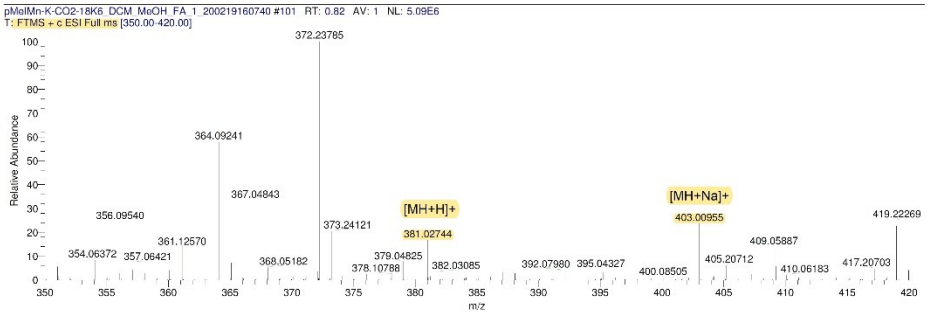

Figure 58S. HRMS-ESI pos CH_2Cl_2/CH_3OH(0.1% formic acid) spectrum of *fac*-[K(18-crown-6)][Mn(*amidopy-COO*)$(CO)_3$] (**4-K-crown**).

pMeIMn-K-CO2-18K6_DCM_MeOH_FA_1_200219160740#151 RT: 1.30
T: FTMS + c ESI Full ms2 381.03@cid9.00 [100.00-420.00]

m/z	Intensity	Relative	Composition
108.17307	34611.6	13.80	
279.03229	34782.4	13.87	$C_{14}H_{12}ON_2Mn$
297.04279	159941.4	63.78	$C_{14}H_{14}O_2N_2Mn$
381.02762	250787.7	100.00	$C_{17}H_{14}O_5N_2Mn$
381.20670	113363.1	45.20	

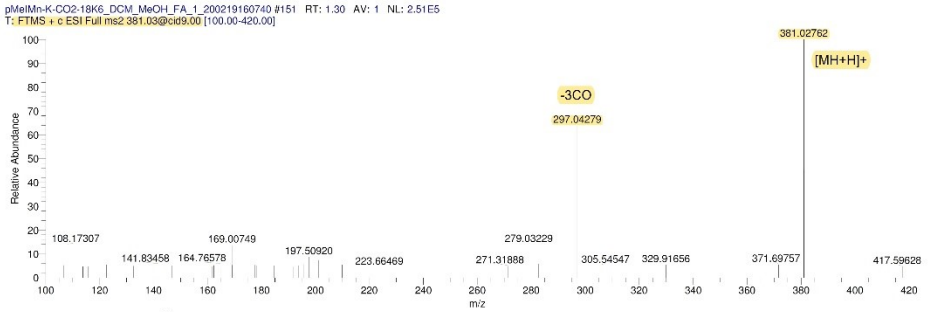

Figure 59S. $HRMS^2$-ESI pos CH_2Cl_2/CH_3OH(0.1% formic acid) spectrum of m/z 381.03@cid9.

pMeIMn-K-CO2-18K6_DCM_MeOH_FA_1_200219160004#190 RT: 1.61
T: FTMS + c ESI Full ms2 403.01@cid11.00 [110.00-1000.00]
m/z= 110.0000-435.0000

m/z	Intensity	Relative	Composition
169.00763	23855.7	1.21	$C_{14}H$
229.96211	45139.4	2.29	$C_7H_8O_3NMnNa$
319.02512	1970998.5	100.00	$C_{14}H_{13}O_2N_2MnNa$
403.00974	547671.2	27.79	$C_{17}H_{13}O_5N_2MnNa$
403.19168	399169.1	20.25	

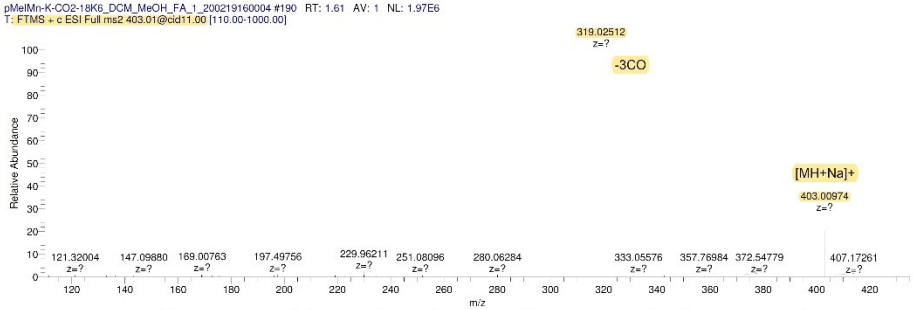

Figure 60S. HRMS^2-ESI pos CH_2Cl_2/CH_3OH(0.1% formic acid) spectrum of m/z 403.01@cid11.

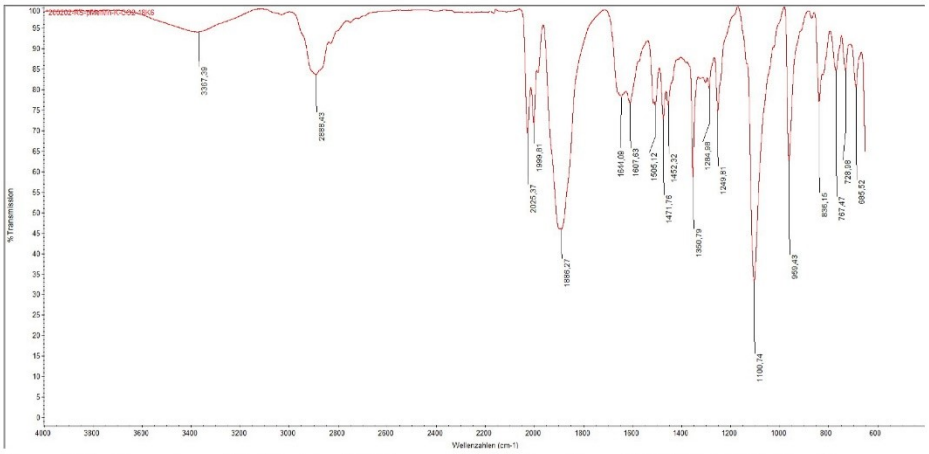

Figure 61S. IR spectrum (FT-IR) of *fac*-[K(18-crown-6)][Mn(*amidopy-COO*)$(CO)_3$] (**4-K-crown**).

Complex *fac*-[Na(15-crown-5)][Mn(*amidopy-COO*)$(CO)_3$] (**4-Na-crown**)

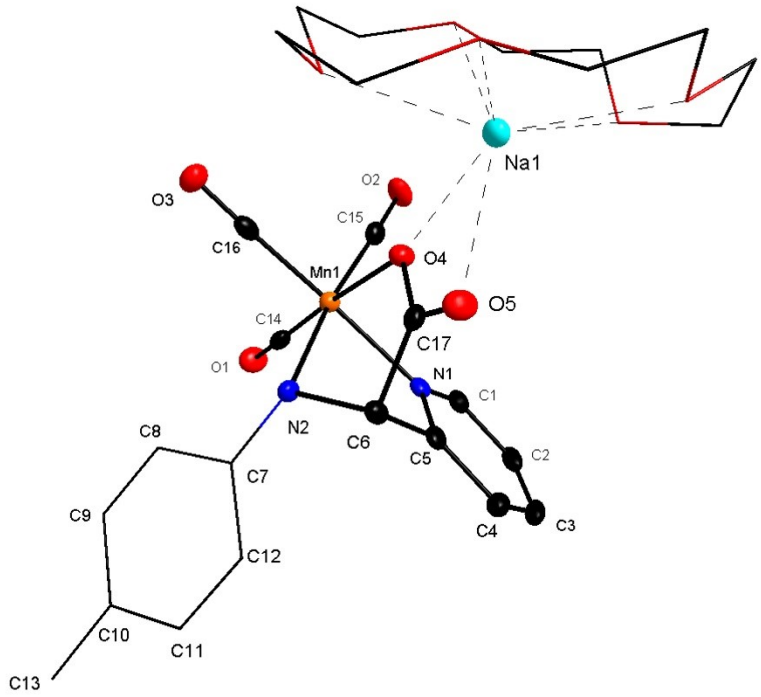

Figure 62S. Diamond plot of *fac*-[Na(15-crown-5)][Mn(*amidopy-COO*)$(CO)_3$] (**4-Na-crown**) (thermal ellipsoids at 50% probability, H atoms neglected for clarity. Selected bond lengths [Å] for **4-*crown***: C1–C2 = 1.381(4), C2–C3 = 1.391(5), C3–C4 = = 1.381(5), C4–C5 = 1.389(4), C5–C6 = 1.510(4), C6–C17 = 1.522(4), C17–O4 = 1.285(3), C17–O5 = 1.241(4), C6–N2 =1.464(4), C5–N1 = 1.360(4), Mn1–N1 = 2.072(3), Mn1–N2 = 2.050(2), Mn1–O4 = 2.070(2), Na1–O4 = 2.649(2), Na1–O5 = 2.307(2).

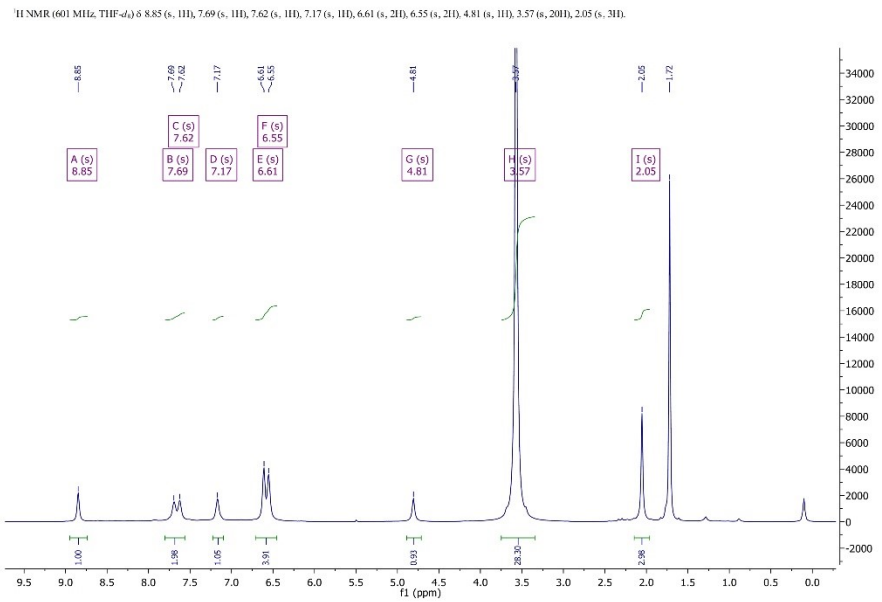

Figure 63S. ^{1}H NMR [600 MHz, THF-d_8, 298 K] spectrum of *fac*-[Na(15-crown-5)][Mn(*amidopy-COO*)(CO)$_3$] (**4-Na-crown**).

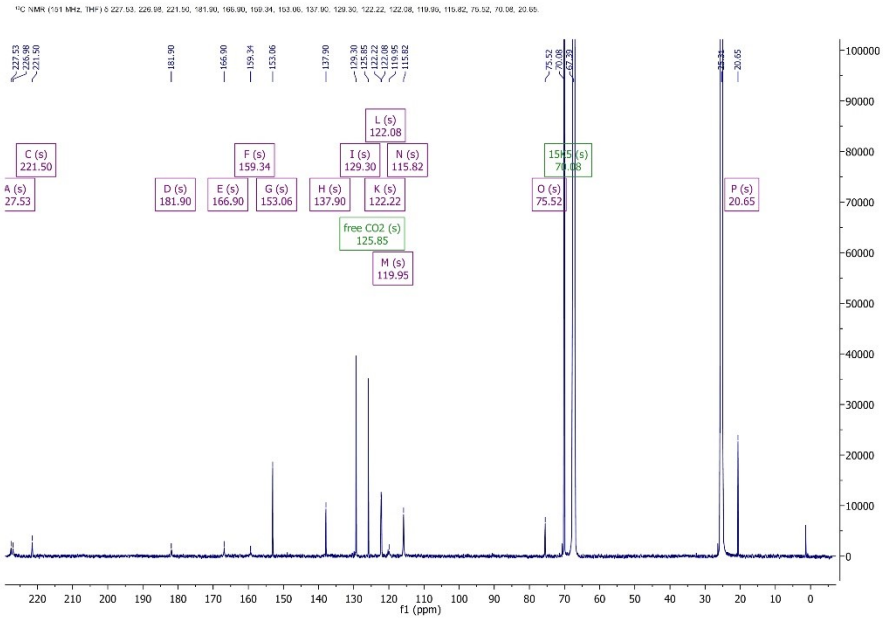

Figure 64S. ^{13}C{^{1}H} NMR [151 MHz, THF-d_8, 298 K] spectrum of *fac*-[Na(15-crown-5)][Mn(*amidopy-COO*)(CO)$_3$] (**4-Na-crown**).

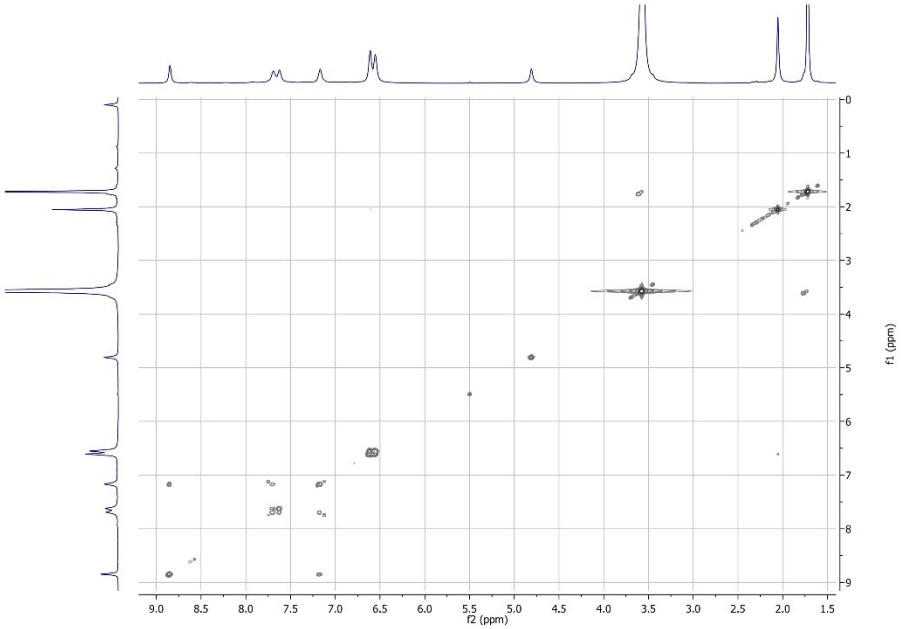

Figure 65S. $^{1}H^{1}H$ COSY NMR [600 MHz, THF-d_8, 298 K] spectrum of *fac*-[Na(15-crown-5)][Mn(*amidopy-COO*)$(CO)_3$] (**4-Na-crown**).

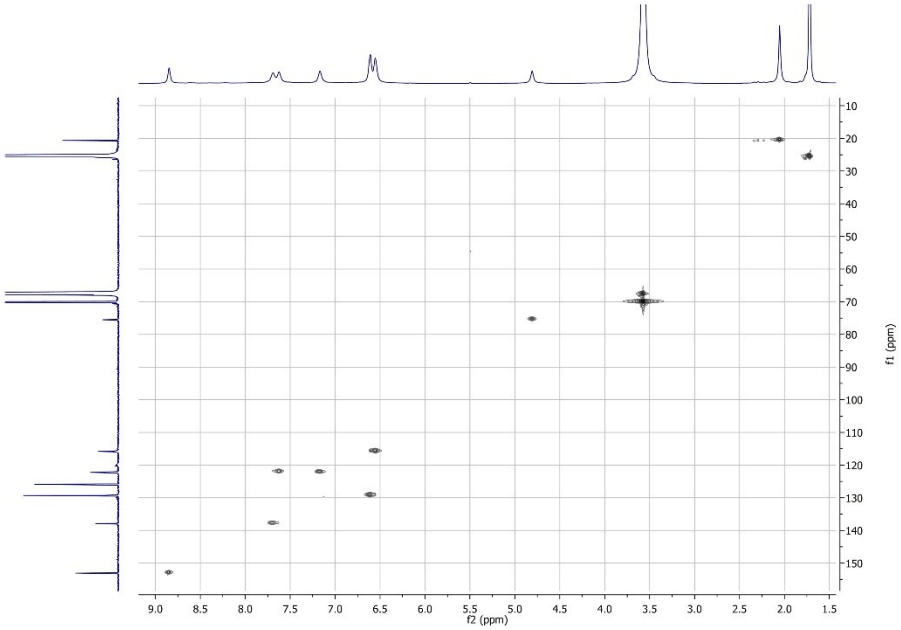

Figure 66S. $^{1}H^{13}C$ HSQC NMR [600 MHz/151 MHz, THF-d_8, 298 K] spectrum of *fac*-[Na(15-crown-5)][Mn(*amidopy-COO*)$(CO)_3$] (**4-Na-crown**).

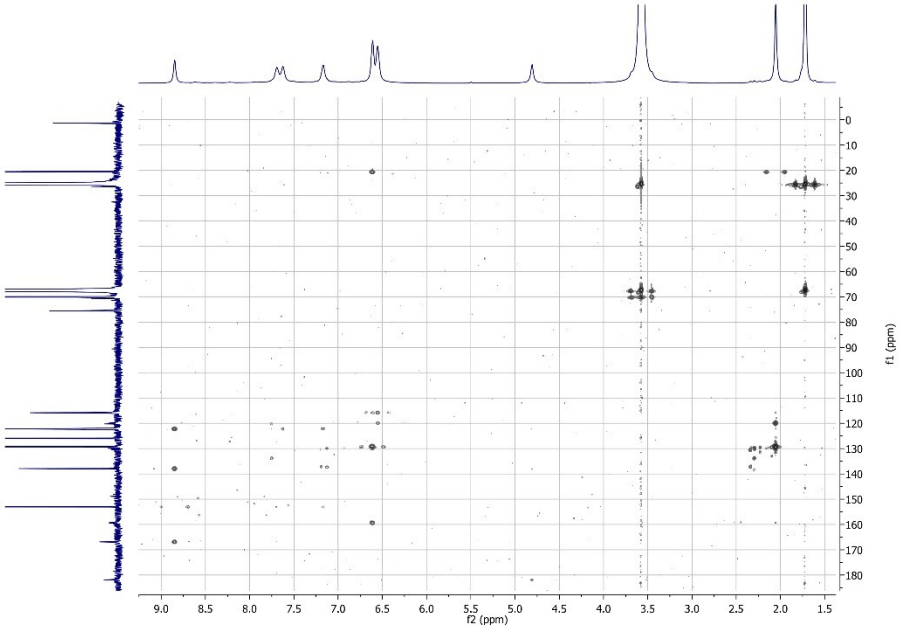

Figure 67S. $^{1}H^{13}C$ HMBC NMR [600 MHz/151 MHz, THF-d_8, 298 K] spectrum of *fac*-[Na(15-crown-5)][Mn(*amidopy-COO*)$(CO)_3$] (**4-Na-crown**).

pMeIMn-Na-CO2-15K5_DCM_EtOH_1#189 RT: 1.96
T: FTMS - c ESI Full ms [250.00-500.00]
m/z= 250.0000-400.0000

m/z	Intensity	Relative	Composition
251.03908	100818.0	1.88	$C_{13}H_{12}N_2Mn$
257.99722	437634.1	8.15	$C_{11}H_9O_3NMn$
268.88937	130484.2	2.43	$C_2O_{11}NMn$
270.88730	123612.2	2.30	$CO_{11}N_2Mn$
295.02878	1689028.6	31.47	$C_{14}H_{12}O_2N_2Mn$
296.03223	251030.3	4.68	$C_9H_{13}O_4N_4Mn$
300.99484	496186.9	9.24	$C_2H_{10}O_8N_6Mn$
302.99197	154628.9	2.88	$C_9H_{12}O_8Mn$
321.98471	562863.4	10.49	$C_6H_3O_4N_9Mn$
323.98181	352310.6	6.56	$C_{13}H_7O_4N_3Mn$
332.98514	325835.5	6.07	$C_{17}H_4N_5Mn$
335.02338	5367490.5	100.00	$C_{16}H_{12}O_3N_2Mn$
336.02667	963215.9	17.95	$C_{11}H_{13}O_5N_4Mn$
379.01324	3468590.5	64.62	$C_{17}H_{12}O_5N_2Mn$

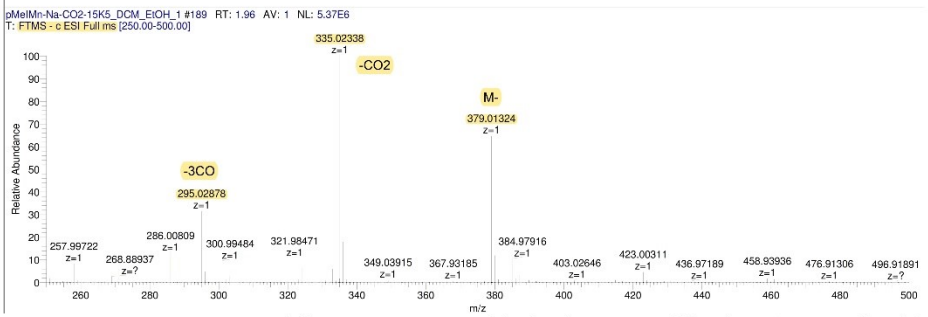

Figure 68S. HRMS-ESI neg CH_2Cl_2/C_2H_5OH spectrum of *fac*-[Na(15-crown-5)][Mn(*amidopy-COO*)$(CO)_3$] (**4-Na-crown**).

pMeIMn-Na-CO2-15K5_DCM_EtOH_1#379 RT: 4.40
T: FTMS - c ESI Full ms2 379.01@cid20.00 [100.00-500.00]
m/z= 100.00000-400.00000

m/z	Intensity	Relative	Composition
108.13130	1238.4	0.46	
168.94225	1933.9	0.71	
191.97321	1491.8	0.55	
205.96507	2501.2	0.92	
206.97276	16044.5	5.90	
251.03773	3545.6	1.30	$C_{13}H_{12}N_2Mn$
254.07500	1327.3	0.49	
295.02731	271873.3	100.00	$C_{14}H_{12}O_2N_2Mn$
313.03778	19246.8	7.08	$C_{14}H_{14}O_3N_2Mn$
335.02225	11525.9	4.24	$C_{16}H_{12}O_3N_2Mn$

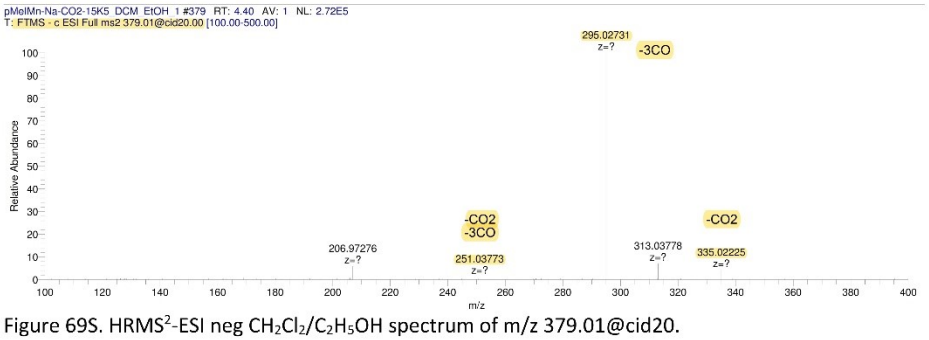

Figure 69S. HRMS^2-ESI neg CH_2Cl_2/C_2H_5OH spectrum of m/z 379.01@cid20.

pMeIMn-Na-CO2-15K5_DCM_EtOH_1_200219150934#158 RT: 1.51
T: FTMS + c ESI Full ms [150.00-500.00]

m/z	Intensity	Relative	Composition
219.08949	806939.4	0.84	$C_{13}H_{12}N_2Na$
243.12042	95908584.0	100.00	$C_{10}H_{20}O_5Na$
244.12370	10822638.0	11.28	$C_3H_{16}O_5N_8$
259.09427	10697578.0	11.15	$C_{14}H_{15}ONNa_2$
260.09753	1147861.4	1.20	$C_5H_{12}O_4N_8$
287.14661	6198338.5	6.46	$C_{12}H_{24}O_6Na$
288.14984	800079.8	0.83	$C_5H_{20}O_6N_8$
303.12057	2809061.0	2.93	$C_{16}H_{19}O_2NNa_2$
449.15347	972177.5	1.01	$C_{21}H_{24}O_3N_4Na_3$
481.14328	1247304.8	1.30	$C_{20}H_{25}O_8N_3Na_2$

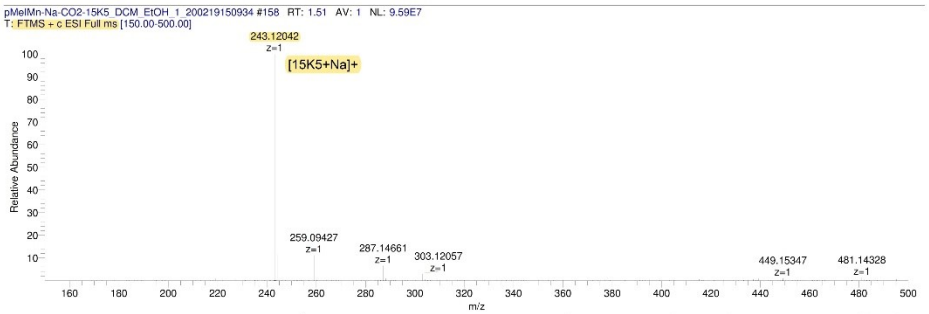

Figure 70S. HRMS-ESI pos CH_2Cl_2/C_2H_5OH spectrum of *fac*-[Na(15-crown-5)][Mn(*amidopy-COO*)$(CO)_3$] (**4-Na-crown**).

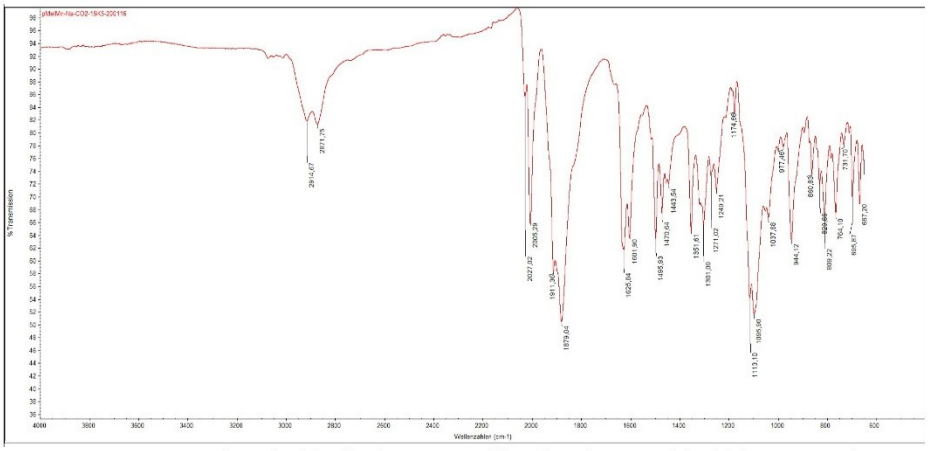

Figure 71S. IR spectrum (FT-IR) of *fac*-[Na(15-crown-5)][Mn(*amidopy-COO*)$(CO)_3$] (**4-Na-crown**).

Complex *fac*-K[Mn(*amidopy-ba*)(CO)$_3$] (**5-K**)

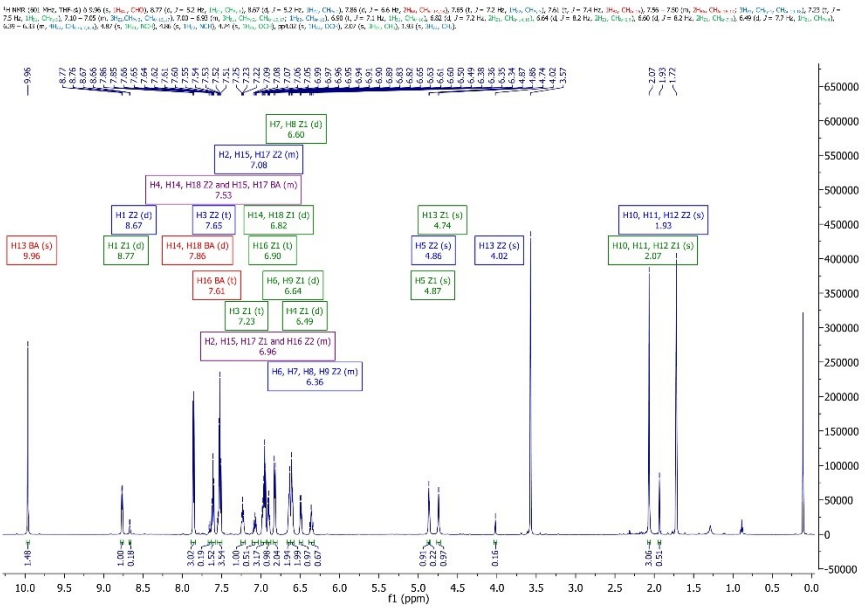

Figure 72S. ^{1}H NMR [600 MHz, THF-d$_8$, 298 K] spectrum of *fac*-K[Mn(*amidopy-ba*)(CO)$_3$] (**5-K**).

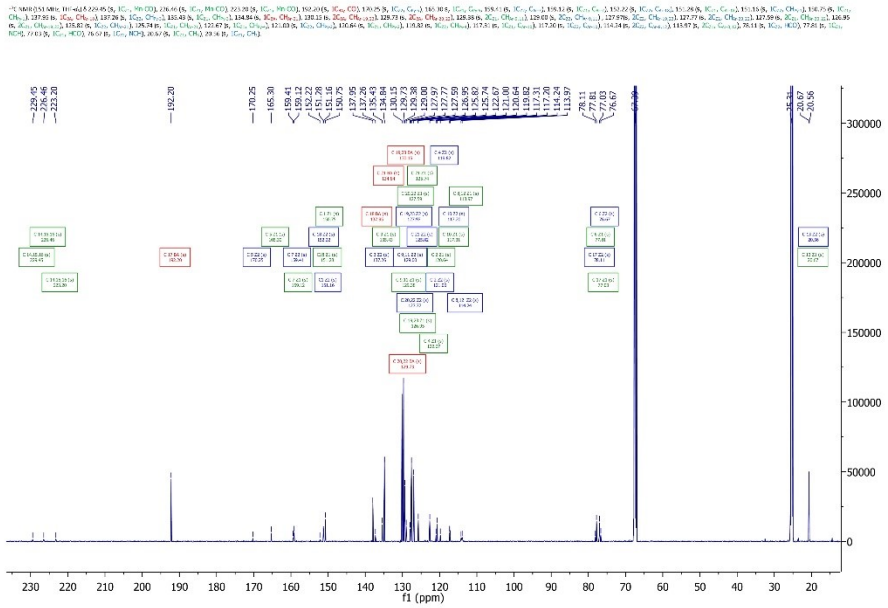

Figure 73S. ^{13}C{^{1}H} NMR [151 MHz, THF-d$_8$, 298 K] spectrum of *fac*-K[Mn(*amidopy-ba*)(CO)$_3$] (**5-K**).

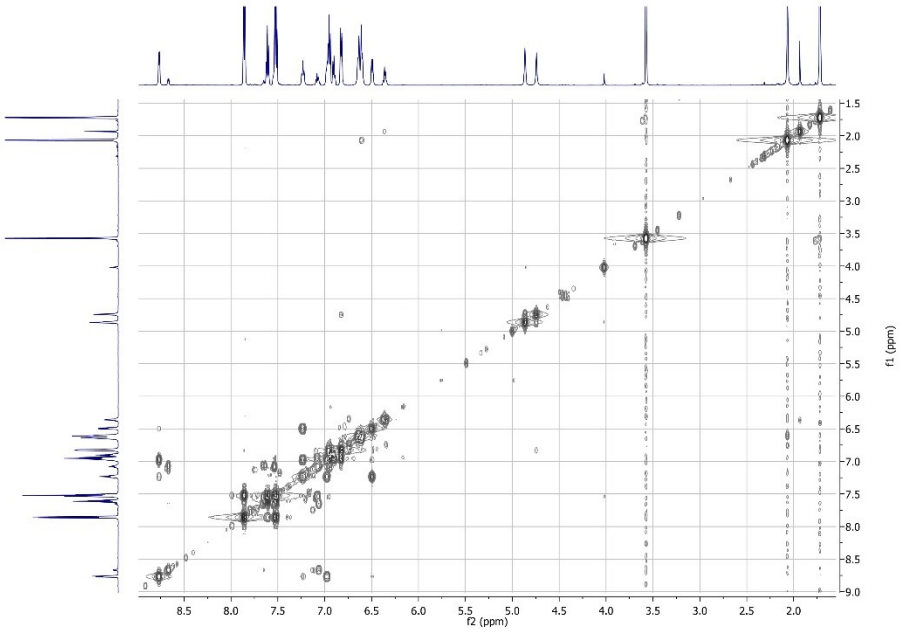

Figure 74S. $^{1}H^{1}H$ COSY NMR [600 MHz, THF-d_8, 298 K] spectrum of *fac*-K[Mn(*amidopy-ba*)$(CO)_3$] (**5-K**).

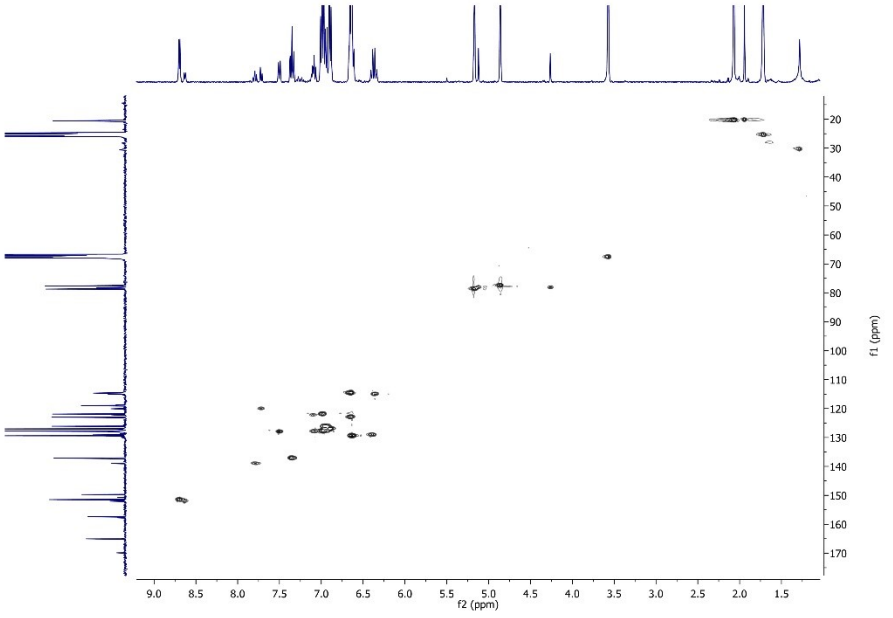

Figure 75S. $^{1}H^{13}C$ HSQC NMR [600 MHz/151 MHz, THF-d_8, 298 K] spectrum of *fac*-K[Mn(*amidopy-ba*)$(CO)_3$] (**5-K**).

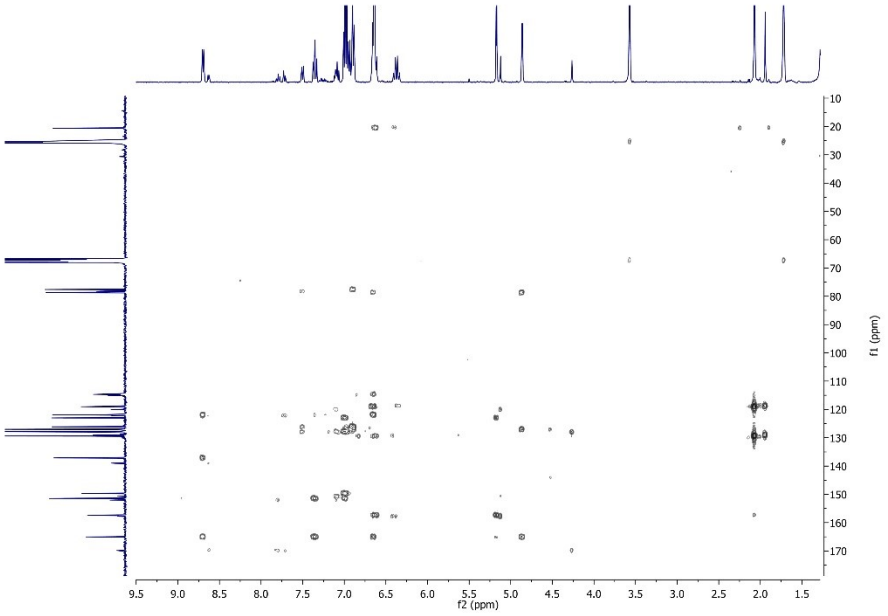

Figure 76S. $^{1}H^{13}C$ HMBC NMR [600 MHz/151 MHz, THF-d_8, 298 K] spectrum of *fac*-K[Mn(*amidopy-ba*)$(CO)_3$] (**5-K**).

pMeIMn-K-BA_neg_10#44 RT: 0.37
T: FTMS - p ESI Full ms [50.00-1000.00]

m/z	Intensity	Relative	Composition
112.98605	277425.2	9.79	
121.02989	2832954.8	100.00	$C_7H_5O_2$
128.95990	495388.8	17.49	H_2ON_4Mn
145.94200	263905.3	9.32	$C_2H_3O_4Mn$
154.91853	280106.9	9.89	C_3O_4Mn
174.96001	442269.7	15.61	$C_7H_4O_2Mn$
183.08180	1642731.4	57.99	$C_{13}H_{11}O$
189.93181	409896.0	14.47	$C_3H_3O_6Mn$
204.99104	258581.1	9.13	$C_4H_4N_7Mn$
251.03874	287515.5	10.15	$C_{13}H_{12}N_2Mn$
265.96292	587571.1	20.74	$C_9H_7O_6Mn$
281.00168	1812487.3	63.98	$C_{14}H_{10}O_3Mn$
304.95007	261399.5	9.23	$C_{11}H_6O_7Mn$
335.02344	1860417.5	65.67	$C_{16}H_{12}O_3N_2Mn$
336.02686	283028.8	9.99	$C_4H_{18}O_3N_8Mn_2$

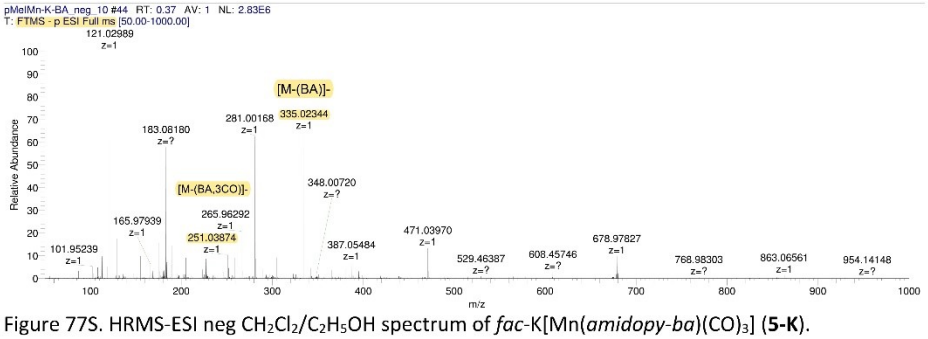

Figure 77S. HRMS-ESI neg CH_2Cl_2/C_2H_5OH spectrum of *fac*-K[Mn(*amidopy-ba*)$(CO)_3$] (**5-K**).

pMeIMn-K-BA_neg_10#154 RT: 1.73
T: FTMS - p ESI Full ms2 335.02@cid20.00 [90.00-500.00]

m/z	Intensity	Relative	Composition
107.95796	4876.2	1.15	
168.68434	3330.0	0.79	
251.03839	423889.7	100.00	$C_{13}H_{12}N_2Mn$
302.91205	5299.9	1.25	$C_{14}O_5Mn$
335.02298	174763.1	41.23	$C_{16}H_{12}O_3N_2Mn$

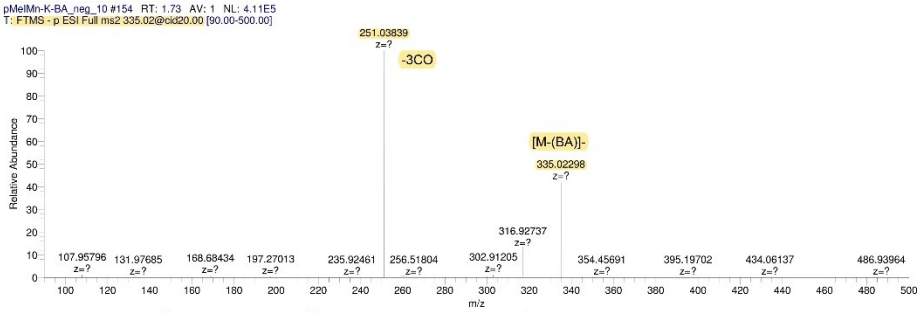

Figure 78S. HRMS^2-ESI neg CH_2Cl_2/C_2H_5OH spectrum of m/z 355.05@cid20.

pMeIMn-K-BA_pos_10#35 RT: 0.27
T: FTMS + c ESI Full ms [50.00-1000.00]
m/z= 100.0000-700.0000

m/z	Intensity	Relative	Composition
131.96114	3266020.3	12.11	$C_2H_3O_3Mn$
197.10732	4240037.0	15.72	$C_{13}H_{13}N_2$
199.12292	2147413.5	7.96	$C_{13}H_{15}N_2$
287.10989	2841555.8	10.53	$C_9H_{15}O_5N_5$
287.15436	2902997.0	10.76	$C_{26}H_{19}N_2$
301.13220	7816873.0	28.98	$C_{18}H_{15}N_3$
303.14914	3383895.5	12.54	$C_{26}H_{19}ON_2$
305.16483	9688036.0	35.92	$C_{26}H_{21}ON_2$
317.16495	12467157.0	46.22	$C_{27}H_{21}ON_2$
318.16812	2465132.5	9.14	$C_9H_{27}ON_6Mn$
357.09201	8958762.0	33.21	$C_{21}H_{20}ONMn$
359.09537	5983423.5	22.18	$C_6H_{22}O_7N_7Mn$
443.07980	26974246.0	100.00	$C_{23}H_{20}O_4N_2Mn$
444.08365	6674545.5	24.74	$C_{18}H_{21}O_5N_4Mn$

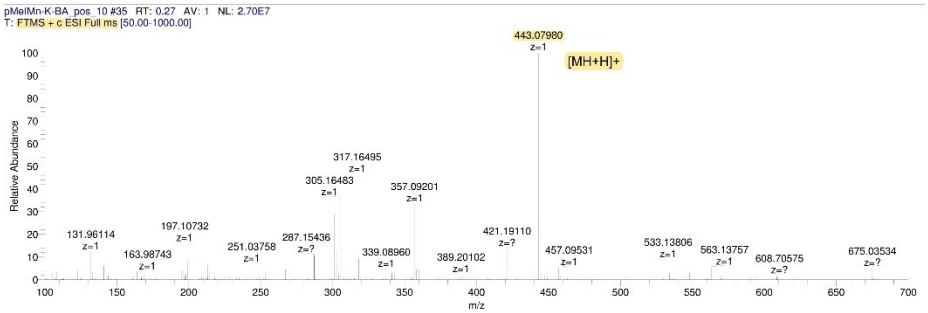

Figure 79S. HRMS-ESI pos CH_2Cl_2/CH_3OH(0.1% formic acid) spectrum of *fac*-K[Mn(*amidopy-ba*)$(CO)_3$] (**5-K**).

pMeIMn-K-BA_pos_10#101 RT: 0.90
T: FTMS + c ESI Full ms2 443.08@cid12.00 [120.00-500.00]

m/z	Intensity	Relative	Composition
168.76204	52790.6	5.06	H_4Mn_3
197.35600	22254.0	2.13	$C_{14}H_{29}$
300.02124	20718.6	1.98	$C_8H_6O_8N_5$
341.08459	44005.2	4.21	$C_{20}H_{18}N_2Mn$
359.09509	1044250.6	100.00	$C_{20}H_{20}ON_2Mn$
443.07974	253764.8	24.30	$C_{23}H_{26}O_4N_2Mn$
443.14102	10018.0	0.96	$C_{19}H_{33}ON_4Mn_2$
443.16110	16980.5	1.63	$C_{21}H_{30}O_4N_3Mn$
443.18436	16349.7	1.57	$C_{12}H_{27}O_{10}N_8$
443.22253	60362.7	5.78	$C_{24}H_{38}O_3NMn$

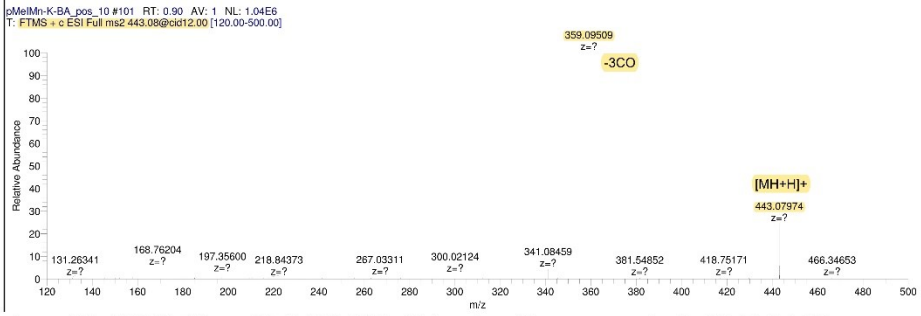

Figure 80S. HRMS^2-ESI pos CH_2Cl_2/CH_3OH(0,1% formic acid) spectrum of m/z 443.08@cid12.

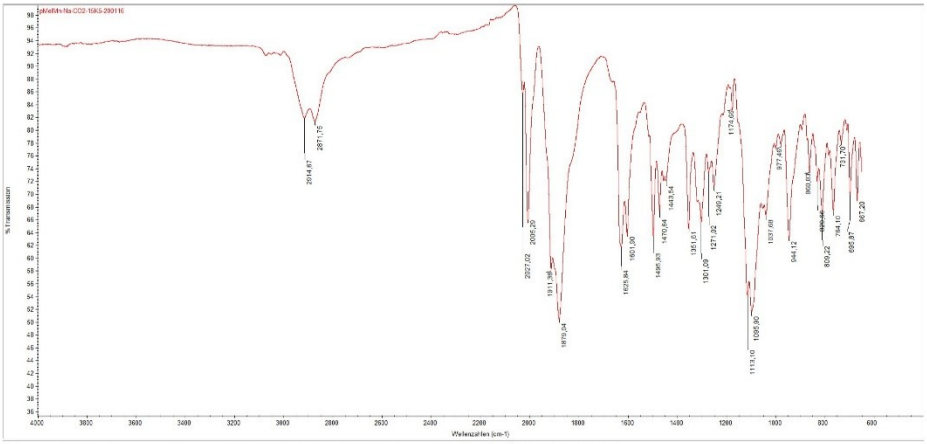

Figure 81S. IR spectrum (FT-IR) of *fac*-K[Mn(*amidopy-ba*)(CO)$_3$] (**5-K**).

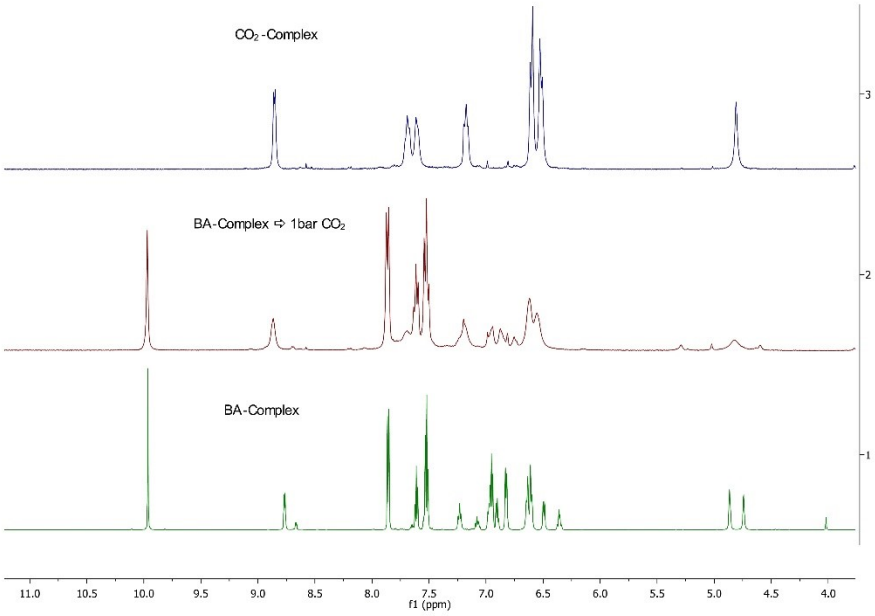

Figure 82S. ^{1}H NMR [600 MHz, THF-d_8, 298 K] spectrum of *fac*-K[Mn(*amidopy-ba*)$(CO)_3$] (**5-K**) with 1 bar CO_2 (red).

fac-[K(18-crown-6)][Mn(*amidopy-ba*)(CO)$_3$] (**5-K-crown**)

pMeIMn-K-BA-18K6_DCM_EtOH_1#96 RT: 0.83
T: FTMS - c ESI Full ms [150.00-1000.00]

m/z	Intensity	Relative	Composition
152.87187	487473.1	3.59	
160.84256	1050892.8	7.75	C K Mn$_2$
162.83952	1036952.4	7.65	
191.98671	1931230.0	14.24	C$_5$ H$_{10}$ N$_2$ K Mn
195.81136	573162.3	4.23	
197.80836	773257.7	5.70	H O$_2$ Mn$_3$
257.99713	798128.9	5.89	C$_9$ H$_{12}$ O N$_2$ K Mn
300.99500	502567.7	3.71	C$_9$ H$_5$ O$_{10}$ N$_2$
317.97397	477923.5	3.52	C$_{11}$ H$_{14}$ O$_3$ N Mn$_2$
332.98526	818812.0	6.04	C$_{17}$ H$_4$ N$_5$ Mn
335.02338	13560084.0	100.00	C$_{16}$ H$_{12}$ O$_3$ N$_2$ Mn
336.02673	2371611.5	17.49	C$_2$ H$_8$ O$_{12}$ N$_8$
384.97968	810814.3	5.98	C$_{15}$ H$_{14}$ O N$_3$ K$_2$ Mn
516.96533	3415229.3	25.19	C$_{25}$ H$_7$ O$_2$ N$_5$ K Mn
517.96869	788378.3	5.81	C$_{15}$ H$_{18}$ O$_4$ N$_6$ K$_3$ Mn

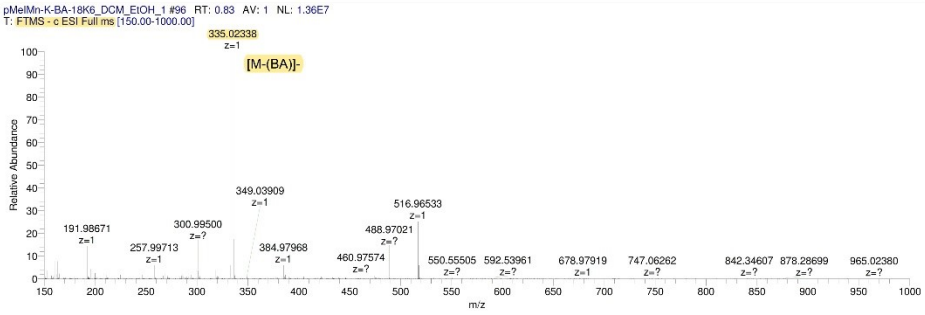

Figure 83S. HRMS-ESI neg CH_2Cl_2/C_2H_5OH spectrum of *fac*-[K(18-crown-6)][Mn(*amidopy-ba*)(CO)$_3$] (**5-K-crown**).

pMeIMn-K-BA-18K6_DCM_MeOH_FA_1_200219165109#346 RT: 3.55
T: FTMS + c ESI Full ms [95.00-500.00]

m/z	Intensity	Relative	Composition
267.03235	6772796.5	2.74	C$_{13}$ H$_{12}$ O N$_2$ Mn
287.14651	8659934.0	3.51	C$_{12}$ H$_{21}$ O$_5$ N$_3$
303.12024	246792192.0	100.00	C$_{12}$ H$_{24}$ O$_6$ K
304.12344	34708400.0	14.06	C$_{14}$ H$_{26}$ N K Mn
305.11823	17914842.0	7.26	C$_{15}$ H$_{24}$ O$_2$ N Mn
359.09479	15820804.0	6.41	C$_{20}$ H$_{20}$ O N$_2$ Mn
364.09207	7135176.0	2.89	C$_{16}$ H$_{21}$ O$_7$ K
391.08453	10417890.0	4.22	C$_{23}$ H$_{16}$ O$_2$ N$_2$ K
443.07944	26400288.0	10.70	C$_{23}$ H$_{26}$ O$_4$ N$_2$ Mn
444.08310	5982970.0	2.42	C$_{15}$ H$_{28}$ O$_8$ N K Mn

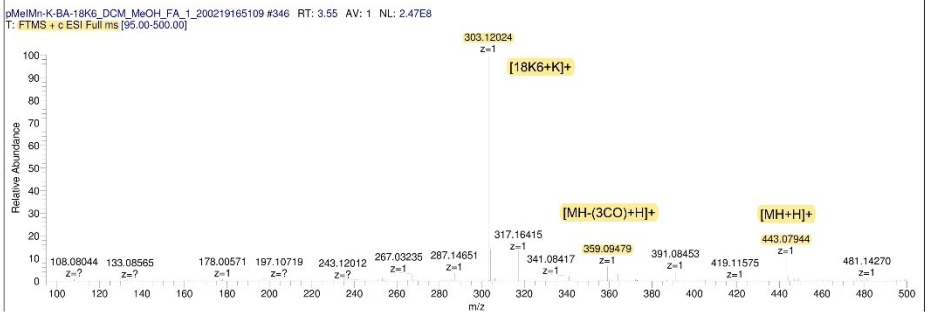

Figure 84S. HRMS-ESI pos CH_2Cl_2/CH_3OH(0,1% formic acid) spectrum of *fac*-[K(18-crown-6)][Mn(*amidopy-ba*)(CO)$_3$] (**5-K-crown**).

pMeIMn-K-BA-18K6_DCM_EtOH_1_200219163511#191 RT: 1.64
T: FTMS + c ESI Full ms2 443.08@cid11.00 [120.00-470.00]

m/z	Intensity	Relative	Composition
169.00827	25361.6	2.79	$C_{14}H$
253.02907	25576.0	2.81	$C_{13}H_{12}ONMn$
341.08365	123892.3	13.63	$C_{20}H_{18}N_2Mn$
359.09433	738601.4	81.24	$C_{20}H_{20}ON_2Mn$
443.07892	909207.6	100.00	$C_{23}H_{20}O_4N_2Mn$

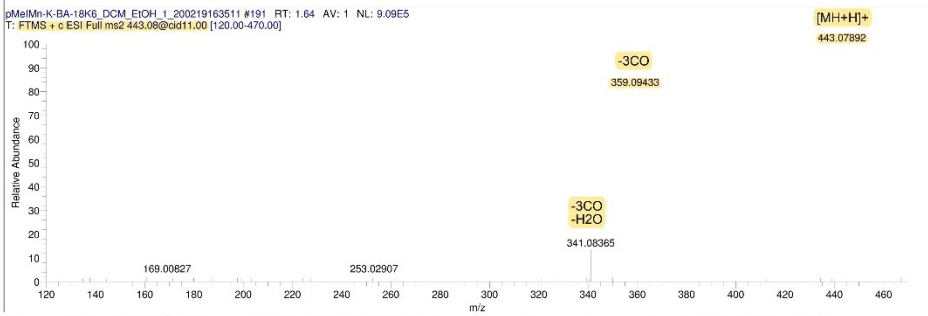

Figure 85S. HRMS^2-ESI pos CH_2Cl_2/CH_3OH(0.1% formic acid) spectrum of m/z 443.06@cid11.

pMeIMn-K-BA-18K6_DCM_MeOH_FA_1_200219165109#201 RT: 1.77
T: FTMS + c ESI Full ms2 359.09@cid15.00 [95.00-500.00]

m/z	Intensity	Relative	Composition
108.15791	3936.8	0.65	$CH_{12}N_6$
159.99521	10520.9	1.75	C_7H_7NMn
169.00941	4073.5	0.68	$C_2H_5O_7N_2$
178.00583	96496.1	16.04	C_7H_9ONMn
252.02122	6119.1	1.02	$C_4H_6O_8N_5$
253.02933	286432.3	47.61	$C_{13}H_{12}ONMn$
341.08441	601589.4	100.00	$C_{20}H_{18}N_2Mn$
341.09821	4646.5	0.77	$C_{14}H_{17}O_8N_2$
359.07477	4949.9	0.82	$C_{15}H_7O_2N_{10}$
359.09485	277901.8	46.19	$C_{20}H_{20}ON_2Mn$

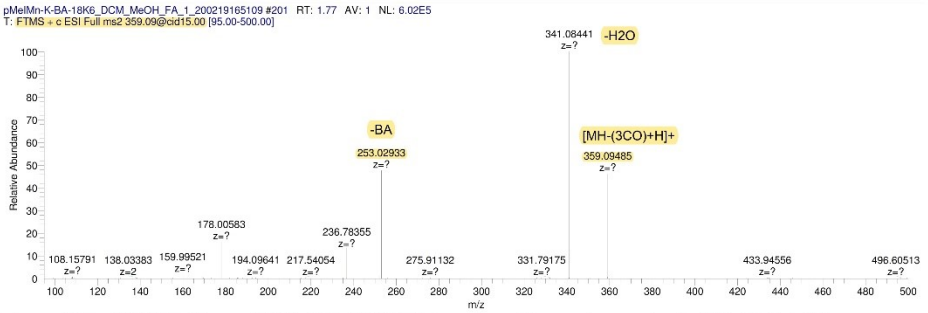

Figure 86S. HRMS^2-ESI pos CH_2Cl_2/CH_3OH(0.1% formic acid) spectrum of m/z 359.09@cid15.

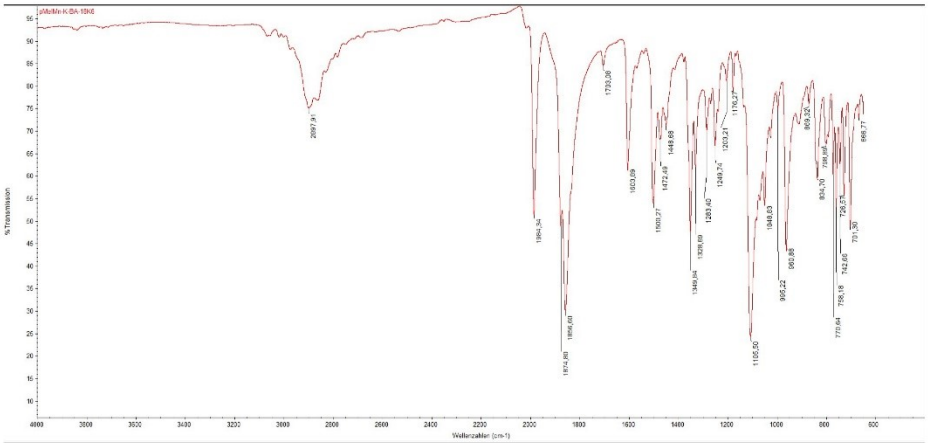

Figure 87S. IR spectrum (FT-IR) of *fac*-[K(18-crown-6)][Mn(*amidopy-ba*)$(CO)_3$] (**5-K-crown**).

.

Computational Details

Quantum chemical investigations were performed using the program package Gaussian16. [M. J. Frisch, G. W. Trucks, H. B. Schlegel, G. E. Scuseria, M. A. Robb, J. R. Cheeseman, G. Scalmani, V. Barone, G. A. Petersson, H. Nakatsuji, et al., Gausssian16, **2016**]. All reported structures were optimized by the density functional theory (DFT)[1] with Grimme's B97D3 functional[2] and the def2-SVP basis set[3,4] Frequency analysis calculations of optimized structures were performed at the same level of theory (B97D3/def2-SVP) to characterize the structures to be minima (no imaginary frequency) or transition states (one imaginary frequency). Intrinsic reaction coordinate (IRC) calculations were performed to confirm the connection between two correct minima for a transition state. The bulky solvation effect of tetrahydrofurane (ε = 7.4257) was simulated by SMD[5] continuum solvent mode at the B97D3/def2-SVP level of theory.

Figure plots of DFT-optimized structures:

[3]$^{-}$

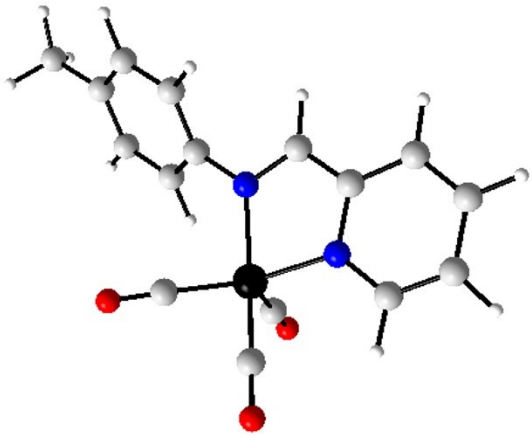

Figure 88S. Plot of the DFT optimized structure of **[3]**$^{-}$ (red: O, blue: N, grey: C, black: Mn, white: H).

[3]Li

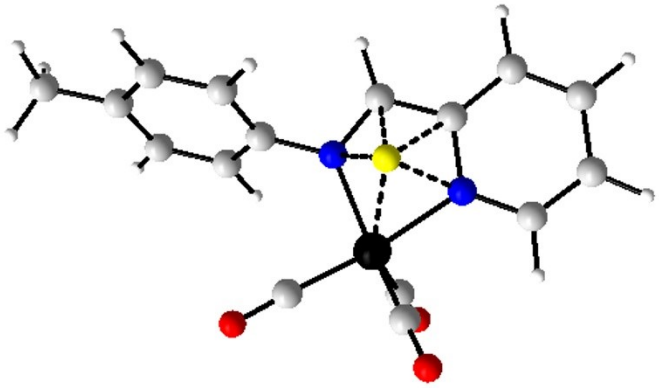

Figure 89S. Plot of the DFT optimized structure of **[3]Li** (red: O, blue: N, grey: C, black: Mn, white: H, yellow: Li).

[3]Na

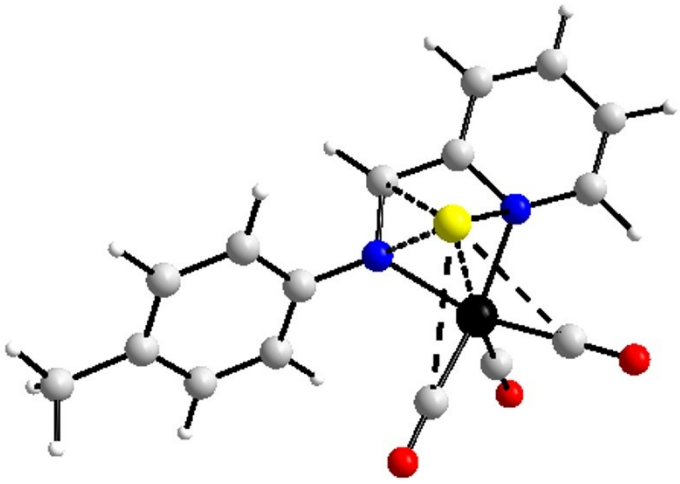

Figure 90S. Plot of the DFT optimized structure of **[3]Na** (red: O, blue: N, grey: C, black: Mn, white: H, yellow: Na).

[3]K

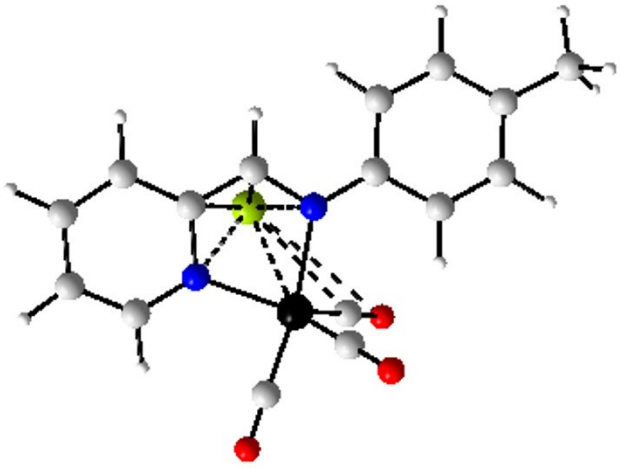

Figure 91S. Plot of the DFT optimized structure of **[3]K** (red: O, blue: N, grey: C, black: Mn, white: H, green: K).

[3][K(18-crown-6)(thf)]

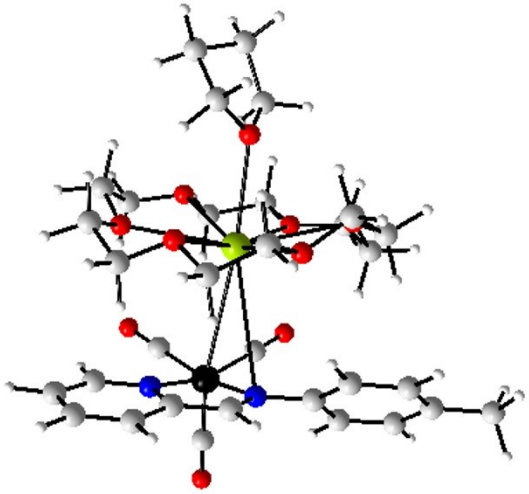

Figure 92S. Plot of the DFT optimized structure of **[3][K(18-crown-6)(thf)]** (red: O, blue: N, grey: C, black: Mn, white: H, green: K).

[4]Li

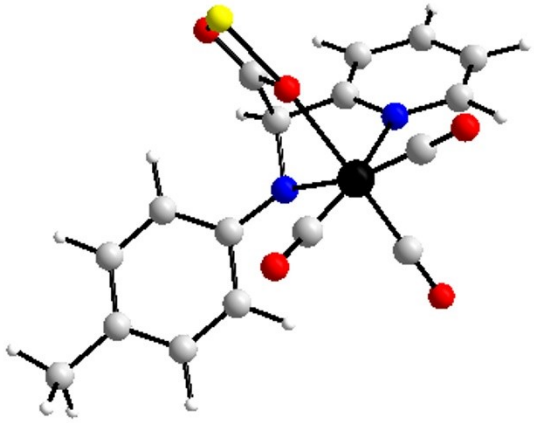

Figure 93S. Plot of the DFT optimized structure of **[4]Li** (red: O, blue: N, grey: C, black: Mn, white: H, yellow: Li).

[4]Na

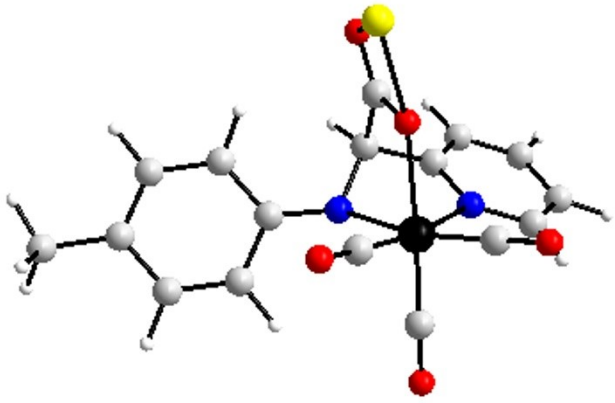

Figure 94S. Plot of the DFT optimized structure of **[4]Na** (red: O, blue: N, grey: C, black: Mn, white: H, yellow: Na).

[4]K

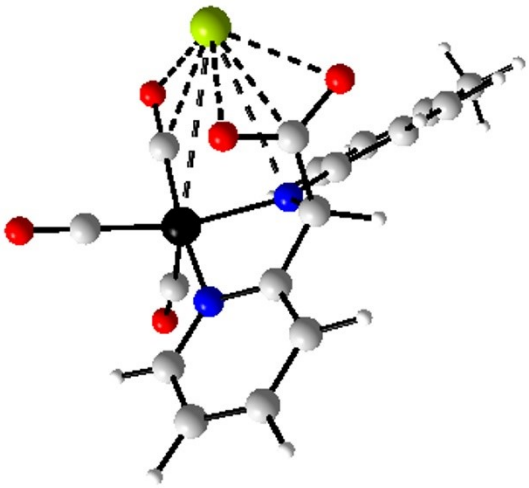

Figure 95S. Plot of the DFT optimized structure of **[4]K** (red: O, blue: N, grey: C, black: Mn, white: H, green: K).

[4][K(18-crown-6)(thf)]

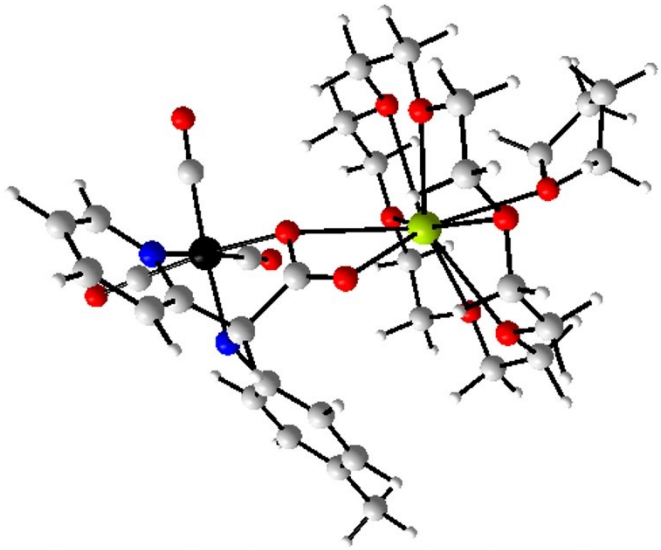

Figure 96S. Plot of the DFT optimized structure of **[4][K(18-crown-6)(thf)]** (red: O, blue: N, grey: C, black: Mn, white: H, green: K).

Benzaldehyde

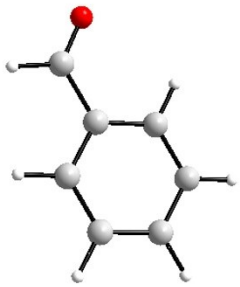

Figure 97S. Plot of the DFT optimized structure of **benzaldehyde** (red: O, grey: C, white: H).

CO_2

Figure 98S. Plot of the DFT optimized structure of **CO_2** (red: O, grey: C, white: H).

References

[1] P. Hohenberg, W. Kohn, *Phys. Rev.* **1964**, *136*, B864.
[2] S. Grimme, *J. Comput. Chem.* **2006**, *27*, 1787–1799.
[3] F. Weigend, R. Ahlrichs, *Phys. Chem. Chem. Phys.* **2005**, *7*, 3297–3305.
[4] F. Weigend, *Phys. Chem. Chem. Phys.* **2006**, *8*, 1057–1065.
[5] A. V. Marenich, C. J. Cramer, D. G. Truhlar, *J. Phys. Chem. B* **2009**, *113*, 6378–6396.

7.4 Supporting Information for

Reversible Binding of Benzaldehyde and Benzophenone *via* Cooperative C-C and Re-O Bond Formation with Bidentate Pyridine-Based Rhenium(I) Triscarbonyl Complexes

Index

Spectroscopic, scXRD analysis and Mass spectrometric data for compound:

***fac*-K[Re(*amidopy-ba*)(CO)$_3$] (80)**

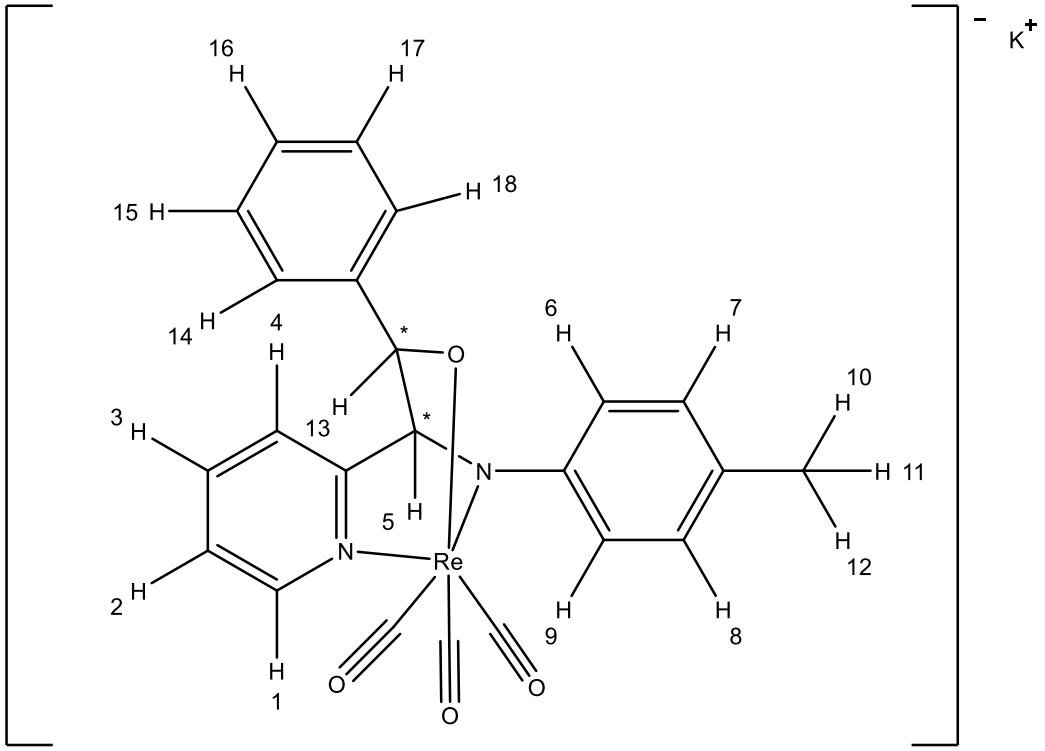

Figure S7.4-1: Structural formula of ***fac*-K[Re(*amidopy-ba*)(CO)$_3$] (80)** for the assignment of ^{1}H NMR signals.

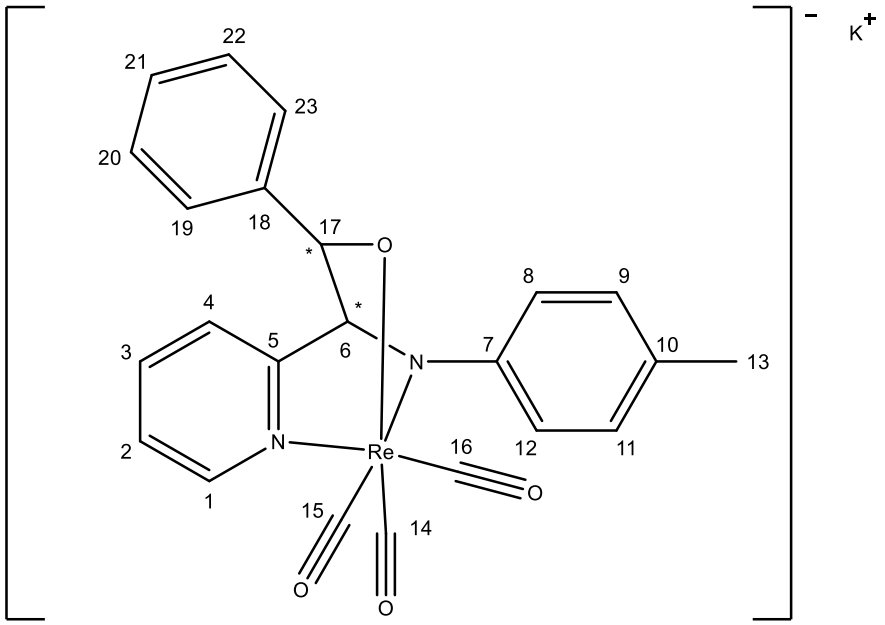

Figure S7.4-2: Structural formula of ***fac*-K[Re(*amidopy-ba*)(CO)$_3$] (80)** for the assignment of ^{13}C NMR signals.

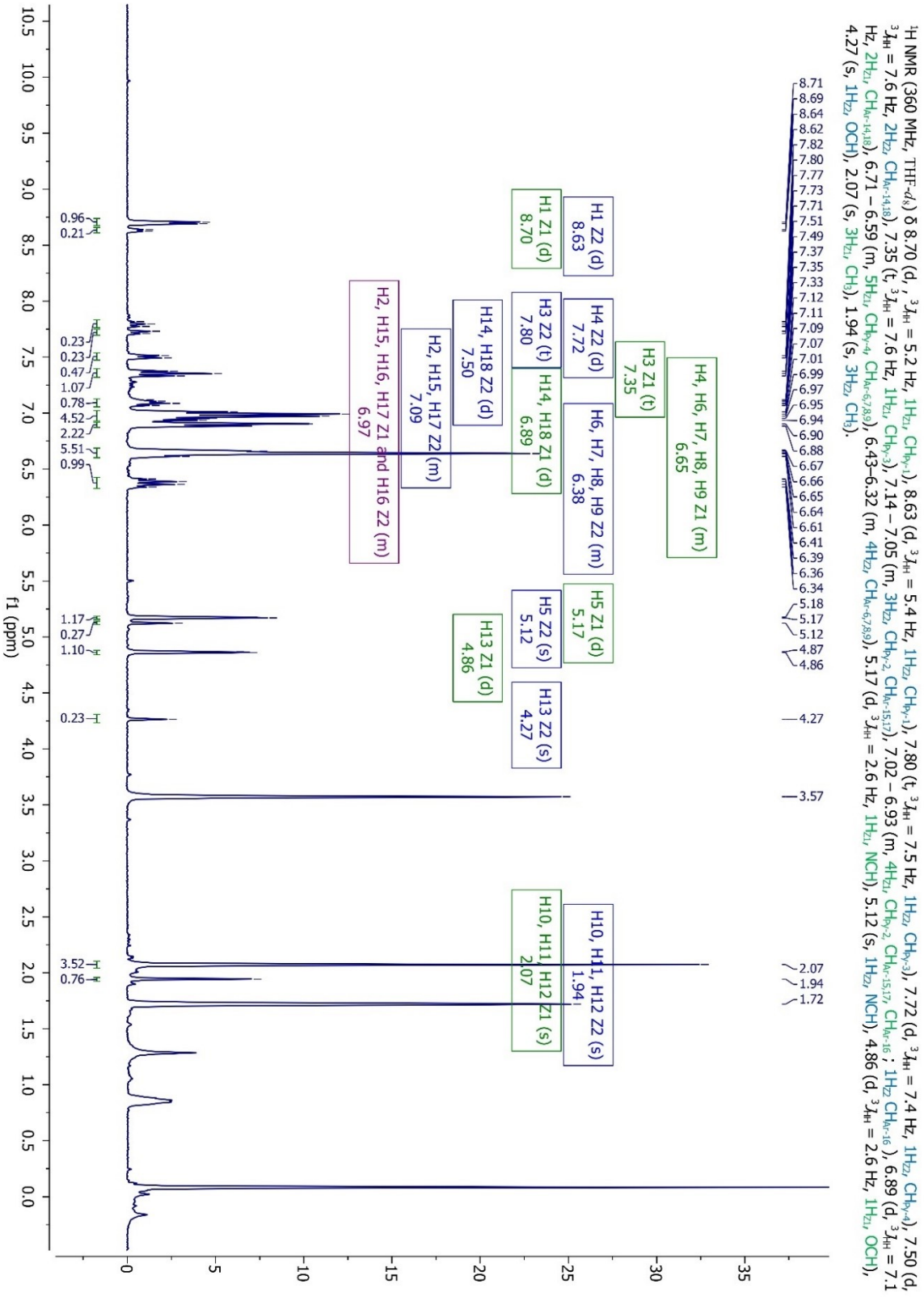

^{1}H NMR (360 MHz, THF-d_8) δ 8.70 (d, $^3J_{HH}$ = 5.2 Hz, 1H$_{Z1}$, CH$_{Py-1}$), 8.63 (d, $^3J_{HH}$ = 5.4 Hz, 1H$_{Z2}$, CH$_{Py-1}$), 7.80 (t, $^3J_{HH}$ = 7.5 Hz, 1H$_{Z2}$, CH$_{Py-3}$), 7.72 (d, $^3J_{HH}$ = 7.4 Hz, 1H$_{Z2}$, CH$_{Py-4}$), 7.50 (d, $^3J_{HH}$ = 7.6 Hz, 2H$_{Z2}$, CH$_{Ar-14,18}$), 7.35 (t, $^3J_{HH}$ = 7.6 Hz, 1H$_{Z1}$, CH$_{Py-3}$), 7.14 – 7.05 (m, 3H$_{Z2}$, CH$_{Py-2}$, CH$_{Ar-15,17}$), 7.02 – 6.93 (m, 4H$_{Z1}$, CH$_{Py-2}$, CH$_{Ar-15,17}$, CH$_{Ar-16}$; 1H$_{Z2}$ CH$_{Ar-16}$), 6.89 (d, $^3J_{HH}$ = 7.1 Hz, 2H$_{Z1}$, CH$_{Ar-14,18}$), 6.71 – 6.59 (m, 5H$_{Z1}$, CH$_{Py-4}$ CH$_{Ar-6,7,8,9}$), 6.43–6.32 (m, 4H$_{Z2}$, CH$_{Ar-6,7,8,9}$), 5.17 (d, $^3J_{HH}$ = 2.6 Hz, 1H$_{Z1}$, NCH), 5.12 (s, 1H$_{Z2}$, NCH), 4.86 (d, $^3J_{HH}$ = 2.6 Hz, 1H$_{Z1}$, OCH), 4.27 (s, 1H$_{Z2}$, OCH), 2.07 (s, 3H$_{Z1}$, CH$_3$), 1.94 (s, 3H$_{Z2}$, CH$_3$).

Figure S7.4-3: ^{1}H NMR [360 MHz, THF-d_8, 298 K] spectrum of ***fac*-K[Re(*amidopy-ba*)(CO)$_3$] (80)**.

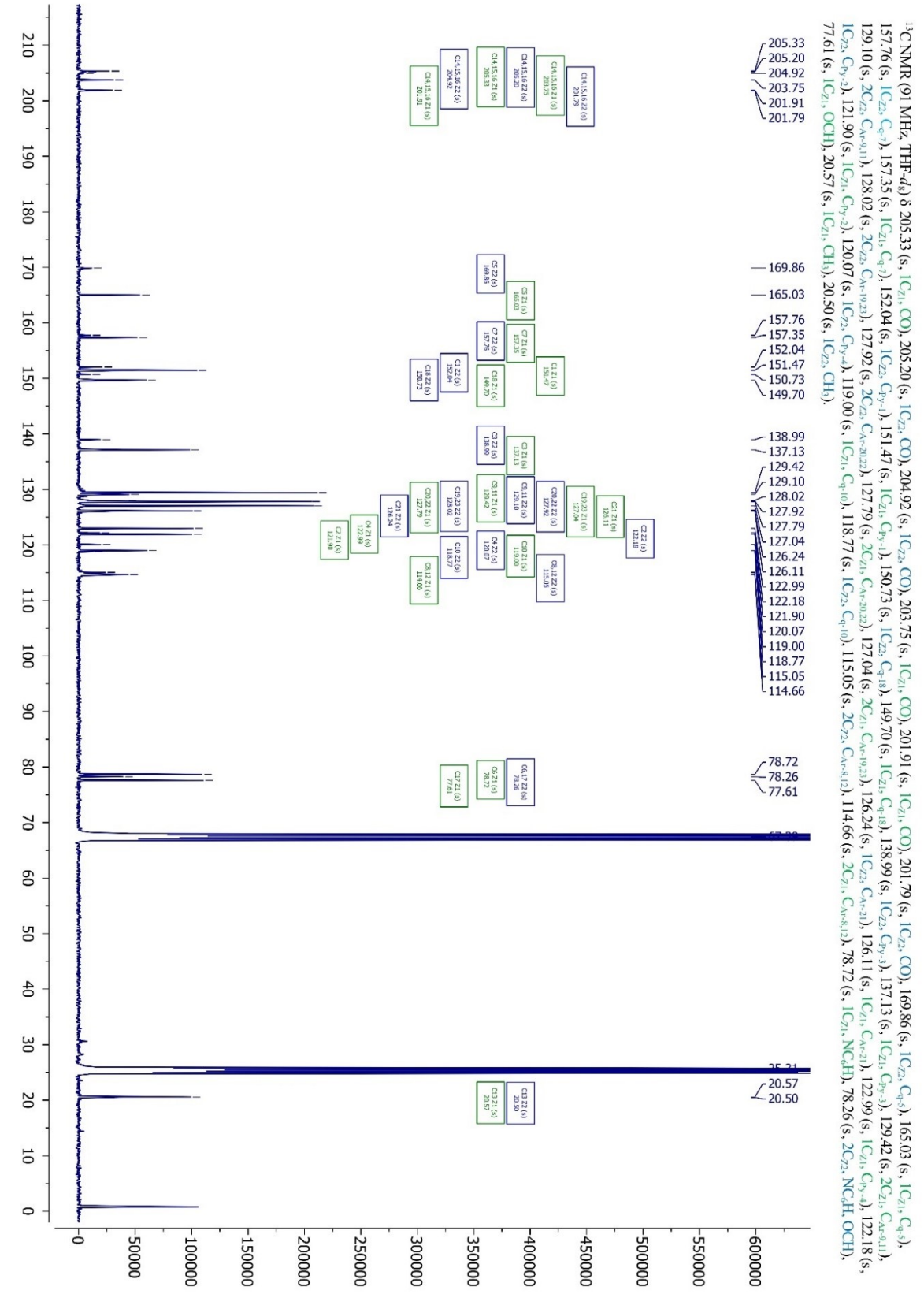

^{13}C NMR (91 MHz, THF-d_8) δ 205.33 (s, $^{1}C_{Z1}$, CO), 205.20 (s, $^{1}C_{Z2}$, CO), 204.92 (s, $^{1}C_{Z2}$, CO), 203.75 (s, $^{1}C_{Z1}$, CO), 201.91 (s, $^{1}C_{Z1}$, CO), 201.79 (s, $^{1}C_{Z2}$, CO), 169.86 (s, $^{1}C_{Z2}$, $C_{q\text{-}5}$), 165.03 (s, $^{1}C_{Z1}$, $C_{q\text{-}5}$), 157.76 (s, $^{1}C_{Z2}$, $C_{q\text{-}7}$), 157.35 (s, $^{1}C_{Z1}$, $C_{q\text{-}7}$), 152.04 (s, $^{1}C_{Z2}$, $C_{Py\text{-}1}$), 151.47 (s, $^{1}C_{Z1}$, $C_{Py\text{-}1}$), 150.73 (s, $^{1}C_{Z2}$, $C_{q\text{-}18}$), 149.70 (s, $^{1}C_{Z1}$, $C_{q\text{-}18}$), 138.99 (s, $^{1}C_{Z2}$, $C_{Py\text{-}3}$), 137.13 (s, $^{1}C_{Z1}$, $C_{Py\text{-}3}$), 129.42 (s, $^{2}C_{Z1}$, $C_{Ar\text{-}9,11}$), 129.10 (s, $^{2}C_{Z2}$, $C_{Ar\text{-}9,11}$), 128.02 (s, $^{2}C_{Z2}$, $C_{Ar\text{-}19,23}$), 127.92 (s, $^{2}C_{Z2}$, $C_{Ar\text{-}20,22}$), 127.79 (s, $^{2}C_{Z1}$, $C_{Ar\text{-}20,22}$), 127.04 (s, $^{2}C_{Z1}$, $C_{Ar\text{-}19,23}$), 126.24 (s, $^{1}C_{Z2}$, $C_{Ar\text{-}21}$), 126.11 (s, $^{1}C_{Z1}$, $C_{Ar\text{-}21}$), 122.99 (s, $^{1}C_{Z1}$, $C_{Py\text{-}4}$), 122.18 (s, $^{1}C_{Z2}$, $C_{Py\text{-}4}$), 121.90 (s, $^{1}C_{Z1}$, $C_{Py\text{-}2}$), 120.07 (s, $^{1}C_{Z2}$, $C_{Py\text{-}2}$), 119.00 (s, $^{1}C_{Z1}$, $C_{q\text{-}10}$), 118.77 (s, $^{1}C_{Z2}$, $C_{q\text{-}10}$), 115.05 (s, $^{2}C_{Z2}$, $C_{Ar\text{-}8,12}$), 114.66 (s, $^{2}C_{Z1}$, $C_{Ar\text{-}8,12}$), 78.72 (s, $^{1}C_{Z1}$, NC_5H), 78.26 (s, $^{2}C_{Z2}$, NC_5H, OCH), 77.61 (s, $^{1}C_{Z1}$, OCH), 20.57 (s, $^{1}C_{Z1}$, CH_3), 20.50 (s, $^{1}C_{Z2}$, CH_3).

Figure S7.4-4: $^{13}C\{^{1}H\}$ NMR [91 MHz, THF-d_8, 298 K] spectrum of ***fac*-K[Re(*amidopy-ba*)(CO)$_3$] (80)**.

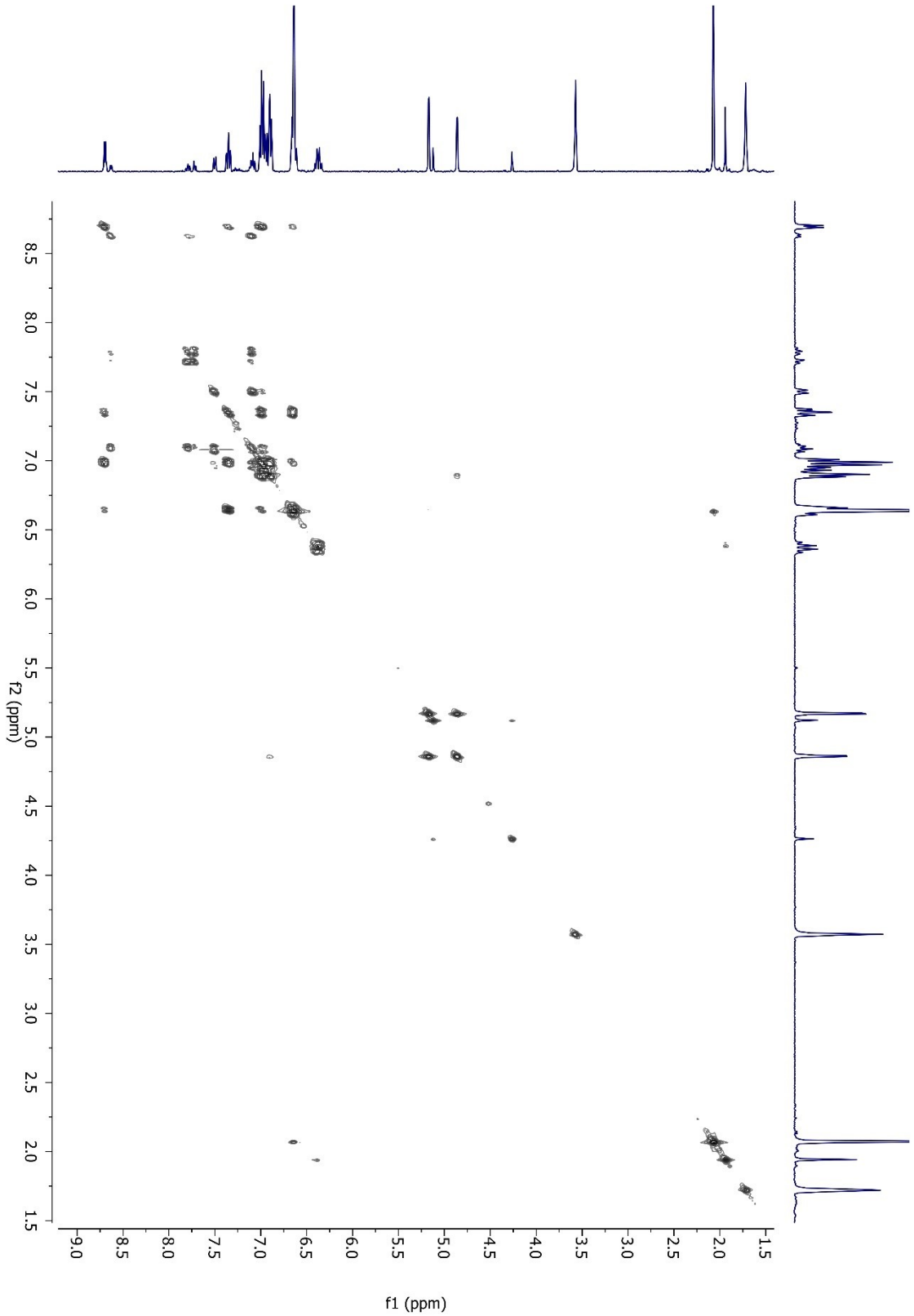

Figure S7.4-5: $^{1}H^{1}H$ COSY NMR [360 MHz, THF-d_8, 298 K] spectrum of ***fac*-K[Re(*amidopy-ba*)(CO)$_3$] (80)**.

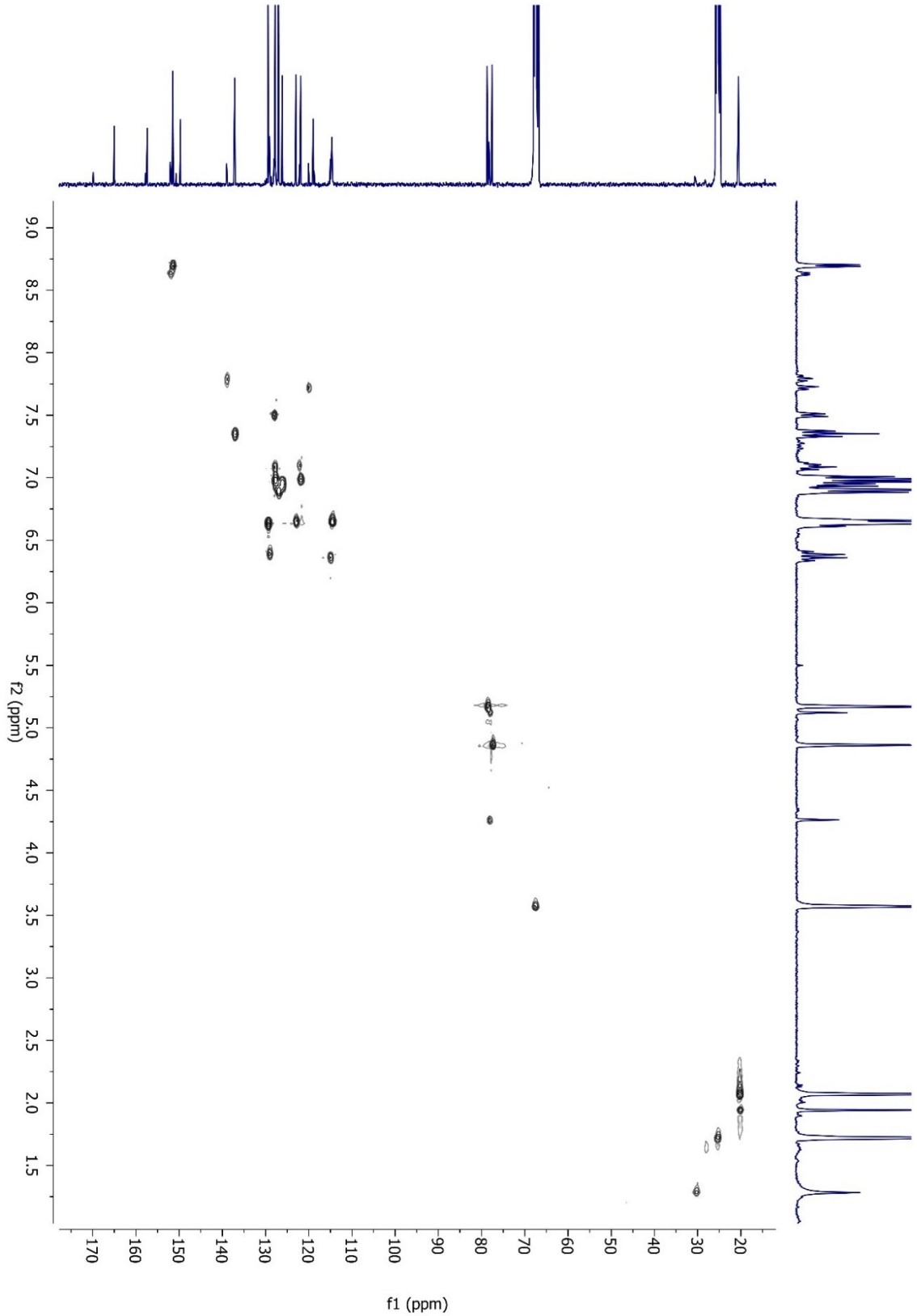

Figure S7.4-6: $^{1}H^{13}C$ HSQC NMR [360 MHz/ 91 MHz, THF-d_8, 298 K] spectrum of ***fac*-K[Re(*amidopy-ba*)(CO)$_3$] (80)**.

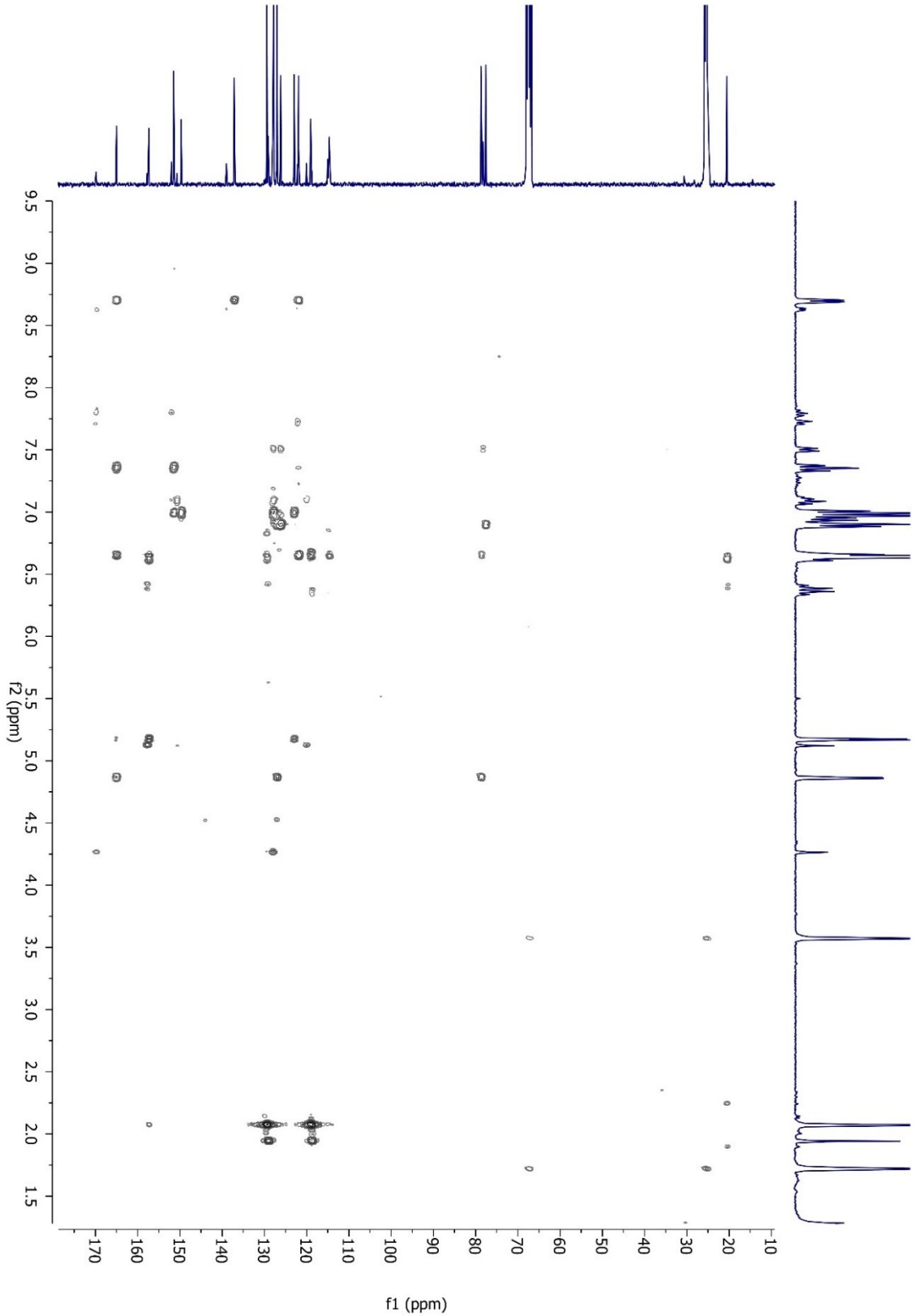

Figure S7.4-7: $^{1}H^{13}C$ HMBC NMR [360 MHz/ 91 MHz, THF-d_8, 298 K] spectrum of ***fac*-K[Re(*amidopy-ba*)(CO)$_3$] (80)**.

U:\Rasmus\...\pMeIRe-K-BA_MeOH-AF_1 3/8/2021 10:53:10 AM

pMeIRe-K-BA_MeOH-AF_1#161 RT: 1.55
T: FTMS - p ESI Full ms [120.00-1000.00]
m/z= 150.0000-1000.0000

m/z	Intensity	Relative	Composition
250.93587	379994.3	19.36	O_4 Re
272.95654	455096.4	23.18	$C_3H_2O_3$ Re
296.88217	329808.4	16.80	
297.95181	274785.3	14.00	C_4HO_3NRe
314.94363	686488.8	34.97	$C_4H_2O_5$ ^{185}Re
316.94632	1098319.5	55.94	$C_4H_2O_5$ Re
358.93344	745505.4	37.97	$C_3O_6N_3$ ^{185}Re
360.93616	1236364.5	62.98	$C_2O_6N_4$ ^{185}Re
390.96201	264799.0	13.49	$C_{10}H_4O_5$ Re
436.96753	389389.1	19.83	H_7ON_3 ^{185}Re Re
465.03827	1166024.4	59.39	$C_{16}H_{12}O_3N_2$ ^{185}Re
467.04086	1963227.8	100.00	$C_{16}H_{12}O_3N_2$ Re
468.04437	333087.2	16.97	$C_{11}H_{13}O_5N_4$ Re
630.93109	396654.6	20.20	$C_{11}H_5O_5N_3$ ^{185}Re Re

Figure S7.4-8: HRMS-ESI neg [CH_2Cl_2/CH_3OH] spectrum of ***fac*-K[Re(*amidopy-ba*)$(CO)_3$] (80)**.

pMeIRe-K-BA_MeOH-AF_1_210308111510 3/8/2021 11:15:11 AM

pMeIRe-K-BA_MeOH-AF_1_210308111510#442 RT: 4.25
T: FTMS + c ESI Full ms [150.00-1000.00]

m/z	Intensity	Relative	Composition
465.03699	421687.1	27.47	$C_{17}H_{12}O_3NRe$
467.04047	710357.9	46.28	$C_{15}H_{12}O_3N_3{}^{185}Re$
469.05560	335547.6	21.86	$C_{16}H_{14}O_3N_2Re$
479.05258	231984.4	15.11	$C_{18}H_{14}O_3NRe$
481.05545	382004.5	24.89	$C_{17}H_{14}O_3N_2Re$
525.09460	237049.2	15.44	$C_{19}H_{20}O_4N_2{}^{185}Re$
527.09735	387714.1	25.26	$C_{19}H_{20}O_4N_2Re$
573.09491	927779.2	60.45	$C_{23}H_{20}O_4N_2{}^{185}Re$
575.09741	1534856.5	100.00	$C_{23}H_{20}O_4N_2Re$
576.10107	384256.0	25.04	$C_9H_{24}ON_4{}^{185}Re\ Re$
663.15399	340542.3	22.19	$C_{21}H_{25}N{}^{185}Re\ Re$
665.15588	642918.1	41.89	$C_{20}H_{25}N_2{}^{185}Re\ Re$
666.15845	211993.0	13.81	$C_{20}H_{26}N_2{}^{185}Re\ Re$
991.12848	270776.4	17.64	
993.13184	284639.0	18.54	

Figure S7.4-9: HRMS-ESI pos [CH_2Cl_2/CH_3OH(0,1% FA)] spectrum of ***fac*-K[Re(*amidopy-ba*)$(CO)_3$] (80)**.

pMeIRe-K-BA_DCM_MeOH_FA_200219171829 2/19/2020 5:27:41 PM

pMeIRe-K-BA_DCM_MeOH_FA_200219171829#263 RT: 3.52
T: FTMS + c ESI Full ms2 575.10@cid23.00 [155.00-700.00]

m/z	Intensity	Relative	Composition
197.10759	39358.3	9.20	$C_{13}H_{13}N_2$
384.03973	39760.4	9.29	$C_{13}H_{11}ONRe$
413.06631	71790.8	16.78	$C_{14}H_{14}ON_2Re$
441.06128	99366.9	23.22	$C_{15}H_{14}O_2N_2Re$
467.04068	59961.8	14.01	$C_{16}H_{12}O_3N_2Re$
469.05627	42824.3	10.01	$C_{16}H_{14}O_3N_2Re$
473.10272	230211.7	53.80	$C_{20}H_{18}N_2Re$
489.09760	148102.3	34.61	$C_{20}H_{18}ON_2Re$
491.11322	104773.5	24.48	$C_{20}H_{20}ON_2Re$
501.09753	72057.0	16.84	$C_{21}H_{18}ON_2Re$
517.09253	62385.9	14.58	$C_{21}H_{18}O_2N_2Re$
519.10815	348111.1	81.35	$C_{21}H_{20}O_2N_2Re$
547.10309	427928.0	100.00	$C_{22}H_{20}O_3N_2Re$
557.08734	74931.8	17.51	$C_{23}H_{18}O_3N_2Re$
575.09790	161776.5	37.80	$C_{23}H_{20}O_4N_2Re$

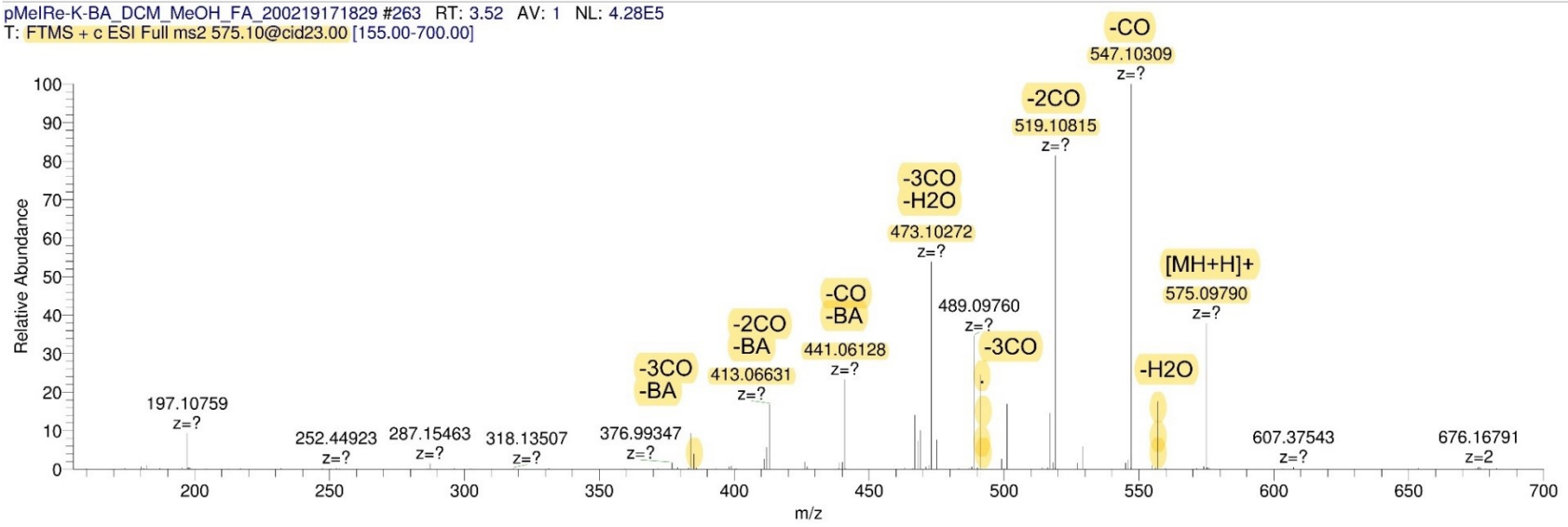

Figure S7.4-10: HRMS-ESI pos [CH_2Cl_2/CH_3OH(0,1% FA)] spectrum of m/z 575.10@cid23.

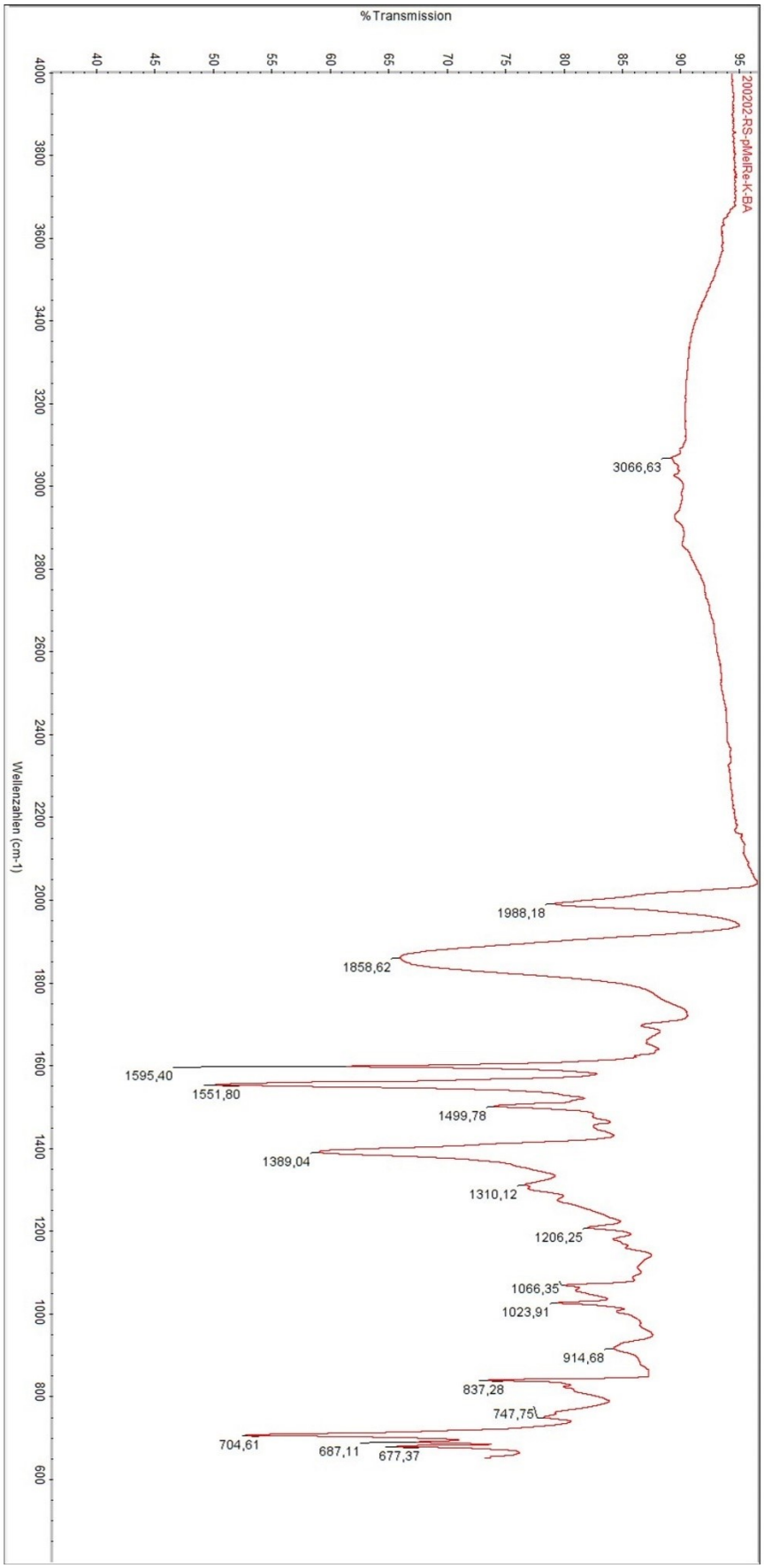

Figure S7.4-11: IR spectrum (FT-IR) of ***fac*-K[Re(*amidopy-ba*)(CO)$_3$] (80)**.

Table 7: Crystal data and structure refinement of ***fac*-K[Re(*amidopy-ba*)(CO)$_3$] (80)**.

checkCIF/PLATON report

Structure factors have been supplied for datablock(s) stichauerr180924_0m

THIS REPORT IS FOR GUIDANCE ONLY. IF USED AS PART OF A REVIEW PROCEDURE FOR PUBLICATION, IT SHOULD NOT REPLACE THE EXPERTISE OF AN EXPERIENCED CRYSTALLOGRAPHIC REFEREE.

No syntax errors found. CIF dictionary Interpreting this report

Datablock: stichauerr180924_0m

Bond precision: C-C = 0.0034 A Wavelength=0.71073

Cell: a=11.8072(5) b=12.3481(5) c=14.2532(5)
alpha=76.999(1) beta=69.975(1) gamma=61.929(1)
Temperature: 100 K

	Calculated	Reported
Volume	1717.65(12)	1717.65(12)
Space group	P -1	P -1
Hall group	-P 1	-P 1
Moiety formula	C70 H84 K2 N4 O14 Re2	C35 H42 K N2 O7 Re
Sum formula	C70 H84 K2 N4 O14 Re2	C35 H42 K N2 O7 Re
Mr	1656.03	828.00
Dx,g cm-3	1.601	1.601
Z	1	2
Mu (mm-1)	3.708	3.708
F000	832.0	832.0
F000'	830.72	
h,k,lmax	14,15,17	14,15,17
Nref	6939	6925
Tmin,Tmax	0.313,0.411	0.538,0.747
Tmin'	0.283	

Correction method= # Reported T Limits: Tmin=0.538 Tmax=0.747
AbsCorr = MULTI-SCAN

Data completeness= 0.998 Theta(max)= 26.247

R(reflections)= 0.0143(6592) wR2(reflections)= 0.0332(6925)

S = 1.146 Npar= 429

The following ALERTS were generated. Each ALERT has the format
test-name_ALERT_alert-type_alert-level.
Click on the hyperlinks for more details of the test.

Alert level C

PLAT220_ALERT_2_C	Non-Solvent Resd 1 C Ueq(max)/Ueq(min) Range	3.6 Ratio
PLAT410_ALERT_2_C	Short Intra H...H Contact H6 ..H8 .	1.95 Ang.
	x,y,z =	1_555 Check
PLAT910_ALERT_3_C	Missing # of FCF Reflection(s) Below Theta(Min).	7 Note
PLAT911_ALERT_3_C	Missing FCF Refl Between Thmin & STh/L= 0.600	7 Report

Alert level G

PLAT042_ALERT_1_G	Calc. and Reported MoietyFormula Strings Differ	Please Check
PLAT045_ALERT_1_G	Calculated and Reported Z Differ by a Factor ...	0.50 Check
PLAT154_ALERT_1_G	The s.u.'s on the Cell Angles are Equal ..(Note)	0.001 Degree
PLAT230_ALERT_2_G	Hirshfeld Test Diff for O4 --C24 .	5.5 s.u.
PLAT232_ALERT_2_G	Hirshfeld Test Diff (M-X) Re1 --C23 .	7.1 s.u.
PLAT232_ALERT_2_G	Hirshfeld Test Diff (M-X) Re1 --C24 .	9.9 s.u.
PLAT232_ALERT_2_G	Hirshfeld Test Diff (M-X) Re1 --C25 .	7.7 s.u.
PLAT764_ALERT_4_G	Overcomplete CIF Bond List Detected (Rep/Expd) .	1.13 Ratio
PLAT774_ALERT_1_G	Suspect X-Y Bond in CIF: K1 --K1 ..	4.03 Ang.
PLAT793_ALERT_4_G	Model has Chirality at C6 (Centro SPGR)	R Verify
PLAT793_ALERT_4_G	Model has Chirality at C14 (Centro SPGR)	S Verify
PLAT883_ALERT_1_G	No Info/Value for _atom_sites_solution_primary .	Please Do !
PLAT978_ALERT_2_G	Number C-C Bonds with Positive Residual Density.	11 Info

0 **ALERT level A** = Most likely a serious problem - resolve or explain
0 **ALERT level B** = A potentially serious problem, consider carefully
4 **ALERT level C** = Check. Ensure it is not caused by an omission or oversight
13 **ALERT level G** = General information/check it is not something unexpected

5 ALERT type 1 CIF construction/syntax error, inconsistent or missing data
7 ALERT type 2 Indicator that the structure model may be wrong or deficient
2 ALERT type 3 Indicator that the structure quality may be low
3 ALERT type 4 Improvement, methodology, query or suggestion
0 ALERT type 5 Informative message, check

It is advisable to attempt to resolve as many as possible of the alerts in all categories. Often the minor alerts point to easily fixed oversights, errors and omissions in your CIF or refinement strategy, so attention to these fine details can be worthwhile. In order to resolve some of the more serious problems it may be necessary to carry out additional measurements or structure refinements. However, the purpose of your study may justify the reported deviations and the more serious of these should normally be commented upon in the discussion or experimental section of a paper or in the "special_details" fields of the CIF. checkCIF was carefully designed to identify outliers and unusual parameters, but every test has its limitations and alerts that are not important in a particular case may appear. Conversely, the absence of alerts does not guarantee there are no aspects of the results needing attention. It is up to the individual to critically assess their own results and, if necessary, seek expert advice.

Publication of your CIF in IUCr journals

A basic structural check has been run on your CIF. These basic checks will be run on all CIFs submitted for publication in IUCr journals (*Acta Crystallographica*, *Journal of Applied Crystallography*, *Journal of Synchrotron Radiation*); however, if you intend to submit to *Acta Crystallographica Section C* or *E* or *IUCrData*, you should make sure that full publication checks are run on the final version of your CIF prior to submission.

Publication of your CIF in other journals

Please refer to the *Notes for Authors* of the relevant journal for any special instructions relating to CIF submission.

PLATON version of 07/08/2019; check.def file version of 30/07/2019

Datablock stichauerr180924_0m - ellipsoid plot

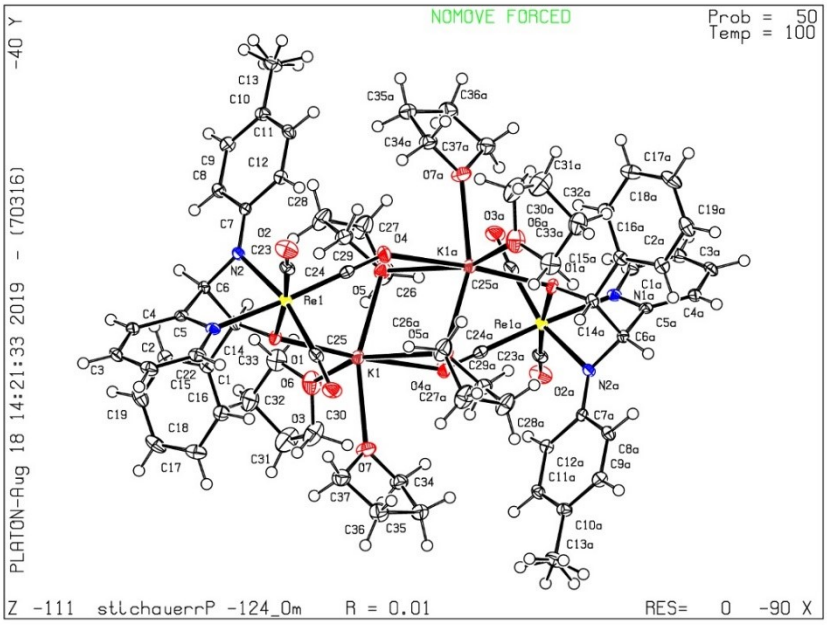

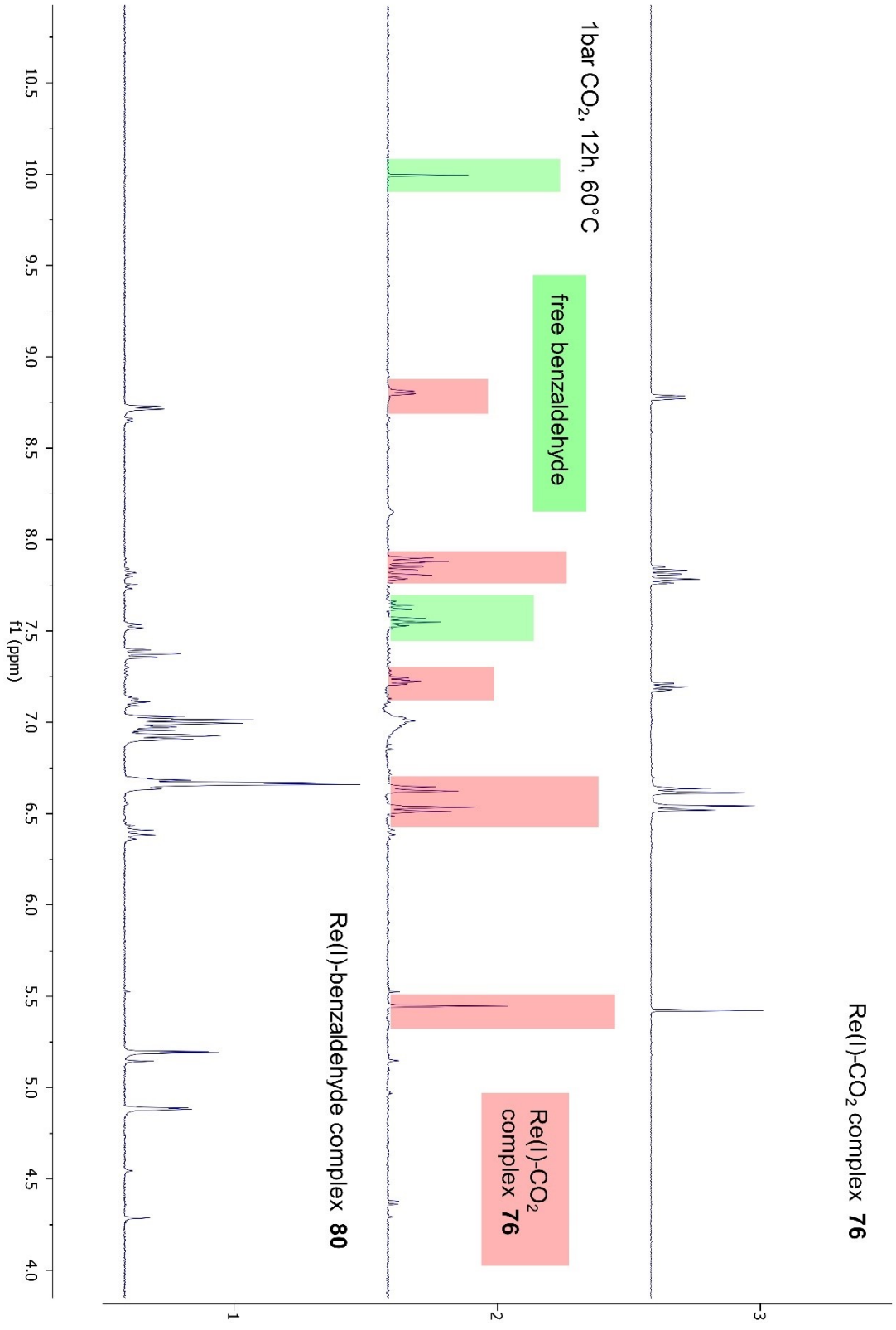

Figure S7.4-12: ^{1}H NMR [360 MHz, THF-d_8, 298 K] spectrum of ***fac*-K[Re(*amidopy-ba*)(CO)$_3$]** (**80**) with 1 bar CO_2 (middle).

***fac*-K[Re(*amidopy-bph*)(CO)$_3$] (81)**

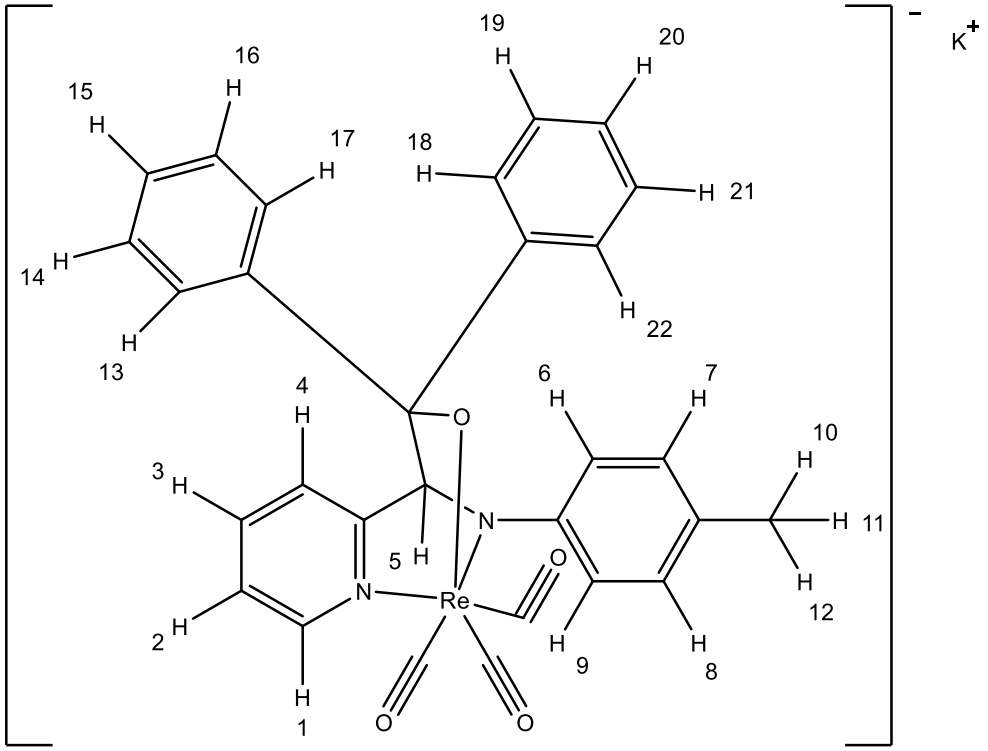

Figure S7.4-13: Structural formula of ***fac*-K[Re(*amidopy-bph*)(CO)$_3$] (81)** for the assignment of ^{1}H NMR signals.

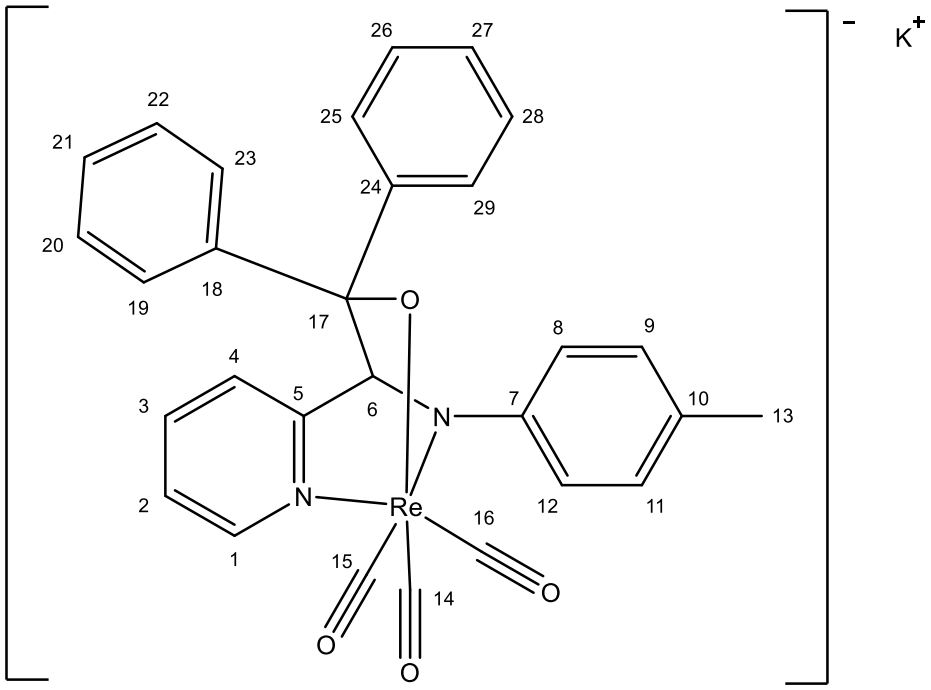

Figure S7.4-14: Structural formula of ***fac*-K[Re(*amidopy-bph*)(CO)$_3$] (81)** for the assignment of ^{13}C NMR signals.

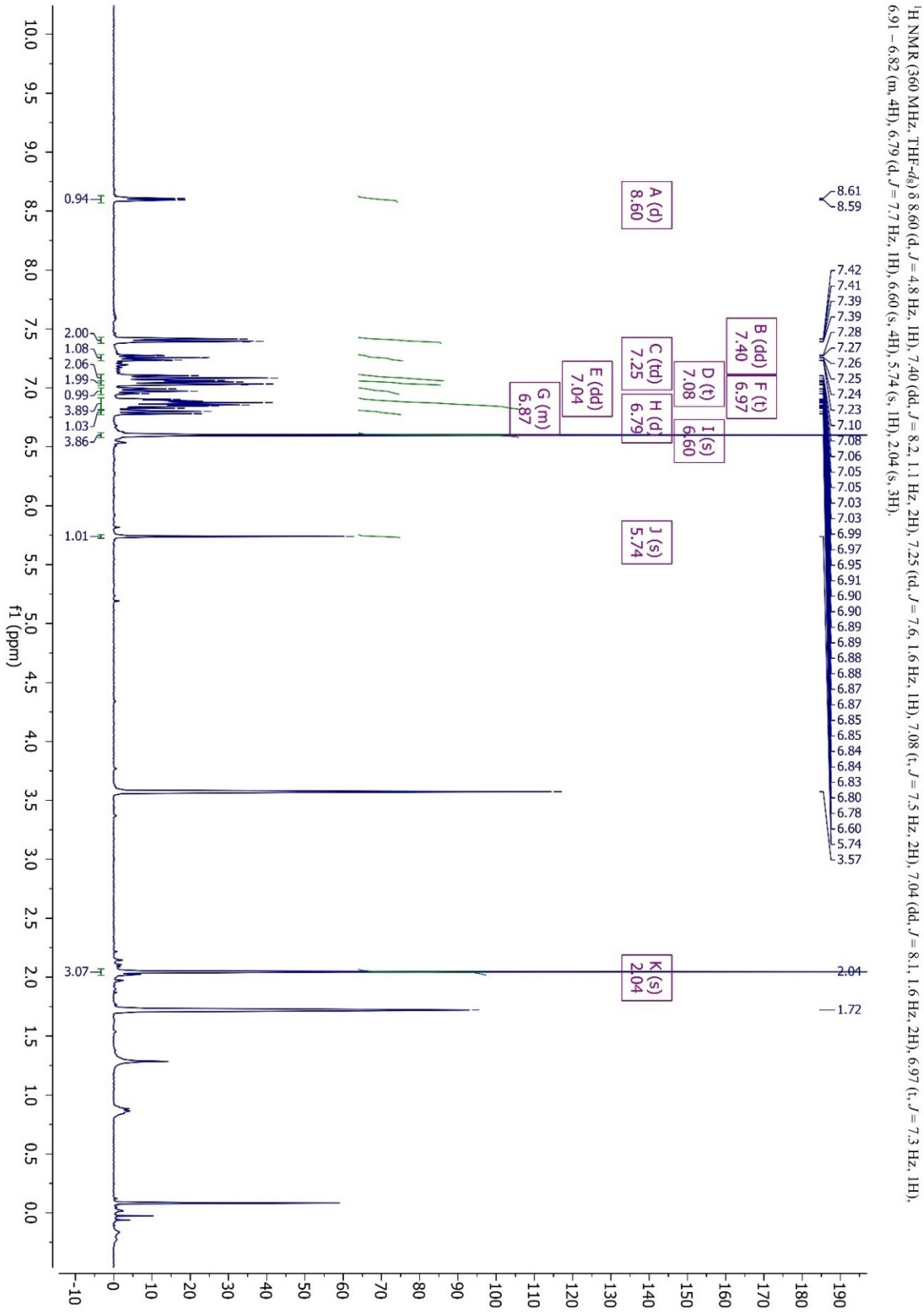

Figure S7.4-15: ^{1}H NMR [360 MHz, THF-d_8, 298 K] spectrum of ***fac*-K[Re(*amidopy-bph*)(CO)$_3$] (81)**.

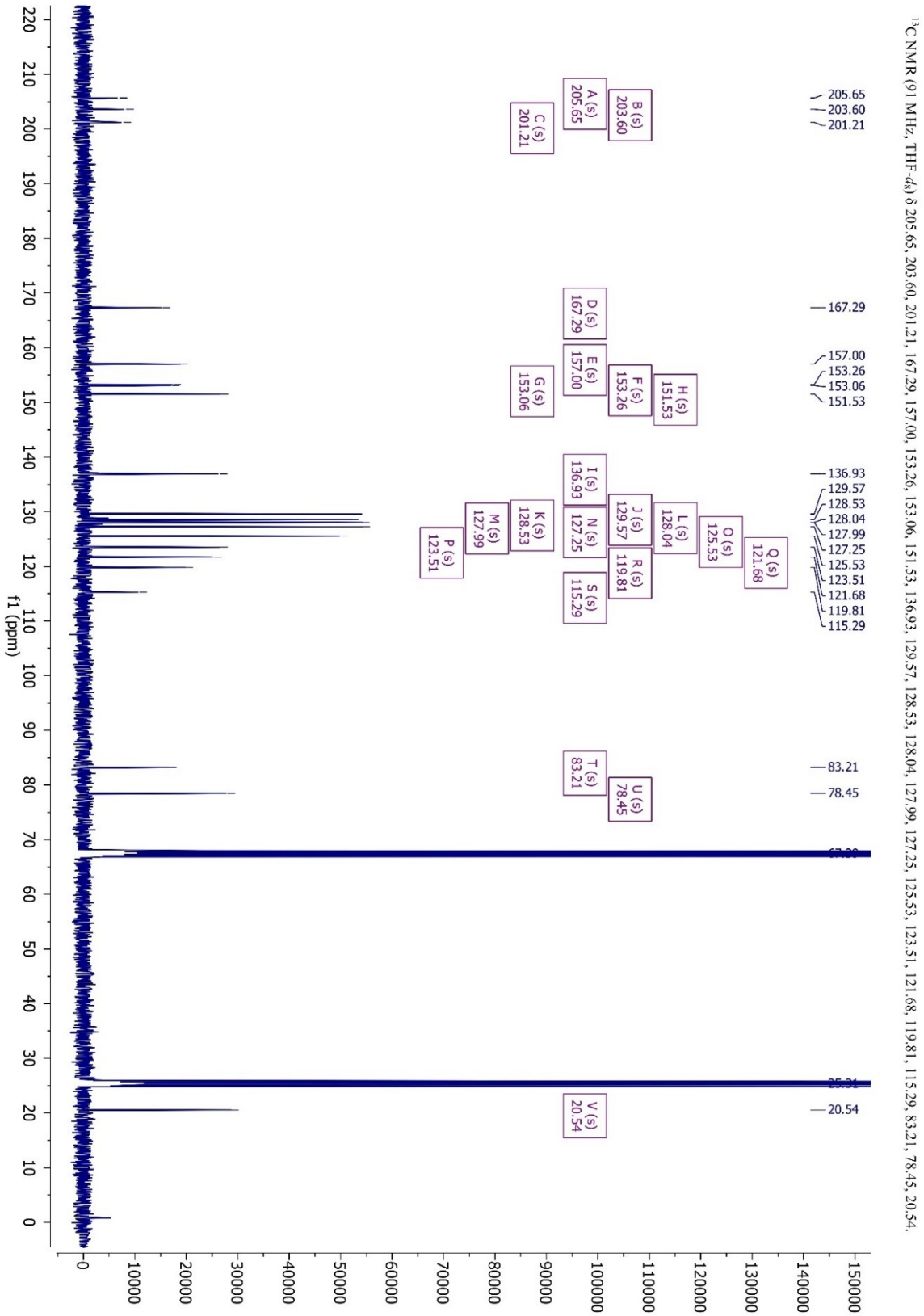

Figure S7.4-16: $^{13}C\{^1H\}$ NMR [91 MHz, THF-d_8, 298 K] spectrum of ***fac*-K[Re(*amidopy-bph*)(CO)$_3$] (81)**.

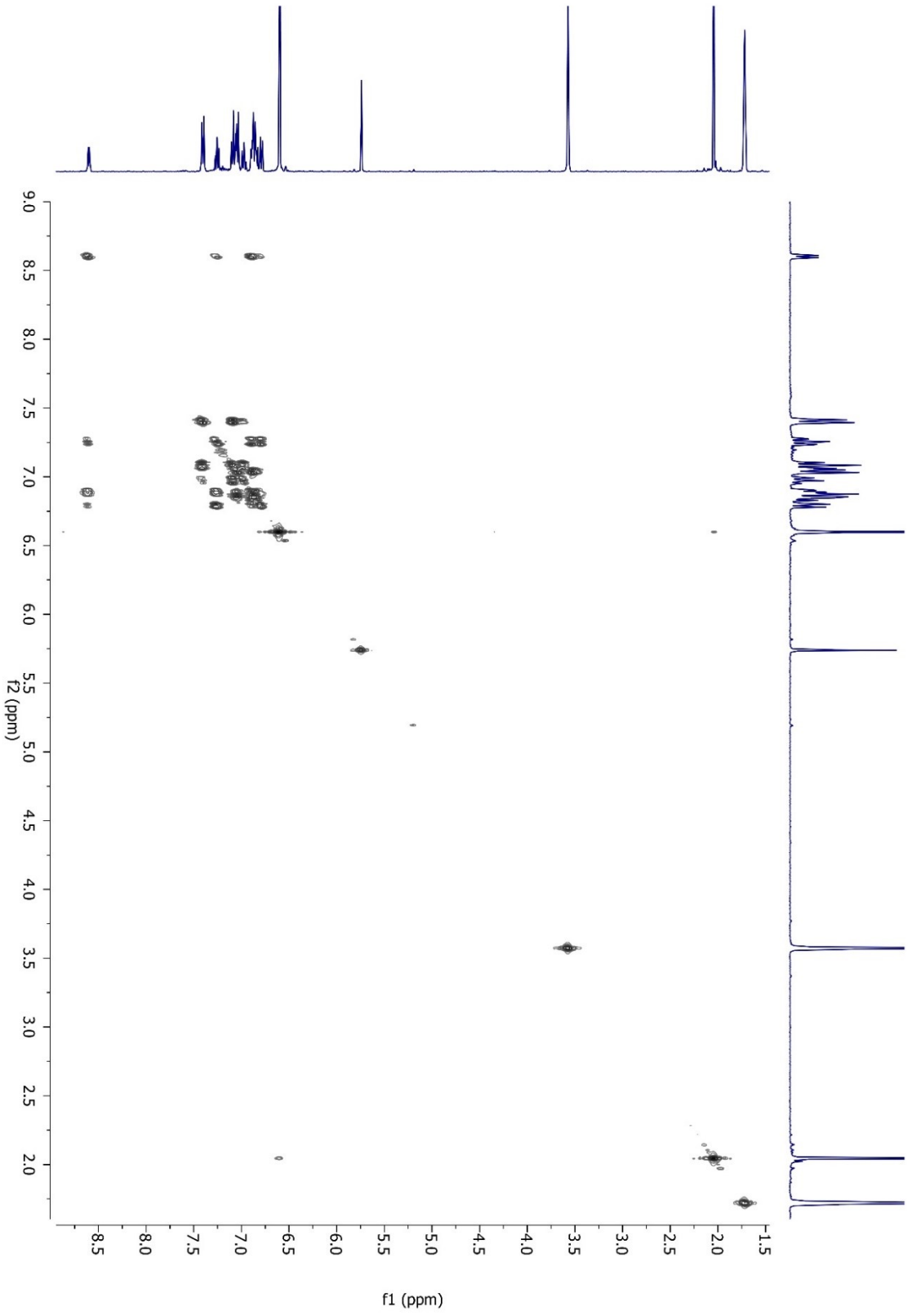

Figure S7.4-17: $^{1}H^{1}H$ COSY NMR [360 MHz, THF-d_8, 298 K] spectrum of ***fac*-K[Re(*amidopy-bph*)(CO)$_3$] (81)**.

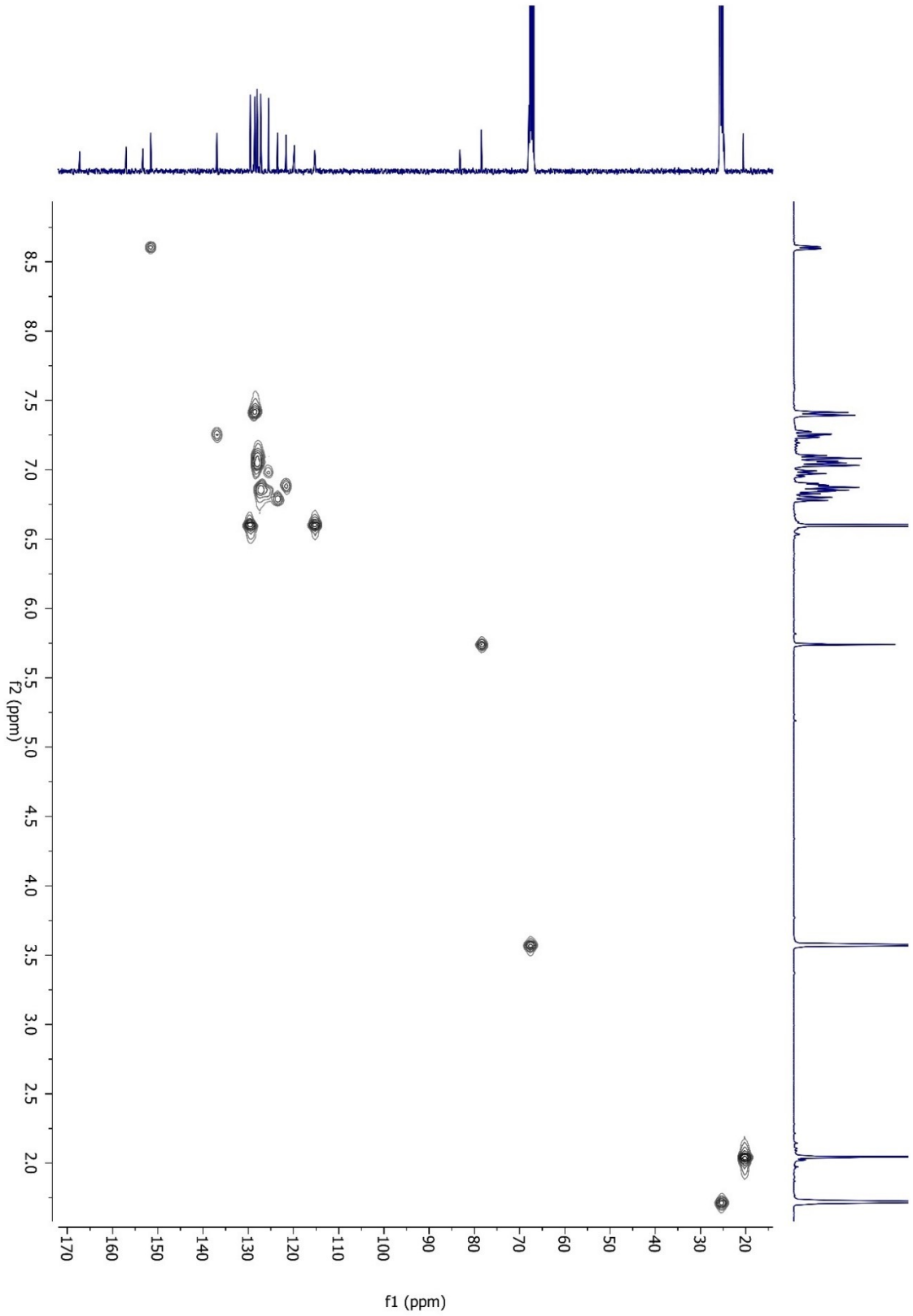

Figure S7.4-18: $^{1}H^{13}C$ HSQC NMR [360 MHz/ 91 MHz, THF-d_8, 298 K] spectrum of ***fac*-K[Re(*amidopy-bph*)(CO)$_3$] (81)**.

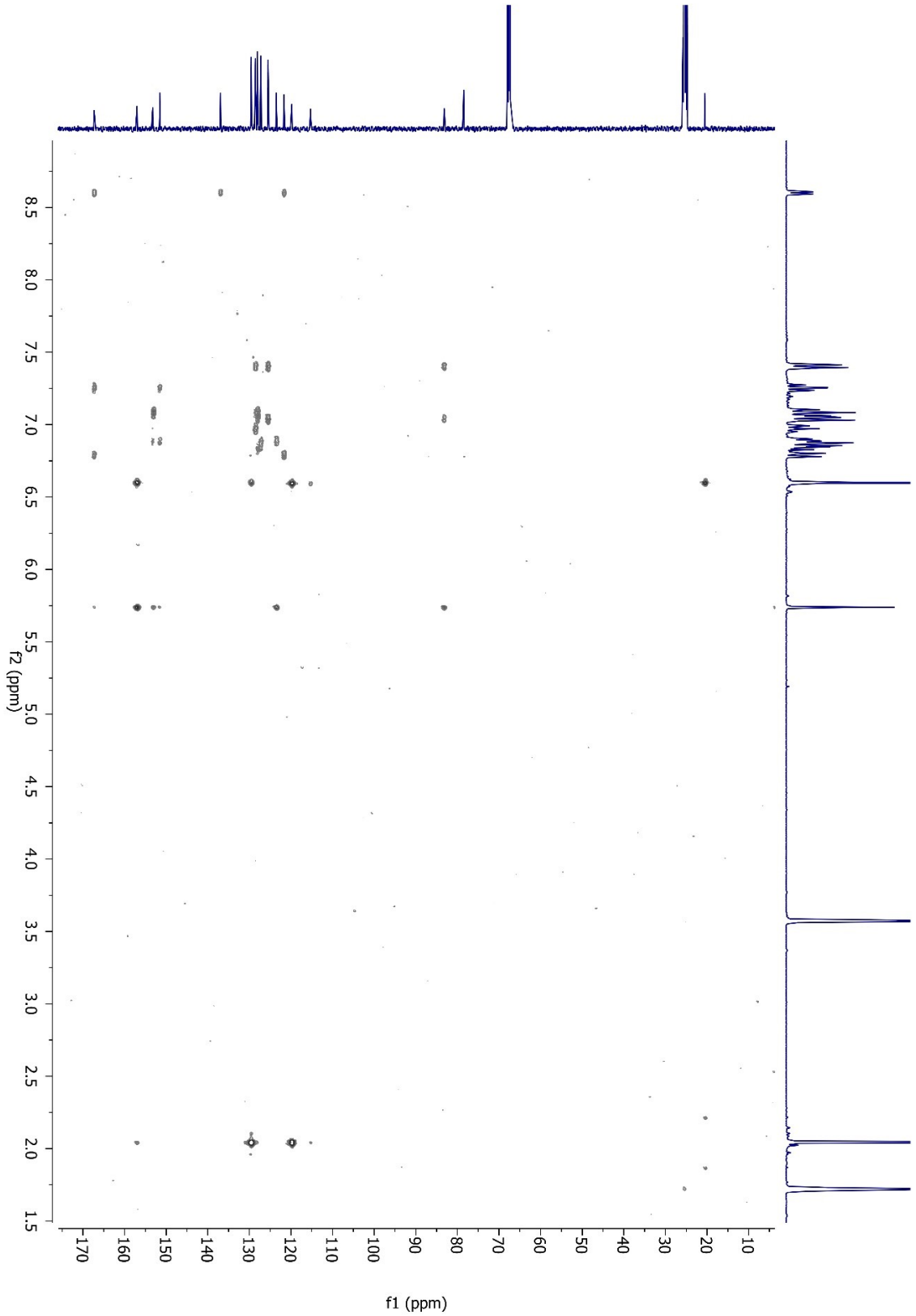

Figure S7.4-19: $^{1}H^{13}C$ HMBC NMR [360 MHz/ 91 MHz, THF-d_8, 298 K] spectrum of ***fac*-K[Re(*amidopy-bph*)(CO)$_3$] (81)**.

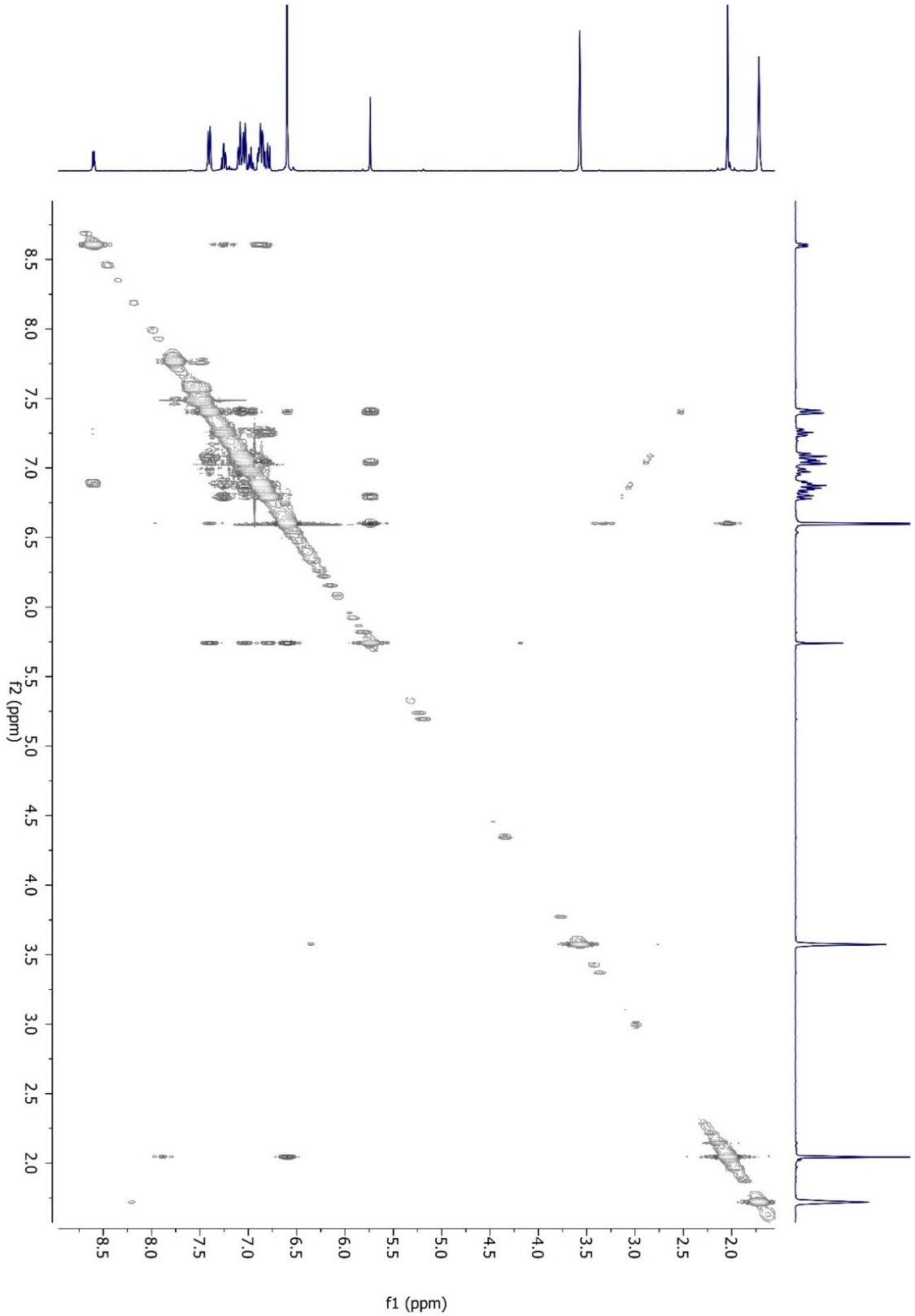

Figure S7.4-20: $^{1}H^{1}H$ NOESY NMR [360 MHz, THF-d_8, 298 K] spectrum of ***fac*-K[Re(*amidopy-bph*)(CO)$_3$] (81)**.

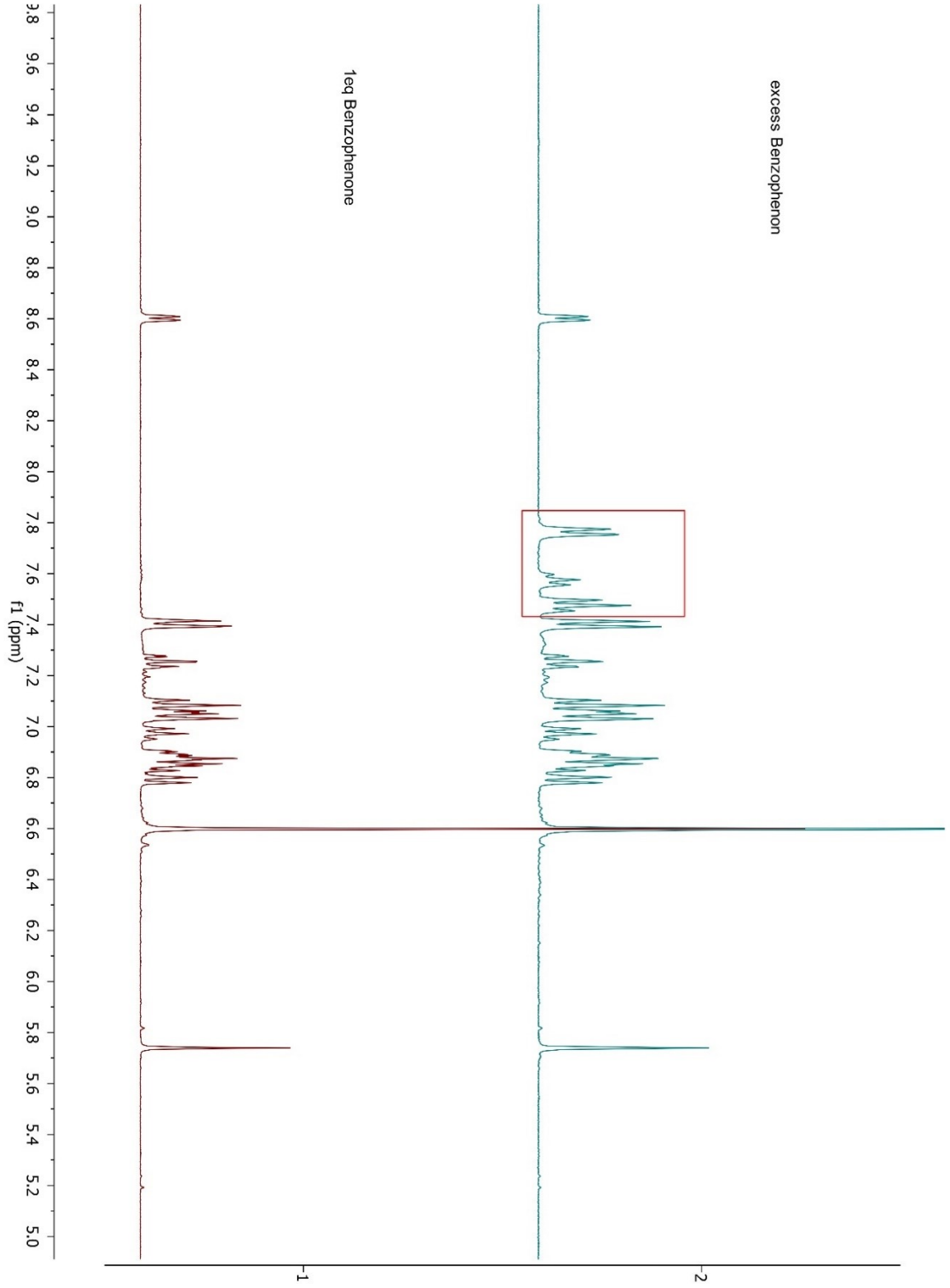

Figure S7.4-21: ^{1}H NMR [360 MHz, THF-d_8, 298 K] spectrum of ***fac*-K[Re(*amidopy-bph*)(CO)$_3$] (81**) with 1 eqiv. benzophenone (buttom) and excess of benzophenone (top) (signals of free benzophenone in the red box).

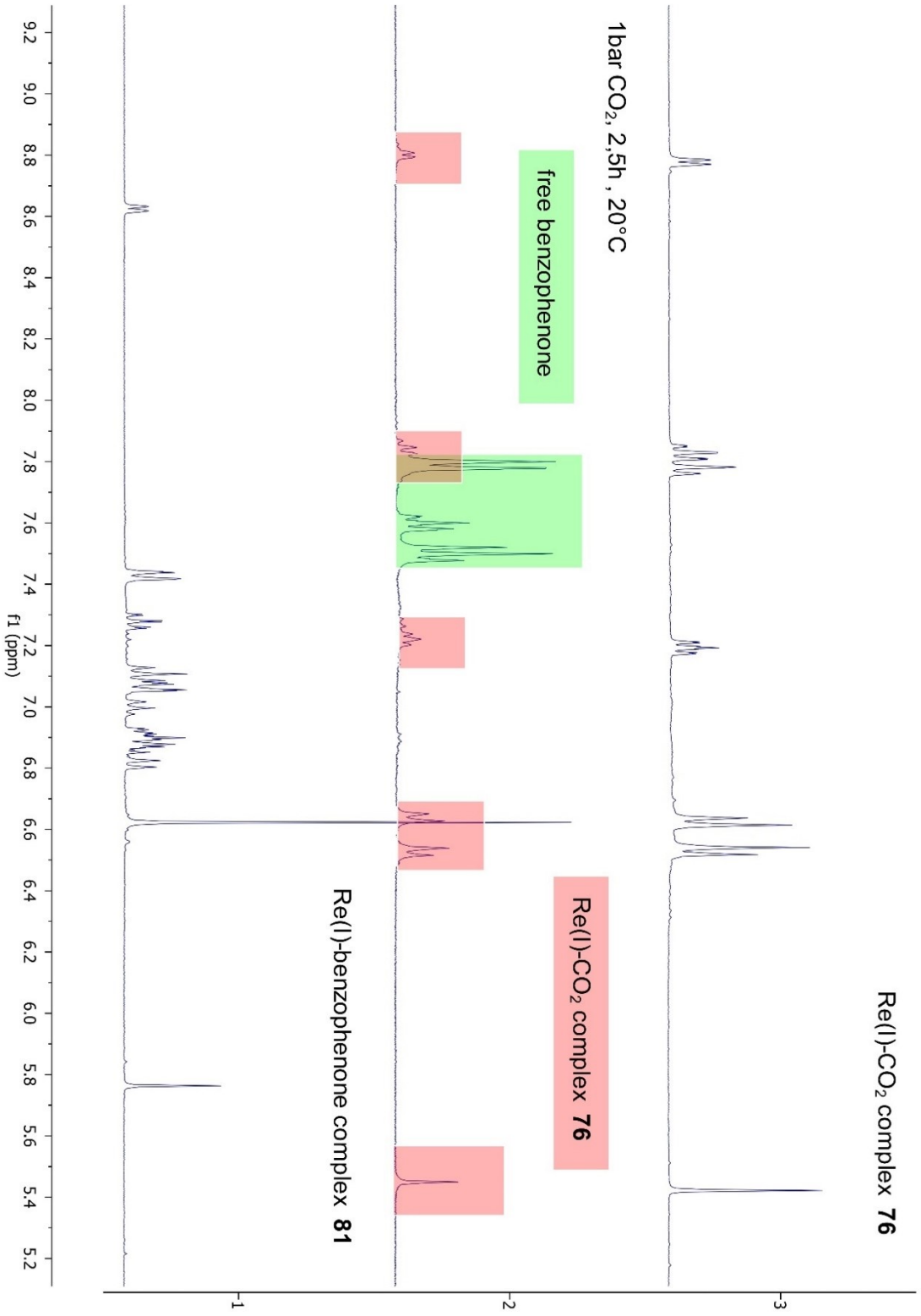

Figure S7.4-22: ^{1}H NMR [360 MHz, THF-d_8, 298 K] spectrum of ***fac*-K[Re(*amidopy-bph*)(CO)$_3$] (81)** with bar CO_2 (middle). Spectrum of complex **81** (buttom) and **76** (top) for comparison.

***fac*-[K(18-*crown*-6)][Re(*amidopy-bph*)(CO)$_3$] (81-crown)**

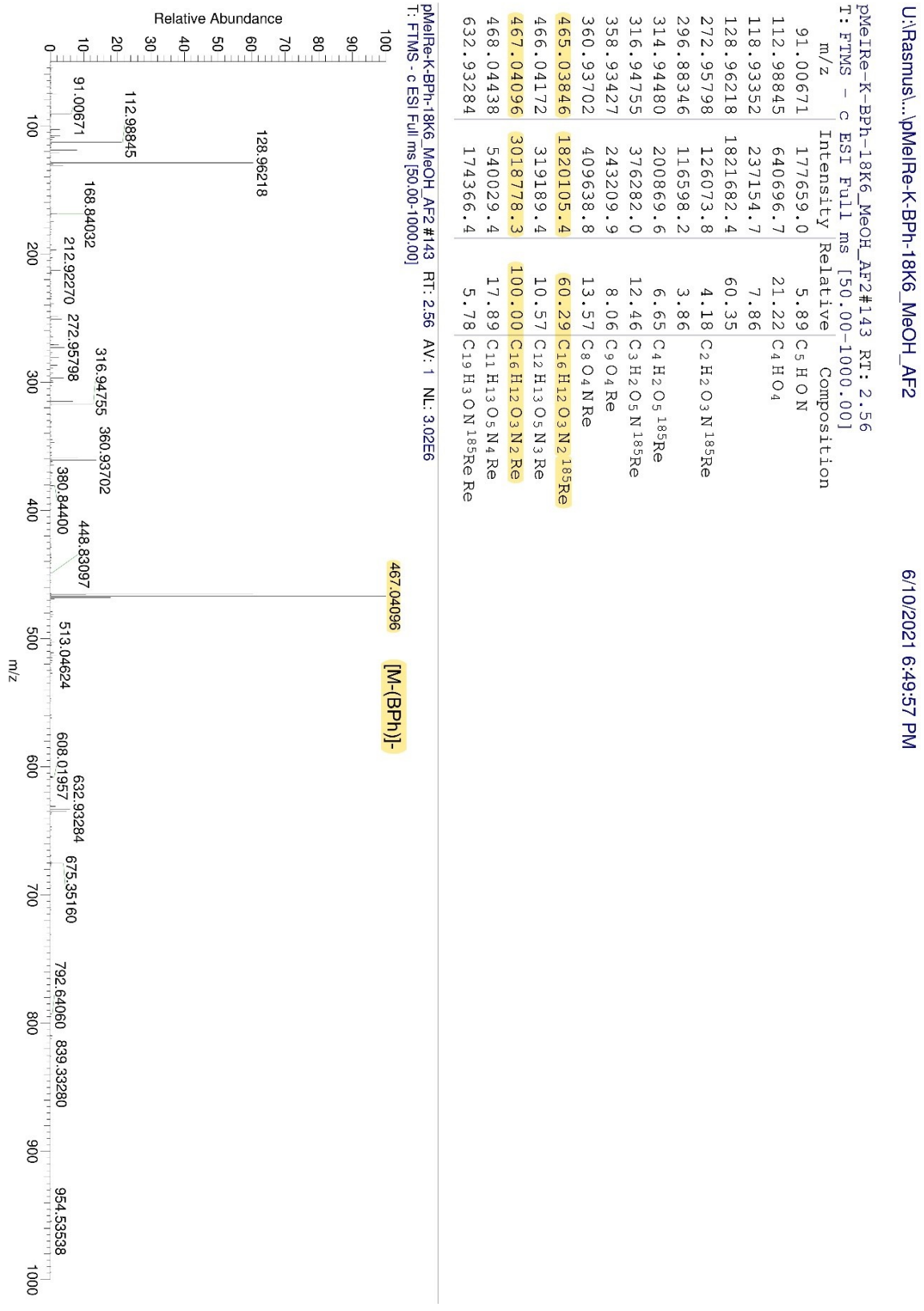

Figure S7.4-23: HRMS-ESI neg [CH_2Cl_2/CH_3OH] spectrum of ***fac*-[K(18-*crown*-6)][Re(*amidopy-bph*)(CO)$_3$] (81-crown)**.

U:\Rasmus\...\pMeIRe-K-BPh_DCM_MeOH_FA 2/19/2020 6:10:21 PM

pMeIRe-K-BPh_DCM_MeOH_FA#546 RT: 5.90
T: FTMS + c ESI Full ms [175.00-800.00]

m/z	Intensity	Relative	Composition
287.14670	5009463.5	1.18	$C_{12}H_{21}O_5N_3$
303.12048	423694656.0	100.00	$C_{12}H_{24}O_6K$
304.12369	58467756.0	13.80	$C_9H_{22}O_{10}N$
305.11844	31056410.0	7.33	$C_8H_{21}O_{10}N_2$
499.22015	4424592.0	1.04	$C_{29}H_{27}O_6N_2$
649.12610	13638659.0	3.22	$C_{29}H_{24}O_4N_2{}^{185}Re$
651.12891	23822736.0	5.62	$C_{29}H_{24}O_4N_2Re$
652.13208	6827581.0	1.61	$C_{26}H_{27}O_7NRe$

Figure S7.4-24: HRMS-ESI pos [CH_2Cl_2/CH_3OH(0.1% FA)] spectrum of ***fac*-[K(18-*crown*-6)][Re(*amidopy-bph*)$(CO)_3$] (81-crown)**.

Figure S7.4-25: HRMS-ESI pos [CH_2Cl_2/CH_3OH(0.1% FA)] spectrum of ***fac*-[K(18-*crown*-6)][Re(*amidopy-bph*)$(CO)_3$] (81-crown)**. (section m/z = 640-665)

Figure S7.4-26: HRMS-ESI pos [CH_2Cl_2/CH_3OH(0.1% FA)] spectrum of m/z 651.13@cid20.

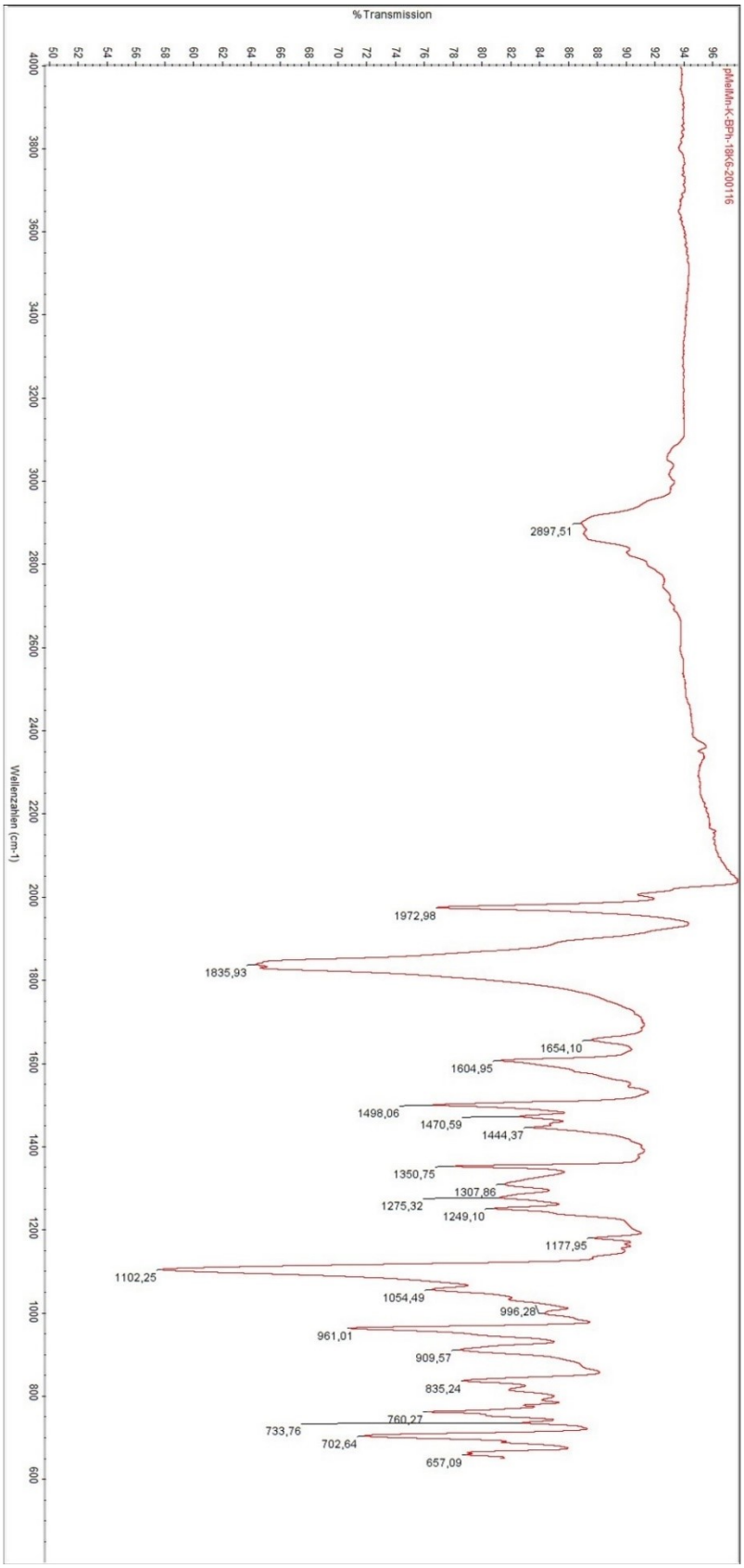

Figure S7.4-27: IR spectrum (FT-IR) of ***fac*-[K(18-*crown*-6)][Re(*amidopy-bph*)(CO)$_3$] (81-crown)**.

Table 8: Crystal data and structure refinement from Olex report of ***fac*-[K(18-*crown*-6)][Re(*amidopy-bph*)(CO)$_3$] (81-crown)**.

StichauerR171124_0m

Table 1 Crystal data and structure refinement for StichauerR171124_0m.

Identification code	StichauerR171124_0m
Empirical formula	$C_{41}H_{46}N_2O_{10}KRe$
Formula weight	952.135
Temperature/K	252.99
Crystal system	triclinic
Space group	P-1
a/Å	11.8426(5)
b/Å	16.5537(7)
c/Å	17.1026(7)
α/°	68.517(1)
β/°	79.232(1)
γ/°	80.949(1)
Volume/Å^3	3050.4(2)
Z	4
ρ_{calc}g/cm^3	2.073
μ/mm^{-1}	4.198
F(000)	1919.4
Crystal size/mm^3	N/A × N/A × N/A
Radiation	Mo Kα (λ = 0.71073)
2Θ range for data collection/°	4.62 to 49.46
Index ranges	-13 ≤ h ≤ 13, -19 ≤ k ≤ 19, -20 ≤ l ≤ 20
Reflections collected	28246
Independent reflections	10306 [R_{int} = 0.0570, R_{sigma} = 0.0640]
Data/restraints/parameters	10306/0/458
Goodness-of-fit on F^2	1.066
Final R indexes [I>=2σ (I)]	R_1 = 0.0477, wR_2 = 0.1336
Final R indexes [all data]	R_1 = 0.0687, wR_2 = 0.1466
Largest diff. peak/hole / e Å^{-3}	2.58/-1.01

7.5 Supporting Information for

Nitrile Activation *via* Cooperative C-C and Re-N Bond Formation with Bidentate Pyridine-Based Rhenium(I) Triscarbonyle Complex

Index

Spectroscopic, scXRD analysis and Mass spectrometric data for compound:

***fac*-K[Re(*amidopy-phacn*)(CO)$_3$] (82)**

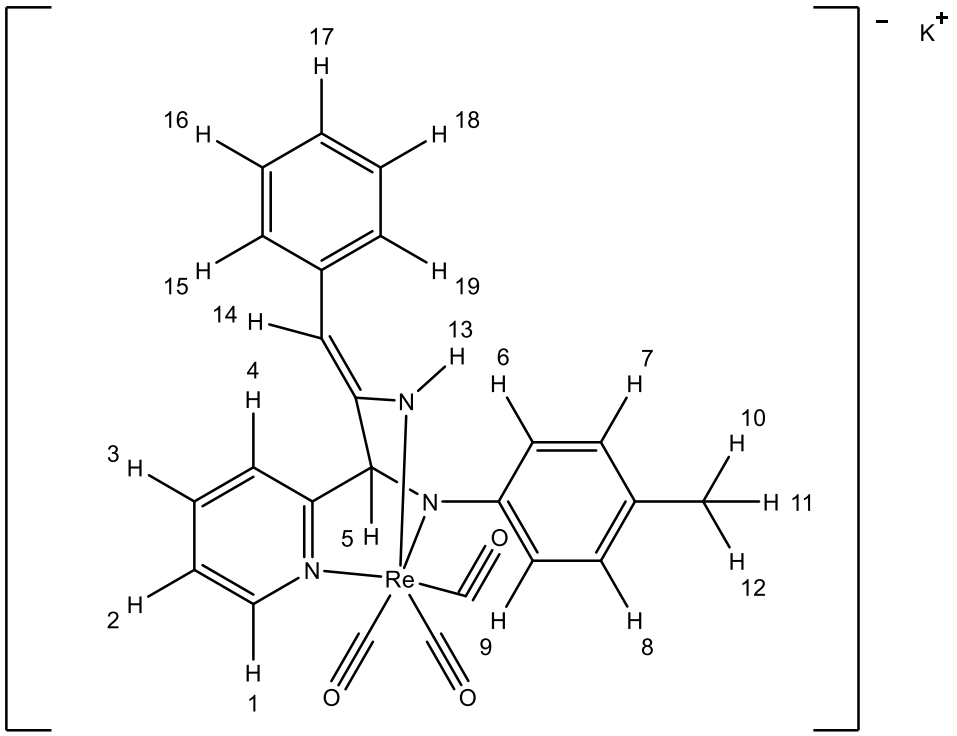

Figure S7.5-1: Structural formula of ***fac*-K[Re(*amidopy-phacn*)(CO)$_3$] (82)** for the assignment of ^{1}H NMR signals.

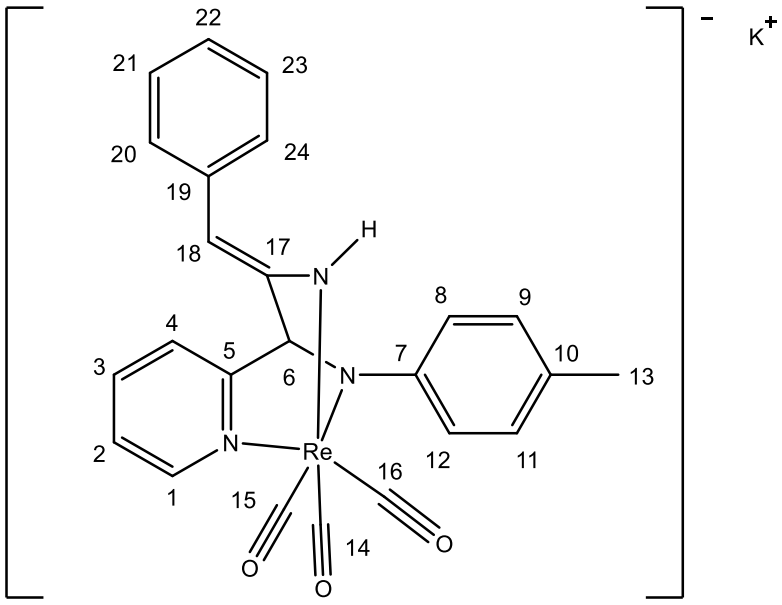

Figure S7.5-2: Structural formula of ***fac*-K[Re(*amidopy-phacn*)(CO)$_3$] (82)** for the assignment of ^{13}C NMR signals.

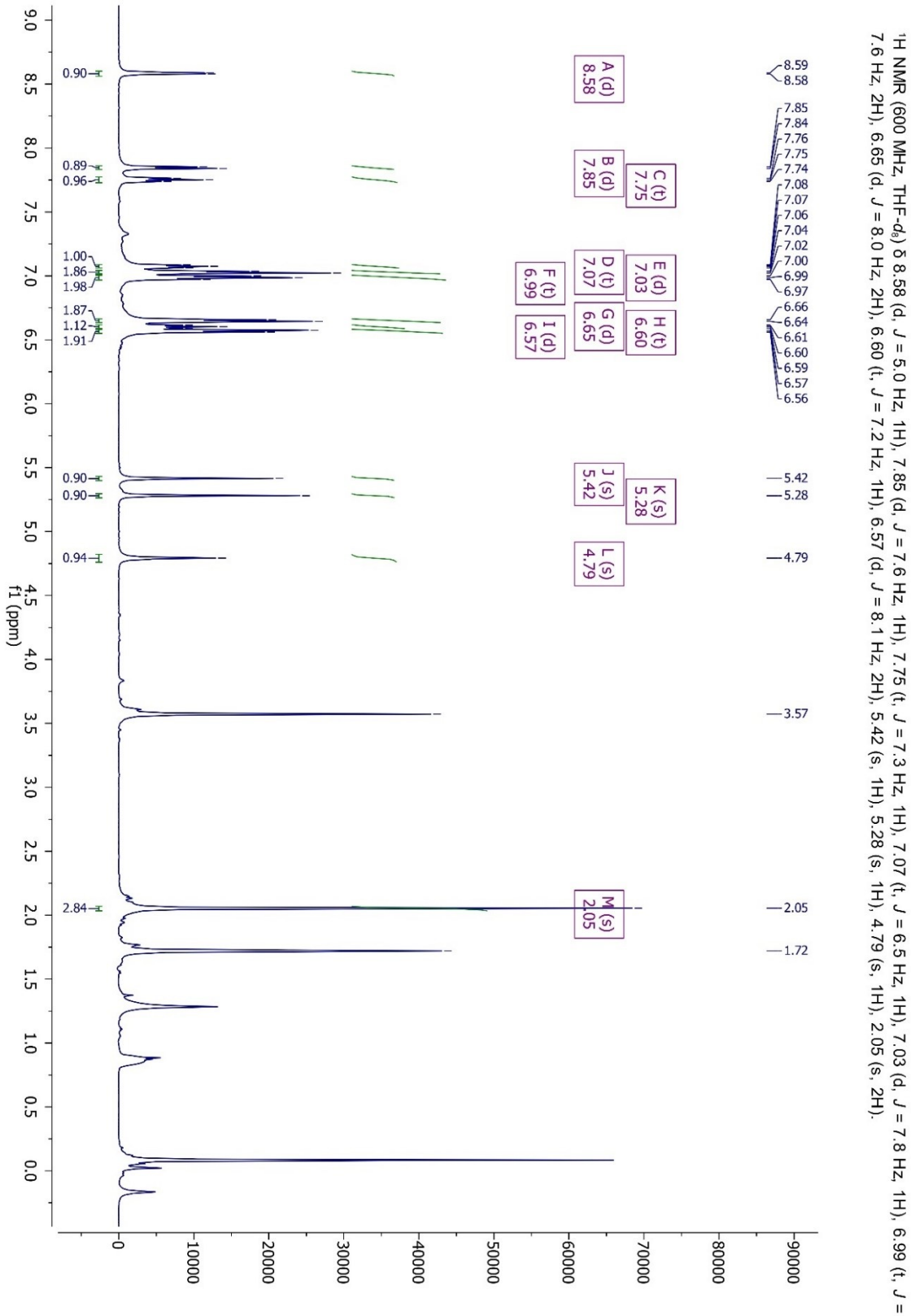

Figure S7.5-3: ^{1}H NMR [600 MHz, THF-d_8, 298 K] spectrum of ***fac*-K[Re(*amidopy-phacn*)(CO)$_3$] (82)**.

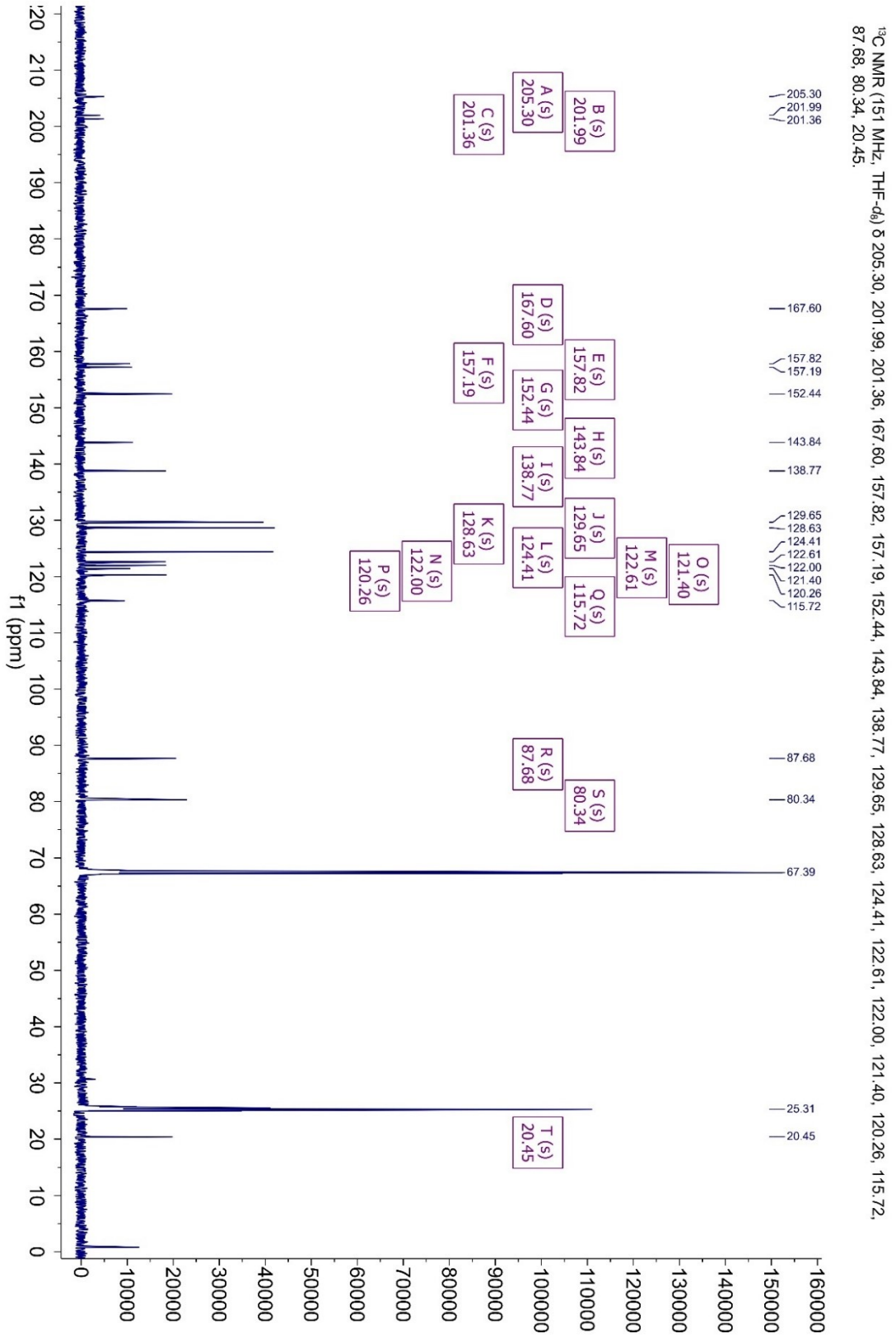

Figure S7.5-4: $^{13}C\{^{1}H\}$ NMR [151 MHz, THF-d_8, 298 K] spectrum of ***fac*-K[Re(*amidopy-phacn*)(CO)$_3$] (82)**.

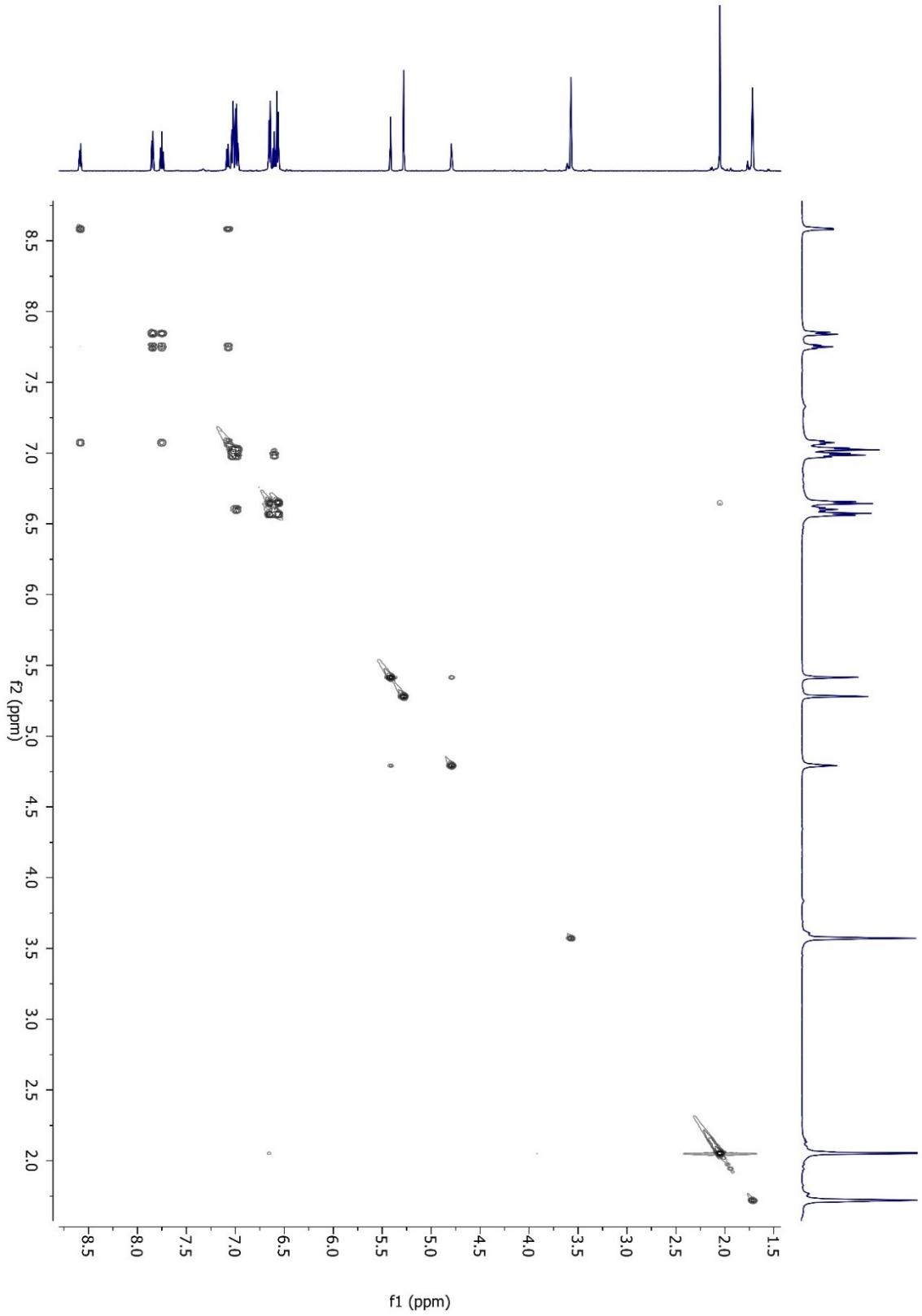

Figure S7.5-5: $^{1}H^{1}H$ COSY NMR [600 MHz, THF-d_8, 298 K] spectrum of ***fac*-K[Re(*amidopy-phacn*)(CO)$_3$] (82)**.

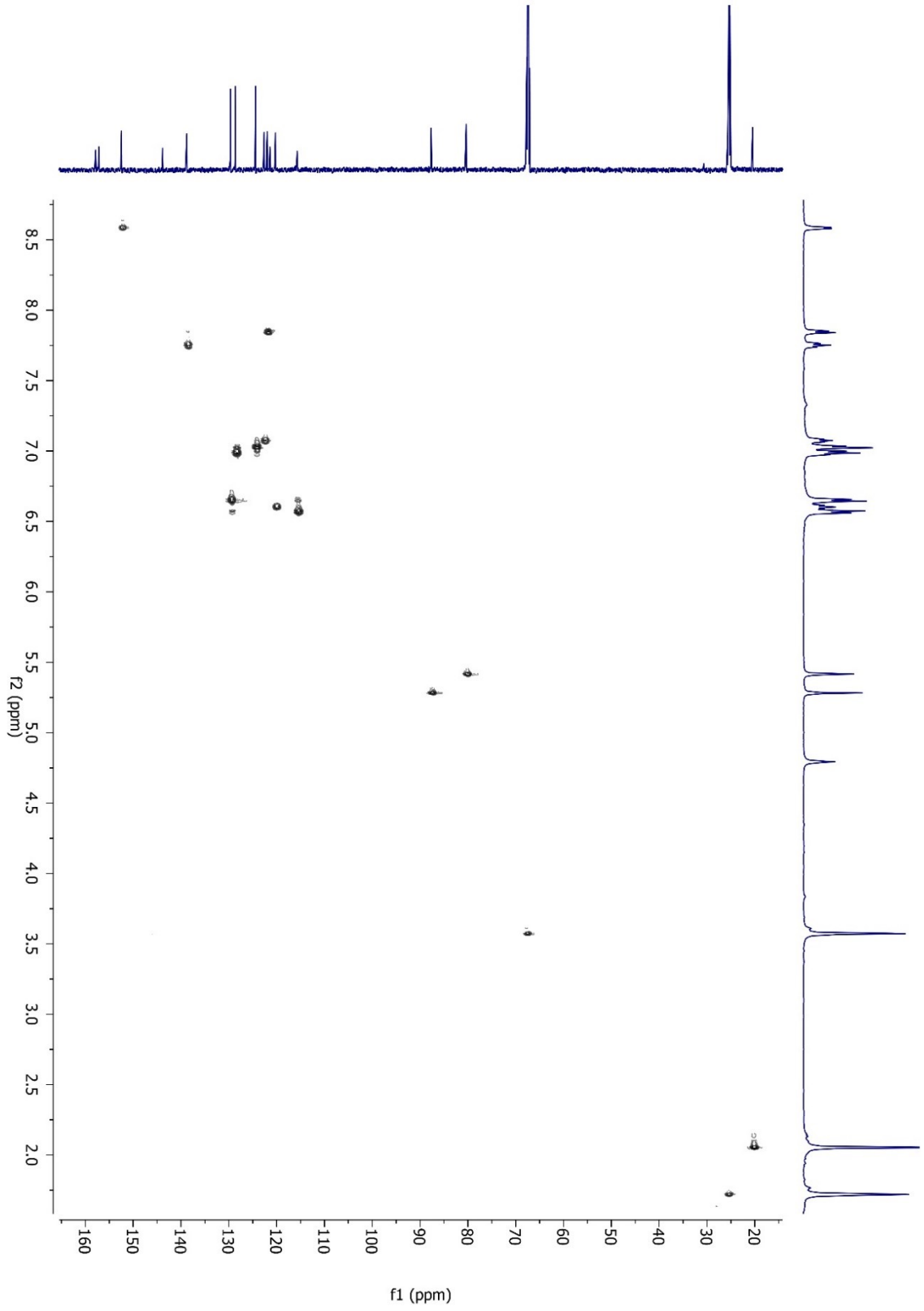

Figure S7.5-6: $^{1}H^{13}C$ HSQC NMR [600 MHz/ 151 MHz, THF-d_8, 298 K] spectrum of ***fac*-K[Re(*amidopy-phacn*)(CO)$_3$] (82)**.

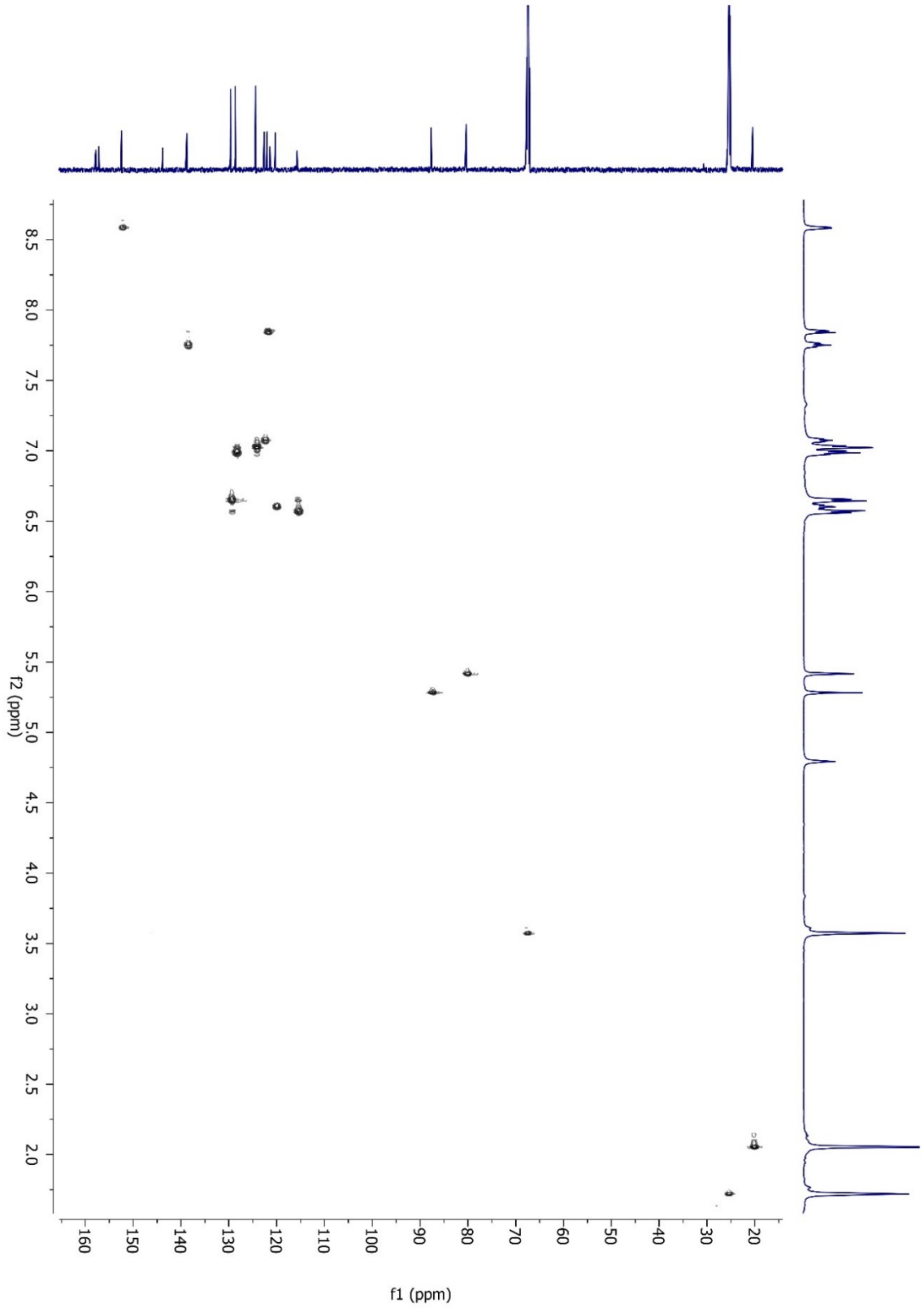

Figure S7.5-7: $^{1}H^{13}C$ HMBC NMR [600 MHz/ 151 MHz, THF-d_8, 298 K] spectrum of ***fac*-K[Re(*amidopy-phacn*)(CO)$_3$] (82)**.

U:\Rasmus\...\pMeIRe-K-PhACN_MeOH_AFFA 3/8/2021 2:09:01 PM

pMeIRe-K-PhACN_MeOH_AFFA#187 RT: 2.93
T: FTMS - c ESI Full ms [50.00-1000.00]
m/z= 150.0000-1000.0000

m/z	Intensity	Relative	Composition
174.95630	109641.0	3.04	
180.97327	120157.8	3.33	
196.94713	110251.8	3.05	
264.93436	144238.3	3.99	
314.94363	133176.0	3.69	$C_4H_2O_5{}^{185}Re$
316.94653	258240.8	7.15	$C_4H_2O_5Re$
358.93344	155247.8	4.30	
360.93625	281582.7	7.80	
465.03842	114962.7	3.18	$C_{16}H_{12}O_3N_2{}^{185}Re$
467.04114	220564.0	6.11	$C_{16}H_{12}O_3N_2Re$
582.09613	2149770.8	59.53	$C_{24}H_{19}O_3N_3{}^{185}Re$
583.09955	515759.7	14.28	$C_{20}H_{20}O_5N_4Re$
584.09863	3611516.3	100.00	$C_{24}H_{19}O_3N_3Re$
585.10217	909119.1	25.17	$C_{19}H_{20}O_5N_5Re$

Figure S7.5-8: HRMS-ESI neg [CH_3OH(0.1% FA, 2mM AF)] spectrum of ***fac*-K[Re(*amidopy-phacn*)$(CO)_3$] (82)**.

Figure S7.5-9: HRMS-ESI neg [CH_3OH(0.1% FA, 2mM AF)] spectrum of m/z 584.10@lcid17.

Figure S7.5-10: HRMS-ESI pos [CH_3OH(0.1% FA, 2mM AF)] spectrum of ***fac*-K[Re(*amidopy-phacn*)$(CO)_3$] (82)**.

U:\Rasmus\...\pMeIRe-K-PhACN_MeOH_AFFA_4 6/14/2021 5:44:06 PM

pMeIRe-K-PhACN_MeOH_AFFA_4#101 RT: 1.52
T: FTMS + c ESI Full ms2 586.11@cid20.00 [160.00-600.00]

m/z	Intensity	Relative	Composition
168.92345	275563.2	1.27	
395.05404	245325.6	1.13	$C_{22}H_9O_5N_3$
502.12783	10665193.0	49.12	$C_{21}H_{21}N_3Re$
530.12292	21711756.0	100.00	$C_{22}H_{21}ON_3Re$
531.12621	244140.7	1.12	$C_{17}H_{22}O_3N_5Re$
558.11797	767662.4	3.54	$C_{23}H_{21}O_2N_3Re$
586.11333	2427962.0	11.18	$C_{24}H_{21}O_3N_3Re$
587.11669	882725.6	4.07	$C_{19}H_{22}O_5N_5Re$

Figure S7.5-11: HRMS-ESI pos [CH_3OH(0.1% FA, 2mM AF)] spectrum of m/z 586.11@lcid20.

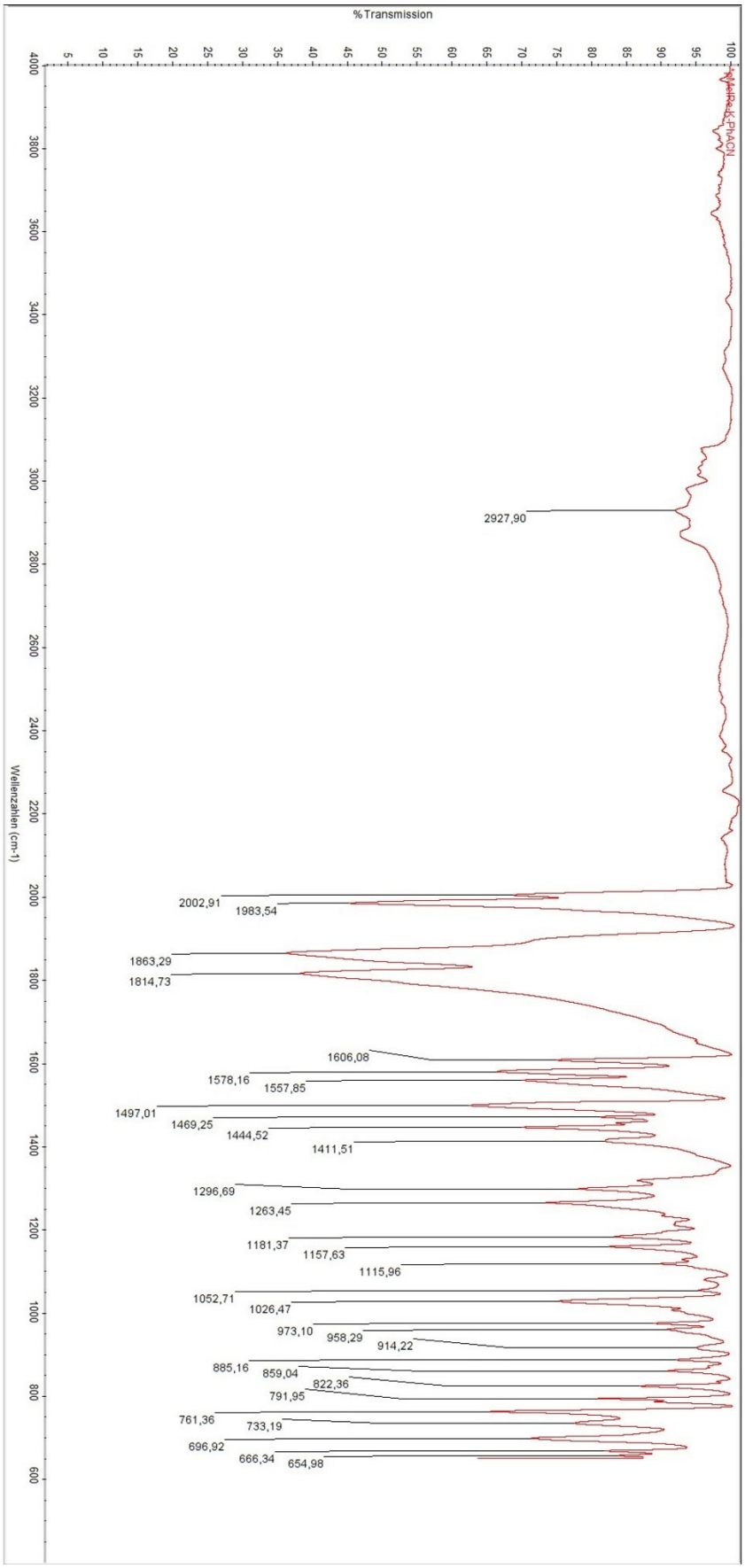

Figure S7.5-12: IR spectrum (FT-IR) of ***fac*-K[Re(*amidopy-phacn*)(CO)$_3$] (82)**.

Table 9: Crystallographic data and structure refinement of ***fac*-K[Re(*amidopy*-p*hacn*)(CO)$_3$] (82)**.

checkCIF/PLATON report

Structure factors have been supplied for datablock(s) stichauerr180827_0m

THIS REPORT IS FOR GUIDANCE ONLY. IF USED AS PART OF A REVIEW PROCEDURE FOR PUBLICATION, IT SHOULD NOT REPLACE THE EXPERTISE OF AN EXPERIENCED CRYSTALLOGRAPHIC REFEREE.

No syntax errors found. CIF dictionary Interpreting this report

Datablock: stichauerr180827_0m

Bond precision: C-C = 0.0066 A Wavelength=0.71073

Cell: a=15.6087(8) b=8.1898(4) c=21.3065(11)
alpha=90 beta=101.769(2) gamma=90
Temperature: 100 K

	Calculated	Reported
Volume	2666.4(2)	2666.4(2)
Space group	P 21/n	P 1 21/n 1
Hall group	-P 2yn	-P 2yn
Moiety formula	C28 H27 K N3 O4 Re	C28 H27 K N3 O4 Re
Sum formula	C28 H27 K N3 O4 Re	C28 H27 K N3 O4 Re
Mr	694.84	694.82
Dx,g cm-3	1.731	1.731
Z	4	4
Mu (mm-1)	4.752	4.752
F000	1368.0	1368.0
F000'	1365.31	
h,k,lmax	18,9,25	18,9,25
Nref	4822	4816
Tmin,Tmax	0.418,0.652	0.629,0.746
Tmin'	0.354	

Correction method= # Reported T Limits: Tmin=0.629 Tmax=0.746
AbsCorr = MULTI-SCAN

Data completeness= 0.999 Theta(max)= 25.247

R(reflections)= 0.0266(4573) wR2(reflections)= 0.0568(4816)

S = 1.358 Npar= 339

The following ALERTS were generated. Each ALERT has the format
test-name_ALERT_alert-type_alert-level.
Click on the hyperlinks for more details of the test.

Alert level C

PLAT220_ALERT_2_C	Non-Solvent Resd 1 C Ueq(max)/Ueq(min) Range	3.4 Ratio
PLAT222_ALERT_3_C	Non-Solv. Resd 1 H Uiso(max)/Uiso(min) Range	10.0 Ratio
PLAT420_ALERT_2_C	D-H Without Acceptor N3 --H3 .	Please Check
PLAT906_ALERT_3_C	Large K Value in the Analysis of Variance	2.882 Check
PLAT911_ALERT_3_C	Missing FCF Refl Between Thmin & STh/L= 0.600	2 Report
PLAT978_ALERT_2_C	Number C-C Bonds with Positive Residual Density.	0 Info

Alert level G

PLAT004_ALERT_5_G	Polymeric Structure Found with Maximum Dimension	1 Info
PLAT007_ALERT_5_G	Number of Unrefined Donor-H Atoms	1 Report
PLAT083_ALERT_2_G	SHELXL Second Parameter in WGHT Unusually Large	9.94 Why ?
PLAT164_ALERT_4_G	Nr. of Refined C-H H-Atoms in Heavy-Atom Struct.	1 Note
PLAT232_ALERT_2_G	Hirshfeld Test Diff (M-X) Re1 --C22 .	7.0 s.u.
PLAT232_ALERT_2_G	Hirshfeld Test Diff (M-X) Re1 --C24 .	7.0 s.u.
PLAT343_ALERT_2_G	Unusual Angle Range in Main Residue for	C14 Check
PLAT367_ALERT_2_G	Long? C(sp?)-C(sp?) Bond C6 - C14 .	1.53 Ang.
PLAT764_ALERT_4_G	Overcomplete CIF Bond List Detected (Rep/Expd) .	1.30 Ratio
PLAT774_ALERT_1_G	Suspect X-Y Bond in CIF: K1 --K1 ..	4.02 Ang.
PLAT909_ALERT_3_G	Percentage of I>2sig(I) Data at Theta(Max) Still	88% Note
PLAT910_ALERT_3_G	Missing # of FCF Reflection(s) Below Theta(Min).	4 Note
PLAT913_ALERT_3_G	Missing # of Very Strong Reflections in FCF	1 Note
PLAT960_ALERT_3_G	Number of Intensities with I < - 2*sig(I) ...	1 Check

0 **ALERT level A** = Most likely a serious problem - resolve or explain
0 **ALERT level B** = A potentially serious problem, consider carefully
6 **ALERT level C** = Check. Ensure it is not caused by an omission or oversight
14 **ALERT level G** = General information/check it is not something unexpected

1 ALERT type 1 CIF construction/syntax error, inconsistent or missing data
8 ALERT type 2 Indicator that the structure model may be wrong or deficient
7 ALERT type 3 Indicator that the structure quality may be low
2 ALERT type 4 Improvement, methodology, query or suggestion
2 ALERT type 5 Informative message, check

It is advisable to attempt to resolve as many as possible of the alerts in all categories. Often the minor alerts point to easily fixed oversights, errors and omissions in your CIF or refinement strategy, so attention to these fine details can be worthwhile. In order to resolve some of the more serious problems it may be necessary to carry out additional measurements or structure refinements. However, the purpose of your study may justify the reported deviations and the more serious of these should normally be commented upon in the discussion or experimental section of a paper or in the "special_details" fields of the CIF. checkCIF was carefully designed to identify outliers and unusual parameters, but every test has its limitations and alerts that are not important in a particular case may appear. Conversely, the absence of alerts does not guarantee there are no aspects of the results needing attention. It is up to the individual to critically assess their own results and, if necessary, seek expert advice.

Publication of your CIF in IUCr journals

A basic structural check has been run on your CIF. These basic checks will be run on all CIFs submitted for publication in IUCr journals (*Acta Crystallographica*, *Journal of Applied Crystallography*, *Journal of Synchrotron Radiation*); however, if you intend to submit to *Acta Crystallographica Section C* or *E* or *IUCrData*, you should make sure that full publication checks are run on the final version of your CIF prior to submission.

Publication of your CIF in other journals

Please refer to the *Notes for Authors* of the relevant journal for any special instructions relating to CIF submission.

PLATON version of 07/08/2019; check.def file version of 30/07/2019

Datablock stichauerr180827_0m - ellipsoid plot

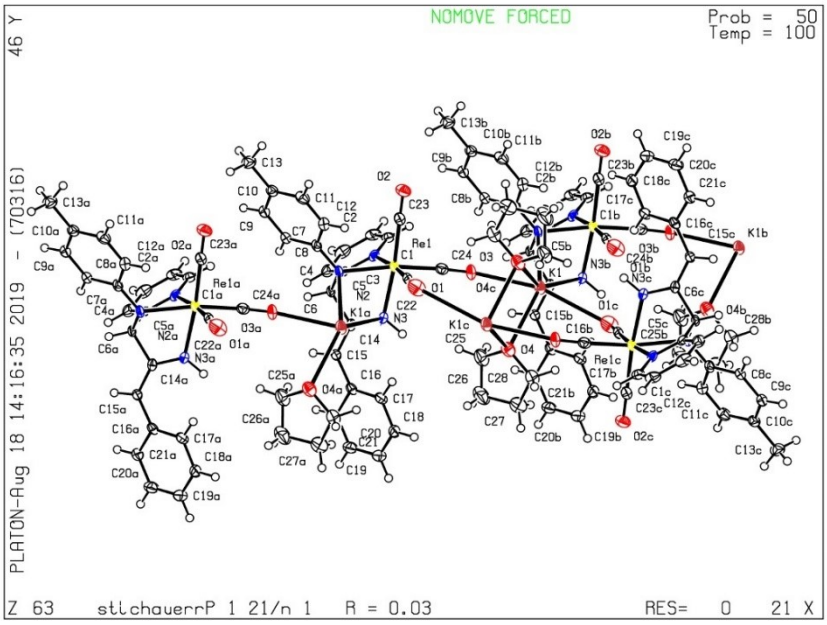

Cyclic coupling product **K-01**

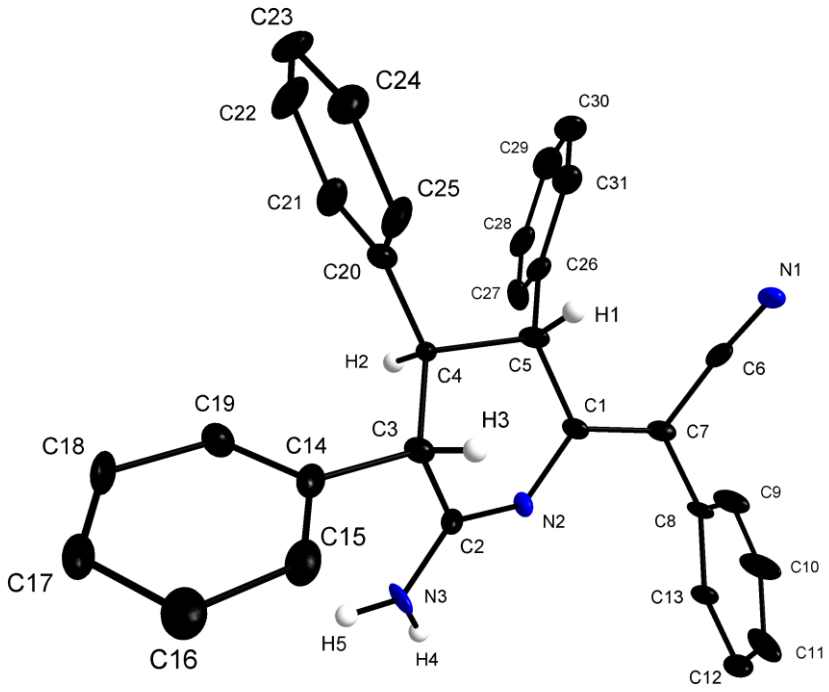

Figure S7.5-14: Diamond plot of cyclic C-C and C-N coupling product **K-01** from phenylacetonitrile with **75*-Re**. (Thermal ellipsoids at 50% probability, H atoms omitted for clarity, except for H1, H2, H3, H4 and H5)

Selected bond lengths [Å] and angle [°] of **K-01** from Diamond plot XRD analysis: C1-N2 = 1.3758(2), N2-C2 = 1.3100(2), C2-C3 = 1.5215(3), C3-C4 = 1.5319(2), C4-C5 = 1.5843(2), C1-C5 = 1.5312(3), C1-C7 = 1.3681(2), C6-N1 = 1.1419(1), C6-C7 = 1.4226(2), C7-C8 = 1.4866(3), C8-C9 = 1.4168(2), C9-C10 = 1.3816(2), C10-C11 = 1.3800(2), C11-C12 = 1.4013(2), C12-C13 = 1.3879(3), C8-C13 = 1.3791(2), C2-N3 = 1.3365(2), C3-C14 = 1.5334(2), C14-C15 = 1.3622(2), C15-C16 = 1.3937(2), C16-C17 = 1.4155(2), C17-C18 = 1.3476(2), C18-C19 = 1.4289(2), C14-C19 = 1.3809(2), C4-C20 = 1.5070(3), C20-C21 = 1.3901(2), C21-C22 = 1.4104(3), C22-C23 = 1.3619(2), C23-C24 = 1.3643(2), C24-C25 = 1.3907(3), C20-C25 = 1.4052(2), C5-C26 = 1.5142(2), C26-C27 = 1.4017(2), C27-C28 = 1.3945(2), C28-C29 = 1.4028(2), C29-C30 = 1.3647(2), C30-C31 = 1.3861(2), C26-C31 = 1.4009(2). C1-N2-C2 = 117.5, N2-C2-C3 = 121.7, C2-C3-C4 = 104.9, C3-C4-C5 = 106.0, C4-C5-C1 = 110.6, C5-C1-N2 = 121.1.

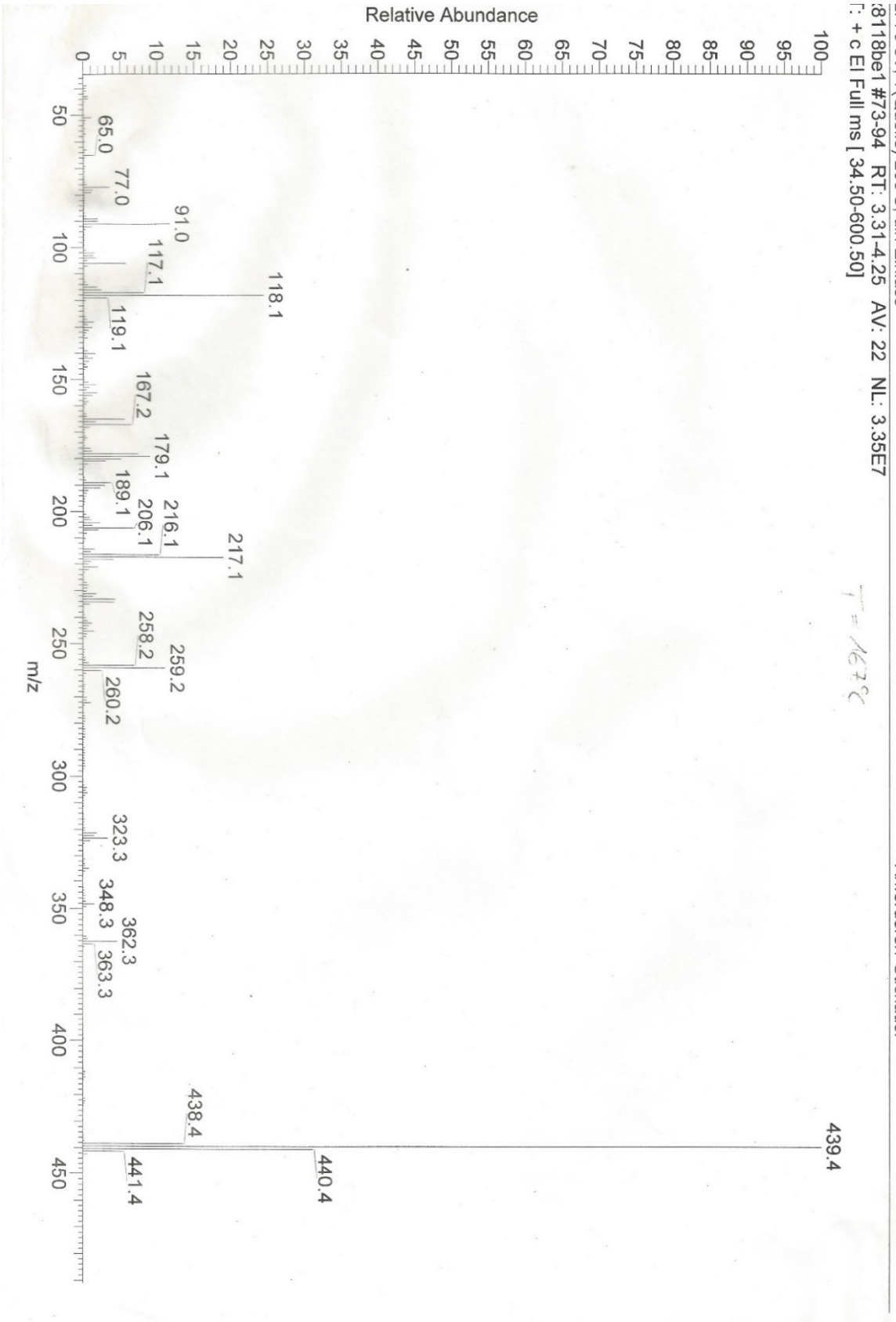

Figure S7.5-14: MS EI, 70eV pos spectrum of cyclic coupling product **K-01**.

Table 10: Crystallographic data and structure refinement from Olex report of cyclic coupling product **K-01**.

StichauerR180226_0ma

Table 1 Crystal data and structure refinement for StichauerR180226_0ma.

Identification code	StichauerR180226_0ma
Empirical formula	$C_{31}H_{25}N_3$
Formula weight	439.564
Temperature/K	100.0
Crystal system	triclinic
Space group	P-1
a/Å	12.292(2)
b/Å	15.971(3)
c/Å	16.894(3)
α/°	115.579(6)
β/°	110.788(5)
γ/°	92.484(6)
Volume/Å^3	2719.6(8)
Z	4
ρ_{calc}g/cm^3	1.074
μ/mm^{-1}	0.063
F(000)	928.3
Crystal size/mm^3	N/A × N/A × N/A
Radiation	Mo Kα (λ = 0.71073)
2Θ range for data collection/°	4.98 to 52.74
Index ranges	-15 ≤ h ≤ 15, -19 ≤ k ≤ 19, -20 ≤ l ≤ 20
Reflections collected	119149
Independent reflections	10603 [R_{int} = 0.1272, R_{sigma} = 0.0663]
Data/restraints/parameters	10603/0/613
Goodness-of-fit on F^2	3.469
Final R indexes [I>=2σ (I)]	R_1 = 0.1833, wR_2 = 0.4691
Final R indexes [all data]	R_1 = 0.2100, wR_2 = 0.4749
Largest diff. peak/hole / e Å^{-3}	1.59/-1.02

7.6

Supporting Information for

A Rh(I) Complex with a Tridentate Pyridine-Amino-Olefin Actor Ligand – Metal-Ligand Cooperative Activation of CO_2 and Phenylisocyanate under C–C and Rh–E (E= O, N) Bond Formation

Isabell Heuermann[#a], Benjamin Heitmann[#a], Rasmus Stichauer[a], Daniel Duvinage[a], and Matthias Vogt*[a]

Universität Bremen, FB 2 Biologie/Chemie, Institut für Anorganische Chemie und Kristallographie, Leobener Str. 7, NW2 C2060, 28359 Bremen, Germany

I. Heuermann, B. Heitmann, R. Stichauer, D. Duvinage, M. Vogt,

Organometallics **2019,** *38*, 1787-1799.

DOI: 10.1021/acs.organomet.9b00094

Index

Spectroscopic Data for compound:

Ligand **1** (**dbap-H**)

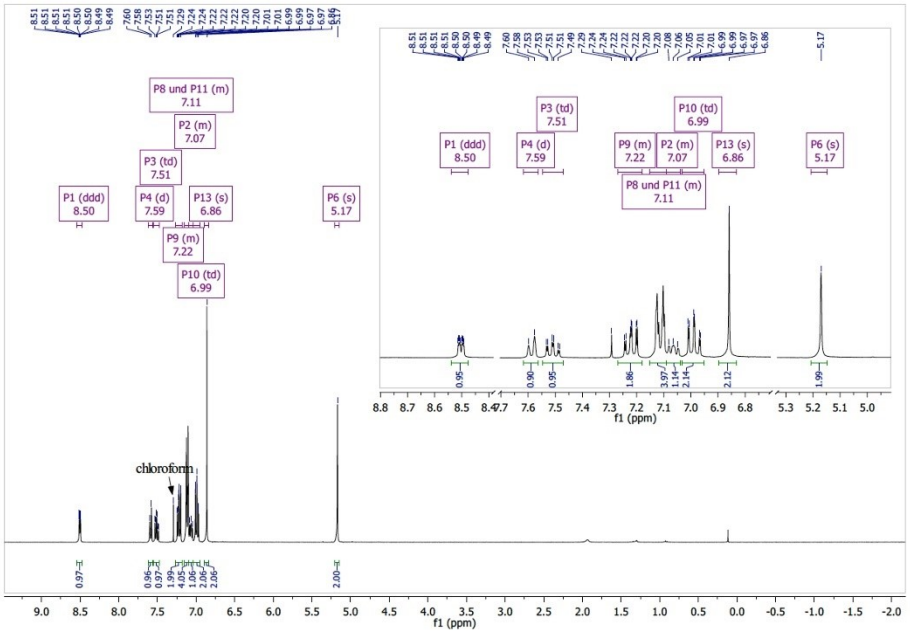

Figure 1S. ^{1}H NMR [360 MHz, $CDCl_3$, 298 K] spectrum of dbap-py (**1**).

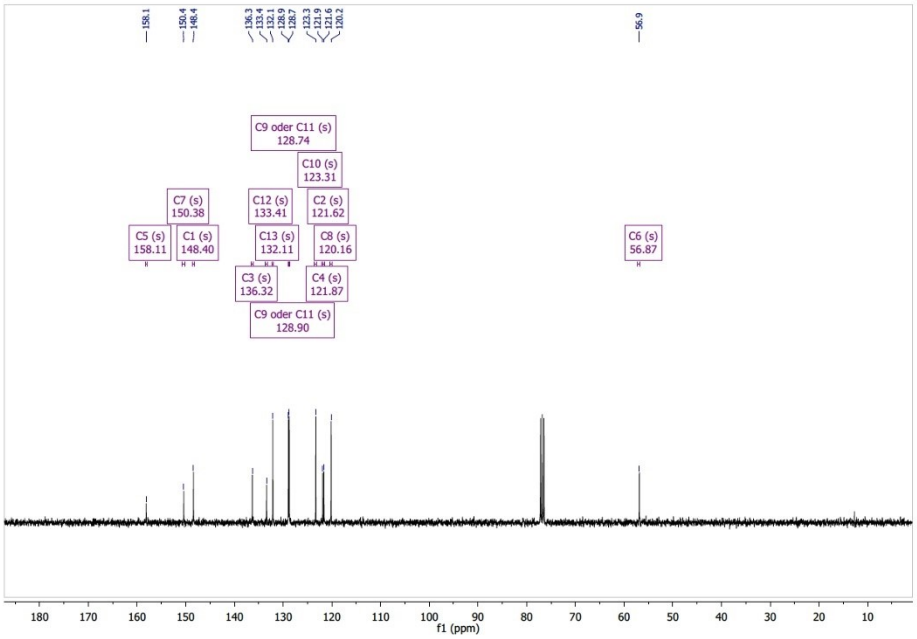

Figure 2S. $^{13}C\{^{1}H\}$ NMR [91 MHz, $CDCl_3$, 298 K] spectrum of dbap-py (**1**).

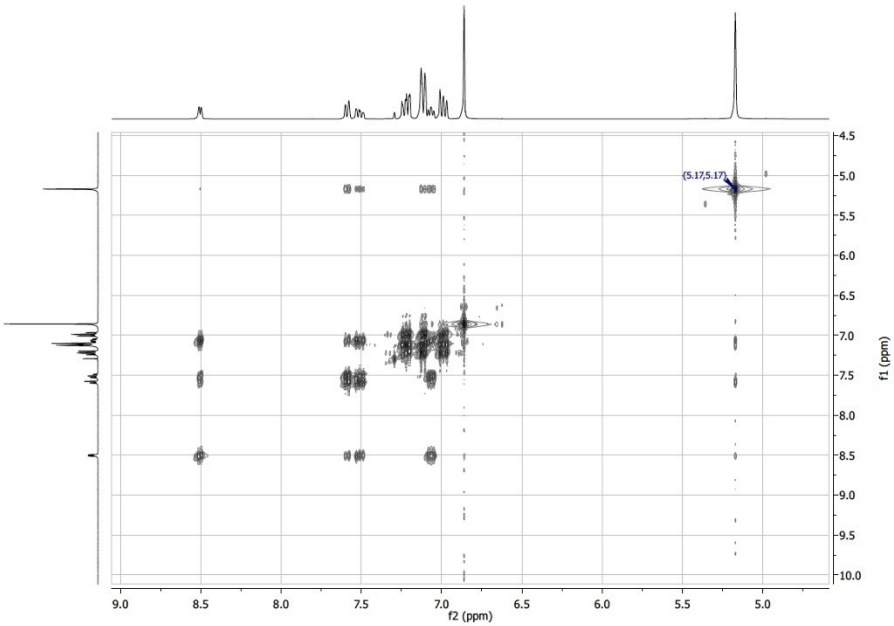

Figure 3S. $^{1}H^{1}H$ COSY NMR [360 MHz, $CDCl_3$, 298 K] spectrum of dbap-py (**1**).

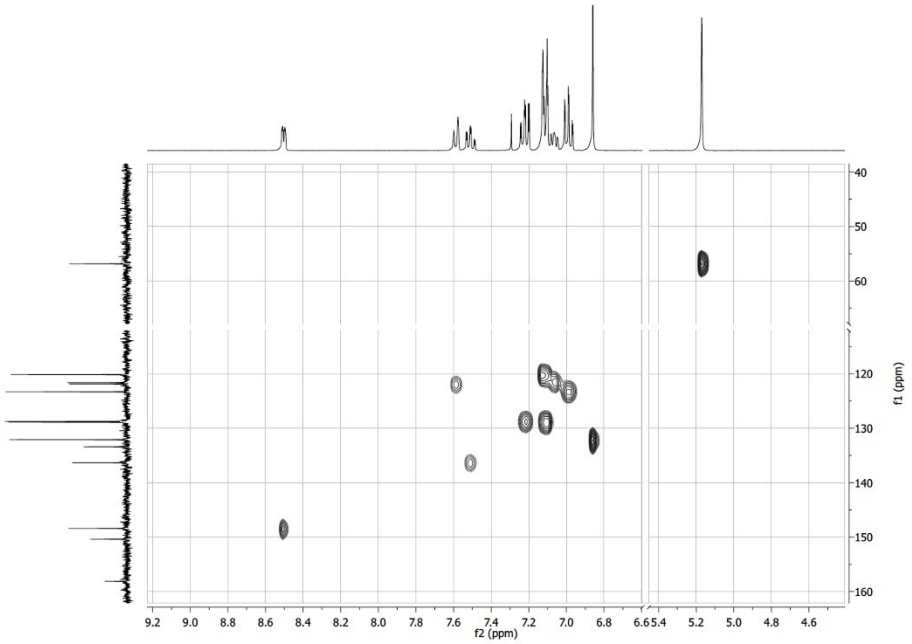

Figure 4S. $^{1}H^{13}C$ HSQC NMR [360 MHz/91 MHz, $CDCl_3$, 298 K] spectrum of dbap-py (**1**).

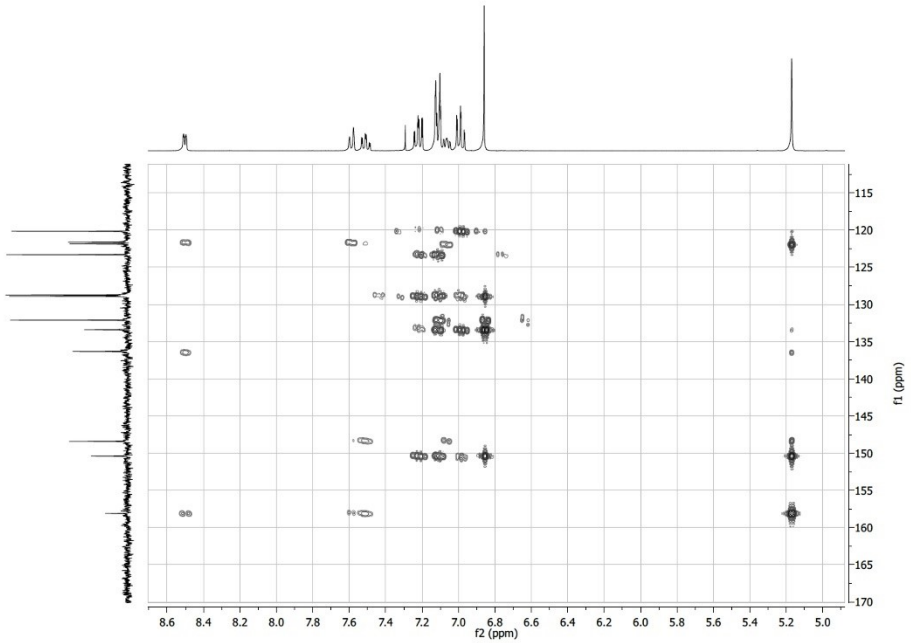

Figure 5S. $^{1}H^{13}C$ HMBC NMR [360 MHz/91 MHz, $CDCl_3$, 298 K] spectrum of dbap-py (**1**).

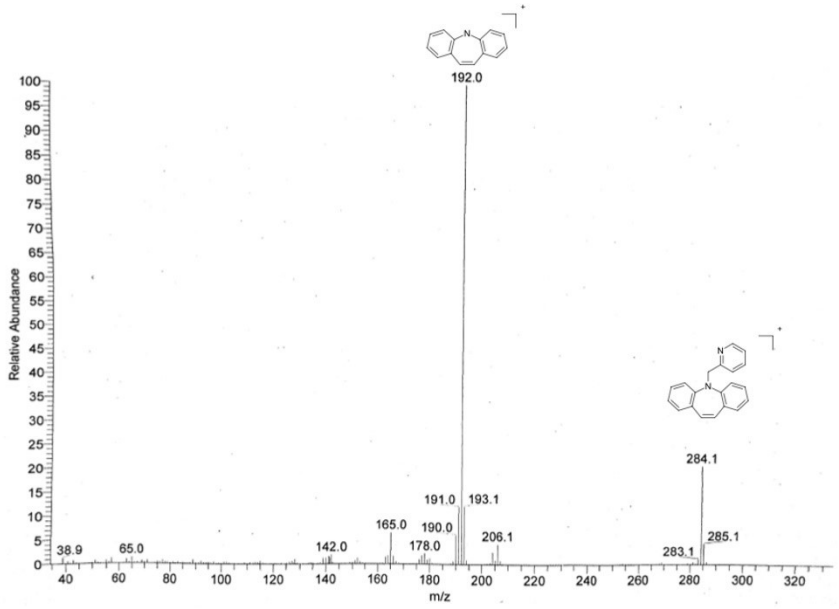

Figure 6S EIMS (70 eV) spectrum of **dbap-py** (**1**).

Complex 2

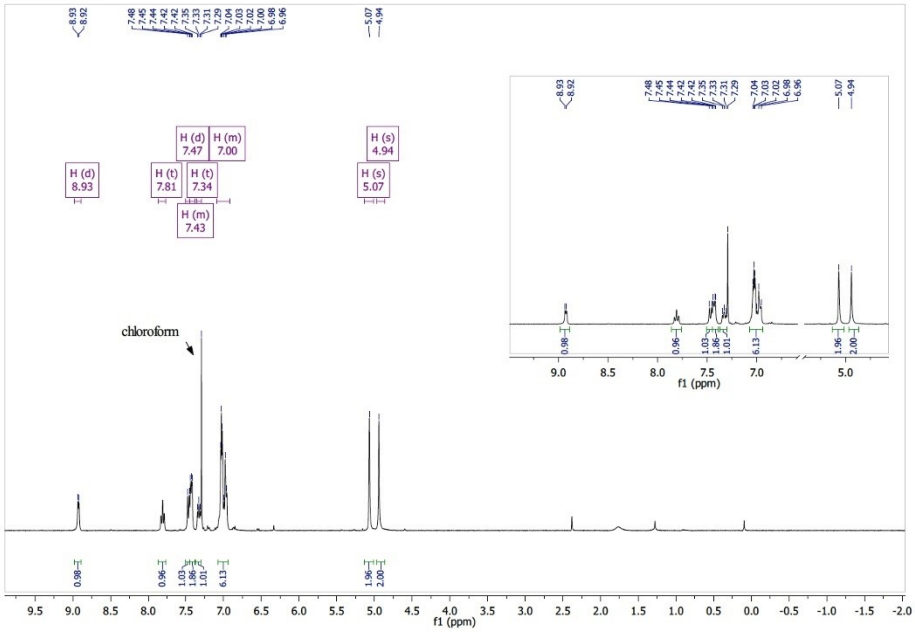

Figure 7S. ^{1}H NMR [360 MHz, $CDCl_3$, 298 K] spectrum of [Rh(dbap-py)Cl)] (**2**).

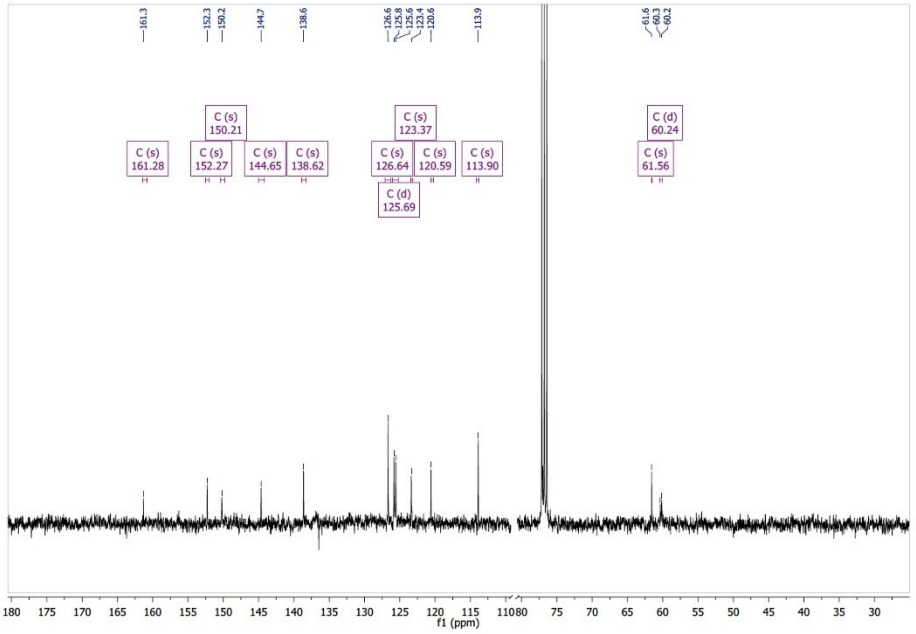

Figure 8S. $^{13}C\{^{1}H\}$ NMR [91 MHz, $CDCl_3$, 298 K] spectrum of [Rh(dbap-py)Cl)] (**2**).

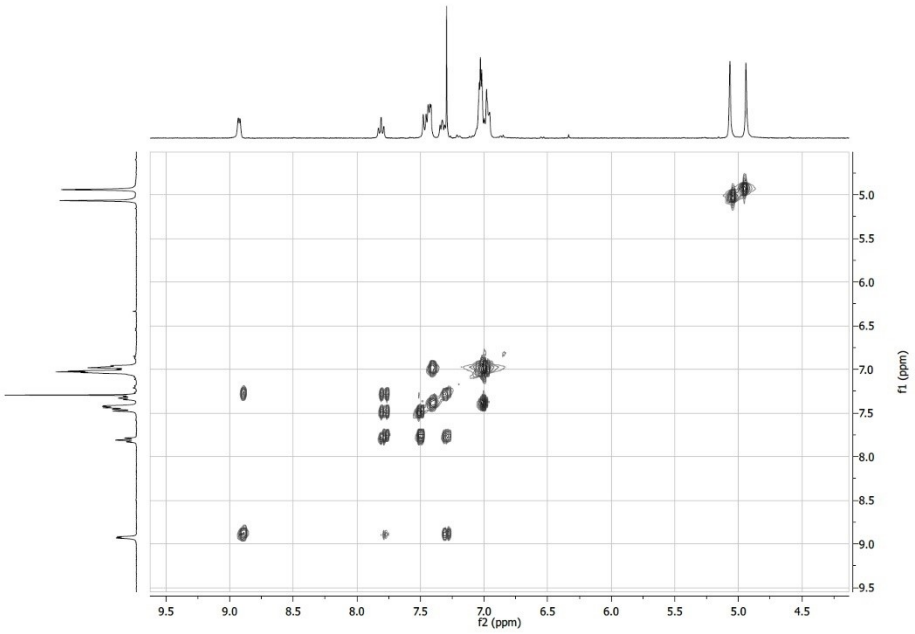

Figure 9S. $^{1}H^{1}H$ COSY NMR [360 MHz, $CDCl_3$, 298 K] spectrum of [Rh(dbap-py)Cl)] (**2**).

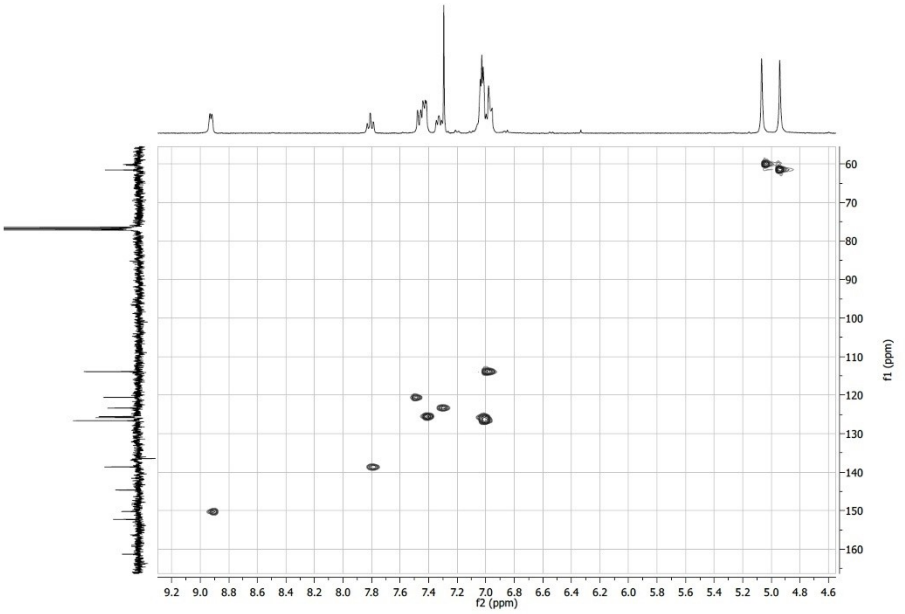

Figure 10S. $^{1}H^{13}C$ HSQC NMR [360 MHz/91MHz, $CDCl_3$, 298 K] spectrum of [Rh(dbap-py)Cl)] (**2**).

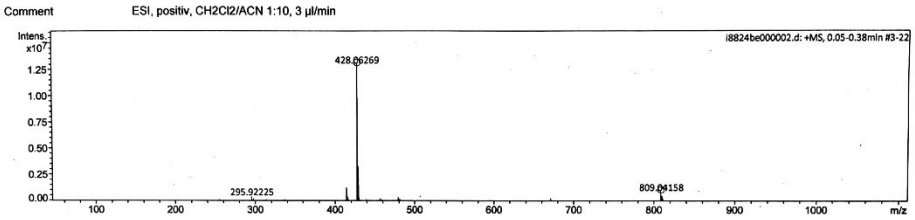

Figure 11S. HRMS-ESI CH_2Cl_2/CH_3CN (*m/z*) spectrum of [Rh(dbap-py)Cl] (**2**).

Complex 3

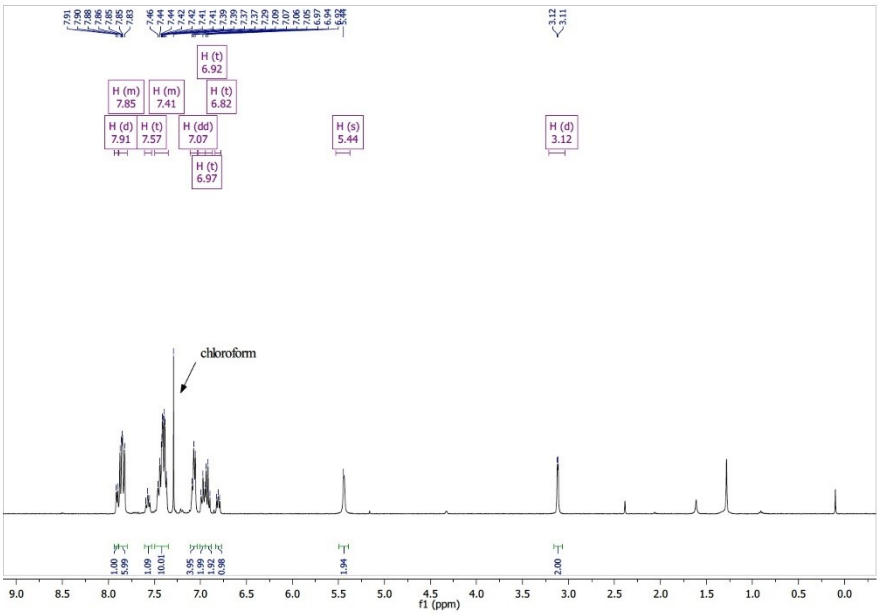

Figure 12S. ^{1}H NMR [360 MHz, $CDCl_3$, 298 K] spectrum of [Rh(dbap-py)PPh_3]Cl (**3**).

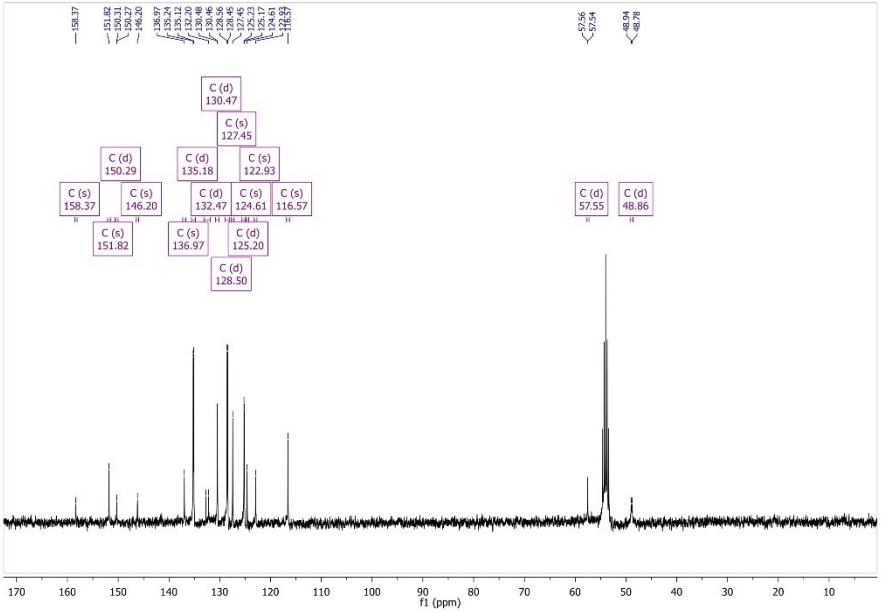

Figure 13S. $^{13}C\{^{1}H\}$ NMR [91 MHz, $CDCl_3$, 298 K] spectrum of [Rh(dbap-py)PPh_3]Cl (**3**).

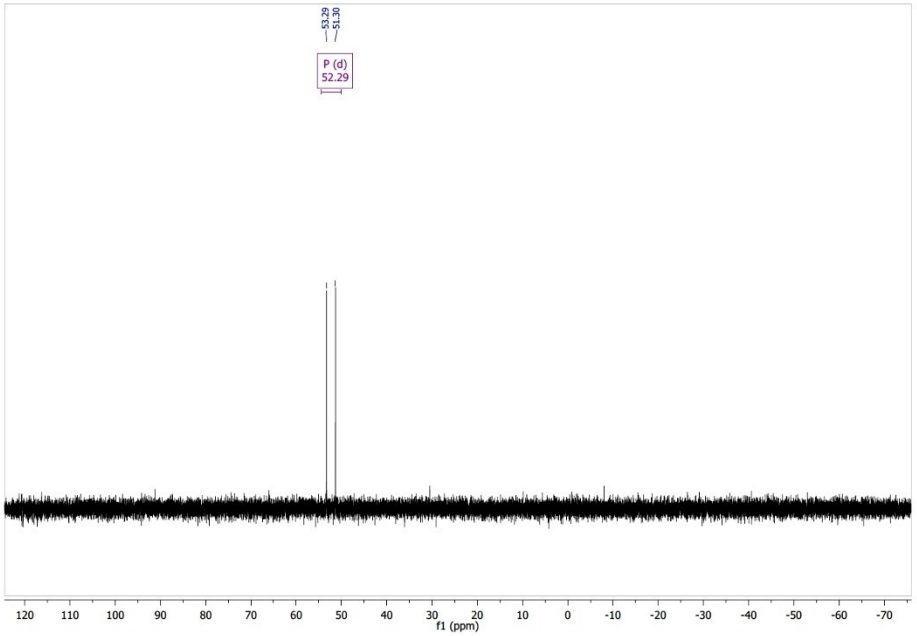

Figure 14S. $^{31}P\{^{1}H\}$ NMR [81 MHz, $CDCl_3$, 298 K] spectrum of [Rh(dbap-py)PPh_3]Cl (**3**).

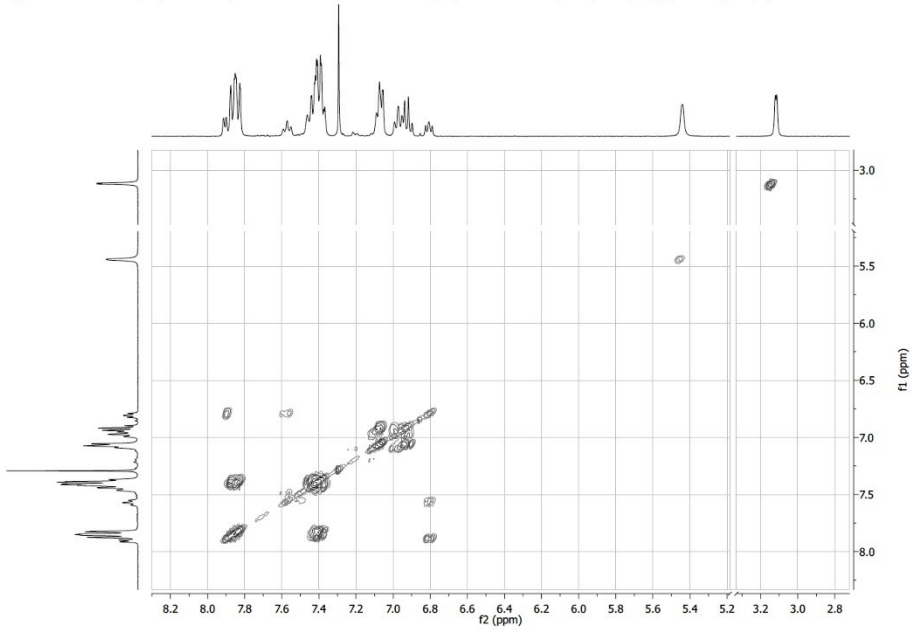

Figure 15S. $^{1}H1H$ COSY NMR [360 MHz, $CDCl_3$, 298 K] spectrum of [Rh(dbap-py)PPh_3]Cl (**3**).

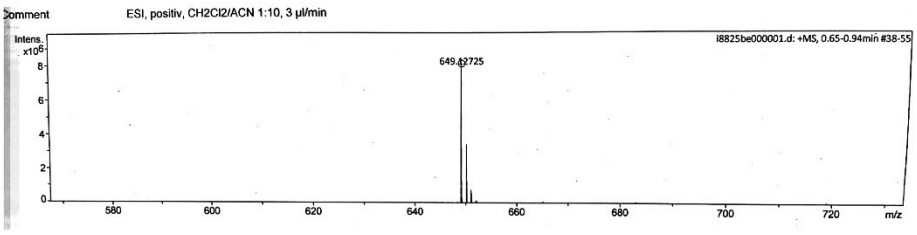

Figure 16S. HRMS-ESI CH_2Cl_2/CH_3CN (*m/z*) spectrum of [Rh(dbap-py)PPh_3]Cl (**3**)

Complex 4

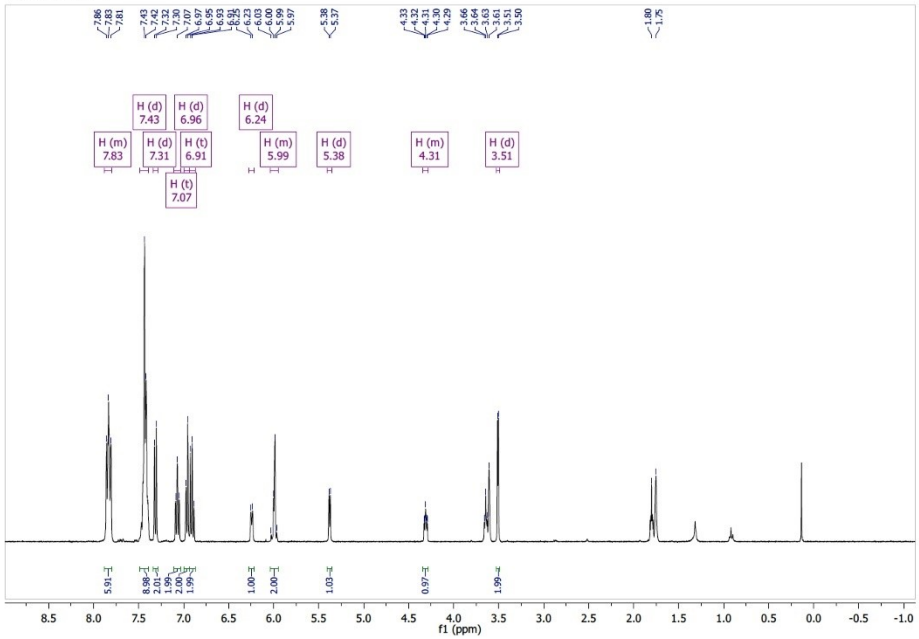

Figure 17S. ^{1}H NMR [360 MHz, THF-d_8, 298 K] spectrum of [Rh(dbap-py*)PPh$_3$] (**4**).

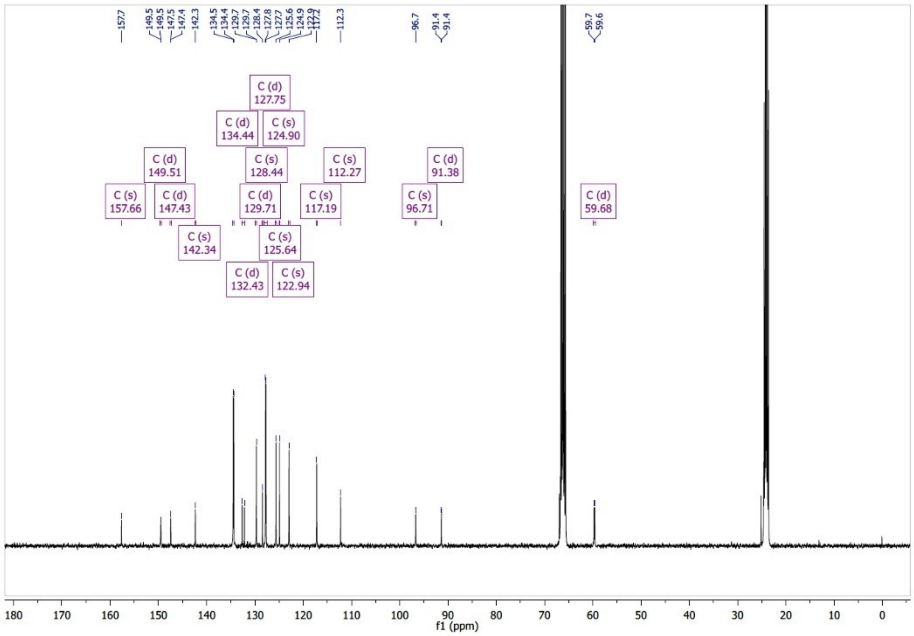

Figure 18S. ^{13}C{^{1}H} NMR [91 MHz, THF-d_8, 298 K] spectrum of [Rh(dbap-py*)PPh$_3$] (**4**).

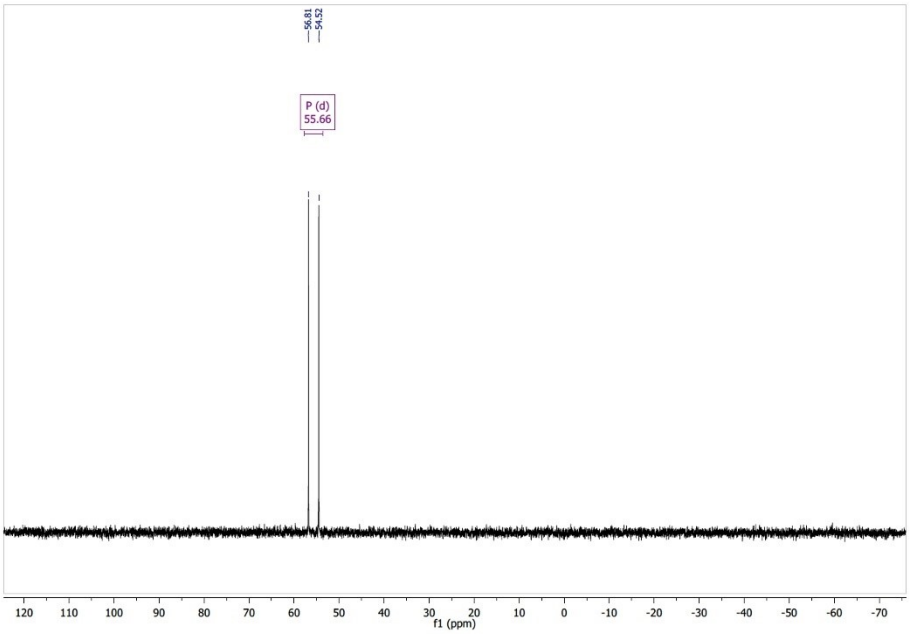

Figure 19S. $^{31}P\{^{1}H\}$ NMR [81 MHz, THF-d_8, 298 K] spectrum of [Rh(dbap-py*)PPh_3] (**4**).

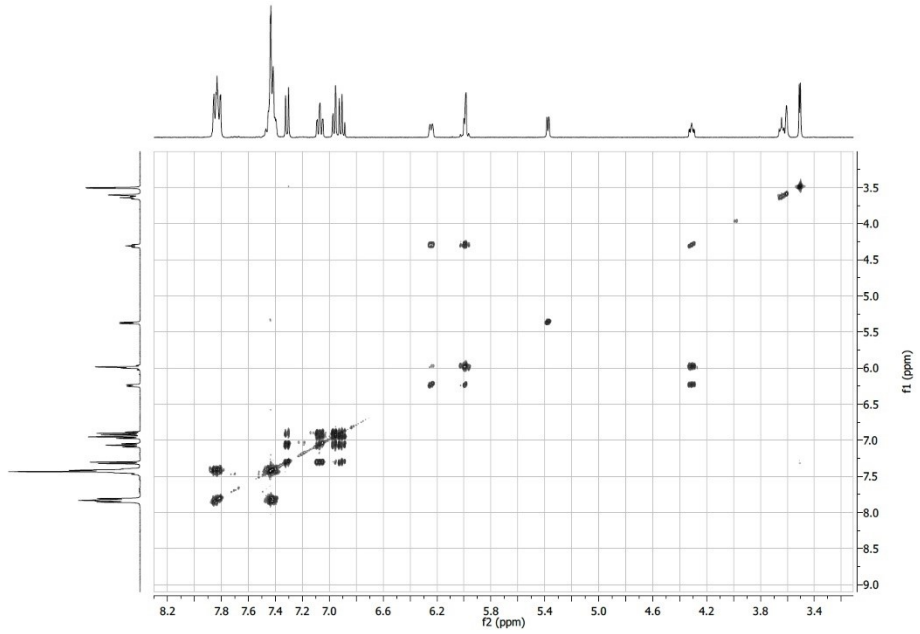

Figure 20S. $^{1}H^{1}H$ COSY NMR [360 MHz, THF-d_8, 298 K] spectrum of [Rh(dbap-py*)PPh_3] (**4**).

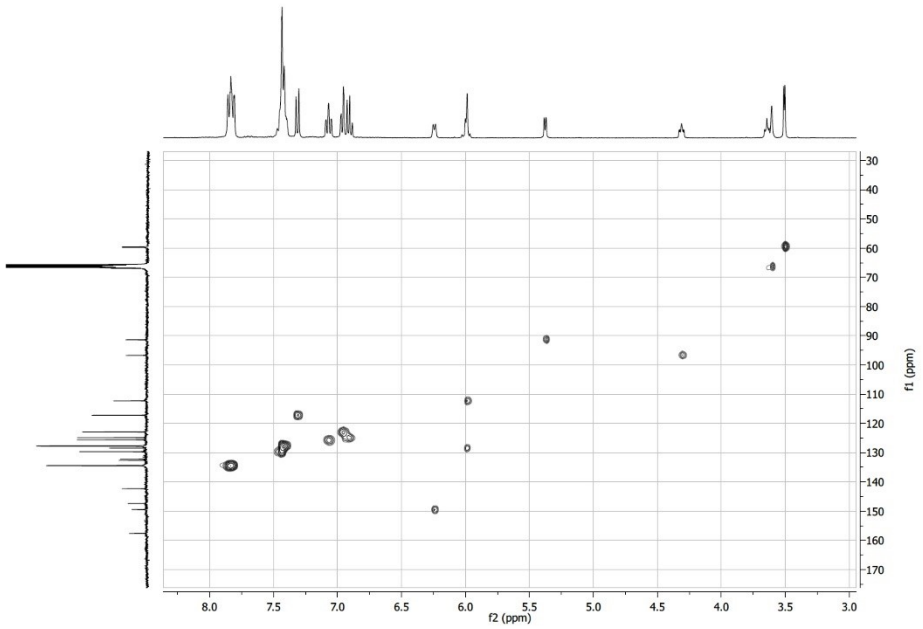

Figure 21S. $^{1}H^{13}C$ HSQC NMR [360 MHz/91MHz, THF-d_8, 298 K] spectrum of [Rh(dbap-py*)PPh_3] (**4**).

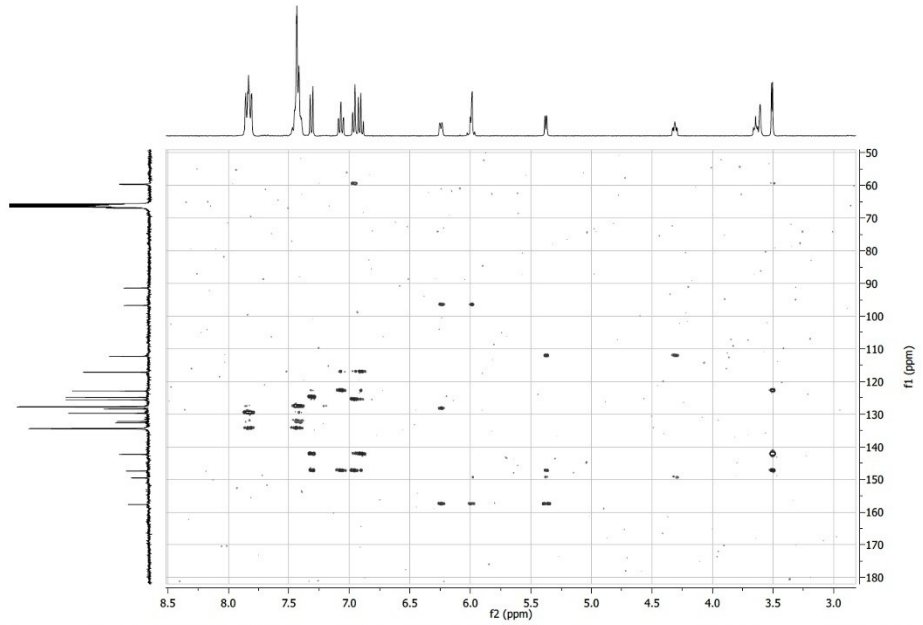

Figure 22S. $^{1}H^{13}C$ HMBC NMR [360 MHz/91MHz, THF-d_8, 298 K] spectrum of [Rh(dbap-py*)PPh_3] (**4**).

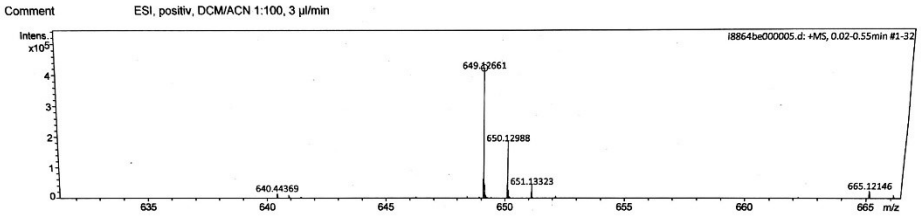

Figure 23S. HRMS-ESI CH_2Cl_2/CH_3CN (*m/z*) spectrum of [Rh(dbap-py*)PPh_3] (**4**).

Complex 5

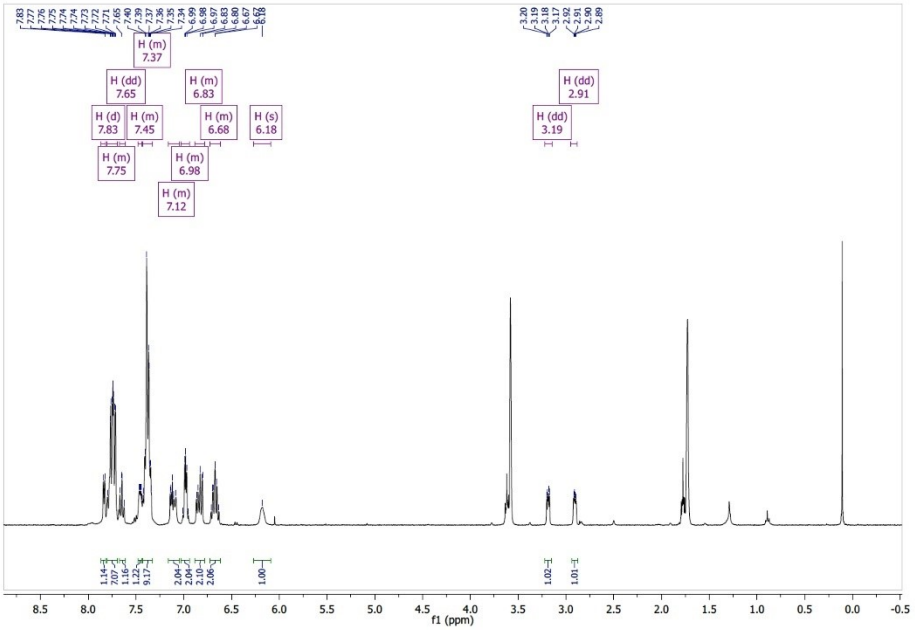

Figure 24S. ^{1}H NMR [360 MHz, THF-d_8, 298 K] spectrum of [Rh(dbap-COO)PPh$_3$] (**5**).

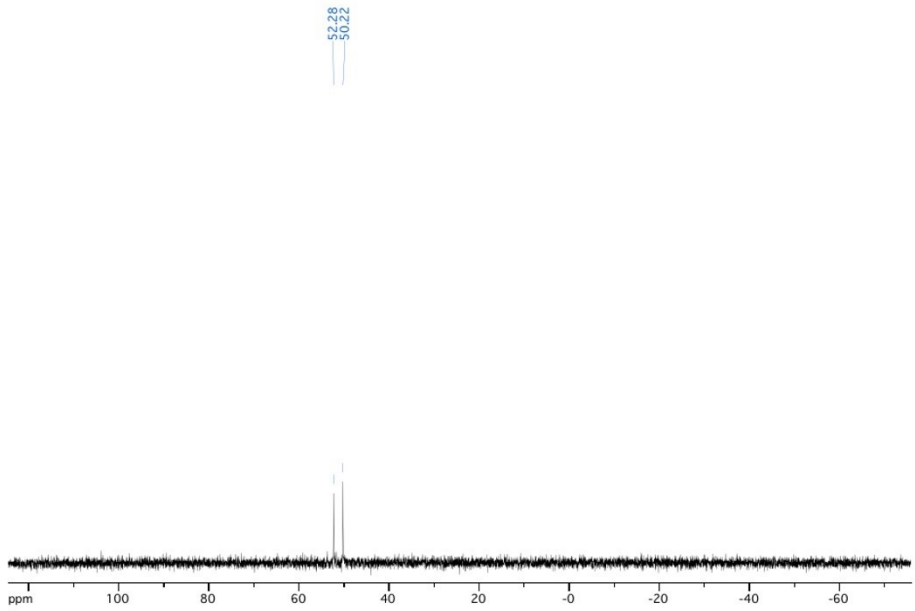

Figure 25S.^{31}P{^{1}H} NMR [81 MHz, $C_6H_4F_2$, 298 K, locked on external THF-d_8] spectrum of [Rh(dbap-COO)PPh$_3$] (**5**).

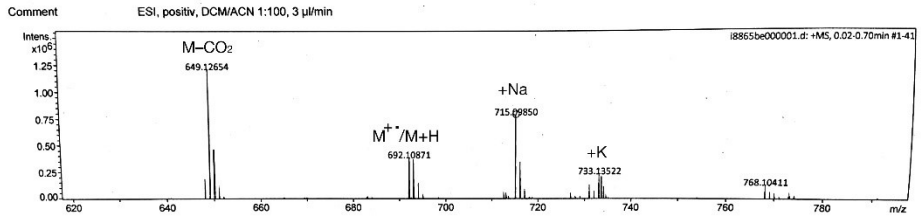

Figure 26S. HRMS-ESI CH_2Cl_2/CH_3CN (*m/z*) spectrum of [Rh(dbap-COO)PPh_3] (**5**).

Complex 6

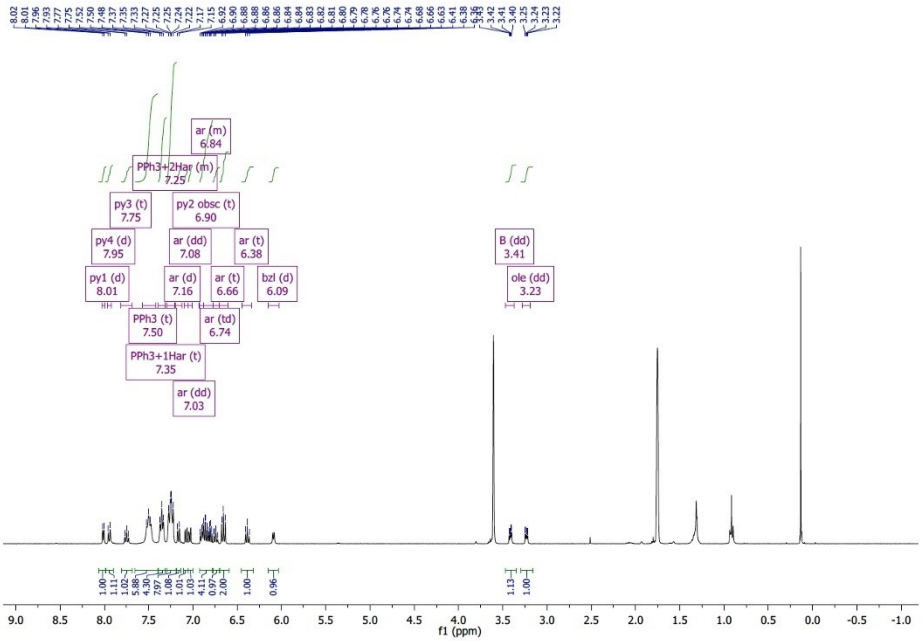

Figure 27S. ^{1}H NMR [360 MHz, THF-d_8, 298 K] spectrum of [Rh(dbap-NCO)PPh$_3$] (**6**).

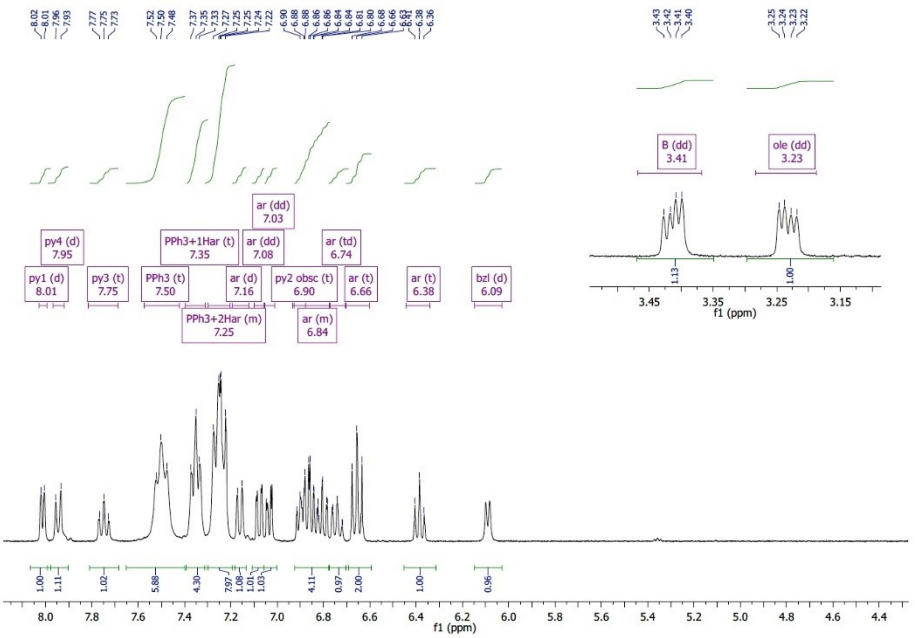

Figure 28S. Section of the ^{1}H NMR [360 MHz, THF-d_8, 298 K] spectrum of [Rh(dbap-NCO)PPh$_3$] (**6**).

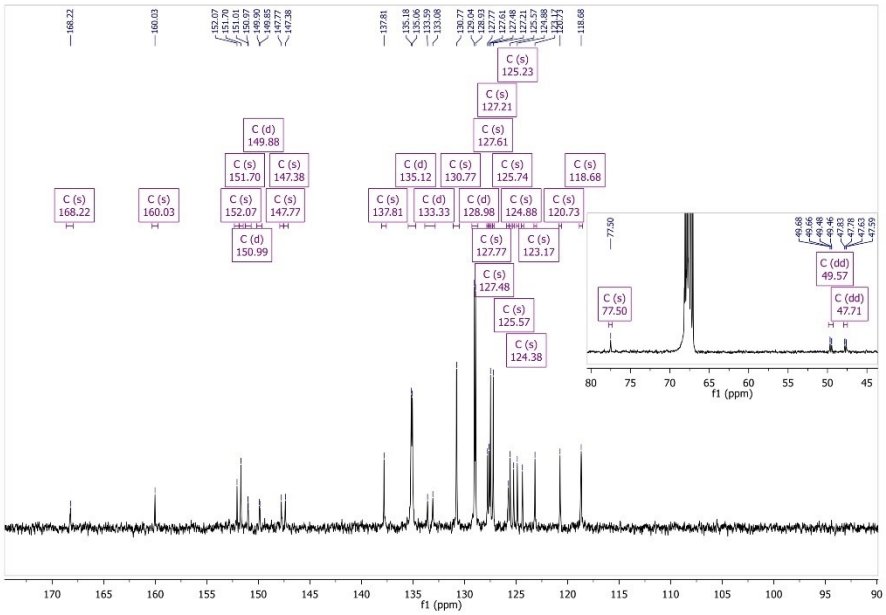

Figure 29S. $^{13}C\{^{1}H\}$ NMR [91 MHz, THF-d_8, 298 K] spectrum of [Rh(dbap-NCO)PPh_3] (**6**).

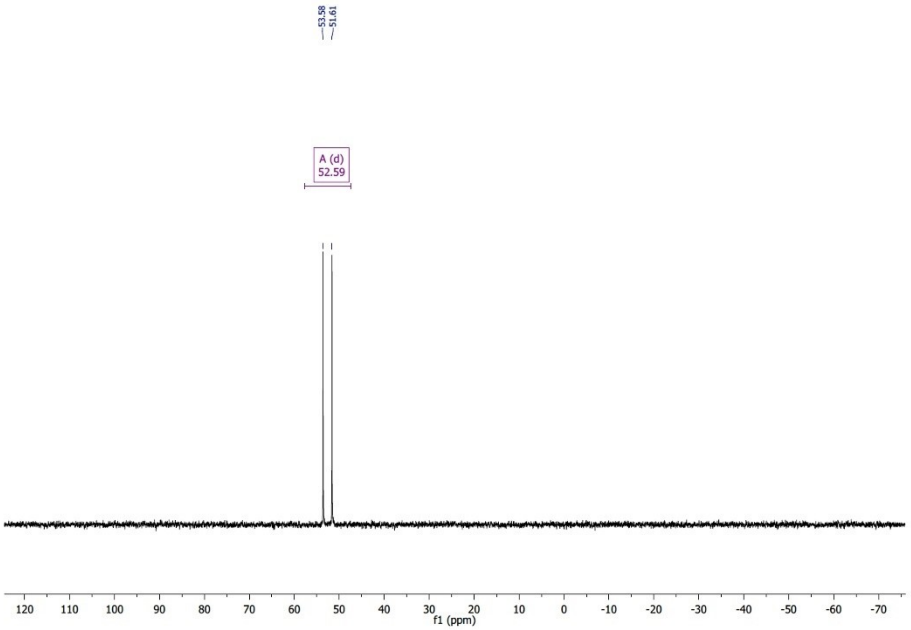

Figure 30S. $^{31}P\{^{1}H\}$ NMR [81 MHz, THF-d_8, 298 K] spectrum of [Rh(dbap-NCO)PPh_3] (**6**).

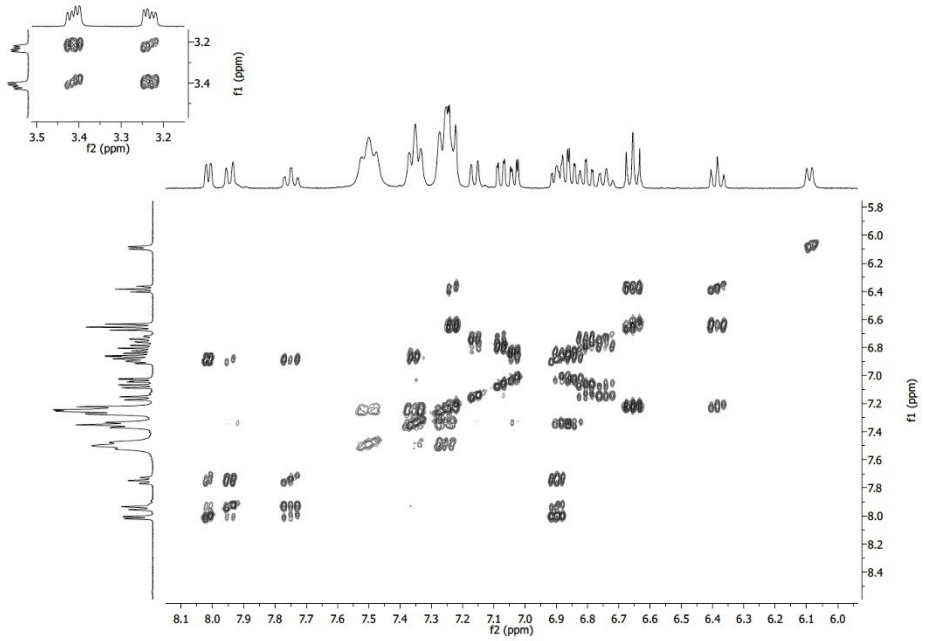

Figure 31S. $^{1}H^{1}H$ COSY NMR [360 MHz, THF-d_8, 298 K] spectrum of [Rh(dbap-NCO)PPh_3] (**6**).

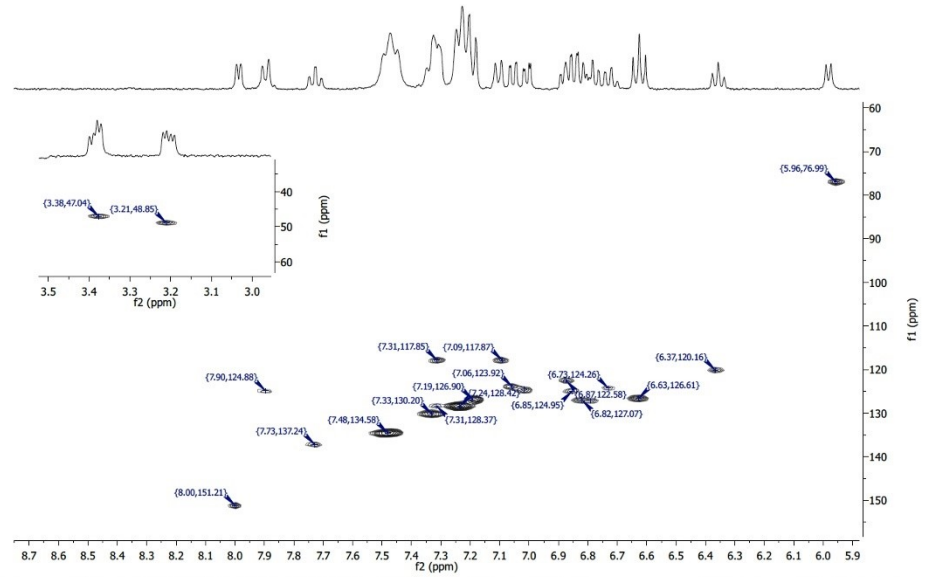

Figure 32S. $^{1}H^{13}C$ HSQC NMR [360 MHz/91MHz, THF-d_8, 298 K] spectrum of [Rh(dbap-NCO)PPh_3] (**6**).

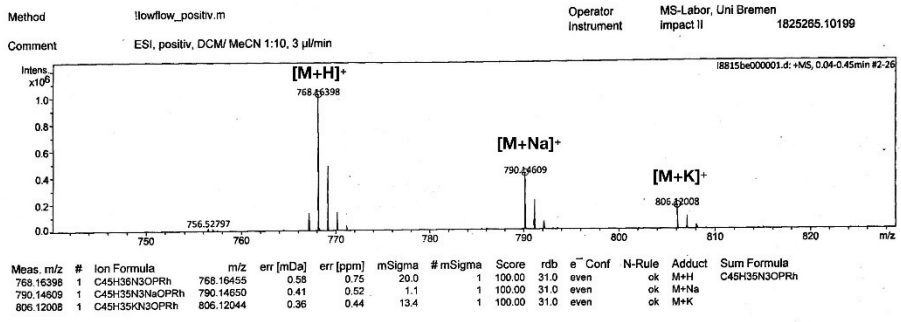

Figure 33S. HRMS-ESI CH_2Cl_2/CH_3CN (*m/z*) spectrum of [Rh(dbap-NCO)PPh_3] (**6**).

Crystallographic details for compounds 1–6

Table S1. Crystallographic details for compounds 1–3.

	1	2	3
Formula	$C_{20}H_{16}N_2$	$C_{20}H_{16}ClN_2Rh$	$C_{38}H_{31}ClN_2PRh$
Formula weight, g mol^{-1}	284.36	422.71	684.98
Crystal system	orthorhombic	Monoclinic	orthorhombic
Crystal size, mm	0.13 × 0.09 × 0.02	0.29 × 0.14 × 0.08	0.24 × 0.21 × 0.09
Space group	Pbca	$P2_1/n$	Pbca
a, Å	10.4562(5)	8.4107(2)	9.2982(3)
b, Å	14.8307(7)	17.1035(4)	20.6219(6)
c, Å	19.4161(8)	11.6098(3)	31.2306(9)
α, °	90	90	90
β, °	90	96.2410(10)	90
γ, °	90	90	90
V, Å^3	3010.9(2)	1660.20(7)	5988.4(3)
Z	8	4	8
ρ_{calcd}, Mg m^{-3}	1.2545	1.691	1.520
μ (Mo $K\alpha$), mm^{-1}	0.074	1.192	0.745
F(000)	1200.4	848.0	2800.0
θ range, deg	5.20 to 52.00	5.698 to 61.19	4.734 to 56.678
Index ranges	$-12 \le h \le 14$	$-12 \le h \le 12$	$-12 \le h \le 12$
	$-20 \le k \le 20$	$-24 \le k \le 24$	$-26 \le k \le 27$
	$-26 \le l \le 27$	$-16 \le l \le 16$	$-41 \le l \le 41$
No. of reflns collected	20106	213091	133976
Completeness to θ_{max}	99.9%	99.8%	99.8%
No. indep. Reflns	2960	5096	7463
No. obsd reflns with ($I>2\sigma(I)$)	2393	4817	5850
No. refined params	199	217	388
GooF (F^2)	1.046	1.047	1.059
R_1 (F) ($I > 2\sigma(I)$)	0.0400	0.0163	0.0316
wR_2 (F^2) (all data)	0.0915	0.0419	0.0700
Largest diff peak/hole, e Å^{-3}	0.32 / −0.29	0.45 / −0.86	0.60 / -0.56
CCDC number	1894393	1894394	1894395

Table S2. Crystallographic details for compounds 4–6.

	4	5	6
Formula	$C_{38}H_{30}N_2PRh$	$C_{41}H_{34}N_2O_{2.5}PRh$	$C_{49}H_{43}N_3O_2PRh$
Formula weight, g mol^{-1}	648.52	728.58	821.72
Crystal system	monoclinic	Tetragonal	monoclinic
Crystal size, mm	0.13 × 0.08 × 0.05	0.16 × 0.12 × 0.09	0.23 × 0.19 × 0.11
Space group	C2/c	I-42d	$P2_1/n$
a, Å	33.805(3)	20.0935(8)	9.5172(6)
b, Å	13.2119(13)	20.0935(8)	18.8171(9)
c, Å	20.8300(19)	37.4909(18)	25.453(2)
α, °	90	90	90
β, °	127.397(2)	90	94.400(4)
γ, °	90	90	90
V, Å^3	7391.0(12)	15136.9(14)	4544.8(5)
Z	8	16	4
ρ_{calcd}, Mg m^{-3}	1.166	1.279	1.201
μ (Mo $K\alpha$), mm^{-1}	0.530	0.530	0.448
F(000)	2656.0	5984.0	1696.0
θ range, deg	4.76 to 56.996	4.336 to 52.74	4.466 to 56.698
Index ranges	$-45 \le h \le 45$	$-25 \le h \le 25$	$-12 \le h \le 12$
	$-17 \le k \le 17$	$-25 \le k \le 25$	$-25 \le k \le 25$
	$-27 \le l \le 27$	$-46 \le l \le 46$	$-33 \le l \le 33$
No. of reflns collected	119546	182047	147792
Completeness to θ_{max}	99.7%	99.9%	99.3%
No. indep. Reflns	9341	7743	11280
No. obsd reflns with ($I>2\sigma(I)$)	8427	7480	9705
No. refined params	389	452	513
GooF (F^2)	1.155	1.124	1.033
R_1 (F) ($I > 2\sigma(I)$)	0.0748	0.0470	0.0438
wR_2 (F^2) (all data)	0.1790	0.1095	0.1078
Largest diff peak/hole, e Å^{-3}	2.15 / −3.27	0.76 / −0.51	0.80 / -0.72
CCDC number	1894396	1894397	1894398

7.7 Supporting Information for

Rhenium(I)-Triscarbonyl M-O Complexes for CO_2 Activation *via* MLC with Alcohol/Aldehyde and Alcohol/Ketone system

Index

Spectroscopic, scXRD analysis and Mass spectrometric data for compound:

***fac*-[Re(I)(*aldpy*)(CO)$_3$Br] (99a)**

^{1}H NMR (200 MHz, THF-*d8*) δ 10.44 (s, 1H), 9.14 (d, *J* = 4.9 Hz, 1H), 8.59 (d, *J* = 7.6 Hz, 1H), 8.36 (t, *J* = 7.6 Hz, 1H), 7.93 (t, *J* = 6.7 Hz, 1H).

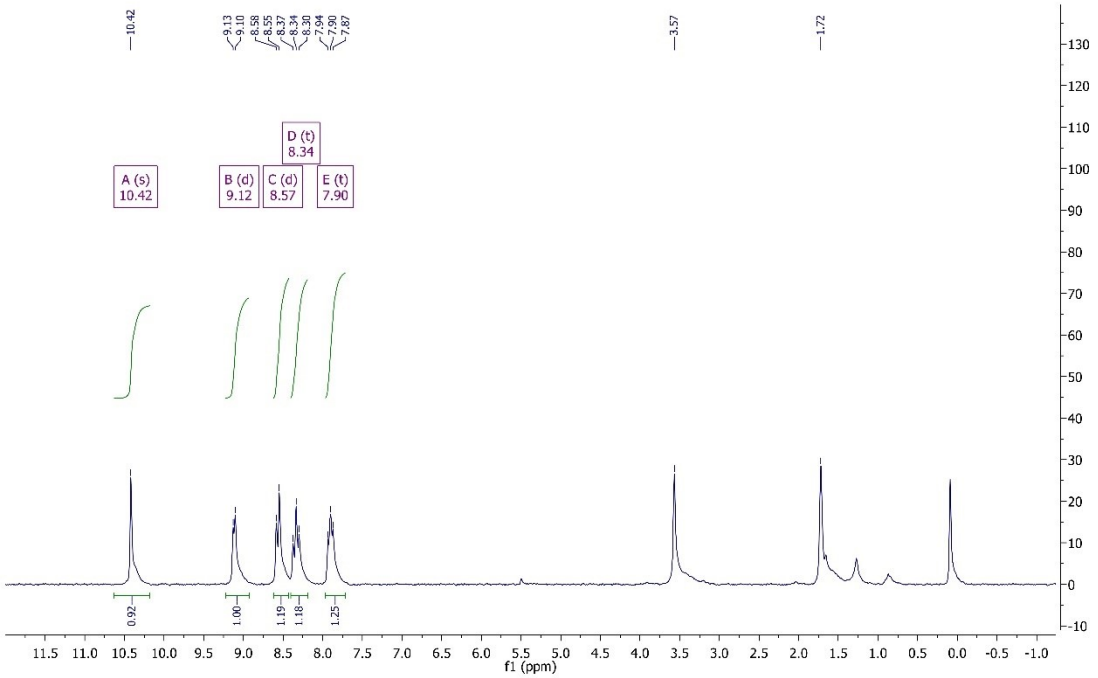

Figure S7.7-1: ^{1}H NMR [200 MHz, THF-d$_8$, 298 K] spectrum of ***fac*-[Re(I)(*aldpy*)(CO)$_3$Br] (99a)**.

^{1}H NMR (360 MHz, Aceton-*d6*) δ 10.76 (s, 1H), 9.24 (d, *J* = 5.2 Hz, 1H), 8.89 (d, *J* = 7.6 Hz, 1H), 8.56 (td, *J* = 7.8, 1.3 Hz, 1H), 8.13 (ddd, *J* = 7.9, 5.3, 1.4 Hz, 1H).

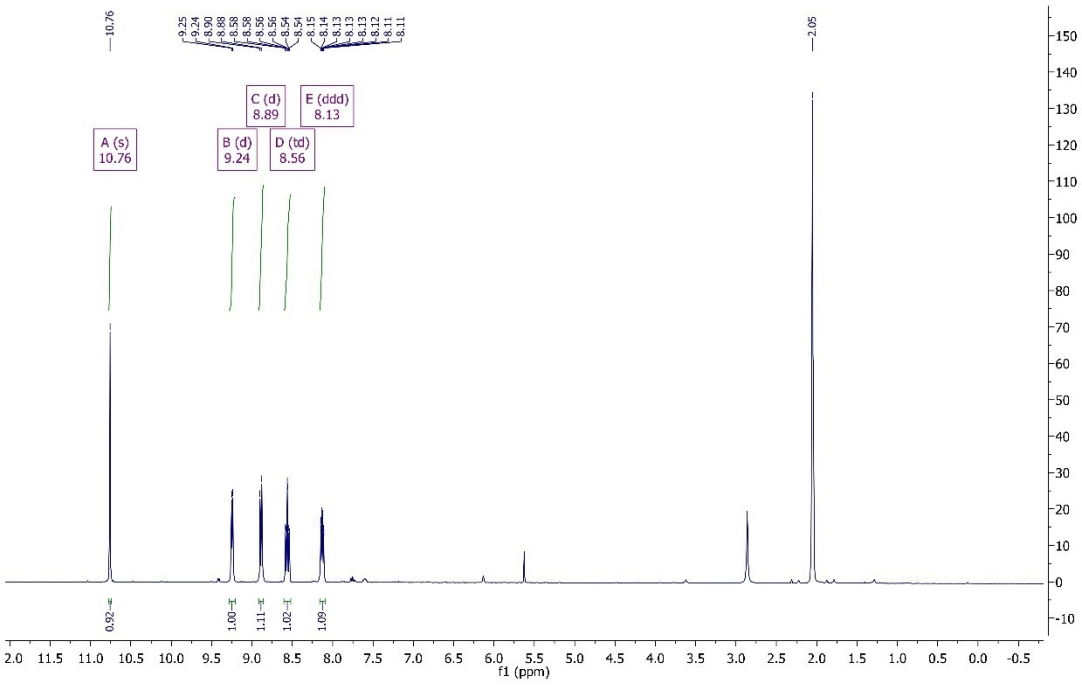

Figure S7.7-2: ^{1}H NMR [360 MHz, Aceton-d$_6$, 298 K] spectrum of ***fac*-[Re(I)(*aldpy*)(CO)$_3$Br] (99a)**.

***fac*-[Re(I)(*ketpy*)(CO)$_3$Br] (99b)**

^{1}H NMR (360 MHz, THF-d_8) δ 9.25 (d, J = 5.1 Hz, 1H), 8.57 (d, J = 7.9 Hz, 1H), 8.31 (td, J = 7.9, 1.6 Hz, 1H), 8.02 (d, J = 7.3 Hz, 2H), 7.93 (ddd, J = 7.8, 5.3, 1.3 Hz, 1H), 7.80 (t, J = 7.5 Hz, 1H), 7.66 (t, J = 7.8 Hz, 2H).

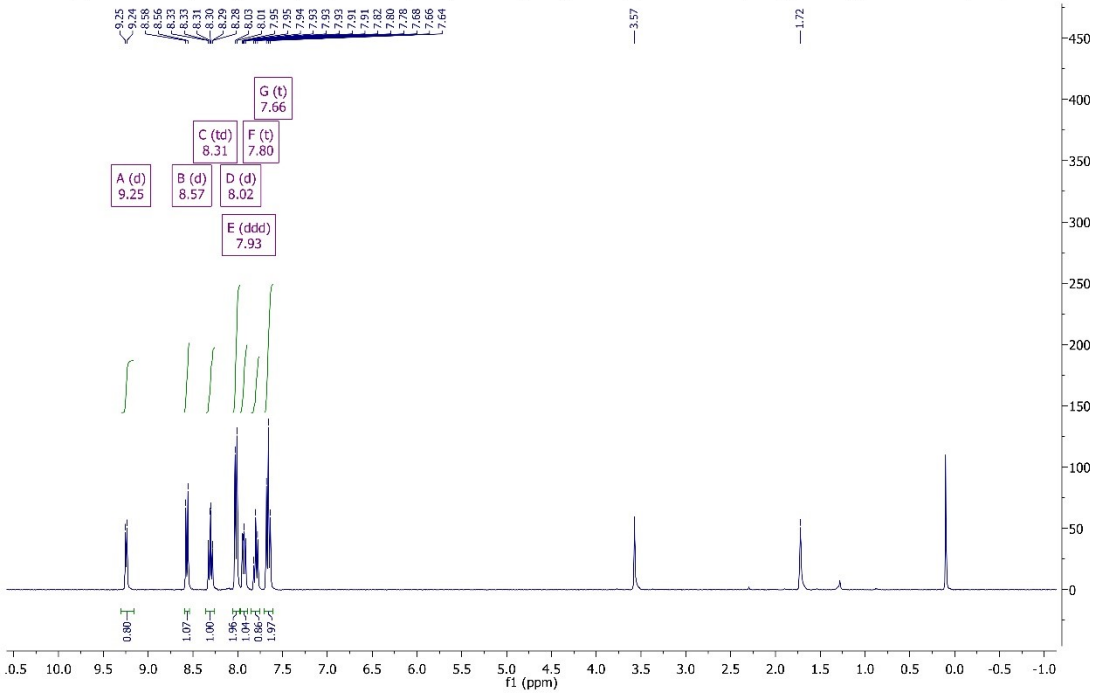

Figure S7.7-3: ^{1}H NMR [360 MHz, THF-d_8, 298 K] spectrum of ***fac*-[Re(I)(*ketpy*)(CO)$_3$Br] (99b)**.

^{13}C NMR (91 MHz, THF-d8) δ 206.46, 198.55, 197.24, 188.56, 154.99, 151.86, 135.83, 135.62, 134.08, 131.98, 131.43, 129.90, 67.39, 25.31.

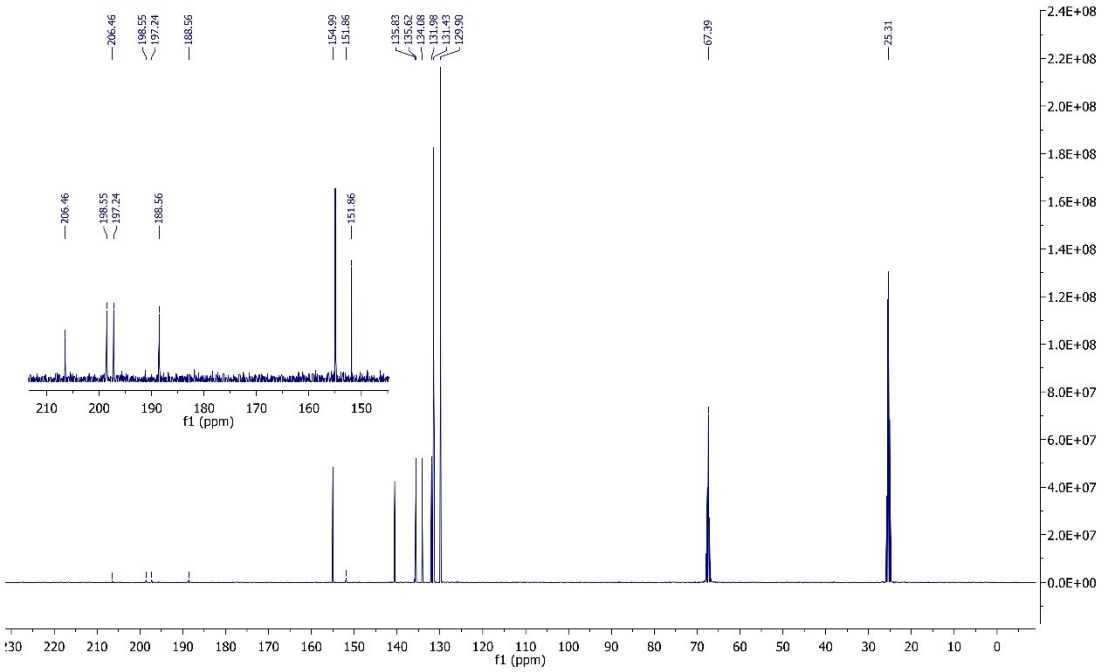

Figure S7.7-4: ^{13}C{^{1}H} NMR [91 MHz, THF-d_8, 298 K] spectrum of ***fac*-[Re(I)(*ketpy*)(CO)$_3$Br] (99b)**.

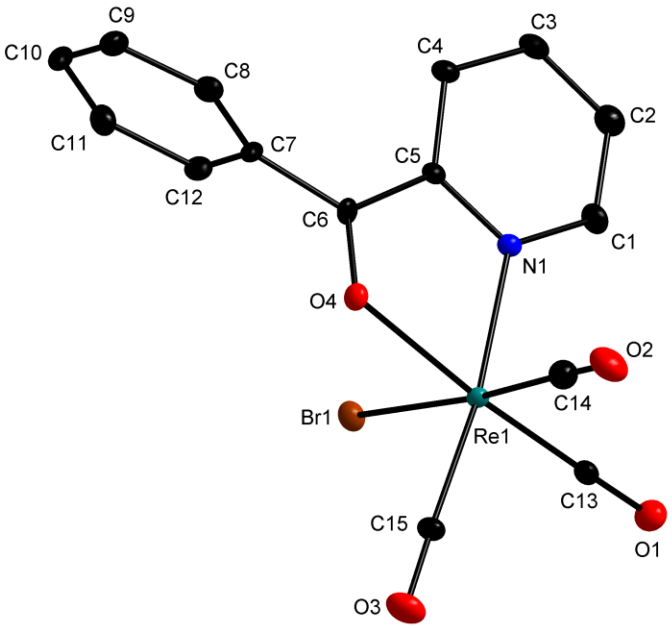

Figure S7.7-5: Diamond plot of ***fac*-[Re(I)(*ketpy*)(CO)$_3$Br] (99b)**. (Thermal ellipsoids at 50% probability, H atoms omitted for clarity)

Selected bond lengths [Å] and angle [°] of **99b** from Diamond plot scXRD analysis: C1-C2 = 1.392(5), C2-C3 = 1.381(6), C3-C4 = 1.395(5), C5-C4 = 1.393(5), C6-C5 = 1.483(5), C6-C7 = 1.467(5), C8-C7 = 1.403(5), C8-C9 = 1.388(5), C10-C9 = 1.397(6) , C10-C11 = 1.390(6) , C12-C11 = 1.397(6) , C7-C12 = 1.397(6), C1-N1 = 1.339(5), N1-C5 = 1.364(5), O4-C6 = 1.245(4), O1-C13 = 1.150(5), O2-C14 = 1.086(6), C15-O3 = 1.138(5), Re1-O4 = 2.162(3), Re1-N1 = 2.175(3), Re1-Br1 = 2.604(1), Re1-C13 = 1.904(4), Re1-C14 = 1.958(5), Re1-C15 = 1.939(4).

Table 11: Crystallographic data and structure refinement from Olex report of ***fac*-[Re(I)(*ketpy*)(CO)$_3$Br] (99b)**.

StichauerD160616_0ma

Table 1 Crystal data and structure refinement for StichauerD160616_0ma.

Identification code	StichauerD160616_0ma
Empirical formula	$C_{15}H_9NO_4BrRe$
Formula weight	533.353
Temperature/K	100.0
Crystal system	monoclinic
Space group	$P2_1/c$
a/Å	15.4407(5)
b/Å	11.4210(4)
c/Å	8.4454(3)
α/°	90
β/°	94.2951(15)
γ/°	90
Volume/Å^3	1485.15(9)
Z	4
ρ_{calc}g/cm^3	2.385
μ/mm^{-1}	10.889
F(000)	989.3
Crystal size/mm^3	N/A × N/A × N/A
Radiation	Mo Kα (λ = 0.71073)
2Θ range for data collection/°	4.44 to 60.2
Index ranges	$-21 \le h \le 21$, $-16 \le k \le 16$, $-11 \le l \le 11$
Reflections collected	85927
Independent reflections	4341 [R_{int} = 0.0464, R_{sigma} = 0.0167]
Data/restraints/parameters	4341/0/199
Goodness-of-fit on F^2	1.046
Final R indexes [I>=2σ (I)]	R_1 = 0.0229, wR_2 = 0.0564
Final R indexes [all data]	R_1 = 0.0255, wR_2 = 0.0574
Largest diff. peak/hole / e Å^{-3}	2.01/-2.00

***fac*-[Re(I)(H-*alkpy*)(CO)$_3$Br] (100a)**

^{1}H NMR (360 MHz, THF-d_8) δ 9.19 (s, 1H), 8.81 (d, J = 5.5 Hz, 1H), 7.96 (td, J = 7.8, 1.6 Hz, 1H), 7.54 (d, J = 7.9 Hz, 1H), 7.43 (t, J = 6.5 Hz, 1H), 5.52 (d, J = 14.8 Hz, 1H), 5.17 (d, J = 14.8 Hz, 1H).

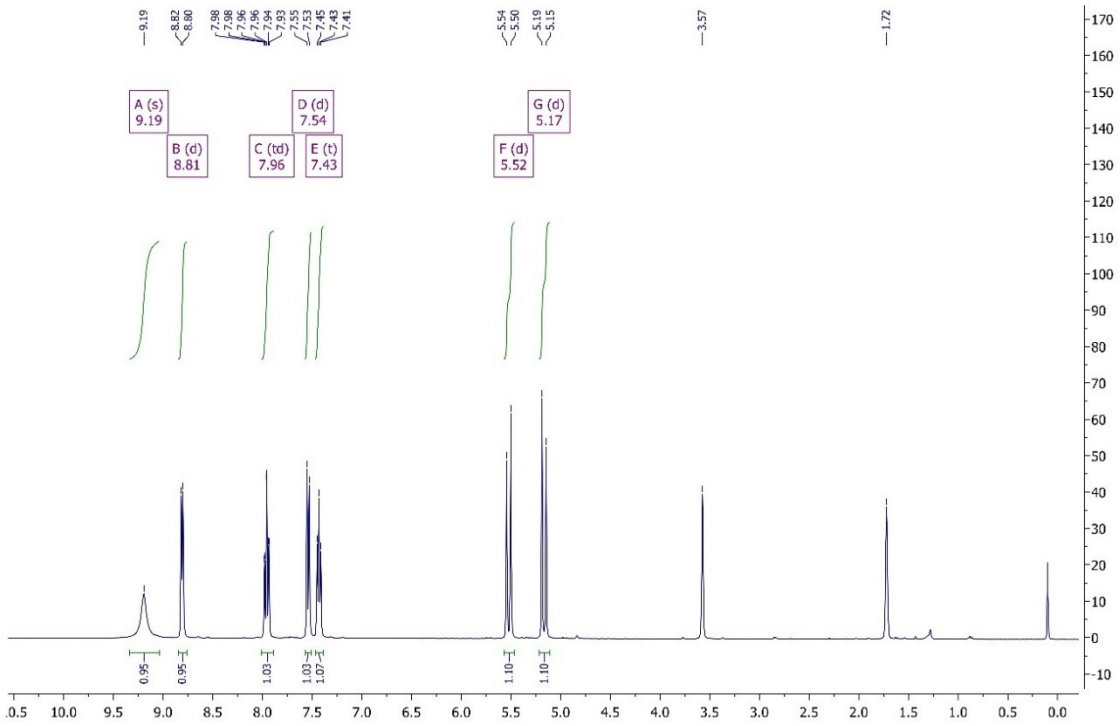

Figure S7.7-6: ^{1}H NMR [360 MHz, THF-d_8, 298 K] spectrum of ***fac*-[Re(I)(H-*alkpy*)(CO)$_3$Br] (100a)**.

***fac*-[Re(I)(Ph-*alkpy*)(CO)$_3$Br] (100b)**

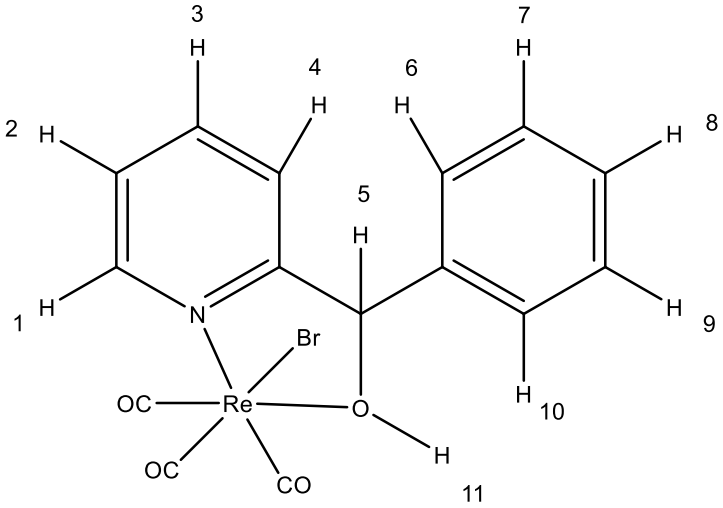

Figure S7.7-7: Structural formula of ***fac*-[Re(I)(Ph-*alkpy*)(CO)$_3$Br] (100b)** for the assignment of ^{1}H NMR signals.

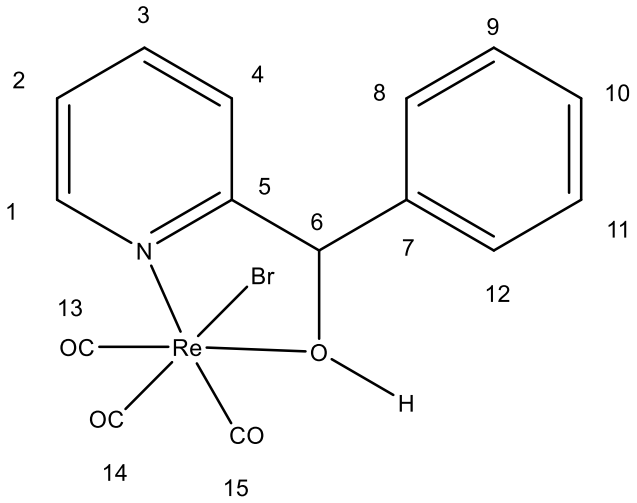

Figure S7.7-8: Structural formula of ***fac*-[Re(I)(Ph-*alkpy*)(CO)$_3$Br] (100b)** for the assignment of ^{13}C NMR signals.

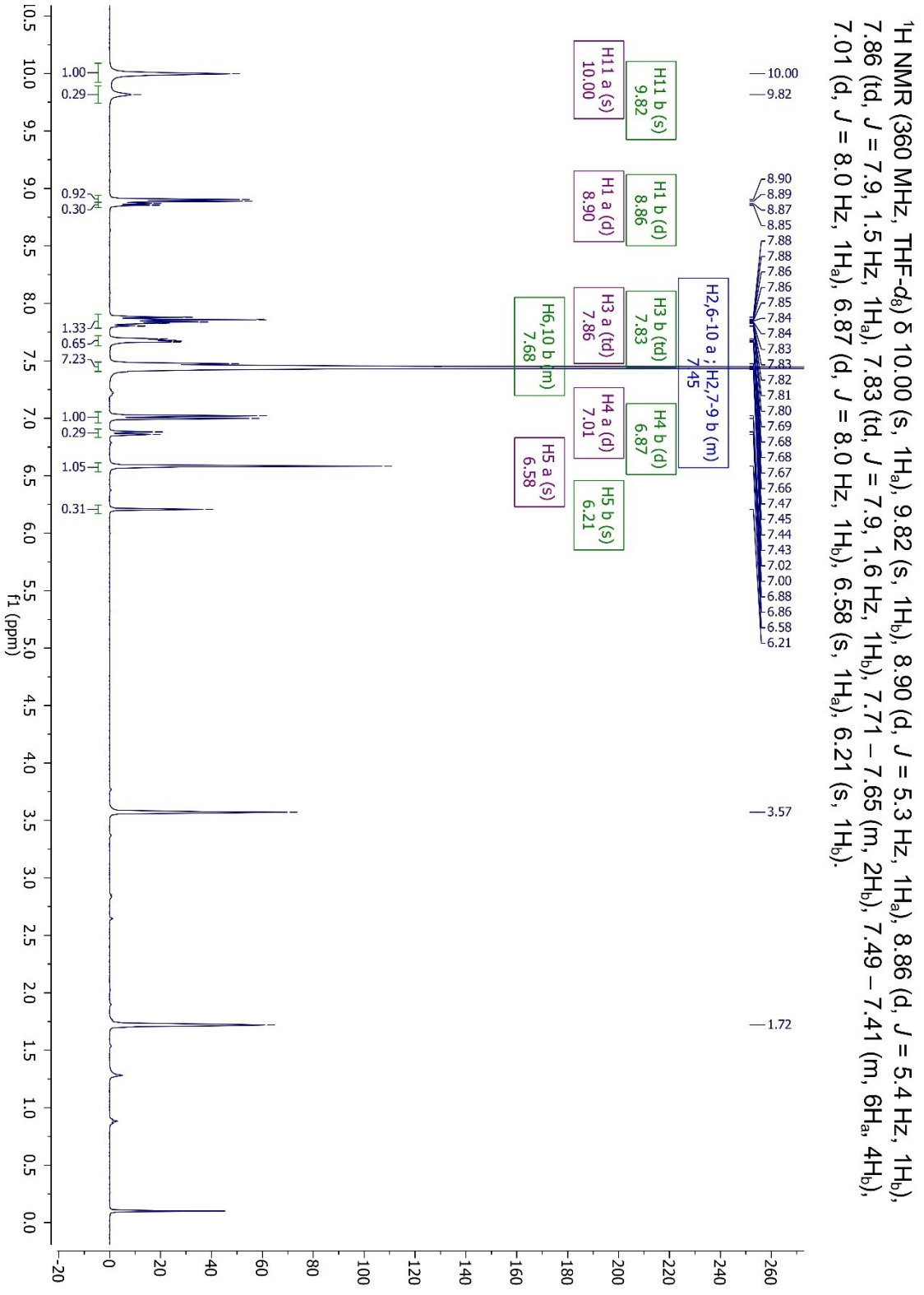

Figure S7.7-9: ^{1}H NMR [360 MHz, THF-d_8, 298 K] spectrum of ***fac*-[Re(I)(Ph-*alkpy*)(CO)$_3$Br] (100b)**.

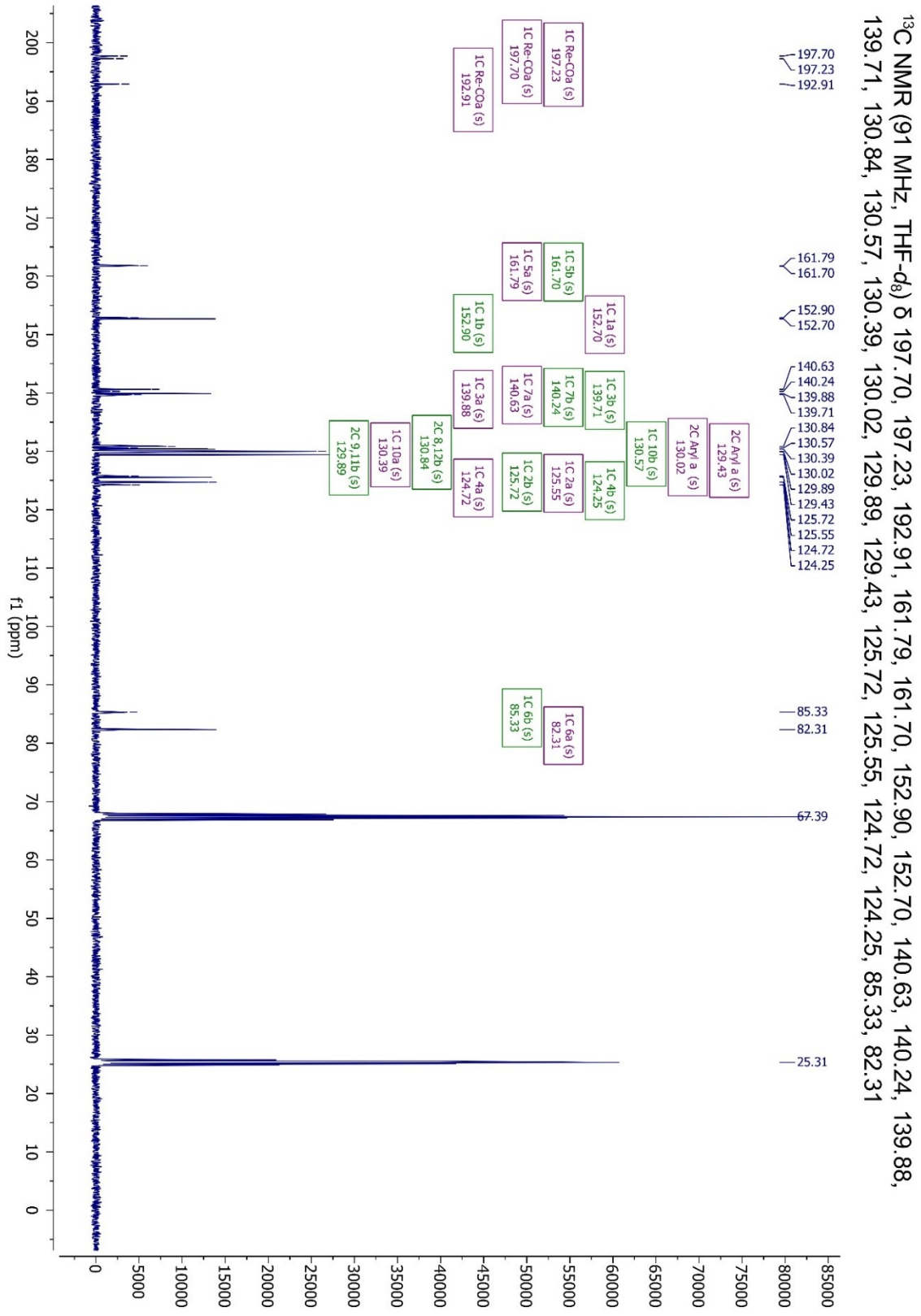

Figure S7.7-10: $^{13}C\{^1H\}$ NMR [91 MHz, THF-d_8, 298 K] spectrum of ***fac*-[Re(I)(Ph-*alkpy*)(CO)$_3$Br] (100b)**.

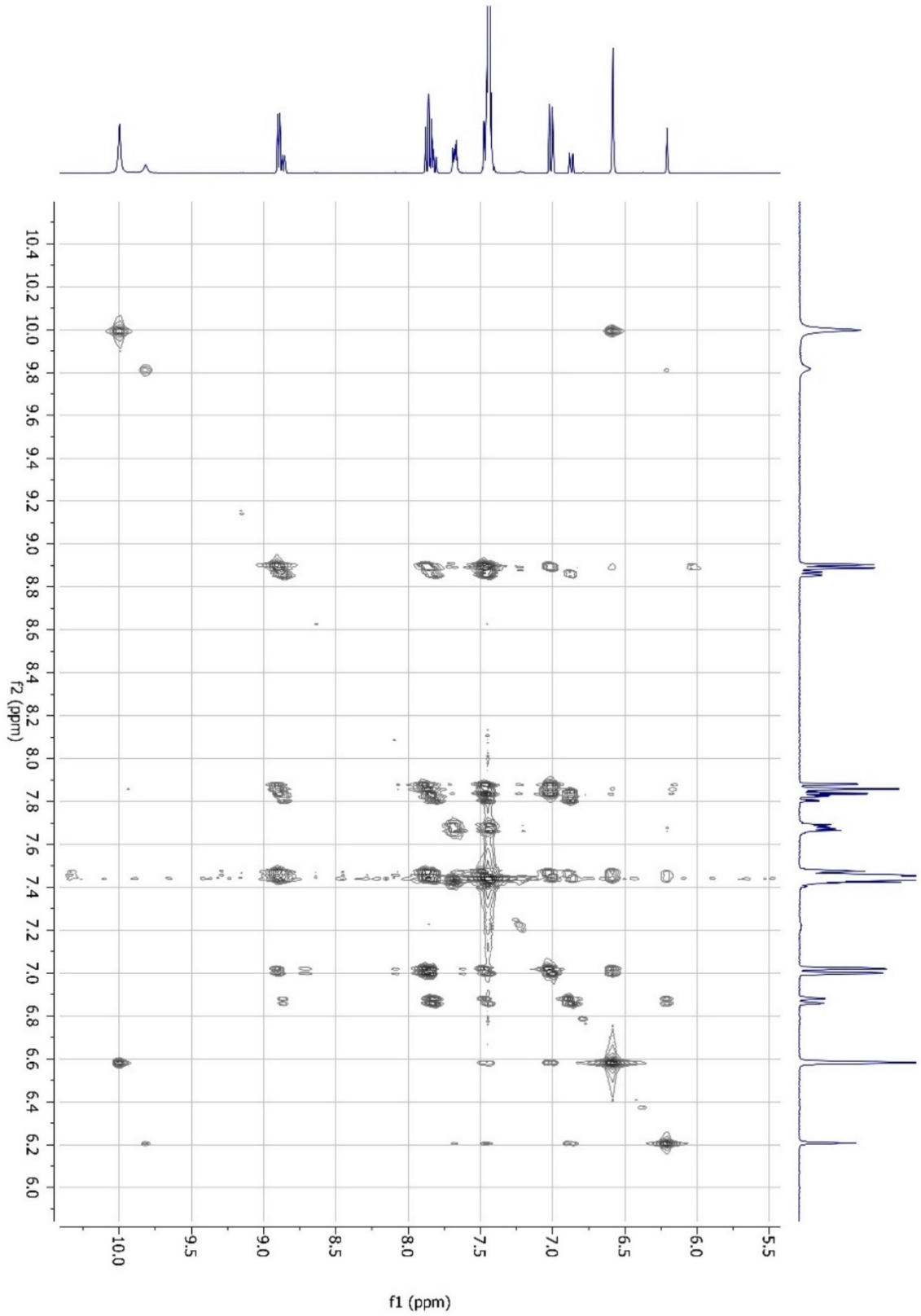

Figure S7.7-11: $^{1}H^{1}H$ COSY NMR [360 MHz, THF-d_8, 298 K] spectrum of ***fac*-[Re(I)(Ph-*alkpy*)$(CO)_3$Br] (100b)**.

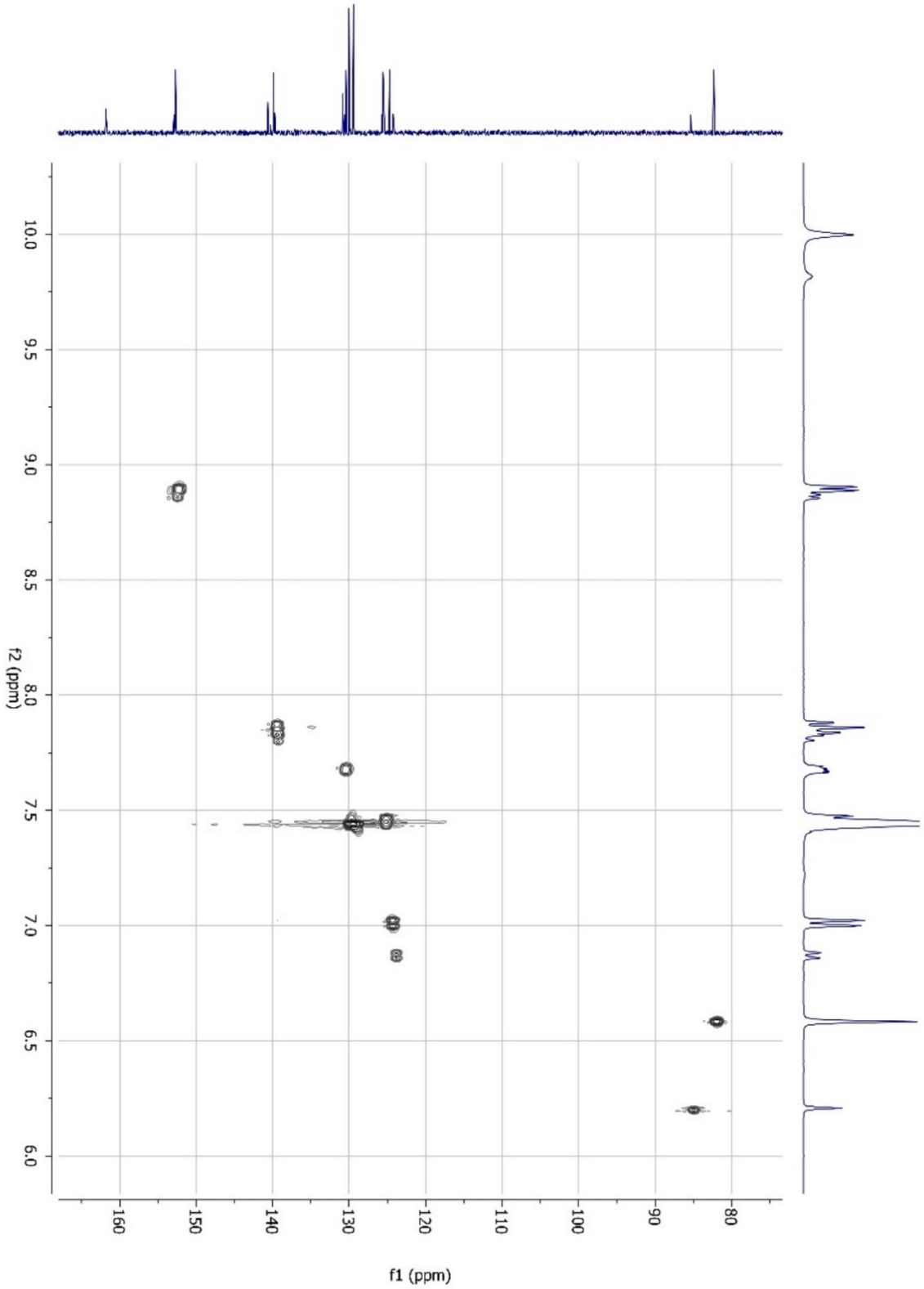

Figure S7.7-12: $^{1}H^{13}C$ HSQC NMR [360 MHz/ 91 MHz, THF-d_8, 298 K] spectrum of ***fac*-[Re(I)(Ph-*alkpy*)(CO)$_3$Br] (100b)**.

Table 12: Crystallographic data and structure refinement from Olex report of ***fac*-[Re(I)(Ph-*alkpy*)(CO)$_3$Br] (100b-R)**

VogtM170726_0m

Table 1 Crystal data and structure refinement for VogtM170726_0m.

Identification code	VogtM170726_0m
Empirical formula	$C_{19}H_{19}BrNO_5Re$
Formula weight	607.477
Temperature/K	100.0
Crystal system	monoclinic
Space group	$P2_1/c$
a/Å	11.3548(4)
b/Å	11.3299(4)
c/Å	15.7145(6)
α/°	90
β/°	91.7337(17)
γ/°	90
Volume/Å^3	2020.73(13)
Z	4
ρ_{calc}g/cm^3	1.997
μ/mm^{-1}	8.019
F(000)	1157.3
Crystal size/mm^3	N/A × N/A × N/A
Radiation	Mo Kα (λ = 0.71073)
2Θ range for data collection/°	4.44 to 70.16
Index ranges	-18 ≤ h ≤ 18, -18 ≤ k ≤ 18, -25 ≤ l ≤ 25
Reflections collected	158422
Independent reflections	8926 [R_{int} = 0.0471, R_{sigma} = 0.0169]
Data/restraints/parameters	8926/3/247
Goodness-of-fit on F^2	2.272
Final R indexes [I>=2σ (I)]	R_1 = 0.0566, wR_2 = 0.2532
Final R indexes [all data]	R_1 = 0.0598, wR_2 = 0.2545
Largest diff. peak/hole / e Å^{-3}	8.30/-8.27

Table 13: Crystallographic data and structure refinement from Olex report of ***fac*-[Re(I)(Ph-*alkpy*)(CO)$_3$Br] (100b-S)**

VogtM170731_0m

Table 1 Crystal data and structure refinement for VogtM170731_0m.

Identification code	VogtM170731_0m
Empirical formula	$C_{15}H_{11}BrNO_4Re$
Formula weight	535.369
Temperature/K	99.99
Crystal system	monoclinic
Space group	$P2_1/c$
a/Å	9.4480(2)
b/Å	11.6086(3)
c/Å	13.9442(3)
α/°	90
β/°	94.4740(13)
γ/°	90
Volume/Å^3	1524.71(6)
Z	4
ρ_{calc}g/cm^3	2.332
μ/mm^{-1}	10.606
F(000)	997.3
Crystal size/mm^3	N/A × N/A × N/A
Radiation	Mo Kα (λ = 0.71073)
2Θ range for data collection/°	4.58 to 65.2
Index ranges	$-14 \le h \le 14$, $-17 \le k \le 17$, $-21 \le l \le 21$
Reflections collected	119428
Independent reflections	5569 [R_{int} = 0.0610, R_{sigma} = 0.0230]
Data/restraints/parameters	5569/3/202
Goodness-of-fit on F^2	0.686
Final R indexes [I>=2σ (I)]	R_1 = 0.0208, wR_2 = 0.0712
Final R indexes [all data]	R_1 = 0.0307, wR_2 = 0.0838
Largest diff. peak/hole / e Å^{-3}	1.10/-1.54

Li[Re(I)(H-*alkoxpy)(CO)$_3$] (101*a-Li)**

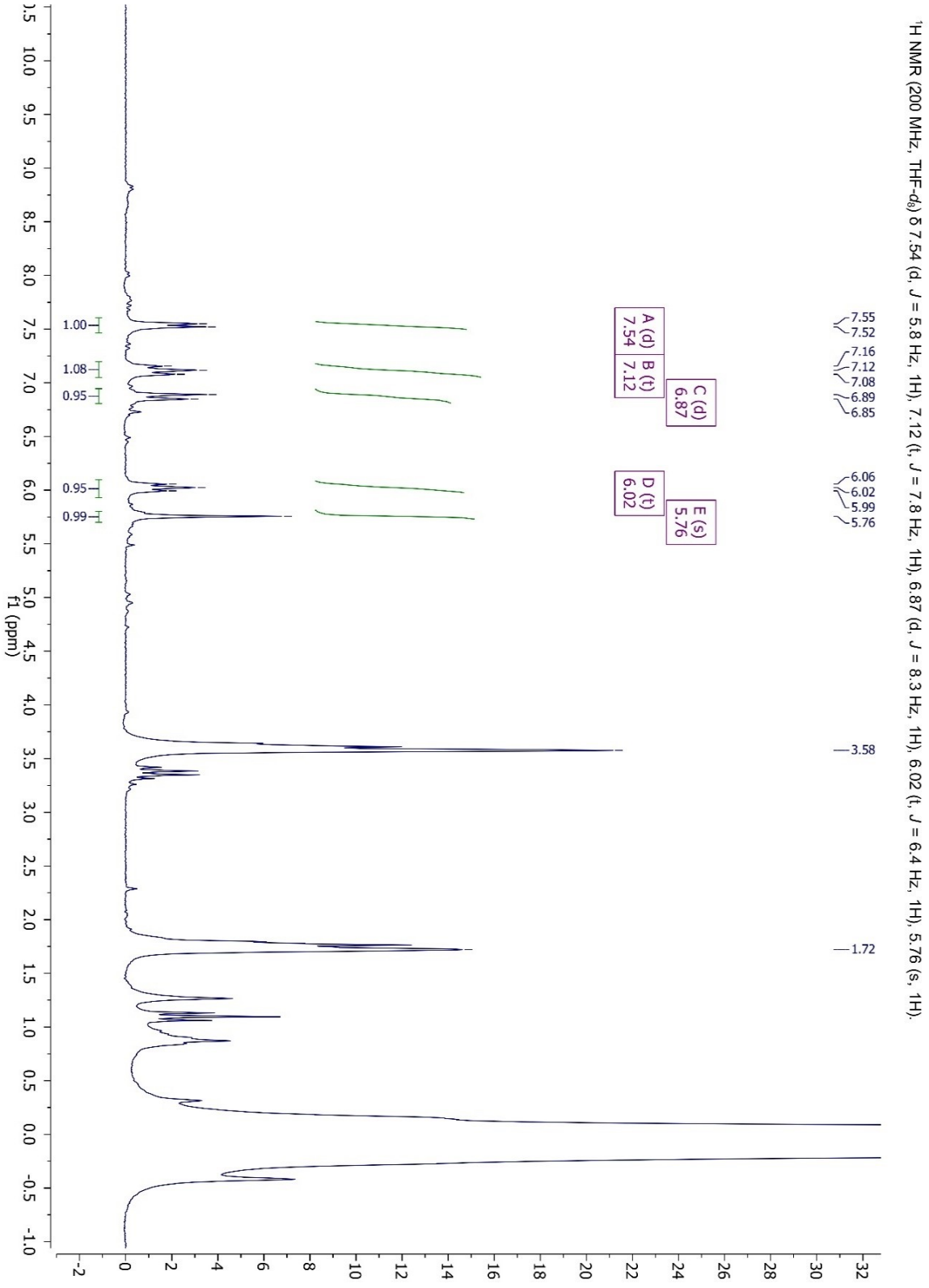

Figure S7.7-13: ^{1}H NMR [200 MHz, THF-d_8, 298 K] spectrum of **Li[Re(I)(H-*alkoxpy**)(CO)$_3$] (101*a-Li).**

K[Re(I)(Ph-*alkoxpy)(CO)$_3$] (101*b)**

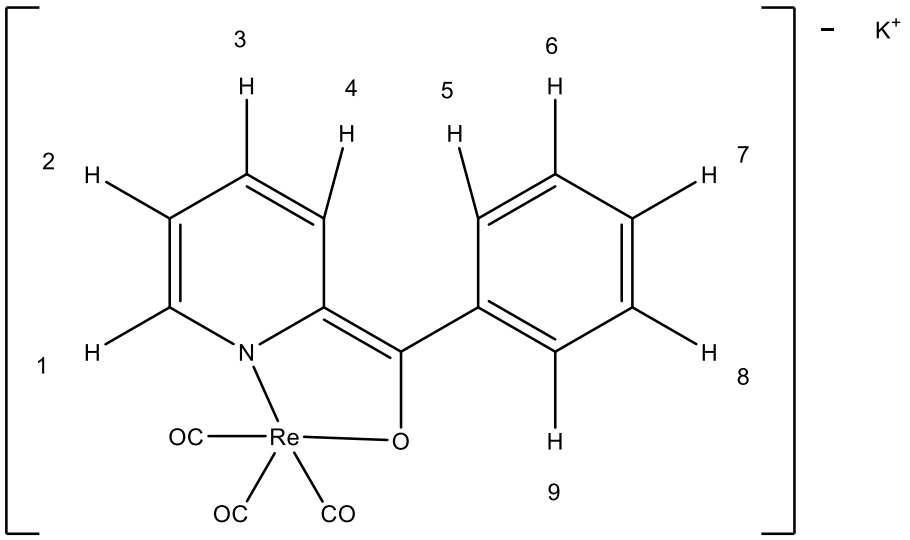

Figure S7.7-14: Structural formula of **K[Re(I)(Ph-*alkoxpy**)(CO)$_3$] (101*b)** for the assignment of ^{1}H NMR signals.

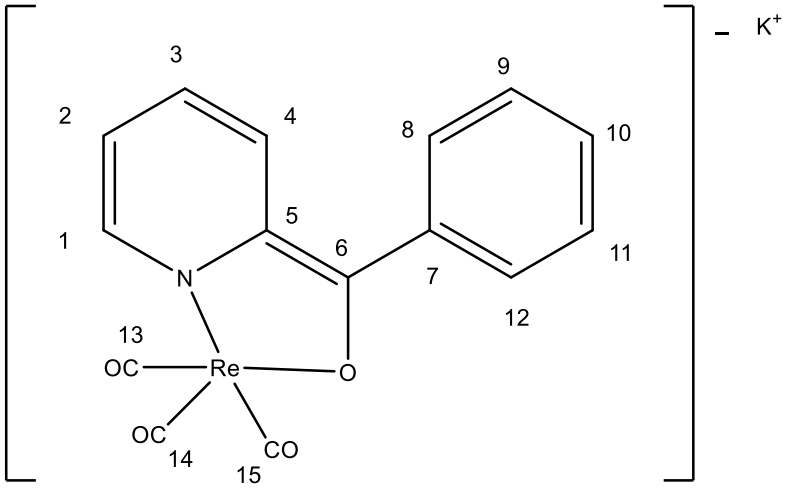

Figure S7.7-15: Structural formula of **K[Re(I)(Ph-*alkoxpy**)(CO)$_3$] (101*b)** for the assignment of ^{13}C NMR signals.

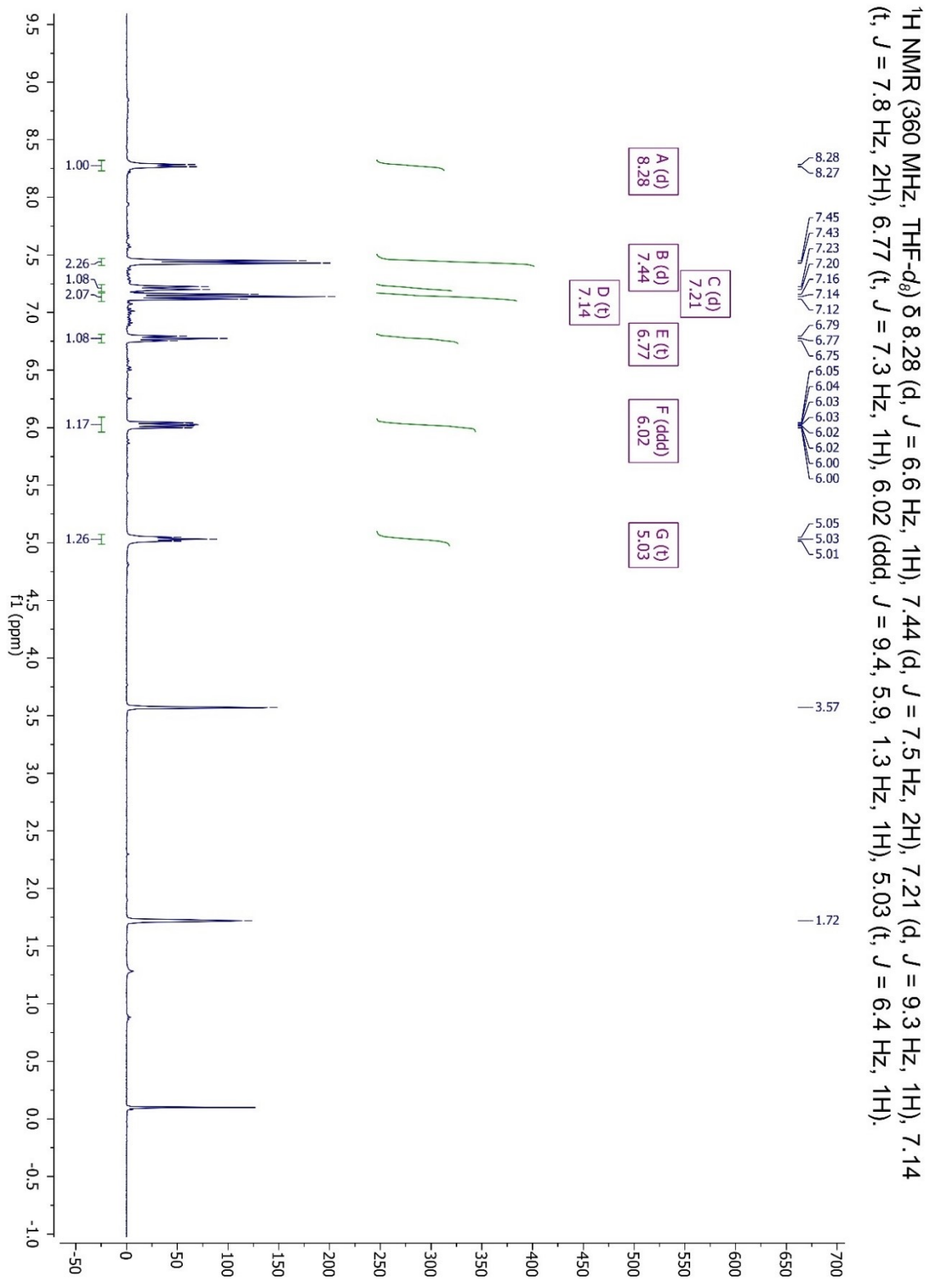

Figure S7.7-16: ^{1}H NMR [360 MHz, THF-d$_8$, 298 K] spectrum of **K[Re(I)(Ph-*alkoxpy**)(CO)$_3$] (101*b).** (Reduction with potassium metal)

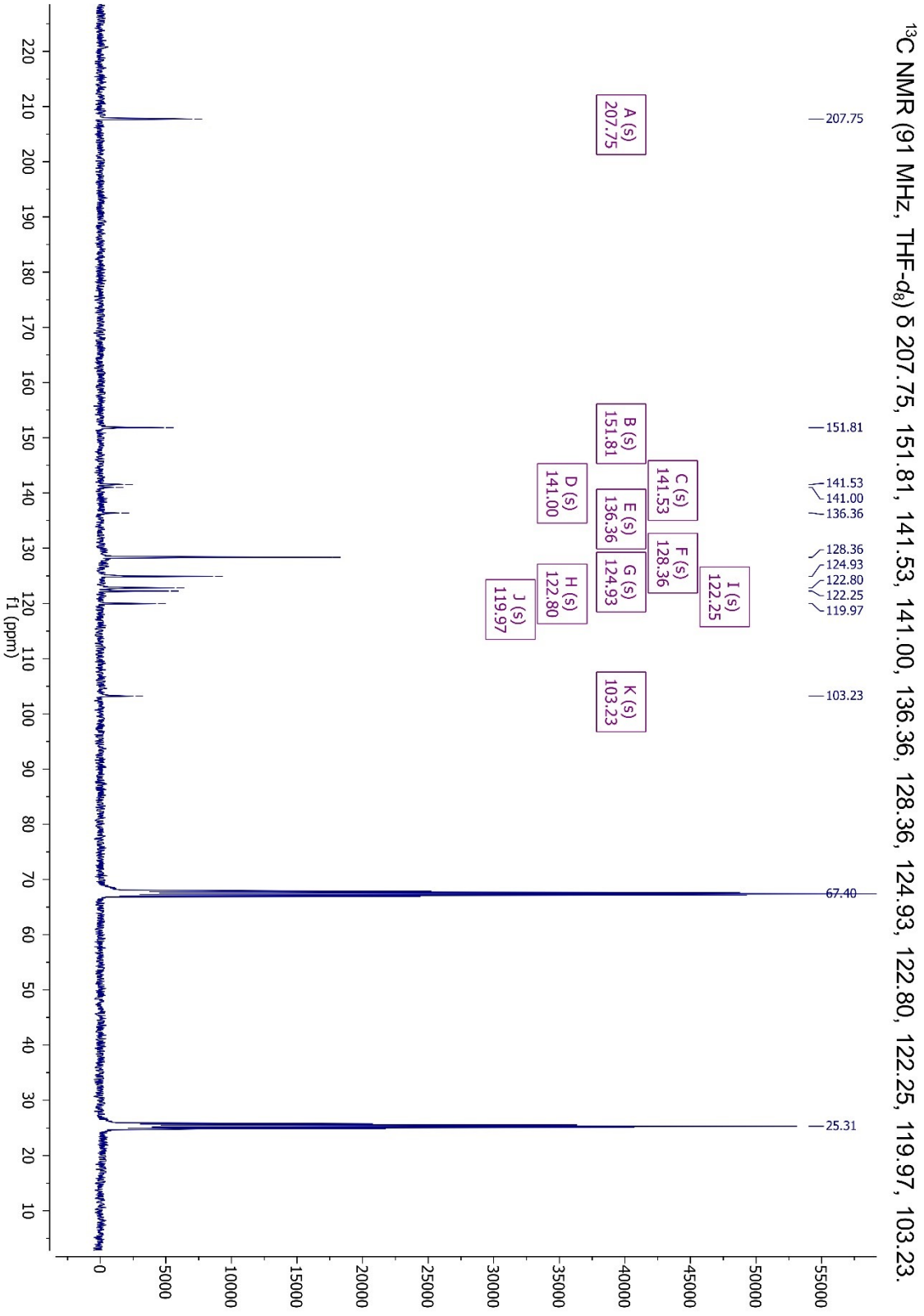

Figure S7.7-17: $^{13}C\{^1H\}$ NMR [91 MHz, THF-d_8, 298 K] spectrum of **K[Re(I)(Ph-*alkoxpy**)$(CO)_3$] (101*b).** (Reduction with potassium metal)

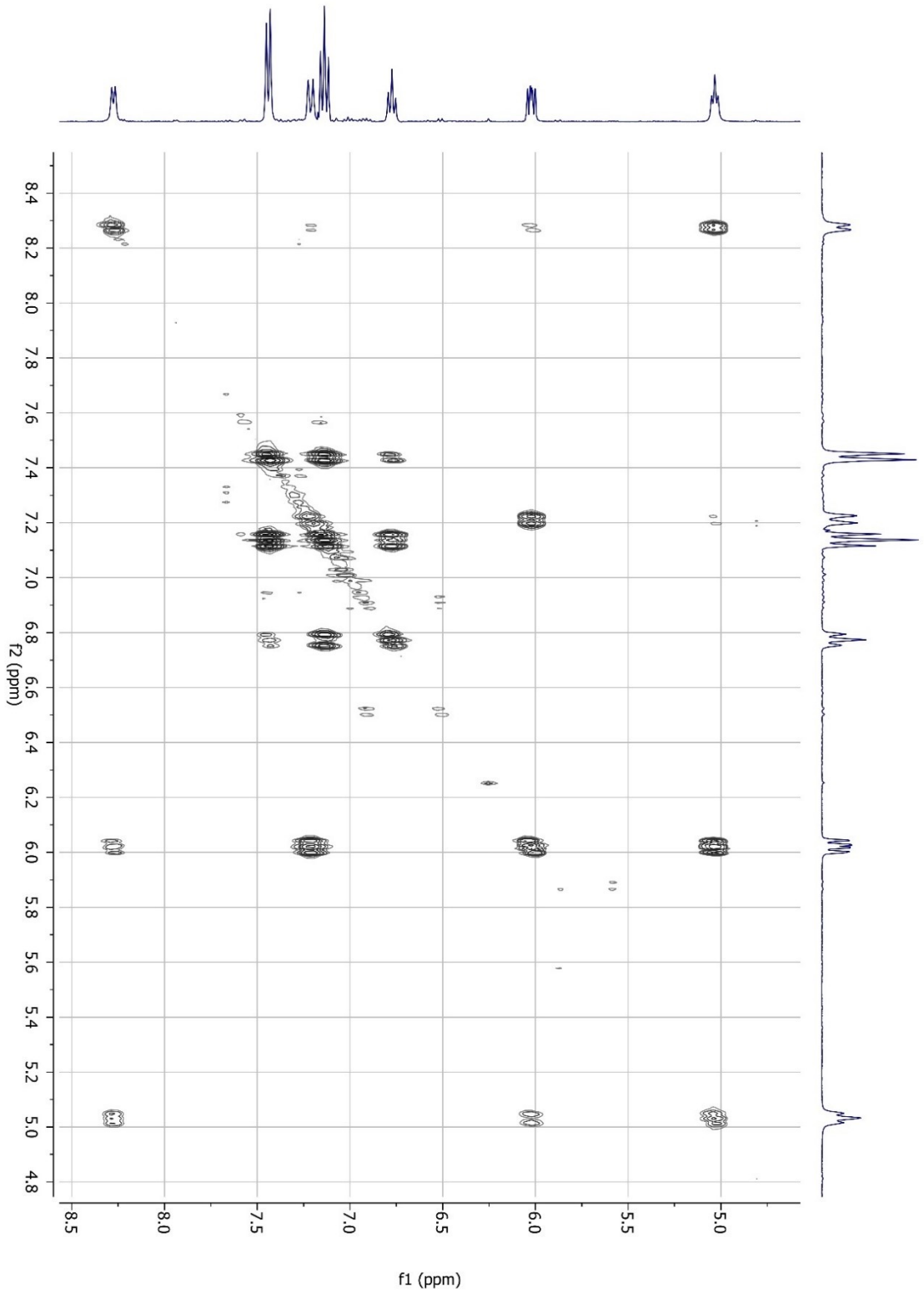

Figure S7.7-18: $^{1}H^{1}H$ COSY NMR [360 MHz, THF-d_8, 298 K] spectrum of **K[Re(I)(Ph-*alkoxpy**)$(CO)_3$] (101*b).** (Reduction with potassium metal)

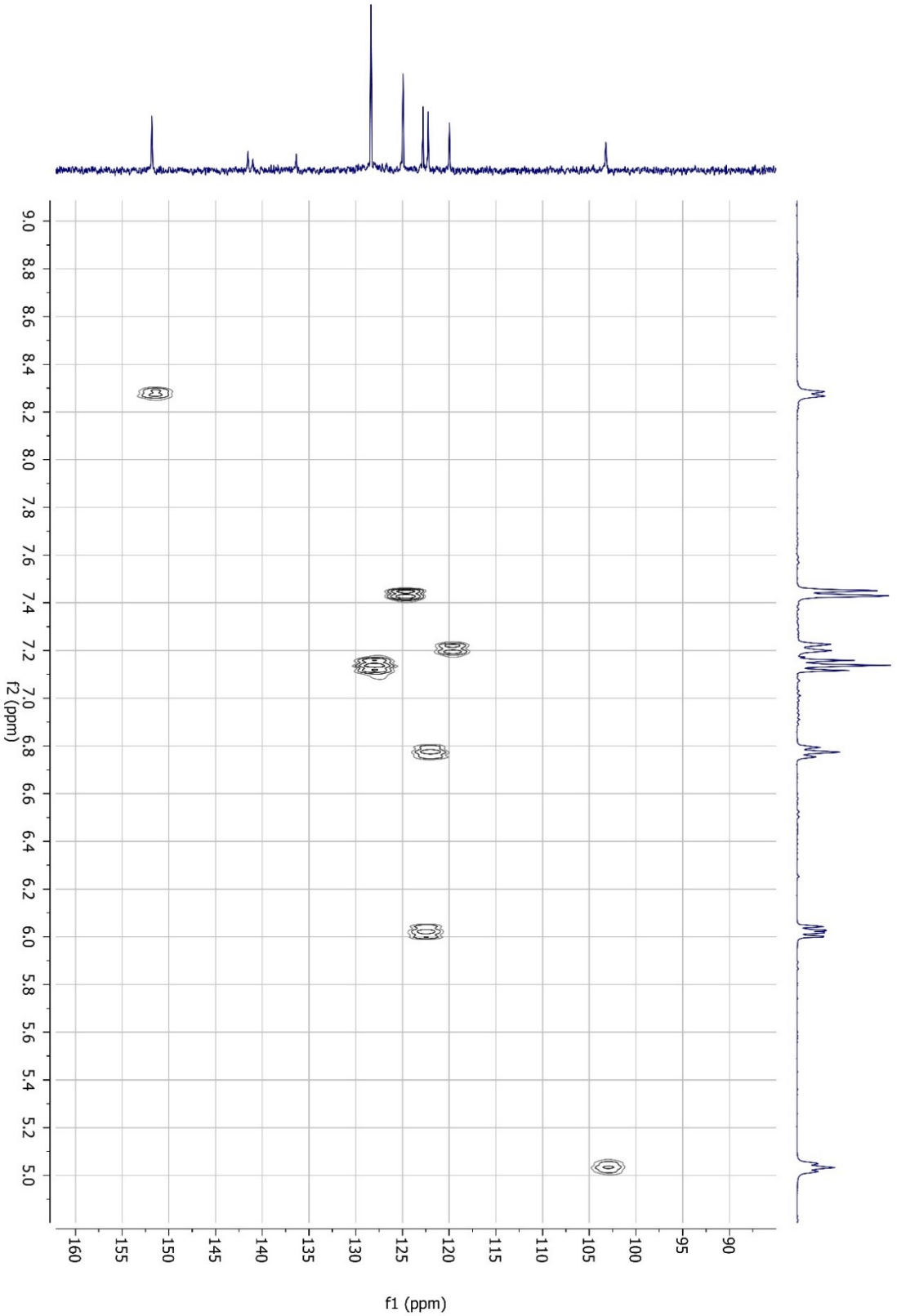

Figure S7.7-19: $^{1}H^{13}C$ HSQC NMR [360 MHz/ 91 MHz, THF-d_8, 298 K] spectrum of **K[Re(I)(Ph-*alkoxpy**)$(CO)_3$] (101*b).** (Reduction with potassium metal)

Li[Re(I)(Ph-*alkoxpy)(CO)$_3$] (101*b-Li)**

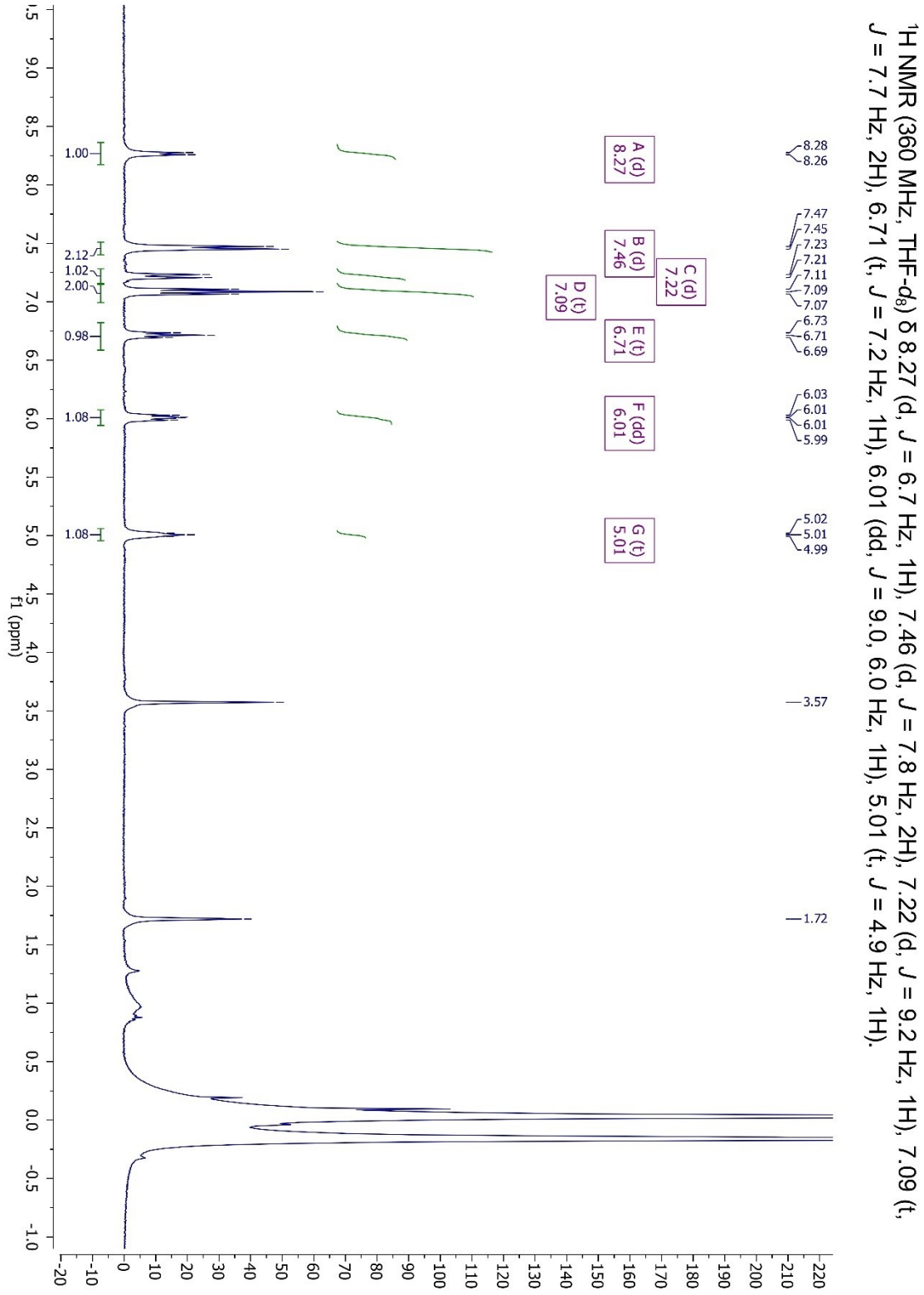

Figure S7.7-20: ^{1}H NMR [360 MHz, THF-d$_8$, 298 K] spectrum of **Li[Re(I)(Ph-*alkoxpy**)(CO)$_3$] (101*b-Li).** (Deprotonation with LiHMDS)

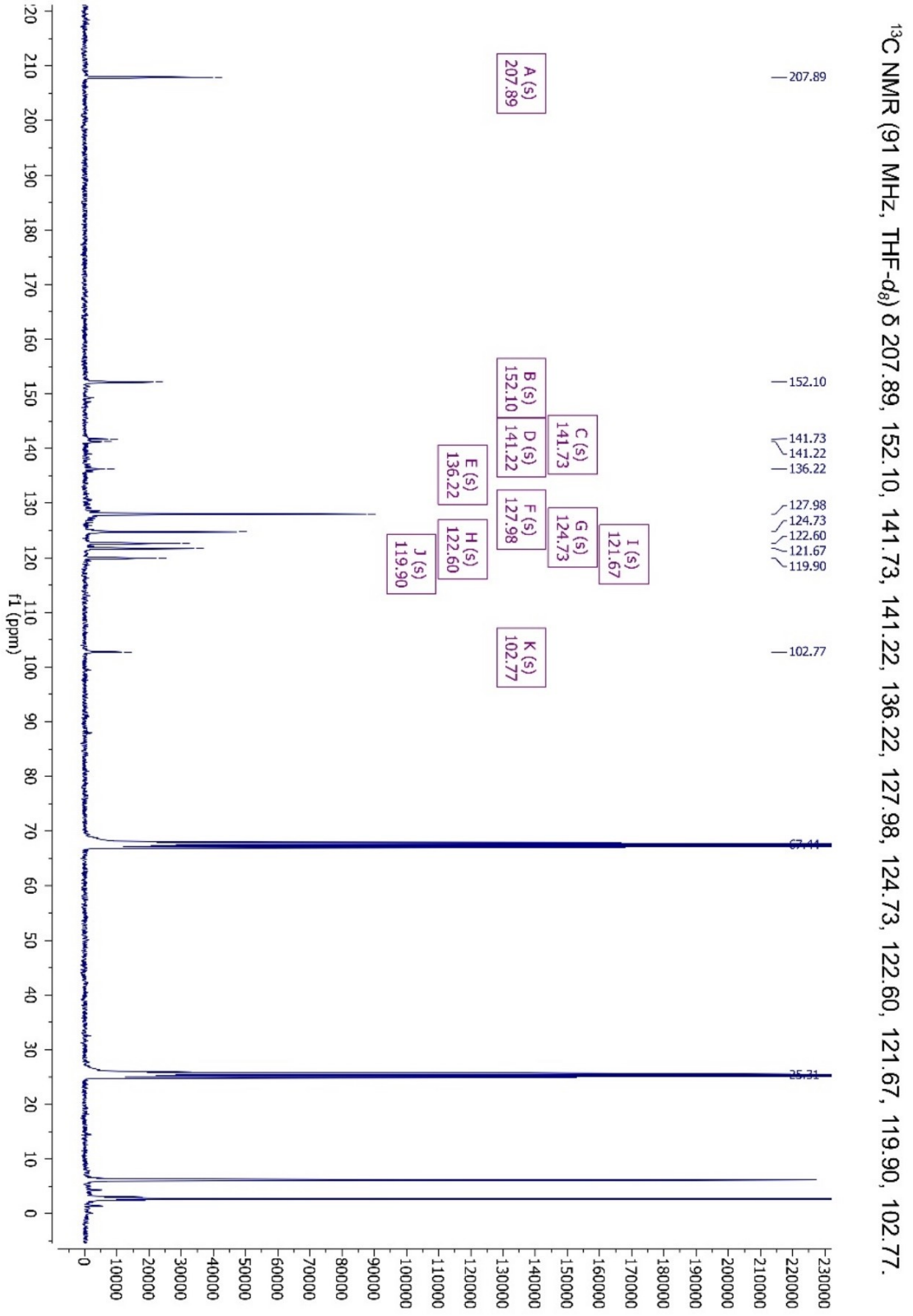

Figure S7.7-21: $^{13}C\{^1H\}$ NMR [91 MHz, THF-d_8, 298 K] spectrum of **Li[Re(I)(Ph-*alkoxpy**)$(CO)_3$] (101*b-Li).** (Deprotonation with LiHMDS)

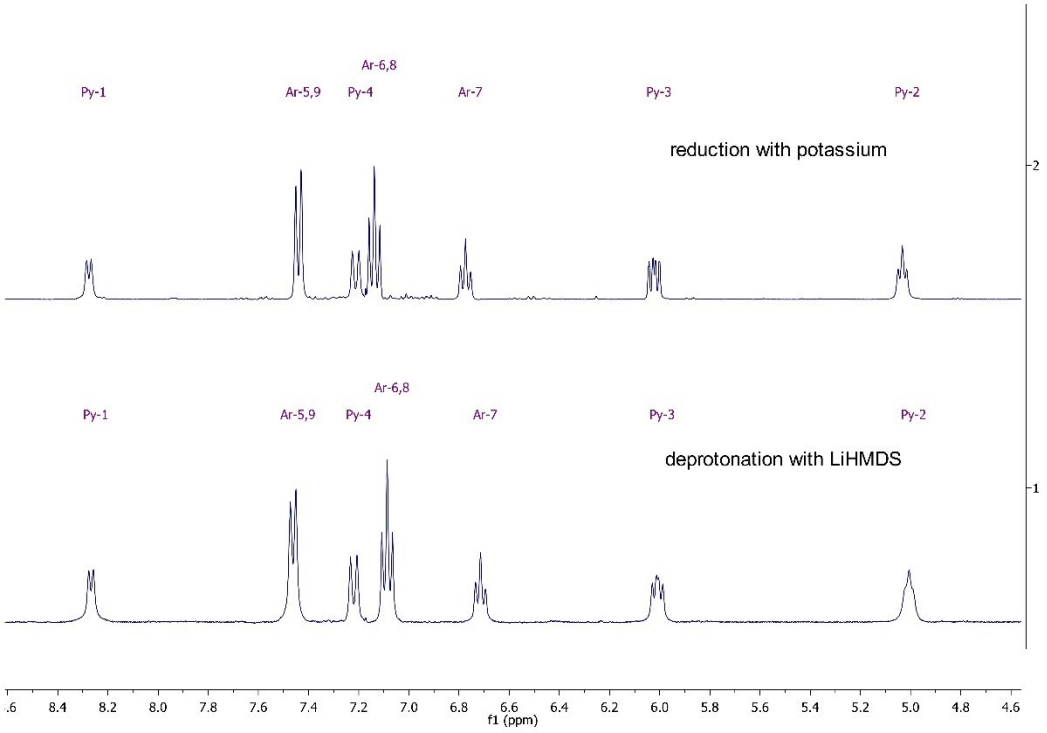

Figure S7.7-22: Sections ^{1}H NMR [360 MHz, THF-d_8, 298 K] spectrum of **101*-b** and **101*b-Li**.

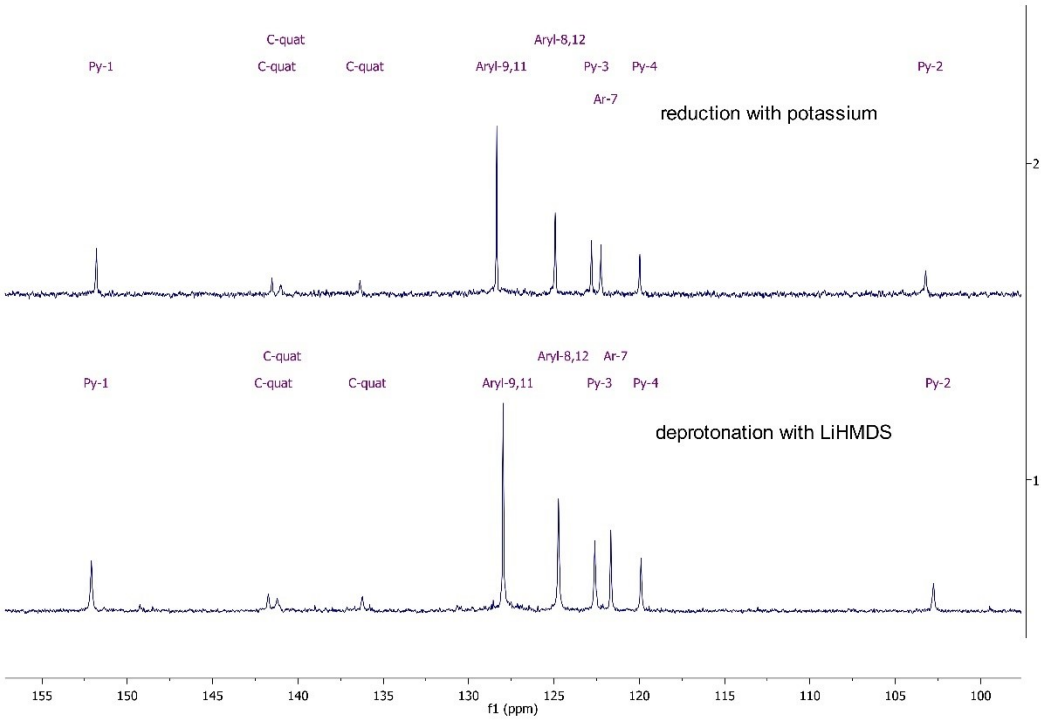

Figure S7.7-23: Sections ^{13}C{^{1}H} NMR [91 MHz, THF-d_8, 298 K] spectrum of **101*-b** and **101*b-Li**.

***fac*-K[Re(I)(Ph-*alkoxpy*-CO_2)$(CO)_3$] (102b)**

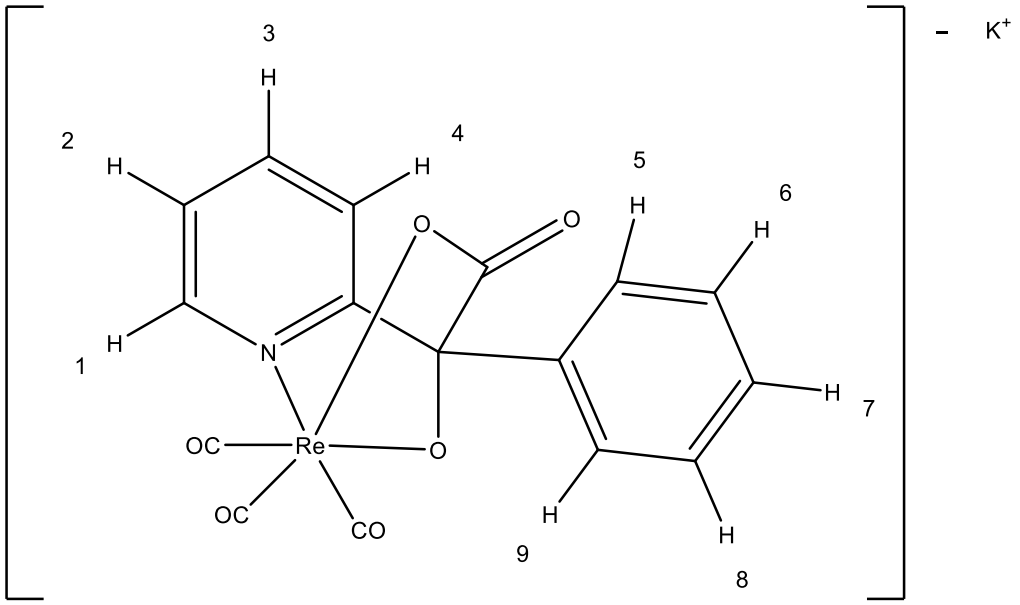

Figure S7.7-24: Structural formula of ***fac*-K[Re(I)(Ph-*alkoxpy*-CO_2)$(CO)_3$] (102b)** for the assignment of ^{1}H NMR signals.

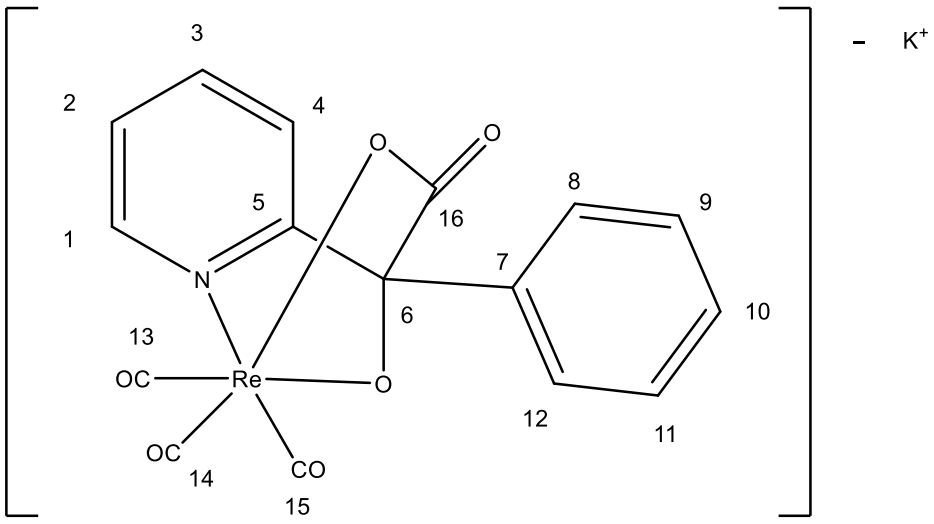

Figure S7.7-25: Structural formula of ***fac*-K[Re(I)(Ph-*alkoxpy*-CO_2)$(CO)_3$] (102b)** for the assignment of ^{13}C NMR signals.

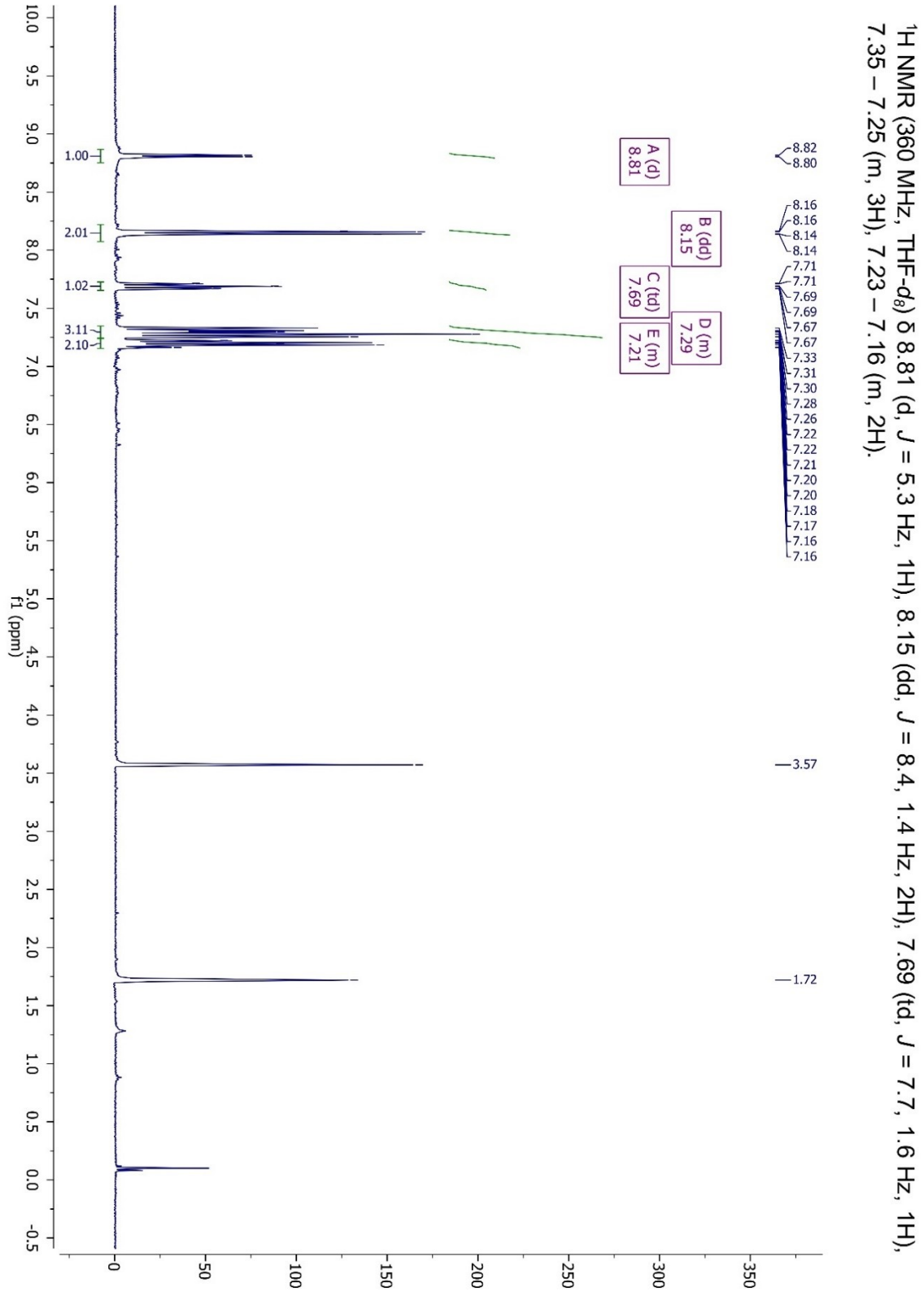

Figure S7.7-26: ^{1}H NMR [360 MHz, THF-d_8, 298 K] spectrum of ***fac*-K[Re(I)(Ph-*alkoxpy*-CO_2)$(CO)_3$] (102b)**.

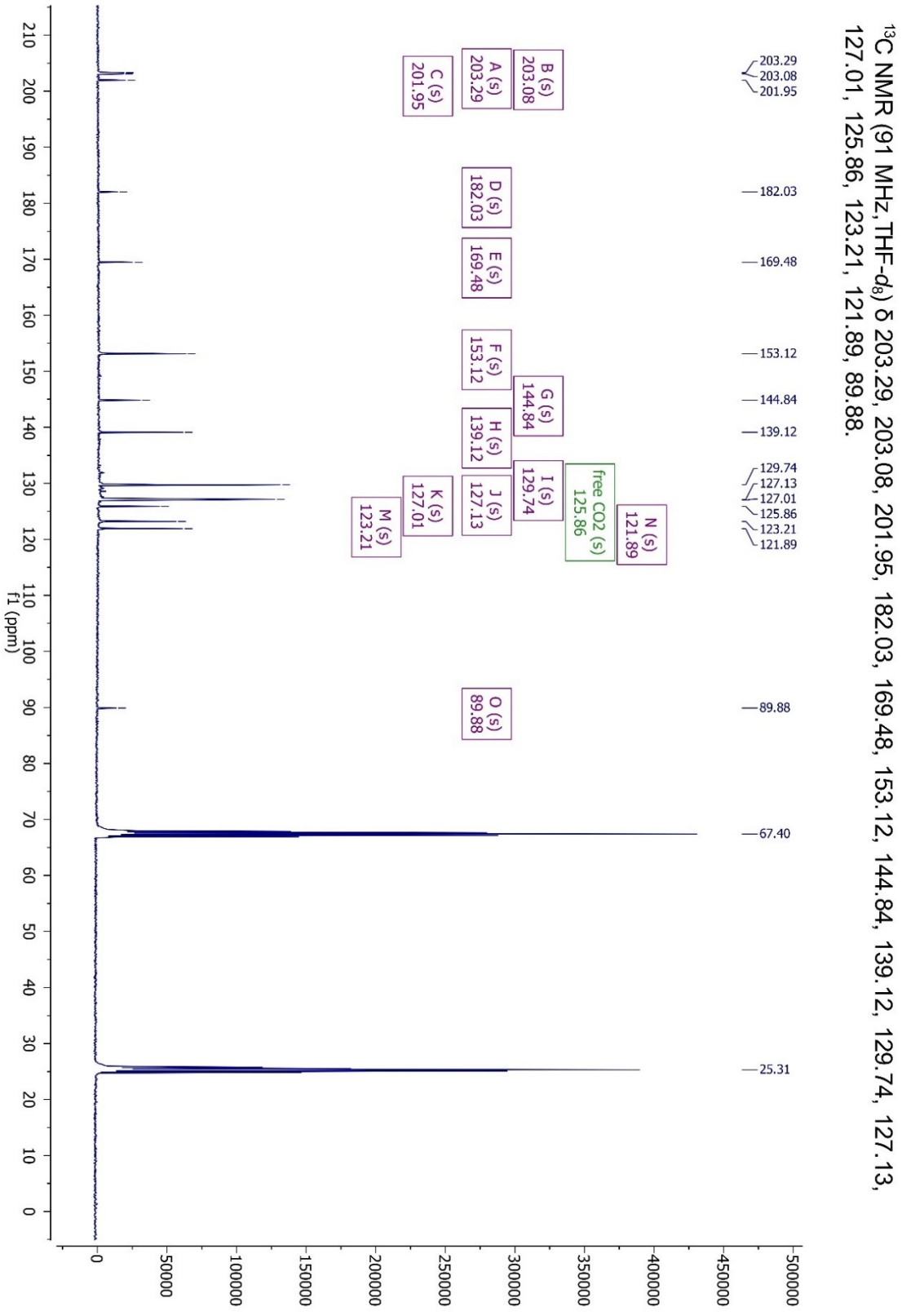

Figure S7.7-27: $^{13}C\{^{1}H\}$ NMR [91 MHz, THF-d_8, 298 K] spectrum of ***fac*-K[Re(I)(Ph-*alkoxpy*-CO_2)$(CO)_3$] (102b)**.

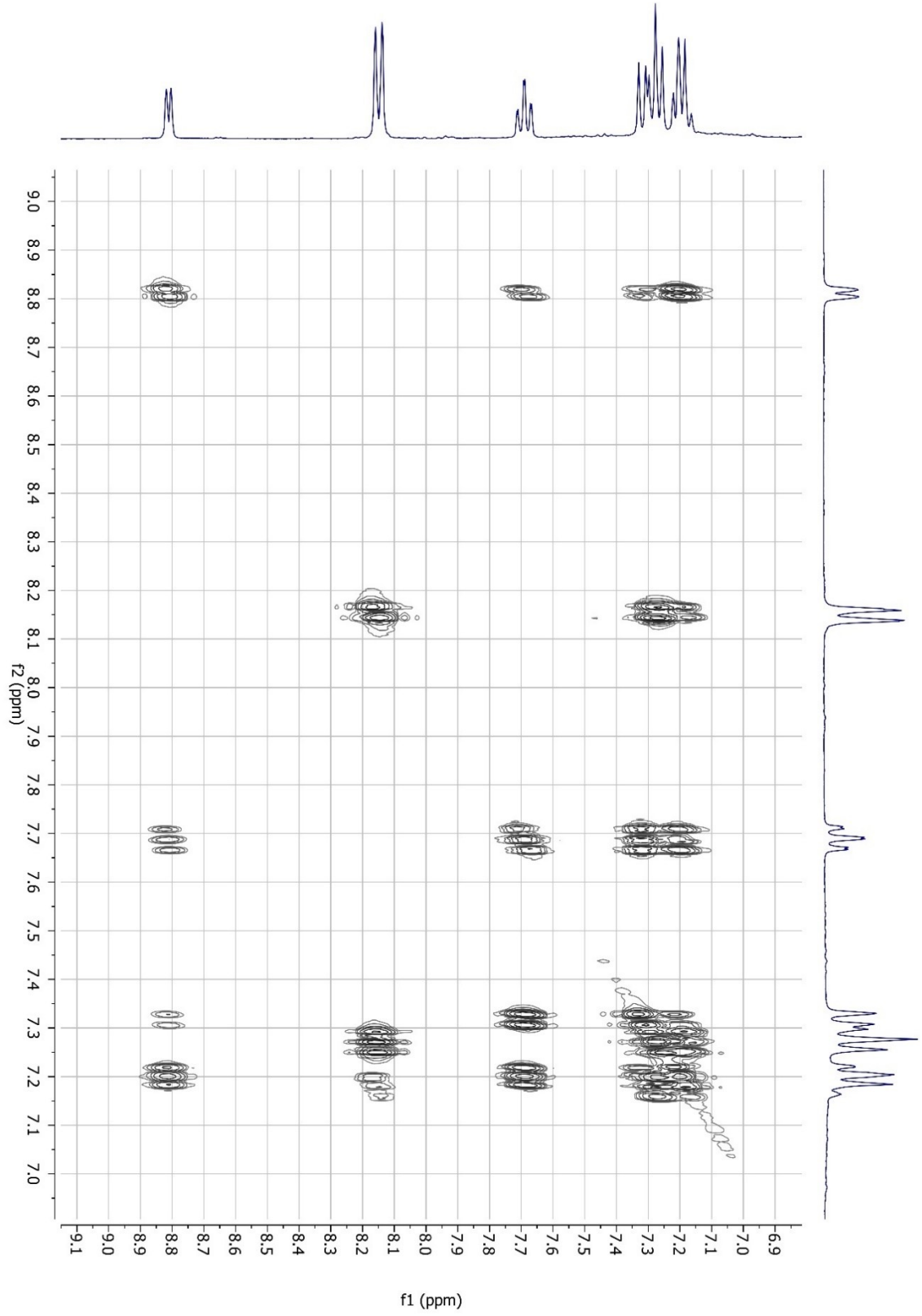

Figure S7.7-28: $^{1}H^{1}H$ COSY NMR [360 MHz, THF-d_8, 298 K] spectrum of ***fac*-K[Re(I)(Ph-*alkoxpy*-CO_2)$(CO)_3$] (102b)**.

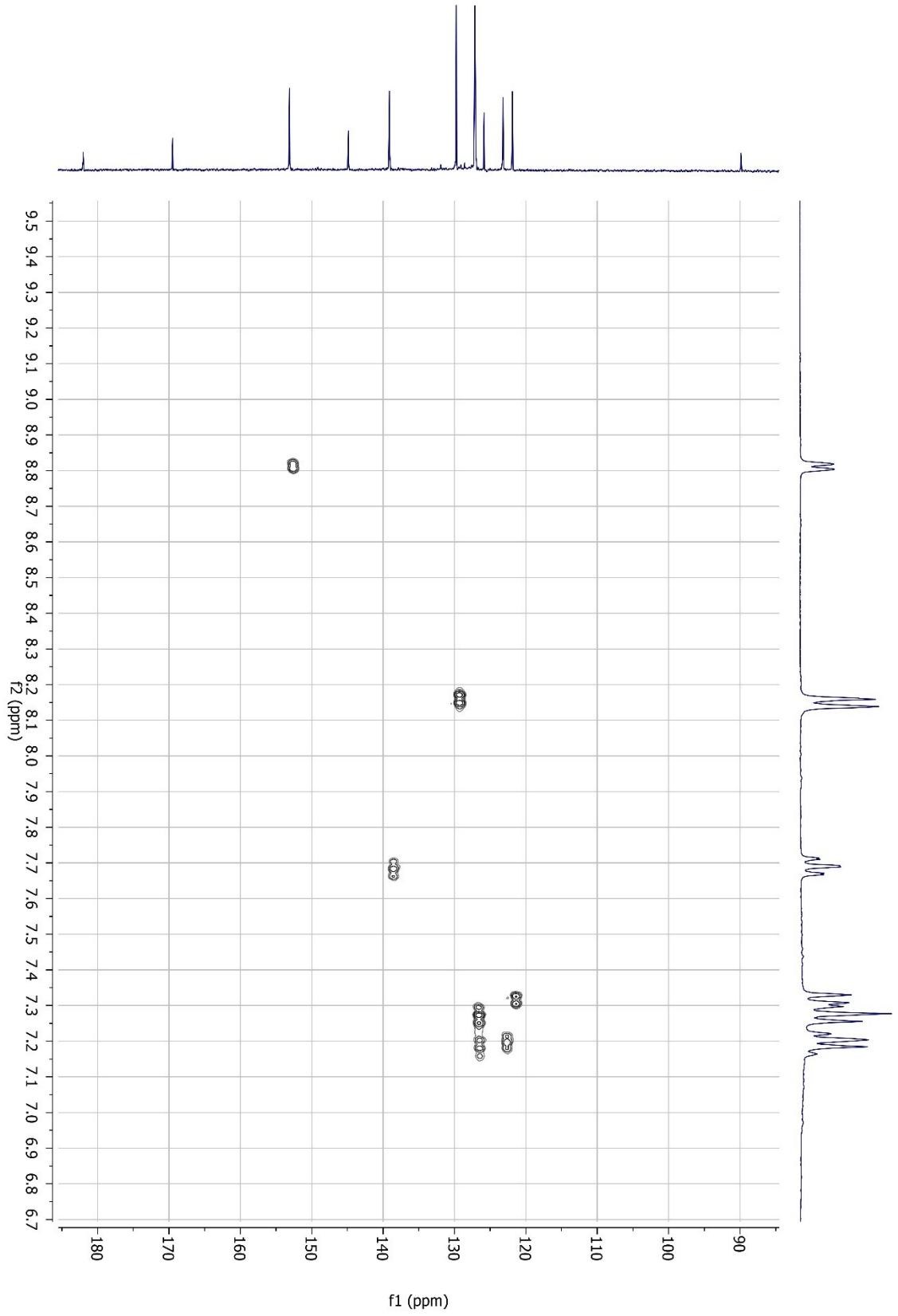

Figure S7.7-29: $^{1}H^{13}C$ HSQC NMR [360 MHz/ 91 MHz, THF-d_8, 298 K] spectrum of ***fac*-K[Re(I)(Ph-*alkoxpy*-CO_2)$(CO)_3$] (102b)**.

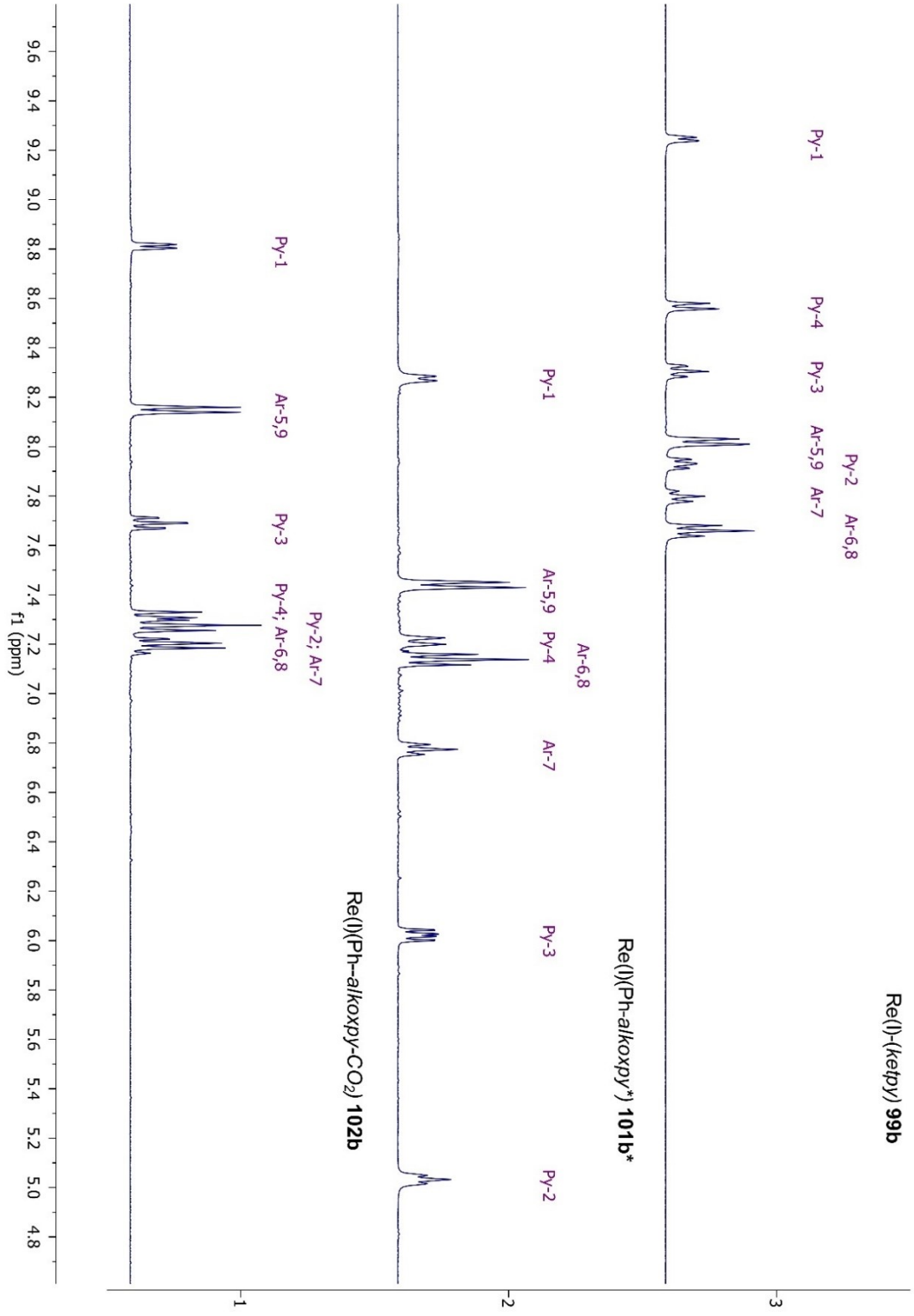

Figure S7.7-30: Section ^{1}H NMR [360 MHz, THF-d_8, 298 K] spectrum of **99b**, **101b*** and **102b.**

***fac*-[K(18-*crown*-6)][Re(I)(Ph-*alkoxpy*-CO_2)$(CO)_3$] (102b-crown)**

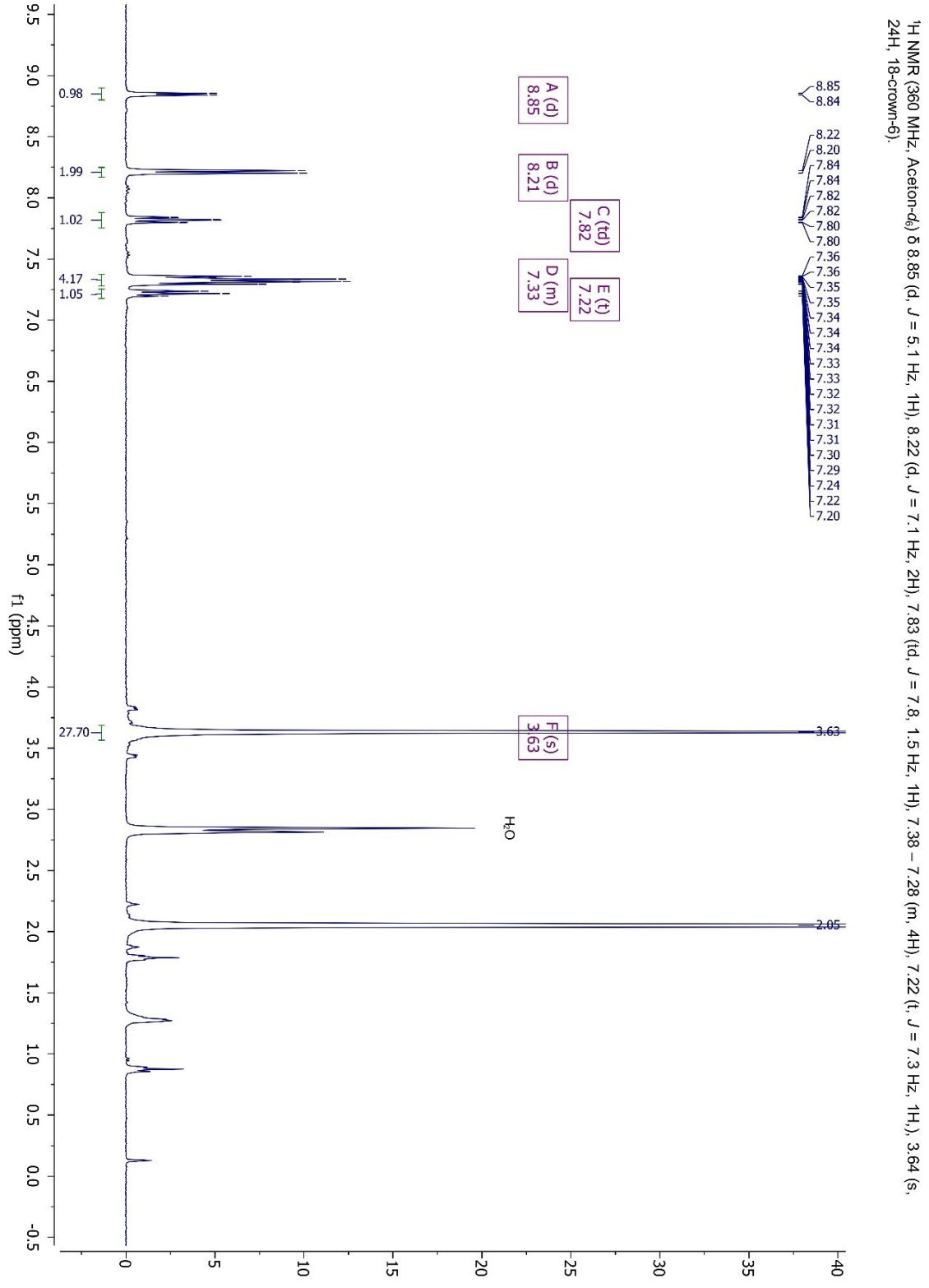

Figure S7.7-31: ^{1}H NMR [360 MHz, Aceton-d_6, 298 K] spectrum of ***fac*-[K(18-*crown*-6)][Re(I)(Ph-*alkoxpy*-CO_2)$(CO)_3$] (102b-crown)**.

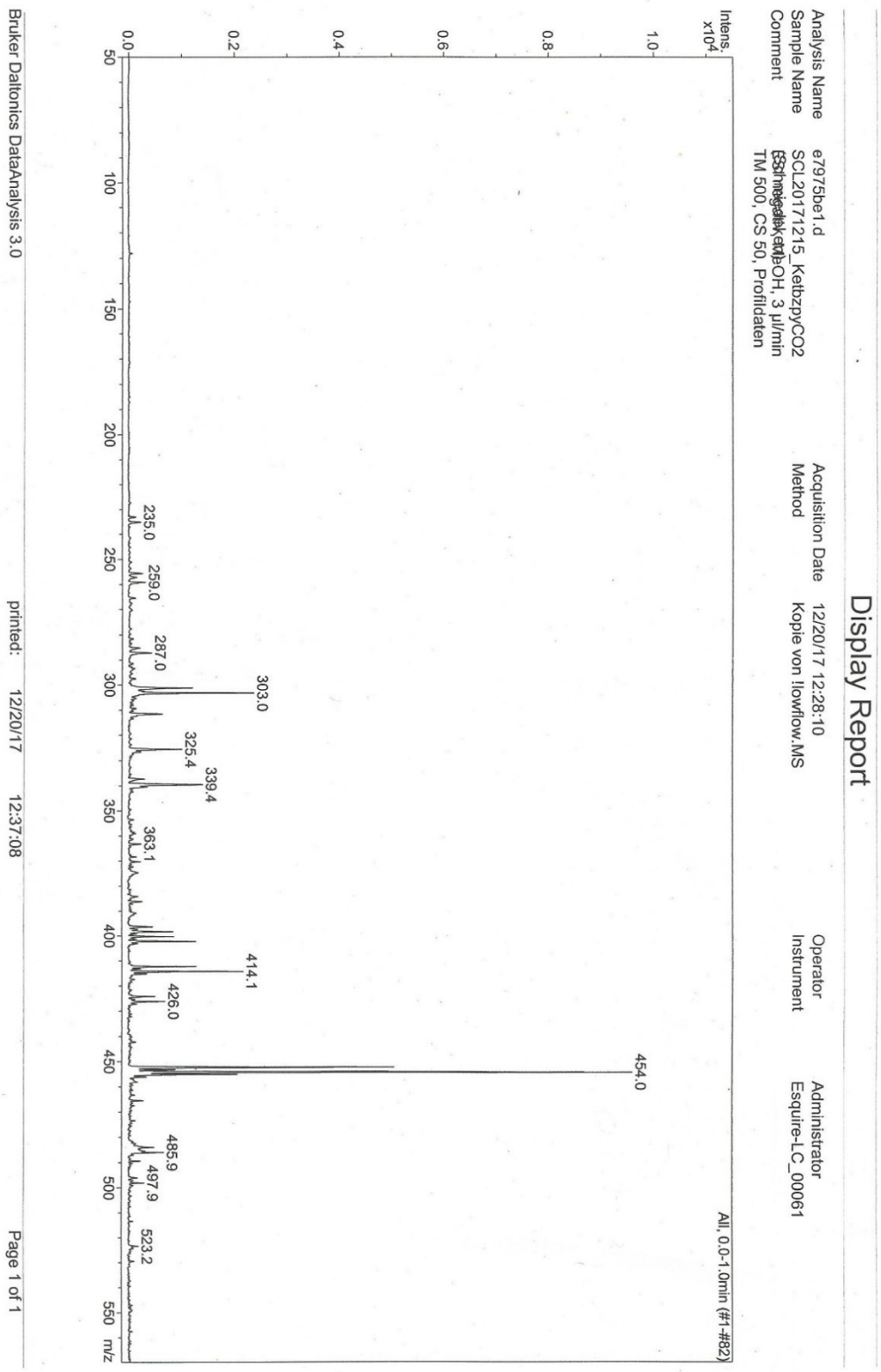

Figure S7.7-32: ESI-MS spectrum [MeOH] neg of ***fac*-[K(18-*crown*-6)][Re(I)(Ph-*alkoxpy*-CO_2)$(CO)_3$] (102b-crown)**.

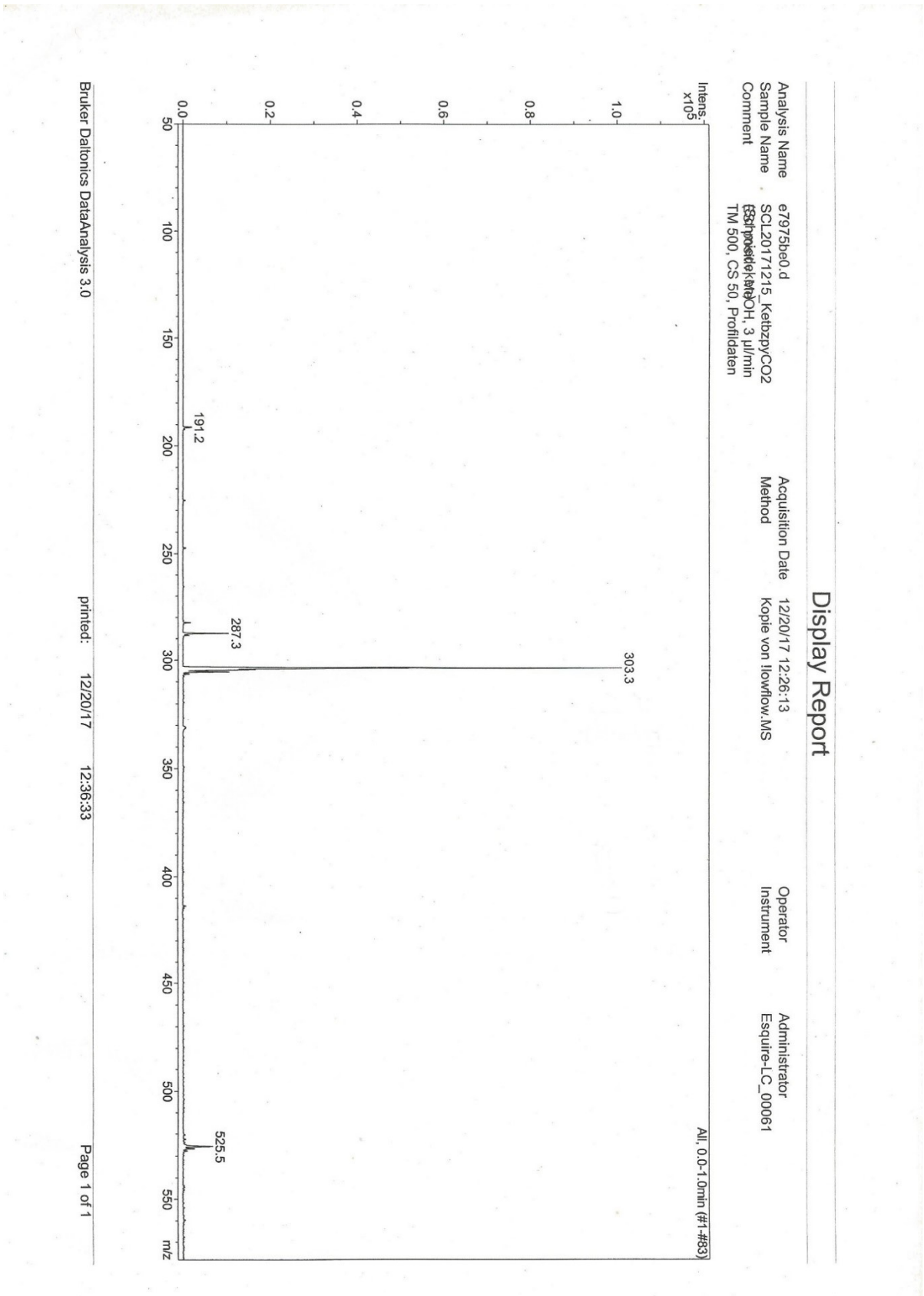

Figure S7.7-33: ESI-MS spectrum [MeOH] pos of ***fac*-[K(18-*crown*-6)][Re(I)(Ph-*alkoxpy*-CO_2)$(CO)_3$] (102b-crown)**.

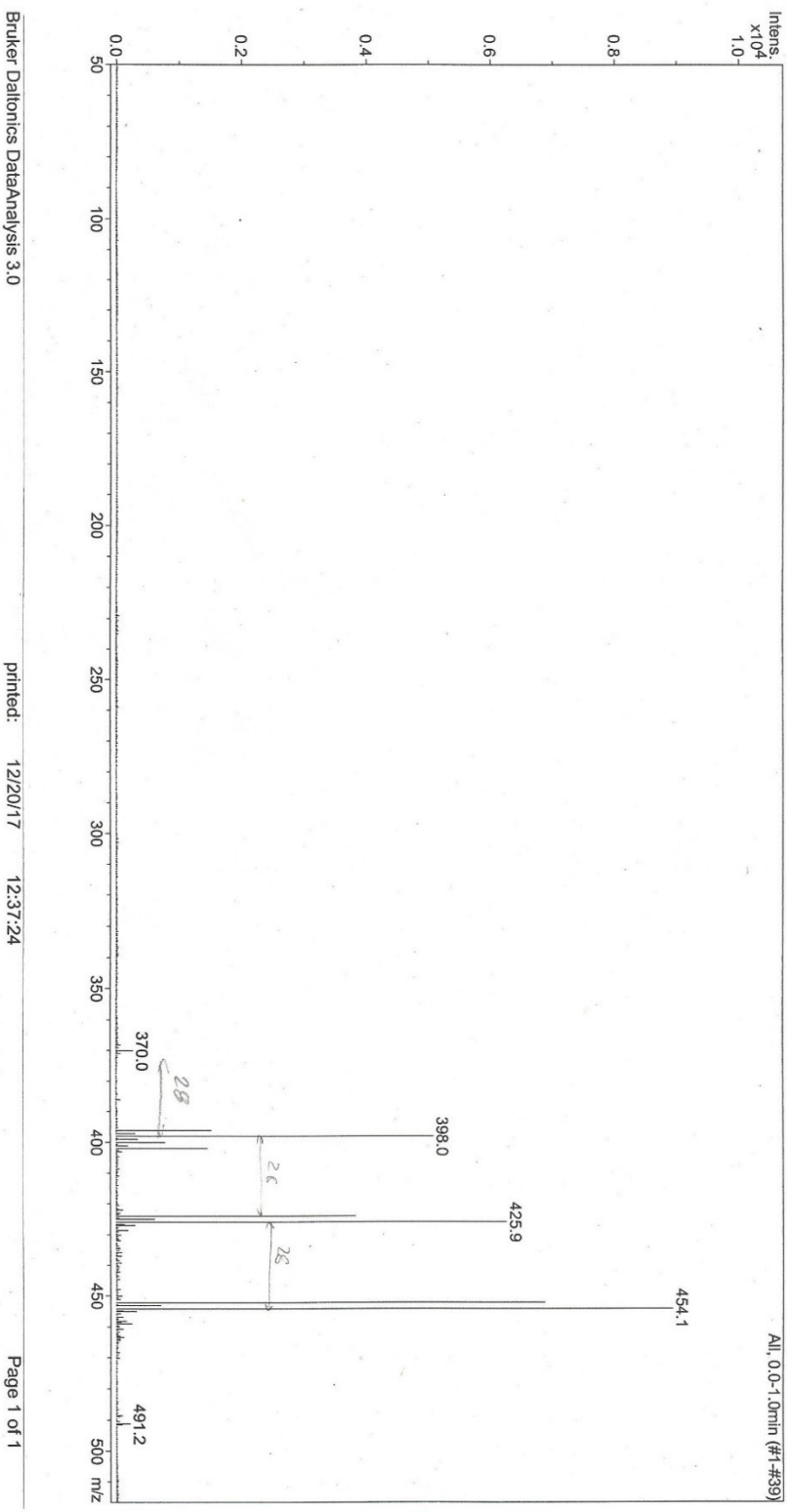

Figure S7.7-34: ESI-MS/MS spectrum [MeOH] neg at m/z = 454 of ***fac*-[K(18-*crown*-6)][Re(I)(Ph-*alkoxpy*-CO_2)$(CO)_3$] (102b-crown)**.

Table 14: Crystallographic data and structure refinement from Olex report of ***fac*-[K(18-*crown*-6)][Re(I)(Ph-*alkoxpy*-CO_2)$(CO)_3$] (102b-crown)**.

StichauerR180109_0m_a

Table 1 Crystal data and structure refinement for StichauerR180109_0m_a.

Identification code	StichauerR180109_0m_a
Empirical formula	$C_{29}H_{35}Cl_2KNO_{12}Re$
Formula weight	885.811
Temperature/K	100.01
Crystal system	triclinic
Space group	P-1
a/Å	7.8396(2)
b/Å	11.1598(3)
c/Å	20.1844(5)
α/°	95.465(2)
β/°	90.626(2)
γ/°	109.353(2)
Volume/Å^3	1656.85(8)
Z	2
ρ_{calc}g/cm^3	1.776
μ/mm^{-1}	4.016
F(000)	880.3
Crystal size/mm^3	N/A × N/A × N/A
Radiation	Mo Kα (λ = 0.71073)
2Θ range for data collection/°	4.58 to 56.82
Index ranges	-10 ≤ h ≤ 10, -14 ≤ k ≤ 14, -26 ≤ l ≤ 27
Reflections collected	34189
Independent reflections	8257 [R_{int} = 0.0740, R_{sigma} = 0.0614]
Data/restraints/parameters	8257/0/431
Goodness-of-fit on F^2	1.055
Final R indexes [I>=2σ (I)]	R_1 = 0.0458, wR_2 = 0.1015
Final R indexes [all data]	R_1 = 0.0606, wR_2 = 0.1081
Largest diff. peak/hole / e Å^{-3}	2.42/-2.83

Erklärung zur elektronischen Version und zur Überprüfung einer Dissertation

Hiermit bestätige ich gemäß §7, Abs. 7, Punkt 4, dass die zu Prüfungszwecken beigelegte elektronische Version meiner Dissertation identisch ist mit der abgegebenen gedruckten Version. Ich bin mit der Überprüfung meiner Dissertation gemäß §6, Abs. 2, Punkt 5 mit qualifizierter Software im Rahmen der Untersuchung von Plagiatsvorwürfen einverstanden.

_____ _____

Ort, Datum Rasmus Stichauer